Molecular mechanism(s) underlying multipartite genome maintenance in radiation resistant bacterium, *Deinococcus radiodurans* R1

By

Ganesh Kumar Maurya

LIFE01201304008

Bhabha Atomic Research Centre, Mumbai

A thesis submitted to the Board of Studies in Life Sciences
In partial fulfillment of requirements
For the Degree of

DOCTOR OF PHILOSOPHY
of
HOMI BHABHA NATIONAL INSTITUTE

February 2019

STATEMENT BY AUTHOR

This dissertation has been submitted in partial fulfillment of requirements for an advanced degree at Homi Bhabha National Institute (HBNI) and is deposited in the library to be made available to borrowers under rules of the HBNI.

Brief quotations from this dissertation are allowable without special permission, provided that accurate acknowledgement of source is made. Requests for permission for extended quotation from or reproduction of this manuscript in whole or in part may be granted by the Competent Authority of HBNI when in his or her judgment the proposed use of the material is in the interests of scholarship. In all other instances, however, permission must be obtained from the author.

Ganesh Kumar Maurya

DECLARATION

I, hereby declare that the investigation presented in the thesis has been carried out by me. The work is original and has not been submitted earlier as a whole or in part for a degree / diploma at this or any other Institution / University.

.

Ganesh Kumar Maurya

List of Publications Arising from the Thesis

Journal

1. ParA proteins of secondary genome elements cross-talk and regulate radioresistance through genome copy number reduction in *Deinococcus radiodurans*; **Maurya, G.K**., Kota, S., Kumar, N.N., Tewari, R. and Misra, H.S.; Biochemical Journal, 15;476(5) (2019), 909-930.
2. Characterisation of ParB encoded on multipartite genome in *Deinococcus radiodurans* and their roles in radioresistance; **Maurya, G.K**., Kota, S. and Misra, H.S.; Microbiological Research, 223–225 (2019), 22–32.
3. Plasmids for making multiple knockouts in a radioresistant bacterium *Deinococcus radiodurans*; **Maurya, G.K**. and Misra, H.S.; Plasmid, 100(2018), 6-13.
4. Divisome and segrosome components of *Deinococcus radiodurans* interact through cell division regulatory proteins; **Maurya, G.K**., Modi, K., and Misra, H.S.; Microbiology (UK), 162(8) (2016), 1321-34.
5. Maintenance of multipartite genome system and its functional significance in bacteria; Misra, H.S., **Maurya, G.K**., Kota, S., and Charaka, V.K.; Journal of Genetics 97(4) (2018), 1013-1038.
6. Interdependence of bacterial cell division and genome segregation and its potential in drug development. Misra, H.S., **Maurya, G.K**., Chaudhary, R. and Misra, C.S. Microbiological Research, 208(2018), 12-24.
7. Functional characterization of cis elements present upstream to *parAB* operon in secondary genome elements in *Deinococcus radiodurans;* **Maurya, G.K**. and Misra, H.S.; (Under preparation).

Symposia/Conference

1. Divisome and segrosome components of *Deinococcus radiodurans* form multiprotein complexes and interact through cell division regulatory proteins; **Maurya, G.K.,** Modi, K., and Misra, H. S.; **XXXIX All India Cell Biology Conference**, (2015) IISER-TVM, Thiruvananthpuram. Abs. No. 371.
2. Secondary genome ParA proteins of *Deinococcus radiodurans* are functionally similar and interact to each other; **Maurya, G.K.,** Kota, S. and Misra, H. S.; **7th Congress of European Microbiologists under Federation of European Microbiological societies (FEMS-2017)** held at Valencia, Spain, (2017) **Ref.No**. **FEMS7-0302**. Poster ID. 101.

   (got **"Early Career Scientist Grant award")**

3. Involvement of centromere binding proteins in genomic stability and radioresistance in *Deinococcus radiodurans;* **Maurya, G.K.,** Kota, S. and Misra, H. S.; **SFR ICRR-HHE** conference held in Hyderabad University, Hyderabad (2018). PP-12 (Abstract No.: 0042) in Journal of Radiation and Cancer Research; Volume 9, Issue 1.

Ganesh Kumar Maurya

Publications from other topics

1. Phosphorylation of FtsZ and FtsA by a DNA Damage-Responsive Ser/Thr Protein Kinase Affects Their Functional Interactions in *Deinococcus radiodurans*.; **Maurya, G.K**.,* Modi, K.,* Banerjee, M., Chaudhary, R., Rajpurohit, Y.S. and Misra, H.S.; mSphere, 3(4)(2018), pp.e00325-18.
2. Studies of protein–protein interactions in Fanconi anemia pathway to unravel the DNA interstrand crosslink repair mechanism; Siddiqui, M.Q., Rajpurohit, Y.S., Thapa, P.S., **Maurya, G.K**., Banerjee, K., Khan, M.A., Panda, P., Hasan, S.K., Gadewal, N., Misra, H.S. and Varma, A.K.; International Journal of Biological Macromolecules, 104, (2017), pp.1338-1344.
3. DrRecQ regulates guadruplex DNA structure dynamics and its impact on radioresistance in *Deinococcus radiodurans*.; NP Khairnar*, **Ganesh K Maurya***, Neha Pandey, Anubrata Das and H. S. Misra; Molecular Microbiology (Accepted), (2019), doi: 10.1111/mmi.14321.

(* - Shares equal authorship)

Ganesh Kumar Maurya

Dedicated to my

beloved parents.....

ACKNOWLEDGEMENTS

I express my deep and heartfelt sincere gratitude to my guide, **Prof. H. S. Misra**, Head, Molecular Biology Division, for suggesting this research problem and for sustained guidance and encouragement throughout the period of research. I also express my utmost gratitude to him for his constructive criticism, valuable suggestions and good wishes.

I express my sincere thanks to Dr. B. L. Das, RB&HSD for her encouragement, moral support and valuable guidance, which inspired me to do my best. I am also grateful to Prof. P. K. Mukherjee (NA&BTD), Dr. Ajay Saini (MBD) and Dr. R. Shashidhar (FTD), members of my doctoral committee, for providing valuable suggestions during annual progress presentation for the completion of this work.

I thank all my lab mates and friends Dr. Swati Kota, Dr. A. D. Das, Dr. Y.S. Rajpurohit, Dr. Suhash Mangoli, Dr. Sheetal Uppal, Dr. Nivedita P. Khairnar, Dr. Vijay K. Charaka, Dr. Kruti Mehta, Ms. Reema Chaudhary, Ms. Shruti Mishra, Mr. Dhirendra K Sharma, Dr. Manisha Banerjee, Dr. Alka Gupta, Dr. Rajinikanth Chitella, Dr. Debes Ray, Dr. R. Tewari, Dr. Naveen, Sunil D. Dhotre, Abhishek P. and all other friends for their constant support. I thank Dr. Hema Rajaram, Dean, Life Sciences for her academic guidance.

I would like to thank all my seniors (Gambhir sir, Rohit sir, Sumit Mehan sir, Mondal Sir, Pankaj Sir, Arvind sir, Gautam sir, Usha, Mahima ma'am and others), batchmates (Ravi dhawan, Francis, Divya T.V., Reema Singh, Gargi, Rakhee, Shankar) and juniors (Shikha, Shridhar, Suresh) for their friendly support and care across my Ph.D.

I acknowledge Department of Atomic Energy, Bhabha Atomic Research Centre for financial assistance during my Ph.D.

At the end, I give my heartfelt gratitude to all my family members (especially my mother) who have always encouraged and supported me.

With the blessing of Lord Shiva, I am thankful to everybody who directly or indirectly was the part of this journey.

February, 2019

MBD, BARC Ganesh Kumar Maurya

HBNI, Mumbai

TABLE OF CONTENTS

Summary

Segregation of duplicated genome is a key step for productive cell division and growth in both bacteria and higher organisms. These processes are interdependent and the molecular machineries controlling them are tightly coordinated and regulated at functional level. Unlike eukaryotic cells where DNA replication, chromosome condensation, sister chromatid segregation and cytokinesis are timely separated, the temporal separation of these molecular events are not very clear in bacteria. In prokaryotes, genome segregation mechanisms are mostly studied in bacteria harbouring single circular chromosome and low copy number plasmids. The tripartite bacterial genome segregation (TGS) system consists of; (i) an origin-proximal centromere or a similar *cis* element, (ii) centromere binding protein, as ParB or its homologs and (iii) P-loop Walker ATPases named ParA or its homologs. Mechanistically, ParBs bind specifically to the centromere-like sequence and form nucleoprotein complex while ParAs polymerize along the DNA and oscillates between the poles in rod shaped bacteria. Depending upon the regulation of polymerisation/depolymerization dynamics of ParA or its homologs, different mechanisms of bacterial genome segregation have been proposed for faithful segregation of DNA molecule.

Unlike bacteria harbouring single circular chromosome and or low copy plasmid, the TGS system is not much studied in multipartite genome harbouring bacteria. Very limited studies have been done in *Vibrio cholerae, Burkholderia cenocepacia*, *Deinococcus radiodurans*, *Brucella abortus* and *Rhodobacter sphearoides*. The multipartite genome of *D. radiodurans,* a radioresistant bacterium, also harbours polyploidy-multipartite genome system consisting of 2 chromosomes and 2 plasmids. Its genome encodes 4 ParA and 4 ParB proteins distributed on both primary (chromosome I) and secondary genome replicons (chromosome II and megaplasmid). This thesis has characterized complete TGS system of both the secondary

genome elements. We observed that P-loop ATPase of chromosome II (ParA2) and megaplasmid (ParA3) are similar in their structure and function. The double mutant showed septum trapped nucleoid phenotype suggesting a cross-talk with cell division proteins of this bacterium. We reported that secondary genome ParAs as well as cognate ParBs interact with cell division regulatory proteins of this organism. Further, direct repeats present upstream to *parA2B2* and *parA3B3* operons were characterized and found to have the features of both origin of replication and centromeres in *D. radiodurans*. The deinococcal ParBs were found as dimeric in nature and interacted to replication initiation proteins viz. DnaA and DnaB. The deletion of *parB1, parB2* and *parB3* genes has increased the ploidy of respective genomic elements suggesting a role of ParBs in DNA replication regulation. The deletion of *parB* genes caused defective segregation and increased sensitivity for γ-ray and H_2O_2. These observations together suggest the role of genome segregation proteins in DNA replication, cell division and radioresistance in this bacterium. In addition, both primary chromosome and secondary genome elements were marked with different fluorescent protein using FROS (Fluorescent Reporter Operator System) approach. The results presented in the thesis have provided evidence that primary chromosome and secondary genome elements segregate independently in *D. radiodurans* by the mechanism that are encoded on them. Interestingly, both the secondary genome elements cross talk for their existence in the dividing population under normal conditions.

List of figures:

List of Tables:

List of abbreviations:

LB	Luria Broth	EDTA	Ethylene diamine tetra acetic
TYG	Tryptone yeast extract Glucose	dsDNA	Double stranded DNA
FISH	Florescence in-situ hybridization	HTH	Helix Turn Helix
PCR	Polymerase chain reaction	MSA	Multiple sequence alignment
PFGE	Pulsed field gel electrophoresis	MGH	Multipartiote genome horboring
RT	Room Temperature	TGS	Tripartite genome system
W/V	Weight/Volume	DAPI	4, 6'diamino -2-phenylindole.2HCl
Ni-NTA	Nickel-nitrilo acetic acid	FITC	Fluorescein isothiocyanate
NBT / BCIP	Nitro blue tetrazolium / 5-bromo-4-chloro-3-indolyl phosphate	TRITC	Tetramethylrhodamine -isothiocyanate

Chapter 1

Introduction and Review of Literature

"The genome is a book that wrote itself, continually adding, deleting and amending over four billion years."

–Matt Ridley

1.1 Genome organization in bacteria

All living organisms contain DNA which is collectively called as genome. DNA is a biological macromolecule that encodes all the information required to program the cell's activities. Inside the cell, genome is arranged in a confined space called nucleoid or nucleus. Such arrangements are highly dynamic and are required for temporal and spatial regulation of genome functions. The physical compaction and functional organization of large genome in tiny cell volume is a multistep event. The organization of genome in bacteria and eukaryotes looks diverse but follows some common principle (Luijsterburg *et al*., 2008; Brocken *et al*., 2018). Like eukaryotic insulator proteins, bacterial H-NS-family proteins (IHF, HU and SMC proteins) hold DNA to form loops at different length scale (Phillips-Cremins, 2013; Van der valk, *et al*., 2014), which are arranged in structural domains known as genome activity (Cavalli, 2013; Brocken *et al*., 2018). The study of bacterial genome organization has advanced with the emergence of fluorescence microscopy where fluorescent *in situ* hybridization (FISH) and fluorescent repressor-operator system (FROS) has been used to define the positioning of different genomic loci and genome elements within the cell (Nath, 2000; Robinett, 1996; Webb, 1997). The emergence of new technologies like chromosome confirmation capture (3C) has helped in better understanding of genome folding and function (Dekker, 2002; Simonis, 2006; Dekker, 2016). In addition, Hi-C (Lieberman-Aiden *et al*., 2009) and genome wide contact matrices have been generated in several organisms including bacteria like *Caulobacater crescentus* (Le, 2013; Tran, 2017), *Bacillus subtilis* (Wang, 2015; Wang, 2017) and *Mycoplasma pneumonia* (Trussart *et al*., 2017). These matrices with modelling approaches have deciphered the global and local features of genome structures (Brocken *et al*., 2018). FROS, 3C and Hi-C have advanced our knowledge of genome organization *in vivo*.

In early 1960s after discovery of DNA structure, first evidence of genome being single circular chromosome came from *E. coli* (Cairns, 1963; Jacob *et al.,* 1963). Till 1980, it was largely believed that bacteria have single circular chromosome with some smaller, nonessential, circular plasmids (diCenzo and Finan, 2017). The chromosome is defined as primary genetic material, which encodes proteins required for essential functions and therefore it is indispensable. The plasmids present in bacteria contribute to the survival of these organisms under adverse conditions (Holden *et al.* 2004; Cooper *et al.* 2010). The diversity occurs in physical organization of chromosome and plasmids in different bacteria. Mostly, circular chromosome and plasmid are confined in separate location inside the cell, but in some bacteria including *Deinococcus radiodurans* (a radioresistant bacterium) they are packed together in a highly compact and doughnut shaped nucleoid (Minsky *et al*., 2006).

1.2 Multipartite genome harboring bacteria

Unlike eukaryotes, the bacterial genome was largely defined as single circular chromosome in less than 2 copies per cell and plasmids as extra chromosomal genetic material. The identification of first linear plasmid in *Streptomyces* in 1979 (Hayakawa *et al*., 1979) and linear chromosome in *Borrelia burgdorferi* in 1989 (Baril *et al*., 1989) had changed the perspective that bacterial genome could be linear. In 1989, pulsed field gel electrophoresis study in *Rhodobacter sphaeroides* reported two circular chromosomes and five large plasmids as its genome (Suwanto and Kaplan, 1989). Thus, *R. sphaeroides* became first multipartite genome harbouring (MGH) bacteria. Usually, primary chromosome contains more conserved housekeeping genes and higher synteny than secondary genome (Lykidis *et al.* 2010). The secondary chromosomes are normally smaller than primary chromosomes (Prozorov, 2008). On the other hand, the secondary genome elements show a greater variability and encode accessory functions associated with adaptation and survival in

different niches, and largely contribute to stress tolerance (Holden *et al.* 2004; Cooper *et al.* 2010; Lykidis *et al.* 2010). Interestingly, in multipartite genome each DNA replicon is physically separate with distinct properties, like differences in codon usage, GC content and dinucleotide relative abundance (diCenzo and Finan, 2017). With advancement in DNA sequencing technology, a large number of bacteria across different phylogenetic groups have been reported whose genome consists of more than one chromosome and megaplasmid (reviewed by Misra *et al*., 2018). It has been also observed that many MGH bacteria are either pathogenic to animals, human and plants or possess tolerance towards abiotic stresses as listed in Table 1.

Table 1.1 The genome composition and inhabitat of known MGH bacteria (replicon size> 50kb) (Misra *et al*., 2018).

Bacteria	Replicons	Size (Mbp)	Specific features	Sources
Agrobacterium radiobacter K84	Chr I	4	Biological control agent againt some pathogenic bacteria.	Slater *et al.,* (2009)
	Megarepli con	2.65		
	pAgK84B	0.184		
Agrobacterium tumefaciens C58	Chr I	2.84	Plant pathogen	Goodner *et al.,* (2001)
	Chr II	2.08		
	pAtC58	0.54		
Agrobacterium vitis S4	Chr I	3.72	Grapevine plant pathogen	Slater *et al.,* (2009)
	Chr II	1.28		
	pAtS4e	0.631		
	pTiS4	0.258		
	pAtS4c	0.211		
	pAtS4b	0.13		
	pAtS4a	0.078		
Anabaena sp 90	Chr I	4.32	Stress tolerant cyanobacteria	Wang *et al*., (2012)
	Chr II	0.81		
	Plasmid A	0.080		
	Plasmid B	0.056		
Brucella abortus A13334	Chr I	2.12	Cattle pathogen	Kim*et al.,* (2012)
	Chr II	1.16		
Brucella canis	Chr I	2.01	Canine pathogen	Kim *et al.,* (2012)
	Chr II	1.17		
Brucella ceti TE10759-12	Chr I	2.11	Dolphins pathogen	Ancora *et al.,* (2014)
	Chr II	1.16		

Brucella melitensis NI	Chr I	2.11	Causes zoonotic brucellosis	Michaux *et al.,* (1993) Jumas-Bilak*et al.,* (1998)
	Chr II	1.17		
Brucella ovis ATCC 25840	Chr I	2.11	Veterinary sheep pathogen	Paulsen *et al.,* (2002) Tsolis *et al.,* (2009)
	Chr II	1.16		
Brucella pinnipedialis B2	Chr I	2.13	Pinnipeds (Seal) pathogen	Audic *et al.,* (2011)
	Chr II	1.26		
Brucella suis VBI22	Chr I	2.1	Causes brucellosis in animals	Tae *et al.,* (2011)
	Chr II	1.2		
Burkholderia ambifaria	Chr I	3.44	Causes cystic fibrosis in human	CP001025.1
	Chr II	2.77		CP001026.1
	Chr III	1.13		CP001027.1
	Plasmid	0.3		CP001028.1
Burkholderia cenocepacia J2315	Chr I	3.87	Causes cystic fibrosis in human	Holden *et al*., (2009)
	Chr II	3.21		
	Chr III	0.87		
	Plasmid	0.092		
Burkholderia dolosa	Chr I	3.31	Opportunistic pathogen in human	Workentine *et al.,* (2014)
	Chr II	2.16		
	Chr III	0.82		
Burkholderia gladioli	Chr I	4.41	Plant pathogen and opportunistic pathogen in human	Seo *et al.,* (2011)
	Chr II	3.7		
	bgla_1p	0.28		
	bgla_2p	0.13		
	bgla_3p	0.13		
	bgla_4p	0.4		
Burkholderia mallei	Chr I	3.51	Etiological agent of glanders	Nierman *et al.,* (2004)
	Chr II	2.33		
Burkholderia multivorans ATCC 17616	Chr I	3.45	Infectious in cystic fibrosis patients	Komatsu *et al.,* (2003)
	Chr II	2.47		
	Chr III	0.92		
	Plasmid	0.17		
Burkholderia phenoliruptrix BR3459a	Chr I	4.15	Stress tolerant symbiont of *Mimosa flocculosa*	Zuleta *et al.,* (2014)
	Chr II	2.71		
	Plasmid	0.78		
Burkholderia pseudomallei	Chr I	4.07	Causative agent of melioidosis	Holden *et al*., (2004)
	Chr II	3.17		
Burkholderia thailandensis MSMB121	Chr I	3.67	Non-pathogenic but opportunistic	Tuanyok *et al.,* (2013)
	Chr II	2.76		
Burkholderia vietnamiensis G4	Chr I	3.65	TCE degrador and cystic fibrosis pathogen	CP000614.1
	Chr II	2.41		CP000615.1
	Chr III	1.24		CP000616.1
	pBVIE01	0.4		CP000617.1
	pBVIE02	0.27		CP000618.1

	pBVIE03	0.23		CP000619.1
	pBVIE04	0.11		CP000620.1
	pBVIE05	0.09		CP000621.1
Burkholderia xenovorans	Chr I	4.89	A polychlorinated biphenyl (PCB) degrader	Chain *et al*. (2006)
	Chr II	3.36		
	MP	1.47		
Butyrivibrio proteoclasticus	Chr I	3.55	Rumen bacterium help in plant polysaccharide degradation	Kelly *et al.,* (2010)
	Chr II	0.3		
	pCY360	0.36		
	pCY186	0.19		
Candidatus Chloracidobacterium thermophilum	Chr I	2.68	Biocidal to microbial mat of alkaline siliceous hot springs	Garcia *et al.,* (2012)
	Chr II	1.01		
Cupriavidus taiwanensis LMG 19424	Chr I	3.41	Nitrogen Fixing Symbiont	Amadou *et al.,* (2008)
	Chr II	2.5		
	pRalta	0.55		
Cyanothece 51142	Chr I Cir.	4.93	Diazotrophic cyanobacterium	Welsh *et al.,* (2008)
	Chr II Lin.	0.42		
Deinococcus radiodurans R1	Chr I	2.64	Extraordinary radioresistance	White *et al.,* (1999)
	Chr II	0.41		
	MP	0.17		
Leptospira interrogans	Chr I	4.33	Leptospirosis in human	Ren *et al.,* (2003)
	Chr II	0.36		
Ochrobactrum anthropi	Chr I	2.89	An opportunistic human pathogen	Jumas-Bilak *et al*., (1998); Chain *et al*., (2011)
	Chr II	1.9		
	pOANT01	0.17		
	pOANT02	0.1		
	pOANT03	0.09		
	pOANT04	0.06		
Ochrobactrum intermedium	Chr I	2.6	Opportunistic gut pathogen in human	Kulkarni *et al*., (2013)
	Chr II	1.91		
	Plasmid	0.06		
Photobacterium angustum	Chr I	3.2	Bioluminescent and a symbiont marine fish	Bjornsdottir-Butler *et al*., (2015)
	Chr II	1.8		
Photobacterium damselae	Chr I	3.2	Pathogenic to marine fishes	NZ_ADBS00000000.1
	Chr II	1.4		
Photobacterium leiognathi	Chr I	3.3	Bioluminescent and a symbiont of ponyfish	NZ_JZSK00000000.1
	Chr II	1.6		
Photobacterium profundum SS9	Chr I	4.09	A barophilic marine bacterium	Vezzi *et al.,* (2005)
	Chr II	2.24		
	pPBPR1	0.08		
Prevotella dentalis DSM	Chr I	1.89	Dental root canol infections	NC_019960.1
	Chr II	1.45		NC_019961.1
Prevotella intermedia	Chr I	0.58	Causes peridontal disease and gingivitis	Nambu *et al*., (2015)
	Chr II	2.12		

Prevotella melaninogenica ATCC 25845	Chr I	1.8	Lives in oral cavity and infect teeth	NC_014370.1
	Chr II	1.37		NC_014371.1
Pseudoalteromonas haloplanktis TAC125	Chr I	3.21	A psychrophilic bacterium	Medigue *et al.,* (2005)
	Chr II	0.635		
Pseudoalteromonas sp. SM9913	Chr I	3.33	Adapted to deep-sea sedimentary life	Qin *et al.,* (2011)
	Chr II	0.7		
Ralstonia eutropha JMP134 (pJP4)	Chr I	3.81	Chloroaromatic pollutants degrador	NC_007347.1
	Chr II	2.73		NC_007348.1
	MP	0.63		NC_007336.1
	Plasmid1	0.087		NC_007337.1
Ralstonia pickettii DTP0602	Chr I	4.49	Degrades 2,4,6-trichlorophenol	Ohtsubo *et al.,* (2013)
	Chr II	2.88		
	Chr III	0.73		
Rhizobium sp. IRBG74	Chr I	2.84	Legume symbiont diazotroph	Crook *et al.,* (2012)
	Chr II (linear)	2.03		
	pIRBG74a	0.58		
Rhodobacter sphaeroides KD131	Chr I	3.05	Purple non-sulpher photosynthetic bacterium	Suwanto *et al*., (1989); Lim *et al.,* (2009)
	Chr II	0.91		
Salinivibrio costicola	Chr I	3.2	a halotolerant facultative anaerobe	AQOF00000000.1
	Chr II	1.3		
Sinorhizobium meliloti	Chr I	3.65	Legumes symbiotic bacterium	Sobral *et al.,* (1991); Galardini *et al.,* (2013)
	pSymA	1.35		
	pSymB	1.68		
Sphingobium japonicum UT26S	Chr I	3.51	Hexachlorocyclohexan degrador	Nagata *et al.,* (2010)
	Chr II	0.68		
	pCHQ1	0.19		
Variovorax paradoxus S110	Chr I	5.8	Biogenic and anthropogenic contaminants degrador	NC_012791.1
	Chr II	1.35		NC_012792.1
Vibrio alginolyticus	Chr I	3.33	Humans and marine animals' pathogen	Liu *et al.,* (2015)
	Chr II	1.81		
Vibrio campbellii ATCC BAA-1116	Chr I	3.77	A bioluminescent marine bacterium	Wang, *et al.,* (2013)
	Chr II	2.2		
	Plasmid	0.09		
Vibrio cholerae O1 biovar eltor str. N16961	Chr I	2.96	An etiological agent of cholera	Heidelberg *et al*., (2000)
	Chr II	1.07		
Vibrio fischeri ES114	Chr I	2.9	Certain fishes and squids' infectious agent	Ruby *et al.,* (2005)
	Chr II	1.3		
Vibrio furnissii	Chr I	3.29	Acute gastroenteritis infections	Lux *et al.,* (2011)
	Chr II	1.62		
Vibrio	Chr I	3.28	Gastroenteritis infections	Makino *et al.,*

parahaemolyticus RIMD 2210633	Chr II	1.87		(2003)
Vibrio splendidus LGP 32	Chr I	3.3	Oyster pathogen	Le Roux *et al.,* (2009)
	Chr II	1.68		
Vibrio vulnificus	Chr I	3.35	Causes seafood-born infections in human	Chen *et al.,* (2003)
	Chr II	1.85		
Vibrio nigripulchritudo	Chr I	4.11	Cause Summer syndrome in Shrimp	Goudenege *et al.* (2013)
	Chr II	2.41		
Vibrio mediterranei	Chr I	3.6	Non-pathogenic, gut colonizer of turbot larvae	NZ_BCUE00000000.1
	Chr II	2.3		
Alivibrio salmonicida	Chr I	3.3	Causes Hitra disease in Atlantic salmon and rainbow trout	Hjerde *et al*., (2008)
	Chr II	1.21		
	pVSAL84	0.08		
Vibrio tubiashii	Chr I	3.3	pathogenic for oyster and clam larvae	Temperton *et al*., (2011)
	Chr II	1.77		
	P251	0.25		
	P123	0.122		
	P57	0.057		
Vibrio natriegens	Chr I	3.3	Non-Pathogenic, halophile	Wang *et al*., (2013)
	Chr II	1.9		
Vibrio nereis	Chr I	3.3	Non-Pathogenic, halophile	NZ_BCUD00000000.1
	Chr II	1.9		
Vibrio fluvialis	Chr I	3.3	Causes gastroenteritis in humans	de Oliveira Veras *et al*., (2015)
	Chr II	1.9		
Vibrio orientalis	Chr I	3.3	Associated with aquaculture farm	NZ_ACZV00000000.1
	Chr II	1.7		
Vibrio aestuarianus	Chr I	3.2	Pathogenic to Oyster	Okada *et al.,* (2005)
	Chr II	1.8		
Vibrio pelagius	Chr I	3.2	Non-Pathogenic	Okada *et al.,* (2005)
	Chr II	1.7		
Vibrio wodanis	Chr I	3.3	Fish pathogen	NZ_LN554846.1
	Chr II	1.52		NZ_LN554847.1
	pAWOD9	0.091		NZ_LN554848.1
Vibrio proteolyticus	Chr I	3.2	Marine Pathogen in Corals	NZ_BATJ00000000.1
	Chr II	1.7		
Vibrio ichthyoenteri	Chr I	3.2	Pathogens of Japanese flounder larvae	Hoffmann *et al.,* (2012)
	Chr II	1.4		
Vibrio pectenicida	Chr I	3.2	A pathogen of scallop larvae	Okada *et al.*, (2005)
	Chr II	1.4		
Vibrio logei	Chr I	3	Bioluminscent organism	AJYJ00000000.2
	Chr II	1.5		
Vibrio mimicus	Chr I	2.97	Human Pathogen	Hasan *et al.,*

	Chr II	1.3		(2010)
Vibrio mytili	Chr I	3	Hosted in Mussels	NZ_JXOK00000000.1
	Chr II	1.5		
Vibrio rumoiensis	Chr I	3	Facultatively Psychrophilic Bacterium	NZ_AJYK00000000.2
	Chr II	1.3		
Vibrio anguillarum	Chr I	3.06	Pathogenic to marine fishes	Naka *et al*., (2011)
	Chr II	0.98		
	pJM1	0.065		
Vibrio gazogenes	Chr I	3	Non-pathogenic to human, marine bacteria	FQUH00000000.1
	Chr II	1.2		
Vibrio halioticoli	Chr I	3	Alginolytic marine bacterium isolated from the gut	NZ_BAUJ00000000.1
	Chr II	1.1		
Vibrio hollisae	Chr I	3.22	Occasional human pathogen	NZ_CP014055.1
	Chr II	0.78		NZ_CP014056.1
Vibrio ordalii	Chr I	3	Pathogenic to marine fishes	Naka *et al*., (2011)
	Chr II	0.9		
Vibrio metschnikovii	Chr I	3	Occasional human pathogen	NZ_ACZO00000000.1
	Chr II	0.9		

The organization of multipartite genome is better known in few of the listed MGH bacteria such as *V. cholerae, B. cenocepacia, B. abortus, R. sphaeroides, S. meliloti* and *D. radiodurans* (Trucksis *et al*. 1998; Fogel and Waldor, 2005; Komatsu *et al*. 2003; Kim *et al*., 2012; Suwanto and Kaplan, 1989; Deghelt *et al*., 2013; Galardini *et al*., 2013; Minsky *et al*., 2006).

1.3 Origin of multipartite genome

Since the discovery of first MGH bacterium, the origin of multipartite genome remains a point of discussion among genome biologist. Currently, there are two hypotheses: the schism hypothesis and the plasmid hypothesis that are debated regarding origin of secondary replicons in bacteria and a large amount of information in support and/or opposition to these hypotheses have been reported in literature (Moreno, 1998; Prozorov, 2008; Choudhary *et al*., 2012; Egan *et al*., 2005; diCenzo and Finan, 2017). According to Schism hypothesis the secondary essential replicons are formed as a result of splitting of an ancestral chromosome.

This hypothesis was earlier given to explain the chromid formation in *B. suis* (Jumas-Bilak, 1998) and *R. sphaeroides* (Choudhary *et al*., 1997). If Schism hypothesis is true then two resulting replicons should have higher similarity and equal distribution of core genes between them. However, biased distribution of essential genes on primary chromosome in MGH bacteria is against to this model (Harrison *et al*., 2010). The plasmid hypothesis on the otherhand states that secondary essential replicon originates from a megaplasmid. According this hypothesis, the coevolution of a megaplasmid with a chromosome will result in loss of genomic features of megaplsmid to that of the chromosome and the gain of essential genes through transfer from the chromosome (diCenzo and Finan, 2017). The resulting replicon i.e. chromid has replication and segregation machinery similar to megaplasmid (Harrison *et al*., 2010). The plasmid hypothesis provides the most favorable explanation for the origin of essential secondary replicons to date.

1.4 Importance of multipartite genome

The origin of multipartite or divided genome has brought certain advantages to their hosts, which are listed below.

1. The average size of a multipartite genome in bacteria is larger than non-multipartite which allow increased gene accumulation (diCenzo and Finan, 2017).

2. The multipartite genome may affect bacterial growth by adjusting the time required for DNA duplication, as each replicon will have to replicate and segregate before cell division can take place (Rasmussen *et al*. 2007; Deghelt *et al*., 2013; Frage *et al*., 2016). But this feature may not be a driving force for the evolution of multipartite genome in bacteria (diCenzo and Finan, 2017). The multipartite genome is not a requirement for fast growth. For example, *R. sphaeroides*, an MGH bacterium is having long generation times (Egan *et al*., 2005) while *Clostridium perfringens,* a non-MGH bacterium can have a generation times as short as 7 minutes (Labbe and Huang, 1995).

3. The distribution of genes between multiple replicons facilitates their coordinated regulation, possibly through the modulation of gene dosage (diCenzo and Finan, 2017).

4. Each replicon in multipartite genome contributes to adaptation to novel niches (Chain *et al*., 2006; diCenzo, 2014). More specifically, secondary genome elements in several MGH bacteria have been known to encode functions adapted through the course of evolution via. horizontal gene transfer andare required for survival under unique environments (Wiedenbeck and Cohan, 2011). In contrast, the primary chromosome is needed for normal growth and survival under unspecialized conditions or environments (diCenzo and Finan, 2017).

1.5 Segregation of DNA in bacteria

Segregation is defined as biological process that assures faithful and stable inheritance of duplicated genome from one generation to another and helps to maintain continuity of life. The inheritance of different phenotype in daughter cells depends upon precision in DNA duplication followed by segregation. Any defect or mutation in these processes will cause genetic defect which ultimately affect the phenotype. The basic mechanism of chromosome segregation is relatively better understood in eukaryotes where the chromosome replication, segregation and cell division are temporally separated (Yanagida, 2005). During eukaryotic cell cycle, DNA duplication occurs in S-phase followed by partitioning in M-phase, and then cytokinesis occurs once segregated chromosomes have reached to opposite halves of the cell. A large number of proteins work under tight regulation during replication and segregation in eukaryotes to transfer genetic material from one generation to another generation. The two identical sister chromatids produced after duplication are entangled at site of centromere. The microtubule filaments capture centromeric region and separate the sister chromatids to opposite poles through GTP dependent polymerization/depolymerization dynamics and finally cell divides (Tessema *et al*., 2004).

The genome partitioning biology is much explored and found to be conserved in eukaryotes than prokaryotes. Unlike higher organism, the genome segregation study in bacteria is more challenging due to (i) the size of the cell, (ii) inseparable phases of cell cycle, (iii)genetic mutations in segregation machinery exhibit pleiotropic effects like defects in chromosome segregation or cell division (Leonard *et al*., 2005), (iv) organization of chromosome within the bacterial cell (Bloom and Joglekar, 2010) and (v) lack of high resolution microscopic techniques with capability to image < 2µm size bacterial cells.

1.6 Mechanism of genome segregation in bacteria

1.6.1 Components of bacterial genome segregation

Several models have been proposed to illustrate mechanism of bacterial genome segregation. In 1963, Francois Jacob and colleagues proposed a passive model in which DNA segregation was coupled to cell elongation. They stated that duplicated DNA molecules are separated due to formation of the septum in the mid of the cell. Further studies had revealed the role of other factors in segregation of two sister chromosomes which spread throughout the cell (Hiemstra *et al*., 1987; Wientjes and Nanninga, 1989).

Later on, A. D. Grossman proposed an active model of chromosome segregation in bacteria and named as 'extrusion capture' model. According to this model, DNA replisome provides force for separation of duplicated chromosome (Lemon and Grossman, 2001). DNA polymerase of replisome machinery occupies mid position inside the cell and initiates replication and then push replicated DNA outward from replisome. Membrane anchoring factors capture the separated DNA and spooled toward opposite poles from the mid cell. In 2002, Dworkin and Losick proposed the role of RNA polymerase in chromosome segregation in support of extrusion model. They hypothesized that RNA polymerase mediated

transcription of the oppositely oriented genes close to the origin of replication generates force which could result in bulk movement of DNA (Dworkin and Losick, 2002). Later, the extrusion model failed to gain much attention due to variation in spatiotemporal positioning of replisome in different bacteria (for example, mid cell position in *B. subtilis* and 3/4th position in *C. crescentus*) and lack of defined start site of segregation. Recently, well accepted models of segregation utilize the presence of mitotic like machinery where TGS system actively segregates duplicated plasmid or chromosome into daughter cells.

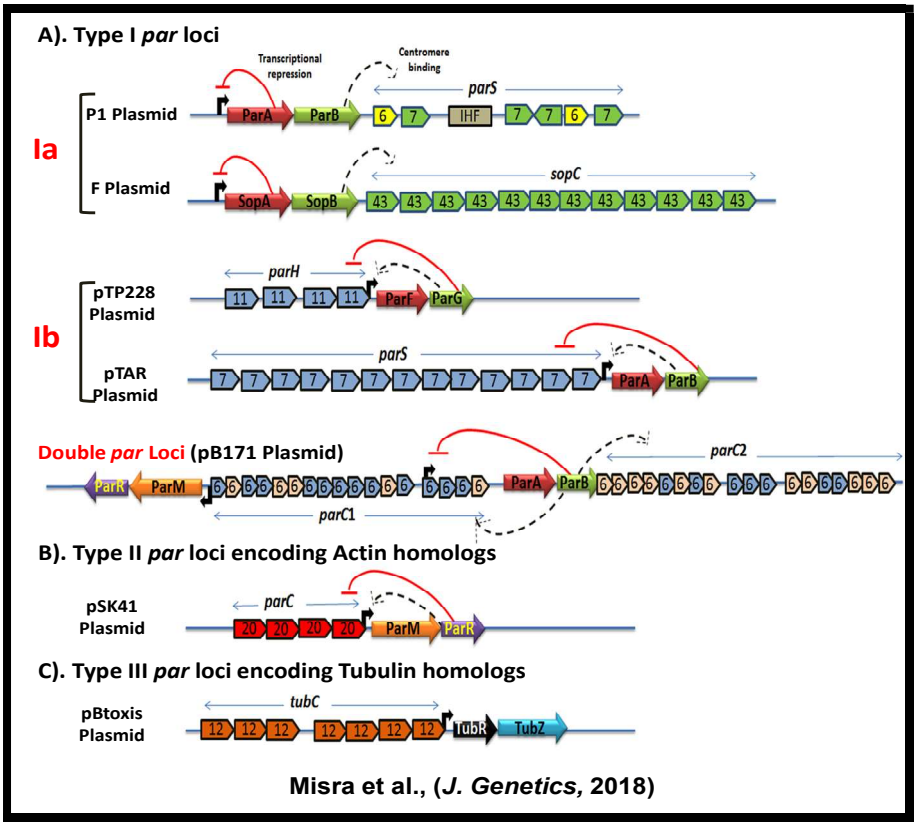

Figure 1.1: The genetic organization of components of different types of partitioning systems present in low copy plasmid. Organization of Type I (A), Type II (B) and Type III (C) partitioning system with their examples has been depicted schematically. In this solid arc indicate regulation of promoter activity and dashed arrows show centromere binding. The boxes with number indicate repeats of centromeric sequences with their nucleotide number.

Basically, centromere-like sequences present near origin or other locations are recognized by ParB or its homologs. The ParB-centromere complex is identified by ParA which help in positioning of duplicated replicons to daughter cells through polymerization/

depolymerization dynamics (Gerdes *et al.,* 2010; Ringgaard *et al*., 2009; Misra *et al.,* 2018). The tripartite genome segregation (TGS) system was initially explored in plasmids (P1 plasmid, F plasmid, pB171 plasmid, R1 plasmid etc.) and later on identified in chromosome of *Bacillus subtilis* and *Caulobacter crescentus.* The genetic organization of TGS components (i.e. *cis* element and their *trans* factors) varies from one genome element to other even in same bacterial host. Thus, TGS is categorized into three types viz. Type I, Type II and Type III (Figure 1).

Table 1.2A brief summary of characterized tripartite genome segregation system in bacteria.

Name of Bacteria	Genome elements	Partitioning elements			References
		NTPase	Adaptor	Centromere	
E. coli	P1 plasmid	ParA	ParB	P1*parS*	Ebersbach and Gerdes, (2005); Ghosh *et al*., (2006); Gitai, (2006); Leonard *et al*., (2005)
E. coli	F plasmid	SopA	SopB	*sopC*	Ebersbach and Gerdes, (2005); Ghosh *et al*., (2006); Gitai, (2006); Leonard *et al*., (2005)
B. subtilis	Chromosome	Soj	Spo0J	*parS*	Draper and Gober, (2002); Lee *et al*., (2003)
C. crescents	Chromosome	ParA	ParB	*parS*	Mohl *et al.* (2001); Mohl and Gober, (1997)
D. radiodurans	Chromosome	ParA1	ParB1	*segS* (1-3)	Charaka and Misra, (2012)
Salmonella enterica	pTP228	ParF	ParG	*parH*	Dobruk-Serkowska *et al*., (2012)
E. coli	pB171	ParA	ParB	*parC*	Ebersbach and Gerdes, (2005)
Streptococcus pyogenes	pSM19035	δ/ω			Volante *et al.,* (2015)
Staphylococcu aureus	pSK41	ParM	ParR	*parC*	Gerdes *et al.,* (2010)

Functional homologues of the proteins involved in segregation (segrosome) are present on both plasmids and chromosomes in different bacteria (Misra *et al.,* 2018). The different mechanisms employed in plasmids and chromosome segregation in different bacteria (including some member of MGH bacteria) have been characterized. Some of them have been functionally characterized and are listed in (Table 1.2).

The studies on bacterial genome segregation have been carried out mostly in some rod-shaped bacteria harboring single circular chromosome and low copy plasmid(s) like F plasmid, R1 plasmid and P1 plasmid of *E. coli* (Ebersbach *et al.,* 2005; Gerdes and Molin, 1986; Ghosh *et al*., 2006; Gitai *et al.,* 2006; Gordon and wright, 2000; Leonard *et al.,* 2005). The bacterial genome segregation machinery is made of tripartite system; (i) cis element (centromere-like sequences) named as *parS* etc., (ii) a centromere binding protein, ParB/Spo0J or their homologs and (iii) a motor NTPase protein, ParA/Soj or their homologs. Based on the sequence and structure of the NTPase, TGS system has been divided mainly into three types viz. types I, II and III (Gerdes *et al*., 2010, Baxter and Funnell, 2015, Oliva, 2016). Type I system encodes Walker box containing P- loop ATPase proteins (present in P1, F, pB171, pTAR, pTP228 plasmids). Type II system consists of actin like ATPase (ParM from R1 plasmid of *E. coli*). Type III system comprised of tubulin like GTPase motor protein (TubZ from pBtoxis plasmid). In addition, a Type IV segregation system has been reported in R388 and pSK+ plasmid.

1.6.1.1 Type I partition system

The type I partition system is most studied and widely distributed system in many plasmids and chromosomes. NTPases encoded by type I system are ParA (P1 plasmid and chromosomes from many bacteria), SopA (F plasmid), Soj (*B. subtilis*), MinD (cell division inhibitor). These NTPase are actually ATPase i.e. hydrolyze ATP that contain Walker type

motifs (Walker A, Walker A' and Walker B). Based on the presence or absence of an additional N-terminal specific DNA binding domain in ParA ATPase, type I group is further divided into two subgroups named as type Ia (for example plasmids P1, F, and RK2) and Ib (plasmidsTP228, pTAR, pB171), respectively (Mohl, 1997; Kim, 2000; Gerdes *et al.,* 2010). Chromosomal ParAs are similar to type Ib.

Type Ia ATPase

Type Ia ATPase family protein has been reported in many plasmids, phase and chromosomes (Oliva, 2016). This includes *parABS* of P1 plasmid and *sopABC* of F plasmid. The size of ATPase ranges from 200 to 400 amino acids, whose N- terminal region contain extra helix turn helix (HTH) region required for auto regulation activity (Austin and Abeles, 1983; Ogura and Hiraga, 1983). The mechanisms underlying segregation of P1 and F plasmids have been described here as the representative examples.

P1 plasmid

First active segregation mechanism was observed in P1 propahase. P1 plasmid occupies mid or 1/4th position within the cell (Erdmann *et al.*, 1999; Ringgaard *et al.*, 2009). P1 *par* system is comprised of 2 Par proteins namely ParA and ParB and a centromeric sequence called *parS*. The *parABS*operon of P1 plasmid encodes P-loop ATPase type ParA protein of 44 kDa, 38kDa ParB and a cis element parS characterized as centromere. Centromeric sequences '*parS'* of P1 plasmid is located downstream to *parAB* operon of plasmid. It contains four copies of heptameric sequences known as A-box (consensus of (G/T)TGAAAT) and two copies of hexameric sequences known as B-box (consensus of TCGCCA). The *parS* can be divided into three main regions left, right and central (Figure 1.2). Left and right regions contain Box-A and Box-B. Central region consists of IHF binding site (consensus

WATCAANNNNTTR (W is dA or dT, R is dA or dG, and N is any nucleotide)), where IHF binds to initiate bending of DNA molecule (Hayes *et al.*, 1994). Bending of *parS* bring left and right arms in close proximity which allow spreading of ParB protein over them simultaneously. P1 ParB initially recognizes *parS* sequences with high affinity and then allow loading of additional ParB molecules onto and around the looped centromere (~500 bp on each side) by specific and nonspecific interaction with the DNA to create large nucleoprotein complex known as segrosome (Schumacher, 2007).

Figure 1.2 *parS* sequence of P1 plasmid showing different boxes (BoxA and BoxB) and IHF binding site.

The minimum region of *parS* required for active segregation was ascertained by mutational analysis which revealed that deletion of box A1 and B1 from left arm had not affected the plasmid stability while deletion of box A2, A3, B2 and A4 from righ arm of *parS* had completely depleted partition activity (Martin *et al.*, 1991). Presence of IHF binding sites is not required for partitioning activity but had reduced the efficiency.

P1 ParA protein plays important role in plasmid segregation and auto regulation of partition genes' expression. P1 ParA contains extended N-terminal α helix region (1-43 residues) required for dimerization, winged HTH region (44-104 residues) for DNA binding and regulation of protein (Bouet and Funnnell, 1999), C-terminal region contains Walker type motif for ATP binding and hydrolysis, as well as ParB interacting domain (Dunham *et al.*, 2009). P1 ParB is a 333-residue long, 38 kDa adaptor protein which binds specifically to centromere like sequences for initiation of segregation. ParB protein contains N-terminal

region (1-141 residues) which interacts to ParA protein, and C-terminal region (142-333) which contains HTH motif helps in recognition of cognate centromere sequences (Surtees and Funnell, 1999). Crystal structure of P1 ParB-(142-333residues) (PDB: 1ZX4) bound to cognate *parS* centromere revealed novel DNA binding properties of ParB (Schumacher and funnell, 2005). The amino acid residues of P1 ParB form seven α helical region (includes HTH) that connected to an independent dimerization domain containing three anti parallel β strands via. 4 flexible linker amino acids (271-274 residues). Linker region permits free rotations of the domains allowing ParB to interact with box elements of *parS* arranged in a variety of orientations (Schumacher *et al*., 2007). During interaction of P1 ParB with *parS,* HTH domains of ParB monomer recognizes heptameric sequence of P1 *parS* followed by independent recruitment of Beta dimer domains to hexameric repeats of P1 *parS*. The IHF (Integrative Host Factor) encoded on *E. coli* genome binds to IHF binding site present in *parS* sequence and bend the DNA molecule (Funnell, 1988). Bending of *parS* allow ParB to spans both arms of P1 *parS* simultaneously (Schumacher and Funnell, 2005), thus *parS*-ParB nucleoprotein complex formation occurs. Bent *parS*-ParB nucleoprotein complex stimulates intrinsic weak ATPase activity of ParA protein to generate force required for segregation.

In 2010, Vechirelli *et al*., proposed diffusion ratchet model to explain the localization of P1 plasmid with in cell (Figure 1.3). According to this model ParA exist in two forms (i) ParA-ATP which is an active form binds to nucleoid and (ii) ParA-ADP, inactive form which is diffusible in cytoplasm. The conversion of ParA-ADP to ParA-ATP is slow and involve an inactive transition form i.e. ParA*-ATP. ParB-*parS* segregation cargo interacts with ParA-ATP (active form) on nucleoid and stimulates the ATPase activity of ParA which leads to conversion of ParA-ATP to ParA-ADP (inactive diffusible form). Since this conversion is slow, ParA-ADP diffuses away from its original site, creates ParA depleted zone. This

activity drags the cargo to the direction of high concentration of ParA-ATP, and removes diffusive motion in orthogonal directions for their segregation (Vecchiarelli *et al.*, 2010; 2014; Baxter and Funnell, 2015, Hu, 2017).

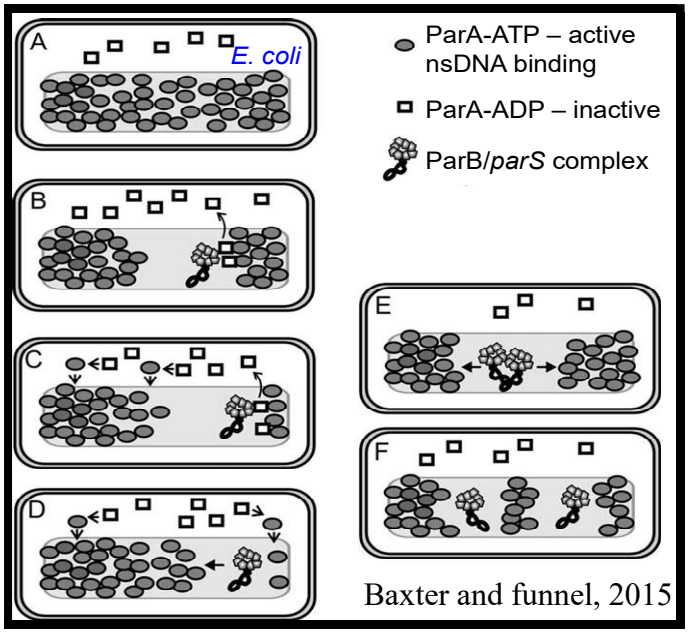

Figure 1.3 Diffusion ratchet model of P1 plasmid segregation. (A) ParA exist as ParA-ATP (active, nucleoid binding form) and ParA-ADP (inactive, diffusible form). (B) ParB/*parS* complex stimulates ATP to ADP conversion on ParA, leaving a void of ParA on nucleoid. (C-D) Diffused ParAs rebind to ATP and became active over nucleoid. (E-F) two segregation complex move toward nearest, high concentration of nucleoid bound ParA which leads their segregation

F Plasmid

F plasmid is 100 kb conjugative plasmid of *E. coli* that contains similar partitioning system as P1 plasmid. TGS system in F plasmid is known as Sop (system of partition) i.e. *sopABC.* Centromeric sequences '*sopC'* consists of 12 direct repeats of 43 bps which is different from P1 *parS*, located downstream of *sopAB* operon (Helsberg and Eichenlaub, 1986). SopB protein interacts to *sopC* by central 25 residues forming HTH structure. SopB also carries a dimerization domain in C-termianl and SopA interaction domain in N-terminal 45 amino acids residues (Ravin *et al*., 2003). Like P1 ParA, SopA binds to nonspecific DNA in ATP dependent manner and their intrinsic ATPase activity is stimulated by (SopB-*sopC*) nucleoprotein complex. SopA polymerizes in the presence of ATP and Mg (II), which is further stimulated by cognate SopB (Hanai and Arai, 2016). Fluorescence microscopic studies have revealed that segregation of F plasmid is assymetric where duplicated DNA is

positioned from 1/4th position to new quarter position within the cell (Onogi *et al.*, 2002). Several models have been given to explain F plasmid segregation. In 2007, Hatano et al., proposed first model where showed that SopA forms an oscillating polymer to interact SopB-*sopC* complex. This interaction moves the plasmid towards higher concentration of SopA (Figure 1.4A). This model has failed to explain the reason behind positioning of SopA foci and F plasmid at ¼ positions of cell (Hatano *et al.*, 2007).

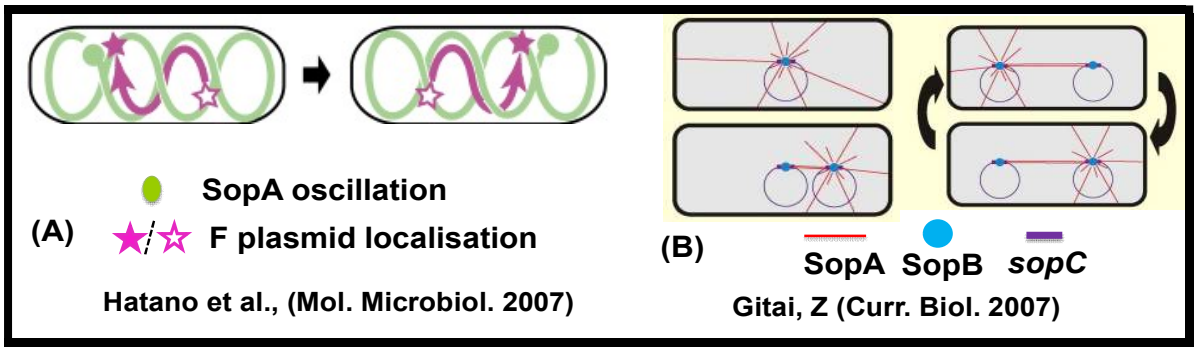

Figure 1.4 Segregation models of F plasmid. (A) Oscillation model (B) Astral model

Later, Astral model had been proposed for F plasmid segregation (Gitai, 2006) which was similar to pushing model of R1 plasmid. According this model, SopA forms long axial filaments in presence of SopB-*sopC* complex to place F plasmid to 1/4th or 3/4th positions within the cell (Figure 1.4B).

Type Ib ATPase

Unlike type Ia, type Ib ATPases are smaller in size and lack N-terminal HTH region. They do not autoregulate gene expression. In this case, ParB regulates the expression of ParA. Type Ib family includes *parABC* from pB171 plasmid, *parFGH* from pTP228 plasmid of *S. enterica* and δ/ω from pSM19035 plasmid (Ebersbash and Gedes, 2005; Dobruk-Serkowska *et al.*, 2012; Volante *et al.,* 2015). Additionally, type Ib ATPase family proteins are also present in

bacterial chromosome. Here we describe type IB segregation mechanism using pB171 as an example.

pB171 plasmid

The virulence plasmid, pB171 of *E. coli* encodes type Ib partitioning system. Unlike other plasmids discussed above, pB171 contains two sets of partition system viz. Par1 (similar to *parMRC* system) and Par2 (similar to *parABS* system). Both of these systems work together for maintenance of plasmid (Ebersbach and Gerdes, 2001; Ebersbach and Gerdes, 2005).

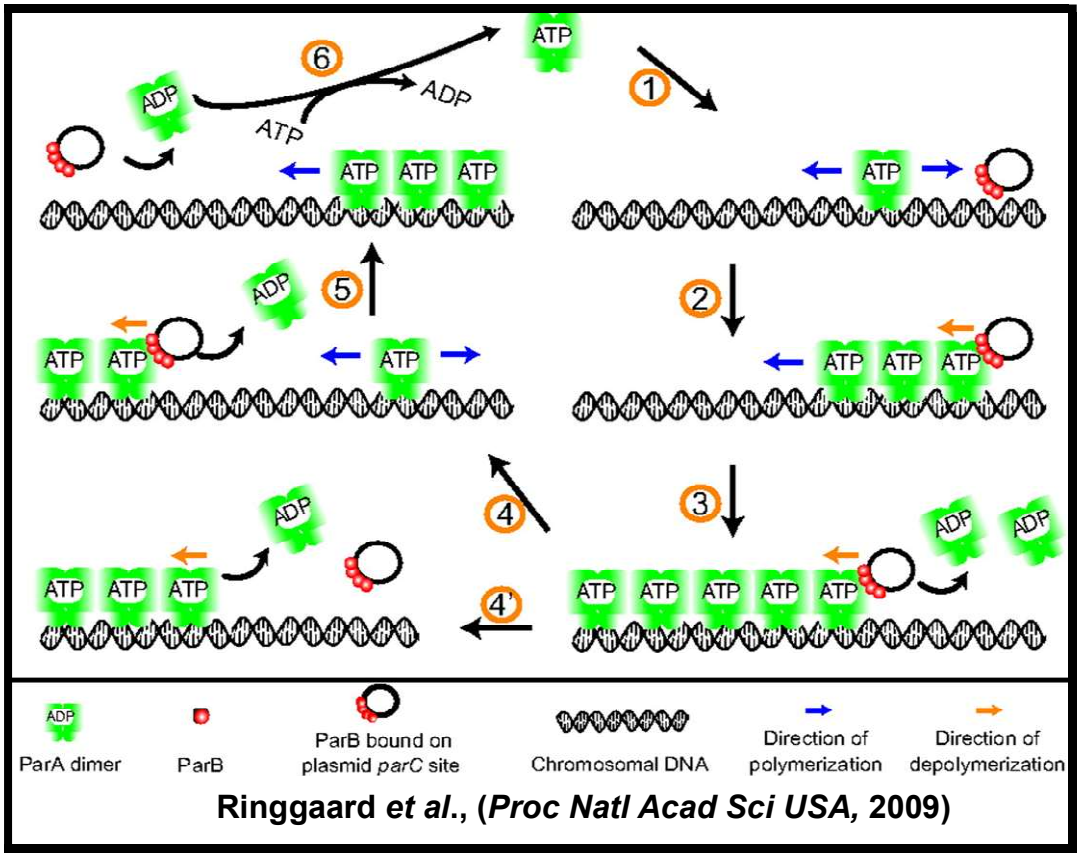

Figure 1.5 Pulling model of plasmid segregation. **1)** Interaction of ParA with ATP. **2)** Binding of ParA-ATP to nucleoid and bidirectional polymerization to meet ParB centromere complex. **3)** Conversion of ParA-ATP to ParA-ADP due to interaction of ParB nucleoprotein complex. **4)** Pulling of plasmid towards higher concentration of ParA due to continued interaction of ParB nucleoprotein complex with next ParA-ATP. **(5&6)** Dispatch of plasmid to the new pole and regeneration of Par-ATP from their ADP form.

Unlike type I, centromere sequences are located upstream to 'par' operon, extended N-terminal region are absent in ATPase motar protein (ParM or ParA) in pB171 plasmid. Hence, ParB not ParA plays role in transcriptional autoregulation. Localization of pB171 in cell was observed similar to type Ia plasmid. Based on fluorescence microscopic observation, Ringgaard and colleagues proposed pulling type model for segregation of pB171 plasmid. According to this model, ATP bound ParAs undergo bidirectional polymerization over nucleoid in search of ParB-*parC* nucleoprotein complex. Once ParA polymer encounters ParB-*parC* complex, it undergoes depolymerization by stimulation of its intrinsic ATPase activity. Depolymerizing ParA filament with continued interaction of ParB-*parC* complex pulls the plasmid DNA toward higher ParA-ATP concentration (Ringgaard *et al*., 2009).

1.6.1.2 Type II partitioning system

Type II partitioning system, also called as *parMRC* system is best studied in R1 and pSK41 plasmids but not in any bacterial chromosome yet. The *parMRC* locus consists of actin like homologue ParM motor protein, centromere binding protein ParR and centromere sequences *parC* (Dam and Gerdes, 1994; Ebersbach and Gerdes, 2001; Schumacher *et al*., 2007a). The *parC* region in R1 plasmid consists of two sets of five 11 bp direct repeats organized in flanking region of the *parA* core promoter sequences while in pSK41, it consists of four 20 bp tandem direct repeats present upstream to *parMR* operon. ParR protein contains an N-terminal domain with a Ribbon-Helix-Helix (RHH) DNA binding motif (similar to type Ib system) and a C-terminal ParM interacting domain. The C-terminal domain with a 3-helix cap reinforces the tight and extensive dimerization of N-terminal domain (Moller-Jensen *et al*., 2007). Electron microscopy studies of *ParR-parC* complex revealed that nucleoprotein complex form a discrete helical arrangement of 15 nm diameter. Here the symmetrical arrangement of six pairs of ParR dimer molecules are formed with distinct negative and

positive electrostatic on the inner (C-terminal region) and outer surface (N-terminal region) of the helix, respectively. The DNA wraps on outer (positively charge outer surface of ParR helical structure) where each ParR dimer binds to one *parC* iteron (Moller-Jensen *et al*., 2007; Oliva, 2016). The conserved C-tails of ParR clustered on inner side of helix binds to growing end of the polar ParM similar to actin polymer (Figure 1.6) (Gayathri *et al*., 2012).

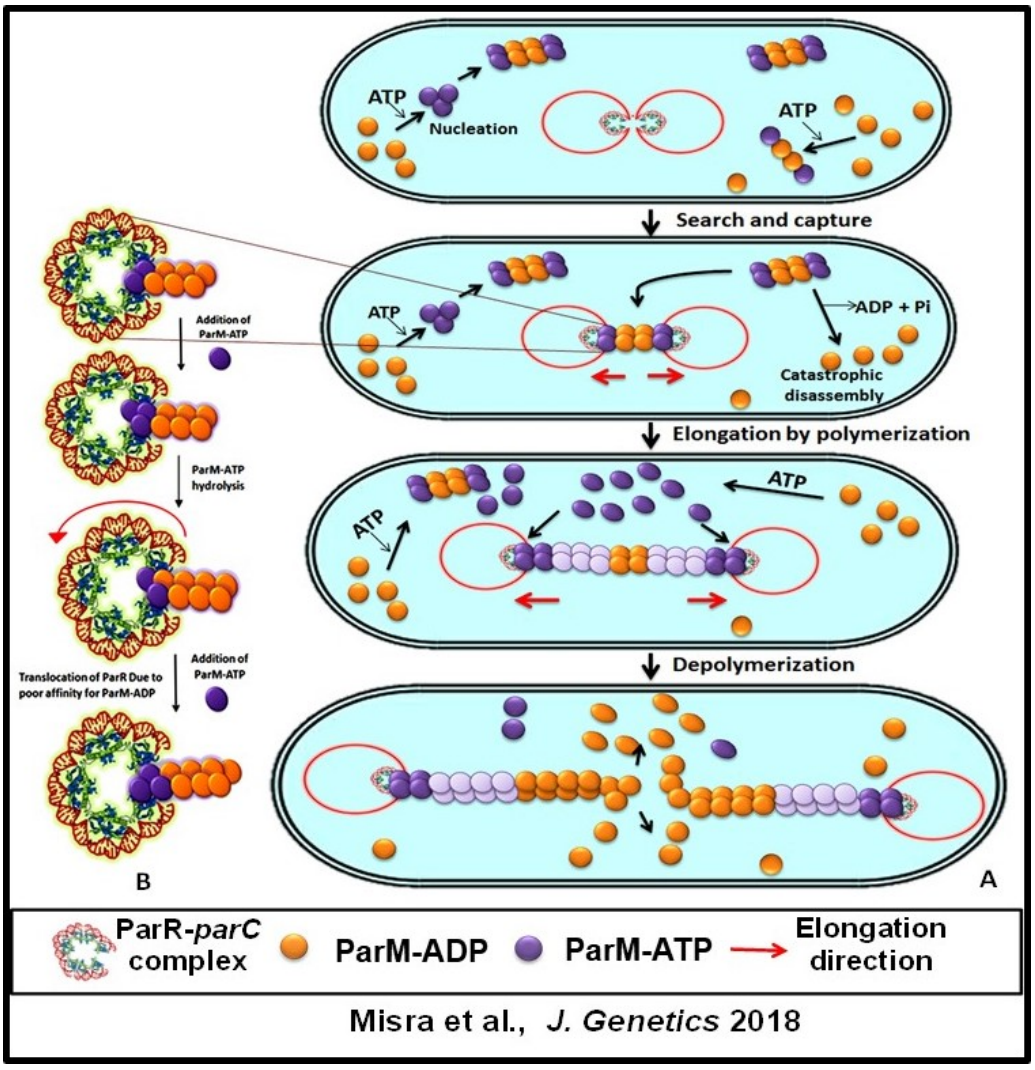

Figure 1.6 Type II partitioning system showing pushing model for pSK41 plasmid. (a) Schematic representation of ParR-*parC* complex formation and polymerization of ParM, which pushes duplicated segregation complex to the opposite direction. (b) Molecular assembly of ParR–*parC* complex (PDB ID: 1Q2 K) and processing of ParM polymers at the site of interaction with ParR–*parC* complex.

Segregation of pSK41 using *parMRC* follows pushing mechanism, where monomeric ParM interacts with each other to form transient unstable polymers which become stable in the presence of ParR- *parC* complex (Galkin *et al.*, 2009). Insertion of monomeric ParM at junction of ParR-*parC* complex and ParM filament allows bidirectional growth of the polymer. Thus, these plasmids are pushed in opposite direction of the cell. Depolymerization of ParM polymer depends upon length. ParM within filament exists in closed form (ParM-ATP) as well as open form (ParM-ADP). Hydrolysis of ATP to ADP +Pi makes inter domain region very rigid which leads to conversion of closed form into open form (Figure 1.6).

1.6.1.3 Type III partitioning system

Type III partitioning system has been recently discovered in pBtoxis plasmid of *Bacillus thuringiensis* and pX101 from *B. anthracis* (Larsen *et al.,* 2007; Ni *et al*., 2010). The TGS system of Type III is *tubZRC* where NTPase is a GTPase. The centromeric region (*tubC*) is localised upstream to *tubZR* operon and contains seven direct repeats of 12 bp arranged in group of three and four repeats in pBtoxis (Aylett and Lowe, 2012). The centromere binding protein TubR is a small winged-helix DNA binding protein that binds to *tubC* as well as acts as a transcriptional repressor of *tubZR.* TubR wraps helically around both sides of *tubC* to form flexible filament of nucleoprotein complex that forms 18 nm wide ring like structure (Aylett and Lowe, 2012; Oliva, 2016). Clustering of TubR in TubR-*tubC* complex allows C-terminal tail of TubZ to interact with TubR (Ni *et al*., 2010, Fink and Lowe, 2015). Initially, TubZ (GTPase) exists as proto-filaments (2-10) and then it forms unidirectional filament from one end to another end of the cell. Once segresome complex of plasmid binds to tread milling TubZ protein, it is transported to the opposite poles and released due to impact of plasmid to membrane layers (Larsen *et al.*, 2007). The dynamics of TubZ polymer depends on concentration of TubZ protein and GTP hydrolysis which are interlinked with each other

like FtsZ protein. Type III partition systemalso called ‘Tram model’ because plasmid molecules move along with the growth of the TubZ polymer like a Tram (Figure 1.7) (Schumacher, 2012).

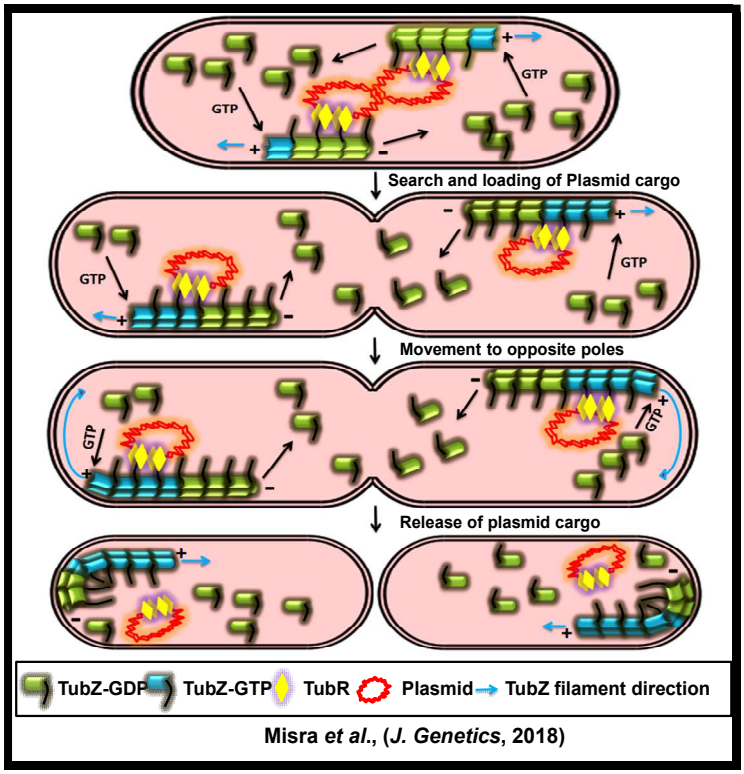

Figure 1.7 Type III partitioning system. TubZRC tripartite system contains *tubC* centromere, TubR adaptor and TubZ, a tubulin like motar GTPase. TubZ-GTP polymerizesat growing ends of the polymer and interacts to TubR-*tubC* complex of plasmid and moves it to opposite pole. Conversion of TubZ-GTP to TubZ-GDP reduces the affinity toTubR–*tubC* complex. So, plasmid molecules move along with the growth of the TubZ polymer like a ‘Tram’.

1.6.2.4 Type IV partitioning system

In addition to three well studied types of partitioning system, a type IV partitioning system has been discovered recently in R388 plasmid of *E. coli*. R388 plasmid encodes homologues of partition system which named as StbA, StbB and *stbC* (Guynet and de la Cruz, 2011). Mutational analysis revealed that StbA is important for partitioning of R388 plasmid. This system required only a *cis*-acting DNA site and DNA binding protein. This suggests the assistance of a host bacteria’s motar protein or passive mechanism for segregation of plasmid (Guynet and de la Cruz, 2011; Oliva, 2016).

1.6.2 Chromosome partitioning in bacteria

The segregation of bacterial chromosome employs three systems, ParAB-*parS*, SMC complexes, and the FtsK translocase. In most cases, all three works in some co-ordination

and no single system is sufficient for segregation. FtsK acts preferentially at *ter* region while both SMC and ParAB-*parS* work at *ori* region to accomplish the job (Reyes-Lamothe *et al.,* 2012). Like plasmid as discussed above, chromosomes from different Gram negative, Gram positive and archea have been identified with '*par*' homologues i.e. (ParA and ParB). These *par* loci play pivotal role in chromosome segregation (Ireton *et al*., 1994; Yamaichi and Niki, 2000; Gerdes *et al*., 2000; Bartosik *et al*., 2005; Fogel and Waldor, 2006; Jakimowicz *et al*., 2007; Toro *et al.,* 2008; Gerdes *et al.,* 2010; Muraleedharan *et al*., 2018). Chromosome segregation is best studied in bacteria harboring single circular chromosome with single independent partition system like *B. subtilis*, *C. crescentus*, *Mycobacterium*, *Psuedomonas, Streptomyces* etc. Beside this, chromosome segregation has been also studied in few MGS bacteria like *V. cholera, D. radiodurans*, *B. cenocepacia*, *B. abortus* and *R. sphaeroides* containing multipartite system (Fogel and Waldor, 2005; Charaka and Misra, 2012; Dubarry *et al*., 2006; Du, 2016; Deghelt *et al*., 2013; Dubarry *et al*., 2019). The '*par*' systems of chromosome and plasmid differ in few aspects such as (i) plasmids contain single centromere sequence whereas chromosomes contain multiple *parS* sites distributed near origin proximal region or some time scattered throughout the genome, (ii) Deletion or point mutation of *par* loci have more effect on segregation process of plasmid than chromosomes. The chromosome segregation system of few well studied bacteria has been described as follows.

Bacillus subtilis

B. subtilis is a Gram-positive bacterium that forms endospore by asymmetric cell division during unfavorable conditions (Errington, 2003). Under favorable condition spores germinate to give vegetative cell which follows symmetrical cell division and genome segregation. Genome segregation has been studied in both vegetative and sporulation conditions. Chromosome of *B. subtilis* encodes SojSpo0J-*parS* system similar to known *parABS* for

segregation and regulation of sporulation. Soj is like Type Ia ParA havingWalker P loop ATPase, which inhibits initiation of sporulation, and Spo0J is like ParB that binds with centromere. Spo0J interaction with centromeric region antagonizes the inhibitory action of Soj and required for initiation of sporulation as well as chromosome segregation (Ireton *et al*., 1994). Mutations in *spo0J* resulted in increased frequency of anucleated cells, increased genomic content possibly due to asynchronous initiation of replication (Lee *et al*., 2003) and perturbed cell size during vegetative cell cycle. Mutations in *soj* have not shown any significant effect. However, thethe stabilization of instable plasmid by Soj implicated its role in genome segregation. A *soj/spo0J* double mutant had shown impaired chromosome partitioning during sporulation (Sharpe and Errington, 1996). The Spo0J showed site-specific interaction with eight 16bp motifs (5'tGTTtCAcGTGAAAAa/g3') located within 20% of origin proximal region known as *parS* (Lin and Grossman, 1998; Draper and Gober, 2002; Lee *et al.*, 2003). In addition to specific interaction, Spo0J can also interact to non-specific DNA present around *parS* sites (Murray *et al*., 2006). With advanced fluorescence microscopic techniques, it was observed that Spo0J mediated bridging and condensation of DNA require both N- and C-terminal domains (Fisher *et al*., 2017; Song *et al*., 2017; Madariaga-Marcos *et al*., 2018). Spo0J helps in loading of Structure Maintenance of Chromosome (SMC) proteins at *parS* sites to initiate condensation during chromosome organization (Gruber and Errington, 2009; Umbarger *et al*., 2011; Broedersz *et al*., 2014; Taylor *et al*., 2015). The *parS* sequences have been reported as highly conserved across the bacterial species (Livny *et al.*, 2007).

Spo0J-GFP forms evenly distributed compact foci in cell whose position and number correspond to *oriC* (Glaser *et al*., 1997, Lee *et al*., 2003). Soj is involved in condensation and compaction of Spo0J foci under influence of Spo0J (Quisel, 2000). Soj being dynamic in

nature oscillates from pole to pole in a co-operative manner under influence of Spo0J. In spo0J deletion mutant, Soj shows even distribution across the nucleoid. In Soj null mutant, Spo0J formed multiple small foci suggesting that binding of Spo0J to the cognate *parS* site is independent of Soj, but formation of compact foci depends on the Soj protein (Bartosik *et al*., 2005).

Caulobacter crescentus

C. crescentus is a Gram-negative dimorphic bacterium existing in two types of cells during its cell cycle; stalk cell and swarmer cell. Only stalk cell undergoes DNA replication and cell division. Swarmer cell sheds their flagellum & chemotaxsis receptor and thus transformed into stalk cell to continue the life cycle (Gober & Marques, 1995). The chromosome partitioning system is *parABS* type, where both *parA* and *parB* are essential for cell viability (Mohl *et al.*, 2001; Mohl and Gober, 1997). Overproduction or reduction of either ParA or ParB affects cell division and chromosome segregation, suggesting an interdependence of cell division and genome segregation in *C. crescentus* (Mohl *et al.,* 2001; Thanbichler and Shapiro, 2006; Thanbichler, 2010). ParB binds specifically to *parS* sites (five sites located within 20 kb regions of origin of replication) via HTH motifs present in central region. ATP bound form of ParA interacts with ParB-*parS* complexes and promotes its dissociation. N-terminal of ParB interacts with ParA and regulates the nucleotide exchange of ParA (Figge *et al*., 2003, Bartosik *et al*., 2005), while C-terminal is involved in dimerization. *C. crescentus* follows polar asymmetric segregation of chromosome where *OriC*, anchored to one pole, undergoes duplication, and one copy of it pulled to opposite pole (new pole) due to retraction of ParA filament before septum formation (Ptacin *et al*., 2010).

Vibrio cholerae

Among MGH bacteria, chromosome partitioning is best studied in *V. cholerae,* a human pathogen. Genome of this bacterium consists of two chromosomes viz. chromosome I (2,961,149 bp) and chromosome II (1,072,315 bp). Both chromosomes have their own 'par' system and exhibit independent segregation mechanism (Egan *et al.,* 2005; Fogel and Waldor; 2005). Genetic and microscopic studies revealed that both the chromosome localized distinctly within the cell viz; origin of chromosome I lies 3/4th position of the cell and follows asymmetric segregation while origin of chromosome II occupies mid position of the cell and undergoes bidirectional segregation. Chromosome I follows pulling type of mechanism where ParB1 binds specifically to a single *parS* site located near origin at 3/4th position of the cell. ParA1 polymerizes from new pole to old pole and capture ParB-*parS* complex and retract them to the new pole by depolymerization kinetics (Fogel and Waldor, 2006).

In contrast to chromosome I, chromosome II contains 9 *parS2* sites located in region of 70 kb of chromosome II whlie one *parS2* on terminus region of chromosome I (Yamaichi *et al*., 2007). Like type I ParA, ParA2 hydrolyses ATP and form left handed helical filaments on non-specific dsDNA (Hui *et al*., 2010). Based on genetic analysis, deletion of *par* genes either from chromosome I or chromosome II has affected the segregation of respective replicon but not other replicon which suggest independent maintenance of both the chromosome in this bacterium (Fogel and waldor, 2005).

Rhodobacter sphearoides

First multipartite genome system was reported in *R. sphearoides,* an alpha proteobacteria*,* that contains two circular chromosomes (Chr I, 3.05 Mb; Chr II, 0.91Mb) (Suwanto and kaplan, 1989). Recently, localization of both Chr I and Chr II in *R. sphearoides* during cell cycle has been studied (Dubarry*et al*., 2019). Positioning of both the chromosome inside the

cell was monitored by tracking respective ParB/*parS* nucleoprotein complex near *OriC*. Like *V. cholerae*, both the chromosomes of *R. sphearoides* occupy different positions inside the cell viz. *OriC1* of Chr I is found close to the poles (15% and 85 % position) while *OriC2* localizes at mid-point of the cell. Segregation mechanism of two chromosomes of *R. sphearoides* is similar to *V. cholera.* Chromosome I follows asymmetric segregation system while chromosome II utilizes symmetric segregation pattern (Dubarry *et al*., 2019). MipZ plays crucial role in interdependent regulation of segregation and cell division in this bacterium and shares similar properties with all the ParA-like proteins. During cell cycle, MipZ forms foci at new pole where FtsZ resides, as well as at old pole where ParB1-*parS*-*OriC1* complex exists. After duplication and segregation of *OriC1,* ParB relocalizes the MipZ focus to a subpolar region at new pole and MipZ is located at ParB at the old pole showing "ParB catching MipZ" phase. Once FtsZ ring formation starts at mid cell, MipZ also colocalize as a single ring and stays till the end of cell division. MipZ shows dynamic localization and oscillation between the pole inside the cell (Dubarry *et al*., 2019).

1.7 *Deinococcus radiodurans:* a model organism

D. radiodurans, a member of *Deinococcaceae* family, is characterized by its ability to withstand the lethal effect of extreme doses of ionizing radiation, ultraviolet (UV) radiation and dessication which cause extensive DNA damage (Cox and Battista, 2005; Slade and Radman, 2011). It was isolated from canned meat that had been treated with 4 kilogray (kGy) of gamma radiation (Anderson *et al*., 1956). It can survive 5kGy ionizing radiation dose without the loss of viability. On the other hand, 5Gy of dose is sufficient to kill a human and 0.2-2kGy sufficient to kill *E. coli*. The ability of *Deinococcus* to survive such high doses of ionizing radiation is not because of prevention of DNA damage but it is due to efficient DNA repair machinery and the strong oxidative stress management system. Lot of studies on the

mechanisms underlying oxidative stress tolerance and repair of DNA have been published (reviewed in Slade and Radman, 2011, Misra *et al.,* 2013; Lim *et al.,* 2018).

1.7.1 Common features and genetic composition

D. radiodurans is a Gram positive, non-motile, non-spore forming, non-pathogenic and pinkish orange pigmented bacteria (Murray, 1986). It is an obligate aerobe and a mesophile with thermal limitation above 39˚C. It is normally grown in TGY medium (0.5% trypton, 0.1% glucose and 0.3% yeast extract) at 32˚C. It is an organotroph and is proteolytic in nature with amino acids being the preferred carbon source (Murray, 1986), however glucose metabolism contributes significantly during the recovery from DNA damaging agents (Zhang *et al*., 2000). Despite staining as Gram-positive, *D. radiodurans* has mutilayered envelope like that of Gram-negative bacteria. Its cell envelope comprises of five layers: (i) the cytoplasmic membrane (ii) the peptidoglycan-holey layer (iii) the compartmentalized layer (iv) the interior layer and (v) the S – layer – fragile soft layer containing hexagonally packed subunits (Work and Griffiths, 1968). It is sensitive to antibiotics which inhibit transcription, translation and peptidoglycan synthesis (Hawiger and Jaljaszewicz, 1967). Cells of *D. radiodurans* are naturally competent. *D. radiodurans* harbour a multipartite genome consists of 3,284,156 base pairs length. It comprises of two chromosomes (2,648,638 bp and 412,348 bp), a megaplasmid (177,466 base pairs), and a small plasmid (45,704 base pairs) (White *et al*., 1999). The genome exists in multiple copies depending upon growth phase with 10 copies present during the exponential phase (Driedger, 1970). The genome consists of approximately 3,187 ORFs and has a GC content of 66.6% (White *et al*., 1999). Genome of this bacterium encodes total 95 gene families, among these P-loop nucleotidase is the largest family consisting of 120 genes while HTH family proteins (DNA binding proteins) consisting of 72 genes is the second largest. The genome contains various mobile genetic elements, for instance, inteins, insertion sequences (ISs), small non-coding repeats (SNRs) and two

prophages. ISs are more prevalent on plasmids while SNRs on chromosome (Makarova, 2001).

Till date more than 50 radiation resistant *Deinococcus* species have been isolated. Majority of genomic components including partitioning system of *D. radiodurans* was found to be closely related to *Thermus thermophilus*. Genome architecture of *D. radiodurans* is like doughnut shaped toroidal structure which remains unaltered after high doses of γ-irradiation and provides close proximity to repair the damaged DNA (Levin-Zaidman *et al.*, 2003; Minsky *et al.*, 2006). Further, multipartite genome of this bacterium shows ploidy. Chromosome I is a primary chromosome and carries most of the essential genes required for replication, division and growth, whereas chromosome II, megaplasmid and small plasmid as secondary genome elements containing genes that play important role in cell response to extreme conditions. Insights into the evolution reveal that horizontal gene transfer during survival under adverse conditions could have played an important role in the evolution of such bacteria and archaea (Nelson *et al*., 1999).

1.7.2 Survival of *D. radiodurans* under oxidative stress

D radiodurans is well known for its extraordinary tolerance to oxidative stress (Cox and Battista, 2005, Slade and Radman, 2011; Lim *et al*., 2018). Oxidative stress is caused due to reactive oxygen species (ROS) generated as a result of metabolism or on exposure to physical and chemical agents like dessication (Potts, 1994), ionizing radiation (Dainton, 1948), UV radiation, mitomycin C (Lown *et al*., 1978) or hydrogen peroxide (Imlay, 2003). The generated ROS damage proteins, lipids, carbohydrates, nucleic acids and also generate single and double strand breaks (SSB and DSB) in the genome. Mitomycin C (MMC) generates DNA interstrand cross-links; UV radiation forms diverse pyrimidine dimers; and H_2O_2, methyl methane sulfonate (MMS), *N*-methyl-*N*_-nitro-*N*-nitrosoguanidine (MNNG), nitrous acid, and hydroxylamine induce severe base and nucleotide damage. Exposure to 5-6 kGy of

ionizing radiation results in the formation of ~200 DSBs, 3000 SSB and 190 cross links for which it takes 4h to completely mend its genome and presumably produces an efficient mutation free DNA repair for its post irradiation survival (Daly and Minton, 1995; Cox and Battista, 2005). However, the radioresistance of *D. radiodurans* cannot only be due to prevention of DNA damage, because in *E. coli* DNA double-strand breaks are formed at the same rate as in *D. radiodurans* (Gerard *et al.*, 2001). Few DSBs are enough to kill an *E. coli* cell (Krasin and Hutchinson, 1977). Yeast and human cells can repair 200 and 400 DSBs respectively produced during meiosis (Burgoyne *et al*., 2007) but cannot tolerate 40 DSBs when exposed to ionizing radiation (Rothkamm and Lobrich, 2003). This difference in handling the DSBs under different conditions indicates that only DNA repair mechanisms are not solely responsible for radioresistance in *D. radiodurans*. Capability to handle high level of oxidative stress has therefore been suggested for survival of *D. radidourans* under such extreme stress (Daly, 2009). The antioxidative mechanisms in *D. radiodurans* includes the presence of enzymatic machinery which includes superoxide dismutases, catalases, peroxidases and Dps proteins (Omelchenko *et. al.*, 2005; Yan *et al*., 2007), unique proteins like PprA (Narumi *et al*., 2004; Kota and Misra, 2006; Adachi *et al*., 2018), small molecules like PQQ (Khairnar *et al*., 2003, Rajpurohit *et al.*, 2008) and carotenoids like deinoxanthin (Tian *et al*., 2004), high Mn:Fe ratio (Daly *et al*., 2007). These mechanisms ensure protection of proteome and the genome from oxidatie damage and are suggested to be one of the principle contributory factors for resistance in *D. radiodurans*. Some links between mechanisms underlying radioresistance and desiccation tolerance have been postulated (Billi *et al.,* 2000). It is demonstrated that both desiccation and ionizing radiation lead to DNA double-strand breaks and extensive oxidative damage (Potts, 1994).

1.7.3 DNA repair mechanisms of *D. radiodurans*

The presence of extremely efficient DNA repair system consisting of direct damage reversal, nucleotide and base excision repair, mismatch repair and recombination repair contributes to the tolerance mechanism in this organism (Slade and Radman, 2011; Lim *et al*., 2018). However, the enzymes involved in these repair mechanisms do not seem to be exceptional. These pathways have a great deal of similarities with those characterized from other bacteria including *E. coli*, with certain exceptions. For instances, it lacks photoreactivation (Moseley and Evans, 1983), RecBC, translesion synthesis polymerase and suppressors of RecBC recombination pathway (Makarova *et al*., 2001). The presence of novel enzymes involved in DNA repair like PprA (Narumi *et al.,* 2004), DdrA (Harris *et al*., 2004), DdrI (Meyer *et al*., 2018), PprI (Hua *et al*., 2003), DNA polymerase X (homologue of DNA polymerase beta, Khairnar and Misra, 2009), and the existing redundancy in DNA repair enzymes have been witnessed (Griffiths and Gupta, 2007). A novel mechanism called ESDSA (Extended Synthesis Dependent Strand Annealing) has been suggested to be active during initial stages of post irradiation recovery. This pathway involves extensive synthesis of long DNA strands with single strand overhangs which can then be used for recombinational repair (Zahradka *et al*., 2006). In ESDSA, two enzymes (i) PolA, required for initial DNA synthesis (ii) and RecA, required for maturation of the linear intermediates into full-size circular chromosomes play crucial roles. The deletion mutants of both *polA* and *recA* are highly radiation-sensitive (Zahradka *et al.*, 2006). Presence of proteins like PprA which stimulates ligase function (Narumi *et al*., 2004) and DR_0282, a human Ku like protein and DR2417, a novel beta CASP family nuclease in *D. radiodurans* suggest the possibility of non-homologous end joining pathway (Das and Misra, 2011). However, the existence of NHEJ has not been proved yet. In addition to DNA repair and handling of oxidative damage, the other factors that are important after DNA damage like recycling of oxidized nucleotides by Nudix

hydrolases (Xu *et al*., 2001) and nucleotidases (Kota *et al*., 2010), removal of damaged oligonucleotides, bringing down endogenous ROS production by reduction in respiratory enzymes and enzymes with iron sulphur clusters (Ghosal *et al*., 2005) and proteolytic degradation of damaged and selected undamaged protein substrates (Servant *et al*., 2007) have been located in the genome of this bacterium. Unlike majority of known bacteria, *D. radiodurans* lacks classical SOS response to manage its transciptome and proteome in response to DNA damage. But many genes involved in DNA repair, oxidative stress resistance, and metabolism are induced at the gene expression and protein synthesis levels in *D. radiodurans* cells recovering from ionizing radiation (Zhang *et al*., 2005).

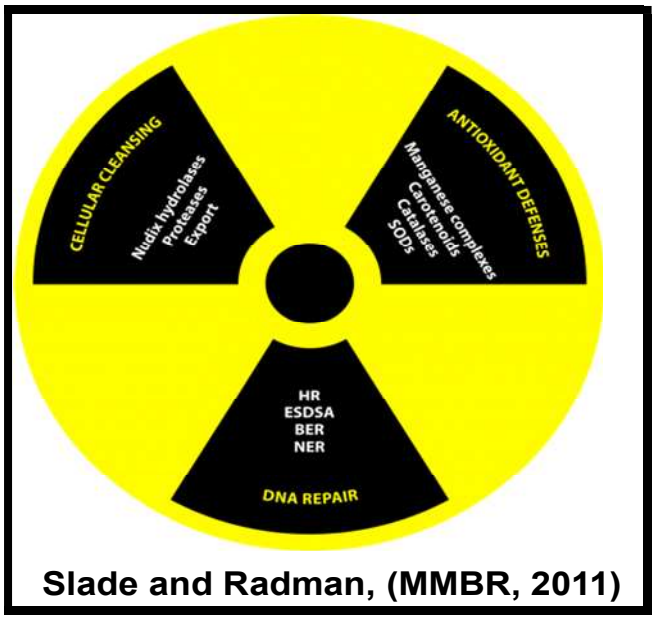

Figure 1.8: Mechanisms of DNA damage tolerance in *D. radiodurans*. Factors contributing to ionizing radiation resistance in *D. radiodurans* involve cellular cleansing, antioxidant defenses, and DNA repair.

Post translational modification especially protein phosphorylation plays an important role in DNA damage signalling pathways both in prokaryotes and eukaryotes (Subramanian and Hochwagen, 2014; Garcia-Garcia *et al*., 2016). Role of DR2518 (RqkA) in radioresistance of *D. radiodurans* has been already established (Rajpurohit *et al.*, 2008 and Rajpurohit and Misra, 2010). A large number of proteins belonging to DNA metabolism (including PprA and RecA) and cell division (Including FtsZ and FtsA) has been observed as a substrate for RqkA which upon

phosphorylation play important role in radiation resistance (Rajpurohit and Misra, 2013, Rajpurohit *et al*., 2016; Maurya *et al*., 2018).

1.7.4 Chromosome partitioning system in *Deinococcus radiodurans*

Genome of *D. radiodurans* encodes partitioning elements (*par* loci) involved in chromosome segregation. Except small plasmid, other genomic replicons have their own sets of putative *parAB* operon viz. *parA1B1* on Chr I, *parA2B2* on Chr II, *parA3B3* and *parA4B4* on megaplasmid (White *et al.,* 1999). Recently, Par elements of chromosome I have been functionally characterized and functional interaction of ParA1, ParB1 and three putative centromeric sites of 14-16 bp *segS* (*segS1*, *segS2*, and *segS3*) has been demonstrated both *in vitro* and *in vivo* (Charaka and Misra, 2012). In brief, ParA1 showed ATP dependent interaction with non-specific dsDNA while ParB1 binds specifically to all three *segS* (*segS*1/*segS*2/*segS*3) with nearly similar affinity. ParA1 protein undergoes polymerisation in the presence of ATP, which upon interaction with ParB-*segS* complex results in to depolymerisation. The deletion mutant of *parB1* exhibited slower growth and anucleation. The centromeric sequences *segS* were able to stabilize pDAG203, an instable mini-F plasmid in the presence of cognate ParA and ParB in *E. coli*. Further, GFP-ParB1 showed distinct foci in *D. radiodurans,* and cellular dyanmcis of ParA of chromosome I requires its congate ParB1 and *segS* elements. This study together has suggested pulling type of segregation mechanism for chromosome I in *D. radiodurans* (Charaka and Misra, 2012). Identification of centromere like *cis* elements and functional characterization of 'Par' proteins have not been studied for chromosome II and megaplasmid, except that involvement of ParA2 in the regulation of cell division especially when its cognate ParB2 was absent has been demonstrated in *E. coli* host (Charaka *et al*., 2013). Involvement of PprA, a pleiotorpic protein of radioresistance in *D. radiodurans* in genome maintenance and cell division has been demonstrated (Devigne *et al*., 2013; Kota *et al.,* 2014). Recently, cell division proteins (FtsZ and

FtsA) of *D. radiodurans* have been characterised to elucidate the cell cycle progression during post irradiation recovery (Modi *et al*., 2014; Modi and Misra 2014). Presence of multiple *par* loci over different genomic replicon has generated a possibility of functional redundancy. In present study, we have characterised *par* system present on secondary genome elements in *D. radiodurans*.

Aims and Objectives

Objective 1. Purification of recombinant ParA and ParB proteins encoded on chromosome II and megaplasmid, and their functional characterization.

Objective 2. Functional characterization of Origin–proximal *cis* elements of chromosome II and megaplasmid.

Objective 3. Preparation of translation fusion of LacI and TetR proteins with fluorescent reporter proteins for expression in *D. radiodurans.*

Objective 4. Real time monitoring of fluorescent tagged protein's interaction with genome elements during growth of *D. radiodurans.*

Chapter 2

Materials and Methods

"An experiment is a question which science poses to Nature, and a measurement is the recording of Nature's answer"

- Max Planck

1.1 Materials

Plasticware and glassware

Disposable polypropylene microcentrifuge tubes (1.5 ml and 2 ml), PCR tubes (0.2 ml or 0.5 ml), micropipette tips (10µl – 1.0 ml), plastic Petri dishes, polypropylene oak ridge tubes and GSA bottles were obtained from Tarsons, India or Axygen, USA. Conical flasks, glass beakers and measuring cylinders were purchased from Borosil, India. All these plasticwares and glasswares were sterilized by autoclaving. Cryovials (2 ml) and low temperature storage boxes were procured from Laxbro, India and Axygen, USA.

Chemicals and media ingredients

Dehydrated culture media components (Bacto-tryptone, Bacto-yeast extract and Bacto-agar) were purchased from Difco Laboratories, USA. Fine chemicals were purchased either from Sigma-Aldrich, USA, Qualigens (Glaxo) India Ltd., USB-Amersham, UK, E. Merck, Germany, Roche Biochemicals GmbH, Germany or Pharmacia LKB, Sweden, SRL, India or Bangalore Genei (P) Ltd., India. Inorganic and organic salts, urea, organic solvents of Excel-R and Anal-R quality were purchased either from Sigma-Aldrich, USA or Qualigens (Glaxo) India Ltd.

Enzymes and other molecular biology reagents

PCR reagents were from New England Biolabs, USA or Roche Biochemicals GmbH, Germany. Restriction enzymes, T4 polynucleotide kinase, alkaline phosphatase from calf thymus were purchased from New England Biolabs, USA. Ligation kits were obtained either from New England Biolabs, USA or Roche Biochemicals GmbH, Germany. Lysozyme (from chicken egg-white), DNAase I (from bovine pancreas) and RNAase (from bovine pancreas) were procured from Sigma-Aldrich Chemical Company, USA. Protein markers and DNA

molecular weight standards were obtained from Sigma-Aldrich, USA or New England Biolabs. PCR purification kit, Gel extraction kit, plasmid isolation kit and bacterial genomic DNA isolation kit were from QIAGEN, Germany or Sigma-Aldrich, USA.

Protein purification matrices and columns

Immobilized metal affinity chromatography matrices were obtained from GE Healthcare, USA as fast flow metal chelating materials and NINTA agarose from QIAgen, Germany or Sigma-Aldrich, USA. Ion exchange and gel filtration columns were purchased from GE Healthcare, USA.

Vectors and DNA

Vector pDsRed was obtained from Invitrogen, USA. Nicked circular DNA ϕXRFII was purchased from New England Biolabs, USA. Oligonucleotides used in this study were synthesized by either IDT technologies, USA or Eurofins Scientific, India.

Radionucleotides and Photographic materials

[^{32}p]γ-ATP and [^{32}p]α-ATP were obtained from Board of Radiation and Isotope Technology (BRIT), India. X-ray films of medical type were purchased from Fujifilm, India.

1.2 Media preparation

Luria Bertani medium (LB)

Bacto-tryptone, 10g; Bacto-yeast extract, 5g; and NaCl, 10g were dissolved in distilled water; pH was adjusted to 7.0 with NaOH solution and volume made to 1 litre.

For LB agar, Bacto-agar was added to a final concentration of 1.5%.

TYG Medium (Tryptone Yeast extract Glucose medium)

Bacto-tryptone, 5g; Bacto-yeast extract, 3g; and glucose, 1g were dissolved in distilled water, pH was adjusted to 7.4 with NaOH solution and volume made to 1 litre.

For TYG agar, Bacto-agar was added to a final concentration of 1.5%.

The media after preparation were autoclaved at 15psi, 121ºC for 20min and stored at RT. The required antibiotics were added in lukewarm media and poured in Petri plates. These plates were stored at 4ºC and used within one week.

1.3 Stock solutions of different chemicals

1M Tris-HCl solution (pH 7.6)

121.14g of Trizma base was dissolved in 800 ml of DW and pH was adjusted using conc. HCl. Volume was made to 1 litre. The solution was autoclaved and stored at RT.

0.75M Potassium phosphate monobasic solution (KH_2PO_4) (pH 3.5)

102g of KH_2PO_4 was dissolved in 800ml of DW and pH was adjusted to 3.5 with phosphoric acid. Volume was made to 1 litre and solution was autoclaved and stored at RT.

1M NaH_2PO_4 solution

119.98g of $NaH2PO_4$ was dissolved in 800 ml of DW and volume made to 1 litre. The solution was autoclaved and stored at RT.

1M Na_2HPO_4 solution

141.96g of $Na2HPO_4$ was dissolved in 800 ml of DW and volume made to 1 litre. The solution was autoclaved and stored at RT.

Phosphate buffered saline

8g of NaCl, 0.2g of KCl, 1.44g of Na_2HPO_4 and 0.2g KH_2PO_4 were dissolved in 800 ml of DW. The pH was adjusted to 7.4 with HCl and volume made to 1 litre. The solution was autoclaved and stored at RT.

5M Sodium chloride (NaCl) solution

292g of sodium chloride was dissolved in 700 ml of DW and volume made to 1 litre. The solution was filtered, autoclaved and stored at RT.

0.85% Saline

0.85g of NaCl was dissolved in 100 ml of DW. The solution was autoclaved and stored at RT.

2.5M Potassium chloride (KCl) solution

46.60g of potassium chloride was dissolved in 700 ml of DW and volume made to 1 litre. The solution was autoclaved and stored at RT.

10N NaOH solution

4g of NaOH pellets were dissolved in 10 ml autoclaved ultrapure milliQ water, stored at RT.

8M Imidazole solution

54.46g of imidazole was dissolved in 80 ml of DDW. The pH was adjusted to 8.0 using NaOH pellets and volume was made to 100 ml. The solution was autoclaved and stored at 4˚C.

1M Magnesium chloride ($MgCl_2$) solution

9.52g of $MgCl_2$ was dissolved in 80ml of DDW and volume made to 100 ml. Solution was autoclaved and stored at RT.

1M Magnesium sulphate ($MgSO_4$) solution

12.03g of $MgSO_4$ was dissolved in 70 ml of DDW and volume made to 100 ml. Solution was autoclaved and stored at RT.

1M Calcium chloride ($CaCl_2$) solution

14.7g of $CaCl_2$ dihydrate was dissolved in 70 ml of DDW and volume made to 100 ml. Solution was autoclaved and stored at 4˚C.

100mM $CaCl_2$ solution

1.47g of $CaCl_2$ dihydrate was dissolved in 70 ml of DDW and volume made to 100 ml. Solution was autoclaved and stored at 4˚C.

0.5M Nickel chloride ($NiCl_2$) solution

23.77g of $NiCl_2$ hexahydrate was dissolved in 150 ml of DW and volume made to 200 ml. Solution was autoclaved and stored at RT.

2% Uranyl acetate solution

0.2g of uranyl acetate was dissolved in 10 ml of autoclaved DDW. The solution was filter sterilized and stored as 1 ml aliquots at 8˚C. The solution was spun before use.

0.5M EDTA solution

186.1g of disodium EDTA.$2H_2O$ was dissolved in 800 ml of DW and pH adjusted to 8.0 using NaOH pellets. The final volume was made to 1 litre, autoclaved and stored at RT.

0.5M Dithiothreitol (DTT) solution

1.54g of Dithiothreitol powder was dissolved in 20 ml of autoclaved DDW and the solution was filter sterilized. Aliquots of 1 ml were stored at -20ºC.

100% Glycerol

100% glycerol was autoclaved and stored at RT.

50% Glycerol solution

50 ml of glycerol was mixed with equal volumes of DDW. The solution was autoclaved and stored at RT.

$T_{10}E_1$ solution

For this, 10 mM Tris.HCl (pH= 8.0) and 1 mM EDTA (pH = 8.0) were diluted in DW from respective stock solution, autoclaved and stored at RT.

100mM PMSF

348mg of phenylmethylsulfonyl fluoride powder was dissolved in 20 ml isopropanol/ absolute ethanol and vortexed vigorously to dissolve the contents. It was stored at -20ºC.

1M IPTG solution

2.38g of IPTG (isopropyl-beta-D-thiogalactopyranoside) powder was dissolved in 7ml of autoclaved DDW and volume made to 10 ml. The solution was filter sterilized and aliquots of 1ml stored at -20ºC.

Lysozyme (100mg/ml)

1g of lyophilised lysozyme powder was dissolved in 10ml of 10mM Tris-HCl (pH 8.0) and stored at -20ºC.

10 mM dNTPs solution (for PCR)

10µl each of the four deoxyribonucleotide triphosphate solutions (100mM stock) were mixed and the volume was adjusted to 100 µl with autoclaved ultrapure MQ water and stored at -20˚C.

10mM ATP/ADP/ATPγS solution

10µl of adenosine triphosphate/adenosine diphosphate/adenosine-5'-(γ-thio) triphosphate solution (100mM stock) was added to 90µl of autoclaved ultrapure MQ water. 25µl aliquots were stored at -20˚C.

X-gal solution (100 mg/ml)

10g of 5-bromo-4-chloro-3-indolyl-β-D-galactopyranoside (X-gal) was dissolved in 10 ml of sterile DMSO (Dimethyl sulfoxide). The solution was filter sterilized and stored as 1 ml aliquots at -20ºC.

RIPA buffer

It is used for cell lysis during coimmunoprecipitation. It consists of 50mM Tris-base, 150mM NaCl, 5mM EDTA, containing 0.5 % triton-X 100, 0.5 % sodium deoxycholate, 0.3 % SDS, 1mM PMSF, 1mM DTT, 0.5 mg/ml lysozyme and 50 µg protease inhibitor cocktail tablets (Cat No S8830, Sigma-Aldrich, Inc).

Note - Prepare fresh before use

Z-Buffer (10X)

It was prepared by diluting the respective stock solutions to 60 mM Na_2HPO_4, 40 mM NaH_2PO_4, 10 mM KCl, 10 mM Mg SO_4 and 50 mM β-mercaptoethanol. Its pH was adjusted to 7 and stored at 8˚C.

DAPI solution (2.5 mg/ml)

2.5mg of DAPI (4, 6'diamino-2-phenylindole.2HCl) was dissolved in 1 ml of DDW. The solution was aliquoted in dark tubes and stored at -20ºC.

1mg/ml Nile red solution

1mg of Nile red powder was dissolved in 1ml of dimethyl sulfoxide (DMSO). The solution was aliquoted in dark tubes and stored at -20ºC.

Reagents for agarose gel electrophoresis

10 x TBE

108g of Tris base, 55g of boric acid (borate) and 40 ml of 0.5 M EDTA (pH = 8.0) were resuspended in distilled water and the volume was made up to 1 litre.

50X TAE (Tris acetate EDTA) buffer

242g of Tris base was dissolved in 700 ml of DDW and 57.1 ml of glacial acetic acid was added to it. Further, 100 ml of 0.5M EDTA at pH 8.0 was added and pH was adjusted to 8. Buffer was autoclaved and stored at RT.

6X DNA loading dye

25mg bromophenol blue or xylene cyanol and 4g of sucrose were dissolved in autoclaved DDW and volume was made to 10ml. The dye was autoclaved and aliquoted before storing at -20ºC.

Ethidium bromide solution (10mg/ml)

100mg of ethidium bromide (EtBr) was dissolved in 10ml of autoclaved ultrapure MQ water, aliquoted and stored at RT.

Precaution: Wear gloves while handling ethidium bromide as it is mutagenic.

Reagents for SDS-polyacrylamide gel electrophoresis

30% Acrylamide solution

29.2g of acrylamide and 0.8g of N, N'-bisacrylamide was dissolved in 60 ml of DW and volume made to 100 ml. The solution was filtered in dark and stored at 4ºC in dark bottle.

Precaution: Wear gloves and mask while handling acrylamide as it is neurotoxic.

1.5M Tris-Cl, pH 8.8

90.75g of Tris base was dissolved in 400ml of DW. The pH was adjusted to 8.8 with conc. HCl and volume was made to 500ml. The solution was autoclaved and stored at RT.

0.5M Tris-Cl, pH 6.8

30.25g of Tris base was dissolved in 400ml of DW. The pH was adjusted to 6.8 with conc. HCl and volume was raised to 500ml. The solution was autoclaved and stored at RT.

10% SDS solution

10g of sodium dodecyl sulphate (SDS) was dissolved in 100ml of DW and stored at RT.

10% APS

1g of APS (ammonium per sulphate) was dissolved in 10ml of autoclaved DDW, vortexed to mix and stored in dark at 4ºC.

10X Tris-Glycine-SDS buffer

30g of Tris base and 144g of glycine was dissolved in 800 ml of DW. The pH was adjusted to 8.8. Further, 10g SDS was dissolved to this and volume was made to 1 litre, stored at RT.

2X Leammli dye (Cracking buffer)

460 mg SDS, 7.6mg EGTA, 20mg sodium azide, 2ml 100% glycerol, 2.5ml 0.5M Tris-HCl pH 6.8, 1ml β-mercaptoethanol, 112µl of 100mM PMSF and 40µl of 5%bromophenol blue were dissolved in autoclaved DDW to a final volume of 10ml, stored at RT.

Fixing solution

500ml methanol and 100ml glacial acetic acid were added to 400ml DW and stored at RT.

Staining solution

Coomassie Brilliant Blue R250 at final concentration of 0.5% was dissolved in fixing solution with continuous shaking overnight. The solution was filtered through Whatman filter paper No. 1 and stored at RT.

Destaining solution

100ml methanol, 100ml glacial acetic acid and 20ml glycerol were mixed in 780ml of DW and stored at RT.

Reagents for immunobloting

Transfer buffer for semi dry blot (10X)

24.28g of Tris base (200mM) and 144.14g of glycine (1920mM) was dissolved in 800ml of DW and pH was adjusted to 8.3. Volume was rasied to 1litre with DW.

Working solution: Dilute to 1X with DW and add methanol to final concentration of 10% before use.

Tris buffered saline (TBS)

20 ml of 1M Tris-Cl pH 7.6 and 200 ml of 5M NaCl solution were added to 780 ml DW, mixed well and stored at 4ºC.

Tween20 Tris buffered saline (TTBS)

0.1% Tween-20 was in TBS buffer before use.

Blocking buffer/ antibody buffer

3g of skimmed powder was dissolved in TBS by vortexing. Prepare freshly before use.

Alkaline phosphatase buffer; pH 9.5 (Developing buffer)

100mM Tris-HCl, pH 9.5, 100mM NaCl and 50mM $MgCl_2$ in 500ml DW were made and stored at RT.

SDS-EB buffer

SDS-EB buffer was prepared by diluting the respective solutions to 400mM NaCl, 400mM EDTA and 100mM Tris-Cl, pH 8.0. To this SDS was added to final concentration of 20% and dissolved at 37˚C.

Solutions for plasmid preparation

Solution I- (GTE solution; resuspension buffer)

GTE solution was prepared by diluting the respective stock solutions to 50 mM Glucose, 25 mM Tris-HCl (pH, 8.0); 10 mM EDTA (pH, 8.0). Solution was autoclaved and stored at 4˚C.

Solution II – Lysis buffer

It was prepared freshly before use by diluting the respective stock solutions to 0.2N NaOH (from stock of 10N) and 1% SDS (from 10% stock).

Solution III - 5 M Potassium acetate (neutralization solution)

59g of potassium acetate was dissolved in 100 ml Milli Q grade water and 23 ml of glacial acetic acid was added to get the final pH of 4.8. The volume was made up to 300 ml with sterile water. Solution was autoclaved and stored at 4˚C.

Antibiotic stock solution

All the antibiotics were prepared as described in table 2.2. Table 2.1 List of antibiotic stock solutions

Sr. No.	Antibiotic	Stock solution (mg/ml)	Working concentration (μg/ml)
1	Ampicillin	100 in MQ water	100
2	Kanamycin	25 in MQ water	5-25[a]
3	Spectinomycin	100 in MQ water	70
4	Chloramphenicol	34 in Abs. Ethanol	5-20[b]
5	Gentamycin	100 in MQ water	10

Notes –

a - 5µg/ml for *D. radiodurans* while 25µg/ml for *E. coli* strains.

b- 5µg/ml for *D. radiodurans* while 20µg/ml for *E. coli* strains.

1.4 Methods

1.4.1 Microbiological methods

Maintenance of the bacterial stocks of *Escherichia coli* and *Deinococcus radiodurans*

Bacterial stocks were maintained at RT, 4-8˚C and under frozen conditions. The room temperature stocks were made in soft agar LB or TYG medium containing 0.2 % glycerol. For this, the medium was dissolved by boiling and cooled down to 48°C before it was dispensed to airtight screw capped tubes to 80% of the total capacity. These media containing vials were sterilized by autoclaving and allowed to cool down to RT. These were further incubated at 37˚C overnight. The bacterial cells were stabbed with loop wire and preserved at RT. In addition, we had maintained different bacterial culture on agar containing respective media. They were periodically streaked on new agar plates and maintained at 4-8˚C.

Alternatively, bacterial culture stocks were also preserved at -70˚C in presence of cryoprotectants (glycerol). The exponentially growing bacterial culture was spun and resuspended in fresh medium to cells density of 10^9 cells per ml. The cell suspension was mixed with 20% glycerol in polypropylene screw capped tubes and stored in freezing temperature tolerant boxes, at -70˚C. Each bacterial stock was numbered and entered in the bacterial culture book with full details.

Growth of the bacterial strains

Different bacterial strains used in this study are listed in Table 2.3. Bacterial cultures were taken from long-term storage stocks or agar plates maintained on 4-8°C directly on LB / TGY

agar plates supplemented with appropriate antibiotics, if required. The plates were incubated at appropriate temperature for overnight. Single isolated colonies were inoculated in liquid broth with or without antibiotics and allowed to grow at 37°C for *E. coli* and 32°C for *D. radiodurans* at shaking speed of 150 rpm overnight. Equal number of cells from overnight grown liquid culture was added in 48 or 96 well microtiter plate (1:100 dilutions) containing respective liquid medium with required amount of antibiotics if any. The bacterial growth was monitored using microplate reader (Synergy H1, BioTek) at 600 nm. The obtained values were used to plot the growth curve for determining the different growth phases of the culture for different experiments. In parallel, an appropriate dilution was plated on suitable agar plates and the numbers of colonies were counted. Total number of colonies appeared on agar plates after different treatments of *D. radiodurans* cells were taken for calculating the survival efficiency.

2.4.2 Methods used in molecular studies

2.4.2.1 Isolation of plasmid DNA (mini prep)

Plasmid DNA was prepared using alkaline lysis method as described in (Sambrook and Russell, 2001). In brief, the bacterial cells were grown overnight in 2ml 1X LB broth with appropriate antibiotics. The cells were spun at 10,000 rpm for 30 seconds and washed with PBS. The pellet was suspended thoroughly in 100 µl ice chilled GTE and 200 µl of freshly prepared lysis buffer (0.2N NaOH, 1% SDS) was added. The mixture was mixed gently by hand and incubated at RT for 2 min and 250 µl pre-chilled neutralization buffer (5M potassium acetate) was added and mixed thoroughly and quickly. The mixture was incubated on ice for 5 min and then spun at 12,000 rpm for 15 min. The supernatant was extracted with equal volume of chloroform:isoamyl alcohol (24:1) and 0.6 volume of isopropyl alcohol was added to it. The contents were mixed and incubated at RT for 30 min followed by

centrifugation at 10,000 RPM for 15 min. The obtained pellet was washed with 70% ethanol, air dried and dissolved in milliQ water for downstream purpose.

2.4.2.2 Large scale preparation of plasmid DNA

Large scale preparation of plasmid DNA was carried out as described in (Sambrook and Russell, 2001). In brief, cells harboring high copy plasmid DNA were grown overnight in 50 ml 1X LB broth medium with vigorous shaking. The low copy number plasmid harboring bacterial culture was grown overnight in presence of antibiotics and then diluted 1:100 in 300 ml LB with antibiotic and allowed to grow for 12-16h at 37°C with vigorous shaking. Cells were harvested and washed with PBS. The plasmid DNA was prepared using alkaline lysis method as described above. In brief, the cell pellet was completely suspended in 4 ml GTE resuspension buffer supplemented with RNase A (50µg/ml) and to this 8 ml solution II (lysis buffer) was added. Content was gently mixed and incubated at RT for 2mins. The nucleoprotein-SDS complex was precipitated with 8 ml of pre-chilled solution III (neutralization buffer) on ice for 5 min. The supernatant was collected by centrifugation at 12,000 RPM for 15 min at 4°C and extracted with equal volume of $CHCl_3$: IAA (24:1). The upper layer was precipitated with 0.6 volume of isopropanol at RT for 20 min and centrifuged at 12,000 RPM for 10 minutes. The pellet was washed with 70% ethanol, dried and DNA was dissolved in ultrapure milliQ water. The plasmid DNA concentration and purity were determined by measuring the OD_{260} and OD_{280}, spectrophotometrically. The purity of DNA preparation was assured by finding the ratio of A260/A280. (A_{260} of 1.0 corresponds to 50µg/ml DNA, A260/A280 ratio indicates the purity of the DNA preparation, the ratio more than 1.65 was used).

2.4.2.3 Isolation of genomic DNA

Escherichia coli:

The chromosomal DNA from bacteria was isolated - using protocol as described earlier (Clark, 1971). In brief, the cell pellet was washed with PBS and stored at –70˚C if not processed immediately. The pellet was thawed on ice and suspended in 1/10th volume of 25 % sucrose and lysozyme (200 µg/ ml) and mixed properly. The mixture was incubated for 10 min on ice and 10mM EDTA (pH 8.0) was added and further incubated for 5 min on ice. The cells were lysed with 0.5% SDS and mixed gently to get clear lysate. The RNAase A (50µg/ml) solution was added and incubated at RT for 20 min. The lysate was extracted with equal volume of phenol (pH 8.0) till white precipitate stops coming. The aqueous phase was extracted once with phenol:$CHCl_3$:IAA (25:24:1) and once with $CHCl_3$:IAA. The aqueous phase was mixed with 0.3M sodium acetate and 2.5 volume of chilled ethanol was added from the side of the tube to layer on the top of the DNA solution. The high molecular weight DNA was recovered by spooling on sterilized glass rod, washed with 70% ethanol and air-dried. The DNA pellet was dissolved in autoclaved milliQ water.

D. radiodurans:

The 20 ml culture was overnight grown at 180 RPM at 32°C. The cells were harvested after pelleting, washed with 70% ethanol and resuspended in 1ml TE Buffer. To this 2mg/ml lysozyme and incubated at 37˚C for 30 min. The 600 µg/ml proteinase K and 2% SDS was added and incubated at 37˚C for 3 hours. After centrifugation supernatant was mixed with equal volumes of phenol-chloroform, incubated on ice for 10 min and centrifuged at 10,000 rpm for 10 min. The upper aqueous layer was extracted with equal volumes of chloroform:isoamyl alcohol (24:1) mixture. The supernatant was mixed with $1/10^{th}$ volume of

3M sodium acetate (pH 4.5) followed by 2.5 volumes of ethanol and incubated at -20°C for overnight. DNA was collected at 12,000 RPM for 15 min, air dried and dissolved in sterile water. DNA concentration was ascertained with OD_{260} and in agarose gel electrophoresis (Battista *et al*., 2001, Kota and Misra, 2008).

2.4.2.4 Agarose gel electrophoresis

Agarose gel electrophoresis was used for the qualitative and quantitative analysis of DNA. The agarose powder was dissolved in 1X TAE buffer by heating in microwave oven and the solution was cooled to around 50°C before ethidium bromide (EtBr) (0.5µg/ml) was added and poured in cassettes. It was allowed to solidify at RT for 30 min. The DNA samples mixed with gel loading dye solution were loaded and electrophoresed till tracking dye has reached to 3/4th of the gel length or depending on the experimental requirement. Similar procedure was followed for preparation of the low melting point (LMP) agarose gel but the ethidium bromide (0.5µg/ml) was added at 50°C and gel was polymerized at low temperature.

After the electrophoresis has completed, the DNA bands were imaged on a gel documentation system (G:box; Syngene).

2.3.2.5 PCR amplification

Primer design and synthesis

Primers were designed manually using the corresponding nucleotide sequences from *D. radiodurans* genome database and different primers used in this study are summarized in Table 2.4. The sequence of the DNA to be amplified was taken and restriction enzyme analysis was carried out using NEB cutter online tool (http://nc2.neb.com/NEBcutter2/). The unique restriction sites were noted and suitable restriction enzyme sites were incorporated into the forward and reverse primer sequences. Further some nucleotides as overhangs that

are required for efficient cutting by the corresponding restriction endonuclease were added at the upstream to the 5′end of both the primers. The composition of the primers was adjusted to have at least 50 % G+C content (wherever possible). The approximate Tm values were determined as Tm= 2x (A+T) +4 x (G+C). Care was taken to avoid repetitive sequences at the 3′ end which might results in primer dimer formation and 3′ base was necessarily kept A or T while C or G was preferred as penultimate base. The complete primer sequence was searched for its match on the other sites of the genome. The mismatch if any was adjusted in such a manner that 8-10 nucleotides of the 3′ end should not have perfect match on any other site on the genome. The primers were commercially synthesized and purified to best purity by manufacturers.

PCR

Polymerase chain reaction is a very common and sensitive method used for the amplification of desired DNA fragment of a few kilo bases from large genome size. PCR amplification was mostly carried out in 25 or 50µl volume. A typical PCR contains template (50ng), primers 400µM, dNTP's 200µM, *Taq* DNA polymerase buffer 1X, 1.5 mM $MgCl_2$ and *Taq* DNA polymerase 2.5U. In addition, DMSO or GC resolution buffer was also incuded for PCR amplifications from GC rich genome.

PCR using band-stab PCR technique

In some cases, where PCR amplification gives non-specific PCR products with desired product due to incompatibility in Tm values of primers, band-stab PCR technique is used. In this, PCR product is separated in agarose gel and desired band is stabbed with sterile hypodermic needles and suspend in the PCR mixture containing all the components. The PCR was carried out and products were analyzed on agarose gel. This technique enriches the

desired band to reasonable purity. However, this need to be further purified for ligation and cloning purpose.

PCR product purification using agarose gel electrophoresis

PCR products were separated on molecular biology grade low melting point (LMP) agarose. Once electrophoresis is complete, the DNA was visualized with handset UV lamp in long wavelength and desired DNA band was cut with sterile blade. DNA extraction was performed using manufacturer protocol from QIAquick gel extraction kit. In brief, gel pieces were dissolved in 3 volume of buffer QG at 50°C for 15 min. and mixed with 1 volume of isopropanol. The mixture was passed from DNA spin column by centrifugation and washed with buffer PE (ethanol added). Empty column was spun to remove traces of wash buffer. DNA was eluted by high speed centrifugation from column using prewarmed autoclaved milliQ water. The eluted DNA was analyzed on agarose gel and their concentration was measured using Nanodrop.

2.4.2.6 DNA manipulation

Different vectors used in this study

Different plasmids used in this study are summarized in Table 2.4. The plasmids were prepared by using genelute plasmid miniprep kit (Sigma-Aldrich, USA) and digested with restriction enzymes as required.

Restriction digestion

The restriction digestion with a particular enzyme was performed largely as described by manufacturers. The restriction digestion of DNA was carried out in the presence of specific buffers and minimum amount of enzymes (10 units per µg DNA in 50µl reaction for 3-4h to

overnight) as required used for the digestion of DNA. The ratio of enzyme to DNA was kept less than 10 and the concentration of glycerol in reaction mixture was maintained less than 10% in overall reaction. Restriction digestion of plasmid DNA or PCR products has been normally carried out by diluting DNA volume to ten-fold in final reaction mixture. Restriction digestion has been mostly carried in 20-50µl. After every digestion reaction, the samples were analyzed on agarose gel to make sure of enzyme activity. The linearized plasmid DNA and digested PCR products were gel purified and used for subsequent studies.

Dephosphorylation of DNA for ligation

In cloning experiment, the phosphodiester bond formation could be either intermolecular or intra molecular. Intra molecular ligation between plasmid vector molecules results increase in negative clones. The intermolecular ligation between vector and inserts would lead to the cloning of the insert in the vector which would give positive clones. The intra molecular ligation can be avoided by dephosphorylation of digested vector specifically for blunt end cloning.

The dephosphorylation of digested vector was performed using standard protocols for alkaline phosphatase activity. In brief 1 µg vector DNA was incubated with 10U of Calf Intestinal Phosphatase (CIP) in 20 µl reaction volume in presence of CIP Buffer (Roche, Mannheim, Germany) and incubated at 37°C for 1h. The reaction was stopped by heating the mixture at 65°C for 15min. The dephosphorylated vector was further purified with phenol: $CHCl_3$: IAA and followed by DNA precipitation by using ethanol, washed, air dried and dissolved in 10 µl sterile water. 1.0 µl of DNA sample was analyzed on agarose gel and 100 ng of it was used for one cohesive end ligation reaction.

End flushing of PCR amplified products

The PCR products used for blunt end ligation were end filled using T4 DNA polymerase from quick blunting kit (New England Biolabs, USA). To suppress exonuclease activity the relatively higher concentration of dNTPs was used as suggested in supplier protocols. A typical reaction mixture contains DNA, 1 µg; T4 DNA polymerase buffer, 1X (New England Biolabs, USA), T4 DNA polymerase enzyme 10U in a total reaction volume 20 µl. The mixture was incubated at 37°C for 1h and reaction was stopped by heating at 65°C for 15 min. Products were analyzed on agarose gel and purified by using QIAquick PCR purification kit (Qiagen).

Ligation

For cohesive end ligation, normally the insert to vector molar ratios were set to 2:1 to 3:1. The amount of the insert is fixed to around 200ng and then vector amount was adjusted to a particular ratio, according to the size of the vector. For the blunt end ligation reaction, the amount of the insert was increased to 500ng and then amount of vector was adjusted to meet the molar ratio of insert to vector of 3:1 or 4:1. The required amount of the vector and inserts were mixed in one tube and precipitated with sodium acetate salt and ethanol. The precipitated DNA pellet was washed twice with 70% ethanol, air dried and dissolved in minimum volume of autoclaved milliQ water. Further, T4 DNA ligase buffer (1X) and T4 DNA ligase (1µl) (New England Biolabs, USA) and 1mM ATP was added in 15 µl ligation reaction. The ligation conditions for sticky end ligation and blunt end ligation are different. The blunt end ligation is carried out at 20°C for overnight while cohesive ends ligation requires 1mM ATP at 16°C for overnight. However, excess ATP inhibits ligation reaction. (*Precautions: Extreme care is necessary for the preparation of the inserts and vector for*

ligation. DNA molecules should not be incubated to longer duration for restriction digestion. Vector should be aliquoted in small batches to avoid repeated freezing and thawing. Both inserts and vector should be necessarily kept at low temperature to avoid shading of the ends. All the processing of the inserts and vectors should be carried out at 4°C or less unless mentioned).

2.4.2.7 Bacterial transformation

Escherichia coli

Competent cells were prepared using the standard protocol. In brief, the overnight grown culture of desired *E. coli* strain was diluted to 100-fold in fresh LB medium. The culture was allowed to grow at 37°C with vigorous shaking (180 rpm) till OD_{600} reaches to 0.3-0.4 and thereafter the culture was transferred to pre-chilled SS34 tubes and chilled on ice for 30 min. It was centrifuged at 6,000 rpm for 5 min at 4°C. The pellet was gently suspended in half culture volume of chilled 100mM $CaCl_2$ and incubated on ice for 45 min. Thereafter it was centrifuged at 3,600 rpm for 10 min at 4°C. Appearance of bull eye shape on the wall of centrifuge tube was assured. The competent cells were gently resuspended in 0.1 culture volume of 100mM $CaCl_2$ and incubated on ice for 45 min. These competent cells can be stored at 4°C for 16 h and at –70°C in 20 % glycerol for one month without much loss of competence.

The 100µl of the competent cells were aliquoted in 1.5 ml pre-chilled tubes and to it half volume of ligation mixture or ~50ng of the plasmid DNA was added and gently mixed by tapping. The mixture was incubated on ice for 30-45 min and heat shocked at 42°C for 2 min followed by 2-5 min incubation on ice. The transformation mixture was diluted with 900µl of 1X LB broth. For the revival and expression of antibiotic resistance genes, the mixture was

incubated at 37°C for 30 min to 45 min depending on background antibiotic selection. Two different dilution of the transformation mixture was plated on LB agar plates containing appropriate antibiotics. The plates were incubated at 37°C for overnight and transformants were screened and characterized.

D. radiodurans

Competent cells of *D. radiodurans* or their derivatives were made as described in (Maurya et al., 2018). In brief, few colonies of bacterial cells were inoculated into plain TYG media and grown overnight at 32°C. It was further sub-cultured in 1:50 dilution and allowed to grow at 32°C till OD_{600} reaches to 0.3-0.4 O.D. A final concentration of 30mM calcium chloride (from the stock of 1 M) was added in the bacterial culture. This mixture was further incubated at 32°C for 1 h. 1–2 μg of circular or linearized plasmid was added to 1 ml of $CaCl_2$ treated bacterial culture and tube was placed on ice for 45 min. The transformation mixture was incubated on an orbital shaker at 32°C for 30 min at slow speed. It was 10-fold diluted with TGY broth and grown for 15–18 h at 32°C with vigorous shaking at 180 rpm. Different dilutions of overnight grown transformants were plated on TYG agar plates supplemented with required antibiotics and incubated at 32°C for selection. The recombinant cells were maintained under respective selection pressure.

2.4.2.8 Methods used in protein purification

Inducible expression of genes in *E. coli*

E. coli BL21(DE3)pLysS strain was used as an expression host different proteins. Cells harboring different pET 28a (+) containing '*par*' genes or *dnaA* gene was grown overnight in the presence of kanamycin (25μg/ml). The cells were diluted in fresh LB medium containing antibiotics and allowed to grow for 3-4 h at 37°C to get density OD_{600} 0.3-0.4 and then 0.5

mM of IPTG was added and growth was continued for a period of 3h on same temperature. The culture flask was kept at 8°C for overnight and a small aliquot (200µl) was drawn for checking the induction of proteins. Later on, cells were harvested, washed and preserved at –70°C for downstream processing. For protein analysis, the cells were collected and suspended in 50µl TE buffer. To it 50µl of 2X laemmellie SDS dyes was added and mixture was heated at 95°C for 10min and spun at 10,000 RPM for 5min. The supernatant was loaded on SDS-PAGE and electrophoresis was done. Gel was stained in CBB stain for checking induction of protein. Once good quantity induction has been confirmed, the remaining cell pellet was processed for large-scale purification (Charaka and Misra, 2012; Modi *et al*., 2014; Maurya *et al*., 2018)

SDS-PAGE analysis of proteins

On PAGE proteins migrate according to mass / charge ratio and structural topology. However, if charge is equalized then these proteins will migrate based on their mass and that would help in determining their molecular weight. Sodium dodecyl sulfate (SDS) is an ionic detergent which denatures proteins by 'wrapping around' the polypeptide backbone. SDS binds specifically in a mass ratio of 1.4:1 and confers a negative charge to the polypeptide. Individual polypeptide chains form a complex with negatively charged molecules of sodium dodecyl sulfate and therefore migrate as a negatively charged SDS-protein complex through the pores of polyacrylamide gel. In denaturing SDS-PAGE therefore, migration is determined not by intrinsic electrical charge of the polypeptide, but by molecular weight.

Preparation of SDS-PAGE gel

The SDS-PAGE gel with uniform 10 % or 12 % acrylamide concentration was made as below.

Table 2.5 Composition of SDS-PAGE gel

	Resolving gel		**Stacking gel**
Components	10 %	12 %	5%
Acrylamide (30%)	6.8 ml	8.0 ml	830 µl
Tris-HCl	5.8 ml (pH 8.8; 1.5 M)	5.8 ml (pH 8.8; 1.5 M)	630 µl (pH 6.8; 1M)
10% SDS	200 µl	200 µl	50 µl
10% ammonium per sulphate	200 µl	200 µl	50 µl
TEMED	20 µl	20 µl	10 µl
Water	7.0 ml	5.8 ml	3.4 ml
Total volume (ml)	20	20	5

Procedure of gel pouring

Glass plates were wiped with 70% ethanol and sandwiched with 1.0 or 1.5 mm spacers and assembled with vertical gel electrophoresis apparatus. Plates were tightened with clamps and make sure that the screws are properly fitted. All the gaps were sealed with 1% agar solution and SDS-PAGE mixture for resolving gel was poured between plates. It was over layered with isopropanol or water-saturated n-butanol. Once gel was polymerized, the propanol was removed and washed with water. Stacking gel mixture was poured above solidified resolving gel and comb (10 or 12 wells) was fitted in the gel. After 15-20 minutes once the stacking gel is polymerized, the comb is removed and wells were flushed with water 3-4 times using syringe and then protein samples were loaded after filling electrophoresis tank with SDS running buffer (10% SDS-Tris-Glycine, pH 8.8). The protein samples were prepared by heating equal volume of sample and 2X SDS gel loading dye at 95°C for 10 min. The denatured samples were centrifuged at 12,000 RPM for 10 min and clear supernatant was loaded in the gel. The SDS-PAGE was run for 1 h at 100 volts and then at 200 volts for 3 h. The gel assembly was dismantled, glass plates were separated and gel was taken out in plastic container containing staining dye as required.

Coomassie Brilliant blue staining

Coomassie Brilliant blue (CBB) dye binds stronglywith the basic amino acids of the polypeptide. Two variants namely G-250 and R-250 of this dye are available which are used for distinct purposes in protein staining. For CBB staining, the gel was fixed in destain solution I (DSI) and then immersed in CBB stain for 10 minutes or till bromophenol blue dye front changes color to yellow. The stain solution was removed back for repeated use and gel was submerged in DSI for 10 minutes followed by destain solution II (DSII). Gel was washed couple of times in DSII until the background become colorless.

Preparation of cell free extract of *E. coli* for protein purification

The cell pellets having induced protein were thawed on ice and 1 gm pellet was suspended in 10 ml lysis buffer A (20mM Tris-HCl, pH 7.6; 300mM NaCl; 1mM PMSF and 5 % glycerol). Lysozyme was added to a final concentration 500µg/ml and incubated at 37°C for 20 min. To it, 0.1 % Triton X-100 was added and further incubated on ice for 30 min. The cell lysate was sonicated at 30% duty cycle for 10 min with 10 seconds ON and 15 sec OFF mode. The suspension was centrifuged at 12,000 RPM (SS34, Sorvall) for 30 min. The clear supernatant was used native purification and pellet was used for denaturation purification.

Immobilized metal affinity chromatography for purification of recombinant proteins

Immobilized Metal ion Affinity Chromatography (IMAC) exploits affinity of molecules for chelated metal ions. IMAC is widely employed method used to purify recombinant proteins containing a short affinity tag consisting of polyhistidine residues. IMAC is based on the interactions between a transition metal ion (Co^{2+}, Ni^{2+}, Cu^{2+}, Zn^{2+}) immobilized on a matrix and specific amino acid side chains. Histidine is the amino acid that exhibits the strongest interaction with immobilized metal ion matrices, as electron donor groups on the histidine

imidazole ring readily form coordination bonds with the immobilized transition metal. Peptides containing sequences of consecutive histidine residues are efficiently retained on IMAC column matrices. Following washing of the matrix material, peptides containing polyhistidine sequences can be easily eluted by either adjusting the pH of the column buffer or adding free imidazole to the column buffer. IMAC is a versatile method that can be utilized to rapidly purify polyhistidine affinity-tagged proteins, resulting in 100-fold enrichments in a single purification step. Affinity-tagged protein purities can be achieved at up to 95% purity by IMAC in high yield.

Column preparation

The glass or plastic column (Biorad) is first thoroughly rinsed with autoclaved DW and then boiled for 10min in autoclaved DW. The column is then sterilized with 70% ethanol for 10min and then rinsed thoroughly with autoclaved DW. Fast flow chelating sepharose matrix (GE Healthcare) is then poured in the column. The volume of matrix depends on the amount of target protein present in cell free extract to be purified. The matrix is allowed to settle under gravity flow taking care that no air bubbles are trapped and then washed with 10 column volumes (CV) of autoclaved DW. The matrix is charged with 5CV of 0.5mM of autoclaved $NiCl_2$ solution and again rinsed with 20 CV of autoclaved DW to remove unbound Ni^{2+}.

Equilibration of matrix

The charged matrix is then equilibrated in 10 CV buffer A containing 5-10mM imdazole to prevent nonspecific binding of proteins. In cases, where imidazole is not used for elution (purification with decreasing pH – under denaturing conditions), imidazole may not be included.

Loading of protein sample

Cell free extract containing the protein of interest with histidine tag is loaded on the pre-charged column. The liquid is allowed to flow under gravity or peristaltic pump can also be used at flow rate of 1ml/min. Flow through is collected and reloaded.

Washing of non-specifically bound proteins

Non-specifically bound proteins were removed by washing the matrix with 40 CV of buffer A containing 50mM or 70mM imidazole and wash through was collected. Alternately (purification with decreasing pH – under denaturing conditions), buffer with pH 6.3 can be used for washing.

Elution of bound protein

Elution of target protein can be using pulse elution or gradient elution. In pulse elution buffer containing 250mM imidazole is passed through the matrix and the eluted fractions are collected and analysed by SDS-PAGE. For purification under denaturing conditions with reducing pH, buffer with pH 5.9 and 4.5 are used for elution. Gradient elution can be employed instead of pulse elution for better purity of protein. Gradient elution can be performed as continuous gradient from100mM to 300mM imidazole while step gradient can be performed by 100, 200, 250 and 300mM imidazole in steps. All the eluted fractions alongwith flow through and wash through were analysed by SDS-PAGE to check for the purity of target protein.

The composition of buffer with respect to buffering agent, salt concentration and presence of additives depended on the protein to be purified. For purification under denaturing conditions 8M urea was added to all buffers. Protein under denaturing conditions was purified in presence of imidazole or with reducing pH.

Dialysis of protein samples

Preparation of dialysis tubing

Dialysis is an efficient way for buffer exchange. Dialysis tubings of desired mesh size and length were cut and boiled for 5 min in 2% sodium bicarbonate and 1mM EDTA pH 8.0. The tubings were cooled and thoroughly rinsed with autoclaved DW before use or stored at 4°C. The protein sample to be buffer exchanged was filled in dialysis bag and the bag was clamped firmly to prevent any leakage. The clamping was done in such a manner that the membrane was under tension. This ensures efficient dialysis. The dialysis bag was then placed in exchange buffer. The buffer volume was kept 100 times more than the protein volume to be dialysed. Dialysis was carried out at 6-8°C with constant stirring. After dialysis, the samples were centrifuges at 11000 RPM to remove any aggregates and further used.

Gel filtration

The purified proteins from IMAC method were further processed for gel filtration chromatography for additional purity. For this, dialysed proteins were concentrated either by Amicon protein concentrator tubes or by ammonium sulphate precipitation followed by re-solubilisation in R-buffer (20mM Tris pH 7.6; 0.1mM EDTA, 1mM DTT and 5% glycerol) with 200mM NaCl. 0.5ml of concentrated protein was injected in AKTA purifier FPLC instrument (GE Healthcare, Germany) equipped with Superdex™ 200 GL column (Pharmacia). The eluted fractions correspond to isolated peak was collected in tubes and checked on SDS-PAGE for purity of protein.

The fractions with homogenous purity were pooled and dialysed as mentioned above.

Storage of purified proteins

The dialysed proteins were concentrated using Amicon protein concentrator tubes as per manufacturer's instructions. The cutoff depended on the protein size. The concentrated protein samples were dialysed in 50% glycerol containing buffer A and stored at -20°C. The composition of storage buffer with respect to buffering agent, salt concentration and presence of additives depended on the protein of interest.

Protein estimation

Different spectrophotometric methods were used for the estimation of protein in a particular solution. One method is measuring the absorbance maxima of proteins at 280 nm using Nanodrop. Other method used for the estimation of proteins was colorimetric method (Bradford, 1976) using Bradford dye (BioRad) kit protocols. In brief, 200µl of the 5X dye solution was mixed with 800µl of total solution containing proteins and buffer. The content was mixed and incubated at RT for 15 min before color development was monitored spectrophotometrically at wavelength of 595nm. The OD_{595} was compared with a standard curve that was made using standard concentration of BSA protein. Amount of protein present in the solution was estimated from standard curve.

2.4.2.9 Native-PAGE for EMSA (Electrophoretic Mobility Shift Assay)

Radiolabelling of DNA

The labelling of proteins or DNA with radioisotope increases the sensitivity of analysis related to them. We have labelled the DNA (both single stranded as well as double stranded) with ^{32}P from [γ-^{32}P] ATP using T4 polynucleotide kinase. In brief, we have taken variable amount of dsDNA or ssDNA depending upon length of DNA and incubated with T4 polynucleotide kinase buffer and 1 µl enzyme at 37°C for 1h. We have added 5 microcurie activity of [γ-^{32}P] ATP at start of reaction. We have purified radiolabeled dsDNA of >50bps using PCR purification kit while radiolabeled ssDNA <50bps were purified using Sephadex G50 or G20 columns as stated by manufacturer. Purified radiolabelled ssDNA were annealed to their unlabelled complimentary strand before experiment.

Preparation of native-PAGE

Non-denaturing native PAGE is required for separation of nucleoprotein complex. The composition of native PAGE is tabulated below.

Table 2.6 List of composition of Native PAGE gel

Components	**Resolving gel**	
	6 % (20 ml volume)	**10 % (20 ml volume)**
Distilled water	11.8 ml	9.1 ml
30 % Acrylamide	4 ml	6.67 ml
5X TBE	2 ml	2 ml
50 % Glycerol	2 ml	2 ml
10 % APS	200 µl	200 µl
TEMED	25 µl	25 µl

Different components were mix and poured between glass plates spaced with 1.5 mm thick spacer in vertical electrophoresis apparatus. 10 or 12 well comb of similar thickness was placed on top for well formation. Once polymerized, the wells were carefully flushed using syringe. 0.5X chilled TBE buffer was filled in buffer tank and reaction mixture of EMSA was loaded in wells. The gel was run at 50V for 3-4 h.

Gel drying and film development

After the gel run was complete, the buffer chambers were emptied by decanting the buffer carefully in radioactive waste container. The gel was removed from glass plates under tap water and placed on Whatmann 3mm filter paper and the entire assembly was placed on gel dryer with filter paper at base. The gel was covered with saran wrap and vacuum drying was done under heating condition for 1h. The dried gel was wrapped with two layers of saran wrap and exposed to X-ray film in X-ray cassette. The cassette was kept in -20°C for overnight or longer periods as desired, before developing. For developing autoradiograms, the film was taken in dark and developing and fixing was carried out as per instructions mentioned in the developer and fixer's manuals. The developed films were washed with water and air dried before documentation.

2.4.2.10 Thin layer chromatography

Thin layer chromatography was used to check ATP hydrolysis using [α^{32}P]-ATP. The glass chamber was filled with 0.75 M KH_2PO_4/H_3PO_4 pH 3.5 upto 2cm from base. The edge of the

mouth of chamber was rubbed with sealing grease and the chamber closed with glass plate. Reaction mixtures were constituted and 1µl of reaction mixtures were spotted on PEI Cellulose F+ TLC sheets (cut according to chamber size) 3cm from base. The spots were air dried and the TLC sheet was placed inside the chamber with spotted side down and in contact with buffer. Care was taken that spots are not submerged in buffer. The chamber was closed and buffer was allowed to run full length of sheet. The sheet was then removed and air dried. It was covered with two layers of saran wrap and exposed to X-ray film as described above. The autoradiogram was developed as per instructions mentioned in the developer and fixer's manuals.

2.4.2.11 Microscopy

Effect of deletion of '*par'* genes on cell morphology and localization of fluorescent protein fusion of any protein in bacterial cell was monitored using fluorescence microscopy. In principle, the specimen is illuminated with light of specific wavelength which is absorbed by the flurophores or proteins and emits higher wavelength light. For this, exponential growing culture was taken and live cells were stained with DAPI (for nucleoid) and/ or Nile red (membrane) and mounted onto a bed of 1 % agarose in water (w/v) for viewing under the microscope. Images were acquired using an Olympus IX83 inverted fluorescence microscope equipped with an Olympus DP80 CCD monochrome camera. Images were captured, processed, aligned and deconvoluted using inbuilt software, cellSens, Japan.

2.4.2.12 Statistical analyses

Statistical analyses were performed using the software GraphPad prism 5.0 software. In addition, student t-test or ANOVA (Analysis of varience) was used for statistical significance of data. P-values obtained at 95 % confidence intervals are shown as (*) for <0.05, (**) for <0.01 and (***) for <0.001.

Chapter 3

Results

"Science and everyday life cannot and

should not be separated"

- Rosalind Franklin

Chapter 3.1

Functional characterization of P-loop ATPases (ParAs) encoded on chromosome II and megaplasmid in *D. radiodurans*

3.1.1 Introduction: -

Until recently, the bacterial genomes were synonyms of a single circular chromosome and extrachromosomal plasmids. Now we know that there are many bacteria that harbor multipartite genome system (Misra *et al*., 2018). The numbers of copies of these genome elements including primary chromosomes may vary from one to several copies per cell (Misra *et al*., 2018). In general, the primary chromosome is larger and tends to have significantly more conserved housekeeping genes that encode for core cellular functions. On the other hand, the secondary genome elements are smaller, show a greater variability and encode accessory functions associated with adaptation and survival in different niches and largely contribute to stress tolerance (Holden *et al*., 2004; Cooper *et al*., 2010). The faithful inheritance of multipartite genome system and maintenance of ploidy are not fully understood in bacteria. The genome segregation in bacteria harboring single circular chromosome and low copy plasmids occurs largely by the involvement of tripartite genome segregation (TGS) system. The TGS consists of an origin-proximal *cis*-acting (centromere-like) DNA sequences, the centromere binding adaptor proteins like ParB or ParB homologues and the P-loop Walker ATPases like ParA or Par A like motor proteins (Gerdes *et al*., 2010). *Deinococcus radiodurans,* a multipartite genome harboring bacterium, also contain TGS system with 4 sets of *par* loci distributes over different replicons which suggest a possibility of functional redundancy among Par proteins (White *et al*., 1999). Paritionng components of chrosmome I has been recentaly characterized (Charaka and Misra, 2012). In this chapter we have worked on P-loop Walker ATPases of chromosome II and megaplasmid and their role in genome maintainace and radioresistance if any.

3.1.2 Materials and methods:

3.1.2.1 Bioinformatic analysis

Multiple sequence alignment and functional motifs search in ParA2 (DR_A0001) and ParA3 (DR_B0001) proteins were carried out using standard online bioinformatics tools as described earlier (Das and Misra, 2011; Charaka *et al*., 2013). In brief, the amino acid sequences of both the proteins were subjected to a PSI-BLAST search with the SWISSPROT database. After five iterations, the sequences obtained were aligned by ClustalW along with ParA protein of several other bacteria including ParA1, ParA2, ParA3 and ParA4 of *D. radiodurans* and the conserved deviant of Walker box ATP-binding motif and DNA binding motif were searched. The sequences of close homology were aligned by T-COFFEE and the conserved motifs were marked. Homology model of ParA1, ParA2 and ParA3 proteins were generated by I-TASSER server (http://zhanglab.ccmb.med.umich.edu /I-TASSER/) (Yang *et al*., 2015) and were validated by PROCHECK server. The structure of Soj of *T. thermophilus* (PDB ID:2BEK) was used as template for these proteins structure modeling (Leonard *et al*., 2005). Both ParA2 and ParA3 modelled structures were superimposed with Soj structure (PDB ID:2BEK) of *T. thermophilus* as well as with deinococcal ParA1 model structure using Pymol software.

3.1.2.2 Cloning, expression and purification ParA2 and ParA3 proteins

The coding sequences of ParA2 (DR_A0001), ParA3 (DR_B0001) were PCR amplified from genomic DNA using pETA2F and pETA2R primers for *dr_A0001* (*parA2*) and pETA3F and pETA3R for *dr_B0001* (*parB3*) gene as mentioned in Table 2.3. Restriction digested PCR products were ligated at *Nde*I and *Xho*I sites in pET28a(+) to yield pETA2 and pETA3 plasmids, respectively (Table 2.4). These plasmids were sequenced for the presence of cloned genes and further used for protein expression and purification or generation of polyhistidine-tagged translational fusion for *in vivo* interaction study.

For expression and purification of proteins, recombinant plasmids were transformed into *E. coli* BL21(DE3)pLysS host and induced with 0.5mM IPTG. The induction of proteins was confirmed by SDS-PAGE analysis with respect to vector control. For purification of protein, mid-logarithmic phase cells of *E. coli* BL21(DE3)pLysS expressing recombinant proteins were induced with 0.5 mM IPTG and allowed to grow at 37°C for 3 h and kept overnight at 18°C. The cells were pelleted and stored at -70°C. The cell pellet was thawed and suspended in buffer A (20 mM Tris–HCl, pH 7.6, 300 mM NaCl) containing 10 mM imidazole, 0.5 mg/ml lysozyme, 1 mM PMSF, 1 mM $MgCl_2$, 0.05 % NP-40, 0.05 % TritonX-100, protease inhibitor cocktail and 10 % glycerol) and incubated at 37°C for 30 min. The mixture was sonicated for 10 min with 10 sec ON and 15 sec OFF mode at 25 % amplitude.The cell-free extract obtained after centrifugation at 11,000 RPM for 30 min at 4ºC was loaded onto a pre-equilibrated Ni-NTA column. The column was thoroughly washed with buffer A containing 50 mM imidazole and recombinant protein was eluted with buffer A containing 200, 250 and 300 mM imidazole. Fractions were analyzed on SDS-PAGE and those containing nearly pure proteins were pooled and protein was further purified using anion exchange column chromatography. Different fractions containing pure protein were pooled and concentrated using 10 kDa cut-off spin columns. The protein solution was centrifuged at 16,000RPM for 30 min and the supernatant containing mostly soluble protein was dialyzed in a buffer containing 20 mM Tris-HCl pH 7.6, 200 mM NaCl, 50% glycerol and 1 mM PMSF, and stored at -20°C (Fig. 3.1.1). Protein concentration was determined by taking OD at 280 nm in NanoDrop (Synergy H1, Hybrid Multi-Mode Reader Biotek) using mass extinction coefficient of both the proteins. The refolding of purified ParA2 and ParA3 proteins was confirmed by recording Circular Dichroism spectroscopy in phosphate buffer using JASCO, J815, Japan as described earlier (Modi and Misra, 2014) (Fig. 3.1.1). Recombinant ParA1 was purified in similar way as above.

3.1.2.3 DNA binding study using electrophoretic mobility shift assay

DNA binding activity of secondary genome ParA proteins was assayed by electrophoretic mobility shift assay (EMSA) as described in (Leonard *et al*., 2005). In brief, the different concentrations of ParA2 or ParA3 proteins (0-2.5 µM) were incubated with 100 fmol of 3 kb linear dsDNA (*Eco*RI linearized pBluescript II SK(+) in 30 µl reaction volume containing DNA binding buffer B (50 mM Tris-Cl pH 8.5, 75 mM NaCl, 5 mM $MgSO_4$ and 0.5 mM 1,4-Dithiothreitol) for 10 min at 25°C in the absence and presence of 1 mM ATP, ADP or ATP-γ-S. The reaction mixture was mixed with DNA loading dye (without SDS) and loaded in 0.8% agarose gel. Agarose gel electrophoresis was performed in 0.5X TBE buffer at 50 mV at 8°C and gels were stained with ethidium bromide. The gel images were documented and analyzed for a shift in mobility with respect to the free DNA probe. The mobility retardation of nucleoprotein complex (NPC) for each concentration has been calculated as difference in distance (cm) travel at each concentration with respect to total migration of DNA probe. It has been further plotted with respect to the different concentration of ParA2 and ParA3 as mean ± SD.

3.1.2.4 Fluorescence anisotropy

Fluorescence anisotropy has been used to monitor the DNA binding activity of ParA proteins (Leonard *et al*., 2005). In brief, an equimolar concentration of 5' fluorescein labelled oligonucleotide Phi-W (5′fluorescein-CGTTCTTATTACCCTTCTGAATGTCACGCTGA TTATTTTGACTTTGAGCGTATCG-3′) was annealed to its complementary unlabeled oligonucleotide Phi-C to create fluorescein labeled double-stranded DNA (Chittela*et al*., 2006). A 50 µl of reaction mixture containing the different concentrations of protein (0.5 to 2.0 µM) was incubated with 20 nM 5′ fluorescein labeled double-stranded DNA (55 mer) in DNA binding buffer B in the absence and presence of 1 mM ATP at 25°C for 10 min. Fluorescence signals were recorded at an excitation of 480 nm and emission at 520 nm at

25°C on an FLS 980 spectrofluorimeter (Edinburgh Instruments, UK). The data were analyzed and plotted with the curves fitted using GraphPad Prism 5.

3.1.2.5 Sedimentation assay

The sedimentation assay of ParA proteins was done under different conditions as described in (Hui *et al*., 2010; Charaka and Misra, 2012). In brief, both recombinant ParA2 and ParA3 proteins were spun at 22000 X g for 15 min at 4°C to remove aggregates if any. The 2 µM proteins were incubated with 0.5 pmol linear dsDNA of ~3 kb and 1 mM of ATP or ADP or ATP-γ-S in 30 µl reaction volume for 10 min at room temperature. Similarly, a titration of DNA concentration (0-1.5 pmol) was done with both proteins in absence and presence of 1mM ATP or ADP only. Proteins incubated without DNA was used as a negative control. The reaction mixtures were centrifuged at 22000 X g for 30 min at 25°C. The supernatants were removed carefully and mixed with equal volume of 2X SDS loading buffer while pellet was resuspended in 30 µl of Buffer B and mixed with 30 µl of 2X SDS loading buffer. Both supernatant and pellet was heated at 95°C for 10 min, centrifuged and separated on 12 % SDS-PAGE gels. Protein gels were stained with Coomassie Brilliant Blue R250 stain and protein band intensity was measured densitometrically by Image J 2.0 software, NIH. The data were plotted as the ratio of pellet to supernatant using GraphPad Prism 5.

3.1.2.6 Dynamic light scattering

Dynamic light scattering was performed using a Horiba Scientific Nanopartica SZ-100 instrument as described previously (Bouet *et al*., 2007; Charaka and Misra, 2012). In detail, all the solutions were filtered through a 0.2 µm filter and proteins were centrifuged at 22000 X g for 30 min at 4°C before experiment. For this, 2 µM proteins were incubated with 0.1 pmol ~3 kb linear dsDNA in the absence and presence of 1 mM ATP or ADP. Light scattering and particle size at 90° angle was measured at 25°C for 30 min at a regular interval

of 30s. The data obtained was analyzed using in-built software (SZ-100) and intensity of scattered light as kilo counts per second and particle size in term of hydrodynamic radii were plotted using GraphPad Prism 5.

3.1.2.7 Measurement of ATPase activity of ParAs using Thin Layer Chromatography

ATPase activity was measured as the release of [^{32}P]-αADPs from [^{32}P]-αATPs using Thin Layer Chromatography (TLC) method as described earlier (Hue *et al*., 2010; Modi and Misra, 2014). In brief, 2 µM ParA proteins were mixed with 30 nM [^{32}P]-αATP in a total volume of 30 µl containing buffer B with 2 mM Mg^{2+} and incubated at 37°C for 0 - 40 min in absence and presence of 0.1 pmol dsDNA. The reaction was stopped at each time point with 10 mM EDTA solution and 1µl of it was spotted on PEI-Cellulose F^{+} TLC sheet. Spots were air-dried, and components were separated on a solid support in a buffer system containing 0.75 M KH_2PO_4 / H_3PO_4 (pH 3.5) and exposed to X-ray film for overnight. The autoradiograms were developed. Spot intensities of both ADP and ATP forms were determined densitometrically using Image J 2.0 software, NIH, and % ADP to ATP ratios were calculated and plotted using the GraphPad Prism 5 software.

3.1.2.8 Measurement of ATP binding and hydrolysis using intrinsic tryptophan fluorescence

Since, both ParA2 and ParA3 proteins possess 2 Trp residues in polypeptide chain, the nucleotides (ADP/ATP/ ATP-γ-S) binding and hydrolysis by ParA2 and ParA3 in absence and presence of dsDNA was measured as a function of intrinsic tryptophan fluorescence of these proteins. For this, 2µM of recombinant ParAs were incubated in buffer B containing 0.5 mM $MgSO_4$ for 30 minutes in absence and presence of 0.1 mM of ADP or ATP or ATP- γ-S and/or 0.1pmol dsDNA in 30µl reaction volume. The emission spectra of each protein were obtained by excitation at 295 nm and spectral scanning of emission from 315 nm to 401 nm at an interval of 2 nm using FLS 980 spectrofluorimeter (Edinburgh Instruments, UK). To

demonstrate time dependent hydrolysis of ATP by deinococcal ParAs, 2 µM of ParA2 or ParA3 was preincubated in buffer B for 2 minutes and the emission spectra were acquired at 0, 10, 15, 20 and 30 min after the addition of 0.1 mM ATP. Spectra were corrected for background and Raman scattering by subtracting buffer spectra. The obtained spectra for each time points were compared with spectra for each protein incubated with 0.1mM ADP for 30 minutes. The data were analyzed and plotted using GraphPad Prism 5.

3.1.2.9 Measurement of binding affinity of ParAs with fluorescent ATP

We have used fluorescent analogue of ATP viz. (2'-(or-3')-O-(Trinitrophenyl) Adenosine 5'-Triphosphate (TNP-ATP) to determine the binding affinity of deinococcal ParAs with fluorescent as well as natural ATP. Fluorescent emission scanning spectra of TNP-ATP (Sigma–Aldrich) and TNP-ATP complexed with ParA1, ParA2 or ParA3 in absence and presence of 2 nM linear dsDNA of 3kbps were obtained using a FLS 980 spectrofluorimeter (Edinburgh Instruments, UK) with an excitation wavelength of 410 nm and emission spectral scanning from 470 to 630 nm at an interval of 1nm. The protein concentration used for each reaction was 2 µM in a reaction volume of 50 µl in buffer B (50 mM Tris-Cl pH 8.5, 75 mM NaCl, 2 mM $MgSO_4$ and 0.5 mM DTT) containing 3 µM of TNP-ATP. The displacement of the fluorophore was monitored by addition of the natural nucleotide (ATP) to a final concentration of 5 mM. A control experiment was also done in the absence of ParAs to ensure that the fluorescence emission of TNP-ATP is not affected by the presence of ATP. The emission maxima for each protein with TNP-ATP were obtained from fluorescence emission spectrum for the same protein. All other fluorescent measurements for kinetic study (titration of protein or TNP-ATP or ATP) were performed using a Biotek Synergy H1 Hybrid multi-mode microplate reader (Bio-Tek Instruments). All measurements were obtained in 96-well, black side, flat and clear bottom plates (Corning, Sigma) at 37°C, in 50 µl reaction volumes. For analysis of titration data, the observed fluorescence emission intensity of each

sample (at 511 nm for ParA2 and 514 nm for ParA1 &ParA3) was corrected with signal observed in buffer plus TNP-ATP. A 'no ParA' blank titration was used for each ParA titration experiment. Therefore, the observed fluorescence change (ΔF_{obs}) in graphs represents the rise of fluorescence emission intensity due to the formation of complex between ParAs and TNP-ATP. In the absence of ParA, fluorescence emission intensities of TNP-ATP were proportional to its concentration up 1 μM. Above 1 μM 'inner filter effects' caused this relationship to deviate from linearity, so we have applied a correction factor to the fluorescence data collected for TNP-ATP concentrations (>1 μM). This correction factor was calculated by determining the ratio of the theoretical fluorescence intensity (predicted by extrapolating the linear region of plots) to the actually observed fluorescence intensity (Ward, 1985).

Determination of Dissociation constants

To study the interaction between ParAs and ATP, we have carried out titration experiments using TNP-ATP. For that, we have titrated proteins against a fixed concentration of TNP-ATP and vice-versa. In details, increasing concentrations of ParAs were added to a fixed concentration of TNP-ATP (3 μM) in buffer B in 50 mL reaction volumes. The reaction mixtures were set in duplicates in 96 wells plate and gently shaken for 10 min in the machine at room temperature before each read. The samples were excited at 410 nm and emission at 511nm (for ParA2) or 514 nm (for ParA1 &ParA3) was recorded as relative fluorescent units (RFU). These data gave saturation curve that was plotted as ΔF_{obs} / ΔF_{total} versus the total concentration of protein using the GraphPad Prism 5.0 software. ΔF_{obs} is the observed fluorescence signal following nucleotide addition (corrected for inner filter effects, for dilution effects and for the signal observed at that nucleotide concentration in the absence of protein). ΔF_{total} is the maximal value of ΔF_{obs} obtained at saturation.

The dissociation constants [Kd(μM)] were determined by applying Langmuir single-site binding equation for a curve fit as described in (Guarnieri *et al*., 2011).

$$F_{obs} = F_{free} + [\{(F_{bound} - F_{free}) X [([Protein]_{total} + [TNP\text{-}ATP]_{total} + Kd) - (([Protein]_{total} + [TNP\text{-}ATP]_{total} + Kd)^2 – (4[Protein]_{total} X [TNP\text{-}ATP]))^{1/2}]\}/(2[TNP\text{-}ATP]_{total})] \quad \text{(Eq. 1)}$$

Where F_{obs}, F_{free}, and F_{bound} are the relative fluorescence units (RFU) observed, RFU of free TNP-ATP, and RFU of TNP-ATP completely bound to protein, respectively, and [Protein] and [TNP-ATP] are the concentrations of ParAs and TNP-ATP, respectively.

For titration of TNP-ATP, different concentration of TNP-ATP was incubated in buffer B with a constant protein concentration (2μM) in a total volume of 50μL. After 10 minutes' incubation at room temperature the fluorescence emission (as RFU) was recorded as mentioned above for each protein. The ΔF_{obs} / ΔF_{total} versus the different concentration of TNP-ATP were plotted using the GraphPad Prism 5.0 software to obtain a saturation curve. The dissociation constants [Kd(μM)] were determined by applying quadratic equation for a curve fit as described in (Hormaeche*et al*., 2002).

$$F = F_{min} + \{(F_{max}\text{-}F_{min})[([Protein]_{total} + [\ TNP\text{-}ATP] + Kd_{(TNP\text{-}ATP)}) – (([Protein]_{total} + [TNP\text{-}ATP] + Kd_{(TNP\text{-}ATP)})^2 – (4[Protein]_{total} X [TNP\text{-}ATP]))^{1/2}]\}/2[Protein]_{total} \quad \text{(Eq.2).}$$

Where F represents RFU, F_{min} is the RFU at the start of titration, F_{max} is the RFU at the saturating concentration of TNP-ATP, $Protein_{total}$ is the total concentration of ParA2 or ParA3 and $Kd_{(TNP\text{-}ATP)}$ is the apparent dissociation constant of ParA2 or ParA3-(TNP-ATP) complex.

To determine the dissociation constants for natural ATP (act as a competitor for TNP-ATP) we performed a displacement assay. In brief, increasing concentrations of a competitor (natural ATP) were added to pre-incubated ParA1:TNP-ATP, ParA2:TNP-ATP or ParA3:TNP-ATP (2μM:3 μM) complex in a total reaction volume of 50 μl. After 10 minutes' incubation at room temperature the fluorescence emission (as RFU) was recorded as stated

above for each protein. The ΔF_{obs} / ΔF_{total} versus the different concentration of ATP were plotted using the GraphPad PRISM 5.0 software to obtain a saturation curve. The displacement of bound TNP-ATP by ATP was calculated by using following quadric equation.

$$F = F_{max} + \{(F_{max} - F_{min})[([Protein]_{total} + [ATP] + K_{(0.5)}) - (([Protein]_{total} + [ATP] + K_{(0.5)})^2 - (4[Protein]_{total} X [ATP]))^{1/2}]\}/2[Protein]_{total} \quad \text{(Eq.3)}$$

Where F_{max} is the RFU at the start of ATP titration, F_{min} is the RFU at the saturating concentration of ATP, $K_{(0.5)}$ in equation 3 indicates the amount of ATP required to displace half of the bound TNP-ATP and [ATP] shows the ATP concentrations. So, the apparent dissociation constant of ParAs-ATP ($Kd_{(ATP)}$) can be calculated by using the $K_{(0.5)}$ value obtained from the equation 3 and the following equation,

$$Kd_{(ATP)} = K_{(0.5)}/\{1 + ([TNP\text{-}ATP]/Kd_{(TNP\text{-}ATP)})\} \quad \text{(Eq. 4)}$$

Where [TNP-ATP] represents the concentration of TNP-ATP at the start of the titration (Hormaeche*et al*., 2002).

3.1.2.10 Transmission electron microscopy

We have imaged the DNA binding activity of ParAs and their polymerization on DNA with respect to different nucleotides by transmission electron microscopy (TEM) on an electron microscope (Model JEOL2000FX, Japan) using previously described protocols (Leonard *et al.,* 2005; Hue *et al.,* 2010). In brief, 100 ng nicked circular ϕX174 RF II dsDNA was incubated with 1.5 µM ParA2 or ParA3 alone or with 1mM ADP or ATP in buffer B containing 50 mM Tris-Cl pH 8.5, 75 mM NaCl, 5 mM $MgSO_4$ and 0.5 mM DTT in different combinations. Protein without DNA and high-energy phosphates were used as a control. This mixture was incubated at 37°C for 10 min before application to UV- activated carbon-coated 200 mesh containing copper grids. This mixture was diluted 5 times and then dropped on the

charged side of the grid for 2 minutes and then washed in stage II distilled water. The grids were negatively stained with 10 µl of 2% (weight / vol) uranyl acetate and washed twice in stage II distilled water. These were further blotted to dry and incubated for 1 h under vacuum before imaging. Grids were observed under JEOL 2000FX, Japan electron microscope at 100 kV and X50,000 – X200,000 magnifications. Digital images were collected on CCD camera as described earlier (Bouet*et al.,* 2007).

3.1.2.11 Construction of plasmids for protein-protein interaction studies

Protein–protein interactions were monitored using a bacterial two-hybrid system (BACTH) as well as coimmunoprecipitation from *E. coli* and *D. radiodurans* as described in (Karimova *et al*., 1998; Maurya *et al.,* 2018).

For protein-protein interaction studies in *E. coli*, the coding sequences of ParA1 (DR_0013), ParA2, ParA3 and ParA4 (DR_B0031) were PCR amplified using gene-specific primers as given in Table 2.3. The purified PCR amplicons of *parA1* and *parA4* was digested with *Bam*HI-*Eco*RI while *parA2* and *parA3* was digested with *Xba*I-*Bam*HI restriction enzymes. These genes were ligated in Bacterial Two-Hybrid System (BACTH) plasmids viz. pUT18 and pKNT25 as given in Table 2.4 to generate T18 or T25 fusion, respectively. In addition, all four *parB*s were also cloned in different BACTH plasmids (Table 2.4).

For *in vivo* interaction among different deinococcal ParAs, the translational fusion of ParA2 and ParA3 were generated with polyhistidine tag in pRADgro vector (an *E. coli-D. radiodurans* shuttle plasmid). For this, coding sequences of N-terminal hexahistidine tagged ParA2 and ParA3 were PCR amplified (from their pET28a + variants) using PETHisF and PETHisR primers, and ligated in pRADgro plasmid at *Apa*I-*Xba*I sites to obtain pRADhisA2 and pRADhisA3 plasmids, respectively (Table 2.4). Similarly, T18 tag fusions of all 4 *parA*s were PCR amplified from their pUT18 variants using BTHF (PV) and BTHR (PV) primers

and were cloned in pVHS559 at *Nde*I-*Xho*I sites, and resultant plasmids were named as pV18A1, pV18A2, pV18A3 and pV18A4, respectively (Table 2.4).

In order to monitor the cross-talk between ParAs, ParBs and cell division proteins if any, we have made BACTH constructs of different cell division proteins of *D. radiodurans* viz. core divisome proteins; FtsE, FtsK, FtsQ and FtsW as well as cell division regulatory proteins; MinC, MinD and DivIVA (Table 2.3 and Table 2.4). In addition, BACTH constructs of FtsA and FtsZ was used from an earlier study (Modi and Misra; 2014). All the constructs generated for protein-protein interaction study were sequenced for the presence of desire gene. The expression of T18 or T25 or polyhis tagged proteins was confirmed by western blotting using respective antibodies [Anti-T18 for T18 tag (SC-33620), Anti-T25 for T25 (SC-13582) and Anti-polyhistidine for polyhis tag].

3.1.2.11A Protein-protein interaction study using bacterial two-hybrid system

We have used bacterial two-hybrid system for protein-protein interaction as described in (Karimova *et al*., 1998; Battesti *et al*., 2012). In brief, *E. coli* BTH101 was co-transformed with different plasmids like pUT18A1, pUT18A2, pUT18A3 and pUT18A4, and pKNTA1, pKNTA2, pKNTA3, pKNTA3 and pKNTA4 in different combinations. Empty vectors were transformed in different combinations and used as negative controls while pUTEFA and pKNTEFZ were used as positive control. In similar way, different genome partitioning proteins and core cell division as well as regulatory proteins were co-transformed in different combination permutation. The transformants were scored on LB agar plate supplemented with ampicillin (100 μg/ml) and kanamycin (25 μg/ml). Three colonies from transformation plate were grown in LB broth containing required antibiotics for spot assay and β-galactosidase activity. Recombinant cells expressing these proteins in different combinations were spotted on LB agar plate containing 5-romo-4-chloro-3-indolyl-β-D-galactopyranoside (X-Gal) (40 μg/mL), IPTG (0.5 mM) and antibiotics as required. Plates were incubated at

30°C for 18-24 h and the appearance of white-blue color colonies was recorded. In parallel, the levels of β-galactosidase activity were measured from the same liquid cultures grown overnight with 0.5 mM IPTG as described earlier (Battesti *et al*., 2012). The β-galactosidase activity was calculated in Miller units as described in (Karimova *et al*., 1998) and plotted with the standard deviation in GraphPad Prism5.

3.1.2.11B. Protein-protein interaction study using coimmunoprecipitation

Interaction of deinococcal ParAs among themselves as well as with cell division proteins in surrogate *E. coli* (as described above) was monitored by co-immunoprecipitation. In general, BTH 101 cells co-expressing two different proteins with different tags (viz. T25 and T18) were grown and induced with 0.5mM IPTG. The cell pellets were washed with 1X PBS and resuspended in RIPA buffer and incubated on 37°C for 20 min. and then on ice for 30 min. The cell lysate suspension was sonicated for 30 seconds at 30% duty cycle for 10sec On and 15sec Off mode. The cell lysate was centrifuged at 12, 000 RPM for 10 min. The clear supernatant was immunoprecipitated using Anti-T25 antibody in CoIP column using standard protocol as described in Protein G immunoprecipitation kit (Sigma-Aldrich). The immunoprecipate was washed with 1X IP buffer alone as well as with 0.5N NaCl. Immunoprecipitates were separated on SDS-PAGE, transferred to polyvinylidene difluoride (PVDF) membrane and hybridized using Anti-T18 antibody. Hybridization signals were detected using anti-mouse secondary antibodies conjugated with alkaline phosphatase using NBT/BCIP substrates (Roche, Mannheim, Germany).

Interaction among different ParAs was also monitored in *D. radiodurans*by co-immunoprecipitation. For that, the cell-free extracts of *D. radiodurans*expressing ParAs as on pV18A1, pV18A2, pV18A3 and pV18A4 in different combinations with ParA2 from pRADhisA2 and ParA3 from pRADhisA3 (Table 2.4) were prepared and immunoprecipitated using polyhistidine antibodies as described above (Maurya *et al*., 2018). Immunoprecipitate

was purified using Protein G Immunoprecipitation Kit (Cat. No. IP50, Sigma-Aldrich. Inc.). The immunoprecipitates were separated on SDS-PAGE, transferred onto PVDF membrane and hybridized using monoclonal antibodies against T18 tag. The hybridization signals were detected using anti-mouse secondary antibodies conjugated with alkaline phosphatase using NBT/BCIPsubstrates (Roche Biochemical, Mannheim) as described above.

3.1.2.12 Generation of deletion mutant of *parA2* and *parA3* genes

For generation of single (Δ*parA2 or* Δ*parA3*) and double mutants (Δ*parA2*Δ*parA3*) of *parA2* and *parA3* genes, ~1 kb upstream and downstream region from mid *parA2* and *parA3* ORFs were PCR amplified using primers (Table 2.3) and cloned in pNOKOUT and pNOSOUT to yield pNOKA2 and pNOSA3, respectively (Table 2.4). In brief, upstream fragments were cloned at *Kpn*I-*Apa*I and downstream at *Bam*HI-*Xba*I sites. These constructs were linearized by *Xmn*I and transformed into *D. radiodurans* separately as well as together and grew several generations under required selection pressure till the homozygous insertion and replacement of middle portion *parA2* with *nptII* cassette and *parA3* with *aadA*cassettewere achieved in the genome of *D. radiodurans*. This was ascertained by diagnostic PCR using *parA2* and *parA3*gene specific as well as antibiotic cassettes (*nptII* and *aadA*) specific primers in different combination.

3.1.2.13 Determination of Genome copy number using quantitative real time PCR

Wild-type, single and double mutant cells of similar O.D. at 600nm were harvested by centrifugation and their cell number was determined using a Neubauer cell counter under light microscope. Equal number of cells were washed with 70 % ethanol solution and lysed in a lysis solution containing 10mM Tris pH 7.6, 1 mM EDTA and 4mg/ml lysozyme at 37°C. The lysed cells were spun (10000 RPM, 5 min) to remove cell debris. The lysis efficiency was confirmed by plating of lysed supernatant on TYG agar plates. The integrity of genomic

DNA was ascertained by agarose gel electrophoresis. The serial dilutions of cytoplasmic extract were made and 0.1 ml of it was used for further analysis of genomic copy number using quantitative Real-Time PCR as described in (Breuert *et al*., 2006). In brief, a fragment of about 300 bps was amplified using standard PCR protocol from isolated genomic DNA of *D. radiodurans*as a template. The PCR product was gel purified using Qiagen gel extraction kit and the amount of DNA was quantified by Nanodrop and the concentration of DNA molecules were calculated using the molecular mass computed with 'oligo calc' (www.basic.northwestern.edu/biotools). A dilution series was generated for each standard fragment and used for quantitative PCR analysis with the dilution series. Copy number vs cycle threshold (Ct) value was plotted as standard curve. Two different genes per replicon with similar PCR efficiency were used in *D. radiodurans* viz. *ftsE* and *ftsZ* for chromosome I, *dr_A0155* and *pprA* for chromosome II, *dr_B003* and *dr_B0104* for megaplasmid and *dr_C001* and *dr_C018* for small plasmid (Table 2.3). PCR efficiency of each gene was checked and was found to >96% for each. The qPCR was carried out by following the Minimum Information for Publication of Quantitative Real-Time PCR Experiments (MIQE) guidelines using Roche Light cycler (Bustin S.A. *et al*., 2009) and the Cp values were determined. We have used three independent biologic replicates for each sample. The copy number of each replicon was quantified by comparing the Ct values with a dilution series of a PCR product of known concentration which is used as a standard. The copy number of each replicon by both genes per cell was calculated by considering the number of cells present at the time of cell lysis. We represented average of copy number reflected from two genes per replicon with student t-test analysis.

3.1.2.14 Cell survival studies in response to γ-radiation and hydrogen proxide

*D. radiodurans*R1 and its *parA* mutants were subjected to 6 kGy γ-radiation as well as different doses of hydrogen peroxide as described in (Misra *et al*., 2006). In brief, wild type and mutants were grown in TGY medium with appropriate antibiotics at 32°C. They were washed and suspended in sterile phosphate-buffered saline (PBS) and treated with 6 kGy γ-radiation at dose rate 1.81 kGy/h (Gamma Cell 5000, ^{60}Co, Board of Radiation and Isotopes Technology, DAE, India). Equal number of gamma irradiated cells and respective controls maintained under identical conditions (SHAM) controls were washed in PBS and suspended in the fresh TGY medium. These cells were grown in TGY medium in 48 well microtiter plates in replicates at 32°C for 42 h. Optical density at 600 nm was measured during growth in the Synergy H1 Hybrid multi-mode microplate reader. Further, growth rate was determined from growth curve using formula ($Nt = N0 * (1 + r)^t$; where Nt is OD_{600} at time t, N0 is OD_{600} at start of growth curve, r is growth rate and t is time passed) and plotted for each sample type.

For H_2O_2 treatment, the exponentially growing cells were exposed to different concentration of H_2O_2 for 30 minutes. Serial dilutions of them were made and plated on TGY agar medium containing antibiotics as required (Misra *et al*., 2006). The colony-forming units were recorded after 48 h of incubation at 32°C. The surviving fractions were expressed as the percentage of colony forming units obtained after treatment with respect to untreated cells. We have also calculated D_{10} value from survival curve for each sample time and plotted.

3.1.2.15 Microscopic studies

Fluorescence microscopy of *D. radiodurans*, its mutants was done as described previously (Charaka and Misra, 2012), using an Olympus IX83 inverted fluorescence microscope equipped with an Olympus DP80 CCD monochrome camera. In brief, bacterial cells were

grown till the exponential phase, washed in PBS and stained for 10 minutes with DAPI (4',6-diamidino-2-phenylindole, Dihydrochloride) for nucleoid and Nile red for the membrane. These cells were washed twice in PBS and resuspended in small volume of PBS. Two-three microliters of cells were mounted on glass slides coated with 0.8% agarose and covered with glass cover slip. Images were taken in DAPI (for nucleoid) and TRITC (for membrane) channels using fluorescence microscope. Images of different channels from same field were merged and deconvoluted using an inbuilt software, cellSens. The brightness and contrast of all images were adjusted using Adobe Photoshop 7.0. More than 500 cells from both wild-type and mutants were examined from different fields for calculation of cell area using cellSens and plotted. We performed line scan analysis of many cells from each sample type through cellSens software by following its manual. In line scan analysis we scanned fluorescence intensity of DAPI and Nile red signals across a line over a cell to find the relative position of nucleoid and membrane (or septum). The percentage of cells showing septum trapped nucleoids and defect on tetrads separation was calculated and plotted using GraphPad Prism 5 software.

3.1.3 Results:

3.1.3.1 Secondary genome ParAs are structurally similar but distinct from ParA1

The amino acid sequence of ParA1, ParA2, ParA3 and ParA4 was aligned with the known ParA-type proteins from other bacteria using ClustalW program (Fig.3.1.1 A). We found that ParA1 contains extra ~48 amino acids at its N-terminal while rest of the region of all the ParAs is conserved. ParAs of secondary genome elements (ParA2 and ParA3) contain similar Walker A, Walker A' and Walker B motifs like other P-loop Walker ATPases (Fig. 3.1.1A). In addition, they have conserved arginine in the DNA binding motifs. Unlike ParA1 of *D. radiodurans* and other bacterial homologs, the secondary genome ParAs lacks some of the

conserved amino acids. For example, a highly conserved lysine at the beginning of the Walker A motif was substituted with alanine in ParA2 and ParA3 proteins. Additionally, the conserved valine at 4th position in this motif was replaced with alanine in both ParAs (Fig. 3.1.1). Interestingally, the difference of amino acid residues between different walker motifs is similar in both ParAs. Earlier, secondary genome ParAs of *D. radiodurans* was reported evolutionarily different from other chromosomal type ParAs including ParA1 of *D. radiodurans* (Charaka *et al*., 2013). They are placed between chromosomal type ParAs and other small ATPases in the phylogenetic tree.

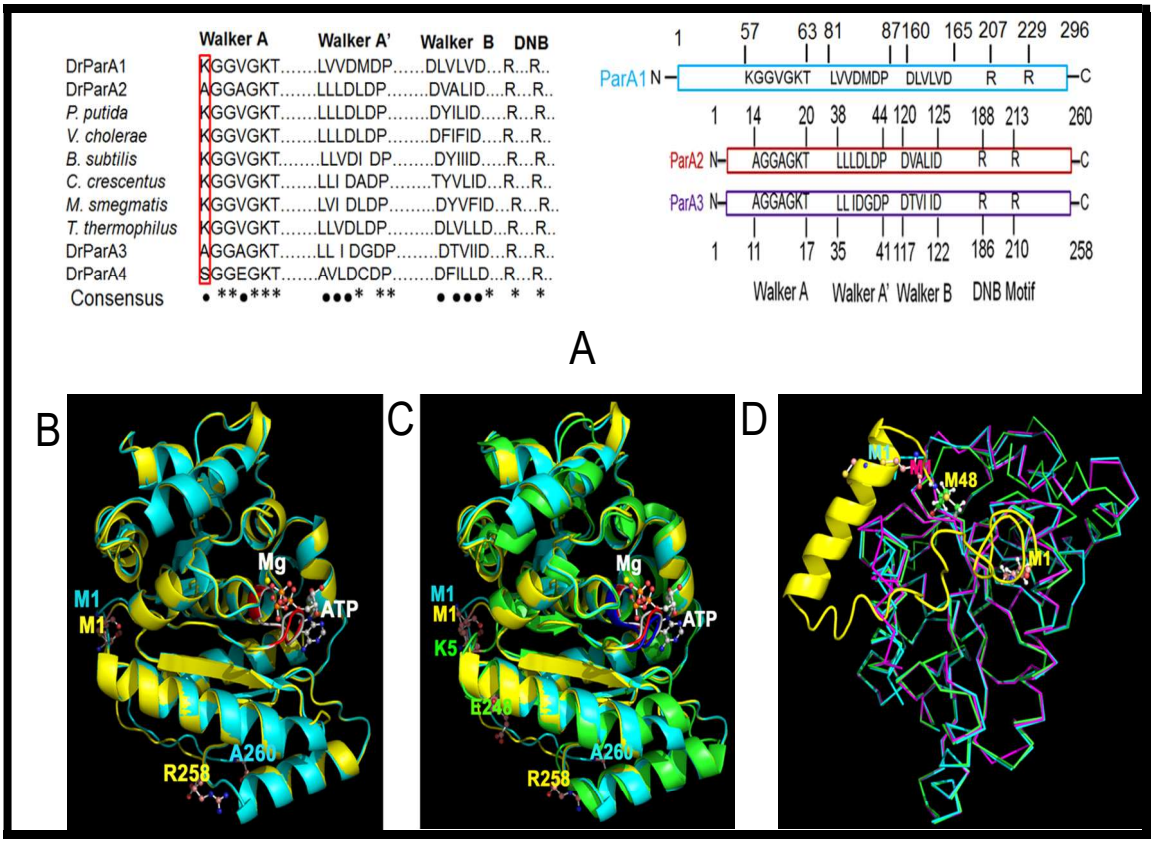

Figure 3.1.1 Functional domain analysis of the putative ParA proteins of *D. radiodurans*. Amino acid sequence of deinococcal ParAs were aligned with known ParAs and searched for the presence of different Walker motifs and DNA-binding (DNB) motifs in these proteins and shown schematically (**A**). Modeled structure of ParA2 (Cyan) and ParA3 (Yellow) were aligned to each other (**B**) as well with Soj of *Thermus thermophilus* (PDB ID-2BEK; Green) (**C**). Ribbon form of modelled structure of ParA1 (Green), ParA2 (Cyan) and ParA3 (hot pink) were aligned in Pymol and the unaligned N-terminal amino acids (1-48) of ParA1 are shown in yellow colour (**D**).

Homology models of different deinococcal ParAs were generated using I-TASSER tool using Soj protein (PDB ID; 2BEK) of *Thermus thermophilus* as template. Structure of ParA2 and ParA3 aligned perfectly to each other as well as to the Soj of *T. thermophilus* (Fig. 3.1.1 B, C). On the other side, the ~48 amino acids extra at the N-terminus in ParA1 hang around and the remaining parts of the 3-D modeled structure were nearly superimposable with secondary ParAs (Fig. 3.1.1D). This finding categories ParA1 as type Ia ParAs while ParA2 and ParA3 as type Ib. The model suggests that both ParA2 and ParA3 proteins of *D. radiodurans* are very similar to each other but seem to be different from ParA1, at least *in silico.*

3.1.3.2 Recombinant ParA2 and ParA3 were expressed in *E. coli* and purified

Genomic DNA of *D. radiodurans* was isolated using standard protocol (Battista *et al*., 2001) and the dr_A0001 (*parA2*) and dr_B0001 (*parA3)* genes were PCR amplified and cloned in pET28a(+) expression plasmid as mentioned in materials and methods section.

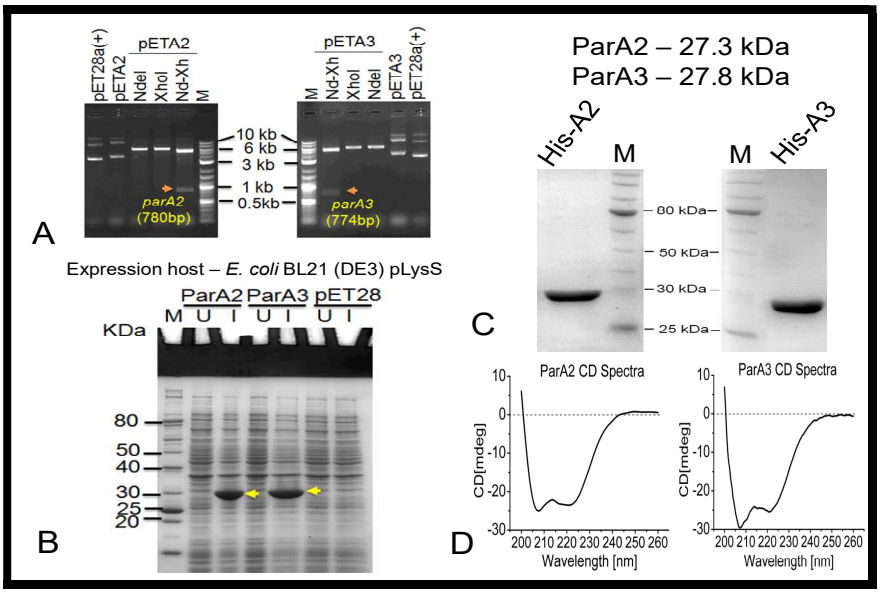

Figure 3.1.2 Cloning, expression and purification of ParA2 and ParA3 (A-C). Circular Dichroism spectra of ParA2 and ParA3 (D)

Recombinant plasmids pETA2 (carrying *parA2*) and pETA3 (carrying *parA3*) were prepared and digested with restriction enzymes used for cloning and the release of DNA fragment by double digestion confirmed the cloning of these genes (Fig 3.1.2). These clones were further sequenced for verification. Verified recombinant plasmids were transformed into *E. coli* BL21(DE3)pLysS cells and induced with 0.5mM IPTG. The expression of $(His)_6$ParA2 of 28.3 kDa and $(His)_6$ParA3 of 28.8 kDa was observed on SDS – PAGE. These proteins were purified under native conditions by using Ni-NTA chelating sepharose followed by ion-exchange and gel filtration chromatography (Fig 3.1.2). Peptide mass fingerprints of both these proteins confirmed their identity as ParA2 and ParA3 of *D. radiodurans*.

3.1.3.3 ParA2 and ParA3 are DNA binding ATPases

We have monitored DNA binding activity of ParA2 and ParA3 by electrophoretic mobility shift assay (EMSA) and fluorescence anisotropy. In EMSA, we incubated both ParAs with dsDNA in absence and presence of ADP, ATP or ATP-γ-S, and electrophoresed in agarose gel. We observed nearly similar binding pattern of both the proteins with non-specific dsDNA and the effect of ATP and ADP on DNA binding activity was also similar (Fig. 3.1.3) For instance, with the increase in protein concentration, the size of the nucleoprotein complex increased progressively (reflected as slower mobility), which was not affected by the presence of ADP. But the presence of ATP or ATP-γ-S as compared to protein controls has clearly stimulated the DNA binding activity of ParA2 and ParA3 (Fig. 3.1.3 A-D). Fluorescence anisotropy experiment revealed that both the proteins interact with fluorescent dsDNA in almost similar fashion. Presence of ATP has significantly increased the anisotropy of ParA nucleoprotein complex possibly due to increased DNA binding activity of ParAs (Fig 3.1.3 E, F).

Since, ATP had significantly affected interaction of ParA2 and ParA3 with DNA, and presumably the assembly of these proteins on dsDNA, the metabolic fate of ATP by these proteins was monitored using [^{32}P]-αATP by TLC.

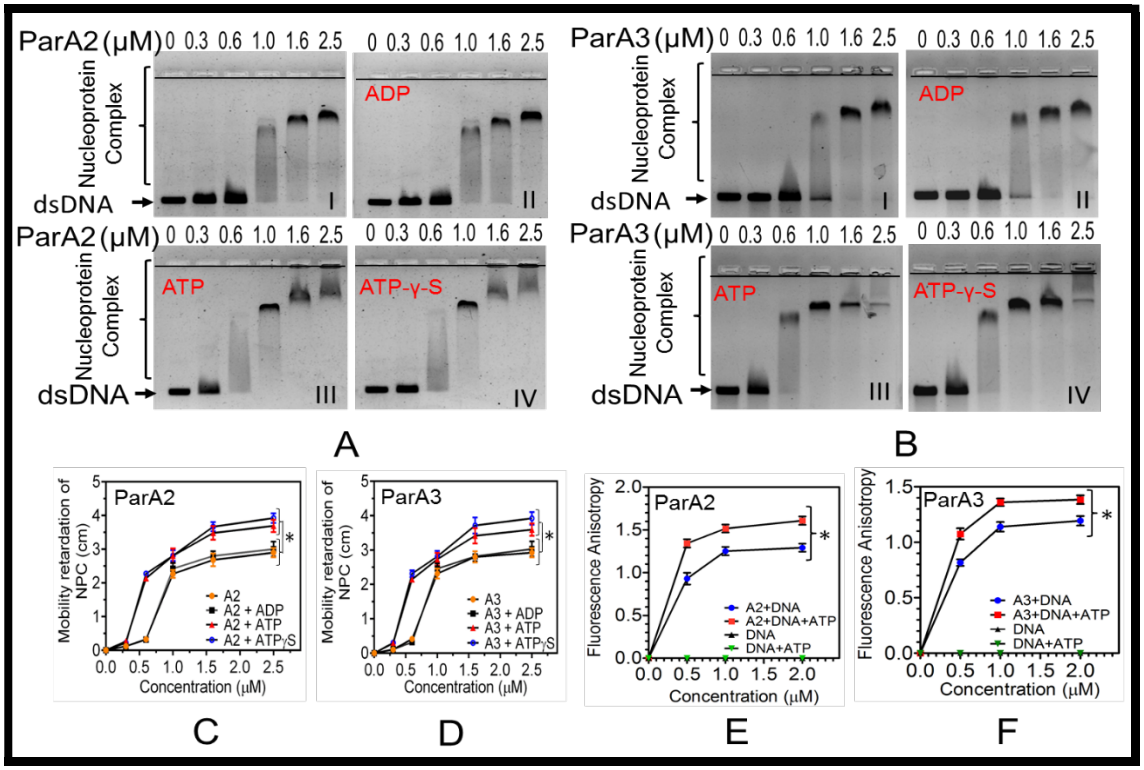

Figure 3.1.3 DNA binding activity of secondary genome ParAs with respect to different nucleotides using EMSA (A-D) and fluorescence anisotropy (E,F).

Both these proteins could hydrolyse ATP into ADP and Pi irrespective of the presence of dsDNA (Fig.3.1.4A-C). Earlier, stimulation of ATP hydrolysis of ParA1 was shown in the presence of centromere-ParB1 complex (Charaka and Misra, 2012). It suggests a possibility of ATPase activity stimulation by secondary genome ParAs in the presence of cognate centromere-ParB nucleoprotein complex, which cannot be ruled out.

3.1.3.4 Secondary ParAs show similar affinity for ATP but distinct from ParA1

The fluorescent analog of ATP, TNP-ATP, has been widely used to characterize ATP binding by a number of eukaryotic and prokaryotic proteins (Dupont *et al*., 1982; Stewart *et al*., 1998; Hiratsuka, 2003 and Treuner-Lange, 2013). TNP-ATP shows minimal fluorescence in free

form. However, upon binding to protein, its fluorescence emission increases several folds which make this fluorescent probe a powerful tool to study ATP binding with the proteins (Hiratsuka and Uchida, 1973).

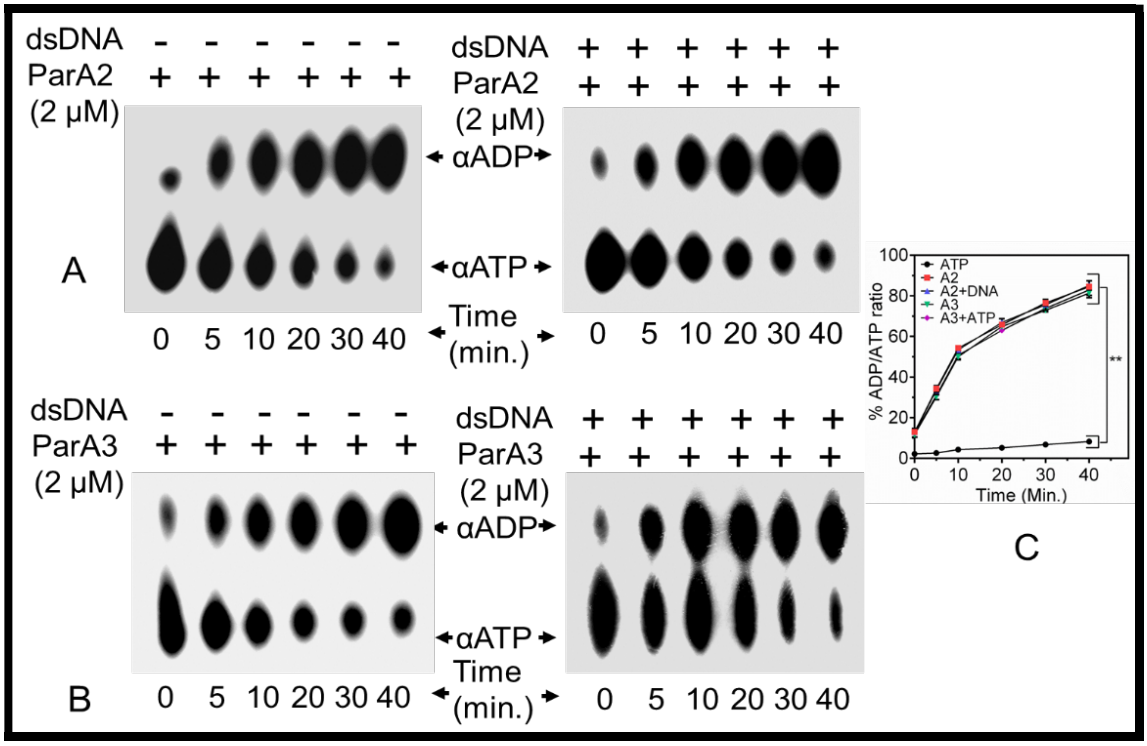

Figure 3.1.4 Time dependent ATP hydrolysis activities of ParA2 (A) and ParA3 (B) studied with respect to dsDNA using [^{32}P]-αATP by TLC. Percent ADP/ATP ratio was ploted based on densitometric analysis of ATP to ADP conversion (**C**).

Here, we monitored the affinity of TNP-ATP for ParA2 and ParA3 with respect to dsDNA and compare it with ParA1. We observed that secondary ParAs display a significant increase of the emission intensity and a blue shift [from 552 to 511 nm (for ParA2) or 514 nm (for ParA1 &ParA3)] in λ_{max} (Fig. 3.1.5A-C). This indicated that TNP-ATP has moved from the aqueous medium to the less polar environment inside the protein. Further, the reduction in fluorescence intensity (RFU) upon addition of natural ATP in protein:TNP-ATP complex indicated a strong possibility of ATP displacing the TNP-ATP with ATP in protein (Fig. 3.1.5A-C). Interestingly, the addition of dsDNA ParAs-TNP-ATP reaction mixture has no significant effect on the fluorescence intensity (Fig. 3.1.5B-C). In comparison to ParA2 or

ParA3, ParA1 showed greater RFU with emission λ_{max} = 517 nm and addition of dsDNA has further increased the RFU at 517nm (Fig. 3.1.5A). These results together suggest that both ParA2 and ParA3 bind to TNP-ATP (or ATP) in similar way and presence of dsDNA has not affected secondary ParAs binding with TNP-ATP (or ATP). However, dsDNA has affected ParA1 interaction with ATP or TNP-ATP.

To find the binding affinity of the TNP-ATP to secondary genome ParAs, a fixed concentration of TNP-ATP in buffer B was titrated with increasing amounts of ParAs as described in the method. Fluorescence intensity versus protein concentration values was plotted and fit into a Langmuir single-site binding equation to determine the dissociation constant (Kd) for the ParA1, ParA2 or ParA3 bound to TNP-ATP. We found an increase in the relative fluorescence unit got saturated as seen in (Fig. 3.1.5 D-F). The similar patterns were observed earlier for ATP-binding proteins (Guarnieri *et al*., 2011; Bilwes, 2001; Plesniak, 2002 and Treuner-Lange, 2013). Our results fitted well the saturation kinetics obtained by equation 1 as given in methods. The Kd values for ParA2 and ParA3 were 2.01 ± 0.13 μM and 1.83 ± 0.2 μM, respectively (Fig. 3.1.5 E, F). In contrast, ParA1 has shown lower Kd value of 1.28 ± 0.26 μM. Although, a very information available on ATP binding affinity of P-loop ATPase using fluorescent ATP, the TNP-ATP binding affinilty of PomZ (a ParA like P-loop ATPase from *Myxococcus xanthus*) having Kd of 4.3 μM (Treuner-Lange,2013) was ~2- 4-fold higher than the Kd of deinococcal ParAs reported in this study. These results suggest that both ParA2 and ParA3 have a very similar affinity for TNP-ATP molecules but higher than ParA1 in *D. radiodurans.* Further, when a constant amount of ParAs was titrated with increasing concentrations of TNP-ATP in the micromolar range (0.5-10 μM), the relative increase in fluorescence intensity got saturated after certain points (Fig. 3.1.5 G-I). Similar trend was earlier reported for many ATP-binding proteins

(Thomas, 1992; Lerner-Marmarosh, 1999; Cho, 2001; Treuner-Lange, 2013 and LaConte *et al*., 2017).

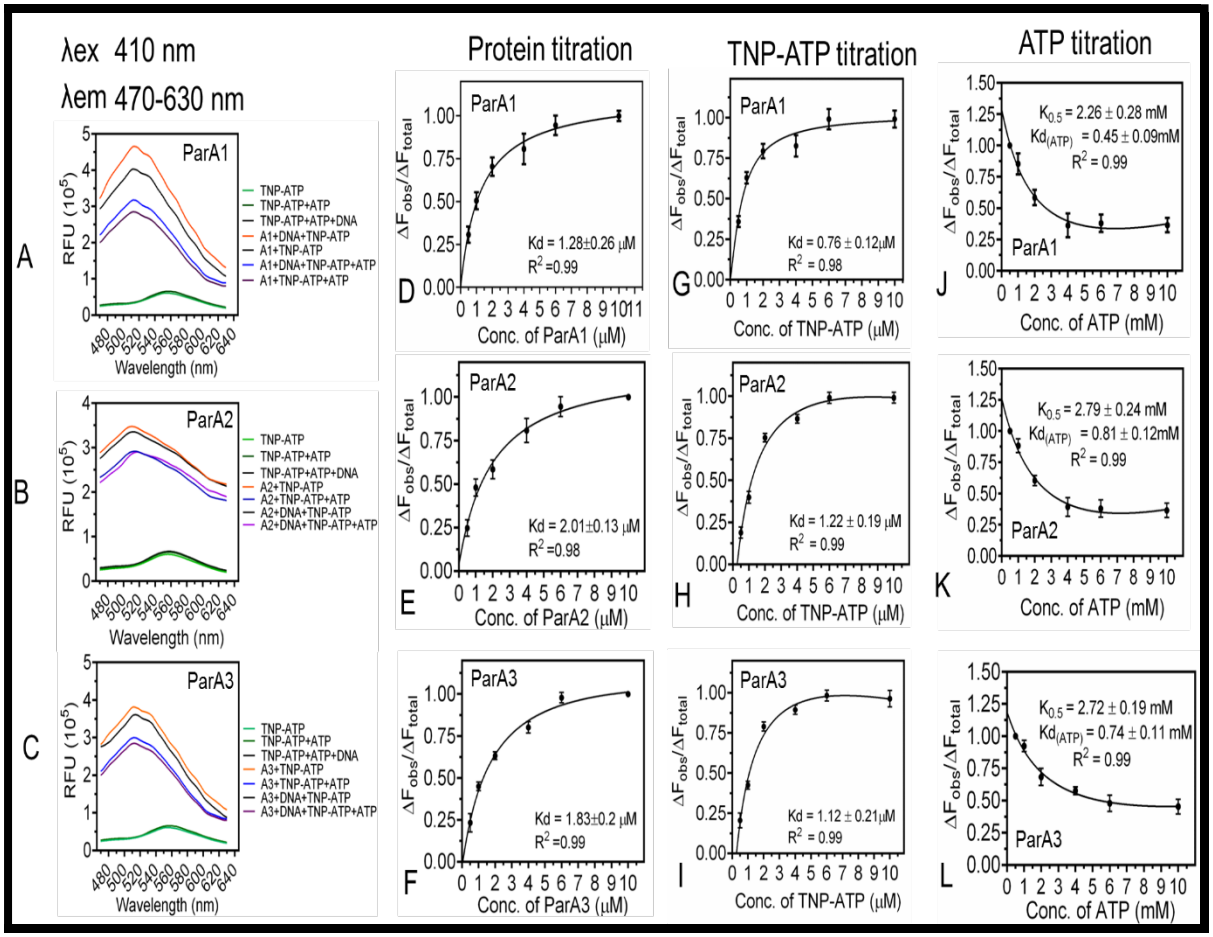

Figure 3.1.5 ATP binding study of deinococcal ParAs using fluorescent TNP-ATP. We monitored the TNP-ATP binding as well as chase by ATP in case of ParA1 (**A**), ParA2 (**B**) and ParA3 (**C**). We have titrated the different ParA proteins (**D-F**), TNP-ATP (**G-I**) as well as ATP (**J-L**) to determine the Kd values.

The apparent dissociation constants for TNP-ATP ($Kd_{(TNP-ATP)}$) was determined using saturation curve fitting equation 2 as given in methods. The calculated $Kd_{(TNP-ATP)}$ values for ParA2 and ParA3 were 1.22 ± 0.19 μM and 1.03 ± 0.21 μM, respectively, which was approximetlay 1.5 fold higher than that of ParA1 (Kd = 0.76± 0.12 μM).

The TNP-ATP binds proteins both specifically to ATP binding pocket as well as non-specifically via TNP moiety to non-polar residues in the vicinity of the ATP-binding site (Hiratsuka and Uchida, 1973). However, TNP-ATP binding to catalytic pocket is several

folds higher than ATP binding to the same site as well as non-specific interaction. The nonspecific component can be removed by addition of excess natural ATP, which progressively replaces TNP-ATP from the nonspecific binding sites in proteins due to competition (Stewart, 1998; Hormaeche*et al.,* 2002 and Guarnieri, 2011). In figure 3.1.5A-C, we have incubated proteins with TNP-ATP alone and then with an excess of natural ATP. The addition of non-fluorescent ATP has reduced the fluorescence intensity which suggests ATP as a competitor to TNP-ATP. Here, we have titrated ATP in millimolar range into an equilibrated TNP-ATP:ParAs complex. The concentration dependent displacement of TNP-ATP from TNP-ATP:ParAs complexes with increasing concentration of natural ATP has been used to determine the Kd of ATP binding to deinococcal ParAs (Fig. 3.1.5 J-L). The curves fitted on equation 3 (as given in methods) were used for calculation of $K_{(0.5)}$ (*i.e.* the amount of ATP necessary to displace half the amount of bound TNP-ATP) for both the proteins. From the results in (Fig. 3.1.5 J-L), a $Kd_{(ATP)}$ of 0.81 ± 0.12 mM for ParA2 and 0.74 ± 0.11 mM for ParA3 was obtained. A $Kd_{(ATP)}$ of 0.45 ± 0.09 mM for ParA1 suggest a ~1.7 fold higher affinity for ATP than secondary genome ParAs. The TNP-ATP binds ~650-fold tighter than natural ATP and such kind of affinity for TNP-ATP was observed for *E. coli* CheA protein (~500 folds) (Stewart, 1998) and HK1 of *Mycobacterium tuberculosis* (~600 folds) (Shrivastava *et al.,* 2007). The results show that both ParA2 and ParA3 have a very similar affinity for ATP but distinct from ParA1.

3.1.3.5 Hydrolysis of ATP into ADP leads conformational change in ParAs

Both ParA2 and ParA3 proteins of *D. radiodurans* contains 2 tryptophan residues in polypeptide chain. We have monitored the conformational change in the protein in absence and presence of dsDNA and different nucleotides, as the change in intrinsic fluorescence of tryptophan. Both secondary ParAs showed excitation maxima (λ_{Ext} 295) at 295 nm and emission maxima (λ_{Em} 327) at 327 nm in the aqueous solution. Therefore, the relative

fluorescence of Trp in these proteins was measured at 327 nm in the presence of different nucleotides (ATP, ADP, ATP-γ-S) and dsDNA (Fig. 3.1.6). We observed an increase in Trp fluorescence in the presence of ATP and ADP but not with non-hydrolysable ATP (ATP-γ-S). This indicated that ParAs hydrolyse ATP into ADP and binding of ADP with protein results in increase in intrinsic fluorescence of the protein perhaps due to a conformational change.

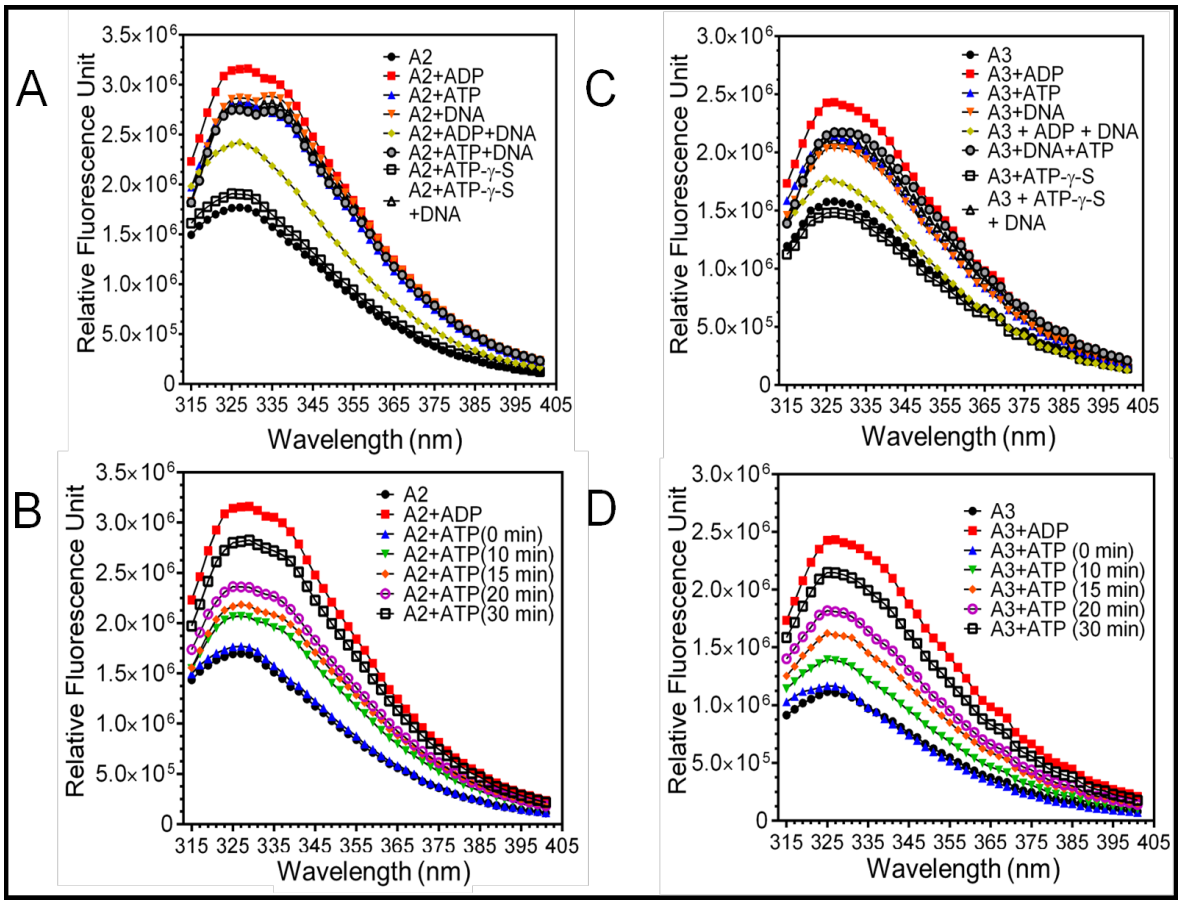

Figure 3.1.6 Effect of nucleotideson Tryptophan fluorescence of ParA2 and ParA3. Intrinsic fluorescence of ParA2 (A2) (**A**) and ParA3 (A3) (**C**) in the absence and presence of dsDNA, 1mM ADP, ATP or ATP-γ-S in different combinations was recorded for tryptophan by excitation at 295 nm and emission from 315 to 401 nm at an interval of 2 nm. Further, emission spectra of A2 (**B**) or A3 (**D**) in presence of 1mM ATP were recorded at 0, 10, 15, 20 and 30 min of incubation after the addition of 0.5mM $MgSO_4$, and compared with 1mM ADP for 30 min.

Such an increase in intrinsic fluorescence would have occurred due to movement of Trp residues in the hydrophobic micro-environment because of conformational changes in the

proteins (Lakowicz, 1983). Interestingly, we found a higher fluorescence intensity with ADP alone, which decreased significantly in the presence of DNA. Presence of ATP and/ or DNA has also shown increase in intrinsic fluorescence which suggests that interaction of ParAs with DNA and ATP creates conformational change perhaps required for protein polymerization on DNA.

We further performed time course kinetics of intrinsic fluorescence change due to ATP hydrolysis in order to understand whether hydrolysis of ATP to ADP by ParAs can affect protein conformation. We incubated the ParAs with ATP and monitored the fluorescence spectrum at different time points. We observed that the fluorescence of ParA increases with incubation time and that reaches close to ADP control (Fig. 3.1.6 B, D). On the other side, we did not find any change in intrinsic fluorescence of ParAs in presence of ATP-γ-S (Fig. 3.1.6 A, C). This clearly suggests that binding of ATP alone with ParA is possibly not causing a structural change in the protein rather it is the conversion of ATP to ADP which leads to conformational changes.

3.1.3.6 Secondary genome ParAs form higher order complexes on DNA, and ATP increases the size of nucleoprotein complex

The possibility of ParA2 and ParA3 proteins forming higher order complexes on DNA as a function of ATP was further analyzed by sedimentation assay and dynamic light scattering (DLS). For sedimentation assay, purified ParA2 and ParA3 were incubated separately with ATP, ADP as well as ATP-γ-S in presence and absence of dsDNA. The reaction mixture was spun at high speed and amount of protein present in the pellet and supernatant was analysed on SDS-PAGE and quantified using densitometry. We observed that the amount of both ParAs in the pellet had increased in the presence of dsDNA as compared to protein control. The presence of ATP with DNA had further increased the protein in pellet in comparison to ATP and DNA controls (Fig 3.1.7 A, B). Interestingly, ADP did not increase the pellet of

these proteins when compared with adequate controls. When we performed similar experiment in the presence of non-hydrolysable ATP (ATP γ-S) and DNA, we found nearly similar results to that of ATP (Fig.3.1.6 C, D). This suggests that ATP hydrolysis *per se* is not necessary for the formation of large nucleoprotein complex by these ParAs. In addition, we performed DLS to measure the size of nucleoprotein complex.

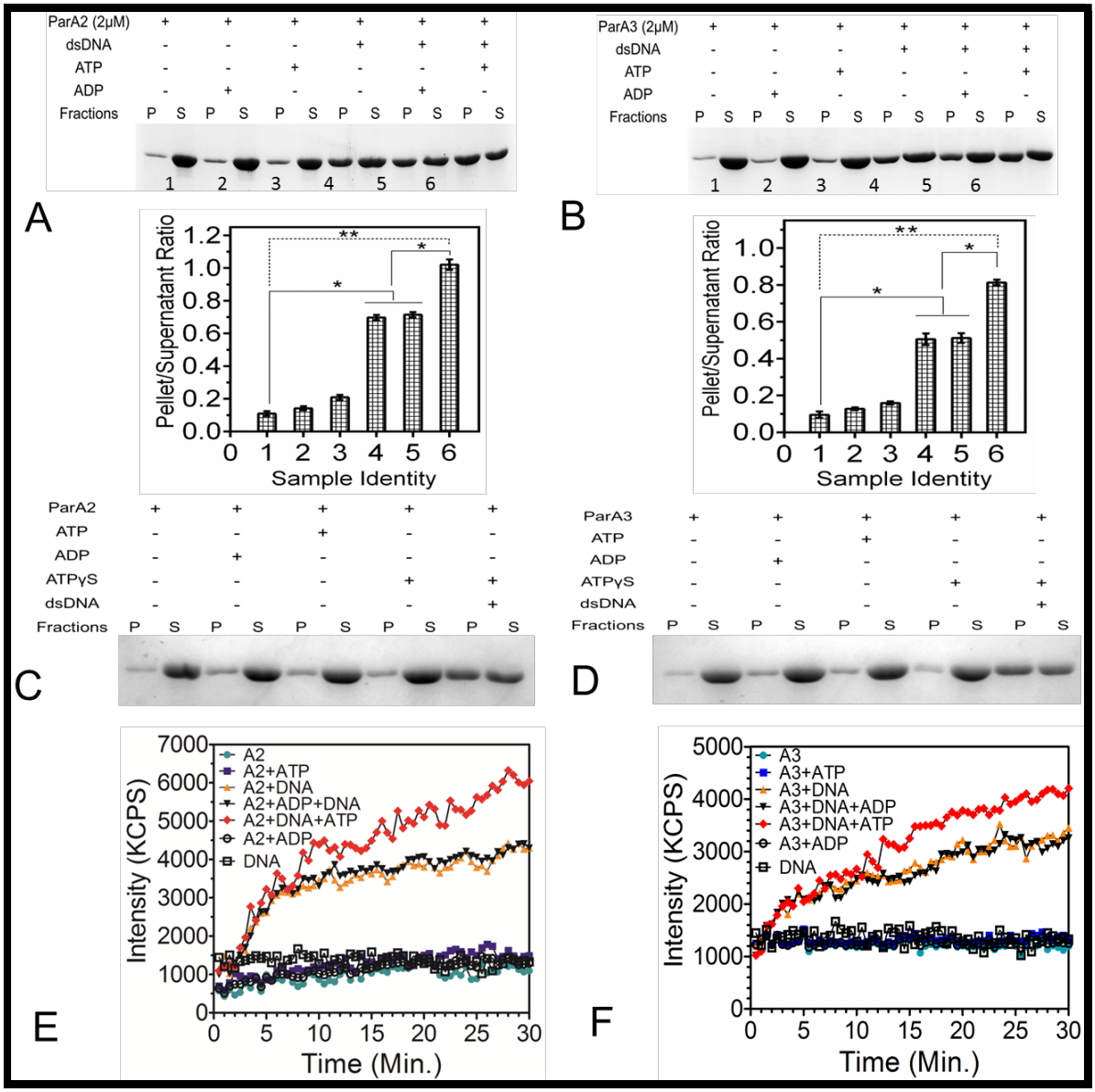

Figure 3.1.7 Effect of different nucleotides on ParAs-DNA interaction. Sedimentation assay was performed for ParA2 (**A, C**) and ParA3 (**B, D**) in absence and presence of ADP/ATP or ATP γ-S (see section 3.1.2.6). Dynamic light scattering of ParA2 (**E**) and ParA3 (**F**) with respect to dsDNA alone or in presence of ADP/ATP was executed (see section 3.1.2.7)

We find similar results as observed in sedimentation assay (Fig. 3.1.7). In detail, the intensity of scattered light with both ParA2 and ParA3 was constant at 900 – 1000 Kilocounts / seconds (KCPS), irrespective of the presence of ATP or ADP. However, in the presence of dsDNA, a rapid increase was noticed and the KCPS increased to more than 3000 in initial 5 min. Presence of ADP has no effect on the size of nucleoprotein particles formed by ParAs and intensity was ~3000 KPCS like DNA control.

Interestingly, the presence of ATP has increased light scattering significantly with KCPS of ~6000 in 30 min as compared to DNA and protein controls (Fig. 3.1.7 E, F). Since, the increase in the intensity of light scattering in the presence of ATP was observed at a ratio of protein to DNA that had reached to saturation in the absence of ATP, this effect of ATP seems to be due to an increase in interaction between ParA and DNA. These observations together suggested that secondary genome ParAs could bind with dsDNA and form nucleoprotein complex, whose size is further increased in presence of ATP *in vitro*. Further, both ParA2 and ParA3 show nearly similar activity with dsDNA in function to ATP at least *in vitro*.

3.1.3.7 ATP but not ADP stimulated polymerization of ParA2 and ParA3 on DNA

We imaged the DNA protein interaction in the presence of ATP and ADP by transmission electron microscopy (TEM). We found that secondary ParAs exist in oligomeric state which did not change in the presence of either ADP or ATP. In the presence of dsDNA, they show beading or nucleation over dsDNA in absence of any nucleotides. However, presence of ATP but not ADP has increased the density of nucleation over dsDNA (Fig. 3.1.8). These findings concurred the observation from sedimentation assay and DLS. Interestingly, ParA interaction with nicked circular dsDNA seems to have affected the helical nature of dsDNA making it a perfect circular geometry rather than irregular folded structure normally dsDNA has been imaged earlier. In conclusion, both secondary ParAs showed nearly similar results in TEM.

3.1.3.8 Both ParA2 and ParA3 showed homotypic as well as heterotypic interactions

The interaction between different ParA proteins was studied using Bacterial-Two-Hybrid System (BACTH) (Karimova *et al*., 1998) and co-immunoprecipitation (co-IP) in *E. coli* as well as in *D. radiodurans* as described in methods. Expression of these chimeras was confirmed by western blotting in *E. coli* (Fig 3.1.9).

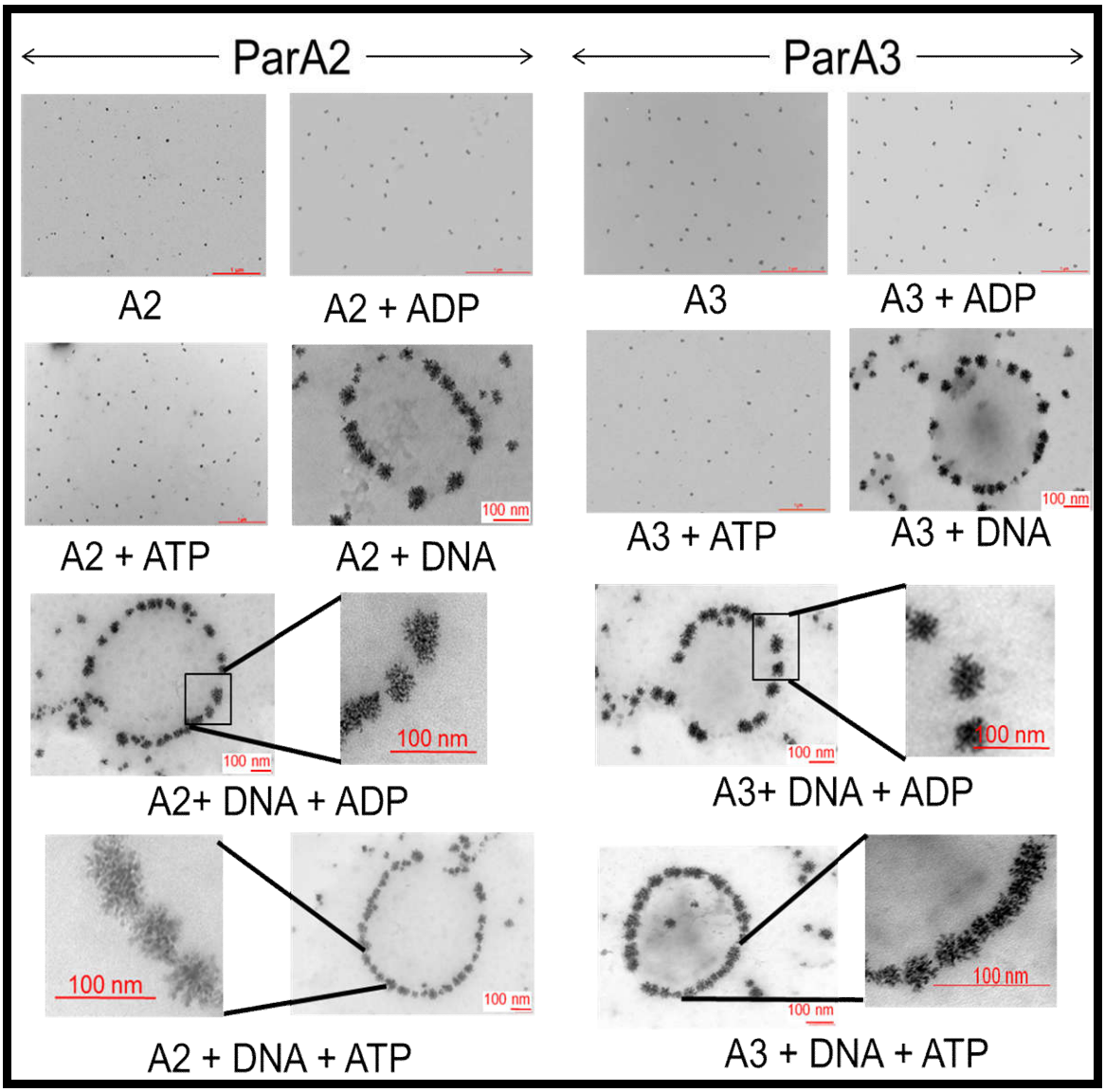

Figure 3.1.8 Electron microscopic studies of ParA protein interactions with nicked circular dsDNA. The interaction of recombinant purified ParA2 (A2) and ParA3 (A3) with nicked circular ϕX174 RF II dsDNA in the presence and absence of ADP or ATP was monitored using TEM as described in methodology (section 3.1.2.10). The scale bar for A2/A3 with or without ADP/ATP is 1 µm while with dsDNA and nucleotides are 100 nm.

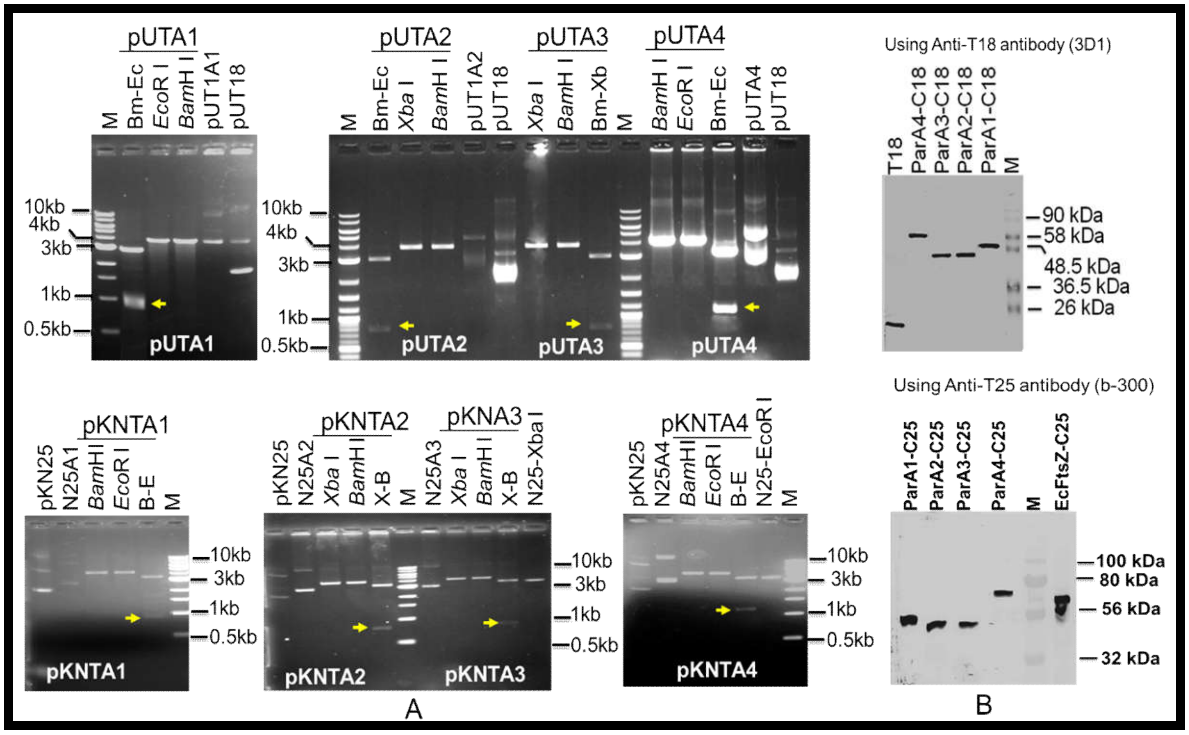

Figure 3.1.9 Cloning and expression of all ParAs in BTH plasmid (pUT18 and pKNT25).

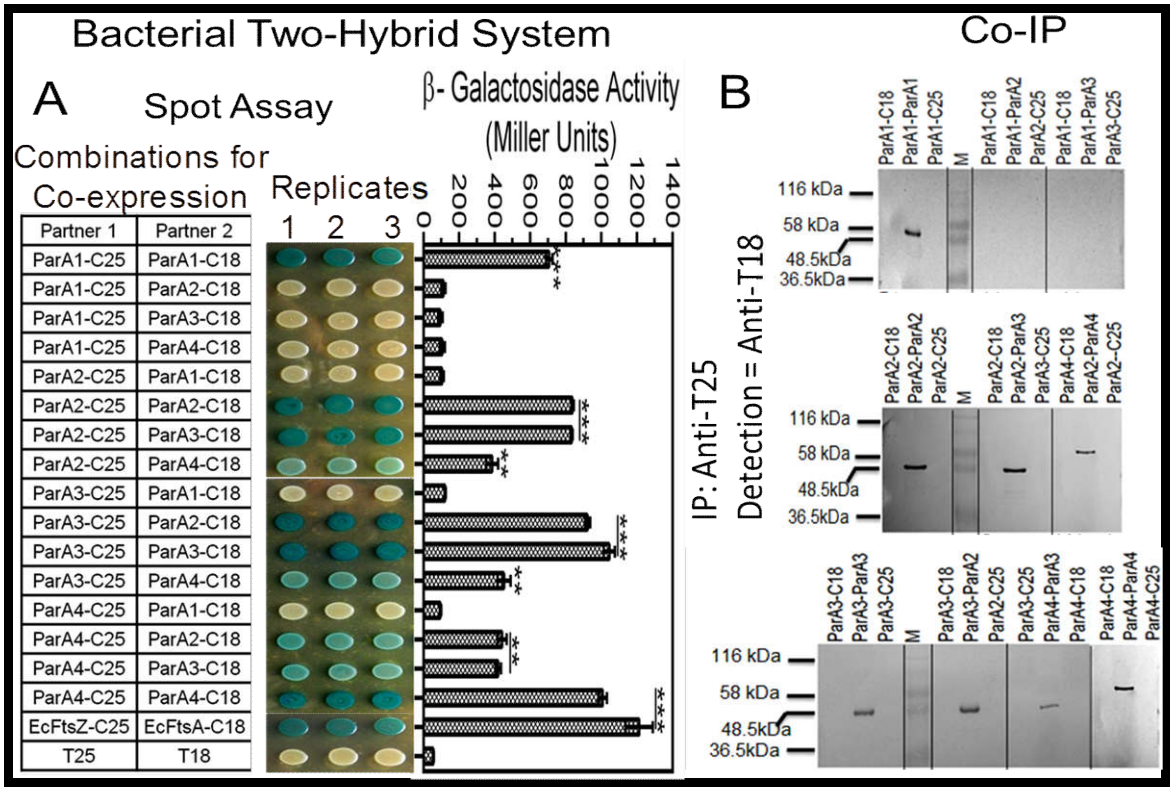

Figure 3.1.10 Protein-protein interaction studies among deinococcal ParAs in *E. coli*. Using Bacterial Two-Hybrid sytem (**A**) and coimmunopreciptation (**B**) (See methods, section 3.1.2.11A, B).

The *E. coli* BTH101 cells (CyaA$^-$) co-expressing ParA1, ParA2, ParA3 and ParA4 on BACTH plasmids in different combinations were screened for CyaA regulated β-galactosidase expression. We performed spot assay as well as β-galactosidase assay to observe interactions if any.

We observed that different ParA proteins showed homotypic interactions (i.e. interact to self) as indicated from the blue color colonies in spot assay and β-galactosidase activity in liquid culture (Fig 3.1.10 A).

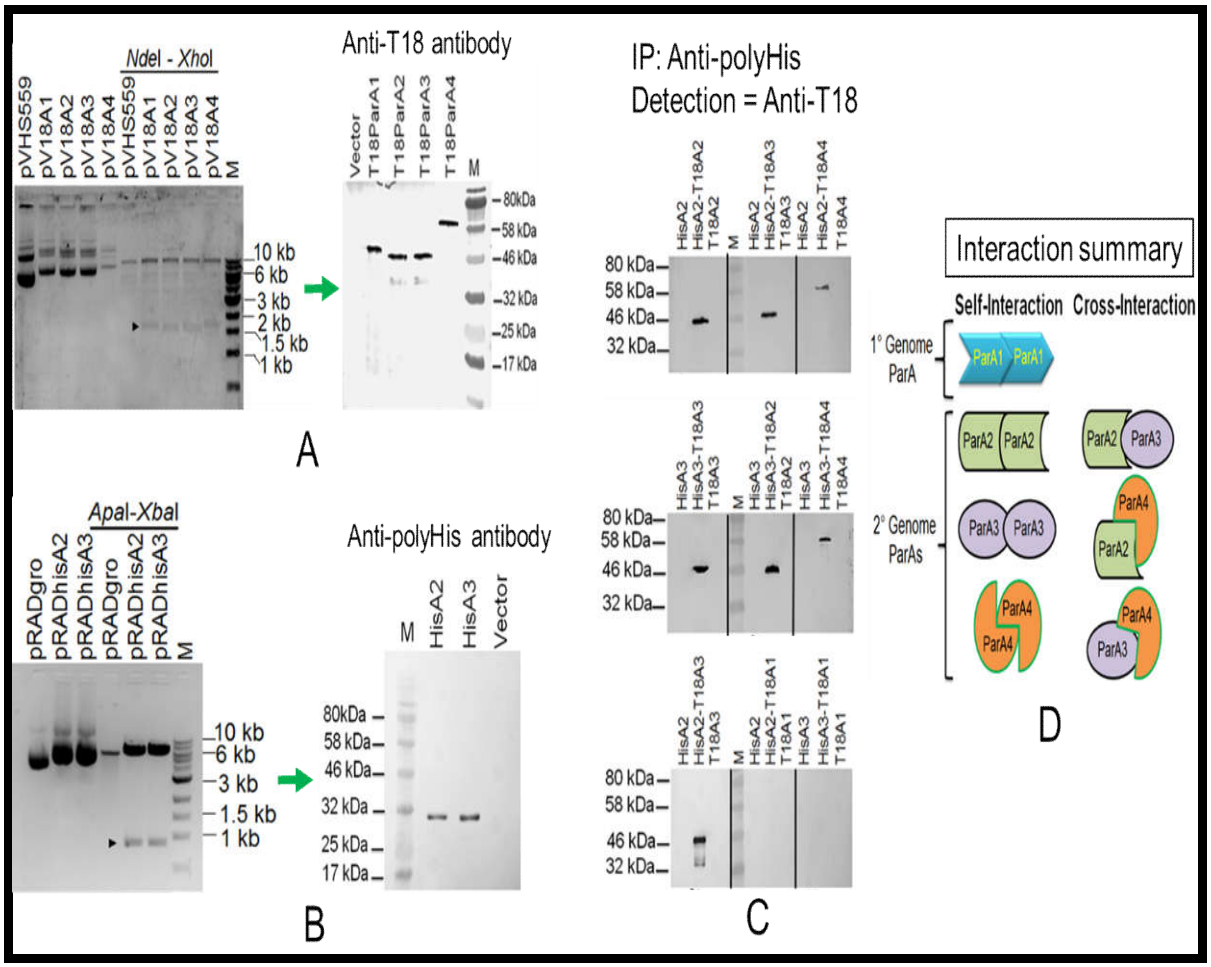

Figure 3.1.11 Protein-protein interaction study among deinococcal ParAs using co-IP from *D. radiodurans*. Cloning and expression of T18 tagged ParA1-4 (**A**) from pVHS559, polyHis tagged ParA2 & ParA3 (**B**) from pRADgro was ascertained in *D. radiodurans* (see section 3.1.2.11). Coimmunopecipatation was performed as described in section 3.1.2.11B (**C**). A cartoon depicting interaction summary among deinococcal ParAs has been given based on observation from both *E. coli* and *D. radiodurans* (**D**).

In addition, secondary genome ParAs (ParA2, ParA3 and ParA4) interacted to each other while none of them showed interaction with ParA1 from Chr I. These observations were further confirmed by co-IP from *E. coli* BTH 101 cells co-expressing these deinococcal ParAs tagged with T18 or T25 domains of CyaA in different combinations. In brief, we immunoprecipitated the cell lysate using anti-T25 antibodies and the presence of interacting partner(s) tagged with T18 was detected by using anti-T18 antibodies. We found similar result as in BTH i.e. secondary genome ParAs showed both homotypic and heterotypic interaction but did not interact to ParA1 (Fig. 3.1.10 B).

We have generated T18 fusion as well as polyhistidine fusion of deinococcal ParA and confirmed their expression in *D. radiodurans* (Fig. 3.1.11A, B). Protein-protein interaction among deinococcal ParAs was also monitored from *D. radiodurans* using co-immunoprecipitation as described in section 3.1.2.11B. We observed nearly similar results as that of BTH and co-IP analysis in surrogate *E. coli* host. These lines of evidences suggest that all the ParAs interacted homotypically while secondary genome ParAs can cross talk to each other but not with ParA1 (Fig. 3.1.11C, D). Thus, there is a possibility of structural and functional similarities among secondary genome's ParAs particularly ParA2 and ParA3 and their role in functional complementation is projected.

3.1.3.9 Deletion of *parA2* and *parA3* has reduced the copy number of secondary genome elements

Since ParAs are know to be actively involved in genome segregation, and deinococcal secondary genome ParA2 and ParA3 shows nearly similar biochemical functions *in vitro,* So the possibility of these ParAs affecting genome maintenance in *D. radiodurans* was tested. We have generated both single (Δ*parA2* and Δ*parA3*) and double (Δ*parA2*Δ*parA3*) mutants of *parA2* and *parA3* in *D. radiodurans* (Fig. 3.1.12 A-D) and determined the copy number of each genomic replicons using qRT-PCR (Breuert *et al*., 2006). In comparison to WT, the

copy numbers of primary Chr I did not change in any of the mutants while the copy number of secondary replicons (Chr II and Mp) has reduced in double mutant but not in their single mutants (Fig. 3.1.12 F). These observations have suggested that deletion of secondary genome ParA2/ParA3 has affected their segregation in dividing cells as well as replication of secondary genome elements by a yet unknown mechanism(s).

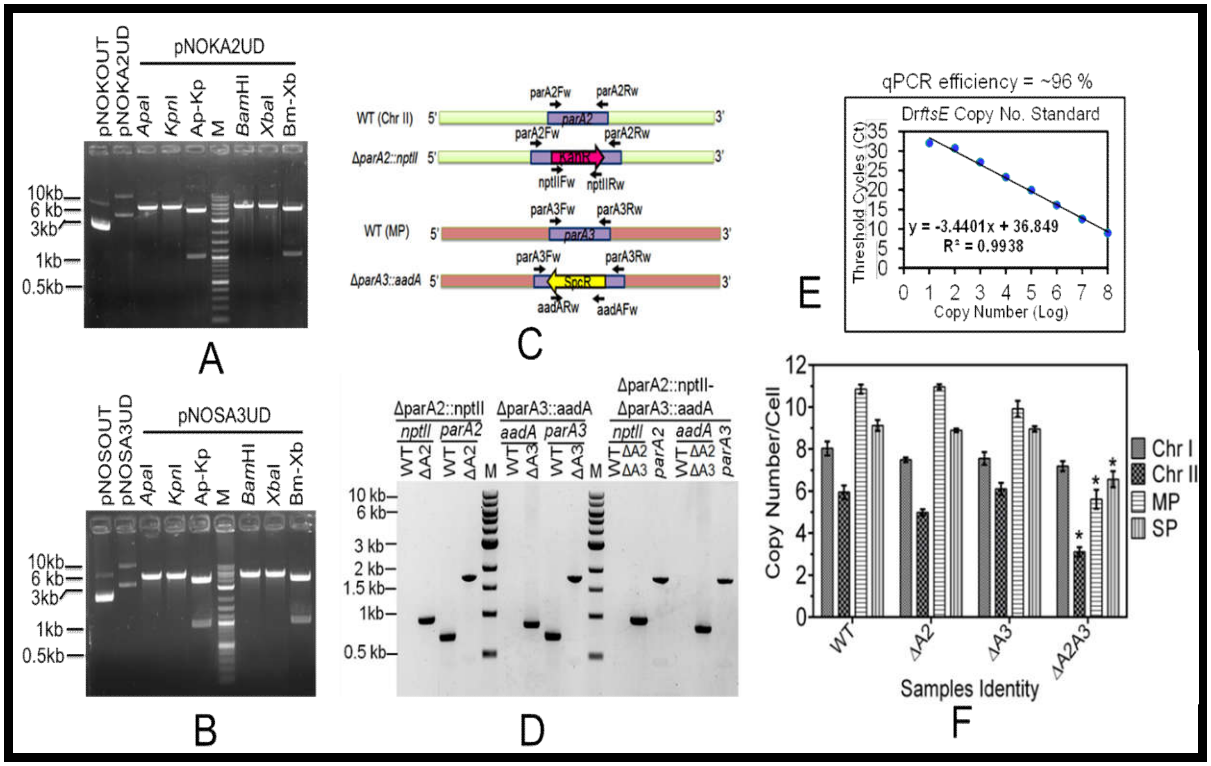

Figure 3.1.12 Genration of *parA2&parA3* mutants and copy number determination. Single and double mutants of both *parA*s were generated using pNOKA2UD (**A**) and pNOSA3UD (**B**) as described in section 3.1.2.12, and verified by diagnostic PCR (**C, D**). The copy number each replicon per cell was determined using qPCR (section 3.1.2.13) (**E, F**).

3.1.3.10 Double mutant of both *parA2* and *parA3* showed sensitivity to γ-radiation and H_2O_2 in *D. radiodurans*

The effect of *parA2* and *parA3* deletion on growth response of *D. radiodurans* was monitored under normal and DNA damaging conditions. The double mutant showed a relatively slow growth under normal conditions as well as higher sensitivity to γ- radiation andH_2O_2 as compared to single mutant and wild type (Fig. 3.1.13). Thus, the double mutant

that had reduced copy number of Chr II and Mp was also found to be more sensitive to γ-radiation and H_2O_2 as compared to the single mutants and the wild-type strain.

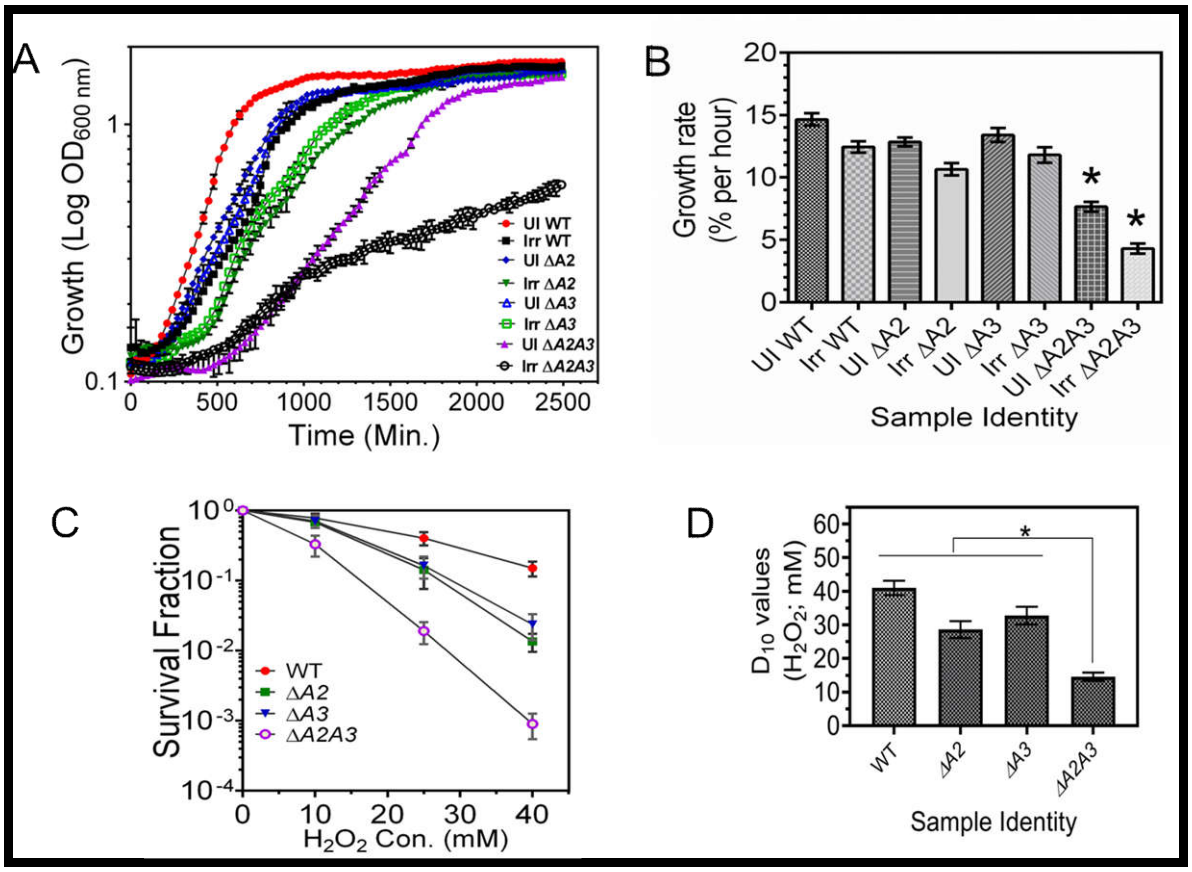

Figure 3.1.13 Effect of *parA2* and *parA3* deletion on growth or survival of *D. radiodurans* in response to 6kGy gamma radiation (A, B) and H_2O_2(C, D) (see section 3.1.2.14).

This clearly indicated the role of secondary genome elements in normal growth and DNA damage tolerance in *D. radiodurans*. Nearly no effect of single deletion on growth, in the resistance to gamma radiation and hydrogen peroxide, and copy number of secondary genome elements further suggested a strong possibility of ParA2 and ParA3 would be complementing each other's roles in these functions *in vivo*.

3.1.3.11 Double mutant of *parA2* and *parA3* showed a different morphology

Cell morphology and nucleoid of wild type, *ΔparA2, ΔparA3* single mutants as well as *ΔparA2ΔparA3* double mutant was monitored under fluorescence microscope (section

3.1.2.15). In comparision to wild type and single mutants, double mutant showed a relatively higher frequency of cells having cell area more than 6µm^2 (Fig. 3.1.14 A, C). Line scan analysis of a large number of cells revealed that double mutant is having higher % of cell whose nucleoid trapped between the septum and showing defect in the separation of tetrads colony that usually happen in wild type cells during normal cell division (Fig. 3.1.14 A, B). Nearly similar phenotype of nucleoid trapped between septum has been reported in Noc null mutant of *Staphylococcus aureus* (Pang *et al*., 2017). Quantitatively, ~ 25% cells were showing septum trapped nucleoid in double mutant as compared to less than 4 % in single mutant and wild type.

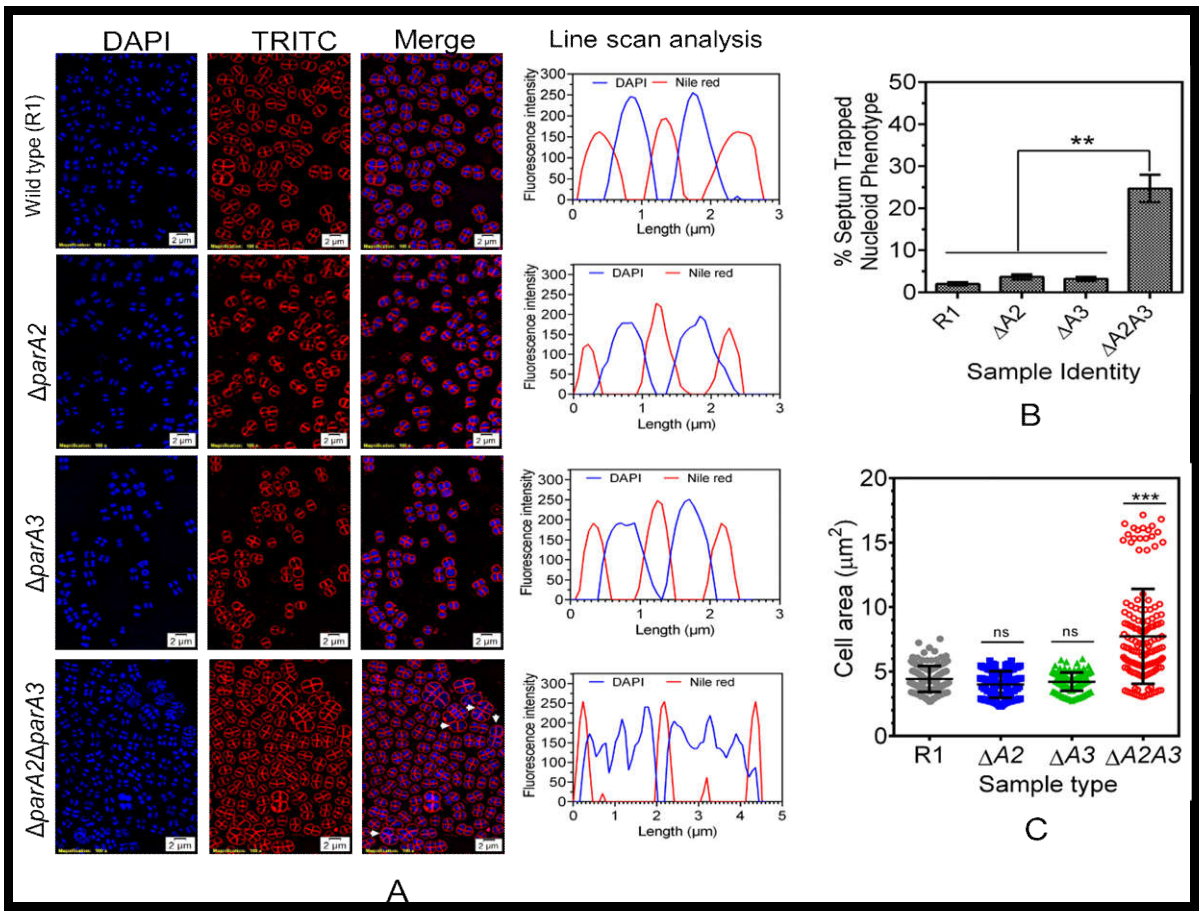

Figure 3.1.14 Microscopic observation of cell morphology and nucleoid in *parA* mutants. Images of DAPI and Nile red stained wild type (R1), different *parA* mutants of *D. radiodurans* were taken and line scan analysis of large number of cells was performed to find % septum trapped phenotype (see section 3.1.2.15) (**A,B**). Cell area (µm^2) was determined for a large number of cells and ploted (**C**).

These finding together suggested that both ParA2 and ParA3 protein regulate DNA translocation during cell division and they could complement the function of each other *in vivo*.

3.1.3.12 Genome segregation proteins interact to divisome components through cell division regulatory proteins in *D. radiodurans*

We observed that deletion of both *parA2* and *parA3* has affected the cell morphology and affected the cell division in *D. radiodurans*.

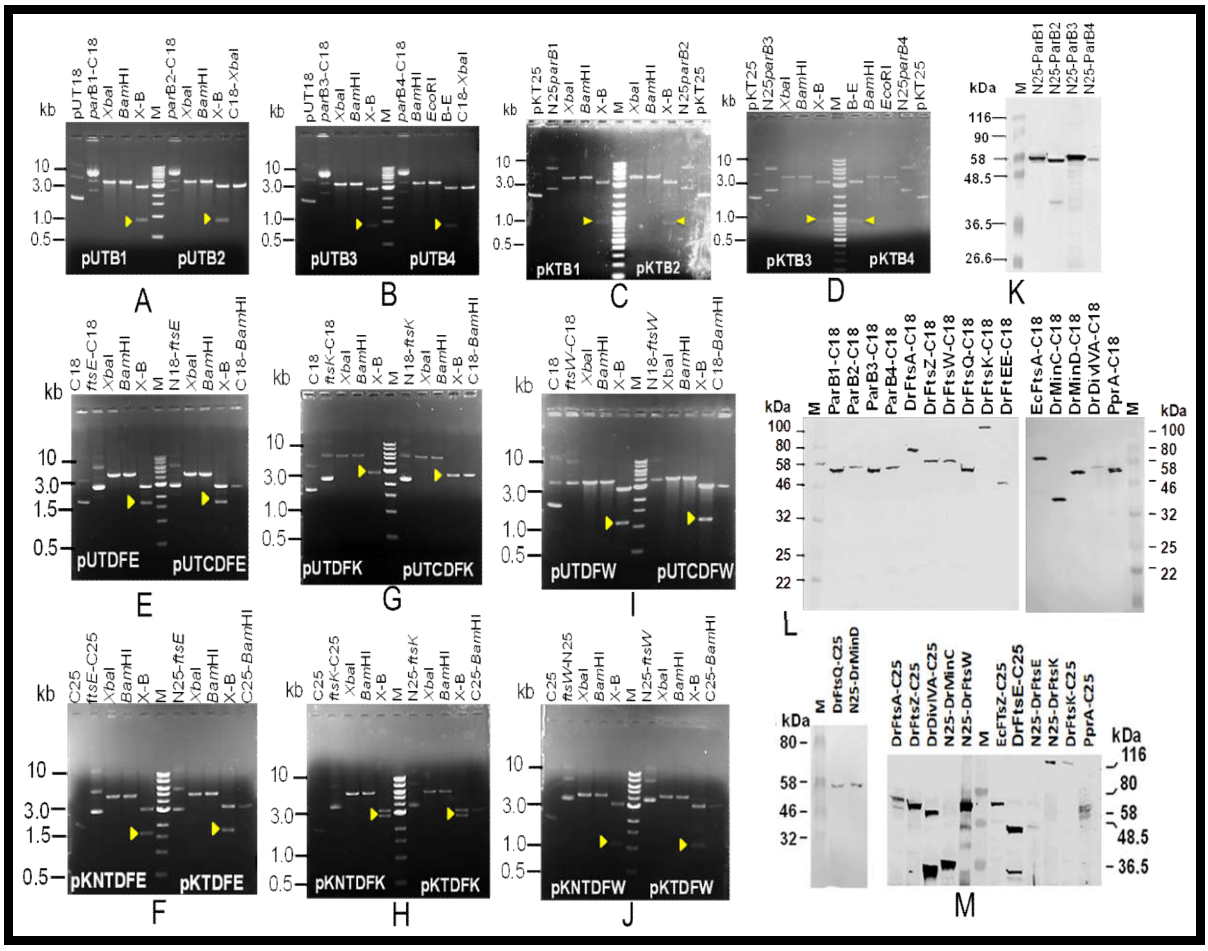

Figure 3.1.15 Cloning and expression of deinococcal ParBs and cell division components from BACTH plasmid in *E. coli* BTH101 cells. Deinococcal *parB1-4* were cloned in pUT18/pKT25 (**A-D**), and *ftsE* (**E, F**), *ftsK* (**G, H**) and *ftsW* (**I, J**) were cloned in pUT18 & pUT18C and pKNT25 & pKT25 plasmids (see Table 2.4; section 3.1.2.11). Cloning of *ftsQ*, *minC*, *minD* and *divIVA* was done in BACTH plasmids, but images are not shown here (see Table 2.4). The expression of fusion protein was monitored using either Anti-T18 or Anti-T25 antibodies in *E. coli* (**K-M**).

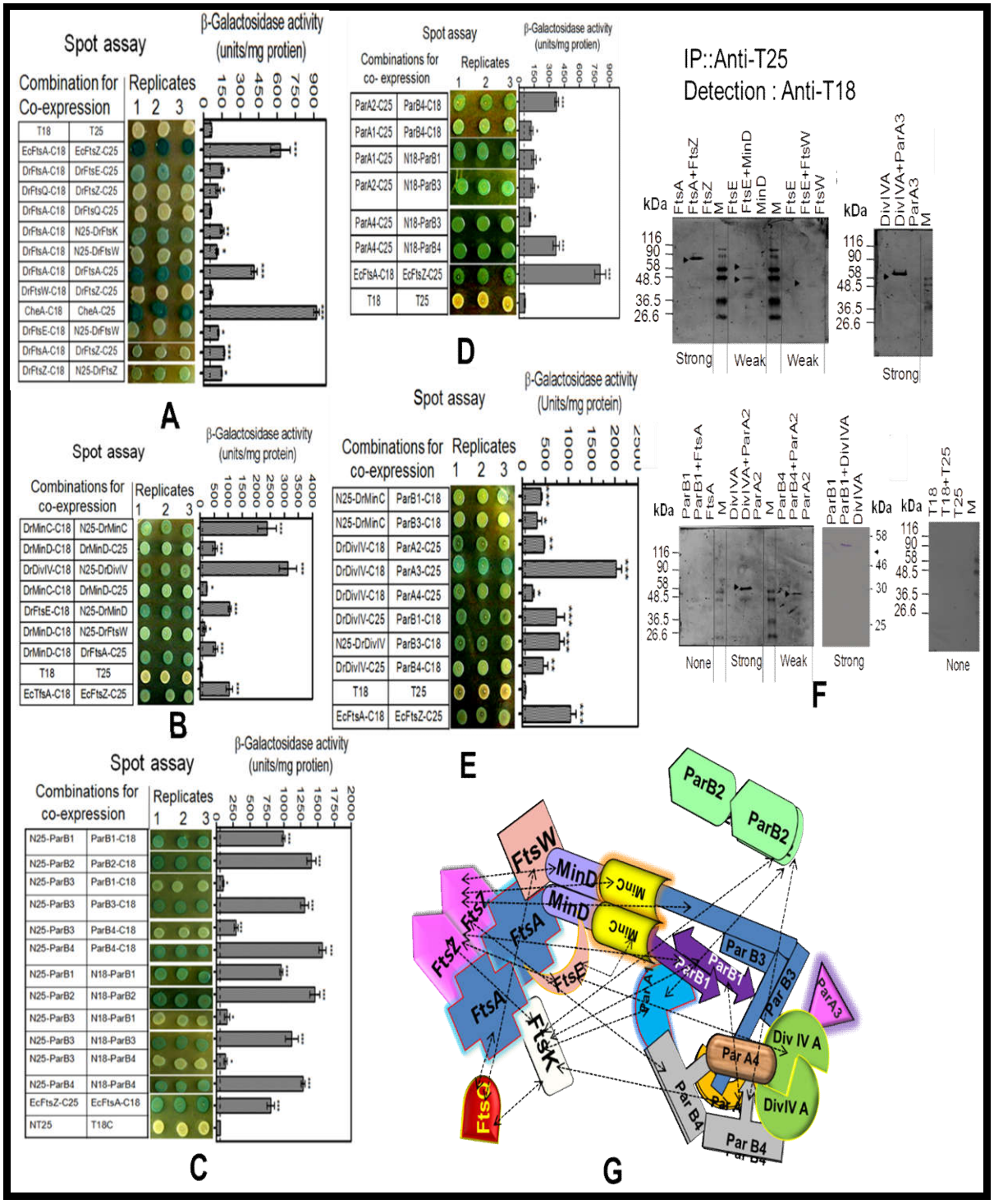

Figure 3.1.16 Protein-protein interactions between segrosome and divisome components of *D. radiodurans.* T18 or T25 fused segrosome and divisome components were used in different combinations to monitored interaction between them with the help of bacterial two-hybrid system (spot assay and β-gal assay) (**A, B;** interaction among divisome components, **C, D**; interaction among segrosome components, **E;** between segrosome and divisome). Few of the total interaction were further ascertained by co-immunoprecipitation (**F**). A conclusive cartoon model depicting summary of interaction has been proposed (**G**). Arrows in cartoon shows interaction based on bioinformatics using STRING tool.

Earlier, role of ParA2 in cell division regulation of *E. coli* host was demonstrated (Charaka *et al*., 2013). We investigated the crosstalk of genome segregation proteins with different cell division proteins of *D. radiodurans* using bacterial two-hybrid system and co-IP from *E. coli.* For that, we made BTH constructs of divisome components (core divisome components like; *ftsE, ftsK, ftsW* & *ftsQ* and regulatory components like*; minC, minD* and *divIVA*) and segrosome components (all 4 *parA*s and *parB*s) (see Table 2.4; section 3.1.2.11; Fig. 3.1.15).

The expression of fusion proteins in *E. coli* BTH101 was ascertained by immunobloting using Anti-T18 or Anti-T25 antibodies (Fig. 3.1.15 K-M). We monitored interactions among different divisome proteins and segrosome proteins separately as well as together using bacterial two hybrid system (spot assay and β-galactosidase assay) and co-IP in *E. coli* host.

The observations have been pointed as (i) deinococcal FtsA, FtsZ, MinD, MinC, DivIVA and all four ParB proteins (ParB1, ParB2, ParB3 & ParB4) showed self interaction (Fig. 3.1.16 A-C). (ii) DrFtsA interacted with DrFtsZ, DrFtsE, DrFtsK, DrFtsW and DrMinD (Fig. 3.1.16 A, B). (iii) DrMinD also interacted with DrFtsW, DrFtsE and DrMinC (Fig. 3.1.16 B). (iv) Deinococcal ParBs showed interaction with their cognate as well as non-cogante ParA proteins, although in absence of their cognate centromeric sequnces in *E. coli* (Fig. 3.1.16 D). (v) Interestingly, septum site determining protein, DrDivIVA showed interactions with secondary genome ParAs (ParA2, ParA3 and ParA4) as well as ParB1, ParB3 and ParB4 while DrMinC interacted with ParB1 and ParB3 (Fig. 3.1.16 E-G). Few of these interaction combinations were subjected to co-IP from *E. coli* to support the result. We observed similar results their also (Fig. 3.1.16 F). These results together suggest the formation of independent multiprotein complexes of 'DrFts' proteins, segrosome proteins and cell division regulatory proteins, and these complexes could interact with each other through DrMinC and DrDivIVA in *D. radiodurans* (Fig. 3.1.16).

Genome duplication followed by its accurate segregation is pre-requisite for productive cell division in all organisms. Interdependent regulation of these processes has not been discussed in greater details. Unlike bacateria harbouring single circular chromosome and low copy plasmid, genome segregation emplyoing TGS system has not been studied much in MGH bacteria. For instance, in *V. cholerae* and *B. cenocepacia*, the TGS of primary and secondary chromosomes have been shown functioning independently (Egan *et al*., 2005; Fogel and Waldor, 2006; Dubarry *et al*., 2006). In *D. radiodurans*, the TGS of primary chromosome has been characterized earlier (Charaka and Misra, 2012). Here, we have brought forth functional characterization of P-loop Walker ATPases encoded on secondary genome elements. We demonstrated that both ParA2 and ParA3 have shown higher sequence similarity at amino acid level, having similar biochemical and biophysical characteristics *in vitro* and could compensate the loss of each other *in vivo*. In brief, we observed that both ParA2 and ParA3 could bind to dsDNA nonspecifically and form large nucleoprotein complex. Both the ParAs could hydrolyze ATP in similar fashion irrespective to presence of dsDNA. Presence of ATP but not ADP has significantly increased the DNA binding activity of these ParA. ParAs of secondary genome showed both homotypic and heterotypic interaction amongst themselves but not with Par proteins of primary chromosome. We observed that the double mutant of *parA2* and *parA3*, in *D. radiodurans* produces phenotypes like reduced copy number of secondary genome elements, growth retardation albeit low under normal conditions, and higher sensitivity to γ-radiation and H_2O_2. Interestingly, we observed that the secondary genome ParA deletion does not affect Chr I copy number indicating that both primary chromosome and secondary genome elements perhaps segregate independently. Interestingly, the phenotypic loss due to secondary genome ParA deletion was not compensated by the presence of primary chromosomal ParA, indicating a strong

possibility of independent segregation of primary chromosome and secondary genome elements.

Earlier, the roles of ParA and ParB in multiple processes like chromosome replication, segregation and cell division have been reported in different bacteria (Murray and Errington, 2008; Lee *et al*., 2003; Mohl *et al*., 2001; Ginda *et al*., 2013). The roles of ParA and ParB in the normal growth of different bacteria have been found to be different. For instance, ParA and ParB encoded on the chromosome in *C. crescentus* has been shown to involve in cell cycle progression and cell division, and their null mutants are lethal (Mohl and Gober, 1997). On the other hand, although the loss of *parAB* in *P. putida*, *P. aeruginosa*, *S. coelicolor* and *B. subtilis* has caused segregation defect, the *parAB* mutants do not show lethality in these bacteria (Lewis *et al*., 2002; Bartosik *et al*., 2004; Kim *et al*., 2000; Ireton *et al*., 1994). In *V. cholerae, parAB* of Chr I is indispensable for normal growth (Saint-Dic *et al*., 2006). Here, we found that double mutant lacking both ParA2 and ParA3 showed reduction in ploidy of secondary replicons, slower growth and higher sensitivity to DNA damaging agents (gamma radiation and H_2O_2) than single mutant and wild type. Interestingly, we found that *ΔparA2ΔparA3* double mutant showed increase in frequency of cells having large cell area and a septum trapped nucleoid phenotype with defective cell division in *D. radiodurans*. However, the loss of ParAs which presumably have arrested DNA segregation, affecting replication i.e. copy number and septum formation i.e. cell division is intriguing, and offers a possibility of an interdependent regulation of segregation, replication and cell division in this bacterium. Our BACTH system-based protein-protein interaction between different divisome and segrosome components suggested that genome segregation proteins (ParA and ParB) interacts to core cell division proteins via cell division regulatory proteins (DivIVA, MinC) in *D. radiodurans.* The real-time demonstration on how genome segregation arrest can affect DNA replication or cell division etc. would be worth pursuing independently.

Chapter 3.2

Roles of centromere binding protein (ParBs) in genome maintenance and radioresistance in *D. radiodurans*

3.2.1 Introduction:

The mechanisms underlying genome segregation is relatively better understood in eukaryotes where all three macromolecular events; chromosome duplication, segregation and cell division, are temporally separated (Yanagida, 2005). In bacteria, which have doubling time in minutes, these processes are not well separated but occur in same order like DNA duplication, segregation and cytokinesis and are believed to be interdependently regulated. Recently, the genome sequencing studies have listed many bacteria that have multipartite genome system (MGS) comprised of more than one chromosome and large plasmids (Egan *et al*., 2005; Misra *et al*., 2018). Multipartite genome harboring bacteria also contain TGS which comprised of *cis* elements termed bacterial centromere, Walker type P-Loop ATPases (ParA or ParA like proteins) and centromere binding proteins (ParB or ParB like proteins). Among the multipartite genome system harboring bacteria, the limited studies on genome maintenance have been reported in *V. cholerae* (Egan *et al*., 2005; Fogel and Waldor, 2006), cystic fibrosis pathogen *B. cenocepacia* (Dubarry *et al*., 2006; Du *et al.*, 2016) and *D. radiodurans* (Charaka and Misra, 2012).

D. radiodurans, a radiation resistant bacterium, contains multipartite genome where chromosome I, chromosome II and megaplasmid encode putative ParA and ParB proteins (White *et al*., 1999). Recently, chromosome I partitioning system has been characterized in *D. radiodurans* (Charaka and Misra, 2012). Molecular mechanisms underlying the evolution and maintenance of multipartite genome system, its inheritance into daughter cells, and their functional significance in extreme phenotypes of *D. radiodurans* are not known and would be worth studying.

Here, we report characterization of ParB proteins *in vitro* and their roles in extraordinary phenotypes in *D. radiodurans in vivo*. We demonstrated that all the ParBs form homodimer

in vitro and do not interact with other ParB homologues of this bacterium *in vivo*. The *ΔparB2, ΔparB3* mutants maintained with antibiotic pressure showed nearly wild type growth under normal and γ-radiation stressed conditions. However, when maintained without selection pressure, a significant population was found to be sensitive to antibiotics and these cells compromised to γ radiation resistance. This indicated that certain population in respective mutant has failed to receive copy of genome element marked with antibiotic resistance. Like earlier report, *ΔparB1* cells showed growth retardation under normal conditions and were sensitive to γ-radiation as compared wild type cells. All the mutants grown under selection pressure showed a significant increase in copy number of respective genome elements. The interaction of ParBs with replication initiation proteins DnaA and DnaB implied a functional interaction of genome duplication and segregation in this bacterium. These results together suggested that ParBs form homodimer and have roles in interdependent regulation of DNA replication and genome segregation as well as in the radioresistance in *D. radiodurans*.

3.2.2 Materials and methods

3.2.2.1 Bacterial strains, plasmids and materials

All the bacterial strains and plasmids used in this study have been listed in Tables 1 and 2, respectively while primers in Table 3 (see annexure I). *D. radiodurans* R1 (ATCC13939) was grown in TGY (Tryptone (1%), Glucose (0.1%) and Yeast extract (0.5%)) medium at 32˚C. *E. coli* strain NovaBlue was used for cloning and maintenance of all the plasmids. *E. coli* strain BL21(DE3)pLysS was used for the expression of recombinant proteins. *E. coli* strain BTH 101 was used for Bacterial Two-Hybrid System (BACTH) based study. *E. coli* cells harboring pET28a (+) and its derivatives were maintained in the presence of kanamycin (25

μg/ml). Standard protocols for all recombinant techniques were used as described in (Green and Sambrook, 2012).

3.2.2.2 Bioinformatic analysis

Multiple sequence alignment and functional motifs search in ParB1 (Dr_0012), ParB2 (DR_A0002), ParB3 (DR_B0002) and ParB4 (Dr_B0030) proteins were carried out using standard online bioinformatics tools as described earlier (Das and Misra, 2011; Charaka *et al*., 2013). In brief, the amino acid sequences of ParB1, ParB2, ParB3 and ParB4 proteins were subjected to a PSI-BLAST search with the SWISSPROT database. After five iterations, the sequences obtained were aligned by ClustalW along with ParB (Spo0J) protein of closest bacteria *T. thermophilus* and *B. subtilis.* The sequences of close homology were aligned by T-COFFEE, and the conserved motifs were marked in ClustalW. The secondary structure was inferred from PSIPRED, JNET, and Prof with the Quick2D server of the MaxPlanck Institute for Developmental Biology. The boundaries of the secondary structure (correspond to Spo0J of *T. thermophilus* (PDB ID: 1VZ0) were defined by using online Espript program. The secondary structure of C-terminal region was analyzed by using Psipred online software and represented in Espript online software. The phylogenetic tree between deinococcal ParBs and known ParB family proteins (Spo0J from *T. thermophilus* and *B. subtilis*) was constructed using PHYLIP program showing Neighbour-joining tree without distance corrections.

3.2.2.3 Cloning, expression and purification of ParB1, ParB2 and ParB3 proteins

Genomic DNA of D. radioduransR1 was prepared as reported previously (Battista et al., 2001), and open reading frames (ORFs) DR_A0002 (parB2) and DR_B0002 (parB3) were PCR amplified from genomic DNA by using primers pETB2F and pETB2R for the parB2 gene and primers pETB3F and pETB3R for the parB3 gene (see Table 2; Annexure I).

PCR products were ligated at the *Nde*I and *Xho*I sites in pET28a (+) to yield pETB2 and pETB3, respectively. For ParB1, pET0012 plasmid (Charaka and Misra, 2012) was used. These plasmids were used for overexpression of recombinant proteins. Recombinant ParB1, ParB2 and ParB3 were expressed on pET0012, pETB2 and pETB3 respectively in *E. coli* BL21(DE3)pLysS. The recombinant proteins were purified by nickel affinity chromatography, as described earlier (Charaka and Misra, 2012). In brief, overnight grown cultures of *E. coli* BL21(DE3)pLysS expressing recombinant proteins were diluted 1:100 in fresh LB broth containing 25 µg/ml kanamycin and 0.5 mM IPTG was added at 0.3 OD at 600 nm and after 2 h culture was kept at 4°C for overnight. It was further allowed to grow at 37°C for 1 h and harvested to keep cell pellet in -70°C. Cell pellet was thawed and suspended in buffer A (20 mM Tris–HCl, pH 7.6, 300 mM NaCl and 10% glycerol) containing 10 mM imidazole, 0.5 mg/ml lysozyme, 1 mM PMSF, 1mM $MgCl_2$, 0.05 % NP-40, 0.05 % TritonX-100, protease inhibitor cocktail) and incubated at 37°C for 30 min. Cells were sonicated for 5 min with 10s ON and 15s OFF mode at 25 % amplitude. The cell lysate was centrifuged at 11,000 RPM for 30 min at 4°C. The supernatant was dialysed in Buffer A containing 1mM PMSF at 4°C. The dialysed cell-free extract was loaded onto $NiCl_2$ charged-fast-flow-chelating-sepharose column (GE Healthcare) pre-equilibrated with buffer A containing 10mM imidazole. The column was washed with 40 column volumes of buffer A containing 50 mM imidazole and 10 column volumes of buffer A containing 70 mM imidazole till proteins stop coming from the column. Recombinant proteins eluted in steps using 100 mM, 200 mM, 250 mM and 300 mM imidazole in buffer A and analyzed on 10% SDS-PAGE. Fractions containing more than 95% pure protein were pooled and dialyzed in buffer A containing 100 mM NaCl and processed for ion exchange chromatography using HiTrap Q HP anion exchange column (GE Healthcare Life sciences). Different fractions were analyzed on SDS-PAGE and fractions containing pure protein were pooled and concentrated using 10

kDa cut-off spin columns. Concentrated protein was centrifuged at 16,000 RPM for 30 minutes to remove aggregates. Supernatant containing mostly soluble proteins were used for size exclusion chromatography. For storage in -20˚C, proteins were dialyzed in dialysis buffer containing 20 mM Tris-HCl pH 7.6, 100 mM NaCl, 50% glycerol, 1mM $MgCl_2$ and 1 mM PMSF. Protein concentration was determined by taking OD at 280 nm in Nanodrop (Synergy H1, Hybrid Multi-Mode Reader Biotek) using mass extinction co-efficient of the proteins.

3.2.2.4 Size exclusion chromatography and glutaraldehyde cross linking

For determination of the molecular weight of deinococcal ParB proteins in its native state, molecular size exclusion chromatography was performed using Superdex™ 200 GL column (Pharmacia) on AKTA purifier (GE Healthcare, USA). For this, ~1 mg of purified ParB1, ParB2 and ParB3 proteins were loaded separately onto the column in storage buffer containing 20 mM TrisHCl, 100 mM NaCl, pH 7.6 and eluted at a flow rate of 0.5 ml/min. The column was formerly calibrated with gel filtration molecular weight markers (Amersham-Pharmacia: Chymotripsinogen- 25 kDa, Ovalbumin – 44 kDa, Bovine serum albumin – 66.5 kDa, Aldolase- 158 kDa and Catalase- 250 kDa). Standard calibration curve was plotted with elution volume of marker against the logarithm of molecular weight of markers. The molecular weight of the purified ParBs in the native condition was determined by fitting the elution volume into the calibration curve.

For glutaraldehyde cross linking of protein in their native state, ~10µg of the purified recombinants ParB1, ParB2 and ParB3 proteins were diluted in 20mM phosphate buffer pH 8.0 in a reaction volume of 30µl. Further, protein solutions were incubated at 37°C for 5 minutes in absence and presence of 2 µl of freshly prepared 0.02 % glutaraldehyde solution. To this, equal volume of 2X cracking dye was added and heated at 80˚C for 5 min. These samples were separated on 10 % SDS-PAGE and stained with coomassie brilliant blue and documented.

3.2.2.5 *In vivo* protein-protein interaction studies in *D. radiodurans*

Interaction among ParB1, ParB2 and ParB3 was monitored in *D. radiodurans* by co-immunoprecipitation. For that, the T18 tagged *parB*s were PCR amplified using BTHF(pv) and BTHR(pv) primers from their BACTH derivative plasmids (see Table 2; Annexure I) and cloned in pVHS559 plasmid (Charaka and Misra, 2012) at *Nde*I-*Xho*I sites to yield pV18B1, pV18B2 and pV18B3 (Table 3; Annexure I). Similarly, N-terminal hexahistidine tagged *parB1, parB2* and *parB3* were amplified using pETHisF and pETHisR primers from their pET28a+ derivatives (Table 2; Annexure I) and cloned in pRADgro plasmid (Misra *et al*., 2006) at *Apa*I-*Xba*I sites to yield pRADhisB1, pRADhisB2 and pRADhisB3 plasmids (Table 3; Annexure I). The expression of fusion proteins in *Deinococcus* from these constructs was monitored using anti-T18 antibodies or anti-polyhistidine antibodies (as described in section 3.1.2.11) (Fig. 3.2.4 B, D). The cell-free extracts of *D. radiodurans* expressing all three ParBs under IPTG induction as on pV18B1, pV18B2 and pV18B3 in different combinations with hexahistidine tagged all three ParBs under constitutive promoter from pRADgro were prepared and immunoprecipitated using Anti-polyhistidine antibodies as described earlier (Maurya *et al*., 2018). The T18 fused or polyhistidine fused ParBs alone were used as controls. The immunoprecipitates were separated on SDS-PAGE, blotted onto PVDF membrane and hybridized using monoclonal antibodies against T18 tag. The hybridization signals were detected using anti-mouse secondary antibodies conjugated with alkaline phosphatase using BCIP/NBT substrates (Roche Biochemical, Mannheim). Likewise, interactions between polyHis tagged ParBs (ParB1-3) and T18 tagged ParAs (ParA1-3) (see section 3.1.2.11; Table 3; Annexure I) were also monitored using coimmunoprecipitation from *D. radiodurans.*

The interaction between replication initiator protein, DnaA and deinococcal ParBs in *D. radiodurans* was monitored by using co-immunoprecipitation. In brief, N-terminal

hexahistidine tagged *dnaA* (Dr_0002) was PCR amplified using pETHisF and pETHisR primers from pETDnaA plasmid (*dnaA* cloned in pET28a (+) at *Bam*HI and *Eco*RI sites) and cloned in pRADgro plasmid at *Apa*I and *Xba*I sites (Table 3; Annexure I). The resulting plasmid named as pRADhisdnaA. The expression of hexahistidine tagged DnaA in *D. radiodurans* from pRADhisdnaA was monitored through western blotting by using Anti-polyhistidine antibody as described above (Fig. 3.2.7). The pRADhisdnaA was co-transformed with T18 tagged deinococcal ParBs expressing plasmid as mentioned above. The expression of T18 tagged ParBs in co-transformants was induced by 5mM IPTG. The cell-free extracts of *D. radiodurans* expressing all three ParBs as on pV18B1, pV18B2 and pV18B3 in different combinations with hexahistidine tagged DnaA under constitutive promoter from pRADgro were prepared and immunoprecipitated using Anti-polyhistidine antibodies as mentioned above (Maurya *et al*., 2018). The T18 fused ParBs or polyhistidine fused DnaA alone were used as controls. The co-immunoprecipitates were separated on SDS-PAGE, blotted onto PVDF membrane and hybridized by Anti-T18 monoclonal antibodies raised in mouse. The hybridization signals were detected as described above.

3.2.2.6 Protein-protein interaction study using BACTH system in surrogate *E. coli*

For protein-protein interaction studies between deinococcal ParBs and replication initiation protein DnaA, coding sequences of Dr_0002 (DnaA)was cloned at *Bam*HI-*Eco*RI sites and *Kpn*I-*Eco*RI sites in pKNT25 to yield pKNTDA while pUTCB1, pUTCB2 and pUTCB3 was used as described in section 3.1.2.11 (Table 3; Annexure I). The expression of T25 tagged DnaA in *E. coli* was monitored using Anti-T25 antibodies (Fig. 3.2.7). *In vivo* interactions of different proteins were monitored using bacterial two-hybrid system (BACTH) as described earlier (section 3.1.2.11). In brief, BTH101 was co-transformed with pKNTDA in different combination with pUTCB1, pUTCB2 and pUTCB3 plasmids expressing target proteins with

T25 or T18 tags. Empty vector pUT18 co-transformed with pKNTDA was used as negative controls while pUTEFA and pKNTEFZ were co-transformed as positive control. The co-transformants were spotted on LB agar plate containing X-Gal (40 μg/mL), IPTG (0.5 mM) and antibiotics as required and the appearance of white-blue color colonies was recorded. Further, β-galactosidase activity of same combinations was measured from liquid cultures and calculated in Miller units as described in (Karimova *et al*., 1998) and plotted with standard deviation in GraphPad Prism 5.

3.2.2.7 Construction of *parB* deletion mutants in *D. radiodurans*

The *parB1* deletion mutant of *D. radiodurans*was used as described in (Charaka and Misra, 2012). For generation of *parB2* and *parB3*deletion mutant of *D. radiodurans,* suicide plasmids pNOKA02 and pNOKB02 respectively were constructed from pNOKOUT (Khairnar *et al.,* 2008) by using a strategy described previously (Charaka and Misra, 2012). In brief, the fragments 1 kb upstream and 1 kb downstream of ORFs Dr_A0002 and Dr_B0002 were PCR amplified with primers (see Table 2; Annexure I) and cloned at the *Kpn*I-*Eco*RI and *Bam*HI-*Sac*I sites in pNOKOUT plasmid, respectively. The recombinant plasmid thus obtained pNOKA02 and pNOKB02, was linearized with *Xmn*I and transformed into *D. radiodurans*cells. Transformants were maintained through several rounds of sub-culturing, and the homozygous replacement of *parB2* and *parB3* with *nptII* was ascertained by PCR amplification using internal primers of both genes (Fig 3.2.6 D). For complementation of deletion mutants, pV18B1, pV18B2 and pV18B3 plasmids (Table 3; Annexure I) were used which express *in trans,* the proteins under IPTG induction. These plasmids were transformed in respective mutants with vector control. The recombinant clones were scored on TGY plates in the presence of kanamycin (8 mg/ml) and spectinomycin (70 mg/ml). The deletion mutants and its complemented forms were used for subsequent studies.

3.2.2.8 Cell survival studies

Deinococcus radiodurans wild type cells, its *parB* mutants and complemented forms were subjected to 6 kGy γ-radiations as described in (Misra *et al*., 2006). In brief, the bacteria grown in TGY medium with or without appropriate antibiotics (kanamycin; 8 mg/ml) at 32°C were washed and suspended in sterile phosphate-buffered saline (PBS) and treated with 6 kGy γ-radiation at dose rate 1.81 kGy/h (Gamma Cell 5000, ^{60}Co, Board of Radiation and Isotopes Technology, DAE, India). Irradiated cells with SHAM controls were washed in PBS and suspended in the fresh TGY medium. Equal numbers of cells were allowed to grow in 48 well microtiter plates (Nunclon; Sigma-Aldrich) containing TGY medium in presence and absence of required antibiotics or 5mM IPTG (for induction ParBs from plasmid during complementation). Growth was monitored in replicates at 32°C for 18 h using Synergy H1 Hybrid multi-mode microplate reader.

In addition, wild type cells and different *parB* mutants were grown in absence and presence of kanamycin (antibiotic selection) and treated with different doses (0 to 8 kGy) of γ-radiations at dose rate of 1.81kGy/h (Misra *et al.*, 2006). The irradiated cells with their SHAM control were washed in PBS and serially diluted. Different dilution from both the conditions (- / + kanamycin) were plated on TYG agar in absence and presence of kanamycin. The colony forming units (CFU) were recorded after 36-40 h of incubation at 32°C. The survival fractions are expressed as a percentage of the number of colonies obtained with respect to untreated cells.

3.2.2.9 Cell disruption and ploidy determination in mutants/complemented forms using quantitative real-time PCR

Wild type, *parB* mutants as well as their complemented cells of similar O.D. at 600nm were harvested from appropriate growth condition by centrifugation. The cell number in all was

determined using a Neubauer cell counter. The cells were washed with 70 % ethanol solution and resuspended in a lysis solution containing 10 mM Tris pH 7.6, 1 mM EDTA and 4mg/ml lysozyme and were incubated at 37°C for complete cell lysis, the cell debris was removed by centrifugation (10000 RPM, 5 min). Lytic efficiency was verified by the densities with a Neubauer counting chamber. The integrity of genomic DNA was confirmed by agarose gel electrophoresis. Further, copy numbers of different genomic replicons in wild type and their *parB* mutants were determined as described in section 3.1.2.13 (Breuert*et al.,* 2006). The qPCR was carried as described in section 3.1.2.13. Three independent biological replicates were used for each sample. The replicon copy number is quantified by comparing the results with a dilution series of a PCR product of known concentration that is used as a standard. The copy number of each replicon by both genes per cell was calculated using the cell number present at the time of cell lysis. Average copy number reflected from two genes per replicon was represented with appropriate bio-statistical analysis.

3.2.3 Results

3.2.3.1 Comparison of ParBs of *D. radiodurans* with ParB family proteins

The multiple sequence alignment of all four ParB proteins with other known ParB (Spo0J) proteins showed that ParB1 had an overall homology with the Spo0J of *T. thermophilus* and ~ 40-60% identity with other chromosomal ParB proteins (Fig. 3.2.1). Secondary genome ParBs like ParB2, ParB3 and ParB4 had only ~30% identity amongst themselves and grossly different from the chromosomal type ParB's. Secondary structure prediction of all 4 ParBs using Spo0J structure template (PDB ID: 1VZ0) (Leonard *et al.,* 2005) showed a characteristic HTH motif formed by helices H6 and H7 and remaining helices help in compaction of the domain (Fig. 3.2.1 A). Further, phylogenetic analysis revealed that secondary genome ParBs form separate clade from primary genome ParB (Fig 3.2.1B) (Dubarry *et al*., 2006).

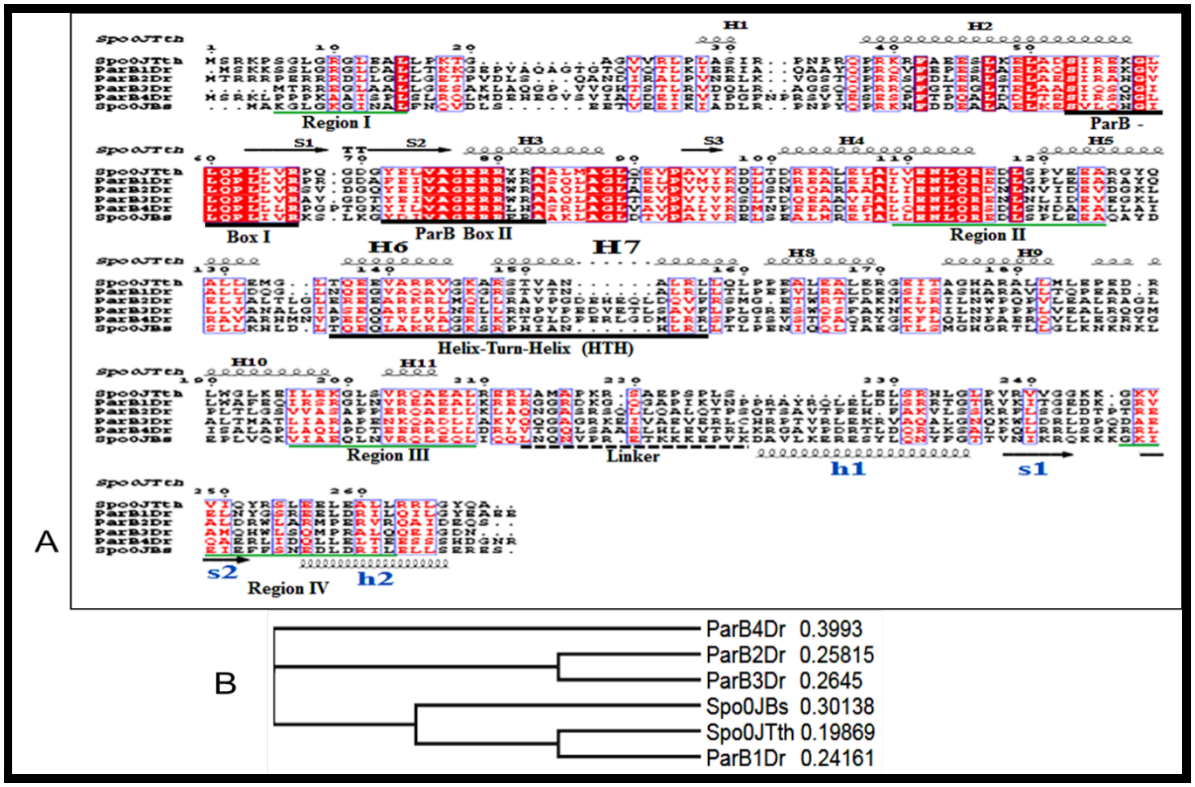

Figure 3.2.1 Multiple sequences alignment of deinococcal ParB proteins with known ParB family proteins using ClustalW. Boundaries of the secondary structure were defined by using online Espript program. The secondary structure shown in this figure corresponds to those of domain of Spo0J of *T. thermophilus* (PDB .ID: 1VZ0) (**A**). The phylogenetic tree between deinococcal ParBs and known ParB family proteins was constructed using Phylip program showing Neighbour-joining tree without distance corrections (**B**).

Except ParB1, the remaining ParBs have an extra sequence in the Helix-Turn-Helix (HTH) region. This might provide flexibility to these ParBs for their interaction with yet uncharacterized centromeric sequences on their cognate genome elements. These proteins also showed different C-terminal region as compared to Spo0J, which might provide specific interaction of these ParB with their cognate ParA during segregation process.

3.2.3.2 ParBs of *D. radiodurans* dimerize *in solution*

Recombinant deinococcal ParBs were purified from *E. coli* BL21(DE3)pLysS host by Ni-NTA affinity chromatography followed by gel filtration (see section 3.2.2.3; Fig. 3.2.2). Since, ParBs in other bacteria are known to function as dimer, the dimerization of purified ParB1, ParB2 and ParB3 was therefore, checked using glutaraldehyde cross-linking and size-

exclusion chromatography approaches. Results showed that a large proportion of total proteins in all ParBs exist as dimer *in solution* (Fig. 3.2.3). For instance, the majority of ParB showed a molecular size of ~ 60 kDa in SDS-PAGE after cross-linking (Fig 3.2.3 A) and these proteins were eluted at volume of BSA (~66 kDa) in size-exclusion chromatography (Fig. 3.2.3B).

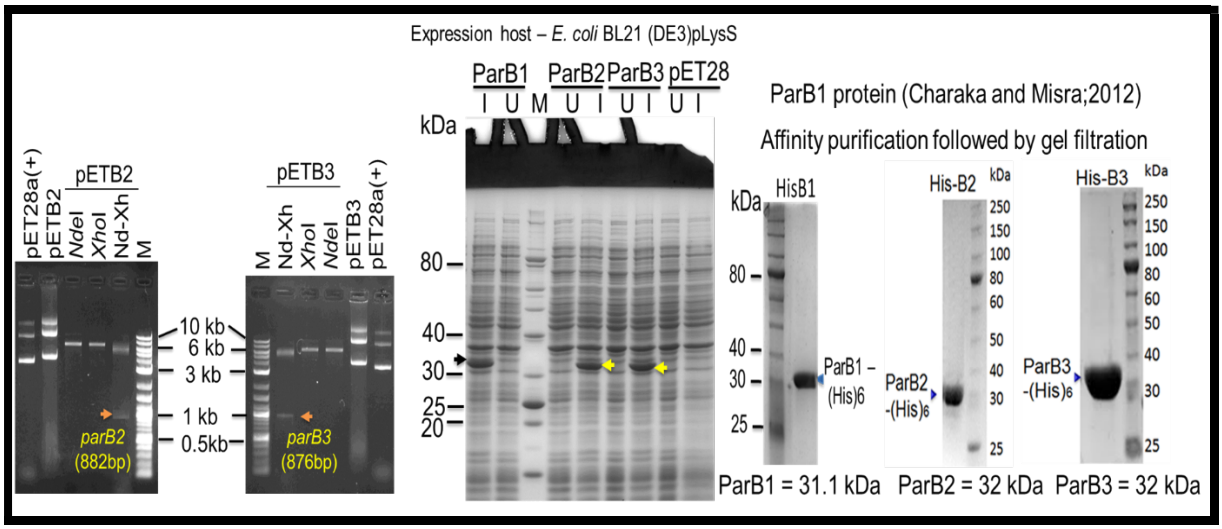

Figure 3.2.2 Cloning, expression and purification of recombinant deinococcal ParBs. Recombinant ParB1 expressing construct was used from earlier study (Charaka and Misra, 2012)**.** Further, parB2 and parB3 genes were cloned in pET28a(+) at *Nde*I-*Xho*I sites, their expression was confirmed in *E. coli* BL21(DE3)pLysS followed by purification.

The *in vivo* oligomeric nature of ParB proteins was checked by immunoprecipitation. For that the different ParBs were tagged with either T18 in pVHS559 or polyhis in pRADgro plasmids and co-expressed in different combinations in *D. radiodurans.* The expression of these fusion products of ParBs was monitored by immunobloting (Fig. 3.2.4 B, D). The total proteins from these cells were immunoprecipitated using polyhis antibody, and the perspective interacting partners duly tagged with T18 was detected by using T18 antibodies. All the ParBs showed homotypic interactions indicating a possibility of homodimerization in *D. radiodurans*. None of them showed heterotypic interactions with other ParBs indicating a little less possibility of cross talk between different ParBs in this multipartite genome harboring bacteria (Fig. 3.2.5).

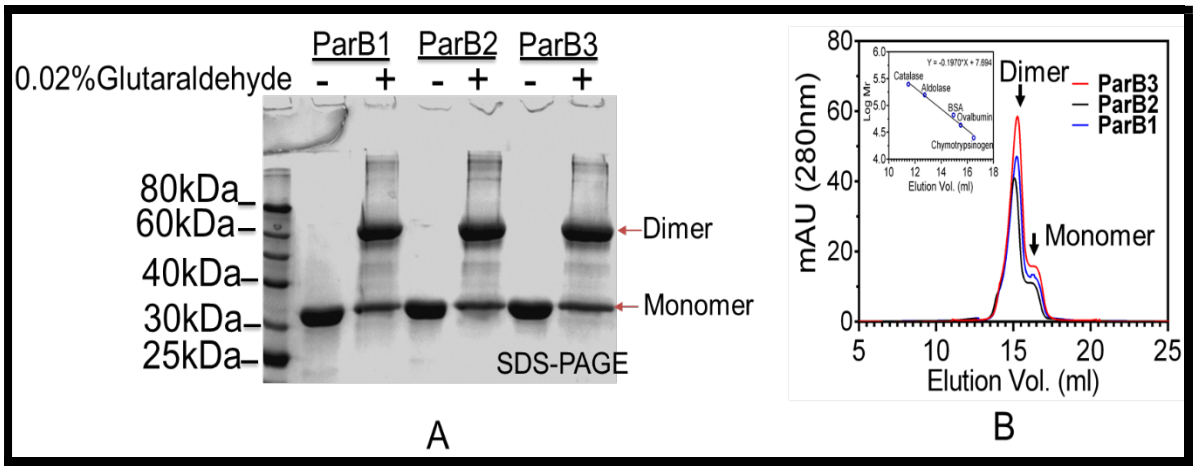

Figure 3.2.3 Molecular size / weight determination of recombinant ParB1, ParB2 and ParB3 proteins in solution. We used gluteraldehyde crosslinking, where ~10µg of the purified recombinants ParB1, ParB2 and ParB3 proteins were cross linked with 0.02 % glutaraldehyde solution and separated on 10 % SDS-PAGE and stained with coomassie brilliant blue (**A**). For size exclusion chromatography, ~1 mg of purified ParB1, ParB2 and ParB3 proteins were separated from Superdex™ 200 GL column (Pharmacia) on AKTA purifier (GE Healthcare, Germany) at a flow rate of 0.5 ml/min. The column was formerly calibrated with gel filtration molecular weight markers and standard calibration curve was plotted with elution volume of marker against the logarithm of molecular weight of markers (given in inset of fig. **B**). The molecular weight of the purified ParBs in the native condition was determined from standard curve (**B**).

These results corroborated earlier finding where full-length Spo0J of *T. thermophilus* was shown to exist in a dimer *in solution.* The roles of C-terminal region in Spo0J of *T. thermophilus* (Leonard *et al*., 2004) and ParB of *Pseudomonas aeruginosa* (Bartosik *et al*., 2004) has been shown in dimerization and these dimers are required for binding to cognate centromeric sequences. These results suggested that ParBs encoded on different genome elements in multipartite genome system are less likely to interact with ParBs encoded on other genome elements.

3.2.3.3 ParBs interact to ParAs *in vivo*

The interaction of ParB1, ParB2 and ParB3 with ParA1, ParA2 and ParA3 in this bacterium was checked in different combinations using co-immunoprecipitation (co-IP) assay. For that, the cell free extract from the cells co-expressing all ParAs tagged with T18, and all ParBs with polyhis tag, on plasmids was subjected to co-IP using anti-polyhis antibodies and interacting partner(s) if any would be detected using T18 antibodies.

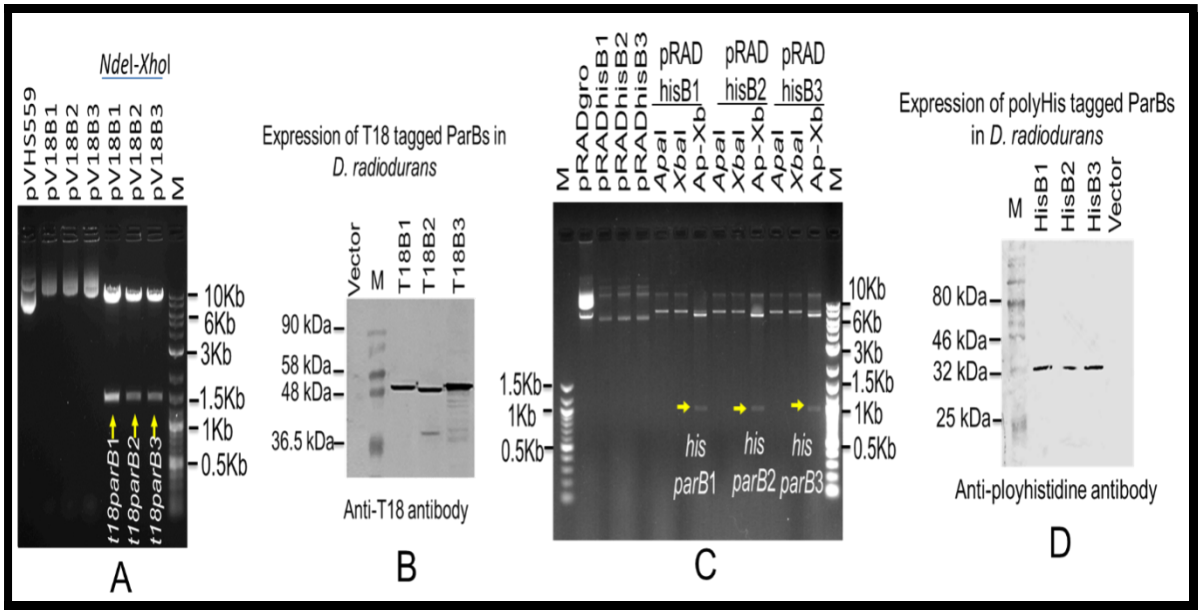

Figure 3.2.4 Cloning and expression of T18 tagged ParB1-3 from pVHS559 (A, B) and polyHis tagged ParB1-3 from pRADgro (C, D) in *D. radiodurans*.

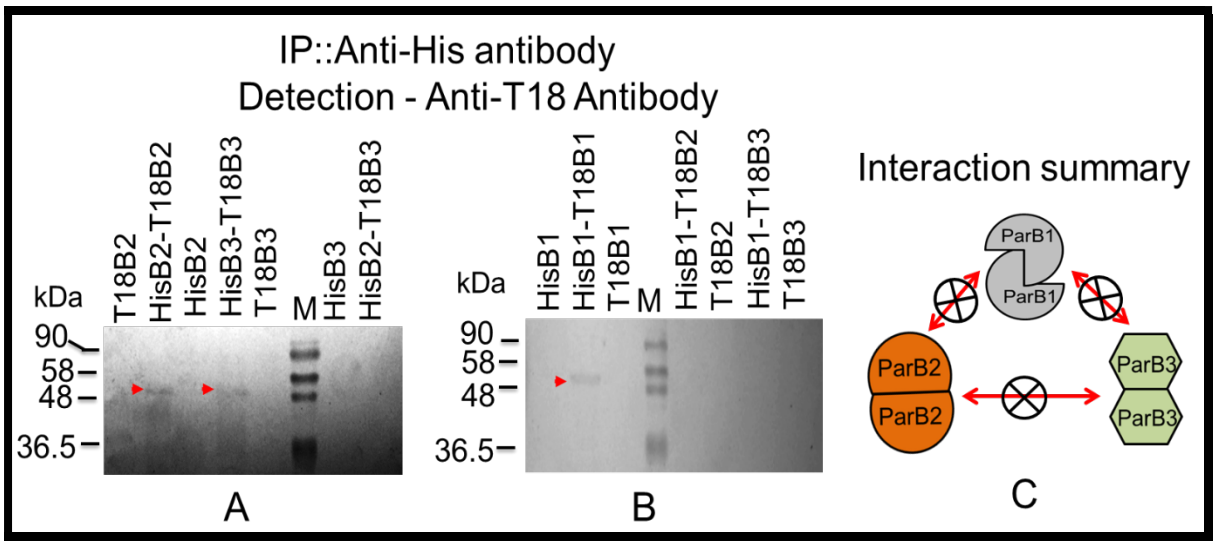

Figure 3.2.5 *In vivo* interaction among deinococcal ParBs using coIP from *D. radiodurans*. Plasmid constructs expressing T18 or polyHis tagged deinococcal ParBs were co-expressed in *D. radiodurans* in different combinations. The cell lysates were immunoprecipitated using Anti-polyhistidine antibodies and interacting partners were detected using Anti-T18 antibodies (**A, B**). A cartoon depicting interaction summary (**C**).

Results showed *in vivo* interaction of all the ParAs with their cognate ParBs. However, the secondary genome ParAs also interacted with non-cognate secondary genome ParBs (Fig. 3.2.5 A-D). Interestingly, ParA1 showed interaction with ParB1 only while none of the

secondary genome ParAs interacted with ParB1. These results suggested a possible functional redundancy in segregation process of secondary genome replicon.

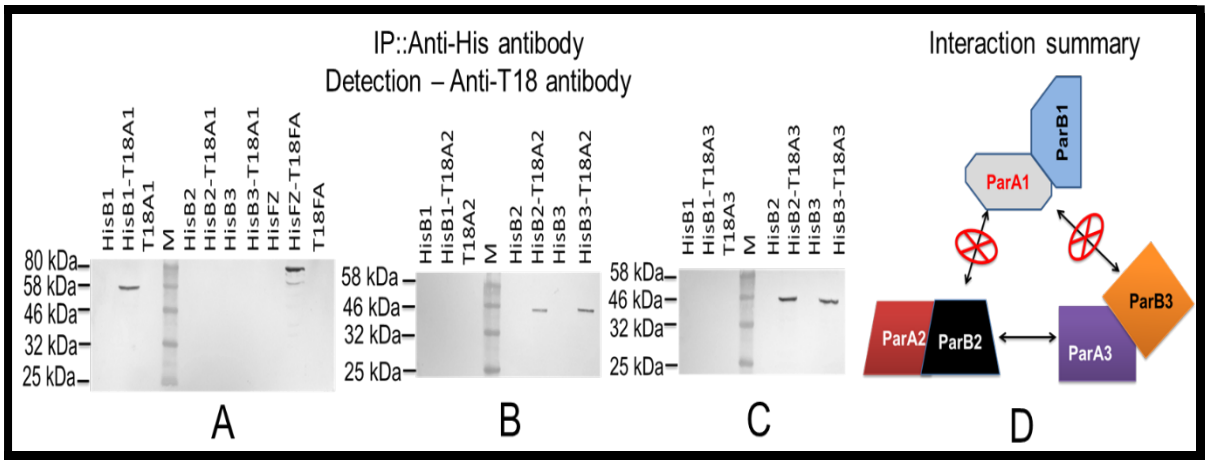

Figure 3.2.5 Protein-protein interaction of deinococcal ParBs with ParAs in *D. radiodurans*. T18 tagged ParAs from pVHS559 and polyHis tagged ParBs from pRADgro were coexpressed in D. radiodurans (section). The cell free extracts were immunoprecipitaed by Anti-polyHis antibodies and interacting partners were detected using Anti-T18 antibodies (**A-C**). A cartoon for interaction summary is given (**D**).

3.2.3.4 Mutation in *parB1, parB2* or *parB3* has affected the ploidy of cognate genome element

To monitor role of deinococcal ParBs in genome maintenance and radioresistance if any, we have generated their deletion mutant using pNOKOUT plasmid. Plasmid pNOKA02 and pNOKB02 were used for generation of *parB2* and *parB3* deletion mutant, respectively (Fig. 3.2.6). Deletion mutant of *parB1* was picked from earlier study (Charaka and Misra, 2012). These mutants were confirmed by diagnostic PCR (Fig. 3.2.6 C, D). *D. radiodurans* harbours 8 to 10 haploid genome copies during exponential growth phase (Harsen, 1978). Since, *parB* proteins are integral part of genome segregation in dividing population, the possibility of *par* deletions affecting the copy number of daughter cells was examined. We monitored the copy number of each replicon using quantitative real time PCR as described in methods. Surprisingly, the copy number of cognate replicon had increased in respective null mutant of deinococcal *parB*s grown in the presence of required selection pressure. For instance, in

Δ*parB1* the copy number of chromosome I has increased from 8 to 10, Δ*parB2* showed chromosome II copy number increase from 6 to 10 and the copy number of megaplasmid was increased from 11-18 in *parB3* mutant (Fig. 3.2.6 F).

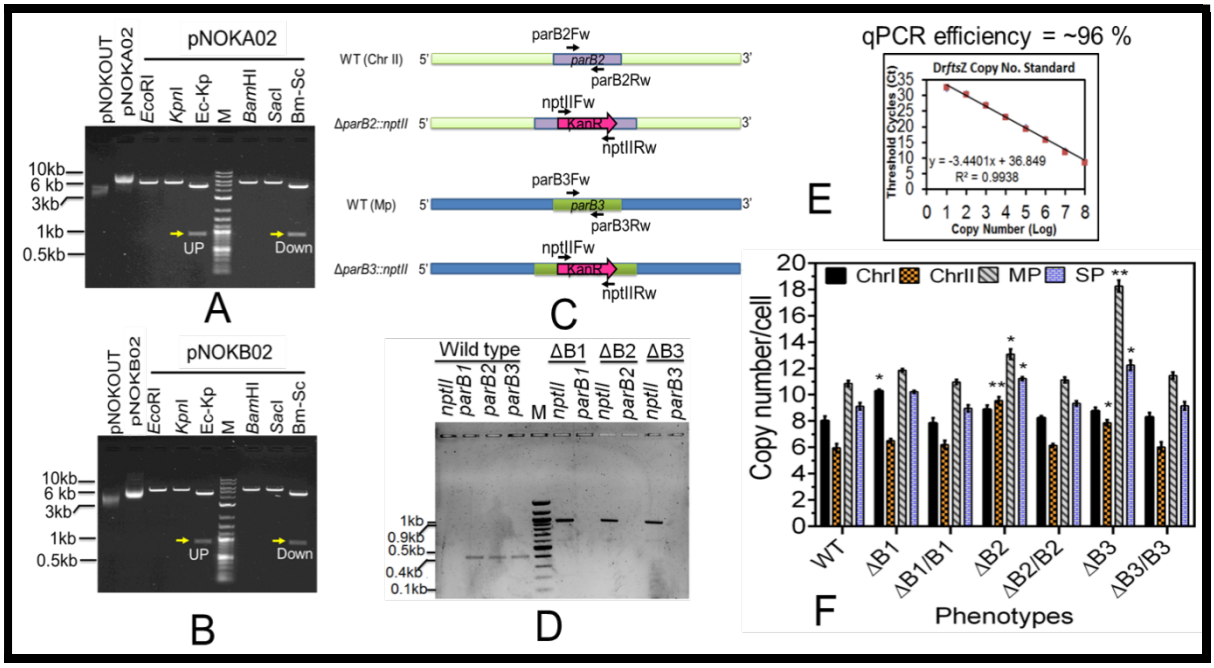

Figure 3.2.6 Construction of *parB2* and *parB3* deletion mutant of *D. radiodurans* and determination of ploidy. Plamids pNOKA02 (**A**) and pNOKB02 (**B**) were linearised and transformed in *D. radiodurans*. The tranformants were subcultured in presence of kanamycin and screened for replacement of target with *nptII* cassettes by diagnostic PCR (see 3.2.2.7; **C, D**). Copy number per cell was determined by qPCR (see section 3.2.2.9; **E, F**).

A marginal increase in the copy number of genome elements which was less than 2 times is intriguing and could not be explained merely by arrest of genome segregation. Earlier, the regulation of DNA replication by genome segregation events has been reported in *B. subtilis* where an increased genomic content was reported upon deletion of *parB* homolog (*spo0J*) in this bacterium (Lee *et al*., 2003; Lee and Grossman, 2006). To be more specific with the involvement of ParBs in copy number variations, the functional complementation by *in trans* expression of these proteins in respective mutants was carried out. Results showed the resumption of original copy number near to wild type, which could suggest that deinococcal

ParBs play the important roles in the regulation of replication initiation by yet uncharacterized mechanisms, in *D. radiodurans*.

3.2.3.5 Deinococcal ParBs interact with replication initiation protein (DnaA) of *D. radiodurans*

Since, the ploidy increase in *parB* mutant was less than 2-fold it indicated a possible cross talk between genome segregation and DNA replication. The *D. radiodurans* genome encodes the replication initiation proteins DnaA and DnaB while *E. coli* homolog of DnaC is missing (White *et al*., 1999). This might suspect the functional redundancy of DnaC with some other proteins of this bacterium. We monitored *in vivo* interaction of ParB1, ParB2 and ParB3 which are DNA binding proteins, with DnaA using BACTH system in surrogate *E. coli* (Karimova *et al*., 1998) as well as using co-immunoprecipitation from *D. radiodurans* (Maurya *et al*., 2018). The *E. coli* (*cyaA*$^{-}$) cells co-expressing DnaA with all three deinococcal ParBs in different combinations on BACTH plasmids were screened for resumption of CyaA regulated expression of β-galactosidase activity. This was monitored by spot assay as well as *in solution* as described in methods. Results show that DnaA interacted with all three ParBs with nearly same levels as evident from the intensity of blue colour colonies in spot assay as well as β-galactosidase activity levels *in solution* (Fig. 3.2.7 C).

In addition, co-immunoprecipitation assay of total soluble proteins of *D. radiodurans* cells co-expressing polyhis tagged DnaA in different combination with T18 tagged ParBs completely supported BACTH findings (Fig. 3.2.7 F). This suggested that replication proteins can interact with all three ParBs encoded on multipartite genome of *D. radiodurans*. The similar observation was reported earlier in *V. cholerae,* where genome segregation proteins (ParA and ParB) were found interacting with DnaA (Kadoya *et al*., 2011).

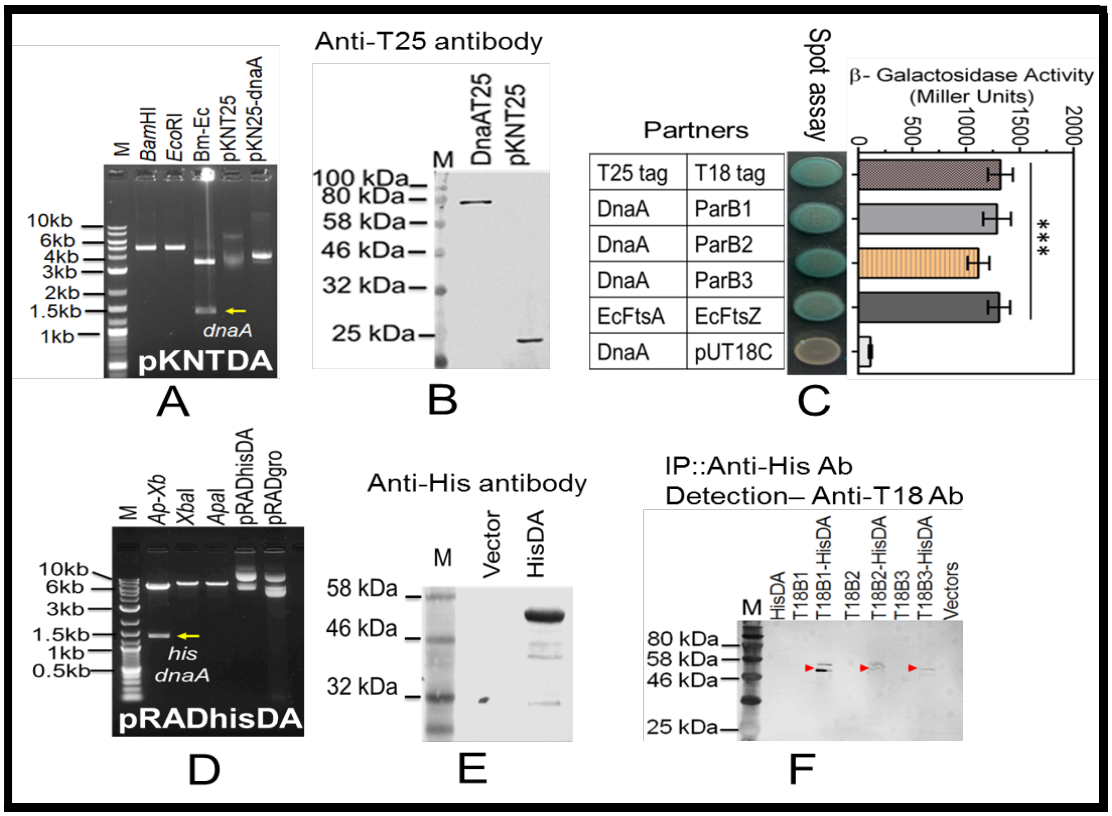

Figure 3.2.7 Interaction of deinococcal ParBs with replication initiation protein DnaA. To generate T25 fusion of DnaA, *dnaA* was cloned in pKNT25 to give pKNTDA (**A**) and its expression in *E. coli* was checked (**B**). PolyHis tagged DnaA was expressed in *D. radiodurans* from pRADhisDA (**D, E**). Further, T18 fused ParBs expressing plasmid were co-expressed with T25 fused DnaA and bacterial two-hybrid assays (spot assay and β-gal assay) were performed (Section 3.2.2.6) (**C**). Interaction of polyHis tagged DnaA from pRADgro with T18 tagged ParBs from pVHS559 in *D. radiodurans* was monitored by co-IP (**F**).

Our results suggested a cross-talk between DNA replication and segregation components of *D. radiodurans* and offers a strong possibility of these macromolecular events are interdependently regulated at least in this bacterium.

3.2.3.6 Secondary genome elements contribute to radioresistance

ParB is key protein that regulates the partitioning of duplicated genome elements into daughter cells in bacteria, and the null mutants of *parBs* in *D. radiodurans* showed increased ploidy of different genome elements. This can be explained on the assumption that genome duplication would have occurred normally at least one round, but segregation that would have kept copy number per cell constant got arrested and led to an increase in copy number under

selection pressure. If this assumption is true, then the cell density of mutants maintained in the presence and absence of selection pressure should be different. To test it, these cells were grown in the presence and absence of antibiotics and then the growth response was monitored under normal and gamma radiation stressed conditions. We observed that Δ*parB1* mutant maintained with or without selection pressure showed nearly similar trends of gamma radiation effects on its growth (Fig 3.2.8 A, B) suggesting the role of primary chromosome in growth irrespective of selection pressure. However, when Δ*parB2* and Δ*parB3* mutants were maintained in the presence or absence of selection pressure, they showed differential growth response under normal and radiation stressed conditions. For instance, the cells maintained under selection pressure showed nearly wild type effects of gamma radiation on their growth (Fig 3.2.8 C, E). When these were maintained in the absence of selection pressure, they showed a significant growth retardation under radiation stressed conditions as compared to that maintained with selection pressure (Fig 3.2.8 D, F). These results might suggest that Δ*parB2* and Δ*parB3* deletion does not affect normal growth of this bacterium while Δ*parB1* does, and the cell population that does not show resistance to antibiotic seems to be the one that is devoid of genome element having replacement of cognate *parB* with antibiotic resistance marker gene. Logically, such population could have arisen when segregation of genome elements having *parB* replaced with antibiotic marker cassette does not occur, and that would support the role of ParBs in segregation of cognate genome element. The slow growth of Δ*parB1* mutant under normal as well as gamma stressed conditions as reported earlier (Charaka and Misra, 2012) further ascertained the indispensability of primary chromosome even in this multipartite genome harboring bacterium.

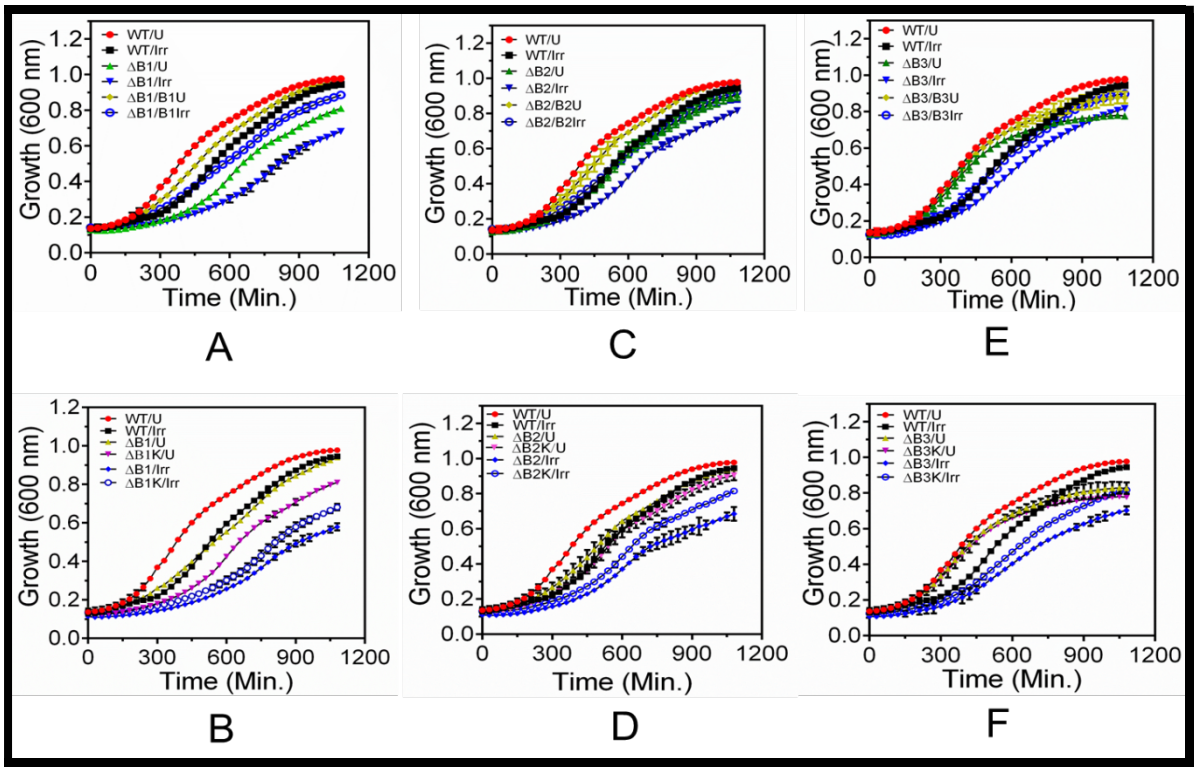

Figure 3.2.8 Survival of *parB1, parB2* and *parB3* mutants and its complemented forms to 6kGy γ-radiation. In brief, wild type (WT) cells, *parB1 (ΔB1), parB2 (ΔB2)* and *parB3 (ΔB3)* mutants and its complemented forms (Δ*B1/B1,* Δ*B2/B2* and Δ*B3/B3* respectively) were grown in presence of kanamycin and treated with 6kGy γ-radiation. Growth of Δ*B1* (**A**), Δ*B2* (**C**) and Δ*B3* (**E**) with respect to SHAM control was recorded in presence of kanamycin. In similar way, Δ*B1* (**B**), Δ*B2* (**D**) and Δ*B3* (**F**) mutants were grown in absence of kanamycin and treated with 6kGy γ-radiation. The radiated cell with SHAM controls were grown in absence and presence of kanamycin (denoted as K; 8µg/ml).

The effect of *parB* deletions (making a phenotype of genome segregation defect) on gamma radiation dose response was checked in all the *parB* mutants. For that all the three mutants were maintained in the presence or absence of antibiotics selection pressure and their survival was monitored at different doses of gamma radiation, again in the presence or absence of antibiotics. Interestingly, the mutants maintained without selection pressure but scored in the presence of antibiotics showed higher sensitivity to gamma radiation as compared to the respective controls maintained under selection pressure (Fig 3.2.9 A). This difference in gamma radiation response was not observed in case of Δ*parB2* and Δ*parB3* mutants when maintained under selection pressure and scored in the presence of antibiotics

(Fig 3.2.9 B). Thus, the cells containing respective genome elements (scored as antibiotic resistance) did not lose resistance to gamma radiation, which implicate the roles of these genome elements in radioresistance.

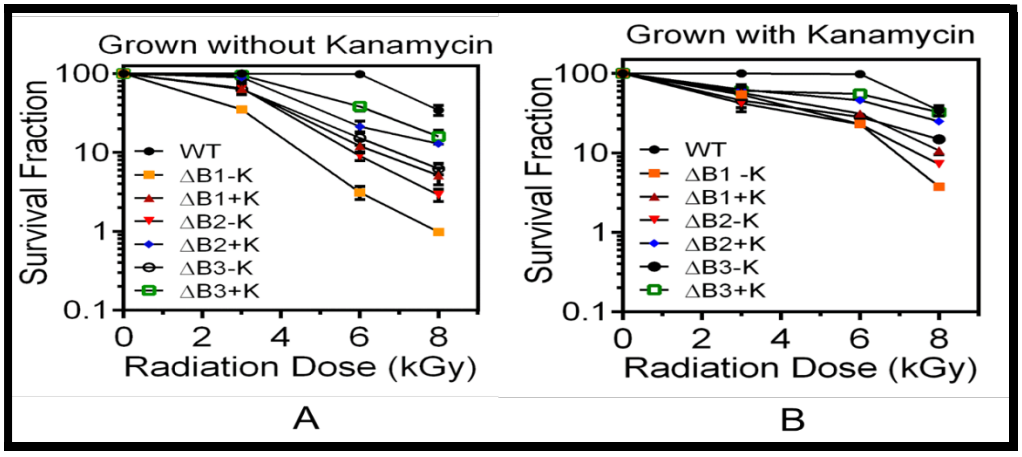

Figure 3.2.9 Effect of γ-radiaiton on survival of *parB* mutants of *D. radiodurans* with respect to antibiotic selection. The deletion mutant of *parB1* (ΔB1), *parB2* (ΔB2) and *parB3* (ΔB3) were grown in absence (A) and presence (B) of kanamycin and subjected to different doses of gamma radiation. Different dilution of irradiated cells as well as their SHAM controls were plated on TYG agar with (+K) and without kanamycin (-K). The survival fraction of each mutant with respect to radiation dose and antibiotics was compared with survival of unirradiated cells and plotted.

These results suggested that ParB deletion can make cells defective in DNA segregation and loss of secondary genome elements can affect gamma radiation resistance without affecting their normal growth while defect in primary chromosome can affect both normal growth and eventually radiation stress tolerance.

The multipartite genome of *D. radiodurans* comprised of 2 chromosomes, megaplasmid and small plasmid, and each of these elements are present in multiple copies presumably packaged together in form of a toroidal nucleoid (White *et al*., 1999; Minsky *et al*., 2006). Functional significance of multiple chromosomes and ploidy in extreme phenotypes, and the mechanisms underlying faithful inheritance of multipartite genome system packaged in form of a compact toroidal nucleoid, into daughter cells are not known and offered the most interesting aspects in bacterial genome biology to investigate. The partitioning system

encoded on primary chromosome of *D. radiodurans* has been characterized and shown expressing characteristics of pulling mechanism of genome segregation (Charaka and Misra, 2012). Here, we have brought forth some evidence to highlight the role of ParBs encoded on chromosome II (ParB2) and megaplasmid (ParB3) in the maintenance of cognate elements and their roles in the survival of *D. radiodurans* under both normal and stressed conditions. We found the homotypic interactions of all the ParBs while these do not talk to its other homologs in *D. radiodurans*. These results were expected because all the ParBs have C-terminal domain, which is similar to ParBs of *T. thermophilus* and *P. aeruginosa* where the roles of C-terminal domain in dimerization of ParB protein have been demonstrated (Leonard *et al*., 2004; Bartosik *et al*., 2004). Further ParBs are known as sequence specific centromere binding proteins that bind to centromere in dimeric form (Funell, 2016) indicating that ParBs in this bacterium are most likely to be functional. This observation was further supported by *in vivo* protein-protein interaction using co-immunoprecipitation study from *D. radiodurans*expressing deinococcal ParBs fused at their N-terminal with different tags, on two plasmids. Additionaly, deinococcal ParAs interacts to their cognate ParBs *in vivo*. Interestingaly, secondary genome ParAs (ParA2 and ParA3) could also interact to non-cognate secondary genome ParBs (i.e. ParB3 and ParB2, respectively) but not with ParB1. This suggests a possiblility of functional redundancy in interaction between secondary genome ParAs and ParBs in *D. radiodurans*. Earlier, we had reported that deletion of *parB1* in *D. radiodurans* imposes slower growth and segregation defects in primary chromosome (Charaka and Misra, 2012). In this study, when we compared the survival of Δ*parB2* and Δ*parB3* under normal and gamma stressed conditions with Δ*parB1* cells, we found that deletion of secondary genome ParBs has a little effect on normal growth as compared to wild type cells. Further, Δ*parB2* and Δ*parB3* mutants have shown sensitivity for γ-radiaiton when grown in absence of antibiotics, suggesting their role in radioresistance. The deletion of

parB1 presumably has arrested the segregation of chromosome I, which is not complemented by the presence of secondary genome ParBs (Fig. 3.2.8 A, B). This suggests that primary chromosome and secondary genome elements are most likely being maintained independently in this bacterium. ParB deletion mutant of *B. subtilis* and *P. aeruginosa* has shown defective genome segregation and growth arrest in these bacteria (Ireton *et al*., 1994; Bartosik *et al.*, 2004). An increase in copy number of replicons in respective *parB* mutants is intriguing and could not be explained with direct evidence. However, a strong interaction of replication initiation protein like DnaA with all the ParB proteins of this bacterium suggests a cross talk of genome segregation and DNA replication. Similar findings have been reported earlier in *V. cholerae* as well as *B. subtilis* (Lee *et al*., 2003; Kadoya *et al*., 2011; Murray and Errington, 2008). Earlier it has been shown that ParABS system regulates the separation and maintenance of origin of replication (containing ParB binding sites near to it) at a characteristic subcellular position in the cells in *B. subtilis*, *C. crescentus* and *Streptomyces coelicolor* A3 bacteria (Mohl and Gober, 1997; Lin and Grossman, 1998; Kim *et al*., 2000). These findings strongly support the interdependent regulation of DNA replication and genome partitioning in bacteria and provide the most plausible explanation for the effect of segregation defects on copy number of genome elements.

Chapter 3.3

Characterization of direct repeats present upstream to *parAB* operons in chromosome II and megaplasmid of *D. radiodurans*

3.3.1 Introduction

Recent advances in molecular, biochemical, biophysical and genetic approaches have improved the understanding of genome segregation in bacteria. Bacterial genome segregation machinery consists of a tripartite system containing (i) *cis* elements or centromere like sequences, (ii) centromere binding protein, ParB or its homologues and (iii) motor protein ParA or its homologues which recognizes ParB-centromere complex and undergo polymerization/depolymerization kinetics to pull or push the duplicated DNA towards opposite poles within cell. The proteins involved in segregation (segrosome) are annotated in the genome of almost all bacteria sequenced till date. The centromeric sequences are mostly undiscovered partly also because of diversity in sequence and structure. However, the centromere like sequences are generally located upstream or downstream to *parAB* operon in the genome of different bacteria (reviewed by Misra *et al*., 2018). They usually occurred in direct repeats of 6-43 bases and repeat number varies depending on their types. There are different types of *cis* elements like *parS* in P1 plasmid, *parC* in R1 plasmid (Gerdes *et al.*, 2010), *parH* in TP228 plasmid (Dobruk-Serkowska*et al*., 2012), and chromosomal centromeres (similar to *Bacillus subtilis*; 16 mer) (Draper and Gober, 2002) have been reported in the bacteria harboring single circular chromosome and/or low copy plasmid. Recently, many bacteria harboring multipartite genome system have been discovered from the diverse phylogenetic groups including *A. tumefaciens, S. meliloti*, *V. cholerae, D. radiodurans, Brucell* sp. and *B. cenocepacia* (Misra *et al*, 2018). Molecular studies have revealed that *V. cholera* has distinct replication and segregation machinery for both the chromosomes (Fogel and Waldor, 2005). *B. cenocepacia* has also shown distinct segregation system for each chromosome (Dubarry *et al*., 2006). The genome of *D. radiodurans* encodes one set of ParAB proteins each on chromosome I and chromosome II, and 2 sets on megaplasmid. These genome elements show the presence of heptameric and hexameric

repeats on chromosome I (Chr I), chromosome II (Chr II) and megaplasmid (Mp). However, the organization of these repeats in all the three genetic elements is found to be different from the typical P1 plasmid type *parS* element (White *et al*., 1999). Recently, partitioning mechanism of Chr I in *D. radiodurans* has been characterized, where three centromere-like sequences (named as *segS1-3*) were located on Chr I at nearly 120° angle to each other but away from *parA1B1* operon (Charaka and Misra, 2012). These *segS* elements seem to be different from origin of replication (*OriI*) sequences of Chr I. We found several direct repeats of 16-18 mer upstream to *parAB* operons in Chr II and Mp. Since, these direct repeats are present close to origin as well as upstream to cognate *parAB* operons in Chr II and Mp, we speculated the role of these direct repeats in replication as well as segregation of Chr II and Mp. In this chapter, we have used different genetic and biochemical approaches to understand the role of these direct repeats asboth origin of replication and centromere for respective genome elements.

3.3.2 Material and methods

3.3.2.1 Bacterial strains, plasmids and oligonucleotides

The bacterial strains, oligonucleotides and plasmids used in this study have been listed in Table 1-3 (Annexure I), respectively. *D. radiodurans* R1 (ATCC13939) was grown in TGY medium at 32˚C. *E. coli* strain NovaBlue was used for cloning and maintenance of all the plasmids while *E. coli* strain BL21(DE3)pLysS was used for the expression of recombinant proteins. The pNOKOUT plasmid (a suicide plasmid for *D. radiodurans*) was used to check the maintenance of different *cis* elements as well as for generation of their knockouts in *D. radiodurans*. Standard protocols for all recombinant techniques were used as described in (Green and Sambrook, 2012). Radiolabeled nucleotides were purchased from Department of Atomic Energy-Board of Radiation and Isotope Technology (DAE-BRIT), India.

3.3.2.2. Bioinformatic analysis

The nucleotide sequences near origin of Chr II (region 150-556) and Mp (region 177403-464) viz. upstream to *parA2B2* and *parA3B3* operons, respectively were analysed for the presence of repeats if any, using Mellina II web tool (Okumura *et al*., 2007). The web logo was generated to represent the consensus sequences for direct repeats (Crooks *et al*., 2004).

3.3.2.3 Cloning of *cis* elements in suicide plasmid of *D. radiodurans*

The 150-556 nucleotide region of Chr II (*cisII*) and 177403- 464 nucleotide region in MP (*cisMP*) were PCR amplified from genomic DNA of *D. radiodurans* using cisIIFw & cisIIRw and cisMPFw & cisMPRw primers, respectively (Table 2; Annexure I). The *cisII*was cloned at *Xba*I while *cisMP* at *Apa*I-*Eco*RI sites in suicide plasmid pNOKOUT (Khairnar *et al*., 2008) and pNOKcisII and pNOKcisMP plasmids, respectively were obtained (Table 3; Annexure I). These plasmids were maintained in *E. coli* for further use. Further, pNOKcisII, pNOKcisMP and pNOKOUT plasmids were transformed in wild type as well as *recA* mutant of *D. radiodurans* as described in material and methods. The transformants were scored TYG agar plates containing kanamycin (6 µg/ml).

3.3.2.4 Plasmid maintenance studies

For studying the maintenance of plasmid, the transformants were purified on kanamycin containing TYG agar plates and growth was monitored in replicates at 32°C for 24 h at O.D. 600 nm using Synergy H1 Hybrid Multi-mode microplate reader Bio-Tek under plasmid encoded selection pressure (kanamycin (6 µg/ml). The presence and maintenance of pNOKcisII and pNOKcisMP plasmids in *Deinococcus* was confirmed by isolation of these plasmids from their host cells as described earlier (Meima and Lidstrom, 2000) using solutions from GenElute Plasmid miniprep kit, Sigma-Aldrich, USA. In brief, pellet of 10

O.D. cells were resuspended in 150 µl of solution I containing lysozyme (10 mg/ml; Sigma, USA) and proteinase K (5 µg/ml; Sigma, USA). The cell suspension was incubated at 50°C for 30 min, followed by 5 min on ice and 1 min in boiling water. Subsequently, 200 µl of solution II was added to achieve cell lysis. To this 200 µl of solution III was added to precipitate chromosomal DNA and proteins. The precipitate was separated by centrifugation at 14000 RPM for 15 min and the aqueous phase was extracted twice with an equal volume of phenol-chloroform-isoamylalcohol (24:24:1) solution. The DNA was precipitated with 2.5 vol of 95% (vol/vol) ethanol in -20°C for 2 h followed by a wash with 70% (vol/vol) ethanol. Finally, the pelleted DNA was resuspended in 20 µl of MilliQ containing RNase A solution (Sigma-Aldrich, USA). The plasmid was checked on 1% agarose gel and verified by restriction digestion viz. pNOKcisII digested with *Xba*I while pNOKcisMP with *Apa*I-*Eco*RI to get the release of *cis* elements from respective plasmids.

3.3.2.5 Construction of knockout mutants

The knockout or deletion mutants of both the *cis* elements were made using pNOKOUT plasmid as described earlier (Charaka *et al*., 2012). In details, ~500 bps upstream and ~500 bps downstream fragments of *cisII* and *cisMP* were PCR amplified with the primers (Table 2; Annexure I) and cloned at the *Kpn*I-*Eco*RI and *Bam*HI-*Xba*I sites in pNOKOUT plasmid, respectively. The recombinant plasmids thus obtained pNOKCIIUD and pNOKCMPUD, respectively was linearized with *Xmn*I and transformed into *D. radiodurans*cells. The transformants were maintained through several rounds of sub-culturing, and the homozygous replacement of *cisII* and *cisMP* with *nptII* was ascertained by diagnostic PCR using flanking primersofthe target gene (Table 2; Annexure I).

3.3.2.6 Purification of DnaA and ParBs

The drdnaA gene (DR_0002) was PCR amplified from the genomic DNA of *D. radiodurans* R1 using pETdnaAF and pETdnaAR primers and cloned in pET28a (+) plasmid at *Bam*HI and *Eco*RI sites to yield pETDnaA plasmid (Table 3; Annexure I). This plasmid was maintained in *E. coli* NovaBlue host and used for purification of recombinant DnaA protein from *E. coli* BL21(DE3)pLysS host. The recombinant proteins were purified by nickel affinity chromatography, as described in (Modi et al., 2014). In brief, *E. coli* BL21 cells harboring pETDnaA was grown till 0.3 OD at 600 nm and then induced with 0.5 mM isopropyl-β-D-thiogalactopyranoside (IPTG). The cells were pelleted and stored in -70°C. For purification, the cell pellet was thawed and suspended in buffer A (20 mM Tris–HCl, pH 7.6, 300 mM NaCl and 10% glycerol) containing 15 mM imidazole, 0.5 mg/ml lysozyme, 1 mM PMSF, 1mM $MgCl_2$, 0.05 % NP-40, 0.05 % TritonX-100, protease inhibitor cocktail) and incubated on ice for 1h. Cells were sonicated for 5 min at 10s pulses with intermittent cooling for 15s at 35 % amplitude.The cell lysate was centrifuged at 11,000 RPM for 30 min at 4°C. The supernatant was loaded onto $NiCl_2$ charged-fast-flow-chelating-sepharose column (GE Healthcare) pre-equilibrated with buffer A containing 15 mM imidazole. The column was washed with 40 column volumes of buffer A containing 50 mM imidazole and 10 column volumes of buffer A containing 70 mM imidazole till proteins stop coming from the column. Recombinant proteins eluted in steps using 100 mM, 200 mM, 250 mM and 300 mM imidazole in buffer A and analyzed on 10% SDS-PAGE. Fractions with more than 95% pure protein were pooled and dialyzed in buffer A containing 200 mM NaCl and purified from HiTrap Heparin HP affinity columns (GE Healthcare, USA) using a linear gradient of NaCl. Different fractions were analyzed on SDS-PAGE and fractions containing pure protein were pooled and precipitated with 30% w/v ammonium sulphate at 8°C. The precipitate was dissolved in R-buffer (20 mM Tris-HCl pH 7.6, 0.1 mM EDTA, 0.5 mM

DTT) containing 1 M NaCl. After centrifugation at 16,000 RPM for 30 minutes, supernatant containing soluble proteins were processed for gel filteration chromatography. The fractions with pure protein were precipitated by ammonium sulphate and dissolved in R-buffer with 200 mM NaCl. The supernatant was dialyzed in dialysis buffer containing 20 mM Tris-HCl pH 7.6, 200 mM NaCl, 50% glycerol, 1mM $MgCl_2$, 0.5mM DTT and 1 mM PMSF. Protein concentration was determined by taking OD at 280 nm in Nanodrop (Synergy H1, Hybrid Multi-Mode Reader Biotek) using mass extinction co-efficient of the proteins. Purification of putative centromere binding protein ParB2 (Chr II) and ParB3 (Mp) was performed as described in chapter 3.2 (section 3.2.2.3).

3.3.2.7 DNA binding study

Electrophoretic mobility shift assay was performed to study the binding of DnaA, ParB2 and ParB3 with both full length *cis* elements and their fragments as described earlier (Charaka and Misra, 2012). In brief, the 400 bp fragment containing 10 direct repeats (*cisII*) or 8 direct repeats (*cisMP*) of 18 mer or 16 mer (Fig. 3.3.1) located upstream to *parA2B2* in chromosome II and *parA3B3* in megaplasmid, respectively were PCR amplified using sequence-specific primers (Table 2; Annexure I). Six or five repeats and three repeats of *cisII* and *cisMP* were also PCR amplified by changing forward primers (Table 2; Annexure I). Two repeats and one repeat were chemically synthesized and annealed with their complimentary strand (Table 2; Annexure I) after radiolabeling with [γ-^{32}P] ATP using T4 polynucleotide kinase. The PCR products were gel purified and radiolabelled at 5' end with [γ-^{32}P] ATP using T4 polynucleotide kinase. Approximately 30 nM radiolabeled substrate of different length from each *cis* element was incubated with different concentrations of purified recombinant DnaA, ParB2 or ParB3 in a reaction buffer containing 50 mM Tris-HCl (pH 8.0), 75mM KCl, 5mM $MgSO_4$ and 0.1mM DTT at 37°C for 15 min. For the competition

assay, saturating concentration of protein was incubated with different length of *cis* sequences followed by addition of different concentration of nonspecific competitor DNA of similar length as per experimental requirements. A 10-fold higher concentration of cold *cis* sequences was also used in competition assay for respective DnaA and ParBs interaction with *cis* elements. Mixtures were separated on 6-10 % native PAGE gels (depends on length of substrate DNA), the gels were dried, and autoradiograms were developed on X-ray films. The band intensity of bound and unbound fraction was determined by using Image J 2.0 software. The fraction of DNA probe bound to the protein was plotted as a function of the protein concentration by using GraphPad Prism 5. The Kdfor the curve fitting of individual plots was determined as described before (Charaka *et al*., 2012).

3.3.2.8 Determination of ploidy

Wild type and *cis* mutants were grown in TYG medium in the presence of required antibiotics if any. Equal OD_{600} nm cells were harvested from appropriate growth condition by centrifugation and were washed with 70 % ethanol solution. The ploidy of *cis* mutants was determined using qPCR as described in section 3.1.2.13 & 3.2.2.9 (Breuer*et al*., 2006).

3.3.3 Results

3.3.3.1. Identification of array of direct repeats present upstream to *parAB* operon in chromosome II and megaplasmid

We searched nucleotide sequence repeats of 16-17 mer upstream to *parAB* operon of Chr II and Mp using Melina II online tool. We found an array of 10 direct repeats of 17 mer upstream to *parA2B2* operon on Chr II (region 150-556) with consensus (CACAAAGTGCCACAGG). Similarly, an array of 8 direct repeats of 16 mer upstream to *parA3B3* operon on Mp (region 177403-464) with consensus (CGCAAAGGTG/ATCGCTA)

(Fig. 3.3.1). The position of these direct repeats near origin region and upstream to respective *parAB* operons has suggested their functional significance in genome replication and /or segregation.

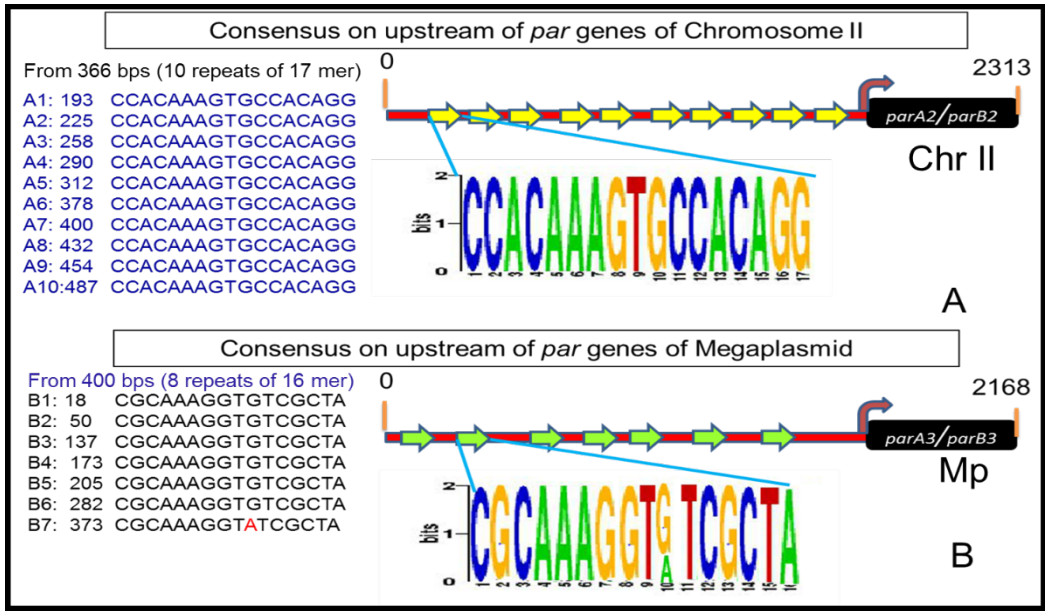

Figure 3.3.1 Organisation of repeats of *cisII* and *cisMP* sequences on chromosome II and megaplasmid in *D. radiodurans,* respectively.

3.3.3.2 Maintenance of non-replicative deinococcal plasmid carrying *cisII* and *cisMP* in *D. radiodurans*

The pNOKOUT, a colE1 origin of replication-based plasmid was defective in replication in *D. radiodurans*. Therefore, the role of *cisII* and *cisMP* in the maintenance of pNOKOUT in *D. radiodurans* was evaluated. For that pNOKcisII and pNOKcisMP plasmids bearing full length *cisII* and *cisMP* elements in pNOKOUT were transformed into *D. radiodurans* and their survival under plasmid born selection pressure (kanamycin:6 µg/ml) was monitored. The cells harboring pNOKcisII or pNOKcisMP were able to grow under selection pressure like untransformed wild type cells while vector control had failed to do so (Fig. 3.3.2 B, D). This was also checked in homologous recombination deficient Δ*recA* mutant of *D. radiodurans*. We observed that pNOKcisII and pNOKcisMP plasmids could

maintain in Δ*recA* mutant too (Fig. 3.3.2 C), which indicated that plasmid marker assited selection of clones bearing these plasmids does not seem to be due to homolgous recombination of these plasmids with respective genome elements.

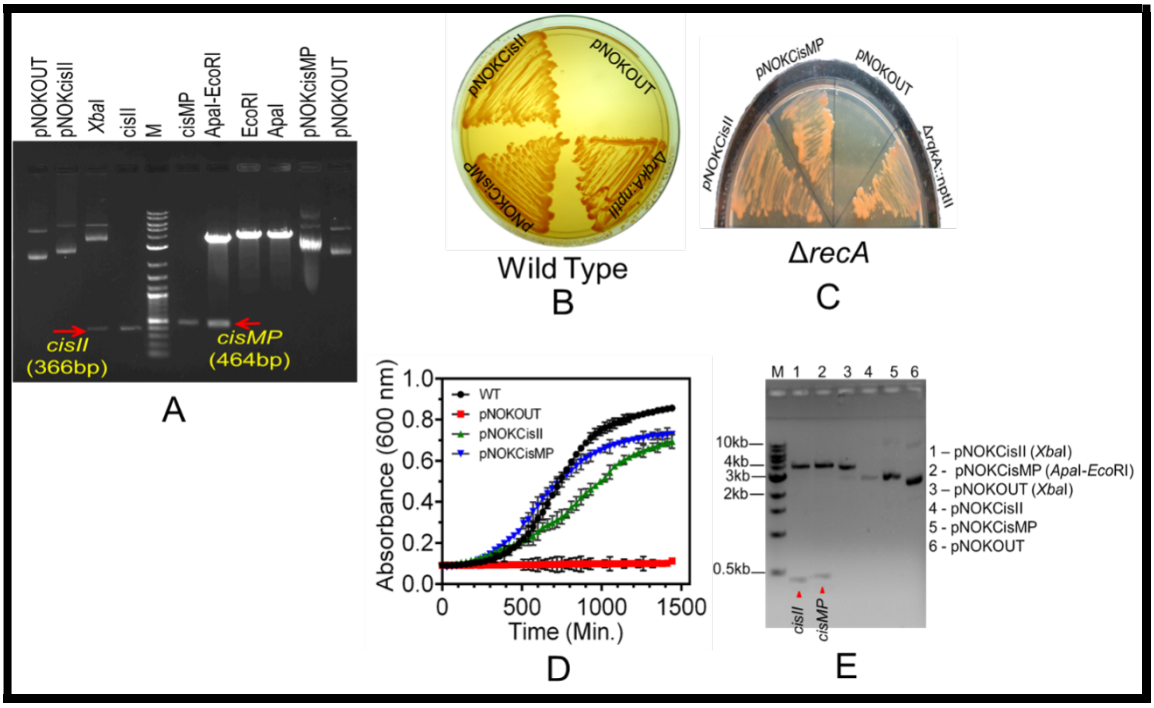

Figure 3.3.2 Cloning, transformation and maintenance of *cis* elements containing pNOKOUT plasmid in *D. radiodurans*. Cloning of *cisII* and *cisMP*elements in deinococcal suicide plasmid (pNOKOUT) yielded pNOKCisII and pNOKCisMP, respectively (**A**). These constructs were transformed in wild type and *ΔrecA* mutant of D. radiodurans, and streaked on TYG/kanamycin plate (**B, C**) as well as in broth (**D**). The respective plasmids were isolated from *ΔrecA* and verified by resitriction digestion (**E**). *ΔrqkA*::nptII used as positive control.

The independent maintenance of these plasmids was further confirmed by isolation of these plasmids followed by restriction analysis. We isolated pNOKcisII and pNOKcisMP plasmids from Δ*recA*cells and verified the presence of *cis* elements by restriction digestion (Fig. 3.3.2 D). This further supported our observation that these *cis* elements are of origin of replication nature as they supported independent maintenance of non-replicative plasmid (pNOKOUT) in *D. radiodurans*.

3.3.3.3. DNA binding studies of *cisII* and *cisMP* elements with deinococcal replication initiator protein DnaA

The *in vivo* role of *cisII* and *cisMP* in replication in *D. radiodurans* was supported with the *in vitro* DNA binding studies of full length as well as smaller fragments of both the *cis* elements with deinococcal replication initiator protein DnaA. The recombinant deinococcal DnaA protein was purified from *E. coli* (Fig.3.3.3 A). The *cis* elements containing multiple direct repeats located near origin of secondary genome elements and upstream to respective *parAB* operons were identified bioinformatically (Fig. 3.3.1). These were found containing the signature of origin of replication (i.e. DnaA boxes). The full length, 6 or 5 repeats and 3 repeats of *cis* element from chromosome II (*cisII*) and megaplasmid (*cisMP*) were PCR amplified while 2 repeats and 1 repeat of them were chemically synthesised and annealed (Fig. 3.3.3 B). The interaction of recombinant DnaA with different number of repeats in *cis* elements was checked *in vitro* by EMSA. DnaA showed sequence-specific interaction with both *cisII* and *cisMP* sequences *in vitro* (Fig. 3.3.3 C, D). The Kd value of interaction between DnaA and substrate having different number of repeats of each *cis* element has been tabulated in table 3.3.1. A comparative analysis of affinity (in term of Kd values) of DnaA with these *cis* elements revealed that both *cisII* and *cisMP* interacts to DnaA *albeit* with different affinity. The *cisII* is having better affinity than *cisMP* with DnaA possibly due to occurrence of perfect DnaA boxes in *cisII* than *cisMP*.

Table 3.3.1 Dissociation constant of *cisII*&*cisMP* interaction with deinococcal DnaA proteins

	Dissociation constant (Kd) (μM)	
Repeat No.	***cisII* variants**	***cisMP* variants**
Full length	0.31 ± 0.004	0.56 ± 0.21
6/5 repeats	0.70 ± 0.35	0.89 ± 0.39
3 repeats	0.80 ± 0.11	1.4 ± 0.7
2 repeats	No significance	No significance
1 repeat	No affinity	No affinity

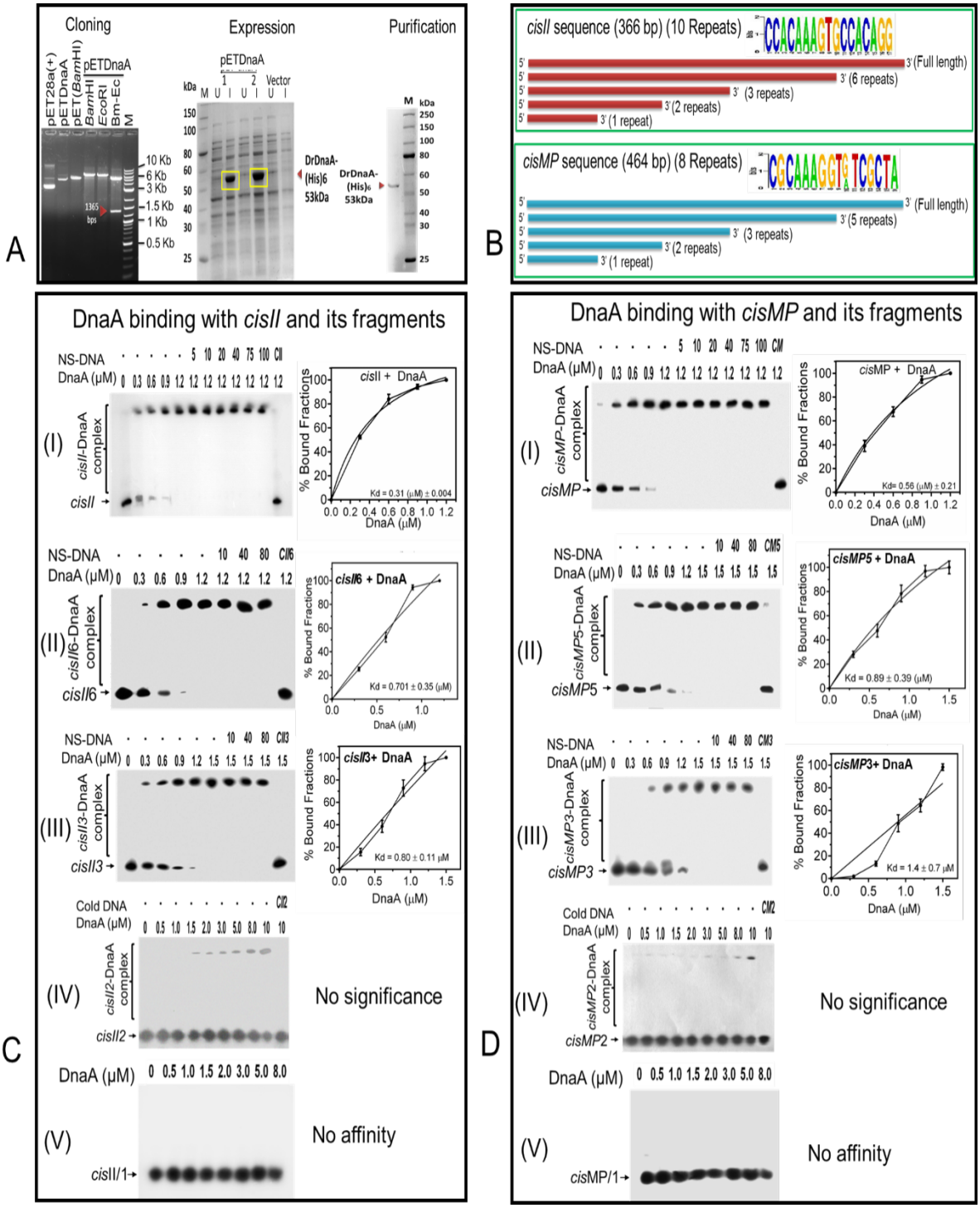

Figure 3.3.3 Purification of recombinant DnaA and its binding with *cisII* and *cisMP* as well as their smaller fragments. Deinococcal *dnaA* was cloned, expressed and purified from *E. coli* BL21 (see section 3.3.2.6) (**A**). Different fragments of *cisII* and *cisMP* were generated by PCR or oligos annealing, and radiolabelled (section 3.3.2.7) (**B**). Different concentrations of DnaA were incubated with diffrernt number of repeats of *cisII* (**C**) and *cisMP* (**D**). Saturating concentration of DnaA was also chased with 5-100 molar excess of non-specific DNA (NS-DNA). Percent bound fraction was calculated by densitometric analysis and ploted with DnaA concentration to find dissociation constant (see section 3.3.2.7).

The affinity analysis suggests that at least 3 direct repeats of both the *cis* elements are required for efficient binding with DnaA (Table 3.3.1). The DnaA bound to either of *cis* elements remained unaffected even in the presence of a 100-fold-higher molar concentration of non-specific DNA while titrated out completely with 10-fold less molar excess of specific DNA as compared to non-specific DNA (Fig. 3.3.3). The interaction of both *cisII* and *cisMP* containing several directs repeats with deinococcal replication initiation protein DnaA suggested the origin of replication feature of both the *cis* elements present on respective genomic replicons.

3.3.3.4. Copy number determination in *cis* mutants

Since both *cisII* and *cisMP* have shown signature of origin of replication, effect of deletion of these *cis* elements from genome on copy number of respective genomic element in *D. radiodurans* was hypothesized and tested. We have individually replaced full length *cisII* and *cisMP* with *nptII* cassettes in Chr II and Mp and mutants were named Δ*cisII* and Δ*cisMP,* respectively (Fig. 3.3.4C-E). Genome copy number in these mutants was determined by qPCR and compared with wild-type cells. We observed that deletion of *cisII* and *cisMP* has significantly affected the copy number of cognate genome elements while the copy number of Chr I was marginally affected (Fig. 3.3.4F). In detail, Δ*cisII* showed reduction in the average copy number of Chr I from 8 to 6, Chr II from 6 to 1.5, Mp from 11 to 6 and no effect on small plasmid. On the other side, deletion of *cisMP* has reduced the average copy number of Chr I from 8 to 7, chr II from 6 to 3, Mp from 11 to 2 and small plasmid (SP) from 9 to 5 (Fig. 3.3.4F). Such reduction in ploidy of secondary genome elements after deletion of their origin proximal *cis* elements could be accounted to their roles in either replication and or segregation of these replicons. These observations together supported the origin of replication nature of these *cis* elements in *D. radiodurans*.

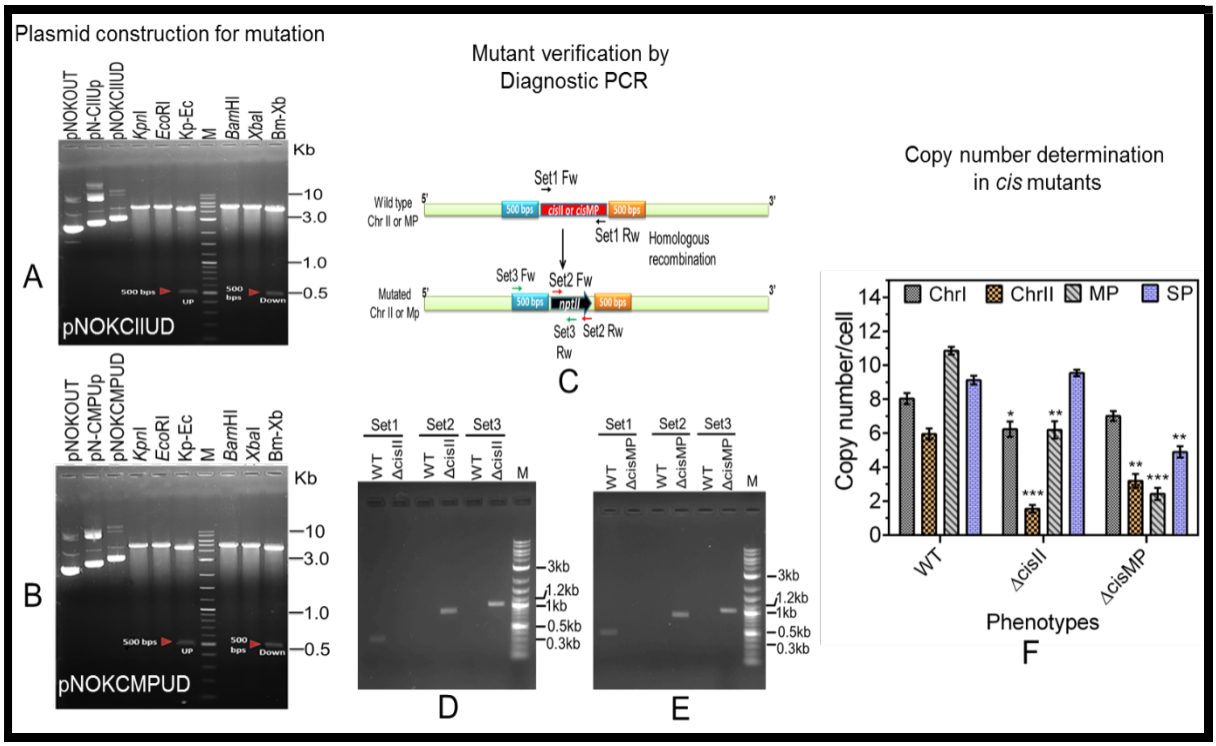

Figure 3.3.4 Generation of *cisII* and *cisMP* deletion mutants and determination of ploidy in *D. radiodurans*. Plasmids pNOKCIIUD (**A**) and pNOKCMPUD (**B**) were constructed from pNOKOUT plasmid (see section 3.3.2.5; Table 2.4), linearized and transformed in *D. radiodurans* to generate Δ*cisII* and Δ*cisMP* mutants. These mutants were confirmed by diagnostic PCR using different primer sets (Set1-3) (**C-E**). Copy number of Chr I, Chr II, megaplasmid (MP) and small plasmid (SP) in these cis mutants was determined by qPCR and compared with wild type (WT) (see section 3.3.2.8; **F**).

3.3.3.5 The *cis* elements have shown specific interaction with secondary genome ParBs of *D. radiodurans*

The *cis* elements (*cisII* and *cisMP*) having multiple direct repeats with signature of putative centromeres located upstream to *parAB* operons were predicted bioinformatically (Fig. 3.3.1). To test the centromeric nature of these cis elements, we monitored their interaction with secondary genome ParBs (ParB2 and ParB3). Both proteins were purified as described in (section 3.2.2.3; Fig. 3.2.2).

Both *cisII* and *cisMP* were PCR amplified from genome and their interaction with both recombinant ParB2 and ParB3 was checked by EMSA. We observed a sequence-specific interaction of both ParB2 and ParB3 with *cisII* and *cisMP* sequences (Fig. 3.3.5) with a Kd

value of 0.39 ± 0.01 µM and 0.58± 0.07 µM, respectively. Interestingly, both ParB2 and ParB3 have also shown sequence specific interaction with non-cognate *cis* elements. For instance, ParB2 interacted with *cisMP* and ParB3 with *cisII*albeitat lower affinity with a Kd of 1.16 ± 0.002 µM and 1.47 ± 0.03 µM, respectively than their cognate *cis* elements (Fig. 3.3.5).

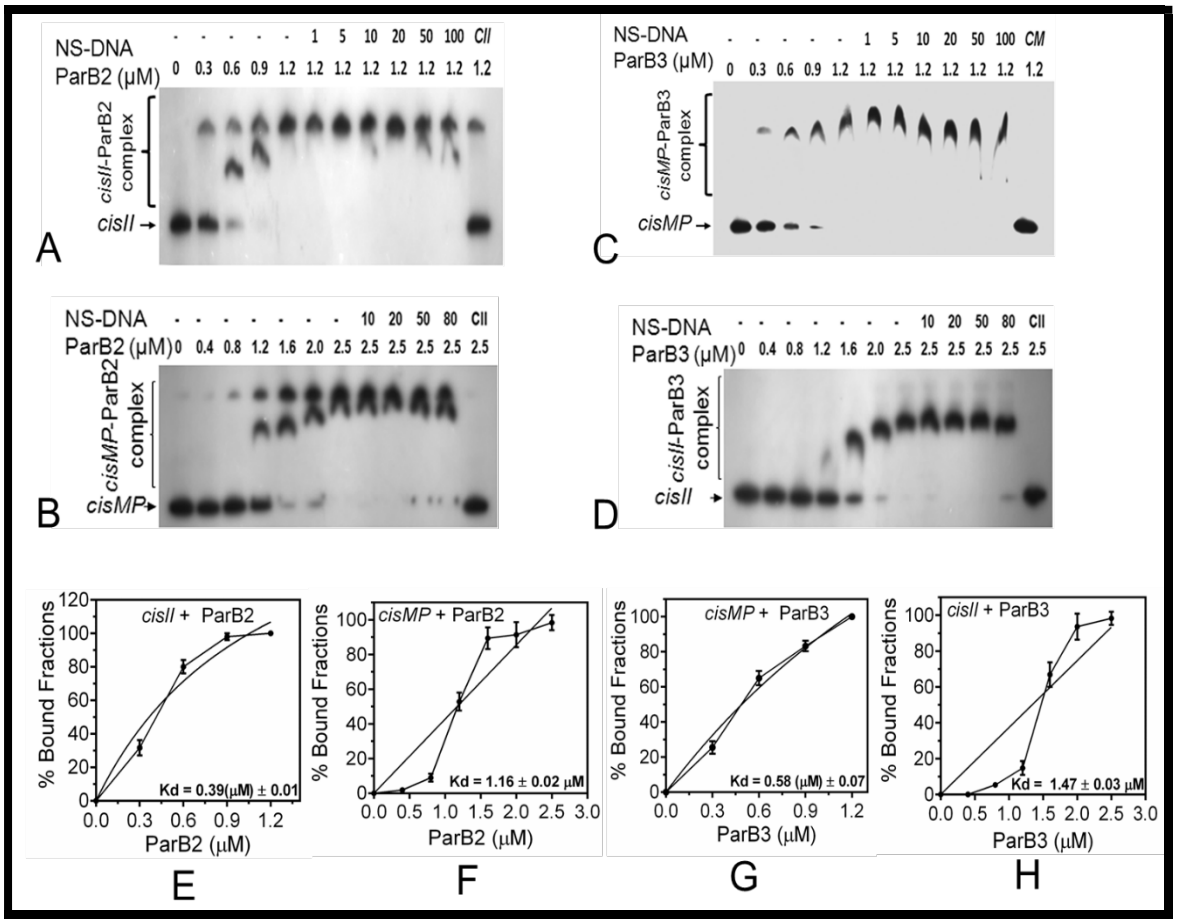

Figure 3.3.5 Interaction of ParB2 & ParB3 with *cisII* and *cisMP* elements. The DNA binding activity of ParB2 (**A, B**) and ParB3 (**C, D**) was checked with *cis* elements present upstream to *parA2B2* (*cisII*) and *parA3B3* (*cisMP*) operon in *D. radiodurans.* PCR amplified *cisII* and *cisMP* were gel purified and radiolabelled with [γ-^{32}P] ATP. 30nM radiolabelled DNA was incubated with different concentrations of recombinant ParBs. For competition assay, the *cis*-elements were incubated with saturating concentration of ParBs and chased with increasing amount (1-100 molar ration) of nonspecific dsDNA (NS-DNA; 400bps) as well as 10 molar excess of cold *cisII* (CII) and *cisMP* (MP), respectively. Products were separated on 6% native PAGE gels and dried. The autoradiograms were developed, and band intensity was quantified and % bound fractions was calculated, plotted for determination of dissociation constant (*Kd*) as described in methods (**E-H**).

These results suggest a possibility of redundancy among secondary genome ParB's interaction with centromeric sequences. The interaction of ParBs to *cis* elements remained unaffected even in the presence of a 80-100 fold higher molar concentration of non-specific DNA while titrated out with less than 10-fold molar concentration of specific DNA (cold *cisII* or *cisMP*) (Fig. 3.3.5).

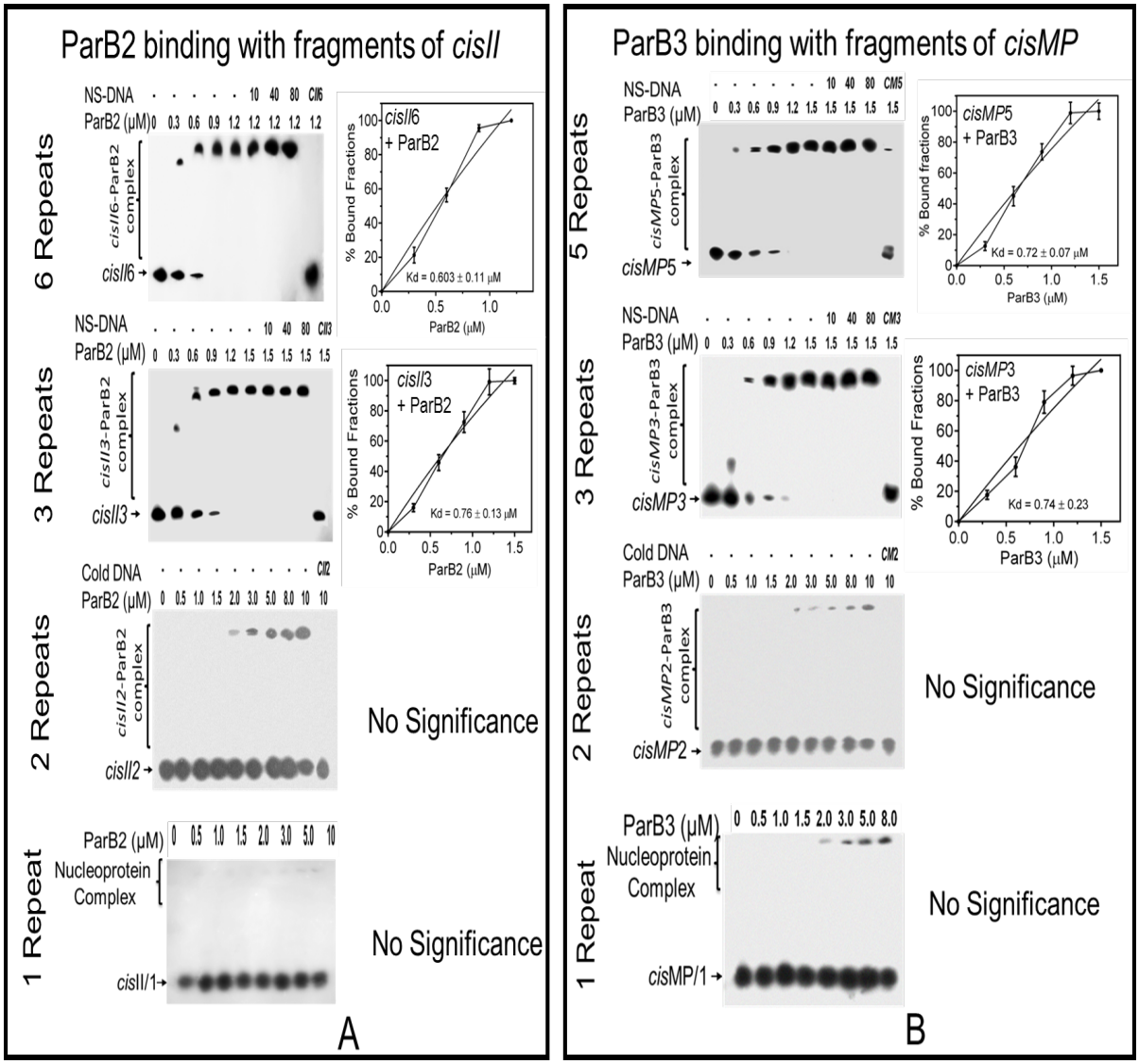

Figure 3.3.6 Binding of ParB2 and ParB3 with different fragments of their cognate *cis* elements. Different fragments of *cisII* and *cisMP* were generated by PCR or oligos annealing, and radiolabelled (section 3.3.2.7). Different concentrations of ParB2 and ParB3 were incubated with diffrernt number of repeats of *cisII* (**A**) and *cisMP* (**B**), respectively. Saturating concentration of DnaA was also chased with 10-80 molar excess of non-specific DNA (NS-DNA). Percent bound fraction was calculated by densitometric analysis and ploted with ParBs concentration to find dissociation constant (see section 3.3.2.7).

Table 3.3.2 Dissociation constant of *cisII* & *cisMP* interaction with deinococcal ParBs.

	***cisII* element**		***cisMP* element**	
Repeat No.	Dissociation constants (Kd) [μM]			
	ParB2	**ParB3**	**ParB2**	**ParB3**
Full length	0.39 ± 0.01	1.47 ± 0.03	1.16 ± 0.02	0.58 ± 0.07
6/5 repeats	0.60 ± 0.11	-	-	0.72 ± 0.07
3 repeats	0.76 ± 0.13	-	-	0.74 ± 0.23
2 repeats	Insignificant	-	-	Insignificant
1 repeat	Insignificant	-	-	Insignificant

In addition, we have determined the minimum size of *cisII* and *cisMP* that could interact with ParB2 and ParB3*in vitro*. We used 6 or 5 repeats, 3 repeats, 2 repeats and 1 repeat versions of both the *cis* elementsand monitored their interaction with cognate ParBs (ParB2 or ParB3) (Fig. 3.3.6). The Kd value of interaction between ParBs and different repeats of each *cis* elements were determined and givenin Table 3.3.2. Results showed that a minum of 3 direct repeats of either *cisII* or*cisMP* is required for efficient binding with cognate ParBs at least *in vitro* (Table 3.3.2). Two repeats and one repeat of *cis* elements have shown insignificant interaction with ParB proteins. These results together suggested that ParB2 and ParB3 bind to both *cisII* and *cisMP* with different affinity such as higher affinity for cognate than non-cognate*cis* elements. Thus, apart from the origin of replication nature, these *cis* elements seem to act as centromerealso for secondary genome elements in *D. radiodurans*.

Segregation of duplicated genome wouldrequire for cytokinesis i.e. cell division. During initiation of replication in bacteria, replication initiation protein DnaA recognizes origin of replication sequnces also called *oriC*. In *E. coli, oriC* is an AT rich region which contains three A–T rich 13 mer repeats and four 9-mer repeats called as DnaA boxes. DnaA binds specifaclly to these DnaA boxes to inititate replication with the subsequent loading of DnaB-DnaC complex (Baker and Wickner, 1992). As discussessd elsehwere in the thesis,

segregation of duplicated genome utilizes a tripartite system where a centromere binding protein, ParB or its homologs binds specifically to a cemtromeric sequence and form segregation complex which get separated to daughter cells through the polymeirzation and depolymerization kinetics of motar protein, ParA or its homologs. The centromeric sequences are usually repeatative in nature and mostly distributed around origin of chromosome (Livny, 2007). There are cases where centromere and *oriC* lie in close vicinity or overlap (for example *P. putida*, *S. coelicolor, B. subtilis*) (Bartosik and Jagura-Burdzy, 2005). Such conditions suggest interdependent regulation of replication and segregation in these bacteria.

D. radiodurans, an extremophile, contains multipartite genome where each replicon is having its own partitioning system. Chromosome I contains three centromeric sequences (*segS*1-3). In this, *segS*1 lies close to $oriC_1$ (origin of replication of chromosome I) while *segS2* and *segS3* are positioned far from $oriC_1$(Charaka and Misra, 2012). Unlike chromosome I, we found an array of 10 direct repeats of 17 bp on chromosome II and 8direct repeats of 16 bp on megaplasmid. These direct repeats are located upstream to respective *parAB* operons near the putative origin. We hypothesized the possibility of these repeats (called as *cis* elements) to be centromere or origin of replication sequences for respective replicons and tested it by utilizing genetic and biochemical approaches. We found that these direct repeats could help to maintain pNOKOUT (a non-replicative plasmid for *D. radiodurans*) plasmid in *D. radiodurans* or its *ΔrecA* mutant as well as replication initiator protein DnaA bound them with high specificity. Reduction in number of repeats in respective motif has reduced their affinity indicating the structural significance of repeats in an array for their function as origin of replication. The *ori* nature of these elements was further confirmed by deletion analysis where deletion mutants of both the *cis* elements have significantly reduced the copy number of secondary genome elements in *D. radiodurans.* The residual levels of copy number also indicated the possible roles of these *cis* elemetns in ploidy

regulation and /or functioning of non-canonical *ori* in maintaining minimal copy numbers of these genome elements in *cis* mutants of this bacterium. These observations together suggested a strong possibility of these *cis* elemenets function as origin of replication in this bacterium. Location of these elements upstream to *parAB* operon, which is typically observed in TGS organization in plasmid or chromosome in many bacteria and the specificity of these elements for ParBs together supported their centromeric nature. Interaction of ParB2 and ParB3 with non-cognate *cis* elements is surprisingly suggesting the functional redundancy amongst secondary genome partitioning system in this bacterium, which has not been reported in limited studies on multipartite genome system in bacteria. The differences in the affinities of both DnaA and ParBs with varying size of these repeats further characterized these elements as *ori* and centromere like elements at least *in vitro*. Thus, these results together report the characterization of an array of direct repeats present upsteam to *parAB*operons of chromosome II and megaplasmid in *D. radiodurans* as origin of replication and an overlap of both *ori* and centromere functions in respective genome elements of this bacterium.

Chapter 3.4

Genome tagging and its localization during growth of *D. radiodurans*

3.4.1 Introduction

The compaction and organization of large genomic DNA in a limited cell volume of both prokaryotes and eukaryotes is an interesting aspect in genome biology. Most of the studies regarding chromosome organization and its dynamics have been done in eukaryotes (Gasser, 2002). In recent times, the availability of high resolution microscopic techniques has helped in understanding of the bacterial chromosome structure and organization. The first method developed for subcellular localization of different loci in bacterial chromosome was FISH (fluorescence *in situ* hybridization) which utilizes the fluorescently-labeled DNA probe against the complimentary region of chromosome (Niki *et al*., 2000). Due to fixation of cell during FISH, it failed to get the understanding of chromosome dynamics during cell growth. This problem was solved by development of another fluorescence-based technique called FROS (Fluorescent Reporter-Operator System). FROS consists of a reporter (*trans* factor) tagged with fluorescent protein, which would specifically bind to its operator (*cis* element) inserted in genome elements (Lau *et al*., 2003). The most studied FROS are *tetO*/TetR and *lacO*/LacI, which have been used in a number of prokaryotic and eukaryotic systems to study genome biology like genome dynamics, position of origin and terminus region of genome, genome segregation etc (Teleman *et al*., 1998; Webb *et al*., 1997; Thrower and Bloom, 2001; Lau *et al*., 2003, Vallet-Gely and Boccard, 2003; Wang *et al*., 2006; Viollier *et al*., 2004; Sellars *et al*., 2017).

D. radiodurans, Gram-positive bacterium resistant to extreme doses of gamma radiation and oxidative stress, harbors multipartite genome system consisting of 2 chromosomes and 2 plasmids. In 2006, Minsky and colleagues demonstrated that the polyploid multipartite genome of *D. radiodurans* is intertwined together in form of a doughnut shaped torroid structure. They implicated torroidal packaging of its genome to extreme resistance of DNA

strand breaks and efficient repair. However, toroidal packaging of polyploid multipartite genome raises several questions related to bacterial genome biology. These include; how each replicon exists in this compact structure and how genome dynamics will regulate replication, segregation, DNA repair & recombination etc., and vice versa, under normal as well as gamma radiation stressed conditions? This chapter describes my efforts of developing *tetO*/TetR and *lacO*/LacI based FROS for the genome elements in *D. radiodurans* and monitoring of real time dynamics of multipartite genome during growth of this bacterium. For that, the different genome elements of *D. radiodurans* were inserted with an array of *tetO* and *lacO* repeats and TetR and LacI were expressed as GFP and RFP fusions in *in trans*. The cells expressing fluorescent proteins fusion of the reporter system in bacterial genome containing *cis* elements were observed under fluorescence microscope. Our results suggest that each cell of tetrad have all replicons as revealed by formation of distinct foci inside the cell. Further, dynamics of FROS taged different genomic replicon of *D. radiodurans* during post irradiation recovery will be interesting and worth to study independently.

3.4.2 Materials and methods

3.4.2.1 Bacterial strain, plasmids and oligonucleotides

For fluorescent tagging of different genomic replicons of *D. radiodurans*, we have used *tetO*/TetR and *lacO*/LacI based Fluorescence Reporter Operator System (FROS). *D. radiodurans* was grown in TYG medium as described in previous chapters. Plasmids like pLAU43 (carrying an array of 240 repeats of *lacO;* a kind gift from Dr. Lucy Shapiro, Stanford University, USA), pLAU44 (carrying an array of 240 repeats of *tetO;* CGSC, Yale University, USA), pLAU53 (carrying *lacI* and *tetR* genes; CGSC, Yale University, USA), pDSW208, pDsRed, pVHS559, pRADgro and their variants were maintained in *E. coli* NovaBlue or DH5α (Table 3; Annexure I). Oligonucleotide primers were used to amplify

different genomic locations for integration and genes for the expression from plasmid to generate fluorescent fusions, and diagnosis of gene integration through PCR have been listed in (table 2; Annexure I).

3.4.2.2 Construction of translational fusion of reporter genes and their expression

The repoter genes, *lacI* and *tetR,* were PCR amplified from pLAU53 (Lau *et al*., 2003) using gene specific primers (Table 2; Annexure I) and cloned in pDsRed (at *Bam*HI and *Kpn*I) and pDSW208 (at *Sac*I and *Sal*I) to give pDRedLacI and pDTRGFP plasmids, respectively. These plasmids express reporter gene having C-terminal fluorescent tag; LacI-RFP from pDRedLacI and TetR-GFP from pDTRGFP. The expression of fluorescent tagged reporters was monitored in *E. coli* by western bloting using Anti-RFP or Anti-GFP antibodies and fluorescence microscopy under FITC or TRITC channels as required.

Since, pDsRed and pDSW208 plasmids are non-replicative in *D. radiodurans* so we subcloned *lacI-rfp* and *tetR-gfp* fusion fragment in *E. coli* - *D. radiodurans* shuttle vectors (pVHS559 and pRADgro) for their expression in *Deinococcus*. In brief, we PCR amplified *lacI-rfp* fragment from pDRedLacI using DsRedFw and DsRedRw primers, and *tetR-gfp* fragment from pDTRGFP using TetRscIApIFw and GFPXbaIRw primers (Table 2 Annexure I). The resulting PCR fragments; *lacI-rfp* was cloned in pVHS559 at *Sac*I-*Xho*I sites to give pVLacIRFP plasmid and *tetR-gfp* was cloned in pRADgro at *Apa*I-*Xba*I to give pRADTRGFP plasmid (Table 3: Annexure I). The expression of translational fusions from their respective plasmids in *E. coli* as well as *D. radiodurans* was confirmed by western bloting and fluorescence microscopy under FITC or TRITC channels as requried.

3.4.2.3 Construction of plasmids for genetic integration of operator in genome of *D. radiodurans.*

We have used *tetO* operator from pLAU44 and *lacO* operator from pLAU43 plasmids as described in (Lau *et al*., 2003). Both the plasmids contain an array of 240 repeats of respective operators. Since, both pLAU43 as well as pLAU44 is non-replicative in *D. radiodurans* due to presence of ColE1 origin of replication so we thought to use whole plasmid as a vehicle to integrate them at defined locations in different genomic replicons of *D. radiodurans.*

We chose the position near origin of Chr I, Chr II and Mp for insertion of operator sequences. In brief, we amplified region (10713-11715) correspond to 1.5˚ of Chr I using ChrI (1.5˚)Fw and ChrI (1.5˚)Rw primers, and region (4659-c5691) correspond to 4˚ of Chr II using ChrII(4˚) Fw and ChrII(4˚)Rw primers. These PCR fragments were cloned in pLAU44 at *Xba*I-*Sca*I sites to yield p44Ch1 or p44Ch2 plasmids having homologous sequences of Chr I and Chr II, respectively. Further, a spectinomycin resistance gene cassete with promoter from pVHS559 was amplified using SpecFw and SpecRw primers and cloned in p44Ch1 as well as p44Ch2 at *Nhe*I-*Xho*I sites to give p44SCh1 or p44SCh2, respectively. Likewise, region (2203-3000) correspond to 4.5˚ of Mp was amplified using Mp(4.5˚)Fw and Mp(4.5˚)Rw and cloned in pLAU43 at *Xba*I-*Sca*I sites to yield p43Mp plasmid (Kan^R). These constructs were confirmed by restriction digestion as well as diagnostic PCR using forward primer specific to insert (as mentioned above) and AmpRw (specific to vector) followed by DNA sequencing.

3.4.2.4 Integration of operators in different replicons of *D. radiodurans*

For integration of different operators at defined genomic location in *D. radiodurans*, we separately transformed p44SCh1 or p44SCh2 or p43Mp plasmids in the bacterium and scored the transformants either on TYG/spectinomycin or TYG/kanamycin as per requirement. Since, these plasmids are non-replicative in this bacterium so will integrate in genome via.

single crossover homologous recombination events. The transformant were maintened under antibiotics selection through several rounds of subculturing to achieve homogenous insertion of operators in genome. We examined the presence of integrated plasmid by diagnostic PCR using different sets of primer pairs (Table 2: Annexure I). The positive clones were stored with 20% glycerol in -70 degrees. The resulting strains were named as R1::ChrI-*tetO,* R1::ChrII-*tetO* and R1::Mp-*lacO* (Table 1: Annexure I).

3.4.2.3 Fluorescence microscopy

We transformed the different modified R1 strains of *D. radiodurans* carrying different operator sequences with their respective fluorescent protein fusions of trans factors containing plasmids. For instances, R1::ChrI-*tetO* was transformed with pRADTRGFP*,* R1::ChrII-*tetO* with pRADTRGFP while R1::Mp-*lacO* was transformed with pVLacIRFP. Theses tansformants were maintained in double antibiotic selection as required. Further, isolated colonies were subcultured in broth containing required antibiotics and induced overnight (for expression of LacI-RFP from pVLacIRFP) with 5mM IPTG once cell OD_{600} reached to 0.5-0.6. The TetR-GFP was expressed under constitutive promoter from pRADgro (Khairnar *et al*., 2008). Overnight grown cultures were harvested, washed with PBS, stained with DAPI and or Nile red and mounted on 0.8% agarose bed made over glass slide. The glass cover slip was placed over mounted samples and used for image aquasition in fluorescence microscope (Olympus IX83). We have imaged each sample in DIC, DAPI, FITC and TRITC channels, and acquired several fields for each sample. Images were scaled and processed using inbuilt software 'CellSens'.

3.4.3 Results

3.4.3.1 Translational fusions of fluorescent proteins of LacI and TetR were made and expressed in *D. radiodurans*

The functional fluorescent reporter operator systems (FROS) have been constructed for monitoring genome dynamics in *D. radiodurans* (Fig 3.4.1 and 3.4.2).

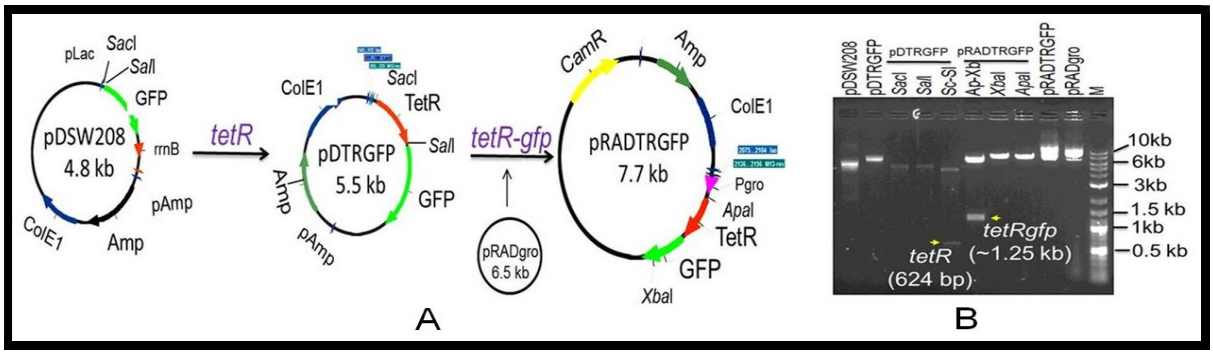

Figure 3.4.1Cloning of GFP tagged TetR in *E. coli* and *D. radiodurans*. A schematic ofcloning of*tetR* gene in pDSW208 to get PDTRGFP, then cloning of *tetR-gfp* in pRADgro to get pRADTRGFP (**A, B**).

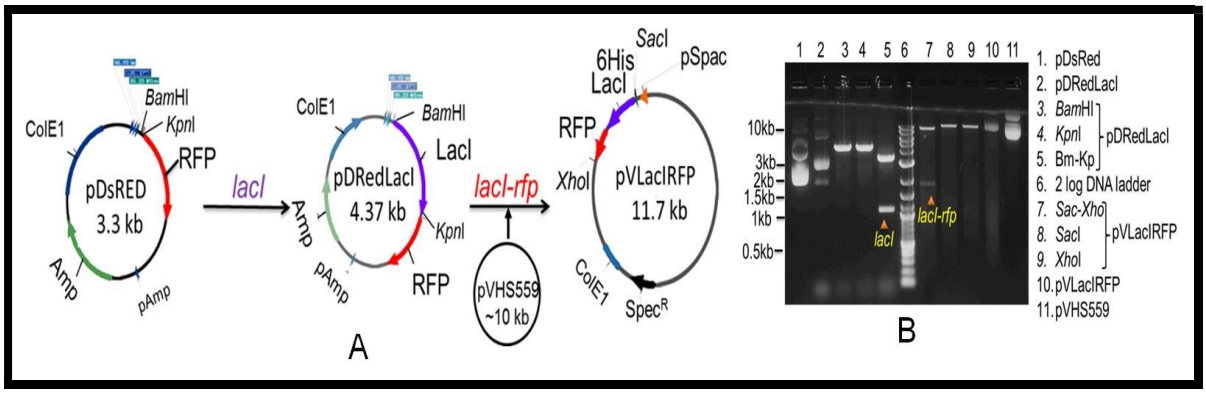

Figure 3.4.2Cloning of RFP tagged LacI in *E. coli* and *D. radiodurans*. A schematic of cloning of *lacI* gene in pDsRed to get pDRedLacI, then cloning of *lacI-rfp* in pVHS559 to get pVLacIRFP (**A, B**).

The GFP tagged TetR and RFP tagged LacI fusions were constructed in *E. coli-Deinococcus* shuttle vectors like pRADgro and pVHS559, respectively. The expression of these fusions was first ascertained in *E. coli* by immunoblotting with antibodies against GFP/RFP as required, and by fluorescence microscopy (Fig 3.4.3 and 3.4.4).

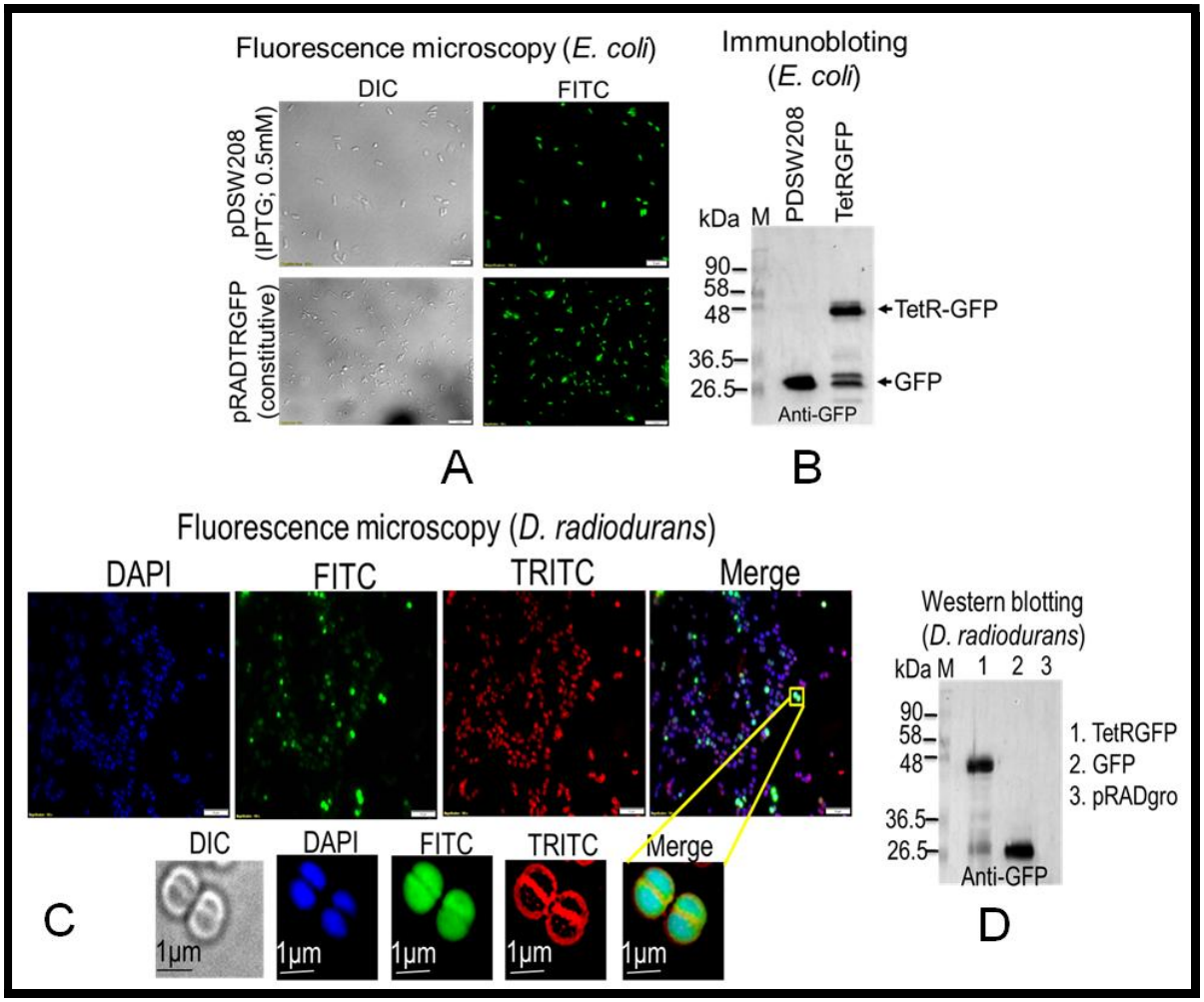

Figure 3.4.3 Expression of GFP tagged TetR in *E. coli* and *D. radiodurans*. Expression of TetRGFP in *E. coli* (**A** (scale 5µm)**, B**) and *D. radiodurans* (**C** (scale 10µm & 1 µm)**, D**) was confirmed by fluorescence microscopy and immunoblotting using Anti-GFP antibody (see section 3.4.2.2).

We observed *E. coli* cells expressing TetR and LacI fusions showed different microscopic patterns in *E. coli*. For instance, TetR expressing cells showed diffused fluorescence while LacI showed descrete foci formation. This result was pleasantly expected because *E. coli* genome contains *lacO* region and LacI-RFP foci formation in untransformed *E. coli* seems to be due its binding to *lacO*. Interestingly, *D. radiodurans* cells expressing TetRGFP or LacIRFP fusions did not form foci and fluorescence was observed throughput the cells (Fig. 3.4.3 and 3.4.4). This was also expected because *D. radiodurans* cells neither

have lac operon i.e. *lacO* nor *tet* operon i.e. *tetO*, hence no foci formation by both the reporter proteins in wild type cells.

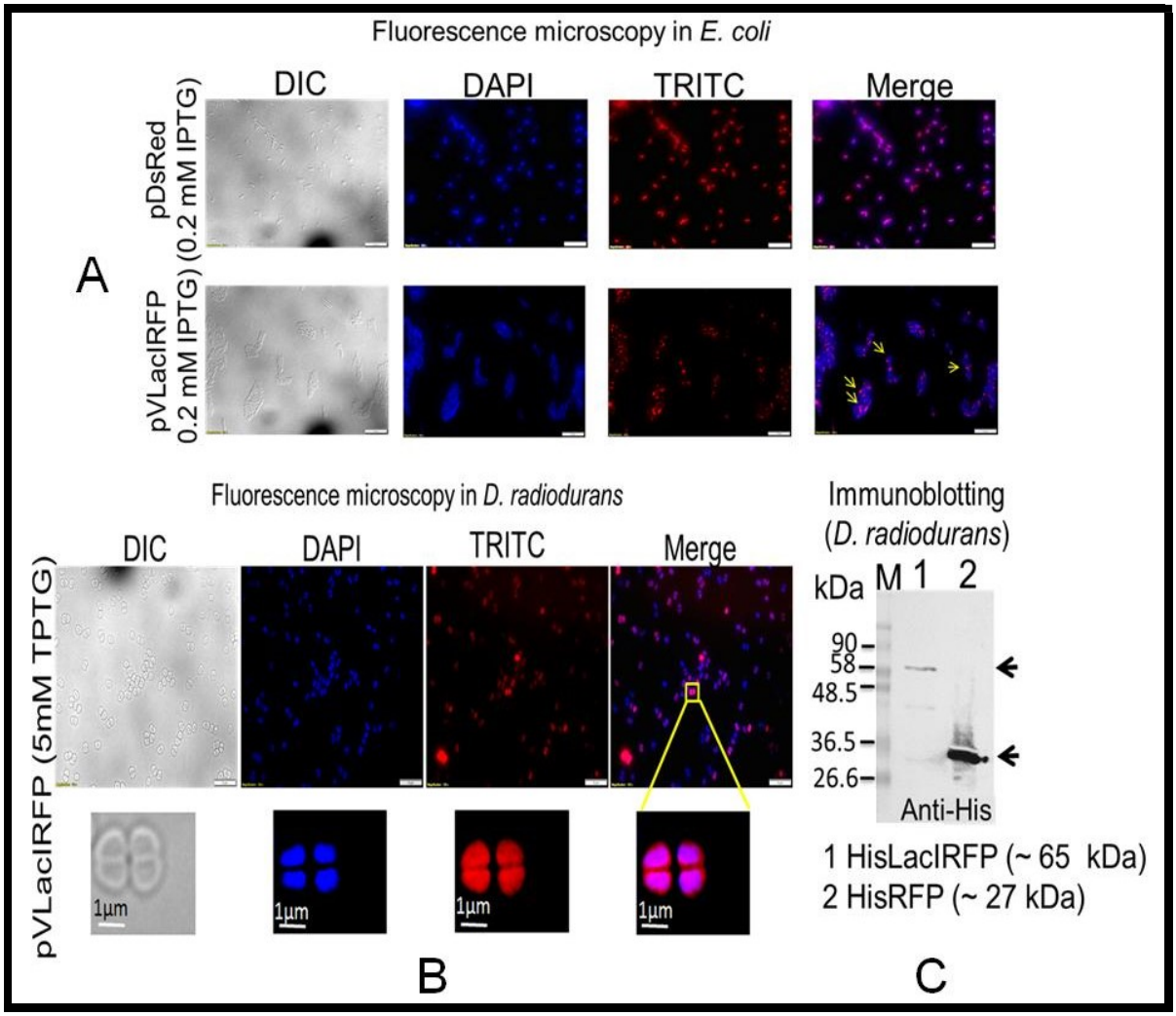

Figure 3.4.4 Expression of RFP tagged LacI in *E. coli* and *D. radiodurans*. Expression of LacIRFP in *E. coli* confirmed by fluorescence microscopy after DAPI stainig (**A** (scale 10µm)), and in *D. radiodurans* (**B** (scale 10µm & 1 µm)) was also confirmed by fluorescence microscopy after DAPI staining, and immunoblotting using Anti-polyHis antibody (**C**) (see section 3.4.2.2).

These results confirmed the successful construction fluorescent protein fusion with reporter genes and lack of non-specific binding with the genome sequence of this bacterium.

3.4.3.2 The binding sites of LacI and TetR were integrated in the genome of *D. radiodurans*

TetR binds to *tetO* and LacI binds with *lacO* sites. The *tetO* and *lacO* operator sequences were used from plasmids pLAU44 and pLAU43, respectively (Lau *et al*., 2003). Since, these plasmids were non-replicative in *D. radiodurans,* we have inserted DNA sequences homologous to genome of bacterium in these plasmids and used them for operator sequence integration at the defined locations in the genome of *D. radiodurans*.

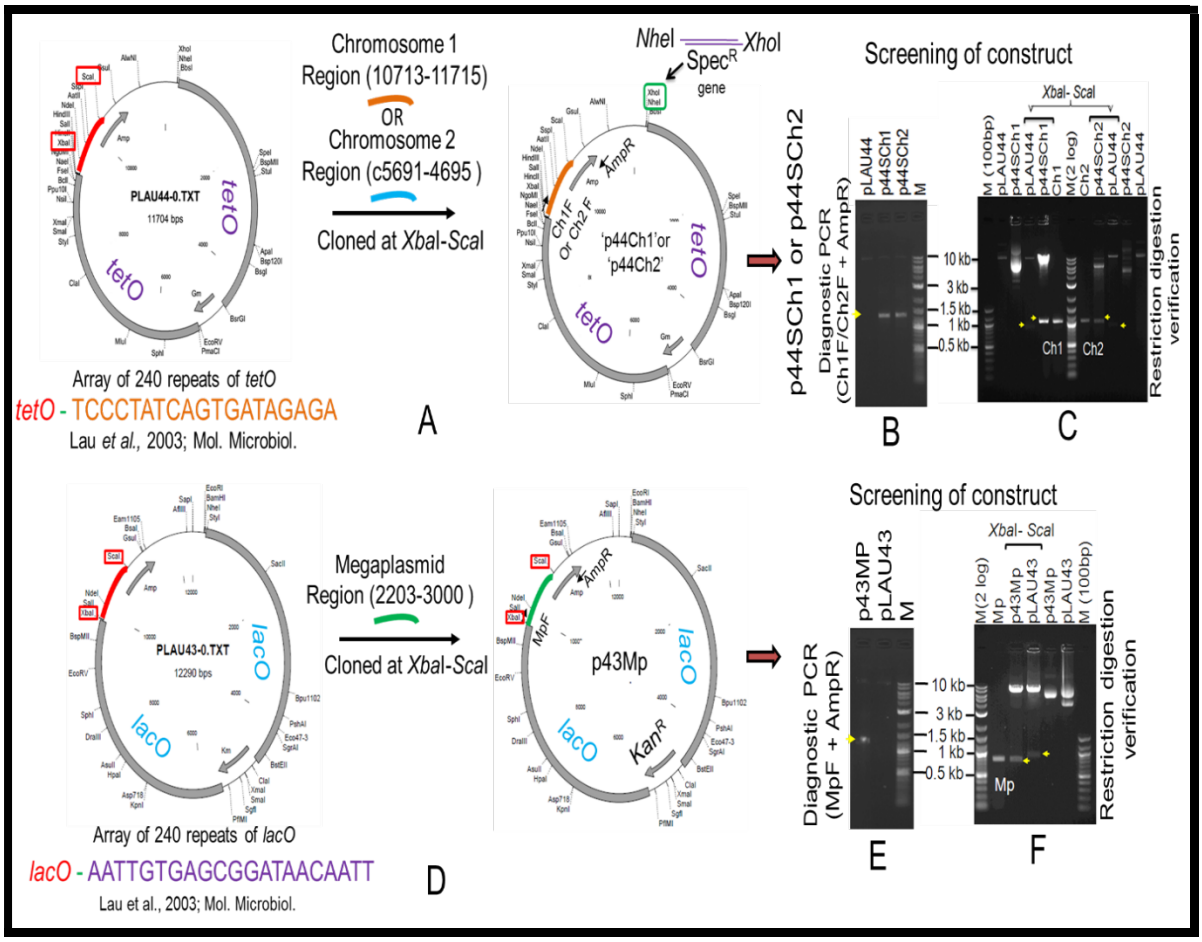

Figure 3.4.5 Construction and verification of suicide plasmids containing *tetO* or *lacO* repeats for integration in *D. radiodurans*. The genomic region 10713-11715 of Chr I, region 4659-c5691 of Chr II were cloned in pLAU44 (plasmid with *tetO*) to yield plasmids namely p44Ch1 or p44Ch2 (**A**; section 3.4.2.3). Further, a spectinomycin gene with promoter was inserted in p44Ch1 and p44Ch2 to give p44SCh1 and p44SCh2, respectively. These constructs were verified by diagnostic PCR (**B**) using target and vector specific primers, and restriction digestion (**C**). Similarly, region 2203-3000 of megaplasmid was inserted in pLAU43 (plasmid with *lacO*) to yield p43Mp, having kanamycin resistance. This was also verified by diagnostic PCR (**E**) and restriction digestion (**F**).

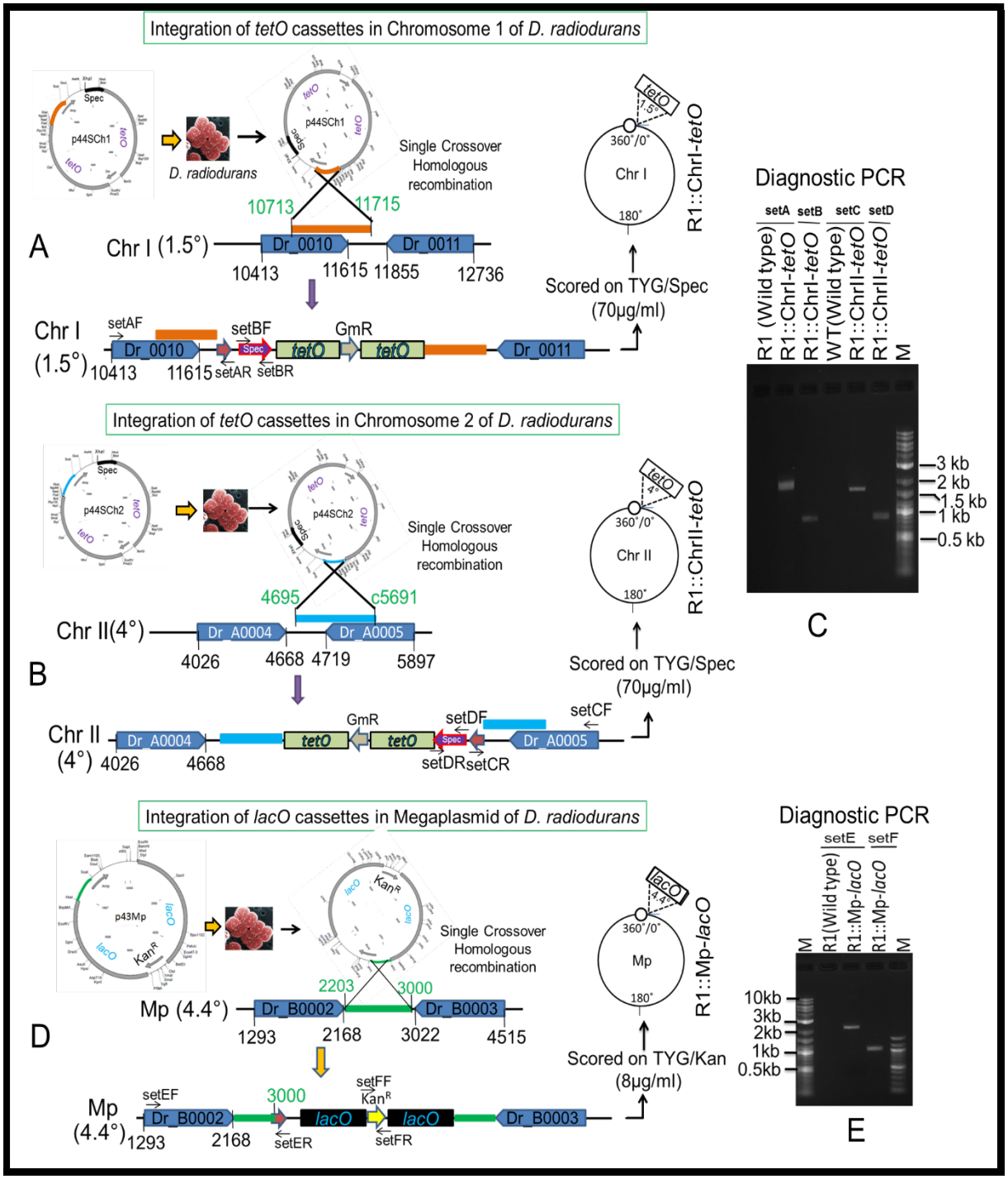

Figure 3.4.6 Integration of *tetO* cassettes in chromosome I & II and *lacO* cassettes in megaplasmid of *D. radiodurans*. Array of *tetO* containing plasmids p44SCh1 and p44SCh2 were intergrated in chromosome I (Chr I; region 10713-11715) and chromosome II (Chr II, region 4596-c5691), respectively by single crossover homologous recombination (**A, B**). The transformants were scored on TYG spectinomycin plates. Like wise, p43Mp plasmid integrated in megaplasmid (Mp; region 2203-3000) and scored at TYG kanamycin plates (**D**). Respective clones were screened by diagnostic PCR using different sets of primers (see section 3.4.2.4; **C, E**).

The 240 repeats of *tetO* were integrated between region 10713-11715 sequences in Chr I and 4659-c5691 region of Chr II separately using integrative plasmids namely p44SCh1 and p44SCh2 derived from p44Ch1 or p44Ch2, respectively and described in methods (section 3.4.2.3). We confirmed the construction of integrative plasmids by restriction digestion (using *Sca*I-*Xba*I) as well as diagnostic PCR. We found the release of insert at appropriate size after restriction digestion and amplication of region in PCR (Fig 3.4.5). These plasmids were used for transformation in *D. radiodurans* for their integration. Transformants were scored in the presence of spectinomycin. Similarly, 240 repeats of *tetO* were inserted in 2203-3000 region in megaplasmid using p43Mp plasmid expressing kanamycin resistance in *D. radiodurans*. We screened the integration of operator in different replicons using diagnostic PCR with the help of different primer sets as detailed in (Table 2: Annexure I). Those clones who have given amplification of required size during PCR were taken for further experiments. They were named as R1::ChrI-*tetO,* R1::ChrII-*tetO* and R1::Mp-*lacO* (Table 1; Annexure I, Fig. 3.4.6). These results provided evidence on successful integration of 240 repeats of *lacO* and *tetO* cis elements in different genome elements of *D. radiodurans*.

3.4.3.3 Functional characterization of FROS system

The FROS systems were checked in *E. coli*. For that, we have co-transformed p44SCh1 containing *tetO* element and pRADTRGFP plasmids in *E. coli* MG1655 and maintained the transformant in the presence of spectinomycin (70 µg/ml) and ampicillin (100 µg/ml). Likewise, p43Mp containing *lacO* and pVLacIRFP plasmids were co-transformed in *E. coli* MG1655 and maintained under selection of spectinomycin (70 µg/ml) and kanamycin (100 µg/ml).

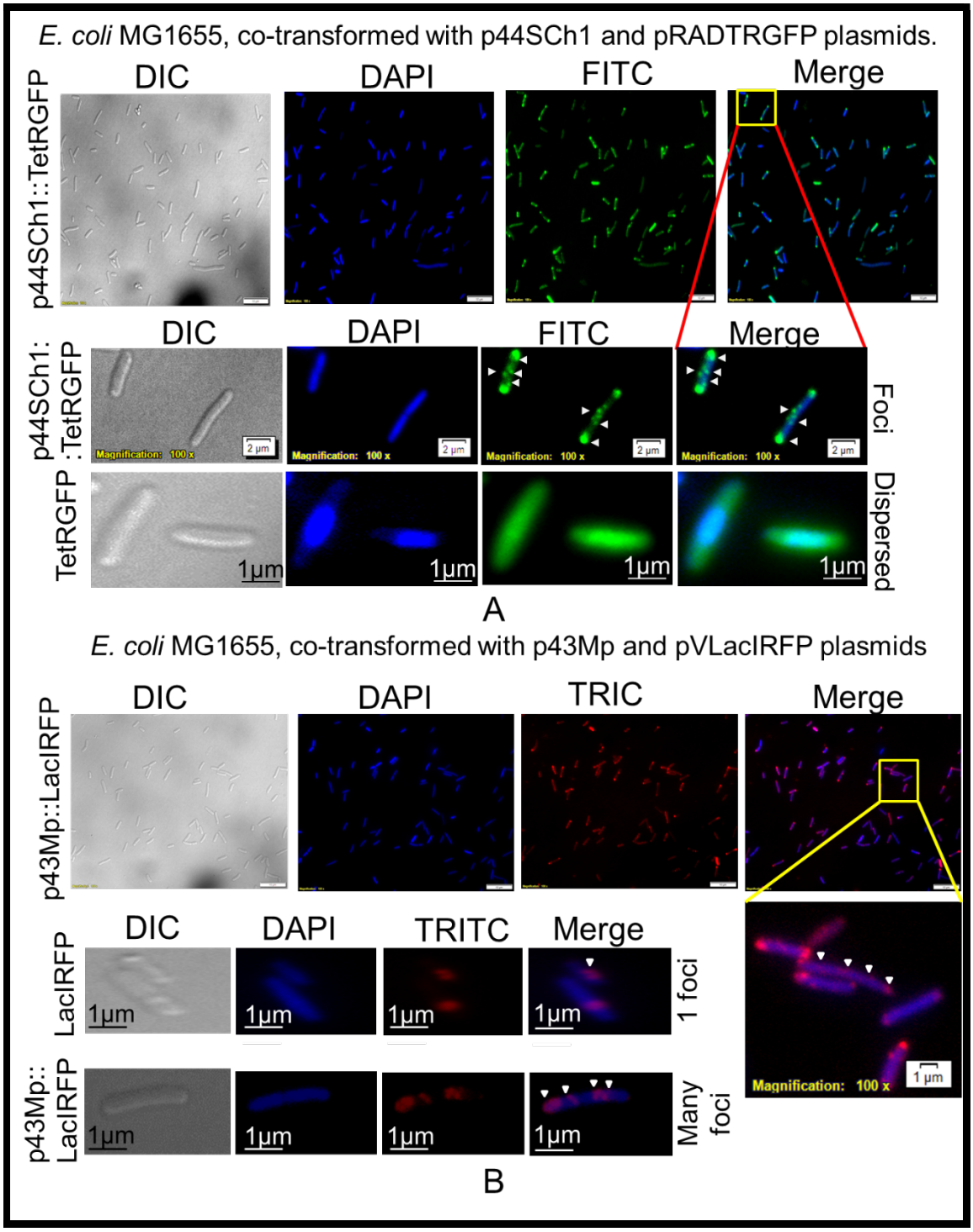

Figure 3.4.7 Verification of constructed *tetO*/TetR and *lacO*/LacI system in *E. coli.* *E. coli* MG1655 cells were cotransformed with *tetO* containing p44SCh1 plasmid and TetRGFP expressing pRADTRGFP plasmid, and fluorescene microscopy under DIC. DAPI (after DAPI staining) and FITC channels was performed. Cells expressing only TetRGFP used as control (**A**). Similarly, *E. coli* MG1655 cells were cotransformed with *lacO* containing p43Mp plasmid and lacIRFP expressing pVLacIRFP plasmid, and fluorescene microscopy under DIC. DAPI (after DAPI staining) and TRITC channels was performed. Cells expressing only LacIRFP used as control (**B**). Scale bar in upper panels of each figure is 10 µm.

We monitored the localization of TetRGFP or LacIRFP indivisualy in these cells and compare with *E. coli* cells carrying only pRADTRGFP or pVLacIRFP plasmid as vector controls, through fluorescence microscopy. We observed that *E. coli* cells carrying both reporter and operators on plasmid form several distinct foci accros the cell lenth, which were not observed in controls expressing only reporter proteins (Fig 3.4.7). These results suggested *tetO* and *lacO* interact specifically with the fusions of TetR and LacI reporter proteins, respectively and FROS system is active *in vivo* at least in *E. coli.*

3.4.3.4 Localization FROS-painted genome elements in *D. radiodurans*

The *D. radiodurans* cells containing tetO repeats in chromosome I (strain R1::ChrI-*tetO*)and in chromosome II (strain R1::ChrII-*tetO*), and lacO repeats in megaplasmid (strain R1::Mp-*lacO*) were expressed with TetR-GFP on pRADTRGFP, and LacI-RFP on pVLacIRFP, as required and these genome elements were localized microscopically. For that these cells were grown in log phase and observed under fluorescence microcope. The cells expressing reporter-fluorescent fusion alone showed fluorescence in whole cell. However, the cells expressing fluorescent protein tagged reporters in the presence of respective *cis* bindings element formed the distinct green or red foci in each cell of tetrad (Fig 3.4.8). This suggest that the foci formation has occurred due to binding of fluorescent tagged reporter proteins to cognate operator inserted near origin in different replicons in *D. radiodurans*. We could vizualise the position of each replicon (chromosomes and megaplasmid) in each cell of tetrad in this bacterium. The formation of distict foci in each cell of tetrad with different FROS system reflected the position of origin of replication of respective replicon (Fig. 3.4.8 A). Interestingly, there were few instances (in case of Chr II) where two distinct foci were observed in a single cell of tetrad possibly due to second round of replication initiation after segregation (Fig. 3.4.8B).

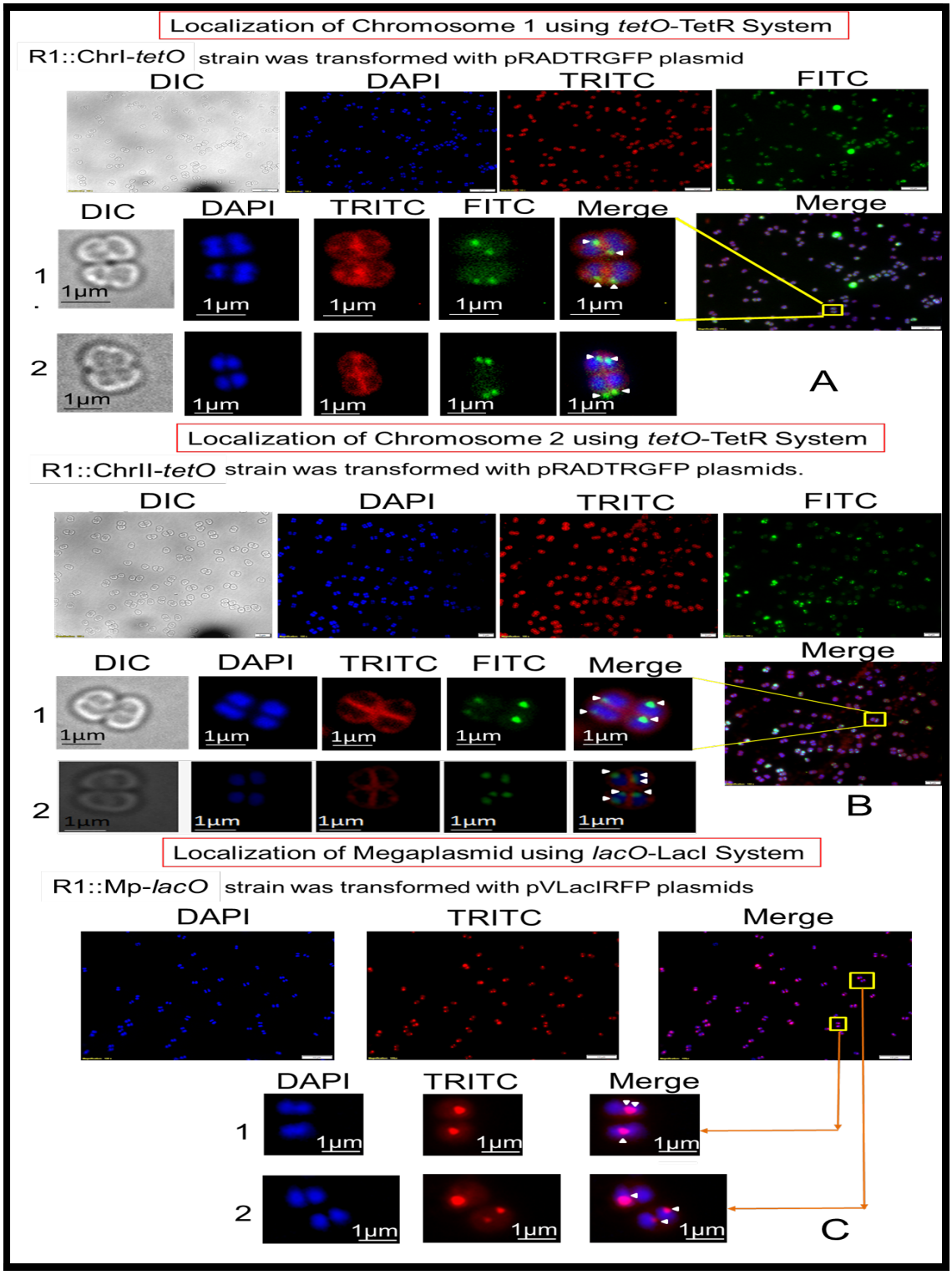

Figure 3.4.6 Localization of different replicons in *D. radiodurans* using FROS. Strain R1::ChrI-*tetO* or R1::ChrII-*tetO* transformed with pRADTRGFP plasmid were stained with DAPI and Nile red and imaged under fluorescene microscope (**A, B**). Strain R1::Mp-*lacO* transformed with pVLacIRFP plasmid was stained with DAPI and imaged as described in (section 3.4.2.3) (**C**). Two replicates of a single cell have been processed in each case for better understanding. Scale for A & C is 10µm while for B is 5µm.

In case of megaplasmid, we observed red foci in mid cell as well as on septum in a tetrad suggesting dynamic positioning of this replicon in growing population of *D. radiodurans* (Fig. 3.4.8 C). Thus, we demonstrated the fucntional FROS system in *D. radiodurans* where each cell of tetrad possesses different genomic replicons at different locations inside the cell. This study for the first time provided evidence to suggest that each cell of the trtrad has at least three of its genome elements and these seem to be dynamic during the growth in this bacterium.

D. radiodurans harbors multipartite genome system and each of these elements are present in multiple copies in similar stoichiometric ratios during the growth of this bacterium (pick up refernce of 1970 research). All these genetic materials are packaged in form of doughnut shaped toroidal structure (Minsky *et al.,* 2006; Zimmerman and Battista, 2005). This type of multipartite genome packaging as a single entity in bacterial cells is found to be unique for this bacterium and implicated to its extreme phenotypes. The positioning and dynamics of bacterial chromosomes have been studies in a number of bacteria by using different fluorescence microscopy methods. For example, the replicated origins occupy at the cell poles in *C. crescentus* (Mohl and Gober, 1997; Figge *et al*., 2003), at the 3/4th in *B. subtilis* (Lin *et al*., 1997; Webb *et al.,* 1997; Sharpe and Errington, 1998) and near the cell quarters or poles in *E. coli* (Gordon *et al*., 1997; Niki *et al*., 2000; Li *et al*., 2002; Lau *et al*., 2003). In multipartite genome harbouring bacteria, their genome elements have been localized in different positions in the cells. For example, in case of *V. cholera* and *R. sphaeroides* the chromosome I position was found to be at sub-polar position while chromosome II at mid cell position (Lin and Grossman, 1998; Stokke *et al*., 2011; Dubarry *et al*., 2019). In case of *S. meliloti*, chromosome I was found at subpolar location, it was quarter for chromosome II and mid for chromosome III (Fragge *et al*., 2016). In case of *Brucella abortus*, both the chromosomes were located at poles (Deghelt *et al*., 2013). Notable, all the

studies of chromosome localization and dynamics were carried out inrod shaped bacteria having predefined poles.

Since, the genome of *D. radiodurans* is packaged in form of torroid; it raises several fundmnetal questions about the localization, duplication and inheritance of all the elements in the cell. This bacterium usualy remains in form of tetrad (a group of four cells). The positioning of each chromosome and plasmid in each cell of tetrad was not explored till now. In this study, we tagged different genomic replicons at their origin with fluorescent proteins using *tetO*/TetR-GFP and *lacO*/LacI-RFP based FROS system and monitored their existence in side the cell. Although, further studies will be required to understand genome dynamics during normal and gamma stressed growth conditions, the available information support that this study for the first time provided evidence that all four cells in the tetrad contain all the three genme elements like ChrI, ChrII and megaplasmid. Furthermore, chromosome II duplication and segregation seem to be occuring at a different location from the location of megaplasmid processing that happens at mid position and located between the septum. The colocalisation of all the replicons tagged at both origin and terminus would be required for better insights in genome dynamics during normal growth as well as radiation stressed condition in this bacterium and should be carried out independently.

Chapter 4

Discussion

"Everything that human being or living animals do is done by protein molecules. And therefore, the kind of proteins that one has and therefore the ability one has is determined by the genes that one has"

- **Har Gobind Khorana**

Unlike bacteria harbouring single circular chromosome and or low copy plasmid, the tripartite genome segregation (TGS) system is not much studied in multipartite genome harbouring bacteria. Very limited studies have been done in *V. cholerae* (Egan *et al*., 2005; Fogel and Waldor, 2006)*, B. cenocepacia* (Dubarry *et al*., 2006), *D. radiodurans* (Charaka and Misra, 2012; Charaka *et al.,* 2013), *B. abortus* (Deghelt *et al*., 2013), and *R. sphearoides* (Dubarry *et al.*, 2019). The multipartite genome of *D. radiodurans* consists of 2 chromosomes and 2 plasmids. Recently, partitioning components of the primary chromosome (Chr I) has been characterized in this bacterium which suggested a pulling type of segregation mechanism for Chr I. Additionally, role of chromosome II encoded ParA2 protein in cell division regulation has also been given (Charaka *et al*., 2013).

In this thesis, we have brought forth functional characterization of secondary genome encoded partitioning components of *D. radiodurans* and their role in extreme tolerance of radiation and oxidative stress if any. We have demonstrated that P-loop Walker ATPases ParA2 (encoded on Chr II) and ParA3 (encoded on Mp) have shown higher sequence similarity at the amino acid levels and nearly similar biochemical and biophysical characteristics *in vitro.* These ParAs could compensate the loss of each other *in vivo*. Briefly, both ParAs showed interactions with nonspecific dsDNA in absence of ATP and form large nucleoprotein complex. Presence of ATP but not ADP has significantly increased the DNA binding activity of these ParAs in a similar way. Both ParA2 and ParA3 has shown similar affinity for TNP-ATP and natural ATP but higher than ParA1 and could hydrolyze ATP in similar fashion irrespective to the presence of dsDNA. Secondary genome encoded ParAs have shown both homotypic and heterotypic interaction amongst themselves but failed to interact with ParA1 encoded on primary chromosome. We have generated single and double mutant of *parA2* and *parA3* and measured the ploidy and survival under abiotic stress conditions. We observed that in comparison to wild type and single mutants, double mutant

has shown a significant reduction in copy number of secodary replicons but not chromosome I, growth retardation under normal conditions, and higher sensitivity to γ-radiation and hydrogen peroxides (Fig. 4.1). Deletion of secondary genome ParAs has not affected the ploidy of chromosome I. Earlier, the roles of ParA and ParB in normal growth of different bacteria have been reported like, loss of ParA and ParB of *C. crescentus* was lethal (Mohl and Gober, 1997), while loss of *parAB* in *P. putida*, *P. aeruginosa*, *S. coelicolor* and *B. subtilis* has caused segregation defect but not lethality (Lewis *et al*., 2002; Bartosik *et al*., 2004; Kim *et al*., 2000; Ireton *et al*., 1994). Further, we observed increased cell size and septum trapped nucleoid phenotype in an approximately 1/3rd population of double mutant than wild type and single mutants. Since, the phenotypic loss due to deletion of secondary genome ParA was not compensated by the presence of primary chromosomal ParA, suggesting a strong possibility of independent regulation of segregation of primary chromosome and secondary genome elements.

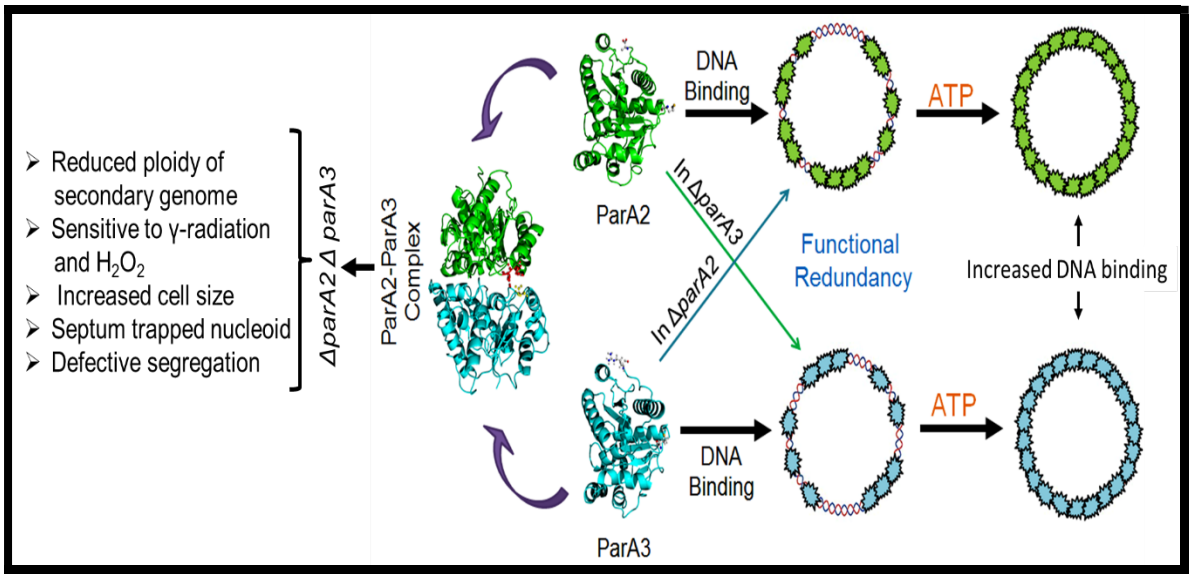

Figure 4.1 Working model forfunctional characterization of secondary genome ParAs (ParA2 and ParA3) in *Deinococcus radiodurans*.

Effect of loss of secondary genome ParAs on ploidy i.e. replication and septum formation i.e. cell division suggested an interdependent regulation of segregation, replication and cell division in this bacterium. Further we monitored the interaction between different divisome and segrosome components using bacterial two hybrid system. We observed that genome segregation proteins (ParA and ParB) interacts to core cell division proteins (different Fts proteins) via cell division regulatory proteins (DivIVA, MinC) in *D. radiodurans.*

The multipartite genome of *D. radiodurans* comprised of 2 chromosomes, megaplasmid and small plasmid, and each of these elements are present in multiple copies presumably packaged together in form of a toroidal nucleoid (White *et al*., 1999; Minsky *et al*., 2006). Functional significance of multiple chromosomes and ploidy in extreme phenotypes, and the mechanisms underlying faithful inheritance of multipartite genome system packaged in form of a compact toroidal nucleoid, into daughter cells are not known and offered the most interesting aspects in bacterial genome biology to investigate. The partitioning system encoded on primary chromosome of *D. radiodurans* has been characterized and shown expressing characteristics of pulling mechanism of genome segregation (Charaka and Misra, 2012).

In addition to role of secondary genome encoded ParAs, we have also characterized ParBs encoded on chromosome II (ParB2) and megaplasmid (ParB3) and outlined their role in the genome maintenance and survival of *D. radiodurans* under both normal and stressed conditions. We observed that ParB1 (Chr II), ParB2 and ParB3 proteins of *D. radiodurans* interact to self and form homodimer in *D. radiodurans* which is reported as a required functional state for specific interaction with centromeric sequences in other bacteria (Funell, 2016). These proteins did not show any cross interaction in *D. radiodurans*. In *T. thermophilus* and *P. aeruginosa,* role of C-terminal domain of ParBs in dimerization had

been reported (Leonard *et al*., 2004; Bartosik *et al*., 2004). Additionaly, deinococcal ParBs have shown interaction with its cognate ParAs *in vivo*. Surprisingly, secondary genome ParBs (ParB2 and ParB3) have also shown interaction with non-cognate secondary genome ParAs (i.e. ParA3 and ParA2, respectively) but not with primary chromosome ParA1. Likewise, primary chromosome ParB1 has not interacted with secondary genome ParAs. These observations together suggested a possibility of functional redundancy in interaction between secondary genome ParA and ParB proteins in *D. radiodurans*. Further, we generated deletion mutants of secondary genome *parB*s and compared their survival with Δ*parB1* (Charaka and Misra, 2012) under normal and gamma radiation stress. We observed that deletion of secondary genome *parB*s has little impact on normal growth than Δ*parB1* as reported eearlier (Charaka and Misra, 2012). Although the deletion of *parB2* and *parB3* has increased the sensitivity for gamma radiation when grown in absence of antibiotic pressure, Δ*parB1* deletion has produced relatively much higher sensitivity for gamma radiation as compared to Δ*parB2* &Δ*parB3* mutants (Fig. 4.2 A, B). Deletion of these proteins would have generated heterogeneous population when grown in the absence of antibiotic selection that would require to retain respective replicons. Loss of gamma radiation resistance when grown in the absence of selection pressure could be accounted to the population that did not have secondary genome element in respective mutants. However, this hypothesis needs to be tested in details. This suggests the role of secondary genome replicons in addition to primary chromosome in radioresistance. Further, we checked the effect of *parB* deletion on ploidy of genome in *D. radiodurans*. We observed that deletion of deinococcal *parB*s has increased the copy number of cognate replicon possibly due to defective segregation and over initiation of replication as reported earlier in case of *B. subtilis* (Lee *et al*., 2003). Interestingly, deletion of secondary genome *parB*s has also increased the copy number of non-cognate secondary replicons also supporting a cross-talk between secondary genome elements. Effect of *parB*

deletion on copy number was further explained by observing a cross-talk between deinococcal ParBs and replication initiation protein (Fig. 4.2 A, B). Similar observations have been reported earlier in *V. cholerae* as well as *B. subtilis* (Lee *et al*., 2003; Kadoya *et al*., 2011; Murray and Errington, 2008). Effect of *parB1*deletion is not complemented by the presence of secondary genome ParBs in this bacterium which further support notion of independent maintenance of primary and secondary genome replicons in *D. radiodurans*. However, a little less impact of deletion of secondary genome *parB*s if due to some functional redundancy between them cannot be ruled out. Thus, these observations strongly support the interdependent regulation of DNA replication and genome segregation in this bacterium (Fig. 4.2 A, B).

The cell cycle starts with replication of DNA followed by its segregation in daughter cells. Replication and segregation of DNA are the key events of cell growth. In bacteria, DNA replication is initiated by binding of DnaA at the origin of replication (*ori*). The *ori* sequences in chromosome, also called *oriC* are AT rich region and contain several DnaA boxes. During replication initiation, DnaA interacts to these DnaA boxes and allow loading of DnaB-DnaC complex (Baker and Wickner, 1992) for progression of replication. During segregation of replicated chromosome, centromere binding protein (ParB or its homologs) recognizes centromere sequences (usually distinct to *oriC*) and form segregation complex which further get separated by polymerization/depolymerization kinetics of motor ATPase (ParA or its homologs). Like *oriC*, the centromeric sequences are also repetitive in nature and mostly distributed around origin of chromosome (Livny, 2007). In some cases, like *P. putida*, *S. coelicolor* and *B. subtilis* (Bartosik and Jagura-Burdzy, 2005) centromere and *OriC* lie in close vicinity or overlap to each other which reflect interdependent regulation of replication and segregation in organism. The multipartite genome of *D. radiodurans* contains separate partitioning system for each replicon. Chromosome I has been reported with three

centromeric sequences (*segS*1-3) which lie far from each other (Charaka and Misra, 2012). Unlike chromosome I, we found an array of 10 direct repeats of 17 mer and 8 direct repeats of 16 mer upstream to *parAB* operon of chromosome II and megaplasmid, respectively. We named them as *cisII* and *cisMP*, respectively.

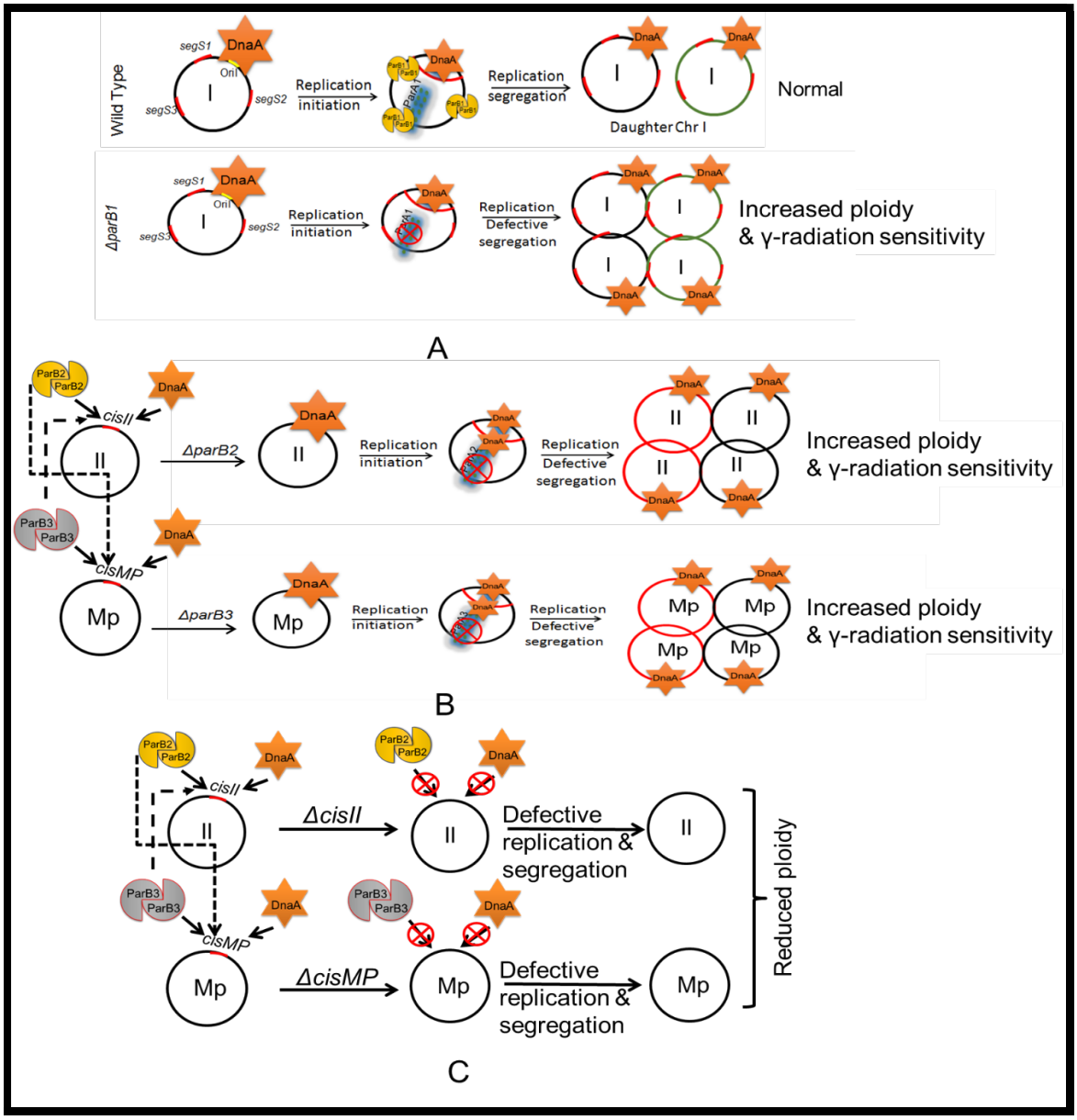

Figure 4.2 Working model for functional characterization of ParB proteins and cis elements present on chromosome II and megaplasmid. Deletion of *parB1* (**A**), *parB2* and *parB3* (**B**) has increased the ploidy of genome as well as sensitivity for gamma radiation in *D. radiodurans*. Secondary genome ParBs as well as DnaA proteins could binds to *cis* elements present upstream to *parAB* operon of Chr II and Mp albeit with different affinity (**B**). Deletion of both *cisII* as well as *cisMP* has drastically reduced the ploidy in *D. radiodurans* (**C**).

We hypothesized the possibility of these *cis* elements to be origin of replication or centromere for respective replicons and tested it. We cloned these *cis* elements in suicide non-replicative plasmid (pNOKOUT) of *D. radiodurans* and monitored the maintenance of derivative plasmids in *D. radiodurans*. The results showed that *cis* element carrying pNOKOUT plasmids were able to replicate and maintain in *D. radiodurans* or its *ΔrecA* mutant which suggested the origin of replication features of these *cis* elements. Further we checked the affinity of these *cis* elements with deinococcal replication initiator protein DnaA protein using EMSA. We observed that these *cis* elements could bind to DnaA with high specificity. At least 3 repeats of both *cisII* and *cisMP* required for significant binding with DnaA. Further, *cisII* showed higher affinity for DnaA than *cisMP*. We have generated deletion mutants of both *cisII* and *cisMP* and measured the copy number of each replicon. We observed a drastic reduction in copy number of secondary genome elements of *cis* mutants than wild type in *D. radiodurans.* Such reduction would have occurred due to defective replication cum segregation events (Fig. 4.2 C). Since, these *cis* elements are located upstream to respective *parAB* operon, which is a typical organization of TGS system in well studied plasmid as well as chromosome in many bacteria. So, we have also tested affinity of these *cis* elements with secondary genome ParBs (ParB2 as well as ParB3). We observed specific interaction of these *cis* elements with their cognate ParB proteins. We have also tested the interaction of deinococcal ParBs with different number of repeats of cognate *cis* elements. The results showed that like DnaA, significant binding of ParB2 or ParB3 to their cognate *cis* elements required at least 3 repeats. Further, affinity of these *cis* elements to their cognate ParBs suggested their centromeric features in addition to origin of replication feature (Fig. 4.2 C). Surprisingly, we also observed a cross talk between secondary genome ParBs and *cis* elements. For instance, ParB2 could binds to *cisMP* and ParB3 to *cisIIalbeit* at lower affinity than their cognate *cis* elements. This raising a serious possibility of functional

redundancy amongst the TGS encoded on chromosome II and megaplasmid in this bacterium. These observations together strengthen the notion of interdependent regulation of DNA replication and its segregation in this bacterium at the level of *cis* factor and raise a strong possibility of redundancy at the levels of ParBs interaction with centromeric region within secondary genome elements.

The genome organization, localization and dynamics are better understood in eukaryotes than prokaryotes. Recent advancement in fluorescence imaging techniques has improved our understanding of genome biology in bacteria. The localization and dynamics of replicated chromosomes has been studied in few bacteria including MGH bacteria. For instance, the replicated origins located at the cell poles in *C. crescentus* (Mohl and Gober, 1997; Figge *et al*., 2003), at the quarter in *B. subtilis* (Lin *et al*., 1997; Webb *et al.,* 1997; Sharpe and Errington, 1998), near the cell quarters or poles in *E. coli* (Gordon *et al*., 1997; Niki *et al*., 2000; Li *et al*., 2002; Lau *et al*., 2003), at sub-polar for chromosome I and at mid for chromosome II in case of *V. cholerae* (Lin and Grossman, 1998; Stokke *et al*., 2011) and *R. sphaeroides* (Dubarry *et al*., 2019), at poles for both the chromosomes of *B. abortus* (Deghelt *et al*. 2013), at subpolar for chromosome I, quarter for chromosome II and mid for chromosome III for *S. meliloti* (Fragge *et al*., 2016). These studies are mostly done in rod shaped bacteria.

The multipartite genome of *D. radiodurans* appears as a donut shaped toroid structure (Minsky *et al*., 2006). How different replicons exist in such toroidal structure in each cell of tetrad was not explored till now. In this study, we developed *tetO*/TetR-GFP and *lacO*/LacI-RFP based FROS system and tagged different genomic replicons near their origin to observe localization and dynamics of genome during normal growth. When TetR-GFP and LacI-RFP expressed alone in *D. radiodurans* have shown diffused expression throughout the cell. We

further inserted *tetO* cassettes in chromosome I & II while *lacO* cassettes in megaplasmid, and expressed their fluorescent protein tagged reporters viz. TetR-GFP and LacI-RFP, respectively in same background. Using fluorescence microscopy, we observed that TetR-GFP forms a single distinct focus in each cell of tetrad for chromosome I as well as chromosome II. Additionally, we observed few populations with 2 or more foci in case of chromosome II that may be undergoing replication cum segregation. Interestingly, we observed LacIRFP foci beaded over *lacO* cassettes in megaplasmid at mid of 2 cells (at septum site) in tetrad, which is undergoing for separation in respective cell. Thus, we found that each cell of tetrad in *D. radiodurans* possesses all the replicons (chromosomes and megaplasmid atleast) to confer multipartite features.

Further colocalization and dynamics of all the replicons tagged at both origin and terminus during normal as well as radiation stressed condition in wild type and different DNA repair mutants or segregation defective mutant background will provide better insight in genome biology of this bacterium.

Chapter 5

Summary, conclusion and future perspectives

Summary

Deinococcus radiodurans, a toughest bacterium on the earth, is known for its tolerance to DNA damaging agents. It has been used as a model system to understand the molecula rmechanisms underlying its extraordinary resistance to several abiotic stressors including ionizing radiation and desiccation. The remarkable capacity to tolerate such a genomic damage has been credited to its unique ability to reconstitute the functional genome with high fidelity. A large number of small molecules has been characterized from this bacterium and shown to help in protecting its proteins from oxidative damage. The cytogenetic features of this bacterium are equally interesting. It has a multipartite genome system made of 2 chromosomes and 2 plasmids. This bacterium being coccus in shape does not have predefined poles and plane of cell division is presumed to be determined by marker protein interaction with macromolecular complexes involved in cell division and genome maintenance. However, it has been shown that the next plane of cell division is perpendicular to the first plane of cell division.

The multipartite genome of *D. radiodurans* encodes proteins involved in segregation but centromeric region for initiation of segregation was not characterized in secondary genome elements like chromosome II and megaplasmid. Each replicon except small plasmid has its own typical tripartite segregation system. The partitioning system of primary chromosome (Chr I) has been characterized earlier and were found to follow pulling mechanism of segregation (Charaka and Misra, 2012). In this thesis, we have characterized TGS of secondary genome elements and summarized the role and maintenance of multipartite genome with special focus on secondary genome (chromosome II and megaplasmid) in extreme phenotype of *D. radiodurans.* I have also showed that segrosome (proteins involved in genome segregation) interact with cell division proteins in this bacterium. Bioinformatics

analysis of ParA1, ParA2 and ParA3 using multiple sequence alignment and homology modeling showed that secondary genome ParAs (both ParA2 & ParA3) have high sequence similarity in different functional domain or motifs (Walker motifs & DNA binding motifs) than ParA1. Unlike ParA2 & ParA3, ParA1 contains extra ~48 amino acids at its N-terminal which hang around while the remaining parts of the 3-D modeled structure were nearly superimposable with secondary ParAs. Both ParA2 and ParA3 have very similar DNA binding and ATP hydrolysis activities. Both ParAs could bind to non-specific DNA in absence of ATP which further increased in the presence of ATP. Binding of ParAs with DNA form large nucleoprotein complex, whose size is further increased in presence of ATP but not ADP. Both ParA2 and ParA3 have shown similar but lower affinity for TNP-ATP as well as natural ATP than ParA1. Interaction of ParAs with DNA and ATP creates conformational change perhaps required for protein polymerization on DNA. Increase in intrinsic fluorescence of the protein bound to ADP and this increase in ATP bound protein required ATP hydrolysis together suggested the different effect of ATP and ADP on ParA protein confirmation in vitro. Based on this result, a possibility of ATP helps this protein as (ParA-ATP) in polymerization and ParA-ADP induces depolymerization could be speculated. Protein-protein interaction studies among Deinococcal ParAs revealed that all secondary genome ParAs interacted to self as well as each other but none of them interacted to ParA1 (showing only homotypic interaction). A cross-talk among secondary genome ParAs suggested a possibility of functional redundancy *in vivo.* Further we have generated deletion mutants of both ParA2 and ParA3 and measured the ploidy level and monitored their survival in presence of gamma radiation and H_2O_2. We observed that the copy numbers of Chr II and Mp reduced significantly in case of double mutant (Δ*parA2*Δ*parA3*) while remain unaffected in their single mutants. Double mutant was more sensitive to gamma radiation and hydrogen peroxide than wild type and single mutants. These observations suggested that ParA2 and

ParA3 complementing the function of each other but ParA1 failed to complement the loss of both ParA2 and ParA3 in *D. radiodurans.* Further, in comparison to wild type and single mutants, double mutant showed a relatively higher frequency of cells having cell area more than 6μm^2 with septum trapped nucleoid phenotype. It suggested the role of secondary genome ParAs in regulation of DNA translocation during cell division and they could complement the function of each other *in vivo*. When we tested the interaction of genome segregation proteins with different cell division proteins using bacterial two-hybrid system, we observed that ParAs & ParBs proteins of segrosome complex interacted to cell division protein, which in turn showed interaction with core divisome components (different Fts proteins). These observations together suggested that secondary genome ParAs are functionally redundant *in vivo* and showed cross-talk with cell division components of *D. radiodurans.*

Like ParAs, deinococcal ParBs also showed self-interaction and form homodimer *in vitro* as well as *in vivo.* Unlike ParAs, none of the ParBs has shown heterotypic interaction or cross-talk to other ParBs *in vivo.* Deinococcal ParBs have shown interaction with their cognate ParA proteins. In addition, the secondary genome ParBs also interacted with non-cognate secondary genome ParAs. Interestingly, ParB1 showed interaction with only ParA1 while none of the secondary genome ParBs interacted with ParA1 and vice versa. These results suggested a possible functional redundancy in segregation process of secondary genome replicons. Further deletion mutants of *parB1, parB2* and *parB3* have increased the copy number of cognate replicons possibly due to over-initiation of replication. Interestingly, deletion of *parB2* or *parB3* has also increased the copy number of non-cognate secondary genome replicons. All deinococcal ParBs showed interaction with DNA replication initiation protein DnaA *in vivo.* These observations together conferred the role of deinococcal ParBs in DNA replication in addition to cell division. Further, Δ*parB2* and Δ*parB3* deletion mutants

have shown sensitivity for gamma radiation when grown in absence of selection pressure *albeit* less than Δ*parB1*, suggesting the role of secondary genome encoded ParBs in radiation resistance.

In addition to ParAB proteins of secondary genome elements, we identified an array several direct repeats of 16-17 mer (called as *cis* elements) upstream to *parAB* operons of chromosome II (*cisII*) and megaplasmid (*cisMP*). During functional characterization of these *cis* elements we found that both *cisII* and *cisMP* can maintain pNOKOUT (a non-replicative suicide plasmid of *D. radiodurans*) in *D. radiodurans.* This suggests the role of these *cis* elements as origin of replication for respective replicons. This observation was further strengthening by specific DNA binding activity of deinococcal DnaA with these *cis* elements. Minimum 3 repeats of both *cisII* and *cisMP* needed for efficient binding with DnaA. Further, deletion of both *cisII* and *cisMP* has drastically decreased the copy number of secondary genome elements possibly due to defective replication. However, presence of few copies of secondary replicons in these mutants suggests the possibility of non-*OriC* based replication initiation. Interestingly, we found that these *cis* elements were also the site of binding of secondary genome ParB proteins (ParB2 and ParB3). Both ParBs could specifically bind either of *cis* elements with different affinity. Thus, our results suggested that direct repeats present upstream to *parAB* operons of chromosome II and megaplasmid have the feature of both origin of replication as well as centromere which play important role in interdependent regulation of segregation and replication for secondary genome replicons. In contrast, chromosome I has shown isolated positioning of origin of replication and centromere.

In order to monitor the localization and dynamics of different genomic replicons of multipartite genome of *D. radiodurans*, we developed *tetO*/TetR-GFP and *lacO*/LacI-RFP based FROS system that compatible to this bacterium. We inserted an array of *tetO* cassettes

near origin in chromosome I & II individually and monitored the localization of TetR-GFP under fluorescence microscope. We observed that each cell of tetrad had a single focus confirming the location of respective replicon inside the tetrad. There were few population showing replication cum segregation event which resulted in formation of two foci in a cell. Tagging of megaplasmid with *lacO*/LacI-RFP system has given similar observation. These observations conclude that each cell of tetrad in *D. radiodurans* contains all the genomic replicons but at different locations

Conclusions

- ParA2 and ParA3 showed similar biochemical and biophysical characteristics, and complement each other's function *in vivo*.
- ParB2 and ParB3 binds centromeric region of secondary genome elements with high specificity but different affinity and tightly regulate the maintenance of respective genome elements.
- Origin of replication in chromosome II and megaplamid also contains centromeric regions.
- Segregation of primary and secondary genome elements are independently regulated in *D. radiodurans.*
- Copy number of secondary genome elements contributes to radioresistance in *D. radiodurans*.
- Macromolecular complexes involved in genome segregation, DNA replication and cell division crosstalk in *D. radiodurans*.
- Functional FROS system has been generated and localisation of different genomic elements in *D. radiodurans* has been ascertained.

Future perspectives

This study has answered some of the questions and tested the proposed hypotheses through different approaches. It has however, raised and left several unanswered questions. The immediate ones may require attention include

- Real-time monitoring of ParB2/ParB3 protein interaction with their centromere and demonstration of dynamic movement of respective ParAs during course of genome segregation.
- How do Par proteins regulate DNA replication and cell division processes *in vivo*?
- Real time monitoring of genome dynamics using fluorescent tagged genomic replicons in wild type, DNA repair and genome segregation mutant background during post irradiation recovery.
- Post translational modification-based regulation of genome segregation process would be an interesting area to explore as this bacterium regulates cell division by phosphorylation.

Bibliography

Adachi, M., Shimizu, R., Shibazaki, C., Satoh, K., Fujiwara, S., Arai, S., ... & Kuroki, R. (2018). Extended structure of pleiotropic DNA repair-promoting protein PprA from *Deinococcus radiodurans*. *The FASEB Journal*, fj-201801506R.

Amadou, C., Pascal, G., Mangenot, S., Glew, M., Bontemps, C., Capela, D., ... & Marchetti, M. (2008). Genome sequence of the β-rhizobium *Cupriavidus taiwanensis* and comparative genomics of rhizobia. *Genome Research*, gr-076448.

Ancora, M., Marcacci, M., Orsini, M., Zilli, K., Di Giannatale, E., Garofolo, G., & Cammà, C. (2014). Complete genome sequence of a *Brucella ceti* ST26 strain isolated from a striped dolphin (*Stenella coeruleoalba*) on the coast of Italy. *Genome Announcements*, *2*(2), e00068-14.

Anderson, A. W. (1956). Studies on a radioresistant micrococcus. 1. Isolation, morphology, cultural characteristics, and resistance to γ radiation. *Food Technol.*, *10*, 575-578.

Audic, S., Lescot, M., Claverie, J. M., Cloeckaert, A., & Zygmunt, M. S. (2011). The genome sequence of *Brucella pinnipedialis* B2/94 sheds light on the evolutionary history of the genus *Brucella*. *BMC Evolutionary Biology*, *11*(1), 200.

Austin, S., & Abeles, A. (1983). Partition of unit-copy miniplasmids to daughter cells: II. The partition region of miniplasmid P1 encodes an essential protein and a centromere-like site at which it acts. *Journal of Molecular Biology, 169*(2), 373-387.

Aylett, C. H., & Löwe, J. (2012). Superstructure of the centromeric complex of TubZRC plasmid partitioning systems. *Proceedings of the National Academy of Sciences USA*, 201210899.

Baker, T. A., & Wickner, S. H. (1992). Genetics and enzymology of DNA replication in *Escherichia coli*. *Annual Review of Genetics*, 26(1), 447-477.

Baril, C., Richaud, C., Baranton, G., & Saint Girons, I. (1989). Linear chromosome of *Borrelia burgdorferi*. *Research in Microbiology, 140*(7), 507-516.

Bartosik, A. A., & Jagura-Burdzy, G. (2005). Bacterial chromosome segregation. *Acta Biochimica Polonica*, *52*(1), 1-34.

Bartosik, A. A., Lasocki, K., Mierzejewska, J., Thomas, C. M., & Jagura-Burdzy, G. (2004). ParB of Pseudomonas aeruginosa: interactions with its partner ParA and its target parS and specific effects on bacterial growth. *Journal of Bacteriology, 186*(20), 6983-6998.

Battesti, A., & Bouveret, E. (2012). The bacterial two-hybrid system based on adenylate cyclase reconstitution in *Escherichia coli*. *Methods*, *58*(4), 325-334.

Battista, J. R., Park, M. J., & McLemore, A. E. (2001). Inactivation of two homologues of proteins presumed to be involved in the desiccation tolerance of plants sensitizes Deinococcus radiodurans R1 to desiccation. *Cryobiology*, *43*(2), 133-139.

Baxter, J. C., & Funnell, B. E. (2015). Plasmid partition mechanisms. In Plasmids: Biology and Impact in Biotechnology and Discovery. *American Society of Microbiology,* (pp. 135-155).

Belmont, A. S. (2001). Visualizing chromosome dynamics with GFP. *Trends in Cell Biology*, 11(6), 250-257.

Billi, D., Friedmann, E. I., Hofer, K. G., Caiola, M. G., & Ocampo-Friedmann, R. (2000). Ionizing-radiation resistance in the desiccation-tolerant cyanobacterium *Chroococcidiopsis*. *Appl. Environ. Microbiol.*, *66*(4), 1489-1492.

Bjornsdottir-Butler, K., McCarthy, S. A., Dunlap, P. V., Timme, R. E., & Benner, R. A. (2015). Draft genome sequences of histamine-producing *Photobacterium kishitanii* and *Photobacterium angustum*, isolated from albacore (*Thunnus alalunga*) and yellowfin (*Thunnus albacares*) tuna. *Genome Announcements*, *3*(2), e00400-15.

Bloom, K., & Joglekar, A. (2010). Towards building a chromosome segregation machine. *Nature, 463*(7280), 446.

Bouet, J. Y., & Funnell, B. E. (1999). P1 ParA interacts with the P1 partition complex at parS and an ATP–ADP switch controls ParA activities. *The EMBO journal, 18*(5), 1415-1424.

Breuert, S., Allers, T., Spohn, G., & Soppa, J. (2006). Regulated polyploidy in halophilic archaea. *PloS One*, *1*(1), e92.

Brocken, D. J., Tark-Dame, M., & Dame, R. T. (2018). The organization of bacterial genomes: towards understanding the interplay between structure and function. *Current Opinion in Systems Biology*, (*8*) 137-143.

Broedersz, C. P., Wang, X., Meir, Y., Loparo, J. J., Rudner, D. Z., & Wingreen, N. S. (2014). Condensation and localization of the partitioning protein ParB on the bacterial chromosome. *Proceedings of the National Academy of Sciences, 111*(24), 8809-8814.

Burgoyne, P. S., Mahadevaiah, S. K., & Turner, J. M. (2007). The management of DNA double-strand breaks in mitotic G2, and in mammalian meiosis viewed from a mitotic G2 perspective. *Bioessays*, *29*(10), 974-986.

Bustin, S. A., Benes, V., Garson, J. A., Hellemans, J., Huggett, J., Kubista, M., ... & Vandesompele, J. (2009). The MIQE guidelines: minimum information for publication of quantitative real-time PCR experiments. *Clinical Chemistry*, *55*(4), 611-622.

Cairns, J. (1963). The bacterial chromosome and its manner of replication as seen by autoradiography. *Journal of Molecular Biology, 6*(3), 208-IN5.

Cavalli, G., & Misteli, T. (2013). Functional implications of genome topology. *Nature Structural & Molecular Biology, 20*(3), 290.

Chain, P. S., Denef, V. J., Konstantinidis, K. T., Vergez, L. M., Agulló, L., Reyes, V. L., ... & Land, M. (2006). *Burkholderia xenovorans* LB400 harbors a multi-replicon, 9.73-Mbp genome shaped for versatility. *Proceedings of the National Academy of Sciences USA*, *103*(42), 15280-15287.

Chain, P. S., Lang, D. M., Comerci, D. J., Malfatti, S. A., Vergez, L. M., Shin, M., ... & Tolmasky, M. E. (2011). The Genome of *Ochrobactrum anthropi* ATCC49188T, a Versatile Opportunistic Pathogen and Symbiont of Several Eukaryotic Hosts. *Journal of Bacteriology*, JB-05335.

Charaka, V. K., & Misra, H. S. (2012). Functional characterization of the role of the chromosome I partitioning system in genome segregation in *Deinococcus radiodurans*. *Journal of Bacteriology*, *194*(21), 5739-5748.

Charaka, V. K., Mehta, K. P., & Misra, H. S. (2013). ParA encoded on chromosome II of *Deinococcus radiodurans* binds to nucleoid and inhibits cell division in *Escherichia coli*. *Journal of Biosciences*, *38*(3), 487-497.

Chen, C. Y., Wu, K. M., Chang, Y. C., Chang, C. H., Tsai, H. C., Liao, T. L., ... & Su, T. L. (2003). Comparative genome analysis of *Vibrio vulnificus*, a marine pathogen. *Genome Research*, *13*(12), 2577-2587.

Choudhary, M., Cho, H., Bavishi, A., Trahan, C., & Myagmarjav, B. E. (2012). Evolution of multipartite genomes in prokaryotes. *In Evolutionary Biology: Mechanisms and Trends* (pp. 301-323). Springer, Berlin, Heidelberg.

Choudhary, M., Mackenzie, C., Nereng, K., Sodergren, E., Weinstock, G. M., & Kaplan, S. (1997). Low-resolution sequencing of *Rhodobacter sphaeroides* 2. A. 1T: chromosome II is a true chromosome. *Microbiology, 143*(10), 3085-3099.

Cooper, V. S., Vohr, S. H., Wrocklage, S. C., & Hatcher, P. J. (2010). Why genes evolve faster on secondary chromosomes in bacteria. *PLoS Computational Biology*, *6*(4), e1000732.

Costas, A. M. G., Tsukatani, Y., Rijpstra, W. I. C., Schouten, S., Welander, P. V., Summons, R. E., & Bryant, D. A. (2012). Identification of the bacteriochlorophylls, carotenoids, quinones, lipids, and hopanoids of "*Candidatus Chloracidobacterium thermophilum*". *Journal of Bacteriology*, *194*(5), 1158-1168.

Cox, M. M., & Battista, J. R. (2005). *Deinococcus radiodurans*—the consummate survivor. *Nature Reviews Microbiology*, *3*(11), 882.

Crook, M. B., Mitra, S., Ané, J. M., Sadowsky, M. J., & Gyaneshwar, P. (2013). Complete genome sequence of the Sesbania symbiont and rice growth-promoting endophyte *Rhizobium sp*. strain IRBG74. *Genome Announcements*, *1*(6), e00934-13.

Crooks, G. E., Hon, G., Chandonia, J. M., & Brenner, S. E. (2004). WebLogo: a sequence logo generator. *Genome Research*, *14*(6), 1188-1190.

Dabrazhynetskaya, A., Brendler, T., Ji, X., & Austin, S. (2009). Switching protein-DNA recognition specificity by single-amino-acid substitutions in the P1 par family of plasmid partition elements. *Journal of Bacteriology, 191*(4), 1126-1131.

Dainton, F. S. (1948). On the existence of free atoms and radicals in water and aqueous solutions subjected to ionizing radiation. *The Journal of Physical Chemistry*, *52*(3), 490-517.

Daly, M. J. (2009). A new perspective on radiation resistance based on *Deinococcus radiodurans*. *Nature Reviews Microbiology*, *7*(3), 237.

Daly, M. J., & Minton, K. W. (1995). Interchromosomal recombination in the extremely radioresistant bacterium *Deinococcus radiodurans*. *Journal of Bacteriology*, *177*(19), 5495-5505.

Daly, M. J., Gaidamakova, E. K., Matrosova, V. Y., Vasilenko, A., Zhai, M., Leapman, R. D., ... & Fredrickson, J. K. (2007). Protein oxidation implicated as the primary determinant of bacterial radioresistance. *PLoS biology*, *5*(4), e92.

Dam, M. J., & Gerdes, K. (1994). Partitioning of plasmid R1 Ten direct repeats flanking the parA promoter constitute a centromere-like partition site parC, that expresses incompatibility. *Journal of Molecular Biology, 236*(5), 1289-1298.

Das, A. D., & Misra, H. S. (2011). Characterization of DRA0282 from *Deinococcus radiodurans* for its role in bacterial resistance to DNA damage. *Microbiology*, *157*(8), 2196-2205.

de Oliveira Veras, A. A., da Silva, M. L., Gomes, J. C. M., Dias, L. M., de Sá, P. C. G., Alves, J. T. C., ... & Rodrigues, M. (2015). Draft genome sequences of *Vibrio fluvialis* strains 560 and 539, isolated from environmental samples. *Genome Announcements*, *3*(1), e01344-14.

Deghelt, M., Mullier, C., Sternon, J. F., Francis, N., Laloux, G., Dotreppe, D., ... & De Bolle, X. (2014). G1-arrested newborn cells are the predominant infectious form of the pathogen *Brucella abortus*. *Nature Communications*, *5*, 4366.

Dekker, J., & Mirny, L. (2016). The 3D genome as moderator of chromosomal communication. *Cell, 164*(6), 1110-1121.

Dekker, J., Rippe, K., Dekker, M., & Kleckner, N. (2002). Capturing chromosome conformation. *Science, 295*(5558), 1306-1311.

Devigne, A., Mersaoui, S., Bouthier-De-La-Tour, C., Sommer, S., & Servant, P. (2013). The PprA protein is required for accurate cell division of γ-irradiated *Deinococcus radiodurans* bacteria. *DNA repair*, *12*(4), 265-272.

DiCenzo, G.C., & Finan, T. M. (2017). The divided bacterial genome: structure, function, and evolution. *Microbiology and Molecular Biology Reviews*, *81*(3), e00019-17.

DiCenzo, G.C., MacLean, A. M., Milunovic, B., Golding, G. B., & Finan, T. M. (2014). Examination of prokaryotic multipartite genome evolution through experimental genome reduction. *PLoS Genetics, 10*(10), e1004742.

Ditkowski, B., Holmes, N., Rydzak, J., Donczew, M., Bezulska, M., Ginda, K., ... & Jakimowicz, D. (2013). Dynamic interplay of ParA with the polarity protein, Scy, coordinates the growth with chromosome segregation in Streptomyces coelicolor. *Open biology, 3*(3), 130006.

Dobruk-Serkowska, A., Caccamo, M., Rodríguez-Castañeda, F., Wu, M., Bryce, K., Ng, I., ... & Hayes, F. (2012). Uncoupling of Nucleotide Hydrolysis and Polymerization in the ParA Superfamily Disrupts DNA Segregation Dynamics. *Journal of Biological Chemistry*, jbc-M112.

Donczew, M., Mackiewicz, P., Wróbel, A., Flärdh, K., Zakrzewska-Czerwińska, J., & Jakimowicz, D. (2016). ParA and ParB coordinate chromosome segregation with cell elongation and division during Streptomyces sporulation. *Open Biology, 6*(4), 150263.

Draper, G. C., & Gober, J. W. (2002). Bacterial chromosome segregation. *Annual Reviews in Microbiology*, *56*(1), 567-597.

Driedger, A. A. (1970). The DNA content of single cells of *Micrococcus radiodurans*. *Canadian Journal of Microbiology*, *16*(11), 1136-1137.

Du, W. L., Dubarry, N., Passot, F. M., Kamgoué, A., Murray, H., Lane, D., & Pasta, F. (2016). Orderly replication and segregation of the four replicons of *Burkholderia cenocepacia* J2315. *PLoS Genetics, 12*(7), e1006172.

Dubarry, N., Pasta, F., & Lane, D. (2006). ParABS systems of the four replicons of Burkholderia cenocepacia: new chromosome centromeres confer partition specificity. *Journal of Bacteriology, 188*(4), 1489-1496.

Dubarry, N., Willis, C. R., Ball, G., Lesterlin, C., & Armitage, J. P. (2019). In Vivo Imaging of the Segregation of the 2 Chromosomes and the Cell Division Proteins of Rhodobacter sphaeroides Reveals an Unexpected Role for MipZ. *mBio, 10*(1), e02515-18.

Dunham, T. D., Xu, W., Funnell, B. E., & Schumacher, M. A. (2009). Structural basis for ADP-mediated transcriptional regulation by P1 and P7 ParA. *The EMBO Journal, 28*(12), 1792-1802.

Dupont, Y., Chapron, Y., & Pougeois, R. (1982). Titration of the nucleotide binding sites of Sarcoplasmic Reticulum Ca2+-ATPase with 2′, 3′-0-(2, 4, 6-trinitrophenyl) adenosine 5′-triphosphate and 5′-diphosphate. *Biochemical and biophysical research communications*, *106*(4), 1272-1279.

Dworkin, J., & Losick, R. (2002). Does RNA polymerase help drive chromosome segregation in bacteria?. *Proceedings of the National Academy of Sciences, 99*(22), 14089-14094.

Ebersbach, G., & Gerdes, K. (2005). Plasmid segregation mechanisms. *Annu. Rev. Genet., 39*, 453-479.

Ebersbach, G., Sherratt, D. J., & Gerdes, K. (2005). Partition associated incompatibility caused by random assortment of pure plasmid clusters. *Molecular Microbiology, 56*(6), 1430-1440.

Egan, E. S., Fogel, M. A., & Waldor, M. K. (2005). MicroReview: Divided genomes: negotiating the cell cycle in prokaryotes with multiple chromosomes. *Molecular Microbiology, 56*(5), 1129-1138.

Erdmann, N., Petroff, T., & Funnell, B. E. (1999). Intracellular localization of P1 ParB protein depends on ParA and parS. *Proceedings of the National Academy of Sciences USA, 96*(26), 14905-14910.

Figge, R. M., Easter, J., & Gober, J. W. (2003). Productive interaction between the chromosome partitioning proteins, ParA and ParB, is required for the progression of the cell cycle in Caulobacter crescentus. *Molecular Microbiology, 47*(5), 1225-1237.

Fink, G., & Löwe, J. (2015). Reconstitution of a prokaryotic minus end-tracking system using TubRC centromeric complexes and tubulin-like protein TubZ filaments. *Proceedings of the National Academy of Sciences USA*, 201423746.

Fisher, G. L., Pastrana, C. L., Higman, V. A., Koh, A., Taylor, J. A., Butterer, A., ... & Moreno-Herrero, F. (2017). The structural basis for dynamic DNA binding and bridging interactions which condense the bacterial centromere. *Elife, 6*, e28086.

Fisher, J. K., Bourniquel, A., Witz, G., Weiner, B., Prentiss, M., & Kleckner, N. (2013). Four-dimensional imaging of *E. coli* nucleoid organization and dynamics in living cells. *Cell, 153*(4), 882-895.

Fogel, M. A., & Waldor, M. K. (2005). Distinct segregation dynamics of the two *Vibrio cholerae* chromosomes. *Molecular Microbiology*, *55*(1), 125-136.

Fogel, M. A., & Waldor, M. K. (2006). A dynamic, mitotic-like mechanism for bacterial chromosome segregation. *Genes & Development*, *20*(23), 3269-3282.

Frage, B., Döhlemann, J., Robledo, M., Lucena, D., Sobetzko, P., Graumann, P. L., & Becker, A. (2016). Spatiotemporal choreography of chromosome and megaplasmids in the *Sinorhizobium meliloti* cell cycle. *Molecular Microbiology*, *100*(5), 808-823.

Funell, A., Shimoni, E., & Englander, J. (2006). Ring-like nucleoids and DNA repair through error-free nonhomologous end joining in *Deinococcus radiodurans. Journal of Bacteriology, 188*(17), 6047-6051.

Galardini, M., Pini, F., Bazzicalupo, M., Biondi, E. G., & Mengoni, A. (2013). Replicon-dependent bacterial genome evolution: the case of *Sinorhizobium meliloti*. *Genome Biology and Evolution*, *5*(3), 542-558.

Galardini, M., Pini, F., Bazzicalupo, M., Biondi, E. G., & Mengoni, A. (2013). Replicon-dependent bacterial genome evolution: the case of *Sinorhizobium meliloti*. *Genome Biology and Evolution, 5*(3), 542-558.

Galkin, V. E., Orlova, A., Rivera, C., Mullins, R. D., & Egelman, E. H. (2009). Structural polymorphism of the ParM filament and dynamic instability. *Structure, 17*(9), 1253-1264.

Garcia-Garcia, T., Poncet, S., Derouiche, A., Shi, L., Mijakovic, I., & Noirot-Gros, M. F. (2016). Role of protein phosphorylation in the regulation of cell cycle and DNA-related processes in bacteria. *Frontiers in Microbiology, 7*, 184.

Gasser, S. M. (2002). Visualizing chromatin dynamics in interphase nuclei. *Science, 296*(5572), 1412-1416.

Gayathri, P., Fujii, T., Møller-Jensen, J., Van Den Ent, F., Namba, K., & Löwe, J. (2012). A bipolar spindle of antiparallel ParM filaments drives bacterial plasmid segregation. *Science, 338*(6112), 1334-1337.

Gerard, E., Jolivet, E., Prieur, D., & Forterre, P. (2001). DNA protection mechanisms are not involved in the radioresistance of the hyperthermophilic archaea *Pyrococcus abyssi* and *P. furiosus*. *Molecular Genetics and Genomics*, *266*(1), 72-78.

Gerdes, K., & Molin, S. (1986). Partitioning of plasmid R1: structural and functional analysis of the *parA* locus. *Journal of Molecular Biology, 190*(3), 269-279.

Gerdes, K., Howard, M., & Szardenings, F. (2010). Pushing and pulling in prokaryotic DNA segregation. *Cell*, *141*(6), 927-942.

Ghosal, D., Omelchenko, M. V., Gaidamakova, E. K., Matrosova, V. Y., Vasilenko, A., Venkateswaran, A., ... & Wackett, L. P. (2005). How radiation kills cells: survival of *Deinococcus*

radiodurans and *Shewanella oneidensis* under oxidative stress. *FEMS microbiology reviews*, *29*(2), 361-375.

Ghosh, S. K., Hajra, S., Paek, A., & Jayaram, M. (2006). Mechanisms for chromosome and plasmid segregation. *Annu. Rev. Biochem., 75*, 211-241.

Ginda, K., Bezulska, M., Ziółkiewicz, M., Dziadek, J., Zakrzewska-Czerwińska, J., & Jakimowicz, D. (2013). ParA of *Mycobacterium smegmatis* co-ordinates chromosome segregation with the cell cycle and interacts with the polar growth determinant DivIVA. *Molecular Microbiology, 87*(5), 998-1012.

Gitai, Z. (2006). Plasmid segregation: a new class of cytoskeletal proteins emerges. *Current Biology*, *16*(4), R133-R136.

Glaser, P., Sharpe, M. E., Raether, B., Perego, M., Ohlsen, K., & Errington, J. (1997). Dynamic, mitotic-like behavior of a bacterial protein required for accurate chromosome partitioning. *Genes & Development, 11*(9), 1160-1168.

Gober, J. W., & Marques, M. V. (1995). Regulation of cellular differentiation in *Caulobacter crescentus*. *Microbiological Reviews, 59*(1), 31-47.

Goodner, B., Hinkle, G., Gattung, S., Miller, N., Blanchard, M., Qurollo, B., ... & Mullin, L. (2001). Genome sequence of the plant pathogen and biotechnology agent *Agrobacterium tumefaciens* C58. *Science*, *294*(5550), 2323-2328.

Gordon, G. S., & Wright, A. (2000). DNA segregation in bacteria. *Annual Reviews in Microbiology*, *54*(1), 681-708.

Goudenège, D., Labreuche, Y., Krin, E., Ansquer, D., Mangenot, S., Calteau, A., ... & Le Roux, F. (2013). Comparative genomics of pathogenic lineages of *Vibrio nigripulchritudo* identifies virulence-associated traits. *The ISME journal*, *7*(10), 1985.

Green, M. R., and Sambrook, J. (2012) *Molecular cloning: a laboratory manual*, 2nd Ed., Cold Spring Harbor Laboratory Press, Cold Spring Harbor, NY

Griffiths, E., & Gupta, R. S. (2007). Identification of signature proteins that are distinctive of the Deinococcus-Thermus phylum. *International Microbiology*, *10*(3), 201.

Gruber, S., & Errington, J. (2009). Recruitment of condensin to replication origin regions by ParB/SpoOJ promotes chromosome segregation in *B. subtilis*. *Cell, 137*(4), 685-696.

Guarnieri, M. T., Blagg, B. S., & Zhao, R. (2011). A high-throughput TNP-ATP displacement assay for screening inhibitors of ATP-binding in bacterial histidine kinases. *Assay and Drug development Technologies*, *9*(2), 174-183.

Guynet, C., & de la Cruz, F. (2011). Plasmid segregation without partition. *Mobile Genetic Elements, 1*(3), 236-241.

Hanai, R., & Arai, Y. (2015). New roles of DNA and SopB in polymerization of SopA of Escherichia coli F plasmid. *The Journal of Biochemistry*, *157*(6), 459-466.

Harris, D. R., Tanaka, M., Saveliev, S. V., Jolivet, E., Earl, A. M., Cox, M. M., & Battista, J. R. (2004). Preserving genome integrity: the DdrA protein of *Deinococcus radiodurans* R1. *PLoS biology*, *2*(10), e304.

Harrison, P. W., Lower, R. P., Kim, N. K., & Young, J. P. W. (2010). Introducing the bacterial 'chromid': not a chromosome, not a plasmid. *Trends in Microbiology, 18*(4), 141-148.

Hasan, N. A., Grim, C. J., Haley, B. J., Chun, J., Alam, M., Taviani, E., ... & Bruce, D. C. (2010). Comparative genomics of clinical and environmental *Vibrio mimicus*. *Proceedings of the National Academy of Sciences USA*, *107*(49), 21134-21139.

Hatano, T., Yamaichi, Y., & Niki, H. (2007). Oscillating focus of SopA associated with filamentous structure guides partitioning of F plasmid. *Molecular Microbiology*, *64*(5), 1198-1213.

Hawiger, J., & Jeljaszewicz, J. (1967). Antibiotic sensitivity of *Micrococcus radiodurans*. *Appl. Environ. Microbiol.*, *15*(2), 304-306.

Hayakawa, T., Tanaka, T., Sakaguchi, K., Otake, N., & Yonehara, H. (1979). A linear plasmid-like DNA in *Streptomyces* sp. producing lankacidin group antibiotics. *The Journal of General and Applied Microbiology, 25*(4), 255-260.

Hayes, F., & Austin, S. (1994). Topological scanning of the P1 plasmid partition site. *Journal of Molecular Biology, 243*(2), 190-198.

Heidelberg, J. F., Eisen, J. A., Nelson, W. C., Clayton, R. A., Gwinn, M. L., Dodson, R. J., ... & Gill, S. R. (2000). DNA sequence of both chromosomes of the cholera pathogen *Vibrio cholerae*. *Nature*, *406*(6795), 477.

Helsberg, M. A. T. T. H. I. A. S., & Eichenlaub, R. U. D. O. L. F. (1986). Twelve 43-base-pair repeats map in a cis-acting region essential for partition of plasmid mini-F. *Journal of Bacteriology*, *165*(3), 1043-1045.

Hiemstra, H., Nanninga, N., Woldringh, C. L., Inouye, M., & Witholt, B. (1987). Distribution of newly synthesized lipoprotein over the outer membrane and the peptidoglycan sacculus of an *Escherichia coli* lac-lpp strain. *Journal of Bacteriology, 169*(12), 5434-5444.

Hiratsuka, T., & Uchida, K. (1973). Preparation and properties of 2′(or 3′)-O-(2, 4, 6-trinitrophenyl) adenosine 5′-triphosphate, an analog of adenosine triphosphate. *Biochimica et Biophysica Acta (BBA)-General Subjects*, *320*(3), 635-647.

Hjerde, E., Lorentzen, M. S., Holden, M. T., Seeger, K., Paulsen, S., Bason, N., ... & Sanders, S. (2008). The genome sequence of the fish pathogen *Aliivibrio salmonicida* strain LFI1238 shows extensive evidence of gene decay. *BMC Genomics*, *9*(1), 616.

Hoffmann, M., Monday, S. R., Allard, M. W., Strain, E. A., Whittaker, P., Naum, M., ... & Brown, E. W. (2012). *Vibrio caribbeanicus* sp. nov., isolated from the marine sponge *Scleritoderma cyanea*. *IJSEM*, *62*(8), 1736-1743.

Holden, M. T., Seth-Smith, H. M., Crossman, L. C., Sebaihia, M., Bentley, S. D., Cerdeño-Tárraga, A. M., ... & Cherevach, I. (2009). The genome of *Burkholderia cenocepacia* J2315, an epidemic pathogen of cystic fibrosis patients. *Journal of Bacteriology*, *191*(1), 261-277.

Holden, M. T., Titball, R. W., Peacock, S. J., Cerdeño-Tárraga, A. M., Atkins, T., Crossman, L. C., ... & Sebaihia, M. (2004). Genomic plasticity of the causative agent of melioidosis, *Burkholderia pseudomallei*. *Proceedings of the National Academy of Sciences USA*, *101*(39), 14240-14245.

Hormaeche, I., Alkorta, I., Moro, F., Valpuesta, J. M., Goñi, F. M., & de la Cruz, F. (2002). Purification and properties of TrwB, a hexameric, ATP-binding integral membrane protein essential for R388 plasmid conjugation. *Journal of Biological Chemistry*. *277*(48), 46456-46462.

Hu, L., Vecchiarelli, A. G., Mizuuchi, K., Neuman, K. C., & Liu, J. (2017). Brownian ratchet mechanism for faithful segregation of low-copy-number plasmids. *Biophysical Journal*, *112*(7), 1489-1502.

Hua, Y., Narumi, I., Gao, G., Tian, B., Satoh, K., Kitayama, S., & Shen, B. (2003). PprI: a general switch responsible for extreme radioresistance of *Deinococcus radiodurans*. *Biochemical and Biophysical Research Communications, 306*(2), 354-360.

Hui, M. P., Galkin, V. E., Yu, X., Stasiak, A. Z., Stasiak, A., Waldor, M. K., & Egelman, E. H. (2010). ParA2, a *Vibrio cholerae* chromosome partitioning protein, forms left-handed helical filaments on DNA. *Proceedings of the National Academy of Sciences USA*, *107*(10), 4590-4595.

Imlay, J. A. (2003). Pathways of oxidative damage. *Annual Reviews in Microbiology*, *57*(1), 395-418.

Ireton, K., & Grossman, A. D. (1994). A developmental checkpoint couples the initiation of sporulation to DNA replication in *Bacillus subtilis*. *The EMBO Journal, 13*(7), 1566-1573.

Ireton, K., Gunther, N. 4., & Grossman, A. D. (1994). spo0J is required for normal chromosome segregation as well as the initiation of sporulation in *Bacillus subtilis*. *Journal of Bacteriology, 176*(17), 5320-5329.

Jacob, F., Brenner, S., & Cuzin, F. (1963, January). On the regulation of DNA replication in bacteria. In Cold Spring Harbor symposia on quantitative biology (Vol. 28, pp. 329-348). *Cold Spring Harbor Laboratory Press*.

Jumas-Bilak, E., Michaux-Charachon, S., Bourg, G., O'callaghan, D., & Ramuz, M. (1998). Differences in chromosome number and genome rearrangements in the genus *Brucella*. *Molecular Microbiology, 27*(1), 99-106.

Kadoya, R., Baek, J. H., Sarker, A., & Chattoraj, D. K. (2011). Participation of a Chromosome Segregation Protein ParAI of *Vibrio cholerae* in Chromosome Replication. *Journal of Bacteriology*, (*193*)1504-14.

Karimova, G., Pidoux, J., Ullmann, A., & Ladant, D. (1998). A bacterial two-hybrid system based on a reconstituted signal transduction pathway. *Proceedings of the National Academy of Sciences USA*, *95*(10), 5752-5756.

Kelly, W. J., Leahy, S. C., Altermann, E., Yeoman, C. J., Dunne, J. C., Kong, Z., ... & Cookson, A. L. (2010). The glycobiome of the rumen bacterium *Butyrivibrio proteoclasticus* B316T highlights adaptation to a polysaccharide-rich environment. *PloS One*, *5*(8), e11942.

Khairnar, N. P., Kamble, V. A., & Misra, H. S. (2008). RecBC enzyme overproduction affects UV and gamma radiation survival of *Deinococcus radiodurans*. *DNA Repair*, *7*(1), 40-47.

Khairnar, N. P., Misra, H. S., & Apte, S. K. (2003). Pyrroloquinoline–quinone synthesized in *Escherichia coli* by pyrroloquinoline–quinone synthase of *Deinococcus radiodurans* plays a role beyond mineral phosphate solubilization. *Biochemical and biophysical research communications*, *312*(2), 303-308.

Kim, H. J., Calcutt, M. J., Schmidt, F. J., & Chater, K. F. (2000). Partitioning of the linear chromosome during sporulation of *Streptomyces coelicolor* A3 (2) involves an oriC-linked *parAB* locus. *Journal of Bacteriology, 182*(5), 1313-1320.

Kim, H., Jeong, W., Jeoung, H. Y., Song, J. Y., Kim, J. S., Beak, J. H., ... & Jung, S. C. (2012). Complete genome sequence of *Brucella abortus* A13334, a new strain isolated from the fetal gastric fluid of dairy cattle. *Journal of Bacteriology*, *194*(19), 5444-5444.

Komatsu, H., Imura, Y., Ohori, A., Nagata, Y., & Tsuda, M. (2003). Distribution and organization of auxotrophic genes on the multichromosomal genome of *Burkholderia multivorans* ATCC 17616. *Journal of Bacteriology*, *185*(11), 3333-3343.

Kota, S., & Misra, H. S. (2006). PprA: a protein implicated in radioresistance of *Deinococcus radiodurans* stimulates catalase activity in *Escherichia coli*. *Applied Microbiology and Biotechnology*, *72*(4), 790.

Kota, S., Charaka, V. K., Ringgaard, S., Waldor, M. K., & Misra, H. S. (2014). PprA contributes to *Deinococcus radiodurans* resistance to nalidixic acid, genome maintenance after DNA damage and interacts with deinococcal topoisomerases. *PLoS One*, *9*(1), e85288.

Kota, S., Kumar, C. V., & Misra, H. S. (2010). Characterization of an ATP-regulated DNA-processing enzyme and thermotolerant phosphoesterase in the radioresistant bacterium *Deinococcus radiodurans*. *Biochemical Journal*, *431*(1), 149-157.

Krasin, F., & Hutchinson, F. (1977). Repair of DNA double-strand breaks in Escherichia coli, which requires recA function and the presence of a duplicate genome. *Journal of Molecular Biology*, *116*(1), 81-98.

Kulkarni, G., Dhotre, D., Dharne, M., Shetty, S., Chowdhury, S., Misra, V., ... & Shouche, Y. (2013). Draft genome of *Ochrobactrum intermedium* strain M86 isolated from non-ulcer dyspeptic individual from India. *Gut Pathogens*, *5*(1), 7.

Labbe, R. G., & Huang, T. H. (1995). Generation times and modeling of enterotoxin-positive and enterotoxin-negative strains of *Clostridium perfringens* in laboratory media and ground beef. *Journal of Food Protection*, *58*(12), 1303-1306.

LaConte, L. E., Srivastava, S., & Mukherjee, K. (2017). Probing Protein Kinase-ATP Interactions Using a Fluorescent ATP Analog. In *Proteomics for Drug Discovery* (pp. 171-183). Humana Press, New York, NY.

Lakowicz, J. R. (1983) *Principles of Fluorescence Spectroscopy*, pp. 257–301, Plenum Press, New York.

Larsen, R. A., Cusumano, C., Fujioka, A., Lim-Fong, G., Patterson, P., & Pogliano, J. (2007). Treadmilling of a prokaryotic tubulin-like protein, TubZ, required for plasmid stability in Bacillus thuringiensis. Genes & development, 21(11), 000-000.

Lau, I. F., Filipe, S. R., Søballe, B., Økstad, O. A., Barre, F. X., & Sherratt, D. J. (2003). Spatial and temporal organization of replicating *Escherichia coli* chromosomes. *Molecular Microbiology*, *49*(3), 731-743.

Le Roux, F., Zouine, M., Chakroun, N., Binesse, J., Saulnier, D., Bouchier, C., ... & Buchrieser, C. (2009). Genome sequence of *Vibrio splendidus*: an abundant planctonic marine species with a large genotypic diversity. *Environmental Microbiology*, *11*(8), 1959-1970.

Le, T. B., & Laub, M. T. (2014). New approaches to understanding the spatial organization of bacterial genomes. Current opinion in microbiology, 22, 15-21.

Le, T. B., Imakaev, M. V., Mirny, L. A., & Laub, M. T. (2013). High-resolution mapping of the spatial organization of a bacterial chromosome. Science, 342(6159), 731-734.

Lee, P. S., & Grossman, A. D. (2006). The chromosome partitioning proteins Soj (ParA) and Spo0J (ParB) contribute to accurate chromosome partitioning, separation of replicated sister origins, and regulation of replication initiation in *Bacillus subtilis*. *Molecular Microbiology, 60*(4), 853-869.

Lee, P. S., Lin, D. C. H., Moriya, S., & Grossman, A. D. (2003). Effects of the chromosome partitioning protein Spo0J (ParB) on oriC positioning and replication initiation in *Bacillus subtilis*. *Journal of Bacteriology, 185*(4), 1326-1337.

Lemon, K. P., & Grossman, A. D. (2001). The extrusion-capture model for chromosome partitioning in bacteria. *Genes & Development, 15*(16), 2031-2041.

Leonard, T. A., Butler, P. J. G., & Löwe, J. (2004). Structural analysis of the chromosome segregation protein Spo0J from *Thermus thermophilus*. *Molecular Microbiology*, *53*(2), 419-432.

Leonard, T. A., Butler, P. J., & Löwe, J. (2005). Bacterial chromosome segregation: structure and DNA binding of the Soj dimer—a conserved biological switch. *The EMBO Journal*, *24*(2), 270-282.

Leonard, T. A., Møller-Jensen, J., & Löwe, J. (2005). Towards understanding the molecular basis of bacterial DNA segregation. *Philosophical Transactions of the Royal Society of London B: Biological Sciences*, *360*(1455), 523-535.

Lerner-Marmarosh, N., Gimi, K., Urbatsch, I. L., Gros, P., & Senior, A. E. (1999). Large Scale Purification of Detergent-soluble P-glycoprotein fromPichia pastoris Cells and Characterization of Nucleotide Binding Properties of Wild-type, Walker A, and Walker B Mutant Proteins. *Journal of Biological Chemistry*, *274*(49), 34711-34718.

Levin-Zaidman, S., Englander, J., Shimoni, E., Sharma, A. K., Minton, K. W., & Minsky, A. (2003). Ringlike structure of the *Deinococcus radiodurans* genome: a key to radioresistance? *Science*, *299*(5604), 254-256.

Lewis, R. A., Bignell, C. R., Zeng, W., Jones, A. C., & Thomas, C. M. (2002). Chromosome loss from par mutants of *Pseudomonas putida* depends on growth medium and phase of growth. *Microbiology, 148*(2), 537-548.

Li, Y., Sergueev, K., & Austin, S. (2002). The segregation of the *Escherichia coli* origin and terminus of replication. *Molecular microbiology*, *46*(4), 985-996.

Lieberman-Aiden, E., Van Berkum, N. L., Williams, L., Imakaev, M., Ragoczy, T., Telling, A., ... & Sandstrom, R. (2009). Comprehensive mapping of long-range interactions reveals folding principles of the human genome. Science, 326(5950), 289-293.

Lim, S. K., Kim, S. J., Cha, S. H., Oh, Y. K., Rhee, H. J., Kim, M. S., & Lee, J. K. (2009). Complete genome sequence of *Rhodobacter sphaeroides* KD131. *Journal of Bacteriology*, *191*(3), 1118-1119.

Lim, S., Jung, J. H., Blanchard, L., & De Groot, A. (2018). Conservation and diversity of radiation and oxidative stress resistance mechanisms in *Deinococcus* species. *FEMS Microbiology Reviews*, *43*(1), 19-52.

Lin, D. C. H., & Grossman, A. D. (1998). Identification and characterization of a bacterial chromosome partitioning site. *Cell, 92*(5), 675-685.

Liu, X. F., Cao, Y., Zhang, H. L., Chen, Y. J., & Hu, C. J. (2015). Complete genome sequence of *Vibrio alginolyticus* ATCC 17749T. *Genome Announcements*, *3*(1), e01500-14.

Livny, J., Yamaichi, Y., & Waldor, M. K. (2007). Distribution of centromere-like *parS* sites in bacteria: insights from comparative genomics. *Journal of Bacteriology*, *189*(23), 8693-8703.

Lown, J. W., Sim, S. K., & Chen, H. H. (1978). Hydroxyl radical production by free and DNA-bound aminoquinone antibiotics and its role in DNA degradation. Electron spin resonance detection of hydroxyl radicals by spin trapping. *Canadian Journal of Biochemistry*, *56*(11), 1042-1047.

Luijsterburg, M. S., White, M. F., van Driel, R., & Dame, R. T. (2008). The major architects of chromatin: architectural proteins in bacteria, archaea and eukaryotes. *Critical Reviews in Biochemistry and Molecular Biology, 43*(6), 393-418.

Lux, T. M., Lee, R., & Love, J. (2011). The Complete Genome Sequence of a free-living *Vibrio furnissii* sp. Nov. strain (NCTC 11218). *Journal of Bacteriology*, *193*:1487–1488

Lykidis, A., Perez-Pantoja, D., Ledger, T., Mavromatis, K., Anderson, I. J., Ivanova, N. N., ... & Kyrpides, N. C. (2010). The complete multipartite genome sequence of *Cupriavidus necator* JMP134, a versatile pollutant degrader. *PloS One*, *5*(3), e9729.

Madariaga-Marcos, J., Pastrana, C. L., Fisher, G. L., Dillingham, M. S., & Moreno-Herrero, F. (2018). ParB dynamics and the critical role of the CTD in DNA condensation unveiled by combined force-fluorescence measurements. *bioRxiv,* 477836.

Makarova, K. S., Aravind, L., Wolf, Y. I., Tatusov, R. L., Minton, K. W., Koonin, E. V., & Daly, M. J. (2001). Genome of the extremely radiation-resistant bacterium *Deinococcus radiodurans* viewed from the perspective of comparative genomics. *Microbiology and molecular biology reviews*, *65*(1), 44-79.

Makino, K., Oshima, K., Kurokawa, K., Yokoyama, K., Uda, T., Tagomori, K., ... & Kubota, Y. (2003). Genome sequence of *Vibrio parahaemolyticus*: a pathogenic mechanism distinct from that of *V cholerae*. *The Lancet*, *361*(9359), 743-749.

Martin, K. A., Davis, M. A., & Austin, S. (1991). Fine-structure analysis of the P1 plasmid partition site. *Journal of Bacteriology, 173*(12), 3630-3634.

Maurya, G. K., Modi, K., Banerjee, M., Chaudhary, R., Rajpurohit, Y. S., & Misra, H. S. (2018). Phosphorylation of FtsZ and FtsA by a DNA Damage-Responsive Ser/Thr Protein Kinase Affects Their Functional Interactions in *Deinococcus radiodurans*. *mSphere*, *3*(4), e00325-18.

Médigue, C., Krin, E., Pascal, G., Barbe, V., Bernsel, A., Bertin, P. N., ... & Fang, G. (2005). Coping with cold: the genome of the versatile marine Antarctica bacterium *Pseudoalteromonas haloplanktis* TAC125. *Genome Research*, *15*(10), 1325-1335.

Meima, R., & Lidstrom, M. E. (2000). Characterization of the minimal replicon of a cryptic *Deinococcus radiodurans* SARK plasmid and development of versatile *Escherichia coli-D. radiodurans* shuttle vectors. *Applied and Environmental Microbiology*, *66*(9), 3856-3867.

Meyer, L., Coste, G., Sommer, S., Oberto, J., Confalonieri, F., Servant, P., & Pasternak, C. (2018). DdrI, a CRP family member, acts as a major regulator for adaptation of *Deinococcus radiodurans* to various stresses. *Journal of Bacteriology,* JB-00129.

Michaux, S., Paillisson, J., Carles-Nurit, M., Bourg., Allardet-Servent, A., & Ramuz, M. (1993). Presence of two independent chromosomes in the *Brucella melitensis* 16M genome. *Journal of Bacteriology*, *175*(3), 701-705.

Misra, H. S., Khairnar, N. P., Kota, S., Shrivastava, S., Joshi, V. P., & Apte, S. K. (2006). An exonuclease I-sensitive DNA repair pathway in *Deinococcus radiodurans*: a major determinant of radiation resistance. *Molecular Microbiology*, *59*(4), 1308-1316.

Misra, H. S., Maurya, G. K., Chaudhary, R., & Misra, C. S. (2018). Interdependence of bacterial cell division and genome segregation and its potential in drug development. *Microbiological Research, 208*, 12-24.

Misra, H. S., Maurya, G. K., Kota, S., & Charaka, V. K. (2018). Maintenance of multipartite genome system and its functional significance in bacteria. *Journal of Genetics*, 1-26.

Misra, H. S., Rajpurohit, Y. S., & Kota, S. (2013). Physiological and molecular basis of extreme radioresistance in *Deinococcus radiodurans*. *Current Science (Bangalore)*, *104*(2), 194-205.

Modi, K. M., Tewari, R., & Misra, H. S. (2014). FtsZDr, a tubulin homologue in radioresistant bacterium *Deinococcus radiodurans* is characterized as a GTPase exhibiting polymerization/depolymerization dynamics in vitro and FtsZ ring formation in vivo. *The international Journal of Biochemistry & Cell Biology*, *50*, 38-46.

Modi, K., & Misra, H. S. (2014). Dr-FtsA, an actin homologue in *Deinococcus radiodurans* differentially affects Dr-FtsZ and Ec-FtsZ functions in vitro. *PloS One*, *9*(12), e115918.

Mohl, D. A., & Gober, J. W. (1997). Cell cycle–dependent polar localization of chromosome partitioning proteins in *Caulobacter crescentus. Cell, 88*(5), 675-684.

Mohl, D. A., Easter Jr, J., & Gober, J. W. (2001). The chromosome partitioning protein, ParB, is required for cytokinesis in *Caulobacter crescentus*. *Molecular Microbiology, 42*(3), 741-755.

Møller-Jensen, J., Ringgaard, S., Mercogliano, C. P., Gerdes, K., & Löwe, J. (2007). Structural analysis of the ParR/parC plasmid partition complex. *The EMBO Journal, 26*(20), 4413-4422.

Moreno, E. (1998). Genome evolution within the alpha Proteobacteria: why do some bacteria not possess plasmids and others exhibit more than one different chromosome?. *FEMS Microbiology Reviews, 22*(4), 255-275.

Moseley, B. E. B., & Evans, D. M. (1983). Isolation and properties of strains of Micrococcus *Deinococcus radiodurans* unable to excise ultraviolet light-induced pyrimidine dimers from DNA: evidence for two excision pathways. *Microbiology*, *129*(8), 2437-2445.

Murray, H., & Errington, J. (2008). Dynamic control of the DNA replication initiation protein DnaA by Soj/ParA. *Cell, 135*(1), 74-84.

Murray, H., Ferreira, H., & Errington, J. (2006). The bacterial chromosome segregation protein Spo0J spreads along DNA from parS nucleation sites. *Molecular Microbiology, 61*(5), 1352-1361.

Murray, R. G. E., & Brooks, B. W. (1986). *Deinococcus*. *Bergey's Manual of Systematic Bacteriology*, *2*, 1035-1043.

Nagata, Y., Ohtsubo, Y., Endo, R., Ichikawa, N., Ankai, A., Oguchi, A., ... & Tsuda, M. (2010). Complete genome sequence of the representative γ-hexachlorocyclohexane-degrading bacterium *Sphingobium japonicum* UT26. *Journal of Bacteriology*, *192*(21), 5852-5853.

Naka, H., Dias, G. M., Thompson, C. C., Dubay, C., Thompson, F. L., & Crosa, J. H. (2011). Complete genome sequence of the marine fish pathogen *Vibrio anguillarum* harboring the pJM1 virulence plasmid and genomic comparison with other virulent strains of *V. anguillarum* and *V. ordalii*. *Infection and Immunity*, IAI-05138.

Nambu, T., Yamane, K., Maruyama, H., Mashimo, C., & Yamanaka, T. (2015). Complete genome sequence of *Prevotella intermedia* strain 17-2. *Genome Announcements*, *3*(4), e00951-15.

Narumi, I., Satoh, K., Cui, S., Funayama, T., Kitayama, S., & Watanabe, H. (2004). PprA: a novel protein from *Deinococcus radiodurans* that stimulates DNA ligation. *Molecular Microbiology*, *54*(1), 278-285.

Nath, J., & Johnson, K. L. (2000). A review of fluorescence in situ hybridization (FISH): current status and future prospects. *Biotechnic & Histochemistry, 75*(2), 54-78.

Nelson, K. E., Clayton, R. A., Gill, S. R., Gwinn, M. L., Dodson, R. J., Haft, D. H., ... & McDonald, L. (1999). Evidence for lateral gene transfer between Archaea and bacteria from genome sequence of *Thermotoga maritima*. *Nature*, *399*(6734), 323.

Ni, L., Xu, W., Kumaraswami, M., & Schumacher, M. A. (2010). Plasmid protein TubR uses a distinct mode of HTH-DNA binding and recruits the prokaryotic tubulin homolog TubZ to effect DNA partition. *Proceedings of the National Academy of Sciences USA, 107*:11763–11768.

Nierman, W. C., DeShazer, D., Kim, H. S., Tettelin, H., Nelson, K. E., Feldblyum, T., ... & Davidsen, T. D. (2004). Structural flexibility in the *Burkholderia mallei* genome. *Proceedings of the National Academy of Sciences USA*, *101*(39), 14246-14251.

Niki, H., Yamaichi, Y., & Hiraga, S. (2000). Dynamic organization of chromosomal DNA in *Escherichia col*i. *Genes & Development, 14*(2), 212-223.

Ogura, T., & Hiraga, S. (1983). Mini-F plasmid genes that couple host cell division to plasmid proliferation. *Proceedings of the National Academy of Sciences USA, 80*(15), 4784-4788.

Ohtsubo, Y., Fujita, N., Nagata, Y., Tsuda, M., Iwasaki, T., & Hatta, T. (2013). Complete genome sequence of *Ralstonia pickettii* DTP0602, a 2, 4, 6-trichlorophenol degrader. *Genome Announcements*, *1*(6), e00903-13.

Okada, K., Iida, T., Kita-Tsukamoto, K., & Honda, T. (2005). Vibrios commonly possess two chromosomes. *Journal of Bacteriology*, *187*(2), 752-757.

Okumura, T., Makiguchi, H., Makita, Y., Yamashita, R., & Nakai, K. (2007). Melina II: a web tool for comparisons among several predictive algorithms to find potential motifs from promoter regions. *Nucleic Acids Research*, *35*(suppl_2), W227-W231.

Oliva, M. A. (2016). Segrosome complex formation during DNA trafficking in bacterial cell division. *Frontiers in Molecular Biosciences, 3*, 51.

Omelchenko, M. V., Wolf, Y. I., Gaidamakova, E. K., Matrosova, V. Y., Vasilenko, A., Zhai, M., ... & Makarova, K. S. (2005). Comparative genomics of *Thermus thermophilus* and *Deinococcus radiodurans*: divergent routes of adaptation to thermophily and radiation resistance. *BMC evolutionary biology*, *5*(1), 57.

Pang, T., Wang, X., Lim, H. C., Bernhardt, T. G., & Rudner, D. Z. (2017). The nucleoid occlusion factor Noc controls DNA replication initiation in *Staphylococcus aureus*. *PLoS Genetics, 13*(7), e1006908.

Paulsen, I. T., Seshadri, R., Nelson, K. E., Eisen, J. A., Heidelberg, J. F., Read, T. D., ... & Daugherty, S. C. (2002). The *Brucella suis* genome reveals fundamental similarities between animal and plant pathogens and symbionts. *Proceedings of the National Academy of Sciences USA*, *99*(20), 13148-13153.

Phillips-Cremins, J. E., & Corces, V. G. (2013). Chromatin insulators: linking genome organization to cellular function. *Molecular Cell, 50*(4), 461-474.

Plesniak, L., Horiuchi, Y., Sem, D., Meinenger, D., Stiles, L., Shaffer, J., ... & Adams, J. A. (2002). Probing the nucleotide binding domain of the osmoregulator EnvZ using fluorescent nucleotide derivatives. *Biochemistry*, *41*(47), 13876-13882.

Potts, M. (1994). Desiccation tolerance of prokaryotes. *Microbiol. Mol. Biol. Rev.*, *58*(4), 755-805.

Prozorov, A. A. (2008). Additional chromosomes in bacteria: Properties and origin. *Microbiology*, *77*(4), 385-394.

Ptacin, J. L., Lee, S. F., Garner, E. C., Toro, E., Eckart, M., Comolli, L. R., ... & Shapiro, L. (2010). A spindle-like apparatus guides bacterial chromosome segregation. *Nature Cell Biology, 12*(8), 791.

Qin, Q. L., Li, Y., Zhang, Y. J., Zhou, Z. M., Zhang, W. X., Chen, X. L., ... & Zhang, Y. Z. (2011). Comparative genomics reveals a deep-sea sediment-adapted life style of *Pseudoalteromonas* sp. SM9913. *The ISME Journal*, *5*(2), 274.

Quisel, J. D., & Grossman, A. D. (2000). Control of sporulation gene expression in Bacillus subtilis by the chromosome partitioning proteins Soj (ParA) and Spo0J (ParB). *Journal of Bacteriology, 182*(12), 3446-3451.

Rajanikant, C., Kumbhakar, M., Pal, H., Rao, B. J., & Sainis, J. K. (2006). DNA strand exchange activity of rice recombinase OsDmc1 monitored by fluorescence resonance energy transfer and the role of ATP hydrolysis. *The FEBS Journal*, *273*(7), 1497-1506.

Rajpurohit, Y. S., & Misra, H. S. (2010). Characterization of a DNA damage-inducible membrane protein kinase from *Deinococcus radiodurans* and its role in bacterial radioresistance and DNA strand break repair. *Molecular Microbiology*, *77*(6), 1470-1482.

Rajpurohit, Y. S., & Misra, H. S. (2013). Structure-function study of deinococcal serine/threonine protein kinase implicates its kinase activity and DNA repair protein phosphorylation roles in radioresistance of *Deinococcus radiodurans*. *The International Journal of Biochemistry & Cell Biology*, *45*(11), 2541-2552.

Rajpurohit, Y. S., Gopalakrishnan, R., & Misra, H. S. (2008). Involvement of a protein kinase activity inducer in DNA double strand break repair and radioresistance of *Deinococcus radiodurans*. *Journal of Bacteriology*, *190*(11), 3948-3954.

Rasmussen, T., Jensen, R. B., & Skovgaard, O. (2007). The two chromosomes of *Vibrio cholerae* are initiated at different time points in the cell cycle. *The EMBO Journal*, *26*(13), 3124-3131.

Ravin, N. V., Rech, J., & Lane, D. (2003). Mapping of functional domains in F plasmid partition proteins reveals a bipartite SopB-recognition domain in SopA. *Journal of Molecular Biology*, *329*(5), 875-889.

Ren, S. X., Fu, G., Jiang, X. G., Zeng, R., Miao, Y. G., Xu, H., ... & Jiang, H. Q. (2003). Unique physiological and pathogenic features of *Leptospira interrogans* revealed by whole-genome sequencing. *Nature*, *422*(6934), 888.

Reyes-Lamothe, R., Nicolas, E., & Sherratt, D. J. (2012). Chromosome replication and segregation in bacteria. *Annual Review of Genetics, 46*, 121-143.

Ringgaard, S., van Zon, J., Howard, M., & Gerdes, K. (2009). Movement and equipositioning of plasmids by ParA filament disassembly. *Proceedings of the National Academy of Sciences, USA*-0908347106.

Robinett, C. C., Straight, A., Li, G., Willhelm, C., Sudlow, G., Murray, A., & Belmont, A. S. (1996). In vivo localization of DNA sequences and visualization of large-scale chromatin organization using lac operator/repressor recognition. *The Journal of Cell Biology, 135*(6), 1685-1700.

Rothkamm, K., & Löbrich, M. (2003). Evidence for a lack of DNA double-strand break repair in human cells exposed to very low x-ray doses. *Proceedings of the National Academy of Sciences*, *USA*, *100*(9), 5057-5062.

Ruby, E. G., Urbanowski, M., Campbell, J., Dunn, A., Faini, M., Gunsalus, R., ... & Schaefer, A. (2005). Complete genome sequence of *Vibrio fischeri*: a symbiotic bacterium with pathogenic congeners. *Proceedings of the National Academy of Sciences USA*, *102*(8), 3004-3009.

Saint-Dic, D., Frushour, B. P., Kehrl, J. H., & Kahng, L. S. (2006). A parA homolog selectively influences positioning of the large chromosome origin in *Vibrio cholerae*. *Journal of Bacteriology*, *188*(15), 5626-5631.

Schumacher, M. A. (2012). Bacterial plasmid partition machinery: a minimalist approach to survival. *Current Opinion in Structural Biology, 22*(1), 72-79.

Schumacher, M. A., & Funnell, B. E. (2005). Structures of ParB bound to DNA reveal mechanism of partition complex formation. *Nature, 438*(7067), 516.

Schumacher, M. A., Glover, T. C., Brzoska, A. J., Jensen, S. O., Dunham, T. D., Skurray, R. A., & Firth, N. (2007). Segrosome structure revealed by a complex of ParR with centromere DNA. *Nature, 450*(7173), 1268.

Schumacher, M. A., Mansoor, A., & Funnell, B. E. (2007). Structure of a four-way bridged ParB-DNA complex provides insight into P1 segrosome assembly. *Journal of Biological Chemistry*, (*282*) 10456–10464.

Sellars, L. E., Bryant, J. A., Sánchez-Romero, M. A., Sánchez-Morán, E., Busby, S. J., & Lee, D. J. (2017). Development of a new fluorescent reporter: operator system: location of AraC regulated genes in Escherichia coli K-12. *BMC Microbiology, 17*(1), 170.

Seo, Y. S., Lim, J., Choi, B. S., Kim, H., Goo, E., Lee, B., ... & Hwang, I. (2011). Complete genome sequence of *Burkholderia gladioli* BSR3. *Journal of Bacteriology*, *193*(12), 3149.

Servant, P., Jolivet, E., Bentchikou, E., Mennecier, S., Bailone, A., & Sommer, S. (2007). The ClpPX protease is required for radioresistance and regulates cell division after γ-irradiation in *Deinococcus radiodurans*. *Molecular Microbiology*, *66*(5), 1231-1239.

Sharpe, M. E., & Errington, J. (1996). The *Bacillus subtilis* soj-spo0J locus is required for a centromere-like function involved in prespore chromosome partitioning. *Molecular Microbiology, 21*(3), 501-509.

Shebelut, C. W., Guberman, J. M., Van Teeffelen, S., Yakhnina, A. A., & Gitai, Z. (2010). *Caulobacter* chromosome segregation is an ordered multistep process. *Proceedings of the National Academy of Sciences USA, 107*(32), 14194-14198.

Shrivastava, R., Ghosh, A. K., & Das, A. K. (2007). Probing the nucleotide binding and phosphorylation by the histidine kinase of a novel three-protein two-component system from Mycobacterium tuberculosis. *FEBS letters*, *581*(9), 1903-1909.

Simonis, M., Klous, P., Splinter, E., Moshkin, Y., Willemsen, R., De Wit, E., ... & De Laat, W. (2006). Nuclear organization of active and inactive chromatin domains uncovered by chromosome conformation capture–on-chip (4C). *Nature Genetics, 38*(11), 1348.

Slade, D., & Radman, M. (2011). Oxidative stress resistance in *Deinococcus radiodurans*. *Microbiology and molecular biology reviews, 75*(1), 133-191.

Slater, S. C., Goldman, B. S., Goodner, B., Setubal, J. C., Farrand, S. K., Nester, E. W., ... & Otten, L. (2009). Genome sequences of three *Agrobacterium* biovars help elucidate the evolution of multichromosome genomes in bacteria. *Journal of Bacteriology*, *191*(8), 2501-2511.

Sobral, B. W., Honeycutt, R. J., Atherly, A. G., & McClelland, M. (1991). Electrophoretic separation of the three *Rhizobium meliloti* replicons. *Journal of Bacteriology*, *173*(16), 5173-5180.

Song, D., Rodrigues, K., Graham, T. G., & Loparo, J. J. (2017). A network of cis and trans interactions is required for ParB spreading. *Nucleic Acids Research, 45*(12), 7106-7117.

Stewart, R. C., VanBruggen, R., Ellefson, D. D., & Wolfe, A. J. (1998). TNP-ATP and TNP-ADP as probes of the nucleotide binding site of CheA, the histidine protein kinase in the chemotaxis signal transduction pathway of Escherichia coli. *Biochemistry*, *37*(35), 12269-12279.

Stokke, C., Waldminghaus, T., & Skarstad, K. (2011). Replication patterns and organization of replication forks in *Vibrio cholerae*. *Microbiology*, *157*(3), 695-708.

Subramanian, V. V., & Hochwagen, A. (2014). The meiotic checkpoint network: step-by-step through meiotic prophase. *Cold Spring Harbor Perspectives in Biology, 6*(10), a016675.

Suwanto, A., & Kaplan, S. (1989). Physical and genetic mapping of the *Rhodobacter sphaeroides* 2.4. 1 genome: presence of two unique circular chromosomes. *Journal of Bacteriology*, 171(11), 5850-5859.

Tae, H., Shallom, S., Settlage, R., Preston, D., Adams, L. G., & Garner, H. R. (2011). Revised genome sequence of *Brucella suis* 1330. *Journal of Bacteriology*, *193*(22), 6410-6410.

Taylor, J. A., Pastrana, C. L., Butterer, A., Pernstich, C., Gwynn, E. J., Sobott, F., ... & Dillingham, M. S. (2015). Specific and non-specific interactions of ParB with DNA: implications for chromosome segregation. *Nucleic Acids Research, 43*(2), 719-731.

Teleman, A. A., Graumann, P. L., Lin, D. C. H., Grossman, A. D., & Losick, R. (1998). Chromosome arrangement within a bacterium. *Current Biology, 8*(20), 1102-1109.

Temperton, B., Thomas, S., Tait, K., Parry, H., Emery, M., Allen, M., ... & Gilbert, J. (2011). Permanent draft genome sequence of *Vibrio tubiashii* strain NCIMB 1337 (ATCC19106). *Standards in Genomic Sciences*, *4*(2), 183.

Tessema, M., Lehmann, U., & Kreipe, H. (2004). Cell cycle and no end. *Virchows Archiv, 444*(4), 313-323.

Thanbichler, M. (2010). Synchronization of chromosome dynamics and cell division in bacteria. *Cold Spring Harbor Perspectives in Biology, 2*(1), a000331.

Thanbichler, M., & Shapiro, L. (2006). MipZ, a spatial regulator coordinating chromosome segregation with cell division in *Caulobacter*. *Cell, 126*(1), 147-162.

Thrower, D. A., & Bloom, K. (2001). Dicentric chromosome stretching during anaphase reveals roles of Sir2/Ku in chromatin compaction in budding yeast. *Molecular Biology of the Cell, 12*(9), 2800-2812.

Tian, B., Wu, Y., Sheng, D., Zheng, Z., Gao, G., & Hua, Y. (2004). Chemiluminescence assay for reactive oxygen species scavenging activities and inhibition on oxidative damage of DNA in *Deinococcus radiodurans*. *Luminescence: the journal of biological and chemical luminescence*, *19*(2), 78-84.

Tran, N. T., Laub, M. T., & Le, T. B. (2017). SMC progressively aligns chromosomal arms in *Caulobacter crescentus* but is antagonized by convergent transcription. *Cell Reports*, *20*(9), 2057-2071.

Treuner-Lange, A., Aguiluz, K., van der Does, C., Gómez-Santos, N., Harms, A., Schumacher, D., ... & Søgaard-Andersen, L. (2013). PomZ, a ParA-like protein, regulates Z-ring formation and cell division in M yxococcus xanthus. *Molecular microbiology*, *87*(2), 235-253.

Trucksis, M., Michalski, J., Deng, Y. K., & Kaper, J. B. (1998). The *Vibrio cholerae* genome contains two unique circular chromosomes. *Proceedings of the National Academy of Sciences*, *95*(24), 14464-14469.

Trussart, M., Yus, E., Martinez, S., Bau, D., Tahara, Y. O., Pengo, T., ... & Turnbull, L. (2017). Defined chromosome structure in the genome-reduced bacterium *Mycoplasma pneumoniae*. *Nature Communications*, 8, 14665.

Tsolis, R. M., Seshadri, R., Santos, R. L., Sangari, F. J., Lobo, J. M. G., De Jong, M. F., ... & DeBoy, R. T. (2009). Genome degradation in *Brucella ovis* corresponds with narrowing of its host range and tissue tropism. *PloS One*, *4*(5), e5519.

Tuanyok, A., Mayo, M., Scholz, H., Hall, C. M., Allender, C. J., Kaestli, M., ... & Settles, E. W. (2017). *Burkholderia humptydooens*is sp. nov., a new species related to *Burkholderia thailandensis* and the fifth member of the *Burkholderia pseudomallei* complex. *Appl. Environ. Microbiol.*, *83*(5), e02802-16.

Umbarger, M. A., Toro, E., Wright, M. A., Porreca, G. J., Bau, D., Hong, S. H., ... & Shapiro, L. (2011). The three-dimensional architecture of a bacterial genome and its alteration by genetic perturbation. *Molecular Cell, 44*(2), 252-264.

Vallet-Gely, I., & Boccard, F. (2013). Chromosomal organization and segregation in *Pseudomonas aeruginosa*. *PLoS Genetics, 9*(5), e1003492.

Van Der Valk, R. A., Vreede, J., Crémazy, F., & Dame, R. T. (2014). Genomic looping: a key principle of chromatin organization. *Journal of Molecular Microbiology and Biotechnology, 24*(5-6), 344-359.

Vecchiarelli, A. G., Han, Y. W., Tan, X., Mizuuchi, M., Ghirlando, R., Biertümpfel, C., ... & Mizuuchi, K. (2010). ATP control of dynamic P1 ParA–DNA interactions: a key role for the nucleoid in plasmid partition. *Molecular Microbiology*, *78*(1), 78-91.

Vecchiarelli, A. G., Neuman, K. C., & Mizuuchi, K. (2014). A propagating ATPase gradient drives transport of surface-confined cellular cargo. *Proceedings of the National Academy of Sciences USA*, 201401025.

Vezzi, A., Campanaro, S., D'angelo, M., Simonato, F., Vitulo, N., Lauro, F. M., ... & Romualdi, C. (2005). Life at depth: *Photobacterium profundum* genome sequence and expression analysis. *Science*, *307*(5714), 1459-1461.

Viollier, P. H., Thanbichler, M., McGrath, P. T., West, L., Meewan, M., McAdams, H. H., & Shapiro, L. (2004). Rapid and sequential movement of individual chromosomal loci to specific subcellular

locations during bacterial DNA replication. *Proceedings of the National Academy of Sciences USA*, *101*(25), 9257-9262.

Volante, A., Carrasco, B., Tabone, M., & Alonso, J. C. (2015). The interaction of ω2 with the RNA polymerase β'subunit functions as an activation to repression switch. *Nucleic Acids Research*, *43*(19), 9249-9261.

Wang, H., Sivonen, K., Rouhiainen, L., Fewer, D. P., Lyra, C., Rantala-Ylinen, A., ... & Liu, B. (2012). Genome-derived insights into the biology of the hepatotoxic bloom-forming cyanobacterium *Anabaena* sp. strain 90. *BMC Genomics*, *13*(1), 613.

Wang, X., Brandão, H. B., Le, T. B., Laub, M. T., & Rudner, D. Z. (2017). *Bacillus subtilis* SMC complexes juxtapose chromosome arms as they travel from origin to terminus. *Science, 355*(6324), 524-527.

Wang, X., Le, T. B., Lajoie, B. R., Dekker, J., Laub, M. T., & Rudner, D. Z. (2015). Condensin promotes the juxtaposition of DNA flanking its loading site in *Bacillus subtilis. Genes & Development, 29*(15), 1661-1675.

Wang, X., Liu, X., Possoz, C., & Sherratt, D. J. (2006). The two *Escherichia coli* chromosome arms locate to separate cell halves. *Genes & Development, 20*(13), 1727-1731.

Wang, Z., Lin, B., Hervey, W. J., & Vora, G. J. (2013). Draft genome sequence of the fast-growing marine bacterium *Vibrio natriegens* strain ATCC 14048. *Genome Announcements*, *1*(4), e00589-13.

Ward, L. D. (1985). Measurement of ligand binding to proteins by fluorescence spectroscopy. In *Methods in Enzymology* (Vol. 117, pp. 400-414). Academic press.

Webb, C. D., Teleman, A., Gordon, S., Straight, A., Belmont, A., Lin, D. C. H., ... & Losick, R. (1997). Bipolar localization of the replication origin regions of chromosomes in vegetative and sporulating cells of *B. subtilis*. *Cell, 88*(5), 667-674.

Welsh, E. A., Liberton, M., Stöckel, J., Loh, T., Elvitigala, T., Wang, C., ... & Aurora, R. (2008). The genome of *Cyanothece* 51142, a unicellular diazotrophic cyanobacterium important in the marine nitrogen cycle. *Proceedings of the National Academy of Sciences USA*, *105*(39), 15094-15099.

White, O., Eisen, J. A., Heidelberg, J. F., Hickey, E. K., Peterson, J. D., Dodson, R. J., ... & Moffat, K. S. (1999). Genome sequence of the radioresistant bacterium *Deinococcus radiodurans* R1. *Science*, *286*(5444), 1571-1577.

Wiedenbeck, J., & Cohan, F. M. (2011). Origins of bacterial diversity through horizontal genetic transfer and adaptation to new ecological niches. *FEMS Microbiology Reviews, 35*(5), 957-976.

Wientjes, F. B., & Nanninga, N. (1989). Rate and topography of peptidoglycan synthesis during cell division in *Escherichia coli*: concept of a leading edge. *Journal of Bacteriology*, *171*(6), 3412-3419.

Work, E., & Griffiths, H. (1968). Morphology and chemistry of cell walls of *Micrococcus radiodurans*. *Journal of Bacteriology*, *95*(2), 641-657.

Workentine, M. L., Surette, M. G., & Bernier, S. P. (2014). Draft genome sequence of *Burkholderia dolosa* PC543 isolated from cystic fibrosis airways. *Genome Announcements*, *2*(1), e00043-14.

Xu, W., Shen, J., Dunn, C. A., Desai, S., & Bessman, M. J. (2001). The Nudix hydrolases of *Deinococcus radiodurans*. *Molecular Microbiology*, *39*(2), 286-290.

Yamaichi, Y., Fogel, M. A., McLeod, S. M., Hui, M. P., & Waldor, M. K. (2007). Distinct centromere-like parS sites on the two chromosomes of *Vibrio* spp. *Journal of Bacteriology, 189*(14), 5314-5324.

Yan, Z. Y., Xu, Z. J., Xu, G. Z., Tian, B., & Hua, Y. J. (2007). Construction of a dps mutant and its functional analysis in *Deinococcus radiodurans*. *Wei sheng wu xue bao= Acta microbiologica Sinica*, *47*(4), 610-615.

Yanagida, M. (2005). Basic mechanism of eukaryotic chromosome segregation. *Philosophical Transactions of the Royal Society of London B: Biological Sciences, 360*(1455), 609-621.

Yang, J., Yan, R., Roy, A., Xu, D., Poisson, J., & Zhang, Y. (2015). The I-TASSER Suite: protein structure and function prediction. *Nature methods*, *12*(1), 7.

Zahradka, K., Slade, D., Bailone, A., Sommer, S., Averbeck, D., Petranovic, M., ... & Radman, M. (2006). Reassembly of shattered chromosomes in *Deinococcus radiodurans*. *Nature*, *443*(7111), 569.

Zhang, C., Wei, J., Zheng, Z., Ying, N., Sheng, D., & Hua, Y. (2005). Proteomic analysis of *Deinococcus radiodurans* recovering from γ-irradiation. *Proteomics*, *5*(1), 138-143.

Zhang, Y. M., Wong, T. Y., Chen, L. Y., Lin, C. S., & Liu, J. K. (2000). Induction of a futile Embden-Meyerhof-Parnas pathway in *Deinococcus radiodurans* by Mn: possible role of the pentose phosphate pathway in cell survival. *Appl. Environ. Microbiol.*, *66*(1), 105-112.

Zimmerman, J. M., & Battista, J. R. (2005). A ring-like nucleoid is not necessary for radioresistance in the Deinococcaceae. *BMC microbiology*, *5*(1), 17.

Zuleta, L., de Oliveira Cunha, C., De Carvalho, F., Ciapina, L., Souza, R., Mercante, F., ... & De Vasconcelos, A. (2014). The complete genome of *Burkholderia phenoliruptrix* strain BR3459a, a symbiont of *Mimosa flocculosa*: highlighting the coexistence of symbiotic.

Annexure I

Table 1. List of bacterial strains used in this study

Strain	Genotype	Source
D. radiodurans	wild type	lab stock
E. coli MG1655	Wild type	lab stock
E. coli DH5α	*F- / endA1 hsdR17 glnV44 thi-1 recA1 gyrA relA* Δ *(lacIZYA-argF) U169 deoR (Φ80dlac*Δ *(lacZ)M15)*	lab stock
E. coli BL21(DE3)pLysS	*F-ompT gal [dcm] [lon] hsdSB DE3::T7RNA*	lab stock
E. coli JM109	*end*A1, *rec*A1, *gyr*A96, *thi*, *hsd*R17 (r_k^-, m_k^+), *rel*A1, *sup*E44, Δ(*lac-proAB*),	lab stock
E. coli BTH 101	F^-, *cya*-99, *ara*D139, *gal*E15, *gal*K16, *rps*L1 (Str^r), *hsd*R2, *mcr*A1, *mcr*B127	Kaimova *et al.*, 1998
Δ *parA2* *D. radiodurans*	DR_A0001 deletion mutant (Kan^R, 8µg/ml)	This study
Δ*parA3* *D. radiodurans*	DR_B0001 deletion mutant ($Spec^R$, 70µg/ml)	This study
Δ *parA2parA3*	Deletion of DR_A0001 and DR_B0001 (Kan^R& $Spec^R$)	This study
Δ*parB1* *D. radiodurans*	DR_0012 deletion mutant (Kan^R, 8µg/ml)	Charaka & Misra, 2012
Δ*parB2* *D. radiodurans*	DR_A0002 deletion mutant (Kan^R, 8µg/ml)	This study
Δ*parB3* *D. radiodurans*	DR_B0002 deletion mutant (Kan^R, 8µg/ml)	This study
Δ*cisII* *D. radiodurans*	*cisII* (region, 150-556 of Chr II) Chr II deletion mutant (Kan^R, 8µg/ml)	This study
Δ*cisMP* *D. radiodurans*	*cisMP* (region 177403-464 of megaplasmid) deletion mutant (Kan^R, 8µg/ml)	This study
R1::ChrI-*tetO*	p44SCh1 plasmid integrated at 1.5˚ position in chromosome I	This study
R1::ChrII-*tetO*	p44SCh2 plasmid integrated at 4˚ position in chromosome II	This study
R1::Mp-*lacO*	p43SMp plasmid integrated at 4.4˚ position in megaplasmid	This study

Table 2. List of primers used in this study

Sr. No.	Primer Name	Oligonucleotide Sequences	Purpose/Plasmid
1	DRBTHA1F	5'CGGGATCCGGCAGCTATGACGGACCACGCGGGCGGGGA3'	pKNTA1 & pUT18A1
2	DRBTHA1R	5'CGGAATTCGCGGCCGCGATTTTTTCGACACGTTGCAGCA 3'	
3	DRBTHA2F	5'GCTCTAGAGGCAGCTATGGTGAGCGCTGTGAAAAC3'	pKNTA2 & pUT18A2
4	DRBTHA2R	5'CGCGGATCCGCGGCCGCTGCGTTTTCCCCCGGA3'	
5	DRBTHA3F	5'GCTCTAGAGGCAGCTATGACGACCATCTTGA3'	pKNTA3 & pUT18A3
6	DRBTHA3R	5'CGGGATCCGCGGCCGCTCGTTCACCTCGCTCA3'	
7	DRBTHB1F	5'GCTCTAGAGGCAGCTGTGTCGAAAAAATCT3'	pUTB1, pUTCB1 & pKTB1
8	DRBTHB1R-	5'CGGGATCCGCGGCCGCTTCCTCGGCCTCGTAAC 3'	
9	DRBTHB1R+	5'CGGGATCCTTATTCCTCGGCCTCGT3	
10	DRBTHB2F	5'GCTCTAGAGGCAGCTATGACCCGGCGTCGTCCA3'	pUTB2, pUTCB2 & pKTB2
11	DRBTHB2R-	5'CGGGATCCGCGGCCGCGCTCTGTTCGTCTATCGCCT3'	
12	DRBTHB2R+	5'CGGGATCCTCAGCTCTGTTCGTCTATCGCCT3'	
13	DRBTHB3F	5'GCTCTAGAGGCAGCTATGACCCGGCGCGAGGGCT3'	pUTB3, pUTCB3 & pKTB3
14	DRBTHB3R-	5'CGGGATCCGCGGCCGCGTTGTCGCCAATCTCT3'	
15	DRBTHB3R+	5'CGGGATCCTTAGTTGTCGCCAATCTCTTGCT3'	
16	DRBTHB4F	5'CGGGATCCGGCAGCTATGAGCCGCAAGTTG3'	pUTB4, pUTCB4 & pKTB4
17	DRBTHB4R-	5'GGAATTCGCGGCCGCCCGGTTCCCATCGTGGGA3'	
18	DRBTHB4R+	5'CGGAATTCCTACCGGTTCCCATCGTGGGA3'	
19	DrfEBTHF	5'GCTCTAGAGGCAGCTTTGAGCGTCCCCGCG3’	BTH variants of DrFtsE
20	DrfEBTHR-	5'CGGGATCCGCGGCCGCTTCCAGTTCCCGCAG3’	
21	DrfEBTHR+	5'CGGGATCCGCGGCCGCTCATTCCAGTTCCCG3’	
22	DrfKBTHF	5'GCTCTAGAGGCAGCTGTGCGGCGCCTGCAAC3	BTH variants of DrFtsK
23	DrfKBTHR-	5'CGCGGATCCGCGGCCGCTTTGCCGAAATACTC3’	
24	DrfKBTHR+	5'CGCGGATCCGCGGCCGCCTATTTGCCGAAATAC3’	
25	DrfQBTHF	5'GCTCTAGAGGCAGCTGTGAAAGACGACCCG3’	BTH variants of DrFtsQ

26	DrfQBTHR-	5'CGCGGATCCGCGGCCGCTTCCTGGACGCTCAC3’	
27	DrfWBTHF	5'GCTCTAGAGGCAGCTGTGAGCCTGCAACTC3’	BTH variants of DrFtsW
28	DrfWBTHR-	5'CGGGATCCGCGGCCGCGTCGTCCGCCGCGGC3’	
29	DrfWBTHR+	5'CGGGATCCGCGGCCGCTCAGTCGTCCGCCGC3’	
30	DrmCBTHF	5'GCTCTAGAGGCAGCTATGCTCACGGCCCAGA3’	BTH variants of DrMinC
31	DrmCBTHR-	5'CGGGATCCGCGGCCGCCTGCACGTCGATCAC3’	
32	DrmCBTHR+	5'CGGGATCCGCGGCCGCTCACTGCACGTCGATC3’	
33	DrmDBTHF	5'GCTCTAGAGGCAGCTTTGCCTTGCTATGCTG3’	BTH variants of DrMinD
34	DrmDBTHR-	5'CGGGATCCGCGGCCGCGCTCCCACCCCCGAAC3’	
35	DrmDBTHR+	5'CGGGATCCGCGGCCGCTCAGCTCCCACCCCCG3’	
36	DrD4BTHF	5'GCTCTAGAGGCAGCTATGAGCTCGCCCAATAAC3’	BTH variants of DrDivIVA
37	DrD4BTHR-	5'CGGGATCCGCGGCCGCTTTCTCGTCGTCCAG3’	
38	DrD4BTHR+	5'CGGGATCCGCGGCCGCTTATTTCTCGTCGTC3’	
39	pETA2F	5’GAATTCCATATGATGGTGAGCGCTGTGAAAAC3’	pETA2
40	pETA2R	5’CCGCTCGAGTCATGCGTTTTCCCCCGGA3’	
41	pETA3F	5’GAATTCCATATGATGACGACCATCTTGACGG3’	pETA3
42	pETA3R	5’CCGCTCGAGTCATCGTTCACCTCGCTCAG3’	
43	pETB2F	5’GAATTCCATATGATGACCCGGCGTCGTC3’	pETB2
44	pETB2R	5’CCGCTCGAGTCAGCTCTGTTCGTCTATC3’	
45	pETB3F	5’GAATTCCATATGATGACCCGGCGCGAGGGCT3’	pETB3
46	pETB3R	5’CCGCTCGAGTTAGTTGTCGCCAATCTC3’	
47	BTHF(PV)	5’GGAATTCCATATGACCATGATTACG3’	pV18, pV18A1-4, pV18B1-4
48	BTHR(PV)	5’GGCCTCGAGCATATTACTTAGTTA3’	
49	pETHisF	5’AAAAGTACTGGGCCCATGGGCAGCAGCCAT3’	pRADhisA2, pRADhisA3, pRADhisB1-3
50	pETHisR	5’CGCTTAAGTCTAGATATCTCAGTGGTGGTG3’	
51	Phi-W	5’CGTTCTTATTACCCTTCTGAATGTCACGCTGATTATTTTGACTTTGAGCGTATCG3	Fluorescence anisotropy
52	Phi-C	5’CGATACGCTCAAAGTCAAAATAATCAGCGTGACATTCAGAAGGGTAATAAGAACG3’	
53	cisIIF	5’GCGGCATGTTCTCACGTC3’	*cisII*/ParB EMSA
54	cisIIR	5’CTTAATAGACCTGTAATTG3’	
55	cisMPF	5’CAAGGACGGCTTCTCTCG3’	*cisMP*/ ParB EMSA
56	cisMPR	5’AGTTGCAGACCATAGGGG3’	

57	RTZ Fw	5'ATCAAGGAATATCTCGA3'	qPCR
58	RTZ Rw	5' CAGCTTTTCGTTGTTCACC 3'	
59	RTEFw	5’ TTGAGCGTCCCCGCGCC3’	
60	RTERw	5’GTGCCCGACGAGGTAGA3’	
61	A155RTFw	5’ TTGGCGCATTTTCCCGGC 3’	
62	A155RTRw	5’ CAGCAGGTTGATCGCCTG 3’	
63	PprARTFw	5’ GTGCTACCCCTGGCCTT 3’	
64	PprARTRw	5’ GCGGCCATCGGTCAGAAT 3’	
65	B03RTFw	5’ CTGAGTCCTGACGAGTCC 3’	
66	B03RTRw	5’ TTCCGGGTGACGCAGCAG 3’	
67	B104RTFw	5’ ATGAAAACTCTTGAGGC3’	
68	B104RTRw	`5 GCCGAGGAAAACGTCCAG 3’	
69	C01RTFw	5’ ATGTGCTCGCCTCCTAGA 3’	
70	C01 RTRw	5’ TCACTGTGAAACCTGATC 3’	
71	C18RTFw	5’ ATGACACAGACGCGGCG 3’	
72	C18RTRw	5’ GTCCGCGAGGCGCATCAT 3’	
73	pETB2F	5’GAATTCCATATGATGACCCGGCGTCGTC3’	pETB2
74	pETB2R	5’CCGCTCGAGTCAGCTCTGTTCGTCTATC3’	
75	pETB3F	5’GAATTCCATATGATGACCCGGCGCGAGGGCT3’	pETB3
76	pETB3R	5’CCGCTCGAGTTAGTTGTCGCCAATCTC3’	
77	pETDAF	5’CGGGATCCGTGCGCAAAAACGTCTC3’	pETDnaA
78	pETDAR	5’GCGAATTCTTACGCCCCGACTTCTTC3’	
79	BTDnaAF	5’CGGGATCCGGCAGCTGTGCGCAAAAACGTCTC3’	pKNTDA
80	BTDnaAR	5’GCGAATTCGCGGCCGCCGCCCCGACTTCTTC3’	
81	A2UPF	5’GGGGTACCTCTTTGCTCGCCATACCCA3’	pNOKA2UD
82	A2UPR	5’GCGGGCCCCATCATCTGGCCTTCCGCCA3’	
83	A2DNF	5’CGGGATCCCCGACGCGACAAAAAG3’	
84	A2DNR	5’GCTCTAGACTGAGGCCAGTTGAGGATAC3’	
85	A3UPF	5’GGGGTACCTTGTTGGGCTTGGGTTTC3’	pNOSA3UD
86	A3UPR	5’GCGGGCCCACCAACCCGACCAGGAATG3’	
87	A3DNF	5’CGGGATCCCCGATCATGACCCGGA3’	
88	A3DNR	5’GCTCTAGAAGTGGCGGAGGATAGTTC3’	
89	B2UPF	5’GGGGTACCGGCGAATTTGACCGGCTG3’	pNOKB2UD
90	B2UPR	5GCGAATTCGAGGGCAGCAGCTCTG3’	
91	B2DNF	5’GTGTTCCGATCAATGG3’	
92	B2DNR	5’GCGAGCTCAGCTTTGCAGCTGGGC3’	
93	B3UPF	5’GGGGTACCCGCGGAGTTGCATGAAAC3’	pNOKB3UD
94	B3UPR	5’GCGAATTCGTCAATGAGGTTCAGG3’	
95	B3DNF	5’CGGGATCCTTCTTACCTCTGGGCC3’	
96	B3DNR	5’GCGAGCTCCGCCGTACGTGCAAGAC3’	
97	nptIIFw	5’GCACGGTGGCCGAGTGG3’	Diagnostic PCR,
98	nptIIRw	5’GTCAGCGTAATGCTCTG3’	

99	aadAFw	5'ATGAGGGAAGCGGTGATC3'	p44SCh1, p44SCh2
100	aadARw	5'TTATTTGCCGACTACCT3'	
101	cisIIFw	5' GC TCTAGA GCG GCA TGT TCT CAC GTC T 3'	pNOKcisII, EMSA (*cisII*; full)
102	cisIIRw	5' GC TCTAGA CTT AAT AGA CCT GTA ATT G 3'	
103	cisMPFw	5' GCGGGCCC CAAGGACGGCTTCTCTC 3'	pNOKcisM, EMSA (*cisMP*; full)
104	cisMPRw	5' CG GAATTC AGTTGCAGACCATAGGGGT 3'	
105	CIIintFw1	5' TCCCCGCGGTCCAAATG 3'	EMSA (*cisII;* 6 repeats)
106	CIIintFw2	5'TCCCCGCGGCAAACGGCCCA 3'	EMSA (*cisII;* 3 repeats)
107	CIIintFw3	5'CTCCACAAAGTGCCACAGGTAATTCCACAA AGTGCCACAGGC 3'	EMSA (*cisII*; 2 repeats)
108	CIIintRw3	5'GCCTGTGGCACTTTGTGGAATTACCTGTGG CACTTTGTGGAG 3'	
109	CIIintFw4	5' CTCCACAAAGTGCCACAGGTG 3'	EMSA (*cisII*; 1 repeat)
110	CIIintRw4	5' CACCTGTGGCACTTTGTGGAG 3'	
111	CMintFw1	5' GCGGGCCCTTTTGCACGTTG 3'	EMSA (*cisMP*; 5 repeats)
112	CMintFw2	5' GCGGGCCCGTCTACAAAGAG 3'	EMSA (*cisMP*; 3 repeats)
113	CMintFw3	5'ACGCAAAGGTGTCGCTATTTTGACCCCAAA TCCCGCAAAGGTGTCGCTAT3'	EMSA (*cisMP*; 2 repeats)
114	CMintRw3	5'ATAGCGACACCTTTGCGGGATTTGGGGTCA AAATAGCGACACCTTTGCGT3'	
115	CMintFw4	5'CCCGCAAAGGTGTCGCTAGG3'	EMSA (*cisMP*; 1 repeat)
116	CMintRw4	5'CCTAGCGACACCTTTGCGGG3'	
117	CIIUPFw.	5'GGGGTACCTCGGTCACGTCGTATGC3'	pNOKCII
118	CIIUPRw	5'CGGAATTCCCTATGATGATGATCATC3'	
119	CIIDNFw	5'CGGGATCCTTTGTGCTGAAGAATCATC3'	
120	CIIDNRw	5'GCTCTAGAAAGGCTAGGCGGACTATC3'	
121	CMPUPFw	5'GGGGTACCGACAGAAGTCTTACGGCC3'	pNOKCMP
122	CMPUPRw	5'CGGAATTCAGCGACACCTTTGCGGGA3'	
123	CMPDNFw	5'CGGGATCCCTTGTAAAATTCACCAAC3'	
124	CMPDNRw	5'GCTCTAGA GCCCGAGAGAAGGGGGAC3'	
125	TetRscIApIFw	5'CGGAGCTCGGGCCCGTGAGATTAGATAAA AG3'	pDTRGFP & pRADTRGFP
126	TetRSalIRw	5'GCGTCGACAGACCCACTTTCACATTTAAG3'	
127	GFPXbaIRw	5'GCTCTAGATTATTTGTATAGTTCATCCA3'	
128	LacIFw	CG GGATCC GGCAGCT GTGAAACCAGTAACG	pDRedLacI
129	LacIRw	GGGGTACCGCGGCCGCCAGCTGCATTA ATGA	
130	HisRedFw	5'CGGAGCTCGGGCCCCACCACCACCACCACA TGACCATGATTACG 3'	pVLacIRFP
131	RedRw	5'CGGATATCTAGACTCGAGGCCGCTACAG 3'	

132	ChI(1.5˚)Fw	5'GCTCTAGAGTCGACGCCTCTTTTCACCGCA AAG 3'	p44Ch1
133	ChI(1.5˚)Rw	5'AAAAGTACTCATATGCCGGACATGTCCGGG CGC3'	
134	Ch2(4˚)Fw	5'GCTCTAGAGTCGACGGCAGCGAGGTCAGG AAG 3'	p44Ch2
135	Ch2(4˚)Rw	5'AAAAGTACTAAGCTTACGTCCGGCAAGCAC CTG3'	
136	MP(4.4˚)Fw	5'GCTCTAGAGTCGACGAAGCTGGTAAAACTT TG3'	p43Mp
137	MP(4.4˚)Rw	5'AAAGTACTCATATGTACGCCCGAAAGCCTA CAG3'	
138	AmpRw	5'TTACCAATGCTTAATCAGTGAGG3'	Diagnostic PCR
139	Dr0010F	5'GTGAAATCACCGCTTCCAATG3'	
140	DrA005F	5'ATGAAAGCAATTGTCTGGCAAG3'	

Table 3. List of plasmids used in this study

Sr. No.	Name of the plasmid	Characteristics	Source	MW of fusion protein
1	pUT18	pUC19 derivative, MCS at N-terminal of T18 fragments of adenylate cyclase, ~3 kb, Amp^R	Karimova *et al.,* 1998	~18 kDa
2	pUT18C	pUC19 derivative, MCS at C-terminal of T18 fragments of adenylate cyclase, ~3 kb, Amp^R	Karimova *et al.,* 1998	~18 kDa
3	pKNT25	pSU40 derivative, MCS at N-terminal of T25 fragment of adenylate cyclase, ~3.4 kb, Kan^R	Karimova *et al.,* 1998	~25 kDa
4	pKT25	pSU40 derivative, MCS at C-terminal of T25 fragment of adenylate cyclase, ~3.4 kb, Kan^R	Karimova *et al.,* 1998	~25 kDa
5	pUTDFA	pUT18 carrying *drftsA* at *Bam*HI and *Kpn*I	Modi & Misra, 2014	~72 kDa
6	pUTCDFA	pUT18C carrying *drftsA* at *Bam*HI and *Kpn*I	Modi & Misra, 2014	~72 kDa
7	pKNTDFA	pKNT25 carrying *drftsA* at *Bam*HI and *Kpn*I	This study	~79 kDa
8	pUTDFE	pUT18 carrying *drftsE* at *Xba*I and *Bam*HI	This study	~81 kDa
9	pUTCDFE	pUT18C carrying *drftsE* at *Xba*I and *Bam*HI	This study	~81 kDa
10	pKNTDFE	pKNT25 carrying *drftsE* at *Xba*I and *Bam*HI	This study	~88 kDa
11	pKTDFE	pKT25 carrying *drftsE at Xba*I and *Bam*HI	This study	~88 kDa
12	pUTDFK	pUT18 carrying *drftsK* at *Xba*I and *Bam*HI	This study	~125 kDa
13	pUTCDFK	pUT18C carrying *drftsK* at *Xba*I and *Bam*HI	This study	~125 kDa
14	pKNTDFK	pKNT25 carrying *drftsK* at *Xba*I and *Bam*HI	This study	~132 kDa
15	pKTDFK	pKT25 carrying *drftsK* at *Xba*I and *Bam*HI	This study	~132 kDa
16	pUTDFQ	pUT18 carrying *drftsQ* at *Xba*I and *Bam*HI	This study	~49 kDa
17	pKNTDFQ	pKNT25 carrying *drftsQ* at *Xba*I and *Bam*HI	This study	~56 kDa
18	pUTDFW	pUT18 carrying *drftsW* at *Xba*I and *Bam*HI	This study	~57 kDa
19	pUTCDFW	pUT18C carrying *drftsW* at *Xba*I and *Bam*HI	This study	~57 kDa
20	pKNTDFW	pKNT25 carrying *drftsW* at *Xba*I and *Bam*HI	This study	~64 kDa

21	pKTDFW	pKT25 carrying *drftsW* at *Xba*I and *Bam*HI	This study	~64 kDa
22	pUTDFZ	pUT18 carrying *drftsZ*	Modi & Misra, 2014	~57 kDa
23	pKNTDFZ	pKNT25 carrying *drftsZ*	Modi & Misra, 2014	~64 kDa
24	pKTDFZ	pKT25 carrying *drftsZ*	Modi & Misra, 2014	~64 kDa
25	pKNTA1	pKNT25 carrying *parA1* at *Bam*HIand *Eco*RI	This study	~56 kDa
26	pKNTA2	pKNT25 carrying *parA2* at *Xba*I and *Bam*HI	This study	~52 kDa
27	pKNTA3	pKNT25 carrying *parA3* at *Xba*I and *Bam*HI	This study	~52 kDa
28	pKNTA4	pKNT25 carrying *parA4* at *Bam*HIand *Eco*RI	This study	~67 kDa
29	pUT18A1	pUT18 carrying Dr_0013 at *Bam*HIand *Eco*RI	This study	~49
30	pUT18A2	pUT18 carrying Dr_A0001 at *Xba*I and *Bam*HI	This study	~45
31	pUT18A3	pUT18 carrying Dr_B0001 at *Xba*I and *Bam*HI	This study	~45
32	pUTB1	pUT18 carrying *parB1* at *Xba*I and *Bam*HI	This study	~50 kDa
33	pUTB2	pUT18 carrying *parB2* at *Xba*I and *Bam*HI	This study	~51 kDa
34	pUTB3	pUT18 carrying *parB3* at *Xba*I and *Bam*HI	This study	~50 kDa
35	pUTB4	pUT18 carrying *parB4* at *Bam*HI and *Eco*RI	This study	~51 kDa
36	pUTDMC	pUT18 carrying *drminC* at *Xba*I and *Bam*HI	This study	~35 kDa
37	pKNTDMC	pKNT25 carrying *drminC* at *Xba*I and *Bam*HI	This study	~42 kDa
38	pKTDMC	pKT25 carrying *drminC* at *Xba*I and *Bam*HI	This study	~42 kDa
39	pUTDMD	pUT18 carrying *drminD* at *Xba*I and *Bam*HI	This study	~48 kDa
40	pKNTDMD	pKNT25 carrying *drminD* at *Xba*I and *Bam*HI	This study	~55 kDa
41	pKTDMD	pKT25 carrying *drminD* at *Xba*I and *Bam*HI	This study	~55 kDa
42	pUTDDiv4	pUT18 carrying *drdivIVA* at *Xba*I and *Bam*HI	This study	~54 kDa
43	pKNTDDiv4	pKNT25 carrying *drdivIVA* at *Xba*I &*Bam*HI	This study	~61 kDa
44	pKTDDiv4	pKT25 carrying *drdivIVA* at *Xba*I and *Bam*HI	This study	~61 kDa
45	pUTCB1	pUT18C carrying Dr_0012 at *Xba*I and *Bam*HI	This study	~50 kDa
46	pUTCB2	pUT18C carrying Dr_A0002 at *Xba*I&*Bam*HI	This study	~51 kDa
47	PUTCB3	pUT18C carrying Dr_B0002 at *Xba*I&*Bam*HI	This study	~50 kDa
48	pUTCB4	pUT18C carrying Dr_B0030 at *Bam*HI&*Eco*RI	This study	~51 kDa
49	pKTB1	pKT25 carrying Dr_0012 at *Xba*I&*Bam*HI	This study	~57 kDa
50	pKTB2	pKT25 carrying Dr_A0002 at *Xba*I&*Bam*HI	This study	~58 kDa
51	PKTB3	pKT25 carrying Dr_B0002 at *Xba*I &*Bam*HI	This study	~57 kDa
52	pKTB4	pKT25 carrying Dr_B0030 at *Bam*HI& *Eco*RI	This study	~58 kDa
53	pUTEFA	pUT18 carrying *E. coli ftsA*	Modi & Misra, 2014	~63 kDa
54	pKNTEFZ	pKNT25 carrying *E. coli ftsZ*	Modi & Misra, 2014	~65 kDa
55	pUTPprA	pUT18 carrying *pprA*	Kota *et al.,* 2014a	~50 kDa
56	pKNTPprA	pKNT25 carrying *pprA*	Kota *et al.,* 2014a	~57 kDa
57	pUTcheA	pUT18 containing vp2229	Ringgaard *et al.,*2011)	~97 kDa
58	pKNTcheA	pKNT25 containing vp2229	Ringgaard *et al.,*2011)	~104 kDa
59	pKNTDA	*drdnaA* in pKNT25at *Bam*HI and *Eco*RI	This study	~78 kDa

60	pET28a(+)	~ 5.3 kb plasmid; N-terminal 6XHis tag (Kan^R)	Novagen	-
61	pETA2	pET28a(+) carrying Dr_A0001 at *Nde*I and *Xho*I	This study	~29 kDa
62	pETA3	pET28a(+) carrying Dr_B0001 at *Nde*I and *Xho*I	This study	~29 kDa
63	pET0012	pET28(+) with *parB1* at *Nde*I and *Xho*I	Charaka & Misra, 2012	~32 kDa
64	pETB2	pET28a(+) carrying Dr_A0002 at *Nde*I and *Xho*I	This study	~33 kDa
65	pETB3	pET28a(+) carrying Dr_B0002 at *Nde*I and *Xho*I	This study	~32 kDa
66	pETDnaA	pET28a(+) carrying Dr_0002 at *Bam*HI and *Eco*RI	This study	~53 kDa
67	pVHS559	p11559 derivative, *D. radiodurans* vector ($Spec^R$)	Charaka & Misra, 2012	-
68	pV18	pVHSM carrying T18 tag from pUT18 at *Nde*I &*Xho*I	This study	~18 kDa
69	pV18A1	pVHS559 carrying ParA1-T18 from pUT18A1 at *Nde*I &*Xho*I	This study	~49 kDa
70	pV18A2	pVHS559 carrying ParA2-T18 from pUT18A2 at *Nde*I &*Xho*I	This study	~45 kDa
71	pV18A3	pVHS559 carrying ParA3-T18 from pUT18A3 at *Nde*I &*Xho*I	This study	~45 kDa
72	pV18B1	pVHS559 carrying T18-ParB1 from pUTCB1 at *Nde*I &*Xho*I	This study	~50 kDa
73	pV18B2	pVHS559 carrying T18-ParB2 from pUTCB2 at *Nde*I &*Xho*I	This study	~51 kDa
74	pV18B3	pVHS559 carrying T18-ParB3 from pUTCB3 at *Nde*I &*Xho*I	This study	~50 kDa
75	pRADgro	pRAD1 derivative, *D. radiodurans* vector (Cam^R)	Khairnar *et al.*, 2006	-
78	pRADhisA2	pRADgro carrying His tagged ParA2 at *Apa*I &*Xba*I from pETA2 plasmid	This study	~29 kDa
79	pRADhisA3	pRADgro carrying His tagged ParA3 at *Apa*I &*Xba*I from pETA3 plasmid	This study	~29 kDa
80	pRADhisB1	pRADgro carrying His tagged ParB1 at *Apa*I &*Xba*I from pET0013 plasmid	This study	~33 kDa
81	pRADhisB2	pRADgro carrying His tagged ParB2 at *Apa*I &*Xba*I from pETB2 plasmid	This study	~34 kDa
82	pRADhisB3	pRADgro carrying His tagged ParB3 at *Apa*I &*Xba*I from pETB3 plasmid	This study	~33 kDa
83	pRADhisDnaA	pRADgro with His tagged *dnaA* at *Apa*I & *Xba*I from pETDnaA plasmid	This study	~53 kDa
84	pVHSFtsA18	pVHSM carrying FtsA-T18 from pUTDFA at *Nde*I & *Xho*I	Maurya *et al*., 2018	~72 kDa
85	pRadHisFZ	pRADgro carrying coding sequence of (his)6-*ftsZ* from pFTSZdr at *Apa*I and *Xba*I	Maurya *et al*., 2018	~40 kDa
86	pNOKOUT	A deinoccocal suicidal vector; Kan^R	Khairnar *et al.*, 2008	-
87	pNOKA2UD	pNOKOUT carrying ~900 bps upstream at *Apa*I &*Kpn*I and ~900 bps downstream at *Bam*HI & *Xba*I from mid of Dr_A0001 gene	This study	-

88	pNOKA02	pNOKOUT with ~900 bps upstream at *Kpn*I &*Eco*RI and ~900 bps downstream at *Bam*HI &*Sac*I of Dr_A0002 gene (Kan^R)	This study	-
89	pNOKB02	pNOKOUT with ~900 bps upstream at *Kpn*I & *Eco*RI and ~900 bps downstream at *Bam*HI &*Sac*I of Dr_B0002 gene (Kan^R)	This study	-
90	pNOKcisII,	pNOKOUT carrying full length *cisII* at *Xba*I	This study	-
91	pNOKcisMP	Full length *cisMPin* pNOKOUT at *Apa*I-*Eco*RI	This study	-
92	pNOKCIIUD	pNOKOUT with ~500 bps upstream at *Kpn*I &*Eco*RI and ~500 bps downstream at *Bam*HI &*Xba*I of *cisII* (Kan^R)	This study	-
93	pNOKCMPUD	pNOKOUT carrying ~500 bps upstream at *Kpn*I &*Eco*RI and ~500 bps downstream at *Bam*HI & *Xba*I of *cisMP* (Kan^R)	This study	-
94	pNOSOUT	pBluescript II SK+ carrying *aadA* gene with promoter from pVHS559 at *Hind*III & *Eco*RI (Spec^R),	This study	-
95	pNOSA3UD	pNOSOUT with ~900 bps upstream at *Apa*I &*Kpn*I and ~900 bps downstream at *Bam*HI & *Xba*I from Dr_B0001 (Spec^R)	This study	-
96	pDSW208	PDSW208-MCS-*gfp* (fusion vector) (Amp^R)	Weiss, 1999	~27 kDa
97	pDTRGFP	pDSW208 with *tetR* at *Sac*I-*Sal*I to give *gfp-tetR*	This study	~48 kDa
98	pRADTRGFP	pRADgro with *gfp-tetR* at *Apa*I-*Xba*I from pDTRGFP	This study	~48 kDa
99	pDsRed	pDsRed-MCS-*rfp* (fusion vector) (Amp^R)	Invitrogen	~27 kDa
100	pDRedLacI	pDsRed with *lacI* gene at *Bam*HI-*Kpn*I to give *rfp-lacI*	This study	~65 kDa
101	pVLacIRFP	pVHS559 with *rfp-lacI* at *Sac*I-*Xho*I from pDRedLacI	This study	~65 kDa
102	pLAU43	Plasmid with an array of 240 repeats of *lacO* (Amp^R& Kan^R)	Lau *et al*., 2003	-
103	P43Mp	pLAU43 with region (2203-3000) from megaplasmid at *Xba*I-*Sca*I	This study	-
104	pLAU44	Plasmid with an array of 240 repeats of *tetO* (Amp^R& Gen^R)	Lau *et al*., 2003	-
105	P44SCh1	pLAU44 with region (10713-11715) from chromosome I at *Xba*I-*Sca*I, with Spectinomycin cassette at *Nhe*I-*Xho*I	This study	-
106	P44SCh2	pLAU44 with region (4695-c5691) from chromosome II at *Xba*I-*Sca*I, with Spectinomycin cassette at *Nhe*I-*Xho*I	This study	-

Biochemical Journal (2019) **476** 909–930
https://doi.org/10.1042/BCJ20180799

Research Article

ParA proteins of secondary genome elements cross-talk and regulate radioresistance through genome copy number reduction in *Deinococcus radiodurans*

Ganesh Kumar Maurya[1,2], Swathi Kota[1,2], N. Naveen Kumar[3], Raghvendra Tewari[3] and Hari S. Misra[1,2]

[1]Molecular Biology Division, Bhabha Atomic Research Centre, Mumbai 400085, India; [2]Life Sciences, Homi Bhabha National Institute, Mumbai 400094, India; [3]Material Science Division, Bhabha Atomic Research Centre, Mumbai 400085, India

Correspondence: Hari S. Misra (hsmisra@barc.gov.in)

Deinococcus radiodurans, an extremely radioresistant bacterium has a multipartite genome system and ploidy. Mechanisms underlying such types of bacterial genome maintenance and its role in extraordinary radioresistance are not known in this bacterium. Chromosome I (Chr I), chromosome II (Chr II) and megaplasmid (Mp) encode its own set of genome partitioning proteins. Here, we have characterized P-loop ATPases of Chr II (ParA2) and Mp (ParA3) and their roles in the maintenance of genome copies and extraordinary radioresistance. Purified ParA2 and ParA3 showed nearly similar polymerization kinetics and interaction patterns with DNA. Electron microscopic examination of purified proteins incubated with DNA showed polymerization on nicked circular dsDNA. ParA2 and ParA3 showed both homotypic and heterotypic interactions to each other, but not with ParA1 (ParA of Chr I). Similarly, ParA2 and ParA3 interacted with ParB2 and ParB3 but not with ParB1 *in vivo*. ParB2 and ParB3 interaction with *cis*-elements located upstream to the corresponding *parAB* operon was found to be sequence-specific. Unlike single mutant of *parA2* and *parA3*, their double mutant (Δ*parA2*Δ*ParA3*) affected copy number of cognate genome elements and resistance to γ-radiation as well as hydrogen peroxide in this bacterium. These results suggested that ParA2 and ParA3 are DNA-binding ATPases producing higher order polymers on DNA and are functionally redundant in the maintenance of secondary genome elements in *D. radiodurans*. The findings also suggest the involvement of secondary genome elements such as Chr II and Mp in the extraordinary radioresistance of *D. radiodurans*.

Introduction

Until recently, the bacterial genomes were synonyms of a single circular chromosome and extrachromosomal plasmids. Now we know that there are many bacteria that harbor multipartite genome system. The numbers of copies of these genome elements, including primary chromosomes may vary from one to several copies per cell [1]. In general, the primary chromosome is larger and tends to have significantly more conserved housekeeping genes that encode for core cellular functions and contribute to greater conservation of the contents. On the other hand, the secondary genome elements show a greater variability and encode accessory functions associated with adaptation and survival in different niches and largely contribute to stress tolerance [2–4]. The secondary chromosomes are normally smaller than primary chromosome [5] and believed to have originated by the mechanisms like the split

Received: 5 October 2018
Revised: 19 February 2019
Accepted: 25 February 2019

Accepted Manuscript online: 25 February 2019
Version of Record published: 15 March 2019

A part of this work was presented in FEMS-2017 congress held at Valencia, Spain and rewarded as the 'Early Career Scientist Award'.

Biochemical Journal (2019) **476** 909–930
https://doi.org/10.1042/BCJ20180799

of a primary chromosome, chromosome duplication or acquisition of a large plasmid with essential genes. The faithful inheritance of multipartite genome system and the maintenance of ploidy are not fully understood in bacteria. The genome segregation in bacteria harboring single circular chromosome and low copy plasmids occurs largely by the involvement of the tripartite genome segregation (TGS) system. The TGS consists of an origin-proximal *cis*-acting (centromere-like) DNA sequences, the centromere binding adaptor proteins like ParB or ParB homologs and the P-loop Walker ATPases like ParA or Par A like motor proteins [6,7].

Deinococcus radiodurans, a radioresistant bacterium, is characterized with an efficient DNA double-strand break repair and the strong oxidative stress tolerance mechanisms [8–10]. The cytogenetic features like multipartite genome system with two chromosomes (2 648 638 bp and 412 348 bp) and plasmids (177 466 bp and 45 704 bp) and their ploidy are equally interesting features in this bacterium [11]. Molecular mechanisms underlying the evolution and maintenance of multipartite genome system and its faithful inheritance into daughter cells, maintenance of ploidy and its functional significance in extreme phenotypes of this bacterium are not clearly understood. The chromosome I (Chr I) and chromosome II (Chr II) contain one putative *parAB* operon each, while megaplasmid (Mp) contains two putative *parAB* operons [11]. Previously, the partitioning system of Chr I including the centromeric sequences (*segS*) of Chr I and 'Par' proteins (ParA1 and ParB1) has been characterized [12]. The partitioning mechanisms of Chr II and Mp (together referred to as secondary genome elements unless specified) are not known and would be worth studying. However, it was shown that ATPase encoded from DR_A0001 in Chr II (ParA2) functions differently in the absence of its cognate ParB2 [13].

Here, we have characterized ParA2 and P-loop ATPase encoded by DR_B0001 (hereafter referred as ParA3) on Mp and established their roles in the cognate genome copy maintenance and in resistance to different abiotic stresses in *D. radiodurans*. We demonstrated that ParA2 and ParA3 have nearly similar functions *in vitro* and can complement each other's phenotype *in vivo*. They produced higher order polymers on DNA in the presence of ATP, and ATP hydrolysis was not stimulated by non-specific DNA, but led to the conformational change that was very similar to the one observed in the presence of ADP. These proteins did interact with each other, but not with ParA1. Also, ParA2 and ParA3 interacted with ParB2 (ParB encoded on Chr II) and ParB3 (ParB encoded on Mp), but not with ParB1 *in vivo*. ParB2 and ParB3 showed sequence-specific interaction with *cis*-elements located upstream to the *parAB* operons of the secondary genome elements. Unlike single mutants, the double mutant of *parA2* and *parA3* (*ΔparA2ΔparA3*) showed a reduction in the copy number of secondary genome elements and was found sensitive to γ-radiation as well as to hydrogen peroxide (H_2O_2). In comparison with single mutant, the double mutant showed an increase in cell size and septum trapped nucleoid phenotype under microscopic observation. These results together suggested that nearly similar *in vitro* characteristics of ParA2 and ParA3 might have allowed them to complement each other's role *in vivo*. Furthermore, ploidy in secondary genome elements seems to play important roles in the radioresistance and oxidative stress tolerance in this bacterium.

Experimental procedures

Bacterial strains, plasmids and materials

Deinococcus radiodurans R1 (ATCC13939) was a kind gift from Professor J. Ortner, Germany [14]. It was grown in TGY (tryptone [1%], glucose [0.1%] and yeast extract [0.5%]) medium at 32°C. *E. coli* strain NOVABLUE was used for cloning and maintenance of all the plasmids. *E. coli* strain BTH101 (*cyaA*$^-$) (hereafter referred to as BTH101) was used for the co-expression of different ParA proteins on BACTH (bacterial two-hybrid system) plasmids to monitor protein–protein interaction in *E. coli*. *E. coli* strain BL21 (DE3) pLysS was used for the expression of recombinant proteins. *E. coli* cells harboring pUT18, pKNT25 and pET28a (+) and its derivatives were maintained in the presence of required antibiotics. Shuttle expression vector pVHS559 [12] and their derivatives were maintained in the presence of spectinomycin (70 μg/ml) in *E. coli* and *D. radiodurans*, whereas pRadgro [15] and their derivatives were maintained in the presence of ampicillin (100 μg/ml) in *E. coli* and chloramphenicol (5 μg/ml) in *D. radiodurans*. Single mutants of *parA2* (ΔparA2::nptII) and *parA3* (ΔparA3::aadA) as well as their double mutant (ΔparA2::nptII–ΔparA3::aadA) from *D. radiodurans* used in this study, has been described recently [16]. Standard protocols for all recombinant techniques were used as described in ref. [17]. All the bacterial strains and plasmids used in this study have been listed in Supplementary Table S2. Antibodies against T18 (SC-33620) and T25 (SC-13582) domains of CyaA of *Bordetella pertussis*, respectively, were procured commercially (Santa Cruz Biotechnology, Inc). Antibody

against polyhistidine tag was purchased from Sigma Chemicals Company, U.S.A. Molecular biology-grade chemicals and enzymes were procured from Sigma Chemicals Company, U.S.A., Roche Biochemicals, Mannheim, Germany, New England Biolabs, U.S.A. and Merk India Pvt. Ltd., India. Radiolabeled nucleotides were obtained from the Board of Radiation and Isotope Technology, Department of Atomic Energy (DAE), India (BRIT, India).

Bioinformatics analysis and molecular modeling

Multiple sequence alignment and functional motif search in ParA1 (DR_0013), ParA2 (DR_A0001) and ParA3 (DR_B0001) proteins were carried out using standard online bioinformatics tools as described earlier [13,18]. In brief, the amino acid sequences of ParA1, ParA2 and ParA3 proteins were subjected to a PSI-BLAST search with the SWISSPROT database. After five iterations, the sequences obtained were aligned by CLUSTALW and the conserved deviant of the Walker box ATP-binding motif and DNA-binding motif were searched. Homologous sequences were aligned by T-COFFEE and the conserved motifs were marked. ParA1, ParA2 and ParA3 proteins were modeled by I-TASSER server (http://zhanglab.ccmb.med.umich.edu /I-TASSER/) [19]. The models were validated by Swiss model workspace encompassing the package of Anolea, DFire, QMEAN, Gromos, DSSP, Promotif and ProCheck (http://swissmodel.expasy.org/workspace/). The template used for the modeling of protein structure was derived from the Soj structure of *Thermus thermophilus* (PDB ID: 2BEK) [20]. The modeled structure of both ParA2 and ParA3 were superimposed with Soj structure (PDB ID: 2BEK) of *T. thermophilus* as well as with deinococcal ParA1 model structure using Pymol software.

Construction of recombinant plasmids

Details of the primers used in the construction of recombinant plasmids and plasmids used in this study are given in Supplementary Tables S1 and S2, respectively. A suicidal plasmid pNOSOUT conferring spectinomycin resistance in *D. radiodurans* was constructed for creating gene knockout in this bacterium and described in ref. [16]. Genomic DNA of *D. radiodurans* R1 was prepared as reported previously [21] and coding sequences of ParA2 (DR_A0001), ParA3 (DR_B0001), ParB2 (DR_A0002) and ParB3 (DR_B0002) were PCR amplified from genomic DNA using gene-specific primers as given in Supplementary Table S1. PCR products were ligated at the *Nde* I and *Xho* I sites in pET28a (+) to yield pETA2, pETA3, pETB2 and pETB3, respectively. These plasmids were sequenced for the presence of cloned genes and further used for protein expression and purification or generation of polyhistidine-tagged translational fusion for *in vivo* interaction study.

For protein–protein interaction studies in *E. coli*, the coding sequences of ParA1 (DR_0013), ParA2 and ParA3 were PCR amplified using gene-specific primers as given in Supplementary Table S1 and ligated in BACTH plasmids, namely pKNT25 and pUT18 as given in Supplementary Table S2. For *in vivo* interaction of ParA and ParB proteins in *D. radiodurans*, the translational fusion of ParA2, ParA3, ParB1, ParB2 and ParB3 were generated with polyhistidine tag (from their pET28a (+) variants) in pRADgro vector using PETHisF and PETHisR primers as given in Supplementary Table S1, and recombinant plasmids obtained were named as pRADhisA2, pRADhisA3, pRADhisB1, pRADhisB2 and pRADhisB3 respectively. Similarly, T18 tag fusions of different *parA*s were PCR amplified from their pUT18 variants and were cloned in pVHS559 using BTHF (PV) and BTHR (PV) primers as given in (Supplementary Table S1), and resultant plasmids were named as pV18A1, pV18A2 and pV18A3, respectively (Supplementary Table S2). *D. radiodurans* cells harboring pVHS559 derivatives as well as pRADgro derivatives in different combinations were induced with 5 mM isopropyl-β-D-thiogalactopyranoside (IPTG) for the expression of recombinant proteins from pVHS559 derivatives while pRADgro variants express recombinant proteins constitutively. The expression of each fusion protein in *D. radiodurans* was ascertained by immunoblotting using antibodies against T18 tag of polyhistidine tag, respectively (Supplementary Figure S1C–E). Recombinant plasmids pKNTA1, pKNTA2 and pKNTA3 used in this study were constructed previously [18].

Generation of insertional deletion mutants of parA2 and parA3

The single (Δ*parA2* or Δ*parA3*) and double mutants (Δ*parA2*Δ*parA3*) of *parA2* and *parA3* genes were generated as described recently [16]. In brief, ∼1 kb upstream and downstream region from mid of *parA2* and *parA3* ORFs were PCR amplified and cloned in pNOKOUT (Kan^R) and pNOSOUT ($Spec^R$) to yield pNOKA2UD and pNOSA3UD, respectively. The upstream fragments were cloned at *Kpn* I–*Apa* I and downstream at *Bam* HI–*Xba* I sites. These constructs were linearized by *Xmn* I and transformed into *D. radiodurans* separately as well as together and transformants were grown for several generations under required, selection pressure until

Biochemical Journal (2019) 476 909–930
https://doi.org/10.1042/BCJ20180799

the homozygous insertion and the replacements of middle portion *parA2* with *nptII* cassette and *parA3* with *aadA* cassette were achieved in the genome of *D. radiodurans*. This was ascertained by PCR amplification using *parA2* and *parA3* gene-specific as well as antibiotic cassettes (*nptII* and *aadA*) specific primers in different combination.

Purification of recombinant proteins

The recombinant ParA2, ParA3, ParB2 and ParB3 were purified from *E. coli* BL21 (DE3) pLysS expressing these proteins on pETA2, pETA3, pETB2 and pETB3, respectively, as described recently [22]. In brief, mid-logarithmic phase cells of *E. coli* BL21 (DE3) pLysS-expressing recombinant proteins were induced with 0.5 mM IPTG allowed to grow at 37°C for 3 h and kept overnight at 18°C. The cells were pelleted and stored at −70°C. The cell pellet was thawed and suspended in buffer A (20 mM Tris–HCl [pH 7.6], 300 mM NaCl) containing 10 mM imidazole, 0.5 mg/ml lysozyme, 1 mM PMSF, 1 mM $MgCl_2$, 0.05% NP-40, 0.05% Triton X-100, protease inhibitor cocktail and 10% glycerol) and incubated at 37°C for 30 min. The mixture was sonicated for 10 min at 10 s pulses with intermittent cooling for 15 s at 25% amplitude. The cell-free extract obtained after centrifugation at 11,000 rpm for 30 min at 4°C was loaded onto a pre-equilibrated Ni-NTA column. The column was thoroughly washed with buffer A containing 50 mM imidazole and recombinant protein was eluted with buffer A containing 200, 250 and 300 mM imidazole. Fractions were analyzed on SDS–PAGE and those containing nearly pure proteins were pooled and protein was further purified using anion exchange column chromatography. Different fractions containing pure protein were pooled and concentrated using 10 kDa cutoff spin columns. The protein solution was centrifuged at 16 000 rpm for 30 min and the supernatant containing mostly soluble protein was dialyzed in a buffer containing 20 mM Tris–HCl (pH 7.6), 200 mM NaCl, 50% glycerol and 1 mM PMSF and stored at −20°C (Supplementary Figure S2). Protein concentration was determined by taking OD at 280 nm in NanoDrop (Synergy H1, Hybrid Multi-Mode Reader Biotek) using mass extinction coefficient of both the proteins. The refolding of purified ParA2 and ParA3 proteins was confirmed by recording Circular Dichroism spectroscopy in phosphate buffer using JASCO, J815, Japan as described previously [23] (Supplementary Figure S2).

Electrophoretic mobility shift assay

The DNA-binding activity of ParA proteins was assayed by electrophoretic mobility shift assay (EMSA) as described in ref. [20]. In brief, different concentrations of proteins (0–2.5 μM) were incubated with 100 fmol of 3 kb linear dsDNA (*Eco*RI linearized pBluescript II SK+) in a total volume of 30 μl containing DNA-binding buffer B (50 mM Tris–Cl (pH 8.5), 75 mM NaCl, 5 mM $MgSO_4$ and 0.5 mM 1,4-dithiothreitol) for 10 min at 25°C in the absence and presence of 1 mM ATP, ADP or ATP-γ-S. The reaction mixture was mixed with 10% glycerol and loaded in 0.8% agarose gel. Agarose gel electrophoresis was performed in 0.5× TBE buffer at 50 mV at 8°C and gels were stained with ethidium bromide. Data were documented and analyzed for a shift in mobility with respect to the free DNA probe. The mobility retardation of the nucleoprotein complex (NPC) for each concentration has been calculated as difference in distance (cm) travel at each concentration with respect to total migration of DNA probe. It has been further plotted with respect to the different concentration of ParA2 and ParA3 as mean ± SD.

Similarly, the ParB2 and ParB3 interaction with *cis*-elements (*cisII* and *cisMP*) as well as non-specific DNA was studied by EMSA as described previously [12]. For that, the ∼400 bp fragment containing 10 direct repeats (*cisII*) or 8 direct repeats (*cisMP*) of 17 mer or 16 mer (Supplementary Figure S3) located upstream to *parA2B2* in chromosome II and *parA3B3* in Mp, respectively, were PCR amplified using sequence-specific primers (see Supplementary Table S1). The PCR products were gel purified. DNA substrates were labeled with [γ^{32}P] ATP using T4 polynucleotide kinase. Approximately, 30 nM labeled substrate was incubated with different concentrations of purified recombinant ParBs in a reaction buffer containing 50 mM Tris–HCl (pH 8.0), 75 mM KCl, 5 mM $MgSO_4$ and 0.1 mM DTT at 37°C for 15 min. For the competition assay, a saturating concentration of ParBs was incubated with *cis* sequences before the different concentration of 400-bp non-specific competitor DNA (mid of *ftsZ* gene; Supplementary Table S1) was added and further incubated as per experimental requirements. A 10-fold higher concentration of cold *cis* sequences was also used in a competition assay for respective ParB and *cis* interaction. Mixtures were separated on 6% native PAGE gels, the gels were dried and autoradiograms were developed on X-ray films. The band intensity of bound and unbound fraction was determined by using ImageJ 2.0 software. The fraction of DNA probe bound to the protein was plotted as a function

of the protein concentration by using GraphPad Prism 5. The K_d value for the curve fitting of individual plots was determined as described before [12].

Fluorescence anisotropy

Fluorescence anisotropy was measured as described in ref. [20]. In brief, an equimolar concentration of 5′ fluorescein-labelled oligonucleotide Phi-W (5′ fluorescein-CGTTCTTATTACCCTTCTGAATGTCACGCTGAT TATTTTGACTTTGAGCGTATCG-3′) was annealed to its complementary unlabeled oligonucleotide Phi-C to create fluorescein labeled double-stranded DNA [24]. A 50 μl of the reaction mixture containing the different concentrations of protein (0.5–2.0 μM) was incubated with 20 nM 5′ fluorescein labeled double-stranded DNA (55 mer) in DNA-binding buffer B in the absence and presence of 1 mM ATP at 25°C for 10 min. Fluorescence signals were recorded at an excitation of 480 nm and emission at 520 nm at 25°C using FLS 980 spectrofluorimeter (Edinburgh Instruments). The data were analyzed and plotted with the curves fitting using GraphPad Prism 5.

Sedimentation analysis

The sedimentation analysis of ParA proteins was performed under different conditions as described in ref. [14,25]. In brief, the recombinant ParA2 and ParA3 proteins were centrifuged at 22 000×*g* for 15 min at 4°C to remove any aggregate. The 2 μM proteins were incubated with 0.5 pmol linear 3 kb dsDNA and 1 mM of ATP, ADP or ATP-γ-S in 30 μl for 10 min at room temperature. Similarly, a titration of DNA concentration (0–1.5 pmol) was done with both proteins in the absence and presence of 1 mM ATP or ADP only. Proteins incubated without DNA was used as a negative control. The mixtures were centrifuged at 22 000×*g* for 30 min at 25°C. The supernatants were removed carefully, and the pellet was resuspended in 30 μl of buffer B and mixed with 30 μl of 2× SDS-loading buffer. The mixture was heated at 95°C for 10 min, centrifuged and components were analyzed on 12% SDS–PAGE gels. Protein gel was stained with Coomassie Brilliant Blue R stain and protein band intensity was measured densitometrically by using ImageJ 2.0 software, and data were plotted as the ratio of pellet to supernatant using GraphPad Prism5.

Dynamic light scattering

Dynamic light scattering (DLS) was measured using a Horiba Scientific Nanopartica SZ-100 instrument as described previously [12,26]. In brief, all the solutions used in this study were passed through a 0.2 μm filter and proteins were centrifuged at 22 000×*g* for 30 min at 4°C. 2 μM proteins were incubated with 0.1 pmol 3 kb linear dsDNA in the absence and presence of 1 mM ATP or ADP. Light scattering at 90° was measured at 25°C for 30 min at a regular interval of 30 s. The data obtained as kilo counts per second (KCPS) were analyzed using in-built software (SZ-100) and plotted. The curve was smoothened using GraphPad Prism 5.

ATPase activity measurement using TLC

ATPase activity was measured as the release of [^{32}P]-αADPs from [^{32}P]-αATPs by TLC as described earlier [23,25]. In brief, 2 μM proteins were mixed with 30 nM [^{32}P]-α ATP and 0.1 pmol dsDNA in different combinations in a total volume of 30 μl containing buffer B containing 2 mM Mg^{2+} and incubated at 37°C for 0–40 min. The reaction was stopped with 10 mM EDTA solution and 1 μl of the reaction mixture was spotted on PEI-Cellulose F^+ TLC sheet. Spots were air-dried, and components were separated on a solid support in a buffer system containing 0.75 M KH_2PO_4/H_3PO_4 (pH 3.5) and autoradiogram was developed. Spot intensities of the samples were determined densitometrically using ImageJ 2.0 software, % ADP to ATP ratios were calculated and plotted using the GraphPad Prism 5 software.

ATP binding and hydrolysis by measurement of intrinsic tryptophan fluorescence

Since both ParA2 and ParA3 proteins have 2 Trp residues, the nucleotides (ADP/ATP/ATP-γ-S) binding and hydrolysis by ParA2 and ParA3 in the absence and presence of dsDNA was measured as a function of intrinsic tryptophan fluorescence of these proteins. In brief, 2 μM of ParA2 or ParA3 were incubated in buffer B containing 0.5 mM $MgSO_4$ for 30 min in the absence and presence of 0.1 mM of ADP, ATP or ATP-γ-S and 0.1 pmol dsDNA in 30 μl reaction volume. The emission spectra of tryptophan were obtained by excitation at 295 nm and spectral scanning of emission from 315 to 401 nm at an interval of 2 nm using FLS 980

Biochemical Journal (2019) 476 909–930
https://doi.org/10.1042/BCJ20180799

spectrofluorimeter (Edinburgh Instruments). Furthermore, 2 μM of ParA2 or ParA3 was preincubated in buffer B for 2 min, and the emission spectra were acquired at 0, 10, 15, 20 and 30 min after the addition of 0.1 mM ATP. Spectra were corrected for background and Raman scattering by subtracting buffer spectra. The obtained spectra for each time points were compared with spectra for each protein incubated with 1 mM ADP for 30 min. The data were analyzed and plotted using GraphPad Prism 5.

Protein–protein interaction studies

Protein–protein interactions were monitored using a BACTH as described in ref. [27,28]. In brief, BTH101 was co-transformed with different plasmids like pUT18A1, pUT18A2 and pUT18A3, and pKNTA1, pKNTA2 and pKNTA3 in different combinations. Empty vectors were transformed in different combinations and used as negative controls while pUTEFA and pKNTEFZ were used as positive control. Recombinant cells expressing these proteins in different combinations were spotted on LB agar plate containing 5-bromo-4-chloro-3-indolyl-β-D-galactopyranoside (X-Gal) (40 μg/ml), IPTG (0.5 mM) and antibiotics as required. Plates were incubated at 30°C overnight and the appearance of white–blue color colonies was recorded. In parallel, the levels of β-galactosidase activity were measured from the same liquid cultures grown overnight with 0.5 mM IPTG as described earlier [27,29]. The β-galactosidase activity was calculated in Miller units as described in ref. [29] and plotted with the standard deviation in GraphPad Prism 5.

Interaction of proteins in surrogate *E. coli* was monitored by co-immunoprecipitation (co-IP). For that, the total proteins of the recombinant *E. coli* BTH101 cells expressing ParA1, ParA2 and ParA3 proteins of *D. radiodurans* on BACTH plasmids (Supplementary Table S2) in different combinations were immunoprecipitated using polyclonal antibodies against T25 tag as described in ref. [29]. The immunoprecipitates were separated on SDS–PAGE, blotted and detected using monoclonal antibodies against T18 tag. Signals were detected using anti-mouse secondary antibodies conjugated with alkaline phosphatase using BCIP/NBT substrates (Roche Biochemical, Mannheim).

Interaction of different ParAs with ParBs was monitored in *D. radiodurans* by using co-IP. For that, the cell-free extracts of *D. radiodurans* expressing ParAs as on pV18A1, pV18A2 and pV18A3 (Supplementary Figure S1) in different combinations with ParA2 from pRADhisA2 and ParA3 from pRADhisA3 (Supplementary Figure S1) were prepared and immunoprecipitated using polyhistidine antibodies as described earlier [22,29]. Similarly, the cell-free extracts of *D. radiodurans* expressing different ParAs (fused to T18 tag as described above) in different combinations with different deinococcal ParBs (fused to polyhistidine tag as expressed from pRADhisB1, pRADhisB2 and pRADhisB3 were prepared and immunoprecipitated using polyhistidine antibodies as described earlier [22,29]. Immunoprecipitate was purified using Protein G Immunoprecipitation Kit (Cat. No. IP50, Sigma–Aldrich, Inc.). The immunoprecipitates were separated on SDS–PAGE, blotted onto PVDF membrane and hybridized using monoclonal antibodies against T18 tag. The hybridization signals were detected using anti-mouse secondary antibodies conjugated with alkaline phosphatase using BCIP/NBT substrates (Roche Biochemical, Mannheim) as described above.

Cell survival studies

Deinococcus radiodurans R1 and its *parA* mutants were treated with 6 kGy γ-radiation as well as different doses of hydrogen peroxide as described in ref. [15]. In brief, the bacteria were grown in TGY medium with appropriate antibiotics at 32°C were washed and suspended in sterile PBS and treated with 6 kGy γ-radiation at dose rate 1.81 kGy/h (Gamma Cell 5000, ^{60}Co, Board of Radiation and Isotope Technology, DAE, India). Gamma irradiated cells and respective controls maintained under identical conditions (SHAM) controls were washed in PBS and suspended in the fresh TGY medium. These cells were grown in TGY medium in 48-well microtiter plates in replicates at 32°C for 42 h. Optical density at 600 nm (OD_{600}) was measured online in the Synergy H1 Hybrid multi-mode microplate reader. The growth rate was calculated from growth curve using formula ($N_t = N_0 \times (1 + r)t$, where N_t is OD_{600} at time t, N_0 is OD_{600} at the start of the growth curve, r is growth rate and t is time passed) and plotted for each sample type.

For hydrogen peroxide treatment, the exponentially growing cells were exposed to different concentration of H_2O_2 for 30 min. The serial dilutions were made and plated on TGY agar medium containing antibiotics as required [15]. The colony-forming units were recorded after 48 h of incubation at 32°C. The surviving fractions were expressed as the percentage of colony-forming units obtained after treatment with respect to untreated cells. We have also calculated D10 values from the survival curve for each sample and plotted.

Genome copy number determination using quantitative real-time PCR

The single and double mutant cells of similar OD at 600 nm were harvested by centrifugation and their cell number was determined using a Neubauer cell counter. The cells were washed with 70% ethanol solution and lysed in a lysis solution containing 10 mM Tris–HCl (pH 7.6), 1 mM EDTA and 4 mg/ml lysozyme at 37°C. The lysed cells were centrifuged (10 000 rpm, 5 min) to remove cell debris. The lysis efficiency was verified by plating of lysed supernatant on TYG agar plates. The integrity of genomic DNA was confirmed by agarose gel electrophoresis. The serial dilutions of cytoplasmic extract were made and 0.1 ml of it was used for further analysis of genomic copy number using quantitative real-time PCR as described in ref. [30]. In brief, a fragment of ∼300 bps was amplified using standard PCRs with isolated genomic DNA from *D. radiodurans* as a template. The PCR product was gel purified and the amount of DNA was quantified by nanodrop and the concentrations of DNA molecules were calculated using the molecular mass computed with 'oligo calc' (www.basic.northwestern.edu/biotools). A dilution series was generated for each standard fragment and used for qPCR analysis with the dilution series. Two different genes per replicon with similar PCR efficiency were selected in *D. radiodurans*, namely *ftsE* and *ftsZ* for chromosome I, *pprA* and Dr_A0155 for chromosome II, Dr_B003 and Dr_B0104 for Mp and Dr_C001 and Dr_C018 for small plasmid (Sp) (Supplementary Table S1). The PCR efficiency of each gene was ascertained and was found to be >96% for each (data not shown). The qPCR was carried out by following the minimum information for publication of quantitative real-time PCR experiments (MIQE) guidelines using Roche Light cycler [31] and the cycle threshold (Ct) values were determined. Three independent biologic replicates were used for each sample. The replicon copy number is quantified by comparing the results with a dilution series of a PCR product of known concentration that is used as a standard (Supplementary Figure S4). The copy number of each replicon by both genes per cell was calculated using the cell number present at the time of cell lysis. An average of copy number reflected from two genes per replicon was represented with appropriate bio-statistical analysis.

Microscopic studies

Fluorescence microscopy of *D. radiodurans* and its mutants was carried out as described previously [12], using an Olympus IX83 inverted fluorescence microscope equipped with an Olympus DP80 CCD monochrome camera. In brief, the cells were grown until the exponential phase, harvested and washed with PBS. Cells were resuspended in PBS and stained with DAPI (4′,6-diamidino-2-phenylindole, dihydrochloride) (0.2 μg/ml) for nucleoid and Nile red (1 μg/ml) for the membrane and washed two times with PBS. These cells were mounted on glass slides coated with 0.8% agarose and imaged for DAPI and Nile red signals using DAPI and TRITC (tetramethylrhodamine isothiocyanate) channels under a fluorescence microscope, respectively. Images were aligned using an in-built software, cellSens. Each image has been presented in isolated as well as merged channels. The brightness and contrast of all images were adjusted using Adobe Photoshop 7.0. Nearly 500 cells from both wild type and mutants were examined for cell area determination using counting and measure tool of cellSens. Furthermore, scatter plot of cell area (μm^2) vs sample type was plotted using GraphPad Prism 5. We performed a line scan analysis of many cells from each sample type through the cellSens software by following its manual. In line scan analysis, we scanned fluorescence intensity of DAPI and Nile red signals across a line in a cell to find the relative position of nucleoid and membrane (or septum). The percentage of cells showing nucleoids located between septum (septum trapped nucleoids) and defect on tetrads separation was calculated in each sample type and plotted using GraphPad Prism 5 software. The experiments were repeated to ensure the reproducibility and significance of these data.

Electron microscopy

The DNA-binding activity of ParAs and their polymerization on DNA was monitored by TEM on an electron microscope (Model JEOL2000FX, Japan) using previously described protocols [20,25]. In brief, 100 ng nicked circular ϕX174 RF II dsDNA was mixed with 1.5 μM ParA2 or ParA3 alone or with 1 mM ADP or ATP in buffer B containing 50 mM Tris–Cl (pH 8.5), 75 mM NaCl, 5 mM $MgSO_4$ and 0.5 mM DTT in different combinations. Protein without DNA and high-energy phosphates were used as a control. This mixture was incubated at 37°C for 10 min before application to UV-activated carbon-coated 200 mesh copper grids. This mixture was placed on the charged side of the grid for 2 min and then washed in stage II distilled water. The grids were negatively stained with 10 μl of 2% (w/v) uranyl acetate followed by a washing in stage II distilled water. These were further blotted to dry and incubated for 1 h under vacuum before imaging. The grids were

Biochemical Journal (2019) **476** 909–930
https://doi.org/10.1042/BCJ20180799

observed under JEOL 2000FX, Japan electron microscope at 100 kV and 50 000–200 000× magnification. Digital images were collected on a CCD camera as described previously [26].

Statistical analysis

To ensure statistical significance of data, we have performed different statistical analysis like 'Student's *t*-test' or ANOVA as required and mentioned in figure legends. Significance value (*P* value) obtained at 95% confidence intervals are shown as (*) for <0.05, (**) for <0.01 and (***) for <0.001.

Results

ParAs encoded on secondary genome elements show higher sequence similarity to each other

It has previously been shown that secondary genome ParAs of *D. radiodurans* are different from chromosome I ParA (ParA1) of *D. radiodurans* [13]. When the amino acid sequences of ParA2 and ParA3 (hereafter referred as secondary genome ParAs) were aligned with chromosomal ParAs using CLUSTALW program (Supplementary Figure S5A), ParA1 contains ∼48 amino acids extra at its N-terminus (Supplementary Figure S5A) while rest of the region of all the ParAs is conserved. The ParAs of secondary genome elements contain Walker A, Walker A′ and Walker B motifs like other known ParAs (Supplementary Figure S5A). ParA2 and ParA3 show higher sequence similarity to each other than to ParA1. For instance, the amino acid sequence of ParA1 is 25% identical with ParA2 and 23% identical with ParA3 while ParA2 and ParA3 show 42% identity with each other. Homology modeling results showed that both ParA2 and ParA3 are structurally closet to Soj protein (PDB ID; 2BEK) of *T. thermophilus*. The structures built on the template of Soj for both the proteins have aligned perfectly to each other as well as to the Soj of *T. thermophilus* (Supplementary Figure S5B,C). However, the ∼48 amino acids at N-terminal in ParA1 was extra and hanged around the remaining parts of the 3D modeled structure, which were nearly superimposable with secondary ParAs (Supplementary Figure S5D). These results suggested that ParA2 and ParA3 proteins of *D. radiodurans* are very similar to each other and seem to be different from ParA1, at least *in silico*.

ParA2 and ParA3 are characterized as the DNA-binding ATPases

The DNA-binding activity of ParA2 and ParA3 was monitored by EMSA and fluorescence anisotropy. Both the proteins showed a nearly similar binding pattern with non-specific dsDNA and the effect of ATP and ADP on DNA-binding activity was also same (Figure 1). For instance, the size of the NPC increased progressively (reflected as slower mobility) with the increase in protein concentration, which did not change in the presence of ADP. ParA3 and ParA2 binding to DNA was significantly stimulated in the presence of ATP and ATP-γ-S as compared with protein controls (Figure 1). Fluorescence anisotropy results further supported that both the proteins interact with dsDNA in almost similar fashion (Supplementary Figure S6). In the presence of ATP, however, these proteins showed a significant increase in anisotropy. Fluorescence anisotropy has been used previously in determining the nature of DNA–protein interaction [20].

Since ATP has made a significant effect on ParA2 and ParA3 interaction with DNA, and presumably, the assembly of these proteins on dsDNA, the metabolic fate of ATP by these proteins was monitored. Both these proteins could hydrolyze ATP into ADP and Pi and this activity was not enhanced in the presence of dsDNA (Figure 2). Previously, dsDNA stimulation of ATP hydrolysis of ParA1 was shown in the presence of centromere-ParB1 complex [12]. A possibility of ATPase activity stimulation in the presence of centromere-ParB NPC cannot be ruled out. The results suggested that ParA2 and ParA3 proteins of *D. radiodurans* coat the DNA in the presence of ATP forming higher order structures independently of ATP hydrolysis, at least *in vitro*. These results together suggested that both the ParAs of secondary genome elements are DNA-binding ATPase.

ParB2 and ParB3 showed specific interaction with the *cis*-element located upstream to parAB operons of the secondary genome in *D. radiodurans*

The recombinant ParB2 and ParB3 proteins were purified to homogeneity from *E. coli* (Supplementary Figure S2D). The *cis*-elements containing multiple direct repeats located upstream to *parAB* operons which are having the signature of putative centromeres were identified bioinformatically (Supplementary Figure S3) The *cis*-elements in chromosome II (*cisII*) and Mp (*cisMP*) were PCR amplified and interaction of the recombinant ParB2 and ParB3 was checked *in vitro* by EMSA. ParB2 and ParB3 showed sequence-specific interaction with *cisII*

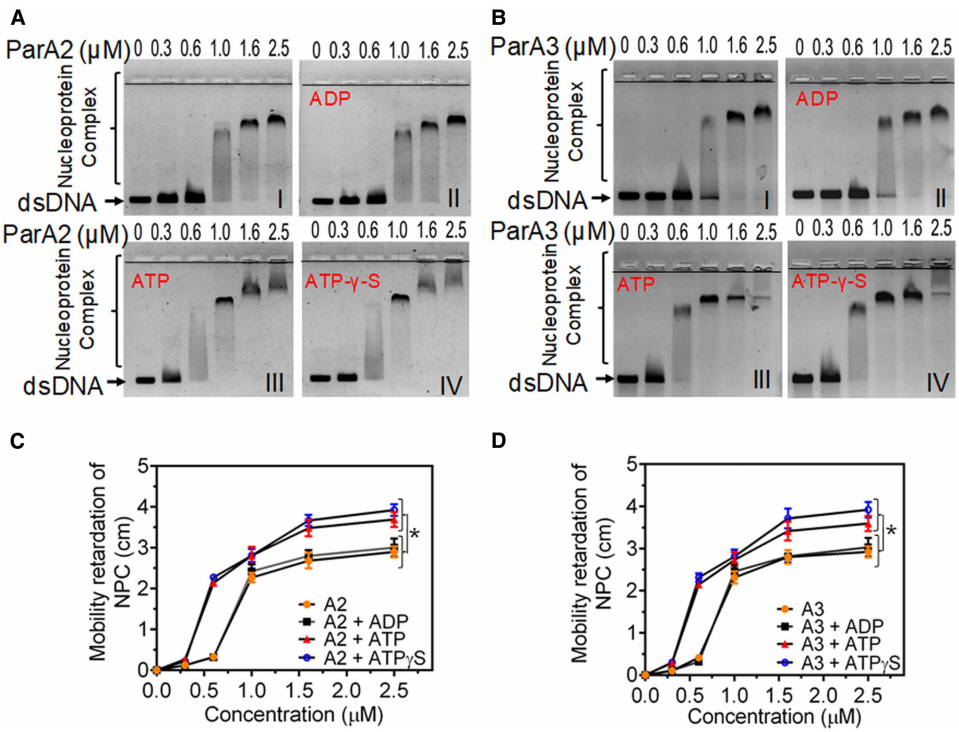

Figure 1. Effect of nucleotides on DNA–protein interaction activity of ParA2 and ParA3.

3.3 nM ~3 kb linear dsDNA was incubated with different concentrations (0.0, 0.3, 0.6, 1.0, 1.6 and 2.5 μM) of ParA2 (**A**,**B**) and ParA3 (**C**,**D**) in the absence (I) and presence of ADP (II), ATP (III) and ATP-γ-S (IV), respectively. The reaction mixture was electrophoresed in 0.8% agarose gel and stained with ethidium bromide. The mobility retardation of NPC in centimeter for each concentration has been calculated with respect to control without protein. Data given are mean ± SD (where $n = 3$). Student's *t*-test was performed and *P* values obtained at 95% confidence intervals are shown as (*) for <0.05, (**) for <0.01 and (***) for <0.001.

and *cisMP* sequences (Figure 3) with a K_d value of 0.41 ± 0.007 μM and 0.60 ± 0.04 μM, respectively. The ParB bound to respective *cis*-elements remained unaffected even in the presence of a 100-fold higher molar concentration of non-specific DNA while titrated out with 10-fold less molar concentration of specific DNA as compared with non-specific DNA (Figure 3). ParB2 or ParB3 also showed specific binding to non-cognate *cis*-elements like *cisMP* and *cisII albeit* with lower affinities. For instance, the K_d of ParB2 for *cisMP* (1.16 ± 0.02 μM) was nearly 3-fold higher than its K_d for *cisII* (0.41 ± 0.007 μM). Similarly, K_d of ParB3 for *cisII* (1.47 ± 0.03 μM) was nearly 2.5 times higher than its K_d for *cisMP* (0.60 ± 0.04 μM) (Figure 3). Surprisingly, both ParBs did not interact with non-specific DNA even at very high concentration (Supplementary Figure S7) indicating the motif specificity of these proteins rather than nucleotide sequence *per se*. These results clearly suggested that ParB2 and ParB3 bind to *cis*-elements present upstream to *parAB* operons with a strong possibility of cross-talk between segregation systems of secondary genome elements in *D. radiodurans*. Whether these motifs as a whole or a few repeats function as centromeres are not known and will be investigated independently.

Secondary genome ParAs produced higher order complexes on DNA, which increased further in the presence of ATP

The possibility of ParA2 and ParA3 proteins forming higher order NPC on DNA as a function of ATP was further investigated by sedimentation assay and DLS. For sedimentation analysis, the purified ParA2 and ParA3 were incubated with ATP, ADP as well as ATP-γ-S in the presence and absence of dsDNA. The amount of protein present in the pellet and supernatant was analyzed on SDS–PAGE and quantified. The amount of protein in the pellet had increased in the presence of DNA as compared with protein control, which significantly increased further in the presence of ATP as compared with ATP and DNA controls (Figure 4A,B). Interestingly, ADP did not increase the

Biochemical Journal (2019) **476** 909–930
https://doi.org/10.1042/BCJ20180799

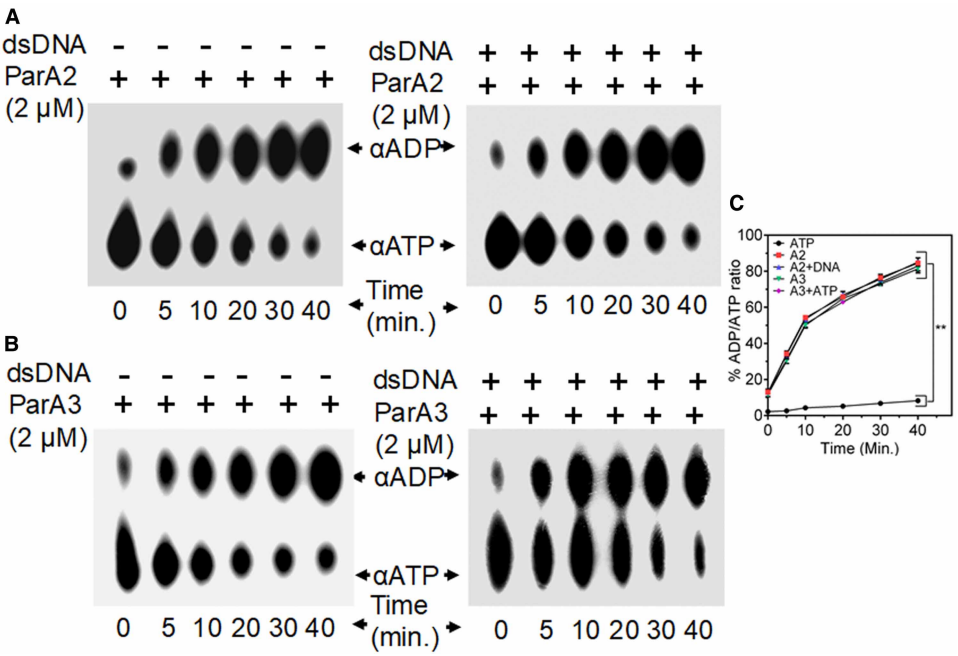

Figure 2. Effect of dsDNA on ATPase activity of ParA2 and ParA3.

2 μM of each ParA2 (**A**) and ParA3 (**B**) proteins were incubated with 30 nM radiolabeled ATP [^{32}P]-αATP in the absence and presence of 3.3 nM dsDNA at 37°C. Aliquots were taken at different time intervals (0–40 min) and separated on PEI-Cellulose F^{+} TLC sheets. Autoradiogram was developed, and the band intensity of each sample was determined densitometrically using ImageJ 2.0 software. The ratios of ADP to ATP were calculated and plotted as mean ± SD in GraphPad Prism 5 (C). Statistical analysis was performed using Student's *t*-test, and *P* values, obtained at 95% confidence intervals, are shown as (*) for <0.05, (**) for <0.01 and (***) for <0.001.

sedimentation of these proteins when compared with protein and DNA controls. To know if the ATP effect on producing bigger pellet was affected by the ATPase activity, the sedimentation of both the proteins was checked in the presence of non-hydrolyzable ATP (ATP γ-S), and the results were nearly similar to that of ATP (Supplementary Figure S8). A similar observation was made previously for ParA2 protein of *Vibrio cholerae* [25].

Furthermore, the increase in the size of the NPC was also measured by DLS (Figure 4C,D). The results fully corroborated the sedimentation assay. For instance, the intensity of light scattering with both ParA2 and ParA3 and dsDNA controls was constant in the range of 900–1000 KCPS, irrespective of the presence of ATP. However, proteins in the presence of dsDNA showed a rapid increase in scattering with the KCPS increasing to more than 3000 in 5 min, which increased further with ATP (KCPS ∼6000 in 30 min) but no effect was seen with ADP (KCPS ∼3000 like DNA + protein) (Figure 4C). Since the increase in the intensity of light scattering in the presence of ATP was observed at a ratio of protein to DNA that had reached to saturation, this effect of ATP seems to be due to an increase in deposition of ParA–ATP complex over DNA. These results together suggested that ParA2 and ParA3 could bind to dsDNA, and the presence of ATP not ADP induced the interaction of ParAs with DNA which resulted in an increase in the size of NPC. Notably, both the proteins showed a similar pattern of interaction with DNA with respect to nucleotides at least *in vitro*.

Unlike ADP, ATP stimulated ParA2 and ParA3 binding on DNA

DNA–protein interaction in the presence of ATP and ADP was imaged by TEM. These proteins appeared as oligomers both in the presence of ATP and ADP. However, they showed nucleation on dsDNA and the density of nucleation had increased further in the presence of ATP but not with ADP (Figure 5). These results concurred the findings from sedimentation assay and DLS. Furthermore, the incubation of DNA with the protein produced the patterns of alternate dark and light spots on DNA, which further increased in the presence of

Biochemical Journal (2019) **476** 909–930
https://doi.org/10.1042/BCJ20180799

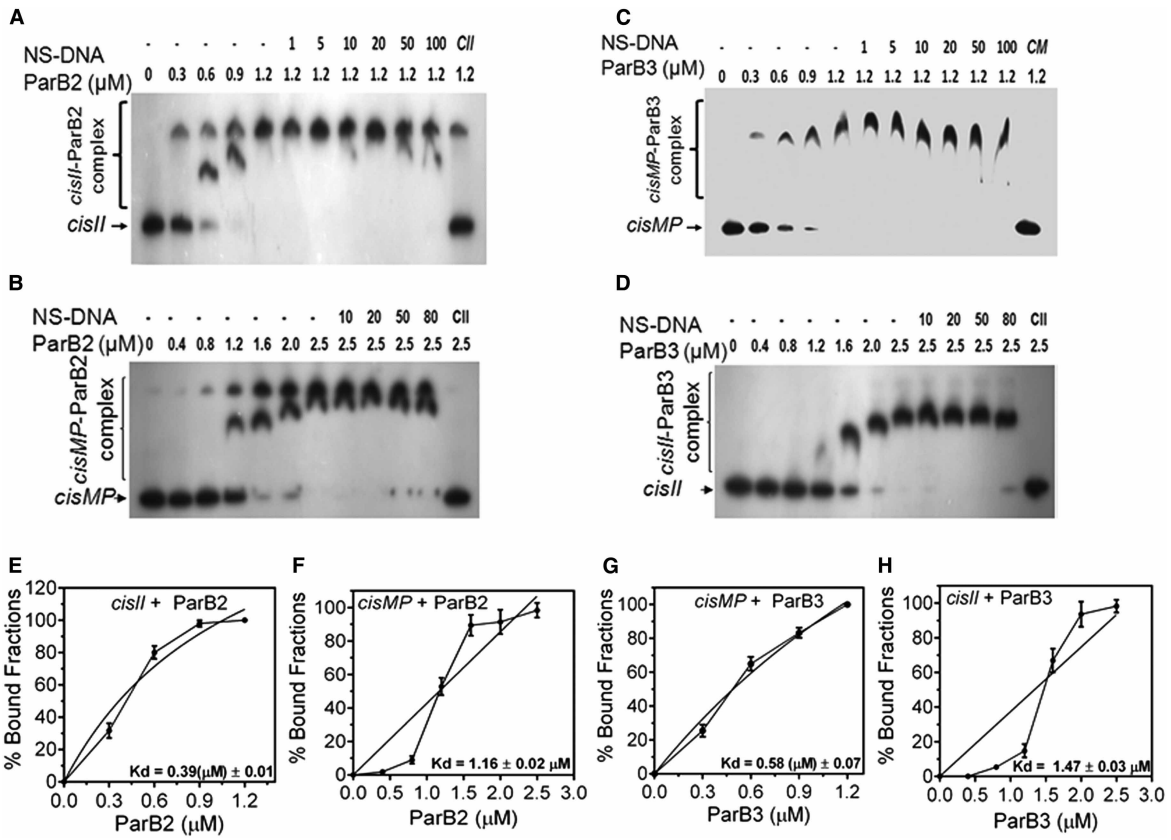

Figure 3. Secondary genome encoded ParB–protein interaction with *cis*-elements located upstream to *parAB* operon in *D. radiodurans*.

The DNA-binding activity of ParB2 (A, B) and ParB3 (C, D) was checked with *cis*-elements present upstream to *parA2B2* (*cisII*) and *parA3B3* (*cisMP*) operon in *D. radiodurans*. PCR-amplified *cisII* and *cisMP* were gel purified and radiolabelled with [γ^{32}P] ATP. 30 nM radiolabelled DNA was incubated with different concentrations of recombinant ParBs. For the competition assay, the *cis*-elements were incubated with saturating concentration of ParBs and chased with the increasing amounts (1–100 molar ratio) of non-specific dsDNA (NS-DNA; 400 bps) as well as 10 molar excess of cold *cisII* (CII) and *cisMP* (MP), respectively. The products were separated on 6% native PAGE gels and dried. The autoradiograms were developed, and the band intensity was quantified and % bound fractions were calculated, plotted for the determination of dissociation constant (K_d) as described in methods (E–H). The experiments were repeated three times, and a representative data of reproducible experiment are presented.

ATP. In conclusion, both ParA2 and ParA3 proteins showed nearly similar results in TEM and ATP but not ADP has affected these proteins binding to dsDNA.

ATP to ADP conversion by ATPase activity of ParAs leads to a conformational change

Conformational change in the protein was monitored as the change in intrinsic fluorescence of tryptophan. Both ParA2 and ParA3 showed excitation maxima ($\lambda_{Ext} = 295$) at 295 nm and emission maxima ($\lambda_{Em} = 327$) at 327 nm in the aqueous solution. Therefore, the relative fluorescence of Trp in these proteins was measured at 327 nm in the presence of different nucleotides (ATP, ADP, ATP-γ-S) and dsDNA (Figure 6A,C). Results showed a significant increase in Trp fluorescence in the presence of ATP and ADP but not with ATP-γ-S. This indicated that ParAs hydrolyze ATP into ADP and it is ADP binding with protein that led to an increase in intrinsic fluorescence of the protein perhaps through a conformational change. Such an increase in intrinsic fluorescence has been implicated in the movement of Trp residues in the hydrophobic micro-environment due to a conformational change in the proteins [32]. Interestingly, the increase in fluorescence was higher when

Biochemical Journal (2019) **476** 909–930
https://doi.org/10.1042/BCJ20180799

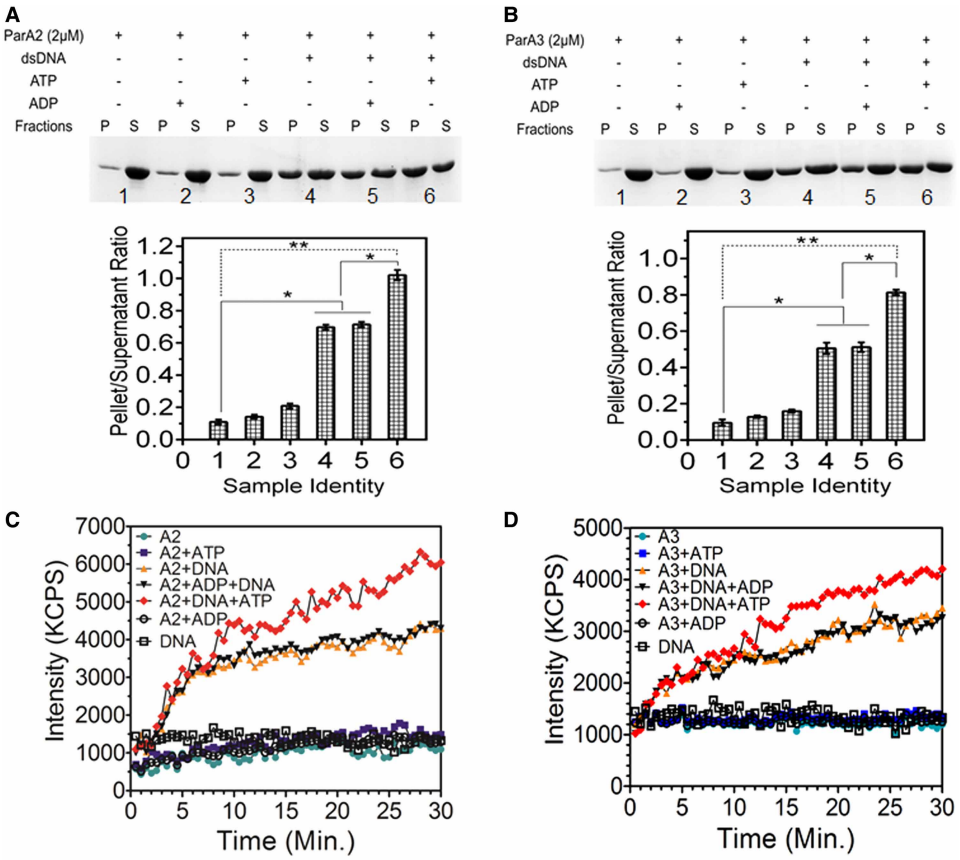

Figure 4. Effect of high-energy nucleotides on ParAs interaction with DNA.

2 μM ParA2 (**A**,**C**) and ParA3 (**B**,**D**) were incubated with 16.6 nM DNA in the presence of 1 mM nucleotides in different combinations. Formation of NPCs was monitored by sedimentation (**A**,**B**) and DLS (**C**,**D**) approaches. For sedimentation, the mixtures were centrifuged and distributions of proteins in the supernatant (S) and pellet (P) fractions were analyzed by SDS–PAGE. Protein band intensity was estimated densitometrically and pellet to supernatant ratios were plotted. The statistical significance of the effect of nucleotides on the size of NPC was ascertained by using Student's *t*-test and *P* values, obtained at 95% confidence intervals, are shown as (*) for <0.05, (**) for <0.01 and (***) for <0.001. Similarly, 2 μM proteins were mixed separately with 3.3 nM DNA and 1 mM nucleotides in different combinations and DLS was recorded as described in methods. The intensity in KCPS was plotted against time (minutes) using GraphPad Prism 5. The intensity of scattering caused by the DNA fragments and proteins alone was also recorded as a control. The graph is representative of a reproducible experiment repeated three times independently.

incubated with ADP alone, which decreased significantly in the presence of DNA. ParA incubated with ATP and DNA separately showed an increase in intrinsic fluorescence, which did not change further when both DNA and ATP were present together. This indicated that ParA protein interaction with DNA and ATP creates conformational change, perhaps required for protein polymerization on DNA. Since the presence of ADP did not increase polymerization, but showed an increase in Trp fluorescence, it indicated the possibility of a conformation change by ADP, and the ATP effects seem to be by the conversion of ATP to ADP by the ATPase activity of these proteins.

To understand if the hydrolysis of ATP to ADP by ParAs can affect protein conformation, time course kinetics of intrinsic fluorescence change due to ATP hydrolysis was monitored. We noticed that the fluorescence of ParA increases with incubation time and that reaches close to ADP control (Figure 6B,D). On the other hand, the change in the intrinsic fluorescence of ParA was not observed in the presence of ATP-γ-S (Figure 6A,C). This clearly suggests that ParA binding with ATP alone is possibly not causing a structural change in the protein rather it is the conversion of ATP to ADP. It has previously been shown that in Type I

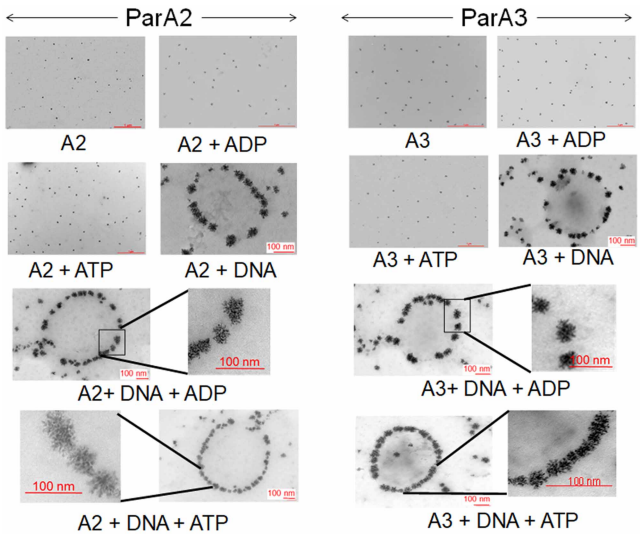

Figure 5. Electron microscopic imaging of ParA–protein interactions with nicked circular dsDNA.

1.5 μM recombinant purified ParA2 (A2) and ParA3 (A3) were incubated with 100 ng nicked circular ϕX174 RF II dsDNA in the presence and absence of 1 mM ADP and ATP as described in methodology. This mixture was incubated at 37°C for 15 min before putting on UV-activated carbon-coated 200 mesh, copper grids and negatively stained with 10 μl of 2% (w/v) uranyl acetate and observed under an electron microscope as described in methods. The scale bar for A2/A3 with or without ADP/ATP is 1 μm whereas with dsDNA and nucleotides is 100 nm. A part of protein interactions with DNA in the presence of ADP (Protein + DNA + ADP) and ATP (Protein + DNA + ATP) is zoomed (Zoomed) and shown.

mechanism of plasmid segregation, the ParA binding to ATP and hydrolysis favors assembly and disassembly of the segregation protein complex with DNA, while ParA–ADP complex is an antagonist to this DNA–protein interaction and exist as a monomer [33]. Therefore, the possibility of ParA–ATP and ParA–ADP ratios determining the polymerization and depolymerization dynamics of secondary ParAs cannot be ruled out and would be worth studying independently.

Para2 and ParA3 showed homotypic and heterotypic interactions

The ParA interaction was studied using BACTH [28] and co-IP in *E. coli*, co-expressing these proteins in different combinations as well as in *D. radiodurans* as described in the experimental procedures. Expression of these chimeras was confirmed by immunoblotting (Supplementary Figure S1). The *E. coli* cells co-expressing ParA1, ParA2 and ParA3 on BACTH plasmids in different combinations were screened for CyaA regulated β-galactosidase expression in *E. coli* BTH101 an *E. coli* host lacking active CyaA (see methods; [22]). Different ParA proteins showed homotypic interactions as indicated from the blue color colonies in spot assay and β-galactosidase activity in liquid culture (Figure 7A). In addition, ParA2 and ParA3 interacted with each other while none of them showed interaction with ParA1. These results were confirmed by co-IP in *E. coli* cells co-expressing these deinococcal ParAs tagged with T18 or T25 domains of CyaA in different combinations. For instance, when immunoprecipitation was carried out using T25 antibodies and the presence of interacting partner(s) tagged with T18 was detected by using T18 antibodies, all ParAs were coimmunoprecipitated with T18-fused species that included ParA2 and ParA3 but not ParA1 (Figure 7B–D).

In *D. radiodurans*, the cell-free extract of the cells co-expressing ParA1, ParA2 and ParA3 tagged with T18, and ParA2 or ParA3 with polyhistidine tag on plasmids was subjected to co-IP using anti-polyhistidine antibodies and interacting partner(s) if any are detected using T18 antibodies (Figure 8A). Nearly similar results were obtained as that of BTH and co-IP analysis in heterologous host *E. coli*. These results provided evidence that all the ParAs interacted homotypically while secondary genome ParAs can cross-talk to each other, but not with their homolog in the primary chromosome (Figure 8B). Thus, there seem to be structural and functional similarities among secondary genome's ParAs particularly ParA2 and ParA3 and a possibility of functional complementation of them for each other *in vivo* cannot be ruled out.

Biochemical Journal (2019) **476** 909–930
https://doi.org/10.1042/BCJ20180799

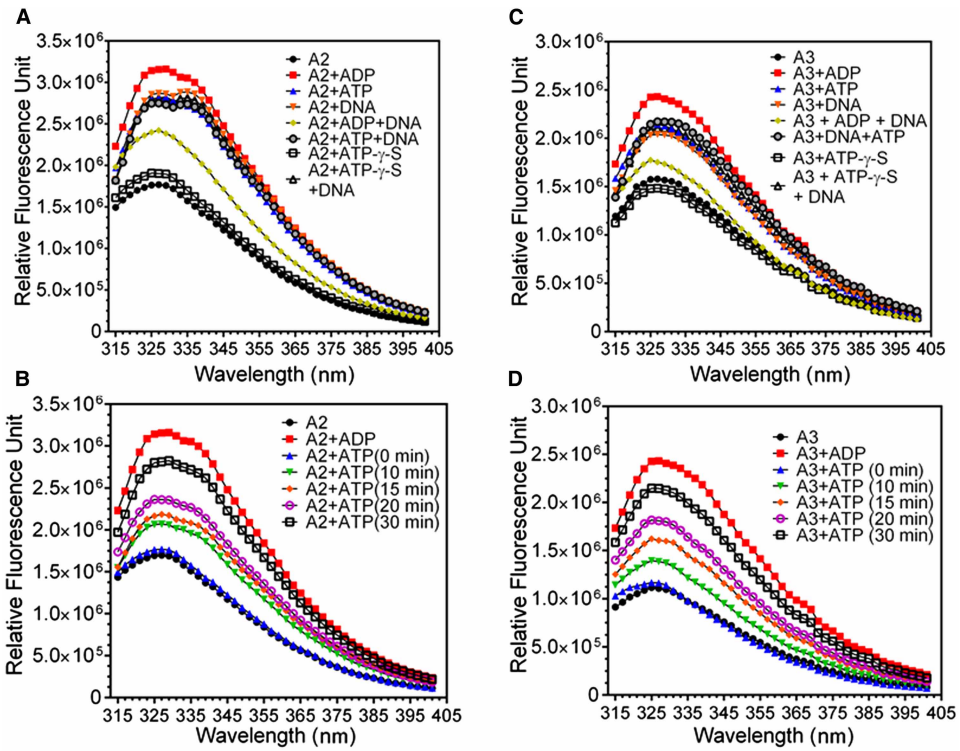

Figure 6. Nucleotides effects on tryptophan fluorescence of secondary genome ParAs.

2 μM ParA2 (A2) (**A**) and ParA3 (A3) (**C**) were incubated with 3.3 nM dsDNA in the absence and presence of 1 mM ADP, ATP or ATP-γ-S in different combinations. Intrinsic fluorescence of proteins was recorded for tryptophan by excitation at 295 nm and emission from 315 to 401 nm at an interval of 2 nm. Furthermore, 2 μM of A2 (**B**) or A3 (**D**) was incubated with 1 mM ATP and emission spectra were recorded at 0, 10, 15, 20 and 30 min of incubation after the addition of 0.5 mM $MgSO_4$. The obtained spectra for each time points were compared with spectra for each protein incubated with 1 mM ADP for 30 min.

ParAs interact to ParBs *in vivo*

The interaction of ParA1, ParA2 and ParA3 with ParB1, ParB2 and ParB3 in this bacterium was checked in different combinations using co-IP assay. For that, the cell-free extract from the cells co-expressing all ParAs tagged with T18, and all ParBs with polyhistidine tag, on plasmids was subjected to co-IP using anti-polyhistidine antibodies and interacting partner(s) if any would be detected using T18 antibodies. Results showed *in vivo* interaction of all the ParAs with their cognate ParBs. However, the secondary genome ParAs also interacted with non-cognate secondary genome ParBs (Figure 9A–C). Interestingly, ParA1 showed interaction with ParB1 only while none of the secondary genome ParAs interacted with ParB1. These results suggested a possible functional redundancy in the segregation process of secondary genome replicons.

ΔParA2ΔParA3 mutant showed a reduction in the copy number of secondary genome elements

Since ParA plays a crucial role in genome segregation, and secondary genome encoded ParA2 and ParA3 show nearly similar functions *in vitro*, the possibility of these ParAs affecting genome maintenance in *D. radiodurans* was tested. Both single (Δ*parA2* and Δ*parA3*) and double (Δ*parA2*Δ*parA3*) mutants of *parA2* and *parA3* were generated in *D. radiodurans* (Figure 10A) [16]. The genome copy number of these mutants was compared with wild-type cells. The copy numbers of Chr I did not change in any of the mutants while the Chr II and Mp copy numbers were reduced in double mutant but not in the single mutants (Figure 10B). This suggested that secondary genome ParA2/ParA3 deletion that may have affected their segregation in dividing cells has also affected replication of secondary genome elements by a yet unknown mechanism(s).

Biochemical Journal (2019) **476** 909–930
https://doi.org/10.1042/BCJ20180799

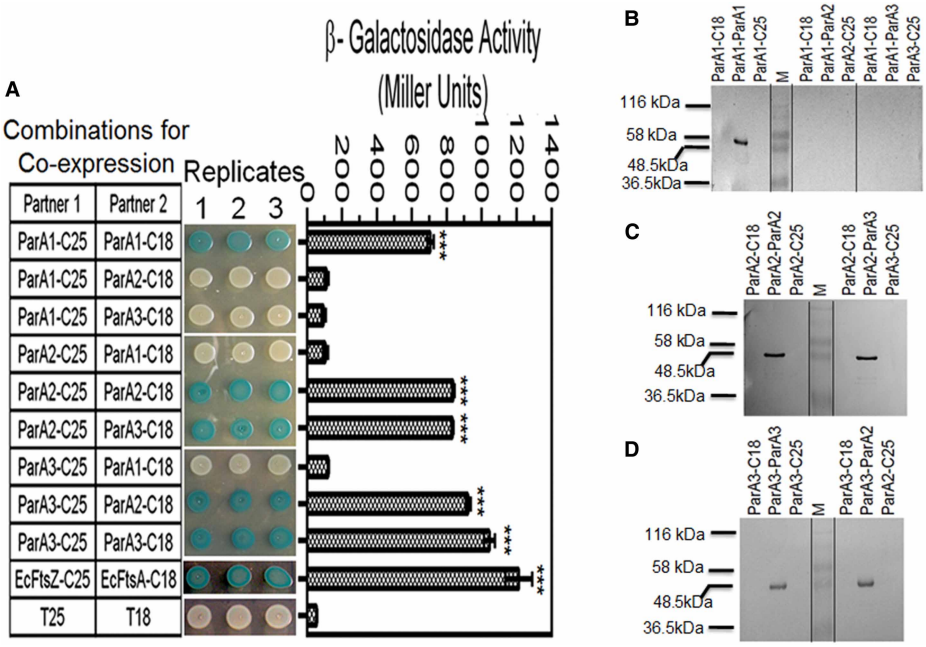

Figure 7. Protein–protein interaction of ParA proteins.

Translation fusion of ParA1, ParA2 and ParA3 was generated with T18 and T25 domains of adenylate cyclase in BACTH plasmids and their co-expression was ascertained by immunoblotting using antibodies against T18/T25 tags (Supplementary Figure S1). These chimeric proteins were expressed in *E. coli* BTH 101 in different combinations and interactions were monitored as white–blue colonies in the presence of X-Gal on the plate and as β-galactosidase activity in liquid culture (**A**). Cells co-expressing T18 or T25 tags on vectors were used as a negative control while *E. coli* FtsA (EcFtsA-C18) with *E. coli* FtsZ (EcFtsZ-C25) as a positive control. The β-galactosidase activity (units/mg protein) is shown here as mean ± SEM ($n = 9$) and the significance of the possible difference was analyzed using Student's *t*-test, and *P* values, obtained at 95% confidence intervals, are shown as (*) for <0.05, (**) for <0.01 and (***) for <0.001. *E. coli* BTH101 was co-expressed with ParA1-C25 (**B**), ParA2-C25 (**C**) and ParA3-C25 (**D**) and different ParAs tagged with T18 in different combinations. Cell-free extracts were immunoprecipitated using T25 antibodies and blotted using T18 antibodies. Results showing interaction of ParA1 with ParA1/ParA2/ParA3 (**B**), ParA2 with ParA2/ParA3 (**C**) and ParA3 with ParA2/ParA3 (**D**) are shown. Data in (**B–D)** are the representatives of a reproducible experiment repeated three times.

D. radiodurans cells lacking both ParA2 and ParA3 showed sensitivity to γ-radiation and H_2O_2

The effect of *parA2* and *parA3* deletion on growth response of *D. radiodurans* was monitored under normal and DNA damaging conditions. The double mutant showed a relatively slow growth under normal conditions as well as higher sensitivity to γ-radiation and H_2O_2 as compared with single mutant and wild type (Figure 10C–F). Thus, the double mutant that had reduced copy number of Chr II and Mp was also found to be more sensitive to γ-radiation and H_2O_2 as compared with their single mutant and wild type. This clearly indicated the role of secondary genome elements in normal growth and DNA damage tolerance in *D. radiodurans*. The single mutants have not shown a significant effect on growth, resistance to γ-radiation and hydrogen peroxide, and change in copy number of secondary genome elements. This further suggested a strong possibility of ParA2 and ParA3 complementing each other's role in these functions *in vivo*.

ΔParA2ΔParA3 double mutant showed a different morphology

Cell morphology and nucleoid phenotype of wild type, *ΔparA2*, *ΔparA3* single mutants as well as *ΔparA2ΔparA3* double mutant were monitored under the fluorescence microscope. Line scan analysis was carried out for a large number of cells in the region of interest (ROI). Figure 11 showed the line scan analysis

Biochemical Journal (2019) **476** 909–930
https://doi.org/10.1042/BCJ20180799

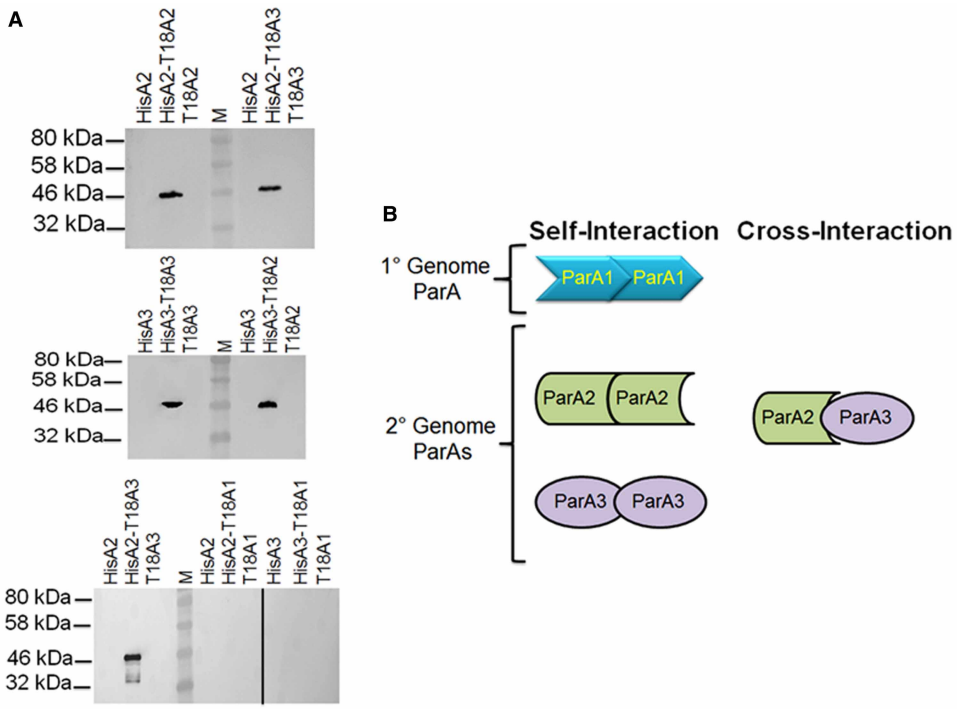

Figure 8. *In vivo* interactions of secondary genome encoded ParA proteins in *D. radiodurans*.

Translational fusions of deinococcal ParAs (ParA1, ParA2 and ParA3) were made with T18 domain of adenylate cyclase, and ParA2 and ParA3 with the polyhistidine tag (Supplementary Table S2). The expression of all these constructs was confirmed in *D. radiodurans* by immunoblotting using respective antibodies (Supplementary Figure S1). Both T18 and polyhistidine chimeras of ParAs were co-expressed in different combinations in *D. radiodurans* and immunoprecipitated using polyhistidine tag antibodies. The interacting partners of ParA2 with ParA2/ParA3, ParA3 with ParA2/ParA3 and ParA2/ParA3 with ParA1 (**A**) if any, were detected in immunoprecipitates by immunoblotting using T18 antibodies and schematically shown (**B**). Data shown are the representative of a reproducible experiment repeated at least three times.

of one ROI as the representative data for each sample. We observe that double mutant has a higher percentage of cells containing their nucleoid trapped between the septum and showing defects in the separation of the tetrads colony that usually happen to wild-type cells during normal cell division (Figure 11A,B). The average cell area of double mutant (~8 μm^2) was significantly higher than the cell areas of wild type and single mutants (~4 μm^2) (Figure 11A,C). A nearly similar phenotype of nucleoid trapped between septum has been reported in Noc null mutant of *Staphylococcus aureus* [34]. Quantitatively, ~25% cells were showing septum trapped nucleoid in double mutant as compared with less than 4% in single mutants and wild type. These finding together suggested that both ParA2 and ParA3 proteins regulate DNA translocation during cell division and they could complement the function of each other *in vivo*.

Discussion

Genome duplication followed by its accurate segregation is pre-requisite for productive cell division in all organisms. Interdependent regulation of these processes has not been discussed in greater details. However, the involvement of TGS in the segregation of the bacterial genome has been studied to a greater extent in bacteria harboring single circular chromosome and low copy plasmids [6,7]. The genome of MGH bacteria also encodes TGS. Very limited studies have been carried out on the mechanisms of genome segregation in MGH bacteria. For instance, in *V. cholerae* and *Burkholderia cenocepacia*, the TGS of primary and secondary chromosomes have been shown to function independently [35–38]. In *V. cholerae*, Chr I segregation shares maximum similarities with the segregation of pB171 [39]. In *D. radiodurans*, the TGS of the primary chromosome has been characterized previously [12].

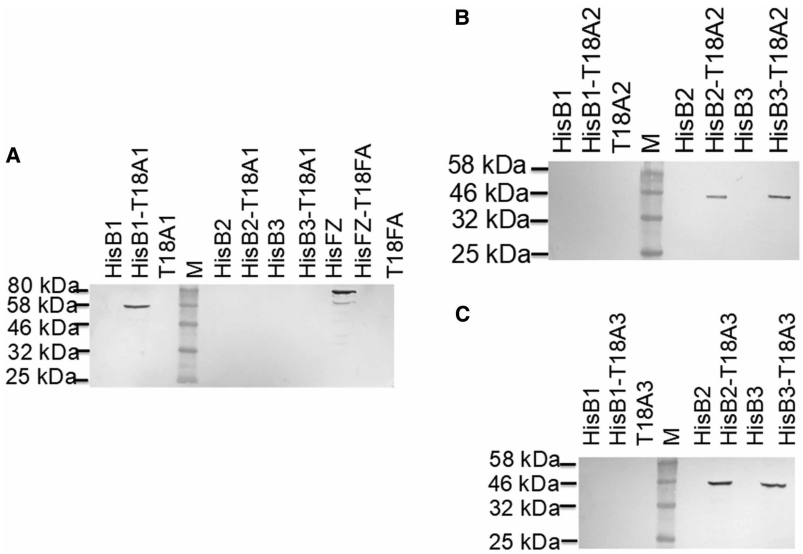

Figure 9. *In vivo* interactions of ParA and ParB proteins in *D. radiodurans*.

Translational fusion of T18 domain of adenylate cyclase was made with deinococcal ParA1 (T18A1), ParA2 (T18A2) and ParA3 (T18A3), while the polyhistidine tag was fused with ParB1 (HisB1), ParB2 (HisB2) and ParB3 (HisB3) (Supplementary Table S2). The expression of all these constructs was confirmed in *D. radiodurans* by immunoblotting using respective antibodies (Supplementary Figure S1). The translational fusions of different ParAs and ParBs were co-expressed in different combinations in *D. radiodurans*. The cell-free extract was immunoprecipitated using polyhistidine tag antibodies and respective interacting partners were detected by immunoblotting using T18 antibodies (**A**–**C**). The histidine-tagged DrFtsZ (HisFZ) and T18-tagged DrFtsA (T18FA) was used as a positive control (**A**). The data given are the representatives of the reproducible experiments repeated two times.

Here, we have brought forth functional characterization of P-loop Walker ATPases encoded on secondary genome elements. We demonstrated that both ParA2 and ParA3 have higher sequence similarity at amino acid levels, show nearly similar biochemical and biophysical characteristics *in vitro* and could compensate for the loss of each other *in vivo*. We found that secondary genome ParAs and or ParBs interact to self as well as to each other, but not with primary genome ParA and/or ParB in *D. radiodurans*. A double mutant lacking both ParA2 and ParA3 showed slower growth and higher sensitivity to DNA damaging agents. These phenotypes could be implicated due to a reduction in copy number of secondary genome elements. Interestingly, the phenotype loss due to secondary genome ParA deletion was not compensated by the presence of primary chromosomal ParA, indicating a strong possibility of independent segregation of primary chromosome and secondary genome elements.

Earlier, the roles of ParA and ParB in multiple processes like chromosome replication, segregation and cell division have been reported in different bacteria [40–47]. The roles of ParA and ParB in the normal growth of different bacteria have been found to be different. For instance, ParA and ParB encoded on the chromosome in *Caulobacter crescentus* has been shown to involve in cell cycle progression and cell division, and their null mutants are lethal [48]. *C. crescentus* follows asymmetric genome segregation where one copy of duplicated *oriC* gets traversed to opposite poles due to retraction of ParA filament upon depolymerization after it encounters to ParB-centromere complex [6,49]. On the other hand, although the loss of *parAB* in *Pseudomonas putida*, *Pseudomonas aeruginosa*, *Streptomyces coelicolor* and *Bacillus subtilis* has caused segregation defect, the *parAB* mutants do not show lethality in these bacteria [50–53]. In *V. cholerae*, *parAB* of Chr I is indispensable for normal growth [54]. Here, we found that the double mutant of *parA2* and *parA3*, in *D. radiodurans* produces phenotypes like reduced copy number of secondary genome elements, growth retardation albeit low under normal conditions, and higher sensitivity to γ-radiation and H_2O_2. Interestingly, we observed that the secondary genome ParA deletion does not affect Chr I copy number indicating that both primary chromosome and secondary genome elements perhaps segregate independently. Interestingly, we found that *ΔparA2ΔparA3* double mutant showed a significantly increased cell size and septum trapped nucleoid phenotype in *D. radiodurans*. However, the loss of ParAs which

Biochemical Journal (2019) **476** 909–930
https://doi.org/10.1042/BCJ20180799

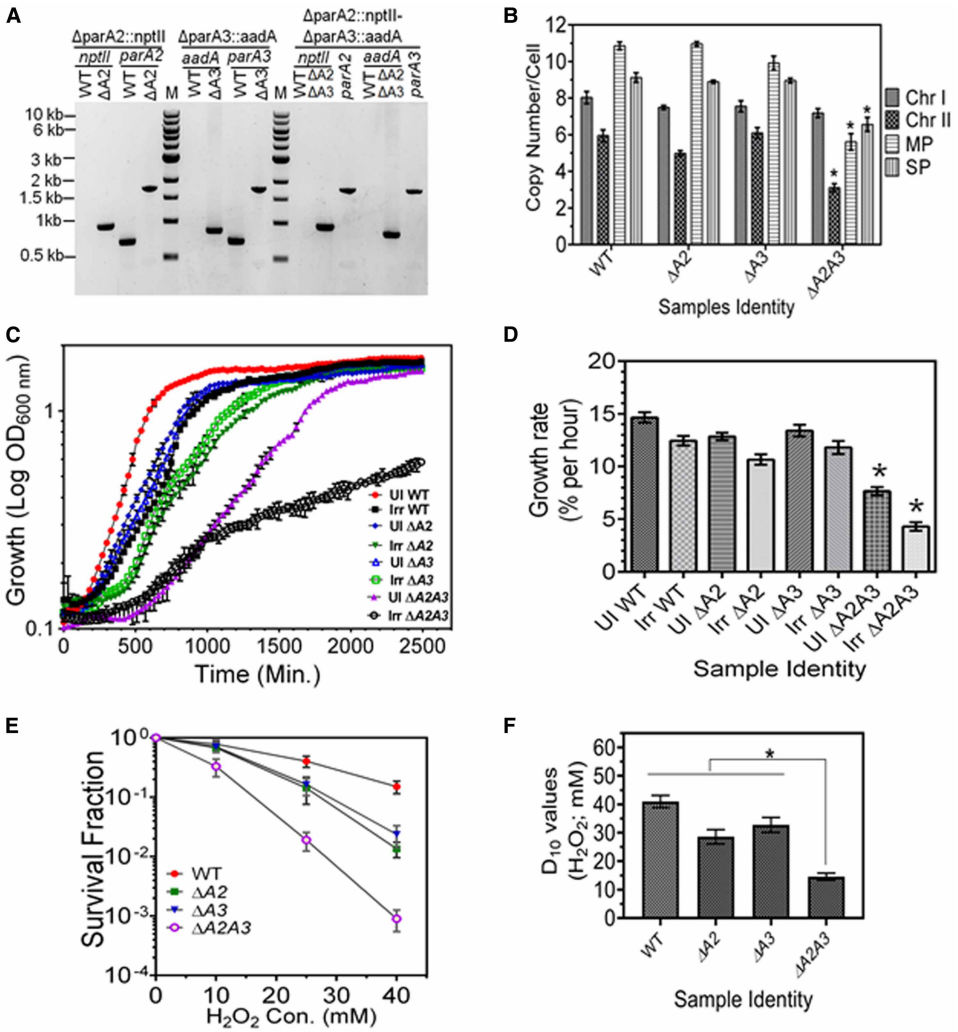

Figure 10. Roles of secondary genome ParAs on genome copy number and extremotolerant phenotypes of *D. radiodurans*.

The single deletion mutants of *parA2* (ΔA2) and *parA3* (ΔA3), as well as their double deletion mutant (ΔA2A3) of *D. radiodurans*, were created and confirmed by diagnostic PCR as described in methods (**A**). The copy number of chromosome I (ChrI), chromosome II (ChrII), Mp and Sp in wild type, ΔA2, ΔA3 and ΔA2A3 mutants was determined by qPCR (**B**). These cells were treated with 6 kGy γ-radiation (Irr) and post-irradiation recovery was compared with untreated controls (**C**) as described in methods. Data shown are the mean ± SEM ($n = 9$). Furthermore, the growth of different samples was monitored (**C**) and growth rate was calculated (**D**) using formula ($Nt = N0 \times (1 + r)t$ as described in methods and statistical significance of growth differences were found out using 'Student's *t*-test'. Similarly, wild type, *ΔA2*, *ΔA3* and *ΔA2A3* mutant cells were exposed to different concentration of H_2O_2 for 30 min and survival was monitored (**E**). The data shown here are mean ± SEM ($n = 6$). The D_{10} value was calculated and plotted (**F**) from the dose–response curve (**E**) and statistical analysis was performed on this using 'Student's *t*-test'. The *P* values obtained at 95% confidence intervals are shown as (*) for <0.05, (**) for <0.01 and (***) for <0.001.

presumably have arrested, DNA segregation affecting replication and thus copy number is intriguing and offers a possibility of an interdependent regulation of segregation and replication in this bacterium.

In summary, we show that the genome partitioning P-loop ATPases ParA2 and ParA3 encoded on secondary genome elements are biochemically and biophysically similar. The ParA proteins interact to its cognate ParB but not with other ParBs. ParAs of the secondary genome showed both homotypic and heterotypic interaction amongst themselves but not with Par proteins of the primary chromosome. The ParB2 and ParB3 proteins

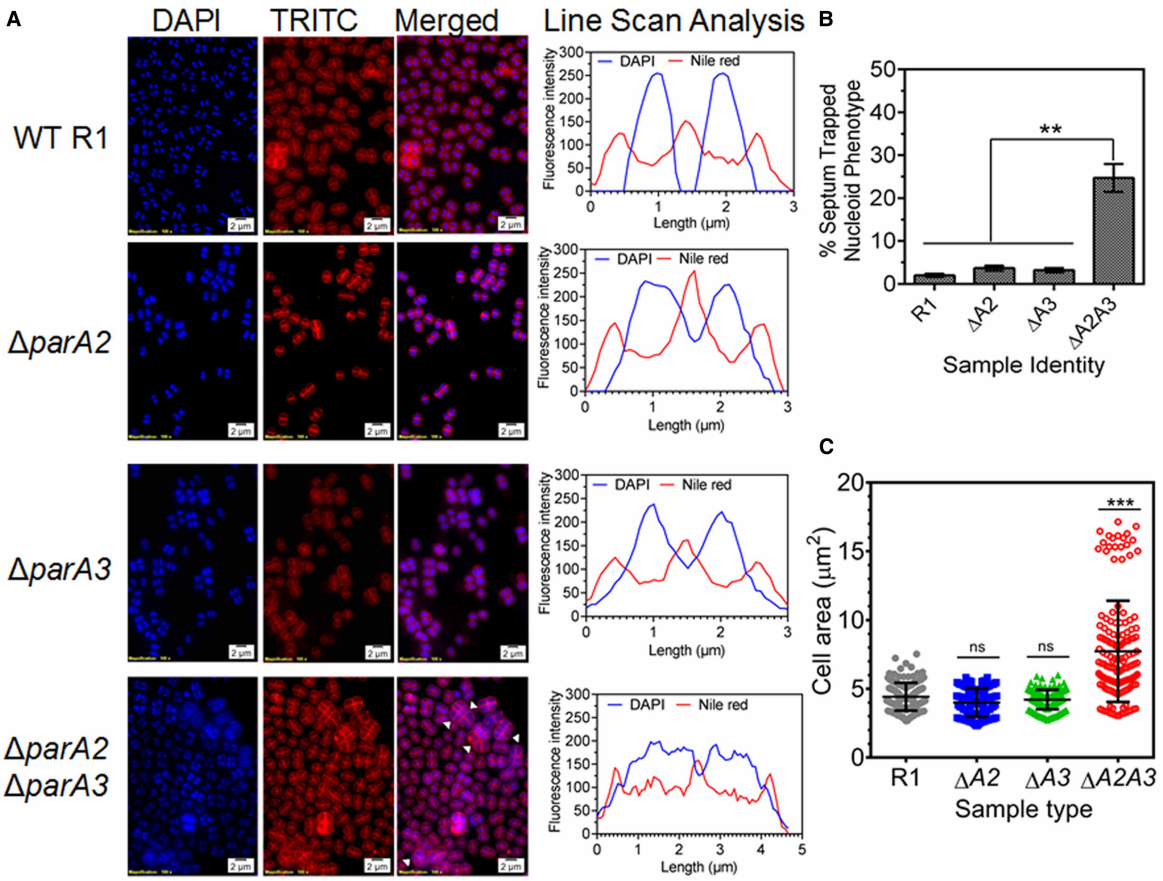

Figure 11. Microscopic studies of *parA*s mutants in *D. radiodurans*.

The wild type (*D. radiodurans*), single mutants of parA2 (Δ*parA2*) and parA3 (Δ*parA3*) and double mutant (Δ*parA2*Δ*parA3*) were stained using DAPI and Nile red. The stained cells were washed twice with PBS and imaged under DAPI and Nile red (TRIC channel) fluorescence in a fluorescence microscope (Olympus IX83). Images were aligned using in-built software cellSens and presented in separate as well as combined channels (**A**). The relative position of nucleoid (as a signal of DAPI) and membrane or septum (as a signal of Nile red) was demonstrated by line scan analysis of a large number of cells for each sample type and a representative plot has been given (**A**) Based on this observation % septum trapped nucleoid (indicated by the white arrow in (**A**)) phenotype has been calculated and plotted (**B**). The given data are representative of an experiment repeated three times independently. The Student's *t*-test was used to find the statistical significance of phenotype among different sample type. The cell area (μm^2) of >500 cells per sample was calculated and plotted (**C**). Two-way ANOVA was performed to find the statistical significance of data. The *P* value for significance has been mentioned in the graph. The *P* values obtained at 95% confidence intervals are shown as (*) for <0.05, (**) for <0.01 and (***) for <0.001.

show specific interaction with both *cisII* and *cisMP* elements *albeit* with different affinity in *D. radiodurans* (Figure 3). Nearly no effect of single deletion of either ParA2 or ParA3 while a profound effect of the double mutant on copy number and response to γ-radiation and H_2O_2 was observed, suggesting a strong possibility of these ParAs complementing the function of each other *in vivo* and seems to be having no role in the maintenance of primary chromosome. While the real-time demonstration on how genome segregation arrest can affect DNA replication would be worth pursuing independently, the available data provide a strong evidence that (i) all the secondary genome ParAs interact with all the ParBs encoded on secondary genome, (ii) arrest of genome segregation (at least secondary genome) affects genome duplication indicating an interdependent regulation of these processes, and (iii) the copy number reduction in ChrII and Mp affects the wild-type response to γ-radiation and oxidative stress in *D. radiodurans*.

Biochemical Journal (2019) **476** 909–930
https://doi.org/10.1042/BCJ20180799

Abbreviations

BACTH, bacterial two-hybrid system; co-IP, co-immunoprecipitation; DAE, Department of Atomic Energy; DLS, dynamic light scattering; EMSA, electrophoretic mobility shift assay; IPTG, isopropyl-β-D-thiogalactopyranoside; KCPS, Kilocounts/seconds; Mp, megaplasmid; NPC, nucleoprotein complex; ROI, region of interest; Sp, small plasmid; TGS, tripartite genome segregation.

Author Contribution

G.K.M. conducted experiments, analyzed data and wrote the paper. S.K. conducted experiments, analyzed data and wrote the manuscript. N.N.K. and R.T. conducted TEM imaging. H.S.M. is a Principal Investigator, conceived idea, analyzed results, discussed, wrote the paper and communicated for publication.

Funding

This work was supported by institutional funds only.

Acknowledgements

The authors are thankful to Ms Shruti Mishra and Dr Anubrata Das for their technical comments on the manuscript. The authors also thank Dr Debes Ray for his help in DLS experiments, Dr Rajani Kant Chittela and Dr Alka Gupta for their help in electron microscopic studies. G.K.M. is grateful to the DAE, Government of India, for research fellowships.

Competing Interests

The Authors declare that there are no competing interests associated with the manuscript.

References

1 Misra, H.S., Maurya, G.K., Kota, S. and Charaka, V.K. (2018) Maintenance of multipartite genome system and its functional significance in bacteria. *J. Genet.* **97**, 1013–1038 https://doi.org/10.1007/s12041-018-0969-x
2 Holden, M.T., Titball, R.W., Peacock, S.J., Cerdeno-Tarraga, A.M., Atkins, T., Crossman, L.C. et al. (2004) Genomic plasticity of the causative agent of melioidosis *Burkholderia pseudomallei*. *Proc. Natl Acad. Sci. U.S.A.* **101**, 14240–14245 https://doi.org/10.1073/pnas.0403302101
3 Lykidis, A., Pérez-Pantoja, D., Ledger, T., Mavromatis, K., Anderson, I.J., Ivanova, N.N. et al. (2010) The complete multipartite genome sequence of *Cupriavidus necator*JMP134 a versatile pollutant degrader. *PLoS ONE* **5**, e9729 https://doi.org/10.1371/journal.pone.0009729
4 Cooper, V.S., Vohr, S.H., Wrocklage, S.C. and Hatcher, P.J. (2010) Why genes evolve faster on secondary chromosomes in bacteria. *PLoS Comput. Biol.* **6**, e1000732 https://doi.org/10.1371/journal.pcbi.1000732
5 Prozorov, A.A. (2008) Additional chromosomes in bacteria: properties and origin. *Microbiology* **77**, 385–394 https://doi.org/10.1134/S0026261708040012
6 Gerdes, K., Howard, M. and Szardenings, F. (2010) Pushing and pulling in prokaryotic DNA segregation. *Cell* **121**, 927–942 https://doi.org/10.1016/j.cell.2010.05.033
7 Hayes, F. and Barillà, D. (2006) The bacterial segrosome: a dynamic nucleoprotein machine for DNA trafficking and segregation. *Nat. Rev. Microbiol.* **4**, 133–143 https://doi.org/10.1038/nrmicro1342
8 Battista, J.R. (2000) Radiation resistance: the fragments that remain. *Curr. Biol.* **10**, R204–R205 https://doi.org/10.1016/S0960-9822(00)00353-5
9 Slade, D. and Radman, M. (2011) Oxidative stress resistance in *Deinococcus radiodurans*. *Microbiol. Mol. Biol. Rev.* **75**, 133–191 https://doi.org/10.1128/MMBR.00015-10
10 Misra, H., Rajpurohit, Y.S. and Kota, S. (2013) Physiological and molecular basis of extreme radioresistance in *Deinococcus radiodurans*. *Curr. Sci.* **104**, 194–206
11 White, O., Eisen, J.A., Heidelberg, J.F., Hickey, E.K., Peterson, J.D., Dodson, R.J. et al. (1999) Genome sequence of the radioresistant bacterium *Deinococcus radiodurans* R1. *Science* **286**, 1571–1577 https://doi.org/10.1126/science.286.5444.1571
12 Charaka, V.K. and Misra, H.S. (2012) Functional characterization of the role of the chromosome I partitioning system in genome segregation in *Deinococcus radiodurans*. *J. Bacteriol.* **194**, 5739–5748 https://doi.org/10.1128/JB.00610-12
13 Charaka, V.K., Mehta, K.P. and Misra, H.S. (2013) Para encoded on chromosome II of *Deinococcus radiodurans* binds to nucleoid and inhibits cell division in *Escherichia coli*. *J. Biosci.* **38**, 487–497 https://doi.org/10.1007/s12038-013-9352-5
14 Schäefer, M.C., Schmitz, R., Facius, G., Horneck, B., Milow, K.H. and Ortner, J. (2000) Systematic study of parameters influencing the action of Rose Bengal with visible light on bacterial cells: comparison between biological effect and singlet-oxygen production. *Photochem. Photobiol.* **71**, 514–523<0514:SSOPIT>2.0.CO;2
15 Misra, H.S., Khairnar, N.P., Kota, S., Srivastava, S., Joshi, V.P. and Apte, S.K. (2006) An exonuclease I sensitive DNA repair pathways in *Deinococcus radiodurans*: a major determinant of radiation resistance. *Mol. Microbiol.* **59**, 1308–1316 https://doi.org/10.1111/j.1365-2958.2005.05005.x
16 Maurya, G.K. and Misra, H.S. (2018) Plasmids for making multiple knockouts in a radioresistant bacterium *Deinococcus radiodurans*. *Plasmid* **100**, 6–13 https://doi.org/10.1016/j.plasmid.2018.09.003
17 Green, M. R. and Sambrook, J. (2012) *Molecular Cloning: A Laboratory Manual*, 2nd edn, Cold Spring Harbor Laboratory Press, Cold Spring Harbor
18 Das, A.D. and Misra, H.S. (2011) Characterization of DRA0282 from *Deinococcus radiodurans* for its role in bacterial resistance to DNA damage. *Microbiology* **157**, 2196–2205 https://doi.org/10.1099/mic.0.040436-0

19 Yang, J., Yan, R., Roy, A., Xu, D., Poisson, J. and Zhang, Y. (2015) The I-TASSER Suite: protein structure and function prediction. *Nat. Methods* **12**, 7–8 https://doi.org/10.1038/nmeth.3213
20 Leonard, T.A., Butler, P.J. and Löwe, J. (2005) Bacterial chromosome segregation: structure and DNA binding of the Soj dimmer – a conserved biological switch. *EMBO J.* **24**, 270–282 https://doi.org/10.1038/sj.emboj.7600530
21 Battista, J.R., Park, M.J. and McLemore, A.E. (2001) Inactivation of two homologues of proteins presumed to be involved in the desiccation tolerance of plants sensitizes *Deinococcus radiodurans* R1 to desiccation. *Cryobiology* **43**, 133–139 https://doi.org/10.1006/cryo.2001.2357
22 Maurya, G.K., Modi, K., Banerjee, M., Chaudhary, R., Rajpurohit, Y.S. and Misra, H.S. (2018) Phosphorylation of FtsZ and FtsA by a DNA damage-responsive Ser/Thr protein kinase affects their functional interactions in *Deinococcus radiodurans*. *mSphere* **3**, e00325-18 https://doi.org/10.1128/mSphere.00325-18
23 Modi, K.M. and Misra, H.S. (2014) Dr-FtsA, an actin homologue in *Deinococcus radiodurans* differentially affects Dr-FtsZ and Ec-FtsZ functions in vitro. *PLoS ONE* **9**, e115918 https://doi.org/10.1371/journal.pone.0115918
24 Chittela, R.K., Kumbhakar, M., Pal, H., Rao, B.J. and Sainis, J.K. (2006) DNA strand exchange activity of rice recombinase OsDmc1 monitored by fluorescence resonance energy transfer and the role of ATP hydrolysis. *FEBS J.* **273**, 1497–1506 https://doi.org/10.1111/j.1742-4658.2006.05170.x
25 Hui, M.P., Galkin, V.E., Yu, X., Stasiak, A.Z., Stasiak, A., Waldor, M.K. et al. (2010) Para2, a *Vibrio cholerae* chromosome partitioning protein, forms left-handed helical filaments on DNA. *Proc. Natl Acad. Sci. U.S.A.* **107**, 4590–4595 https://doi.org/10.1073/pnas.0913060107
26 Bouet, J.Y., Ah-Seng, Y., Benmeradi, N. and Lane, D. (2007) Polymerization of SopA partition ATPase: regulation by DNA binding and SopB. *Mol. Microbiol.* **63**, 468–481 https://doi.org/10.1111/j.1365-2958.2006.05537.x
27 Battesti, A. and Bouveret, E. (2012) The bacterial two-hybrid system based on adenylate cyclase reconstitution in *Escherichia coli*. *Methods* **58**, 325–334 https://doi.org/10.1016/j.ymeth.2012.07.018
28 Karimova, G., Pidoux, J., Ullmann, A. and Ladant, D. (1998) A bacterial two-hybrid system based on a reconstituted signal transduction pathway. *Proc. Natl Acad. Sci. U.S.A.* **95**, 5752–5756 https://doi.org/10.1073/pnas.95.10.5752
29 Maurya, G.K., Modi, K. and Misra, H.S. (2016) Divisome and segrosome components of *Deinococcus radiodurans* interact through cell division regulatory proteins. *Microbiology* **162**, 1321–1334 https://doi.org/10.1099/mic.0.000330
30 Breuert, S., Allers, T., Spohn, G. and Soppa, J. (2006) Regulated polyploidy in halophilic archaea. *PLoS ONE* **1**, e92 https://doi.org/10.1371/journal.pone.0000092
31 Bustin, S.A., Benes, V., Garson, J.A., Hellemans, J., Huggett, J., Kubista, M. et al. (2009) The MIQE guidelines: minimum information for publication of quantitative real-time PCR experiments. *Clin. Chem.* **55**, 611–622 https://doi.org/10.1373/clinchem.2008.112797
32 Lakowicz, J.R. (1983) *Principles of Fluorescence Spectroscopy*, pp. 257–301, Plenum Press, New York
33 Havey, J.C., Vecchiarelli, A.G. and Funnell, B.E. (2012) ATP-regulated interactions between P1 ParA, ParB and non-specific DNA that are stabilized by the plasmid partition site, *parS*. *Nucleic Acids Res.* **40**, 801–812 https://doi.org/10.1093/nar/gkr747
34 Pang, T., Wang, X., Lim, H.C., Bernhardt, T.G. and Rudner, D.Z. (2017) The nucleoid occlusion factor Noc controls DNA replication initiation in *Staphylococcus aureus*. *PLoS Genet.* **13**, e1006908 https://doi.org/10.1371/journal.pgen.1006908
35 Egan, E.S., Fogel, M.A. and Waldor, M.K. (2005) Microreview: divided genomes: negotiating the cell cycle in prokaryotes with multiple chromosomes. *Mol. Microbiol.* **56**, 1129–1138 https://doi.org/10.1111/j.1365-2958.2005.04622.x
36 Fogel, M.A. and Waldor, M.K. (2005) Distinct segregation dynamics of the two *Vibrio cholerae* chromosomes. *Mol. Microbiol.* **55**, 125–136 https://doi.org/10.1111/j.1365-2958.2004.04379.x
37 Fogel, M.A. and Waldor, M.K. (2006) A dynamic, mitotic-like mechanism for bacterial chromosome segregation. *Genes Dev.* **20**, 3269–3282 https://doi.org/10.1101/gad.1496506
38 Dubarry, N., Pasta, F. and Lane, D. (2006) ParABS systems of the four replicons of *Burkholderia cenocepacia*: new chromosome centromeres confer partition specificity. *J. Bacteriol.* **188**, 1489–1496 https://doi.org/10.1128/JB.188.4.1489-1496.2006
39 Ringgaard, S., van Zon, J., Howard, M.K. and Gerdes, K. (2009) Movement and equipositioning of the plasmids by ParA filament disassembly. *Proc. Natl Acad. Sci. U.S.A.* **106**, 19369–19374 https://doi.org/10.1073/pnas.0908347106
40 Murray, H. and Errington, J. (2008) Dynamic control of the DNA replication initiation protein DnaA by Soj/ParA. *Cell* **135**, 74–84 https://doi.org/10.1016/j.cell.2008.07.044
41 Kadoya, R., Baek, J.H., Sarker, A. and Chattoraj, D.K. (2011) Participation of chromosome segregation protein ParAI of *Vibrio cholerae* in chromosome replication. *J. Bacteriol.* **193**, 1504–1514 https://doi.org/10.1128/JB.01067-10
42 Lee, P.S., Lin, D.C.H., Moriya, S. and Grossman, A.D. (2003) Effects of the chromosome partitioning protein Spo0J (ParB) on oriC positioning and replication initiation in *Bacillus subtilis*. *J. Bacteriol.* **185**, 1326–1337 https://doi.org/10.1128/JB.185.4.1326-1337.2003
43 Lee, P.S. and Grossman, A.D. (2006) The chromosome partitioning proteins Soj (ParA) and Spo0J (ParB) contribute to accurate chromosome partitioning, separation of replicated sister origins, and regulation of replication initiation in *Bacillus subtilis*. *Mol. Microbiol.* **60**, 853–869 https://doi.org/10.1111/j.1365-2958.2006.05140.x
44 Mohl, D.A., Easter, J. Jr and Gober, J.W. (2001) The chromosome partitioning protein, ParB, is required for cytokinesis in *Caulobacter crescentus*. *Mol. Microbiol.* **42**, 741–755 https://doi.org/10.1046/j.1365-2958.2001.02643.x
45 Ginda, K., Bezulska, M., Ziółkiewicz, M., Dziadek, J., Zakrzewska-Czerwińska, J. and Jakimowicz, D. (2013) Para of *Mycobacterium smegmatis* co-ordinates chromosome segregation with the cell cycle and interacts with the polar growth determinant DivIVA. *Mol. Microbiol.* **87**, 998–1012 https://doi.org/10.1111/mmi.12146
46 Ditkowski, B., Holmes, N., Rydzak, J., Donczew, M., Bezulska, M., Ginda, K. et al. (2013) Dynamic interplay of ParA with the polarity protein, Scy, coordinates the growth with chromosome segregation in *Streptomyces coelicolor*. *Open Biol.* **3**, 130006 https://doi.org/10.1098/rsob.130006
47 Donczew, M., Mackiewicz, P., Wróbel, A., Flärdh, K., Zakrzewska-Czerwińska, J. and Jakimowicz, D. (2016) Para and ParB coordinate chromosome segregation with cell elongation and division during *Streptomyces* sporulation. *Open Biol.* **6**, 150263 https://doi.org/10.1098/rsob.150263
48 Mohl, D.A. and Gober, J.W. (1997) Cell cycle-dependent polar localization of chromosome partitioning proteins in *Caulobacter crescentus*. *Cell* **88**, 675–684 PMID: 9054507
49 Shebelut, C.W., Guberman, J.M., van Teeffelen, S., Yakhnina, A.A. and Gitai, Z. (2010) Caulobacter chromosome segregation is an ordered multistep process. *Proc. Natl. Acad. Sci. U.S.A.* **107**, 14194–14198 https://doi.org/10.1073/pnas.1005274107

Biochemical Journal (2019) **476** 909–930
https://doi.org/10.1042/BCJ20180799

50 Lewis, R.A., Bignell, C.R., Zeng, W., Jones, A.C. and Thomas, C.M. (2002) Chromosome loss from par mutants of *Pseudomonas putida* depends on growth medium and phase of growth. *Microbiology* **148**, 537–548 https://doi.org/10.1099/00221287-148-2-537

51 Bartosik, A.A., Lasocki, K., Mierzejewska, J., Thomas, C.M. and Jagura-Burdzy, G. (2004) ParB of *Pseudomonas aeruginosa*: interactions with its partner ParA and its target parS and specific effects on bacterial growth. *J. Bacteriol.* **186**, 6983–6998 https://doi.org/10.1128/JB.186.20.6983-6998.2004

52 Kim, H.J., Calcutt, M.J., Schmidt, F.J. and Chater, K.F. (2000) Partitioning of the linear chromosome during sporulation of *Streptomyces coelicolor* A3 (2) involves an oriC-linked parAB locus. *J. Bacteriol.* **182**, 1313–1320 https://doi.org/10.1128/JB.182.5.1313-1320.2000

53 Ireton, K., Gunther, N.W.4th and Grossman, A.D. (1994) Spo0j is required for normal chromosome segregation as well as the initiation of sporulation in *Bacillus subtilis*. *J. Bacteriol.* **177**, 5320–5329 https://doi.org/10.1128/jb.176.17.5320-5329.1994

54 Saint-Dic, D., Frushour, B.P., Kehrl, J.H. and Kahng, L.S. (2006) A parA homolog selectively influences positioning of the large chromosome origin in *Vibrio cholerae*. *J. Bacteriol* **188**, 5626–5631 https://doi.org/10.1128/JB.00250-06

Microbiological Research 223–225 (2019) 22–32

Contents lists available at ScienceDirect

Microbiological Research

journal homepage: www.elsevier.com/locate/micres

Characterisation of ParB encoded on multipartite genome in *Deinococcus radiodurans* and their roles in radioresistance

Ganesh K Maurya[a,b], Swathi Kota[a,b], Hari S. Misra[a,b,*]

[a] Molecular Biology Division, Bhabha Atomic Research Centre, Mumbai, 400085, India
[b] Homi Bhabha National Institute, Mumbai, 400094, India

ARTICLE INFO

Keywords:
Centromere binding protein
Deinococcus
Genome segregation
Interdependence of genome maintenance and cell division
Multipartite genome system
Toroidal nucleoid
Radioresistance

ABSTRACT

The *Deinococcus radiodurans* multipartite genome consists of 2 chromosomes and 2 plasmids Its genome encodes 4 ParA and 4 ParB proteins on different replicons. Multiple sequence alignments of ParBs encoded on these genome elements showed that ParB of primary chromosome (ParB1) is close to chromosomal type ParB and is found to be different from ParBs encoded on chromosome II (ParB2) and megaplasmid (ParB3) elements. We observed that ParB1, ParB2 and ParB3 exist as dimer *in solution* and these proteins interact to self but not to its homologs in *D. radiodurans,* suggesting the specificity in ParBs dimerization. The *parB1* deletion mutant showed slow growth under normal condition and relatively reduced resistance to γ-radiation as compared to wild type. The *parB2* and *parB3* mutants maintained without selection pressure showed loss of radioresistance, which was not observed when maintained with selection pressure. Nearly half of the populations of these mutants showed resistance to antibiotics marked to respective genome elements. Interestingly, all the *parB* mutants showed increased copy numbers of cognate genome element in cells maintained with antibiotics possibly due to arrest in genome segregation. These results suggested that ParB proteins encoded on multipartite genome system in *D. radiodurans* form homodimer and not heterodimer with other ParB homologs, and they independently regulate the segregation of respective genome elements. The roles of ParB1 proteins in normal as well as radiation stressed growth of this bacterium have also been ascertained.

1. Introduction

The mechanisms underlying genome segregation are relatively better understood in eukaryotes where all three macromolecular events; chromosome duplication, segregation and cell division, are temporally separated (Yanagida, 2005). In bacteria, which have doubling time in minutes, these processes are not well separated but occur in same order like DNA duplication, segregation and cytokinesis and are believed to be interdependently regulated. Recently, genome sequencing studies have listed many bacteria that have multipartite genome system (MGS) comprised of more than one chromosome and large plasmids (Egan et al., 2005; Misra et al., 2018). Genome sequence analysis revealed that like bacteria harbouring monopartite genome, multipartite genome system harbouring bacteria also contain classical tripartite genome segregation (TGS) systems. TGS is comprised of *cis* elements termed bacterial centromere, Walker type P-Loop ATPases (ParA or ParA like proteins) and centromere binding proteins (ParB or ParB like proteins) (Hayes and Barilla, 2006; Gerdes et al., 2010). In brief, ParBs or its homologues show site specific interaction with centromeric sequences (usually present close to *parAB* operon in repeats) by HTH motif present in C-terminal region of protein. ParAs or its homologues are non-specific DNA binding ATPases which interact to *parB*-centromere segregation complex and undergo polymerisation / depolymerisation kinetics to segregates duplicated DNA. Different roles of Par proteins in bacterial survival have been reported in different bacteria. For instance, loss of chromosomal *parAB* locus is lethal and essential in *Caulobacter crescentus* (Mohl and Gober, 1997) but found to be dispensable in *Bacillus subtilis*, *Pseudomonas putida*, *Pseudomonas aeruginosa*, *Streptomyces coelicolor*, and *Vibrio cholerae* (chromosome I *parAB*) (Ireton et al., 1994; Lewis et al., 2002; Bartosik et al., 2004; Kim et al., 2000; Saint-Dic et al., 2006). Among multipartite genome system harbouring bacteria, the limited studies on genome maintenance have been reported in *V. cholerae* (Egan and Waldor, 2003; Fogel and Waldor, 2005), cystic fibrosis pathogen *B. cenocepacia* (Dubarry et al., 2006) and *D. radiodurans* (Charaka and Misra, 2012).

D. radiodurans is an extremotolerant bacteria characterized for its extraordinary resistance to DNA damaging agents including radiations and desiccation (Battista, 2000; Slade and Radman, 2011; Misra et al.,

* Corresponding author.
E-mail address: hsmisra@barc.gov.in (H.S. Misra).

https://doi.org/10.1016/j.micres.2019.03.005
Received 14 October 2018; Received in revised form 27 February 2019; Accepted 16 March 2019
Available online 01 April 2019
0944-5013/

2013). Multipartite genome of this bacterium consists of 2 chromosomes and 2 plasmids (White et al., 1999). Chromosome I, chromosome II and megaplasmid encode putative ParA and ParB proteins (White et al., 1999). Recently, chromosome I partitioning system has been characterized in *D. radiodurans* (Charaka and Misra, 2012). Involvement of ParA of chromosome II (ParA2) in the regulation of cell division has been reported (Charaka et al., 2013). Multiple sequence alignments of different ParA and ParB proteins encoded on multipartite genome elements in *D. radiodurans* showed close similarities with their homologs. Therefore, the importance of multiple sets of Par proteins with nearly similar putative structures and their possible functional redundancy in multipartite partite genome maintenance would be a curiosity to understand. Molecular mechanisms underlying the evolution and maintenance of multipartite genome system, its inheritance into daughter cells, and their functional significance in extreme phenotypes of *D. radiodurans* are not known in detail and would be worth studying.

Here, we report characterization of ParB proteins *in vitro* and their roles in extraordinary phenotypes in *D. radiodurans*. We demonstrated that all the ParBs form homodimer *in vitro* and do not interact with other ParB homologues of this bacterium. The *ΔparB2, ΔparB3* mutants maintained with antibiotic pressure showed nearly wild type growth under normal and γ-radiation stressed conditions. However, when maintained without selection pressure, a significant population was found to be sensitive to antibiotics and these cells compromised to γ-radiation resistance. This indicated that certain population in respective mutant has failed to receive copy of genome element marked with antibiotic resistance. The *ΔparB1* cells showed growth retardation under normal conditions and were sensitive to γ-radiation as compared wild type cells. All the mutants grown under selection pressure showed a significant increase in copy number of respective genome elements. Interaction of ParBs with replication initiation proteins DnaA and DnaB implied a functional interaction of genome duplication and segregation in this bacterium. These results together suggested that ParBs form homodimer and have roles in interdependent regulation of DNA replication and genome segregation as well as in radioresistance in *D. radiodurans*.

2. Materials and methods

2.1. Bacterial strains, plasmids and materials

All the bacterial strain and plasmids used in this study have been listed in Table S1 while primers in table S2. *D. radiodurans* R1 (ATCC13939) was a kind gift from Professor J. Ortner, Germany (Schaefer et al., 2000). It was grown in TGY (Tryptone (1%), Glucose (0.1%) and Yeast extract (0.5%)) medium at 32 °C. *E. coli* strain Nova Blue was used for cloning and maintenance of all the plasmids. *E. coli* strain BL21 (DE3) pLysS was used for the expression of recombinant proteins. *E. coli* strain BTH 101 was used for Bacterial Two-Hybrid System (BACTH) based study. *E. coli* cells harbouring pET28a (+) and its derivatives were maintained in the presence of kanamycin (25 μg/ml). Standard protocols for all recombinant techniques were used as described in (Green and Sambrook, 2012). All the molecular biology grade chemicals and enzymes were purchased from Sigma Chemicals Company, USA, Roche Biochemicals, Mannheim, Germany, New England Biolabs, USA and Merk India Pvt. Ltd. India.

2.2. Bioinformatic analysis

Multiple sequence alignment and functional motifs search in ParB1 (Dr_0012), ParB2 (DR_A0002), ParB3 (DR_B0002) and ParB4 (Dr_B0030) proteins were carried out using standard online bioinformatics tools as described earlier (Das and Misra, 2011; Charaka et al., 2013). In brief, the amino acid sequences of ParB1, ParB2, ParB3 and ParB4 proteins were subjected to a PSI-BLAST search with the SWISSPROT database. After five iterations, the sequences obtained were aligned by CLUSTAL-W along with ParB (Spo0J) protein of closest bacteria *T. thermophilus* and *B. subtilis*. The sequences of close homology were aligned by T-COFFEE, and the conserved motifs were marked in CLUSTAL-W. The secondary structure was inferred from PSIPRED, JNET, and Prof with the Quick2D server of the Max Planck Institute for Developmental Biology. The boundaries of the secondary structure (correspond to Spo0J of *T. thermophilus* (PDB. ID: 1VZ0)) were defined by using online Espript program. The secondary structure of C-terminal region was analyzed by using Psipred online software and represented in Espript online software. The phylogenetic tree between deinococcal ParBs and known ParB family proteins (Spo0J from *T. thermophilus* and *B. subtilis*) was constructed using PHYLIP program showing Neighbour-joining tree without distance corrections.

2.3. Cloning, expression and purification of ParB1, ParB2 and ParB3 proteins

Details of the primers used for construction of recombinant plasmids and generation of deletion mutants are given in Table S2. Genomic DNA of D. radiodurans R1 was prepared as reported previously (Battista et al., 2001), and open reading frames (ORFs) DR_A0002 (parB2) and DR_B0002 (parB3) were PCR amplified from genomic DNA by using primers pETB2F and pETB2R for the parB2 gene and primers pETB3F and pETB3R for the parB3 gene (see Table S2). PCR products were ligated at the NdeI and XhoI sites in pET28a (+) to yield pETB2 and pETB3, respectively. For ParB1, pET0012 plasmid (Charaka and Misra, 2012) was used. These plasmids were used for protein purification. Recombinant ParB1, ParB2 and ParB3 were expressed on pET0012, pETB2 and pETB3 respectively in E. coli BL21 (DE3) pLysS. The recombinant proteins were purified by nickel affinity chromatography, as described earlier (Charaka and Misra, 2012). In brief, overnight grown cultures of E. coli BL21 (DE3) pLysS expressing recombinant proteins were diluted 1:100 in fresh LB broth containing 25 μg/ml kanamycin and 0.5 mM isopropyl-β-D-thiogalactopyranoside (IPTG) was added at 0.3 OD at 600 nm and after 2 h culture was kept at 4 °C for overnight. It was further allowed to grow at 37 °C for 1 h and harvested to keep cell pellet in −70 °C. Cell pellet was thawed and suspended in buffer A (20 mM Tris–HCl, pH 7.6, 300 mM NaCl and 10% glycerol) containing 10 mM imidazole, 0.5 mg/ml lysozyme, 1 mM PMSF, 1 mM $MgCl_2$, 0.05% NP-40, 0.05% TritonX-100, protease inhibitor cocktail) and incubated at 37 °C for 30 min. Cells were sonicated for 5 min at 10 s pulses with intermittent cooling for 15 s at 25% amplitude. The cell lysate was centrifuged at 11,000 rpm for 30 min at 4 °C. The supernatant was dialysed in Buffer A containing 1 mM PMSF at 4 °C. The dialysed cell-free extract was loaded onto $NiCl_2$ charged-fast-flow-chelating-sepharose column (GE Healthcare) pre-equilibrated with buffer A containing 10 mM imidazole. The column was washed with 40 column volumes of buffer A containing 50 mM imidazole and 10 column volumes of buffer A containing 70 mM imidazole till proteins stop coming from the column. Recombinant proteins eluted in steps using 100 mM, 200 mM, 250 mM and 300 mM imidazole in buffer A and analyzed on 10% SDS-PAGE. Fractions containing more than 95% pure protein were pooled and dialyzed in buffer A containing 100 mM NaCl and processed for ion exchange chromatography using HiTrap Q HP anion exchange column (GE Healthcare Life sciences). Different fractions were analyzed on SDS-PAGE and fractions containing pure protein were pooled and concentrated using 10 kDa cut-off spin columns. Concentrated protein was centrifuged at 16,000 rpm for 30 min to remove aggregates. Supernatant containing mostly soluble proteins were used for size exclusion chromatography. For storage in −20 °C, proteins were dialyzed in dialysis buffer containing 20 mM Tris-HCl pH 7.6, 100 mM NaCl, 50% glycerol, 1 mM $MgCl_2$ and 1 mM PMSF. Protein concentration was determined by taking OD at 280 nm in Nano drop (Synergy H1, Hybrid Multi-Mode Reader Biotek) using mass extinction co-efficient of the proteins.

Table 1
Copy number of different replicons in wild type (WT) and *parB* mutants with and without expression of respective ParBs *in trans* in *Deinococcus radiodurans*. Two genes per replicon (one near to origin and other near to terminus) were selected and copy number values have been tabulated accordingly.

	Chromosome I		Chromosome II		Megaplasmid		Small Plasmid	
Pheno -type	*ftsZ* 87°	*ftsE* 212°	*pprA* 334°	Dr_A0155 137°	Dr_B0003 6°	Dr_B0076 187°	DrC0001 0.55°	DrC0018 145°
WT	8.03 ± 0.33	7.28 ± 0.3	5.95 ± 0.35	5.55 ± 0.32	10.85 ± 0.32	10.06 ± 0.22	9.12 ± 0.26	8.69 ± 0.24
ΔB1	10.3 ± 0.11	9.62 ± 0.10	6.5 ± 0.16	6.01 ± 0.15	11.86 ± 0.13	11.02 ± 0.12	10.22 ± 0.09	9.59 ± 0.08
ΔB1/B1	7.85 ± 0.39	7.22 ± 0.32	6.2 ± 0.34	5.85 ± 0.31	10.96 ± 0.24	10.23 ± 0.18	8.96 ± 0.25	8.29 ± 0.23
ΔB2	8.89 ± 0.3	7.86 ± 0.27	9.55 ± 0.31	8.89 ± 0.28	13.08 ± 0.29	12.55 ± 0.38	11.22 ± 0.13	10.79 ± 0.12
ΔB2/B2	8.25 ± 0.13	7.88 ± 0.11	6.15 ± 0.13	5.88 ± 0.12	11.12 ± 0.12	10.59 ± 0.21	9.34 ± 0.18	8.9 ± 0.17
ΔB3	8.78 ± 0.24	8.02 ± 0.21	7.86 ± 0.24	7.12 ± 0.22	18.25 ± 0.33	17.55 ± 0.45	12.24 ± 0.38	11.52 ± 0.36
ΔB3/B3	8.31 ± 0.32	7.62 ± 0.29	6.02 ± 0.41	5.78 ± 0.37	11.45 ± 0.35	10.81 ± 0.25	9.15 ± 0.31	8.78 ± 0.29

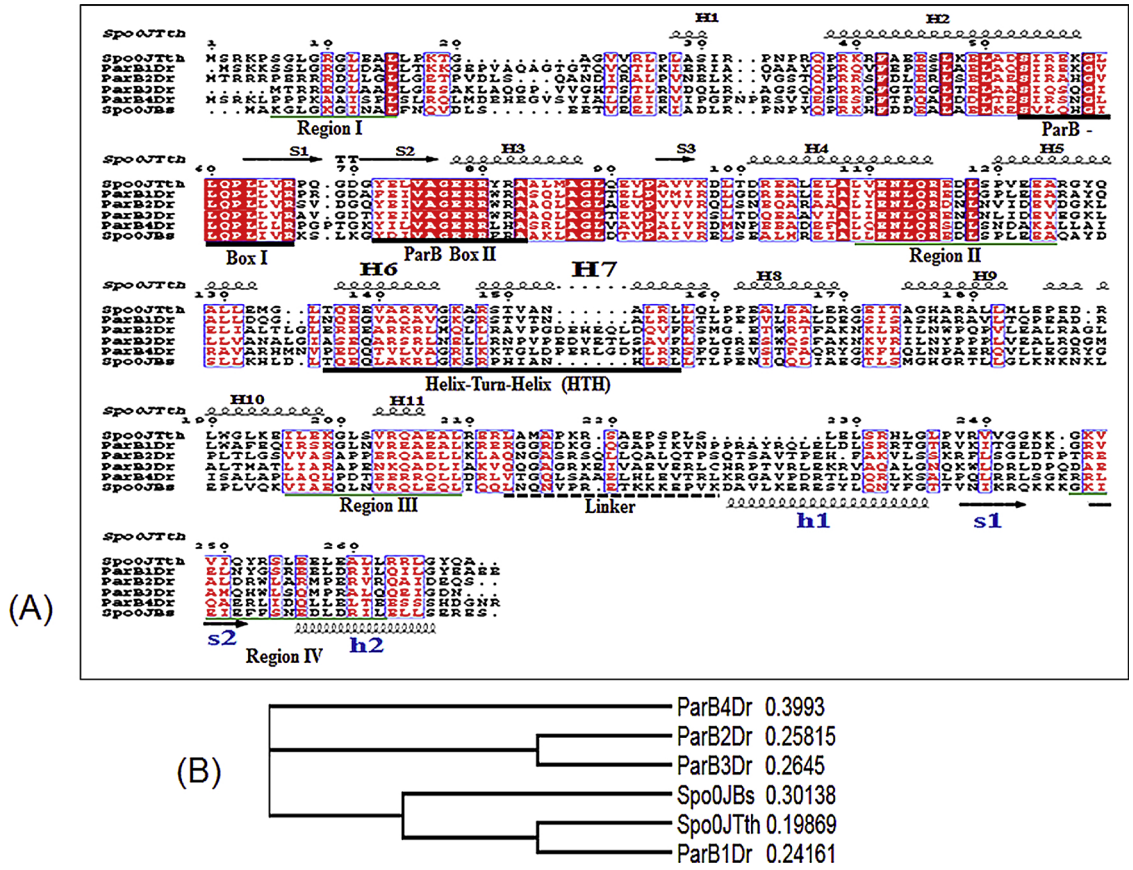

Fig. 1. Multiple sequence alignment of deinococcal ParB proteins with known ParB family proteins. The amino acid sequence of different deinococcal ParB proteins, Spo0J from *B. subtilis* and *T. thermophilus* is retrieved from NCBI and homology between sequences is checked by ClustalW analysis. Boundaries of the secondary structure were defined using online Espript program. The secondary structure shown in this figure corresponds to those of domain of Spo0J of *T. thermophilus* (PDB. ID: 1VZ0). Secondary structure of C-terminal region was analyzed by using Psipred online software and represented in Espript online software (A). The phylogenetic tree between deinococcal ParBs and known ParB family proteins was constructed using PHYLIP program showing Neighbour-joining tree without distance corrections (B).

2.4. Size exclusion chromatography and glutaraldehyde crosslinking

For determination of the molecular weight of deinococcal ParB proteins in its native state, molecular size exclusion chromatography was performed using Superdex™ 200 G L column (Pharmacia) on AKTA purifier (GE Healthcare). For this, ˜1 mg of purified ParB1, ParB2 and ParB3 proteins were loaded separately onto the column in storage buffer containing 20 mM Tris HCl, 100 mM NaCl, pH 7.6 and eluted at a flow rate of 0.5 ml/min. The column was formerly calibrated with gel filtration molecular weight markers (Amersham-Pharmacia: Chymotripsinogen- 25 kDa, Ovalbumin- 44 kDa, Bovine serum albumin – 66.5 kDa, Aldolase – 158 kDa, Catalase- 250 kDa). Standard calibration curve was plotted with elution volume of marker against the logarithm of molecular weight of markers. The molecular weight of the purified ParBs in the native condition was determined by fitting the elution volume into the calibration curve. Eluted peaks were analyzed on native PAGE for reconfirmation of the presence of ParB proteins (data not shown).

For glutaraldehyde crosslinking of protein in their native state, ˜10 µg of the purified recombinants ParB1, ParB2 and ParB3 proteins were diluted in 20 mM phosphate buffer pH 8.0 in a reaction volume of 30 µl. Further, protein solutions were incubated at 37 °C for 5 min in absence and presence of 2 µl of freshly prepared 0.02% glutaraldehyde solution. To this, equal volume of 2X cracking dye was added and

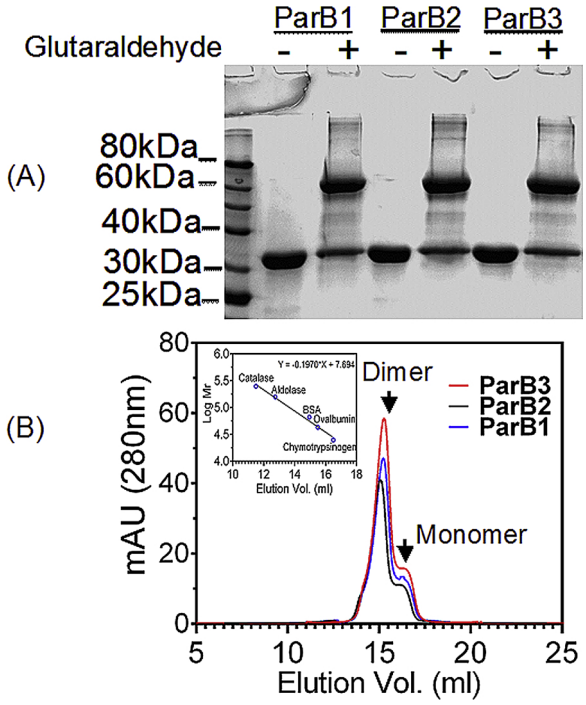

Fig. 2. Molecular size / weight determination of recombinant ParB1, ParB2 and ParB3 proteins in solution using glutaraldehyde crosslinking (A) and size exclusion chromatography (B). In brief, ~10 µg of the purified recombinants ParB1, ParB2 and ParB3 proteins were incubated in 20 mM phosphate buffer pH 8.0 in the absence and presence of 0.02% glutaraldehyde solution at 37 °C for 5 min. The reaction mixture was heated at 80 °C in presence of 2X cracking dye and separated on 10% SDS-PAGE and stained with Coomassie brilliant blue (A). For size exclusion chromatography, ~1 mg of purified ParB1, ParB2 and ParB3 proteins were passed through Superdex™ 200 G L column (Pharmacia) on AKTA purifier (GE Healthcare) at a flow rate of 0.5 ml/min. The column was formerly calibrated with gel filtration molecular weight markers and standard calibration curve was plotted with elution volume of marker against the logarithm of molecular weight of markers (given in inset of Fig. 2B). The molecular weight of the purified ParBs in the native condition was determined from standard curve (B). The given data is representative of experiments repeated three times independently.

heated at 80 °C for 5 min. These samples were separated on 10% SDS-PAGE and stained with Coomassie brilliant blue and documented.

2.5. *In vivo* protein-protein interaction studies in *D. radiodurans*

Interaction among ParB1, ParB2 and ParB3 was monitored in *D. radiodurans* by co-immunoprecipitation. For that, the T18 tagged *parB*s were PCR amplified using BTHF(pv) and BTHR(pv) primers from their BACTH derivative plasmids (Maurya et al., 2016) and cloned in pVHS559 plasmid (Charaka and Misra, 2012) at *Nde*I-*Xho*I sites to yield pV18B1, pV18B2 and pV18B3 (Table S1). Similarly, N-terminal hexahistidine tagged *parB, parB2* and *parB3* were amplified using pETHisF and pETHisR primers from their pET28a + derivatives (Table S1) and cloned in pRADgro plasmid (Misra et al., 2006) at *Apa*I-*Xba*I sites to yield pRADhisB1, pRADhisB2 and pRADhisB3 plasmids (Table S1). The expression of fusion proteins in *Deinococcus* from these constructs was monitored using Anti-T18 antibodies or Anti-polyhistidine antibodies (Maurya et al., 2018) (Fig. S2 A, B). The deinococcal cells co-expressing T18 tagged ParBs with hexahistidine tagged ParBs in different combinations were collected at log phase. The cell-free extracts of *D. radiodurans* expressing all three ParBs under IPTG induction as on pV18B1, pV18B2 and pV18B3 in different combinations with hexahistidine tagged all three ParBs under constitutive promoter from pRADgro were prepared and immunoprecipitated using Anti-polyhistidine antibodies as described earlier (Maurya et al., 2016, 2018). The T18 fused or polyhistidine fused ParBs alone were used as controls. The immunoprecipitates were separated on SDS-PAGE, blotted onto PVDF membrane and hybridized using monoclonal antibodies against T18 tag. The hybridization signals were detected using anti-mouse secondary antibodies conjugated with alkaline phosphatase using BCIP/NBT substrates (Roche Biochemical, Mannheim). The interaction between replication initiator protein, DnaA and deinococcal ParBs in *D. radiodurans* was monitored by using co-immunoprecipitation. In brief, N-terminal hexahistidine tagged dnaA (DR_0002) was PCR amplified using pETHisF and pETHisR primers from pETDnaA plasmid (dnaA cloned in pET28a + at *Bam*HI and *Eco*RI sites) and cloned in pRADgro plasmid at *Apa*I and *Xba*I sites. The resulting plasmid named as pRADhisdnaA. The expression of hexahistidine tagged DnaA in *D. radiodurans* from pRADhisdnaA was monitored through western blotting by using Anti-polyhistidine antibody as described above (Fig. S2 C). The pRADhisdnaA was co-transformed with T18 tagged deinococcal ParBs expressing plasmid as mentioned above. The expression of T18

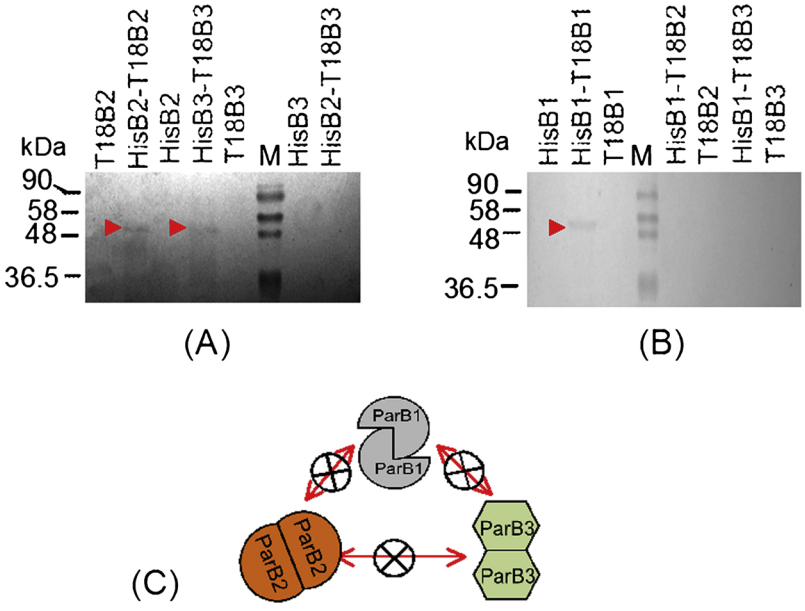

Fig. 3. *In vivo* interaction among deinococcal ParBs from *D. radiodurans* using co-immunoprecipitations. Plasmid bearing polyhis tagged ParB1 (HisB1), ParB2 (HisB2) or ParB3 (HisB3) were co-transformed with plasmid bearing T18 tagged ParB1 (T18B1), ParB2 (T18B2) or ParB3 (T18B3) in different combinations (see table S1). For controls these constructs were co-transformed along with empty vectors. These transformants were grown and induced with required amount of IPTG (see methods). The cell lysate of equal O.D. co-transformants were used for co-immunoprecipitation using polyhistideine antibodies. Equal amount of co-IPs was separated on SDS-PAGE and immunoblotted using T18 antibodies (Fig. 3A–B). Data in panel A and B are the representatives of a reproducible experiment repeated 3 times. Based on these observations from *D. radiodurans,* a cartoon model has been made to show interactions among deinococcal ParBs (C).

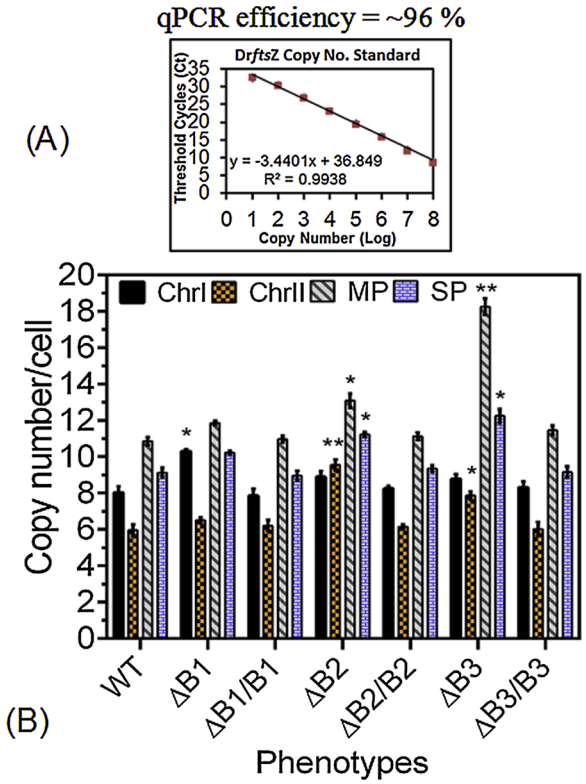

Fig. 4. Effect of *parB1, parB2* and *parB3* mutation on the ploidy of deinococcal genome. The wild type (WT) cells, *parB1 (ΔB1), parB2 (ΔB2)* and *parB3 (ΔB3)* mutants and its complemented forms (*ΔB1/B1, ΔB2/B2* and *ΔB3/B3* respectively) were subjected to copy number determination for each replicon using quantitative Real Time PCR (qRT-PCR) as detailed in method. In brief, a fragment of about 300 bps of *DrftsZ* gene was PCR amplified and their know concentration was used for generating standard curve for copy number determination using qRT-PCR (A). Two different genes per replicon with similar PCR efficiency (> 96%) was selected in *D. radiodurans* (described in methods; Table 1). The qRT-PCR was carried out and the cycle threshold (Ct) values were determined. The replicon copy number is quantified by comparing the Ct values with standard (B). Average of copy number reflected from two genes per replicon was represented as mean ± SD (B). The student *t*-test was used for statistical analysis of obtained data. The P values, obtained at 95% confidence intervals, are shown as (*) for < 0.05, (**) for < 0.01 and (***) for < 0.001. The data is representative of experiments repeated three times.

tagged ParBs in co-transformants was induced by 5 mM IPTG. The cell-free extracts of *D. radiodurans* expressing all three ParBs as on pV18B1, pV18B2 and pV18B3 in different combinations with hexahistidine tagged DnaA under constitutive promoter from pRADgro were prepared and immunoprecipitated using Anti-polyhistidine antibodies as mentioned above (Maurya et al., 2016, 2018). The T18 fused ParBs or polyhistidine fused DnaA alone were used as controls. The co-immunoprecipitates were separated on SDS-PAGE, blotted onto PVDF membrane and hybridized by Anti-T18 monoclonal antibodies raised in mouse. The hybridization signals were detected as described above.

2.6. Protein-protein interaction study using BACTH system in surrogate E. coli

For protein-protein interaction studies between deinococcal ParBs and replication initiation protein DnaA as well as replication helicase DnaB, coding sequences of Dr_0002 (DnaA) and Dr_0549 (DnaB) were cloned at *Bam*HI-*Eco*RI sites and *Kpn*I-*Eco*RI sites in pKNT25 to yield pKNTDA and pKNTDB, respectively while pUTCB1, pUTCB2 and pUTCB3 was used as described in (Maurya et al., 2016) (Table S1). The expression of T25 tagged DnaA and DnaB in *E. coli* was monitored using Anti-T25 antibodies (Fig. S2 D). *In vivo* interactions of different proteins were monitored using bacterial two-hybrid system (BACTH) as described earlier (Karimova et al., 1998; Maurya et al., 2016). In brief, BTH101 was co-transformed with pKNTDA or pKNTDB in different combination with pUTCB1, pUTCB2 and pUTCB3 plasmids expressing target proteins with T25 or T18 tags. Empty vector pUT18 co-transformed with pKNTDA was used as negative controls while pUTEFA and pKNTEFZ were co-transformed as positive control. The co-transformants were spotted on LB agar plate containing 5′ bromo 4 chloro-3-indolyl-β-D-galactopyranoside (X-Gal) (40 μg/mL), IPTG (0.5 mM) and antibiotics as required and the appearance of white-blue color colonies was recorded. Further, β-galactosidase activity of same combinations was measured from liquid cultures and calculated in Miller units as described in (Battesti and Bouveret, 2012; Maurya et al., 2016) and plotted with standard deviation in GraphPad Prizm5.

In addition, co-immunoprecipitation was performed for *in vivo* interaction of deinococcal ParBs with DnaB in surrogate *E. coli.* Briefly, cell lysates of *E. coli* BTH 101 cells co-expressing different ParBs (ParB1, ParB2 and ParB3) with T18 tag from BACTH plasmids (table S2) in combination with DnaB from pKNTDB were immunoprecipitated using Anti-T25 antibodies as described in (Maurya et al., 2016). The immunoprecipitates were separated in 10% SDS-PAGE and blotted on PVDF membrane. The membrane was hybridized with Anti-T18 monoclonal antibodies and the hybridization signals were detected calorimetrically as described above.

2.7. Construction of parB deletion mutants in D. radiodurans

The parB1 deletion mutant of D. radiodurans was used as described in (Charaka and Misra, 2012). For generation of parB2 and parB3 deletion mutant of D. radiodurans, suicide plasmids pNOKA02 and pNOKB02 respectively were constructed from pNOKOUT (Khairnar et al., 2008) by using a strategy described previously (Charaka and Misra, 2012). In brief, the fragments 1 kb upstream and 1 kb downstream of ORFs Dr_A0002 and Dr_B0002 were PCR amplified with primers (see Table S2) and cloned at the *Kpn*I-*Eco*RI and *Bam*HI-*Sac*I sites in pNOKOUT plasmid, respectively. The recombinant plasmid thus obtained pNOKA02 and pNOKB02, was linearized with *Xmn*I and transformed into D. radiodurans cells. Transformants were maintained through several rounds of sub-culturing, and the homozygous replacement of parB2 and parB3 with nptII was ascertained by PCR amplification using internal primers of both genes (Fig S1). For complementation of deletion mutants, pV18B1, pV18B2 and pV18B3 plasmids (Table S1) were used which express trans copy of proteins under IPTG induction. These plasmids were transformed in respective mutants with vector control. The recombinant clones were scored on TGY plates in the presence of kanamycin (8 mg/ml) and spectinomycin (70 mg/ml). The deletion mutants and its complemented forms were used for subsequent studies.

2.8. Cell survival studies

Deinococcus radiodurans wild type cells, its *parB* mutants and complemented forms were subjected to 6 kGy γ-radiations as described in (Misra et al., 2006). In brief, the bacteria grown in TGY medium with and without appropriate antibiotics (kanamycin; 8 mg/ml) at 32 °C were washed and suspended in sterile phosphate-buffered saline (PBS) and treated with 6 kGy γ-radiation at dose rate 1.81 kGy/h (Gamma Cell 5000, ^{60}Co, Board of Radiation and Isotopes Technology, DAE, India). Irradiated cells with SHAM controls were washed in PBS and suspended in the fresh TGY medium. Equal numbers of cells were grown in 48 well microtiter plates (Nunclon; Sigma-Aldrich) containing TGY medium in presence and absence of required antibiotics or 5 mM IPTG (for induction ParBs from plasmid during complementation). Growth was monitored in replicates at 32 °C for 18 h using Synergy H1 Hybrid multi-mode microplate reader. In addition, growth rate was

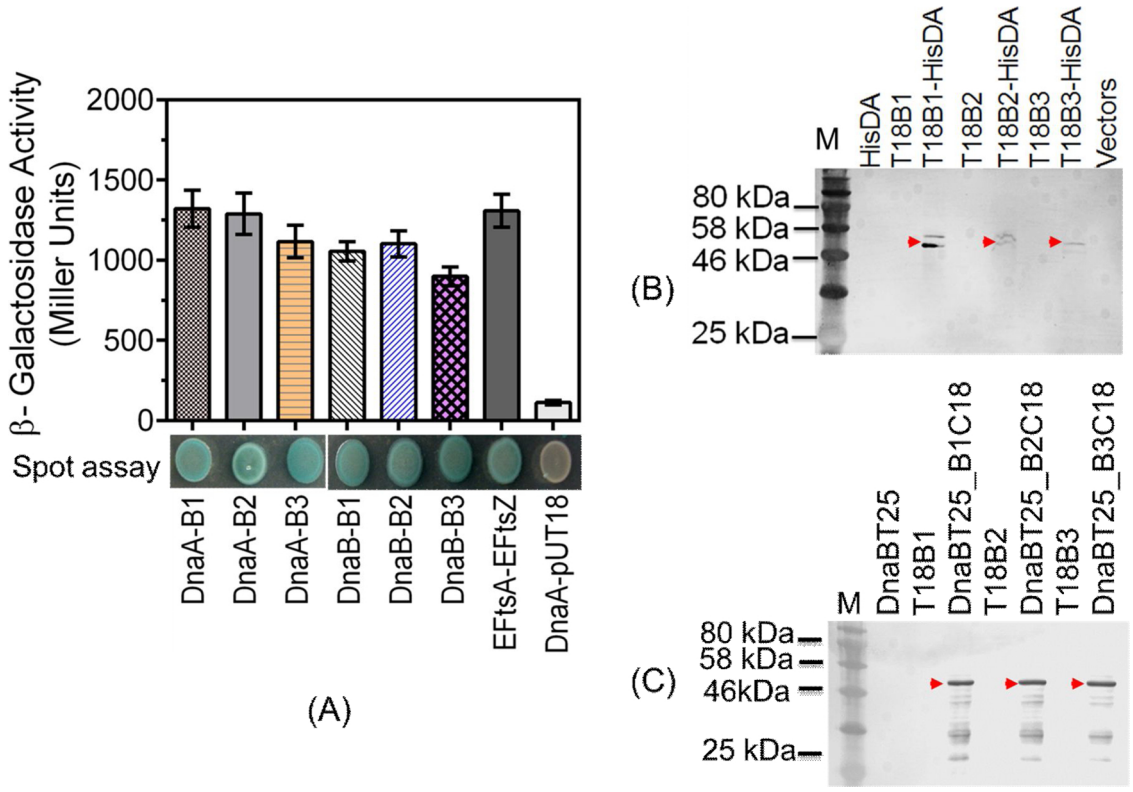

Fig. 5. Interaction of deinococcal ParBs with replication initiation protein DnaA and DnaB helicase. In brief, DnaA and DnaB from pKNT25 (as DnaA or DnaB) and deinococcal ParBs from pUT18C (as B1, B2 and B3) was co-expressed in BTH 101 strain of *E. coli*. Here *E. coli* FtsA from pKNT25 (EFtsA) and FtsZ from pUT18 (EFtsZ) was used as a positive control while DnaA with pUT18 empty vector was used as negative control. The obtained colonies were subjected to blue-green colonies spot and β-galactosidase assay (as described in methods) (A). For interaction of deinococcal ParBs with DnaA in *Deinococcus*, polyhis tagged DnaA (HisDA) from pRADhisDnaA was co-expressed with T18 tagged ParBs (as T18B1, T18B2 and T18B3 from pV18B1, pV18B2 and pV18B3 respectively) in different combinations in *D. radiodurans*. The cell lysate of co-transformants expressing the target proteins were imunoprecipitated by using polyhistidine antibody. The imunoprecipitates were separated on 10% SDS-PAGE and immunoblotted using T18 antibodies (B). For DnaB and ParBs interaction study from *E. coli* using co-IP, E. coli BTH101 cells co-expressing DnaB from pKNT25 (as DnaBT25) and ParBs from pUT18C (as B1C18, B2C18 and B3C18) in different combinations were lysed and immunoprecipitated using Anti-T25 antibody. The imunoprecipitates were separated on 10% SDS-PAGE and immunoblotted using T18 antibodies (C). Data in panel A is representative of reproducible experiment repeated 3 times while in panel B and C are repeated 2 times independently.

calculated for each sample type by following formula ($Nt = N0 * (1 + r)^t$); where Nt is OD_{600} at time t, N0 is OD_{600} at the start of growth curve, r is growth rate and t is time passed. For gamma radiation dose response studies, the wild type cells and different *parB* mutants were grown in absence and presence of kanamycin (antibiotic selection) and treated with different doses (0–8 kGy) of γ-radiations at dose rate of 1.81 kGy/h as described in (Misra et al., 2006). The irradiated cells with their SHAM control were washed in PBS and serially diluted. Different dilution from both the conditions (- / + kanamycin) were plated on TYG agar in absence and presence of kanamycin. The colony forming units (CFU) were recorded after 36–40 h of incubation at 32 °C. The survival fractions are expressed as a percentage of the number of colonies obtained with respect to untreated cells. Additionally, D_{10} value was determined for each sample from the survival curve and plotted.

2.9. Cell disruption and ploidy determination in mutants/complemented forms using quantitative real-time PCR

The mutants as well as their complemented cells of similar O.D. at 600 nm were harvested from appropriate growth condition by centrifugation. The cell number in all was determined using a Neubauer cell counter. The cells were washed with 70% ethanol solution and resuspended in a lysis solution containing 10 mM Tris pH 7.6, 1 mM EDTA and 4 mg/ml lysozyme and were incubated at 37 °C for complete cell lysis, the cell debris was removed by centrifugation (10,000 rpm, 5 min). Lytic efficiency was verified by the densities with a Neubauer counting chamber. The integrity of genomic DNA was confirmed by agarose gel electrophoresis. The aliquots of the cytoplasmic extract were serially diluted and 0.1 ml of it was used as for further analysis of genomic copy number using quantitative Real-Time PCR as described in (Breuert et al., 2006). In brief, a fragment of about 300 bps was amplified using standard PCRs with isolated genomic DNA from *D. radiodurans* R1 (ATCC13939) as a template. It was purified by Gel Extraction kit (Qiagen, Inc) and the amount of DNA was quantified by nanodrop, and the concentration was calculated using the molecular mass computed with 'oligo calc' (www.basic.northwestern.edu/biotools). A dilution was generated for each standard fragment and used for qPCR standardization. Two genes per replicon with similar PCR efficiency were selected in *D. radiodurans viz. ftsE* (212° position) and *ftsZ* (87° position) of chromosome I, Dr_A0155 (137° position) and *pprA* (334° position) of chromosome II, Dr_B0003 (6° position) and Dr_B0076 (187° position) of megaplasmid and Dr_C0001 (0.55° position) and Dr_C0018 (145° position) of small plasmid (Table 1, Table S2). PCR efficiency of each gene for amplification of internal 300 bps fragments was ascertained and was found to > 96% for each (data not shown). The qPCR was carried out by following the MIQE (minimum information for publication of quantitative real-time PCR experiments) guidelines using Roche Light cycler (Bustin et al., 2009) and optimum cycle threshold (Ct) values. Three independent biological replicates were used for each sample. The replicon copy number is quantified by comparing the results with a dilution series of a PCR product of known concentration

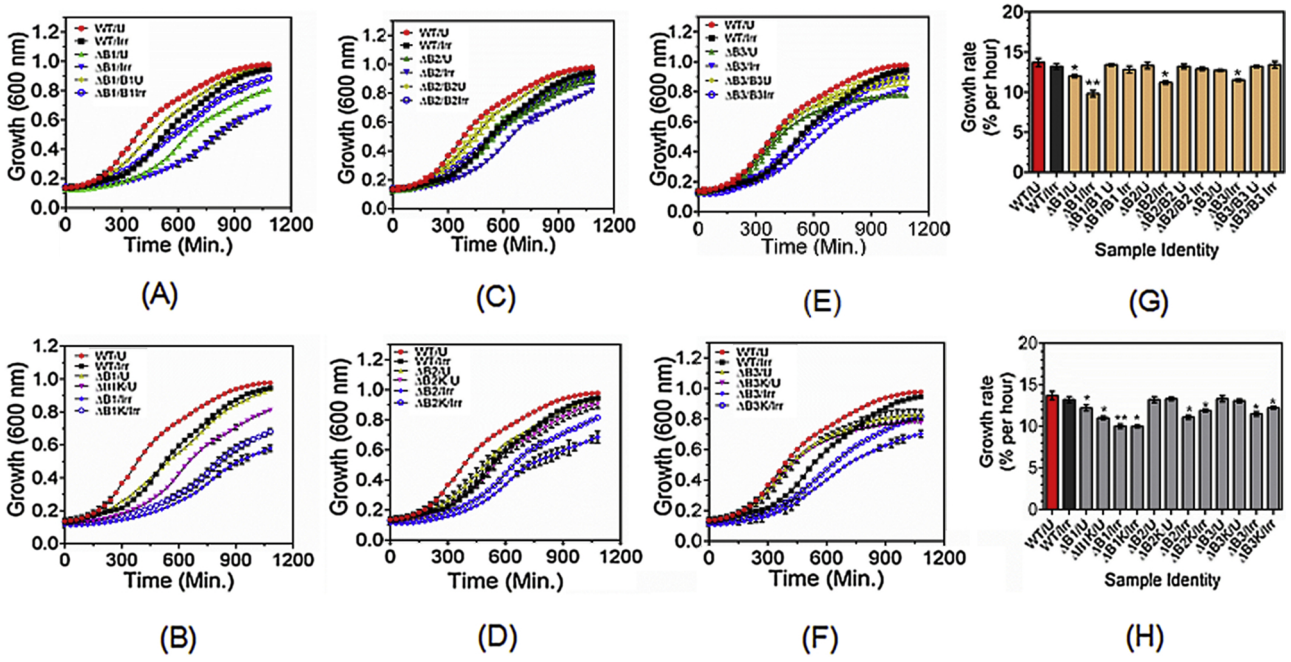

Fig. 6. Survival of *parB1, parB2* and *parB3* mutants to gamma radiation stresses. In brief, wild type (WT) cells, *parB1 (ΔB1), parB2 (ΔB2)* and *parB3 (ΔB3)* mutants and its complemented forms (*ΔB1/B1, ΔB2/B2* and *ΔB3/B3* respectively) were grown in required antibiotics (kanamycin; 8 μg/ml) and treated with 6kGy γ-radiation at dose rate 1.81 kGy/h. Irradiated cells (Irr) with SHAM controls (U; Unirradiated cells) were washed in PBS and suspended in fresh TGY medium. Equal numbers of cells were grown in 48 well microtiter plates containing TGY medium along with required antibiotics at 32 °C for 18 h and their growth was monitored at 600 nm wavelength using microplate reader. The growth curve of *ΔB1* and its complementation (A) *ΔB2* and its complementation (C) as well as *ΔB3* and its complementation (E) is representative of experiments repeated three times in triplicates and shown here as mean ± SEM (n = 9). In addition, wild type (WT) cells, *parB1 (ΔB1), parB2 (ΔB2)* and *parB3 (ΔB3)* mutants were grown in absence of kanamycin and treated with 6kGy γ-radiation. Equal numbers of irradiated cells with SHAM controls were grown in TGY medium in absence and presence of kanamycin (denoted as K; 8 μg/ml) at 32 °C for 18 h and their growth was monitored at 600 nm wavelength using microplate reader. The growth curve of *ΔB1* (B) *ΔB2* (D) as well as *ΔB3* (F) is representative of experiments repeated three times in triplicates and shown here as mean ± SEM (n = 9). The growth rate for each sample in Fig. 6(A–C) as well as (D–F) was calculated using formula ($Nt = N0 * (1 + r)^t$) and plotted in figure G & H, respectively. Statistical analysis was performed on this using 'student *t*-test'. The P values obtained at 95% confidence intervals are shown as (*) for < 0.05, (**) for < 0.01 and (***) for < 0.001.

that is used as a standard. The copy number of each replicon by both genes per cell was calculated using the cell number present at the time of cell lysis. Average copy number reflected from two genes per replicon was represented with appropriate bio-statistical analysis.

3. Results

3.1. Comparison of ParBs of D. radiodurans with ParB family proteins

Multiple sequence alignment of ParB proteins encoded on chromosome I (ParB1); chromosome II (ParB2) and megaplasmid (ParB3 and ParB4) with ParB homologs showed that ParB1 had an overall homology with the Spo0J of *T. thermophilus* and ˜40–60% identity with other chromosomal ParB proteins (Fig. 1A). Secondary genome ParBs like ParB2, ParB3 and ParB4 had only ˜30% identity amongst themselves and grossly different from the chromosomal type ParB's. Secondary structure prediction of all 4 ParBs using Spo0J structure template (PDB ID: 1VZ0) (Leonard et al., 2004) showed a characteristic HTH motif formed by helices H6 and H7 and remaining helices help in compaction of the domain (Fig. 1A). Further, phylogenetic analysis revealed that secondary genome ParBs form separate clade from primary genome ParB (Fig. 1B) (Dubarry et al., 2006). Except ParB1, the remaining ParBs have an extra sequence in the Helix-Turn-Helix (HTH) region. This might provide flexibility to these ParBs for their interaction with yet uncharacterized centromeric sequences on their cognate genome elements. These proteins also showed different C-terminal region as compared to Spo0J, which might provide specific interaction of these ParB with their cognate ParA during segregation process.

3.2. ParBs of D. radiodurans dimerises in solution

Since, ParBs in other bacteria are known to function as dimers, dimerization of purified ParB1, ParB2 and ParB3 was checked using glutaraldehyde cross-linking and size-exclusion chromatography approaches. Results showed that a large proportion of total proteins in all ParBs exist as dimer *in solution* (Fig. 2). For instance, majority of ParB showed a molecular size of ˜ 60 kDa on SDS-PAGE after cross-linking (Fig. 2A) and these proteins were eluted at the same volume where of BSA (˜66.5 kDa) eluted in size-exclusion chromatography (Fig. 2B). *In vivo* oligomeric nature of ParB proteins was checked by immunoprecipitation. For that different ParBs were tagged with either T18 in pVHS559 or polyhis in pRADgro plasmids and co-expressed in different combinations in *D. radiodurans*. Expression of these fusion products of ParBs was monitored by immunobloting (Fig. S2A, S2B). The total proteins from log phase cells were immunoprecipitated using polyhis antibody, and the perspective interacting partners duly tagged with T18 was detected using T18 antibodies. All ParBs showed homotypic interactions indicating a possibility of homodimerization in *D. radiodurans*. None of them showed heterotypic interactions with other ParBs indicating less possibility of cross talk between different ParBs in this multipartite genome harbouring bacteria (Fig. 3A–C). These results corroborated earlier finding where full-length Spo0J of *T. thermophilus* was shown to exist in a dimer *in solution*. The roles of C-terminal region in Spo0J of *T. thermophilus* (Leonard et al., 2004) and in ParB of *Pseudomonas aeruginosa* (Bartosik et al., 2004) has been shown in dimerization and these dimers are required for binding to cognate centromeric sequences. These results suggested that ParBs encoded on different genome elements in *D. radiodurans* are less likely to interact with each other.

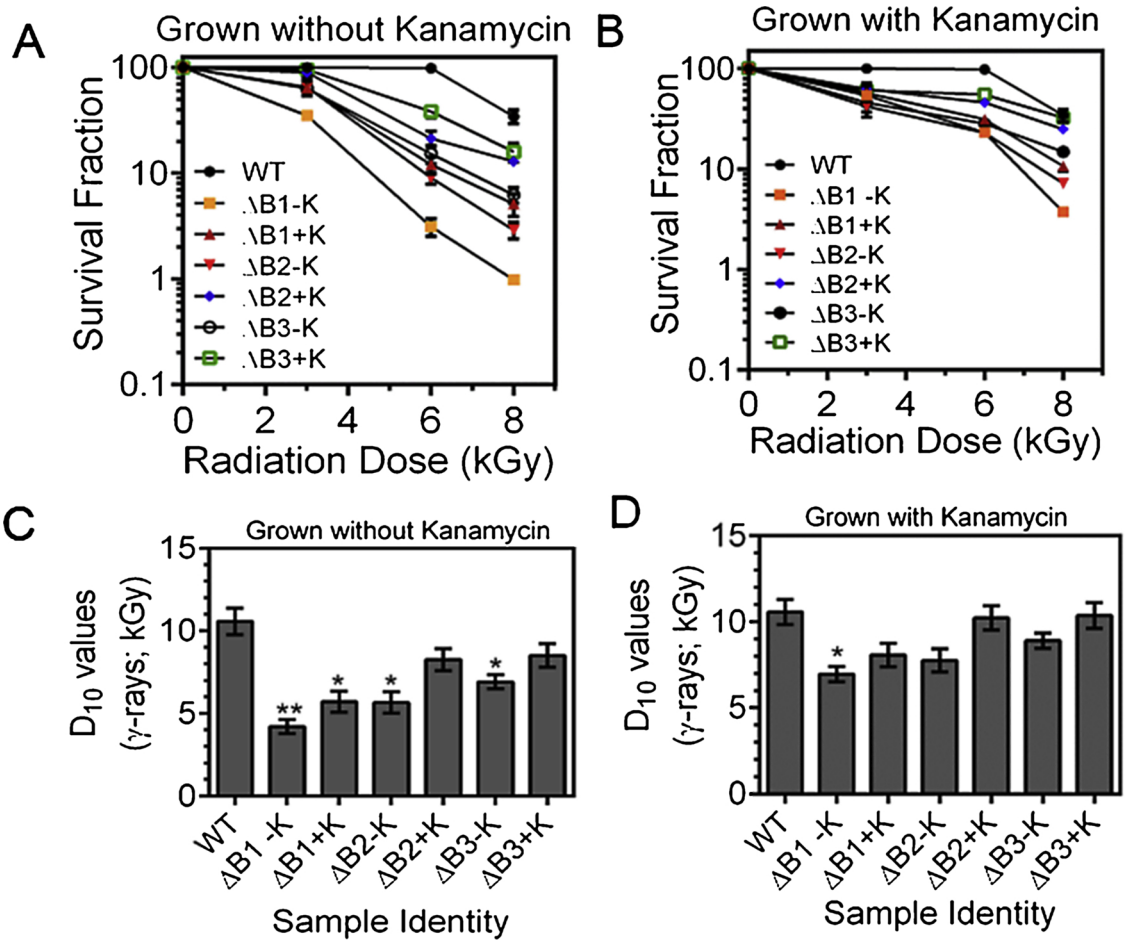

Fig. 7. Gamma radiation response of *parB* mutants of *D. radiodurans* grown with and without selection pressure. The deletion mutant of *parB1* (ΔB1), *parB2* (ΔB2) and *parB3* (ΔB3) were grown in absence (A) and presence (B) of kanamycin in TYG broth. The wild type (WT) and mutant cells were exposed to different doses of gamma radiation. Different dilution of irradiated cells as well as their SHAM controls were plated on TYG agar with (+K) and without kanamycin (-K). The survival fraction of each mutant with respect to radiation dose and antibiotics was compared with survival of unirradiated cells and plotted. The given data is representative of experiment repeated twice independently. The D10 values plot (C, D) was generated from survival curve A & B respectively. Statistical analysis was performed on this using 'student *t*-test'. The P values obtained at 95% confidence intervals are shown as (*) for < 0.05, (**) for < 0.01 and (***) for < 0.001.

3.3. Mutation in parB1, parB2 or parB3 has affected ploidy of cognate genome element

D. radiodurans harbours 8–10 haploid genome copies during exponential growth phase (Hansen, 1978; Harsojo and Matsuyama, 1981). Since, *parB* proteins are integral part of genome segregation in dividing population, the possibility of *parB* deletions affecting the copy number of daughter cells was examined. We monitored copy number of each replicons using quantitative real time PCR as described in methods. We used two genes per replicon (one near origin and other near terminus) and listed the values of copy number per gene per replicon in Table 1. Surprisingly, the copy number of cognate replicons had increased in respective null mutant of deinococcal *parB*s grown in the presence of required selection pressure. For instance, in Δ*parB1* the copy number of chromosome I has increased from 8–10, Δ*parB2* showed chromosome II copy number increase from 6 to 10 and the copy number of megaplasmid was increased from 11 to 18 in *parB3* mutant (Fig. 4). A marginal increase in the copy number of genome elements which was less than 2 times is intriguing and could not be explained merely by arrest of genome segregation. Earlier, the regulation of DNA replication by genome segregation events has been reported in *B. subtilis* where an increased genomic content was reported upon deletion of *parB* homolog (*spo0J*) in this bacterium (Lee et al., 2003, 2006). To be more specific with the involvement of ParBs in copy number variations, the functional complementation by *in trans* expression of these proteins in respective mutants was carried out. Results showed the resumption of original copy number near to wild type, which could suggest that deinococcal ParBs play the important roles in the regulation of replication initiation by yet uncharacterized mechanisms, in *D. radiodurans*.

3.4. ParBs interact with replication initiation proteins of D. radiodurans

Since, ploidy increase in *parB* mutant was less than 2-fold it indicated a strong possibility of arrest of replication progression in the absence of DNA segregation leading a marginal increase in DNA content. Thus, a possible cross talk between genome segregation and DNA replication was hypothesized. The *D. radiodurans* genome encodes replication initiation proteins DnaA and DnaB while *E. coli* homolog of DnaC is missing (White et al., 1999). This might suspect the functional redundancy of DnaC with some other proteins of this bacterium. We monitored *in vivo* interaction of ParB1, ParB2 and ParB3 with DnaA and DnaB using Bacterial Two Hybrid System (BACTH) in surrogate *E. coli* (Karimova et al., 1998; Maurya et al., 2016) as well as using co-immunoprecipitation from *D. radiodurans* (Maurya et al., 2018). The *E. coli* (*cyaA*$^-$) cells co-expressing DnaA / DnaB with all three deinococcal ParBs in different combinations on BACTH plasmids were screened for resumption of CyaA regulated expression of β-galactosidase activity. This was monitored by spot assay as well as *in solution* as described in methods. Results show that both DnaA and DnaB interacted with all three ParBs with nearly same levels as evident from the intensity of blue

colour colonies in spot assay as well as β-galactosidase activity levels *in solution* (Fig. 5A). In addition, co-immunoprecipitation assay of total soluble proteins of *D. radiodurans* cells co-expressing polyhis tagged DnaA in different combination with T18 tagged ParBs completely supported BACTH findings (Fig. 5B). Likewise, the co-immunoprecipitation assay from *E. coli* (*cyaA*$^-$) cells co-expressing DnaB on pKNTDB and ParB1, ParB2 or ParB3 on pUTCB1, pUTCB2 or pUTCB3, respectively in different combinations agreed with BACTH findings (Fig. 5C). This suggested that replication proteins can interact with all three ParBs encoded on multipartite genome of *D. radiodurans*. The similar observation was reported earlier in *V. cholerae,* where genome segregation proteins (ParA and ParB) were found interacting with DnaA (Kadoya et al., 2011). Our results suggested a cross-talk between DNA replication and segregation components of *D. radiodurans* and a strong possibility of interdependent regulation of these macromolecular events at least in this bacterium.

3.5. Secondary genome elements contribute in radioresistance

ParB is key protein that regulates the partitioning of duplicated genome elements into daughter cells in bacteria, and the null mutants of *parBs* in *D. radiodurans* showed increased copy number of genes estimated in different genome elements. This can be explained on the assumption that genome duplication would have occurred normally at least one round, but genome segregation, which maintains constant copy number per cell, got arrested and led to an increase in copy number under selection pressure. If this assumption is true, then cell density of mutants maintained in the presence and absence of selection pressure should be different. To test it, these cells were grown in the presence and absence of antibiotics and then growth kinetics were monitored under normal and gamma radiation stressed conditions. We observed that Δ*parB1* mutant maintained with or without selection pressure showed nearly similar trends of gamma radiation effects on its growth (Fig. 6A, B, G & H) suggesting the role of primary chromosome in growth irrespective of selection pressure. However, when Δ*parB2* and Δ*parB3* mutants were maintained in the presence or absence of selection pressure, they showed differential growth response under normal and radiation stressed conditions. For instance, the cells maintained under selection pressure showed nearly wild type effects of gamma radiation on their growth (Fig. 6C, D, G & H). When these were maintained in the absence of selection pressure, they showed a significant growth retardation under radiation stressed conditions as compared to that maintained with selection pressure (Fig. 6E–H). These results might suggest that Δ*parB2* and Δ*parB3* deletion does not affect normal growth of this bacterium while Δ*parB1* does, and the cell population that does not show resistance to antibiotic seems to be the one that is devoid of genome element(s) having replacement of cognate *parB* with antibiotic resistance marker gene. Logically, such population could have arisen when segregation of genome elements having *parB* replaced with antibiotic marker cassette does not occur, and that would support the role of ParBs in segregation of cognate genome element. The slow growth of Δ*parB1* mutant under normal as well as gamma stressed conditions as reported earlier (Charaka and Misra, 2012) further ascertained the indispensability of primary chromosome even in this multipartite genome harbouring bacterium.

The effect of parB deletions (making a phenotype of genome segregation defect) on gamma radiation dose response was checked in all the *parB* mutants. For that all the three mutants were maintained in the presence or absence of antibiotics selection pressure and their survival was monitored at different doses of gamma radiation, again in the presence or absence of antibiotics. Interestingly, *parB* mutants maintained without selection pressure but scored in the presence of antibiotics, showed higher sensitivity to gamma radiation as compared to the respective controls maintained under selection pressure (Fig. 7 A,C). This difference in gamma radiation response was not observed in case of Δ*parB2* and Δ*parB3* mutants when maintained under selection pressure and scored in the presence of antibiotics (Fig. 7B, D). Thus, the cells containing respective genome elements (scored as antibiotic resistance) did not lose resistance to gamma radiation, which implicate the role of these genome elements in radioresistance. These results suggested that ParB deletion can make cells defective in DNA segregation and loss of secondary genome elements, which can affect gamma radiation resistance without affecting their normal growth while defect in primary chromosome can affect both normal growth and eventually radiation stress tolerance.

4. Discussion

D. radiodurans, an extremotolerant bacterium, characterized for its extraordinary resistance to radiations and other DNA damaging agents (Slade and Radman, 2011). This bacterium also has an interesting cytogenetic feature like a multipartite genome system comprised of 2 chromosomes, megaplasmid and small plasmid, and each of these elements are present in multiple copies presumably packaged together in form of a toroidal nucleoid (White et al., 1999; Minsky et al., 2006). Functional significance of multiple chromosomes and ploidy in extreme phenotypes, and the mechanisms underlying faithful inheritance of multipartite genome system packaged in form of a compact toroidal nucleoid, into daughter cells are not known and offered the most interesting aspects in bacterial genome biology to investigate. Studies on genome partitioning in MGS system is limited to *V. cholera*e and *B. cenocepacica*, where each replicon (either chromosome or plasmids) have their own independent partitioning components responsible for their maintenance (Egan and Waldor, 2003; Egan et al., 2005; Dubarry et al., 2006). In case of *D. radiodurans* another multipartite genome harbouring bacterium, the partitioning system encoded on primary chromosome has been characterized and shown expressing characteristics of pulling mechanism of genome segregation (Charaka and Misra, 2012). Here, we have brought forth some evidence to highlight the role of ParBs encoded on chromosome II (ParB2) and megaplasmid (ParB3) in maintenance of cognate elements and their roles in the survival of *D. radiodurans* under both normal and stressed conditions. We found the homotypic interactions of all the ParBs while these ParBs do not interact to its other homologs in *D. radiodurans*. These results were expected because all ParBs have C-terminal domain, which is similar to ParBs of *T. thermophilus* and *P. aeruginosa* where the roles of C-terminal domain in dimerization of ParB proteins have been demonstrated (Leonard et al., 2004; Bartosik et al., 2004). Further ParBs are known as sequence specific centromere binding proteins that bind to centromere in dimeric form (Funnell, 2016) indicating that ParBs in this bacterium are most likely to be functional. This observation was further supported by *in vivo* protein-protein interaction using co-immunoprecipitation study from *D. radiodurans* expressing deinococcal ParBs fused at their N-terminal with different tags, on two plasmids (Fig. 3A–C). Earlier, we had reported that deletion of *parB1* in *D. radiodurans* imposes slower growth and segregation defects in primary chromosome (Charaka and Misra, 2012). In this study, when we compared the survival of Δ*parB2* and Δ*parB3* under normal and gamma stressed conditions with Δ*parB1* cells, we found that deletion of secondary genome ParBs has a little effect on normal growth as compared to wild type cells. The deletion of *parB1* presumably has arrested the segregation of chromosome I, which is not complemented by the presence of secondary genome ParBs (Fig. 6). This suggests that primary chromosome and secondary genome elements are most likely being maintained independently in this bacterium. Deletion of chromosomal ParB like proteins in *B. subtilis* and *P. aeruginosa* has affected genome segregation and normal growth in these bacteria (Ireton et al., 1994; Bartosik et al., 2004). An increase in copy number of replicons in respective *parB* mutants is intriguing and could not be explained with direct evidence. However, a strong interaction of replication initiation proteins like DnaA and DnaB, with all the ParB proteins of this bacterium allowed us to speculate on the cross talk of genome segregation and DNA replication. Similar findings have been

reported earlier in *V. cholerae* as well as in *B. subtilis* (Kadoya et al., 2011; Lee et al., 2003, 2006; Murray and Errington, 2008). The replicated origins occupying characteristic positions on genome have been shown in many bacteria. For instance, the replicated origins occupy at cell poles in *Caulobacter crescentus* (Mohl and Gober, 1997; Figge et al., 2003), at cell quarters in *Bacillus subtilis* (Lin et al., 1997; Webb et al., 1997, 1998; Sharpe and Errington, 1998) and near cell quarters or poles in *Escherichia coli* and *V. cholerae* (Gordon et al., 1997; Niki et al., 2000; Li et al., 2002; Lau et al., 2003; Figge et al., 2003; Egan and Waldor, 2003). Earlier it has been shown that ParABS system regulates the separation and maintenance of origin of replication (containing ParB binding sites near to it) at a characteristic subcellular position in the cells in *Bacillus subtilis*, *Caulobacter crescentus* and *Streptomyces coelicolor* A3 bacteria (Mohl and Gober, 1997; Lin and Grossman, 1998; Kim et al., 2000). These findings strongly support the interdependent regulation of DNA replication and genome partitioning in bacteria and provide the most plausible explanation for the effect of segregation defects on copy number of genome elements.

In conclusion, we report the functional characterization of ParBs encoded on multipartite genome system in *D. radiodurans* both *in vitro* and *in vivo*. ParB roles in regulation of genome copy number in multiparitte genome harboring bacteria is first time reported in any multipartite genome harboring bacteria. The molecular basis of *ori* regulation by ParBs and real time interaction of DNA replication machinery with multipartite genome segregation components would be the exciting area of bacterial genome biology and would be worth addressing independently. The available results together suggest that all ParBs exist as dimers, regulate genome segregation, and components of both genome segregation and DNA replication seem to interact with each other in this bacterium.

Conflict of interest

The authors declare that they have no conflicts of interest with the content of this article.

Acknowledgments

We thank Dr. Ajay Saini and Ms. Reema Singh for help in q-PCR experiments. GKM is grateful to the Department of Atomic Energy, Government of India for research fellowships.

Appendix A. Supplementary data

Supplementary material related to this article can be found, in the online version, at doi:https://doi.org/10.1016/j.micres.2019.03.005.

References

Bartosik, A.A., Lasocki, K., Mierzejewska, J., Thomas, C.M., Jagura-Burdzy, G., 2004. ParB of *Pseudomonas aeruginosa*: interactions with its partner ParA and its target *parS* and specific effects on bacterial growth. J. Bacteriol. 186 (20), 6983–6998.

Battesti, A., Bouveret, E., 2012. The bacterial two-hybrid system based on adenylate cyclase reconstitution in Escherichia coli. Methods 58, 325–334.

Battista, J.R., 2000. Radiation resistance: the fragments that remain. Curr. Biol. 10, R204–R205.

Battista, J.R., Park, M.J., McLemore, A.E., 2001. Inactivation of two homologues of proteins presumed to be involved in the desiccation tolerance of plants sensitizes *Deinococcus radiodurans* R1 to desiccation. Cryobiology 43, 133–139.

Breuert, S., Allers, T., Spohn, G., Soppa, J., 2006. Regulated polyploidy in halophilic archaea. PLoS One 1, e92.

Bustin, S.A., Benes, V., Garson, J.A., Hellemans, J., Huggett, J., Kubista, M., Mueller, R., Nolan, T., Pfaffl, M.W., Shipley, G.L., Vandesompele, J., 2009. The MIQE guidelines: minimum information for publication of quantitative real-time PCR. Clin. Chem. 55, 611–622.

Charaka, V.K., Misra, H.S., 2012. Functional characterization of the role of the chromosome I partitioning system in genome segregation in *Deinococcus radiodurans*. J. Bacteriol. 194, 5739–5748.

Charaka, V.K., Mehta, K.P., Misra, H.S., 2013. ParA encoded on chromosome II of *Deinococcus radiodurans* binds to nucleoid and inhibits cell division in *Escherichia coli*. J. Biosci. 38, 487–497.

Das, A.D., Misra, H.S., 2011. Characterization of DRA0282 from *Deinococcus radiodurans* for its role in bacterial resistance to DNA damage. Microbiology 157, 2196–2205.

Dubarry, N., Pasta, F., Lane, D., 2006. ParABS systems of the four replicons of *Burkholderia cenocepacia*: new chromosome centromeres confer partition specificity. J. Bacteriol. 188, 1489–1496.

Egan, E.S., Waldor, M.K., 2003. Distinct replication requirements for the two *Vibrio cholerae* chromosomes. Cell 114 (4), 521–530.

Egan, E.S., Fogel, M.A., Waldor, M.K., 2005. Divided genomes: negotiating the cell cycle in prokaryotes with multiple chromosomes. Mol. Microbiol. 56, 1129–1138.

Figge, R.M., Easter, J., Gober, J.W., 2003. Productive interaction between the chromosome partitioning proteins, ParA and ParB, is required for the progression of the cell cycle in Caulobacter crescentus. Mol. Microbiol. 47, 1225–1237.

Fogel, M.A., Waldor, M.K., 2005. Distinct segregation dynamics of the two *Vibrio cholerae* chromosomes. Mol. Microbiol. 55, 125–136.

Funnell, B.E., 2016. ParB partition proteins: complex formation and spreading at bacterial and plasmid centromeres. Front. Mol. Biosci. 3, 44.

Gerdes, K., Howard, M., Szardenings, F., 2010. Pushing and pulling in prokaryotic DNA segregation. Cell 141, 927–942.

Gordon, G.S., Sitnikov, D., Webb, C.D., Teleman, A., Straight, A., Losick, R., et al., 1997. Chromosome and low copy plasmid segregation in *E. coli*: visual evidence for distinct mechanisms. Cell 90, 1113–1121.

Green, M.R., Sambrook, J., 2012. Molecular Cloning: A Laboratory Manual. Cold Spring Harbor Laboratory Press, Cold Spring Harbor N.Y.

Hansen, M.T., 1978. Multiplicity of genome equivalents in the radiation-resistant bacterium Micrococcus radiodurans. J. Bacteriol. 134 (1), 71–75.

Harsojo, K.S., Matsuyama, A., 1981. Genome multiplicity and radiation resistance in Micrococcus radiodurans. J. Biochem. 90, 877–880.

Hayes, F., Barillà, D., 2006. The bacterial segrosome: a dynamic nucleoprotein machine for DNA trafficking and segregation. Nat. Rev. Microbiol. 4 (2), 133.

Ireton, K., Gunther, N.W., Grossman, A.D., 1994. spo0J is required for normal chromosome segregation as well as the initiation of sporulation in Bacillus subtilis. J. Bacteriol. 176 (17), 5320–5329.

Kadoya, R., Baek, J.H., Sarker, A., Chattoraj, D.K., 2011. Participation of chromosome segregation protein ParAI of Vibrio cholerae in chromosome replication. J. Bacteriol. 193 (7), 1504–1514.

Karimova, G., Pidoux, J., Ullmann, A., Ladant, D., 1998. A bacterial two-hybrid system based on a reconstituted signal transduction pathway. Proc. Nat. Acad. Sci. U. S. A. 95, 5752–5756.

Khairnar, N.P., Kamble, V.A., Misra, H.S., 2008. RecBC enzyme overproduction affects UV and gamma radiation survival of Deinococcus radiodurans. DNA Repair 7, 40–47.

Kim, H.J., Calcutt, M.J., Schmidt, F.J., Chater, K.F., 2000. Partitioning of the linear chromosome during sporulation of *Streptomyces coelicolor* A3 (2) involves an oriC-linked parAB locus. J. Bacteriol. 182 (5), 1313–1320.

Lau, I.F., Filipe, S.R., Soballe, B., Okstad, O.A., Barre, F.X., Sherratt, D.J., 2003. Spatial and temporal organization of replicating *Escherichia coli* chromosomes. Mol. Microbiol. 49, 731–743.

Lee, P.S., Grossman, A.D., 2006. The chromosome partitioning proteins Soj (ParA) and Spo0J (ParB) contribute to accurate chromosome partitioning, separation of replicated sister origins, and regulation of replication initiation in Bacillus subtilis. Mol. Microbiol. 60 (4), 853–869.

Lee, P.S., Lin, D.C.H., Moriya, S., Grossman, A.D., 2003. Effects of the chromosome partitioning protein Spo0J (ParB) on oriC positioning and replication initiation in Bacillus subtilis. J. Bacteriol. 185 (4), 1326–1337.

Leonard, T.A., Butler, P.J.G., Löwe, J., 2004. Structural analysis of the chromosome segregation protein Spo0J from Thermus thermophilus. Mol. Microbiol. 53 (2), 419–432.

Lewis, R.A., Bignell, C.R., Zeng, W., Jones, A.C., Thomas, C.M., 2002. Chromosome loss from par mutants of *Pseudomonas putida* depends on growth medium and phase of growth. Microbiology 148 (2), 537–548.

Li, Y., Sergueev, K., Austin, S., 2002. The segregation of the *Escherichia coli* origin and terminus of replication. Mol. Microbiol. 46, 985–996.

Lin, D.C.H., Grossman, A.D., 1998. Identification and characterization of a bacterial chromosome partitioning site. Cell 92, 675–685.

Lin, D.C.H., Levin, P.A., Grossman, A.D., 1997. Bipolar localization of a chromosome partition protein in Bacillus subtilis. Proc. Natl. Acad. Sci. U. S. A. 94, 4721–4726.

Maurya, G.K., Modi, K., Misra, H.S., 2016. Divisome and segrosome components of *Deinococcus radiodurans* interact through cell division regulatory proteins. Microbiology (UK) 162, 1321–1334.

Maurya, G.K., Modi, K., Banerjee, M., Chaudhary, R., Rajpurohit, Y.S., Misra, H.S., 2018. Phosphorylation of FtsZ and FtsA by a DNA damage-responsive Ser/Thr protein kinase affects their functional interactions in *Deinococcus radiodurans*. mSphere 3 (4).

Minsky, A., Shimoni, E., Englander, J., 2006. Ring-like nucleoids and DNA repair through error-free nonhomologous end joining in *Deinococcus radiodurans*. J. Bacteriol. 188 (17), 6047–6051.

Misra, H.S., Khairnar, N.P., Kota, S., Srivastava, S., Joshi, V.P., Apte, S.K., 2006. An exonuclease I sensitive DNA repair pathways in *Deinococcus radiodurans*: a major determinant of radiation resistance. Mol. Microbiol. 59, 1308–1316.

Misra, H.S., Rajpurohit, Y.S., Kota, S., 2013. Physiological and molecular basis of extreme radioresistance in Deinococcus radiodurans. Curr. Sci. 104, 194–206.

Misra, H.S., Maurya, G.K., Kota, S., Charaka, V.K., 2018. Maintenance of multipartite genome system and its functional significance in bacteria. J. Genet. 97 (4), 1013–1038.

Mohl, D.A., Gober, J.W., 1997. Cell cycle–dependent polar localization of chromosome partitioning proteins in *Caulobacter crescentus*. Cell 88 (5), 675–684.

Murray, H., Errington, J., 2008. Dynamic control of the DNA replication initiation protein DnaA by Soj/ParA. Cell 135 (1), 74–84.

Niki, H., Yamaichi, Y., Hiraga, S., 2000. Dynamic organization of chromosomal DNA in *Escherichia coli*. Genes Dev. 14, 212–223.
Saint-Dic, D., Frushour, B.P., Kehrl, J.H., Kahng, L.S., 2006. A parA homolog selectively influences positioning of the large chromosome origin in Vibrio cholerae. J. Bacteriol. 188 (15), 5626–5631.
Schaefer, M.C., Schmitz, R., Facius, G., Horneck, B., Milow, K.H., Ortner, J., 2000. Systematic study of parameters influencing the action of Rose Bengal with visible light on bacterial cells: comparison between biological effect and singlet-oxygen production. Photochem. Photobiol. 71, 514–523.
Sharpe, M.E., Errington, J., 1998. A fixed distance for separation of newly replicated copies of *oriC* in *Bacillus subtilis*: implications for co-ordination of chromosome segregation and cell division. Mol. Microbiol. 28, 981–990.
Slade, D., Radman, M., 2011. Oxidative stress resistance in Deinococcus radiodurans. Microbiol. Mol. Biol. Rev. 75, 133–191.
Webb, C.D., Teleman, A., Gordon, S., Straight, A., Belmont, A., Lin, D.C.H., et al., 1997. Bipolar localization of the replication origin regions of chromosomes in vegetative and sporulating cells of *B. subtilis*. Cell 88, 667–674.
Webb, C.D., Graumann, P.L., Kahana, J.A., Teleman, A.A., Silver, P.A., Losick, R., 1998. Use of time-lapse microscopy to visualize rapid movement of the replication origin region of the chromosome during the cell cycle in *Bacillus subtilis*. Mol. Micribiol. 28, 883–892.
White, O., Eisen, J.A., Heidelberg, J.F., Hickey, E.K., Peterson, J.D., Dodson, R.J., et al., 1999. Genome sequence of the radioresistant bacterium *Deinococcus radiodurans* R1. Science 286, 1571–1577.
Yanagida, M., 2005. Basic mechanism of eukaryotic chromosome segregation. Philos. Trans. R. Soc. Lond. B Biol. Sci. 360, 609–621.

Plasmid 100 (2018) 6–13

Contents lists available at ScienceDirect

Plasmid

journal homepage: www.elsevier.com/locate/yplas

Original Research Article

Plasmids for making multiple knockouts in a radioresistant bacterium *Deinococcus radiodurans*

Ganesh K. Maurya[a,b], Hari S. Misra[a,b,*]

[a] Molecular Biology Division, Bhabha Atomic Research Centre, Mumbai 400085, India
[b] Homi Bhabha National Institute, Mumbai 400094, India

ARTICLE INFO

Keywords:
Deinococcus radiodurans
Gene deletion and disruption
Genome manipulation
Plasmids
Radioresistance

ABSTRACT

The gene knockouts are mostly created using homologous recombination-based replacement of target gene(s) with the expressing cassette of selection marker gene(s). Here, we constructed a series of plasmids bearing the expressing cassettes of genes encoding different antibiotics markers like *nptII* (Kan^R), *aadA* ($Spec^R$), *cat* (Cm^R) and *aac(3)* (Gen^R). *D. radiodurans* is a radioresistant Gram positive bacterium that does not support the independent maintenance of *colE*1 origin-based plasmids. Using these constructs, the disruption mutants of both single and multiple genes involved in segregation of secondary genome elements have been generated in this bacterium. Unlike single mutants, the double and triple mutants showed growth retardation under normal growth conditions and the synergistic effects with Topoisomerase II inhibitor on the growth of this bacterium. Thus, these plasmids could be useful in creating multiple deletions/disruptions in bacteria that do not support independent maintenance of *colE1* origin-based plasmid.

1. Introduction

Deinococcus radiodurans a Gram-positive non-sporulating bacterium is primarily known for its extraordinary resistance to several DNA damaging agents including radiations and desiccation (Makarova et al., 2001; Misra et al., 2013). These phenotypes are attributed to the efficient DNA double strand break repair and the protection of biomolecules from oxidative damage (Slade and Radman, 2011; Misra et al., 2013; Daly, 2009). This bacterium harbours the multipartite genome system comprised on 2 chromosomes and 2 plasmids (White et al., 1999). These genome elements are present in multiple copies per cell (Harsojo Kitayama and Matsuyama, 1981). The multipartite genome system and ploidy make this bacterium relatively difficult to create homogenous deletion of any gene. However, to understand the roles of protein(s) in extraordinary radioresistance of this bacterium, the construction of gene deletion mutant and monitoring the required phenotypes would be required. Earlier the disruption mutant of *recA* was isolated through double crossover events in *D. radiodurans* (Gutman et al., 1994) and of superoxide dismutase (SOD) and catalase gene through single crossover event (Markillie et al., 1999). The double cross-over events leading to the generation of several disruption/deletion mutants have been demonstrated using both PCR and plasmid-based approaches (Narumi et al., 2004; Khairnar et al., 2008; Rajpurohit and Misra, 2010). PCR products based homologous recombination has also been used to create gene knockout in *D. radiodurans* (Slade et al., 2009; Hua et al., 2012). Using these approaches, the deletion mutants of a few genes have been created with different antibiotic resistance markers. However, the studies on the possible roles of multiple proteins in the regulation of multigenic extreme phenotypes would require the genetic tools that could be used for the disruption /deletion of multiple targets with independent scorable markers. Using pBluescriptSK+ (pBSK+) backbone, a series of plasmids like pNOKOUT, pNOSOUT, pNOGOUT and pNOCOUT expressing independent antibiotic resistance genes like *nptII*, *aadA*, *aac(3)* and *cat* and conferring kanamycin, spectinomycin, gentamicin, and chloramphenicol resistance, respectively have been created. Using these recombinant plasmids, the deletion mutants of genome segregation proteins (ParAs and ParBs) required for the segregation of chromosome II and megaplasmid (hereafter referred as secondary genome) have been generated. The phenotypes of these mutants particularly in the maintenance of respective genome elements in dividing population of *D. radiodurans* have been ascertained. Our results suggest that these *colE1* type recombinant plasmids are useful in generating multiple disruption mutants in the same background in *D. radiodurans*. Since the expression of all four antibiotics cassette under their promoter has been shown in different bacteria, the usefulness of these plasmids in creating mutations in the bacteria that do not maintain *colE1* plasmids could be suggested.

* Corresponding author at: Molecular Biology Division, Bhabha Atomic Research Centre, Mumbai 400085, India.
E-mail address: hsmisra@barc.gov.in (H.S. Misra).

https://doi.org/10.1016/j.plasmid.2018.09.003
Received 17 June 2018; Received in revised form 28 August 2018; Accepted 7 September 2018
Available online 24 September 2018
0147-619X/

2. Materials and methods

2.1. Bacterial strains, plasmids, and growth conditions

Bacterial strains, plasmids, and primers used in this study are listed in Table S1. *D. radiodurans* R1 (ATCC13939) was a kind gift from Professor J. Ortner, Germany (Schaefer et al., 2000). It was grown in TGY (Tryptone (1%), Glucose (0.1%) and Yeast extract (0.5%) medium at 32 °C. *E. coli* strain NovaBlue was used for cloning and maintenance of all the plasmids. *E. coli* cells harboring different plasmids viz. pBlueScript II SK(+) (Stratagene), pNOKOUT (Khairnar et al., 2008), pNOCOUT, pNOGOUT and pNOSOUT were grown at 37 °C in Luria-Bertani (LB) medium supplemented ampicillin (100 μg/ml), kanamycin (25 μg/ml), chloramphenicol (20 μg/ml), gentamycin (10 μg/ml) or spectinomycin (70 μg/ml), respectively. Shuttle expression vector p11559 (Mennecier et al., 2004) was maintained in the presence of spectinomycin (70 μg/ml) in *E. coli* and *D. radiodurans*. Standard protocols for all recombinant techniques were used as described in (Sambrook and Russell, 2001). Molecular biology grade chemicals and enzymes were procured from Sigma Chemicals Company, USA, Roche Biochemicals, Mannheim, Germany, New England Biolabs, USA and Merk India Pvt. Ltd. India.

2.2. Construction of recombinant plasmids

Details of the primers used in the construction of recombinant plasmids are given in Table S1. Plasmid pBlueScript II SK (+) (pBSK+), which fails to replicate in *D. radiodurans*, was used as the backbone for generating double-crossover recombination template plasmid. In brief, pBSK+ was digested with *Hin*dIII and *Eco*RI and ligated with ~1.1 kb DNA fragment of spectinomycin resistance gene (*aadA*) with promoter obtained after *Hin*dIII-*Eco*RI digestion of p11559 plasmid to yield pNOSOUT plasmid. Parallelly, a *Sma*I digested pBSK+ plasmid was incubated with alkaline phosphatase (Roche Biochemicals, Germany) at 37 °C for 1 h and purified by a PCR purification kit (Roche Biochemicals, Germany). The ~1.1 kb DNA fragments conferring kanamycin resistance gene (*nptII*) with promoter was PCR amplified from pET28a(+) using nptIIFw and nptIIRw primers and blunt ligated to dephosphorylated *Sma*I digest of pBSK+ plasmid to yield pNOKOUT as described in (Khairnar et al., 2008). Similarly, ~0.8 kb fragment of chloramphenicol resistance gene (*cat*) with promoter was PCR amplified from pRAD1 plasmid (Meima and Lidstrom, 2000) using catFw and catRw primers and blunt ligated to dephosphorylated *Sma*I digest of pBSK(+) plasmid to yield pNOCOUT (Fig. 1C). To construct pNOGOUT, ~0.8 kb fragment of the gentamicin resistance gene (*aac(3)*) with promoter was PCR amplified from a pLAU44 plasmid (Lau et al., 2003) using GentFw and GentRw primers and digested with *Pst*I and *Bam*HI enzymes. This fragment was ligated with *Pst*I – *Bam*HI digest of pBSK+ to create pNOGOUT plasmid. These different ligated plasmid constructs were chemically transformed into *E. coli* NovaBlue strain and plated on LB agar supplemented with respective antibiotics to allow the growth of only positive colonies. Further, these colonies were screened for the presence of respective antibiotic cassettes in different plasmid construct. All constructed plasmids were maintained in *E. coli* NovaBlue strain for future use. Several restriction sites in multiple cloning sites were marked on the flanks of different antibiotic cassettes for insertion of the homologous arms of the target gene.

2.3. Construction of knockout plasmids for D. radiodurans

For generation of the disruption mutant for *parA2* (DR_A0001), *parB2* (DR_A0002), *parA3* (DR_B0001) and *parB3* (DR_B0002) genes, pNOKA2UD, pNOCB2UD, pNOSA3UD and pNOGB3UD plasmids were created from pNOKOUT, pNOCOUT, pNOSOUT and pNOGOUT plasmids, respectively. In brief, ~1 kb upstream and downstream region from the middle of each ORFs were PCR amplified using respective primers (Table S1) from the genome of *D. radiodurans*. PCR products were digested with required restriction enzymes and cloned in MCS1 and MCS2 of these plasmids as given in (Table S1). For instance, the upstream and downstream fragment of *parA2* were cloned at *Apa*I-*Kpn*I and *Bam*HI-*Xba*I sites in pNOKOUT (Kan^R) to give pNOKA2UD, *parB2* at *Xho*I-*Hin*dIII and *Bam*HI-*Xba*I sites of pNOCOUT (Cm^R) to create pNOCB2UD, *parA3* at *Apa*I-*Kpn*I and *Bam*HI-*Xba*I sites of pNOSOUT ($Spec^R$) to make pNOSA3UD and *parB3* at *Kpn*I-*Eco*RI and *Bam*HI-*Sac*I sites of pNOGOUT (Gen^R) to form pNOGB3UD. These plasmids were maintained in *E. coli* NovaBlue for further use.

2.4. Transformation in D. radiodurans

The recombinant plasmids like pNOKOUT (Khairnar et al., 2008), pNOCOUT, pNOGOUT and pNOSOUT confering resistance to kanamycin (8 μg/ml), chloramphenicol (5 μg/ml), gentamycin (10 μg/ml), and spectinomycin (70 μg/ml) respectively, were transformed in *D. radiodurans* using a modified protocol as described in (Udupa et al., 1994). In brief, a final concentration of 30 mM calcium chloride (from the stock of 1 M) was added in the bacterial culture of 0.3–0.4 OD (600 nm). This mixture was further incubated at 32 °C for 1 h. 1–2 μg of circular or linearized plasmid was added to 1 ml of $CaCl_2$ treated bacterial culture and tube was placed on ice for 45 min. The transformation mixture was incubated on an orbital shaker at 32 °C for 30 min at 120 rpm. This transformation mixture was 10 fold diluted with TGY broth and grown for 15–18 h at 32 °C in a shaker incubator at 180 rpm. Different dilutions of overnight grown transformants were plated on TYG agar plates supplemented with required antibiotics and incubated at 32 °C for selection. The recombinant cells were maintained under respective selection pressure. The p11559 plasmid expressing spectinomycin resistance was used as a positive control and pBSK+ conferring Amp^R, was used as a negative control.

For generating knockouts, the *D. radiodurans* cells were transformed with linearized pNOKA2UD, pNOCB2UD, pNOSA3UD and pNOGB3UD plasmids as described above and grown several generations under selection pressure of respective antibiotics (kanamycin 8 μg/ml; chloramphenicol 5 μg/ml; spectinomycin 70 μg/ml and gentamycin 10 μg/ml, respectively) as detailed in (Charaka and Misra, 2012). In brief, pNOKA2UD and pNOCB2UD plasmids were digested with *Xmn*I while pNOSA3UD and pNOGB3UD plasmids with *Kpn*I. Linearized plasmid DNA was gel purified and transformed into *D. radiodurans* cells separately as mentioned above. The transformants were scored on TGY agar plates supplemented with required antibiotics. At least 15 colonies for each combination were streaked on TYG agar plate containing required concentration of antibiotics for selection of only positive colonies. The survived colonies were further sub-cultured in TYG broth containing required antibiotics and grown at 32 °C overnight. Like this, at least 30–35 passages of alternate streaking on TYG agar plate and sub-culturing in TYG broth was performed until diagnostic PCR failed to give amplification of full-length wild type copy of target gene. The selection pressure of respective antibiotics was maintained in each passage to achieve the homozygous disruption of *parA2* with *nptII* cassette, *parB2* with *cat* cassette, *parA3* with *aadA* cassette and *parB3* with *aac(3)* cassette in the genome of *D. radiodurans*. The disruption mutants were designated as Δ*parA2::nptII* for *parA2*, Δ*parB2::cat* for *parB2*, Δ*parA3::aadA* for *parA3* and Δ*parB3::aac(3)* for *parB3*. For generation of double mutant Δ*parA2::nptII* cells were transformed with linearized pNOSA3UD to give Δ*parA2::nptII*-Δ*parA3::aadA* while for generation of triple mutants, Δ*parA2::nptII* cells were transformed with linearized pNOSA3UD and pNOCB2UD plasmids or pNOSA3UD and pNOGB3UD plasmids in different combinations to generate triple mutants represented as Δ*parA2::nptII*Δ*parA3::aadA*Δ*parB2::cat* or Δ*parA2::nptII*Δ*parA3::aadA*Δ*parB3::aac(3)*. These mutants were also subjected to 30–35 rounds of passages in the presence of required combinations of antibiotics as a selection pressure for homozygous disruption of target genes.

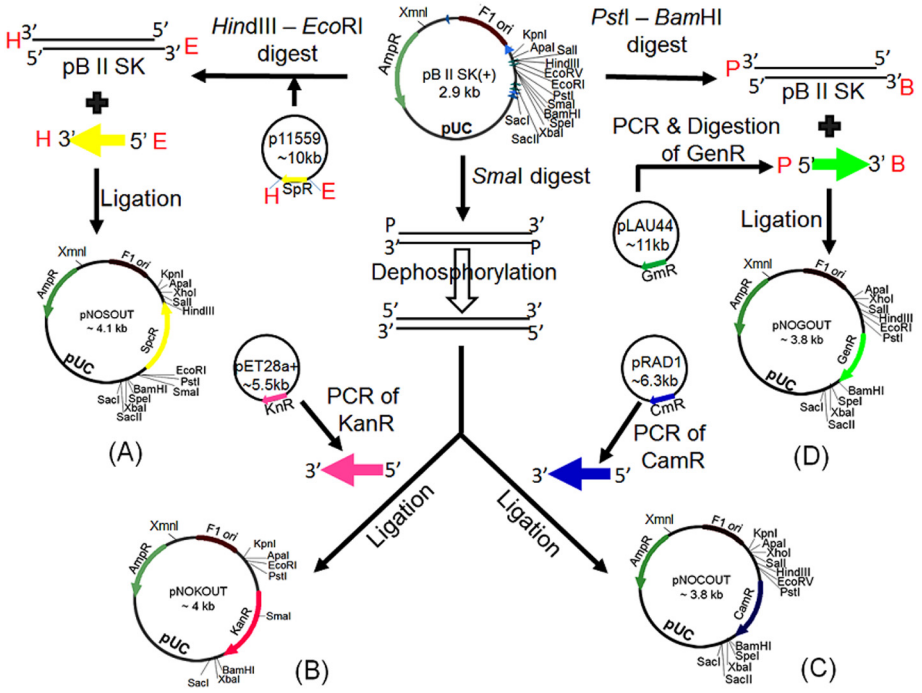

Fig. 1. Schematic representation of the construction of pNOSOUT, pNOKOUT, pNOCOUT and pNOGOUT plasmids. In brief, the expressing cassette of *aadA* (Spec^R) gene obtained from p11559 was cloned at *Hind*III and *Eco*RI sites while *nptII* cassette at *Sma*I site in pBluescript II SK(+) [pBSK(+)] plasmid yielding pNOSOUT (**A**) and pNOKOUT (**B**), respectively. Similarly, the expressing cassette of *cat* gene obtained from pRAD1 was cloned at *SmaI* site while *acc(3)* cassette obtained from pLAU44 plasmid was cloned at *Pst*I and *Bam*HI sites in pBSK(+) yielding pNOCOUT (**C**) and pNOGOUT (**D**) plasmids respectively. H = *Hin*dIII, E = *Eco*RI, P = *Pst*I and B = *Bam*HI.

2.5. PCR screening and verification of gene insertional deletion mutants in D. radiodurans

Total genomic DNA of transformants was isolated as described earlier (Battista et al., 2001) and used as the template for diagnostic PCR. For identification and confirmation of disruption mutation, the gene-specific primers of antibiotic marker genes and target specific primers were used for PCR amplification in different combinations (Table S1). The diagnostic PCR was performed in two groups to verify the mutants. In one group, diagnostic PCR was performed using flanking primers of the target gene as well as flanking primers of the antibiotic gene. In brief, parA2Fw & parA2Rw and nptIIFw & nptIIRw primers for Δ*parA2::nptII,* parB2Fw & parB2Rw and catFw & catRw primers for Δ*parB2::cat,* parA3Fw & parA3Rw and SpecFw & SpecRw primers for Δ*parA3::aadA* and parB3Fw & parB3Rw and GentFw & GentRw primers for Δ*parB3::aac(3)* mutants were used in this study. For screening of triple mutants, similar primers used as said above. In another group, diagnostic PCR was carried out using one of the primers of the target gene and another primer from antibiotic marker gene (Table S1) and depicted in respective figures. For example parA2Fw & nptIIRw (set A) and nptIIFw & parA2Rw (set B) for Δ*parA2::nptII.* parB2Fw & catRw (set C) and catFw & parB2Rw (set D) for Δ*parB2::cat*, parA3Fw & SpecRw (set E) and SpecFw & parA3Rw (set F) for Δ*parA3::aadA* and parB3Fw & GentRw (set G) and GentFw & parB3Rw (set H) for Δ*parB3::aac(3)*, respectively. The PCR was performed using Phusion high-fidelity DNA polymerase and PCR products were analyzed on 1% agarose gel after ethidium bromide staining.

2.6. Cell survival of different mutants of D. radiodurans

To analyze the segregation defects as a function of percent survival of mutants with and without antibiotics, equal number of cells of single, double and triple mutants were plated on TGY agar with and without appropriate antibiotics and grown at 32 °C for 40–48 h. Further, the colony forming units (CFU) were counted for each and plotted as % CFU in presence of antibiotics to its absence. In addition, the phenotype of poor segregation in different *par* mutants of *Deinococcus* was monitored in synergies with topoisomerase II inhibitor (Nalidixic acid) as a function of growth kinetics in liquid culture. In brief, all the single, double and triple mutants of *par* genes were grown in the presence of required antibiotics as mentioned above. The equal OD cells of each mutant along with wild type in triplicates were further grown in absence and presence of nalidixic acid (20 μg/ml) in 48 well microtiter plate (Corning, Sigma-Aldrich) containing TYG broth supplemented with a required amount of antibiotics as used above (Kota et al., 2014). The cells were grown at 32 °C for 18 h using Synergy H1 Hybrid Multi-Mode Microplate Reader, BioTek and growth kinetics was monitored by Gen5 data analysis software.

3. Results and discussion

3.1. Construction of knockout plasmids for D. radiodurans

The pBlueScript II SK(+) (pBSK+) is a high copy number plasmid vector bearing *colE1* origin of replication. It also carries a conditional F1 origin of replication, which allows it to be used as phagemid for packaging of ssDNA with phage capsid. This vector is being used in gene cloning in *E. coli*, as well as a parental molecule for generating other recombinant plasmids. This plasmid should not have maintained in any bacteria that do not replicate both these origins. With this hypothesis, pBSK (+) was used for making recombinant plasmid pNOKOUT (~4.0 kb), which could not be stably maintained in *D. radiodurans* and was used for creating single gene replacement in the genome of *D. radiodurans* (Khairnar et al., 2008). Subsequently, we needed to create multiple disruptions in a single genetic background in this bacterium. Using similar approach therefore, three more recombinant plasmids pNOCOUT (~3.8 kb), pNOSOUT (~4.1 kb) and pNOGOUT (~3.8 kb) containing deinococcal expression cassettes of *cat* gene for chloramphenicol (Cm^R), *aadA* gene for spectinomycin (Spc^R) and *aac(3)* gene for gentamycin (Gen^R), respectively were created (Fig. 1). These cassettes were taken from the plasmids that express these antibiotic resistance in other bacteria including *D. radiodurans*. For instance, the coding sequence of *cat* gene along with the promoter was taken from pRAD1 (Meima and Lidstrom, 2000), *aadA* from p11559 (Mennecier et al., 2004) and *aac(3)* from pLAU44 (Lau et al., 2003) plasmids and cloned in pBSK(+) as described in methods. These plasmids contain multiple cloning sites flanking the respective antibiotic resistant genes and that could be used for making gene replacement

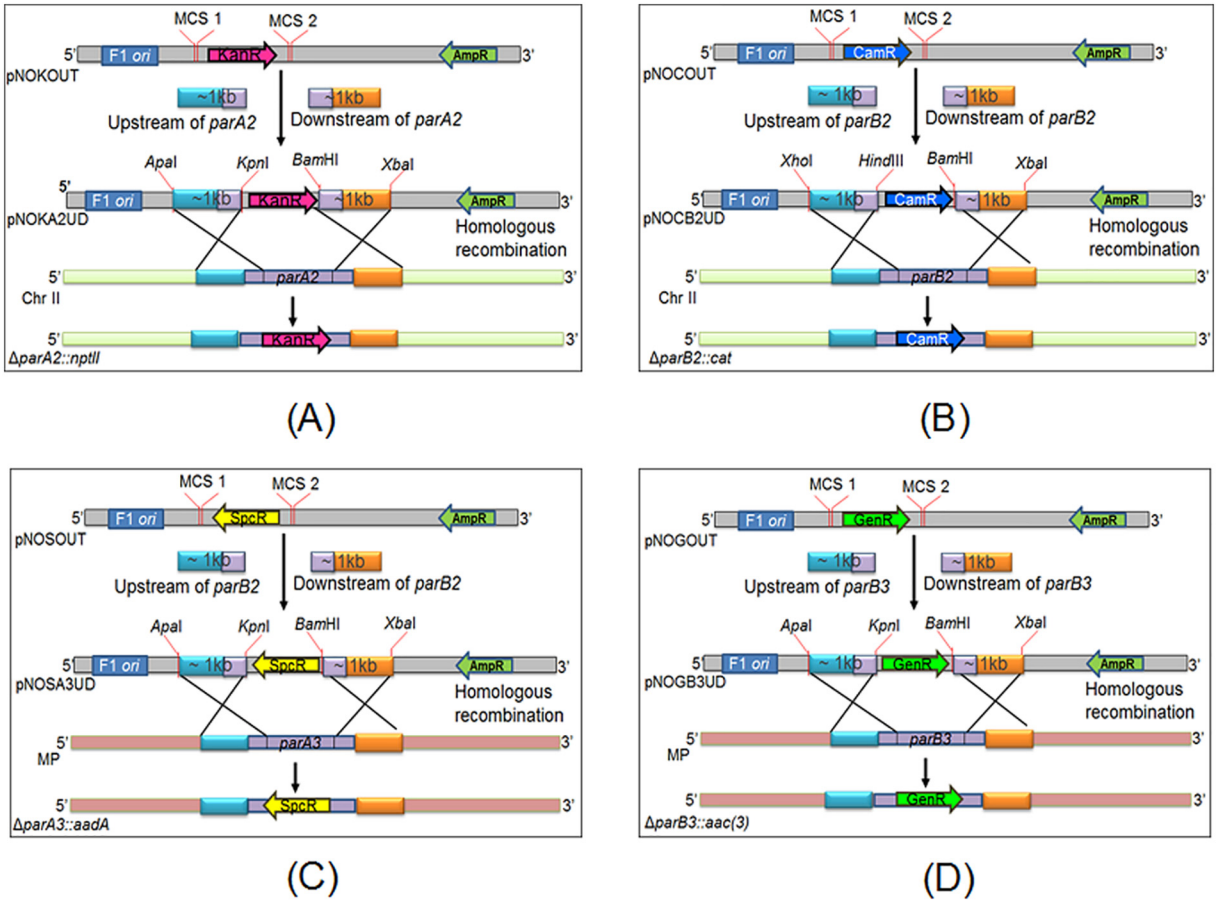

Fig. 2. Schematic representation of the disruption in different genes in the *D. radiodurans* genome using suicide plasmids. In brief, ~1 kb upstream and downstream fragments containing equal half (violet color) of *parA2* (A), *parB2* (B), *parA3* (C) and *parB3* (D) genes along with upstream and downstream sequences (sky blue and orange, respectively) in respective targets were PCR amplified from the genome of the *D. radiodurans*. These fragments were digested appropriately with required restriction enzymes and cloned upstream and downstream to the antibiotic cassettes in pNOKOUT, pNOCOUT, pNOSOUT and pNOGOUT respectively. The resultant plasmids were named pNOKA2UD (**A**), pNOCB2UD (**B**), pNOSA3UD (**C**) and pNOGB3UD plasmids (**D**), respectively. These plasmids were linearized and transformed into *D. radiodurans* and the transformants were selected on TYG plates with respective antibiotics. Crossed marks in the scheme depict the region of homologies and the sites of probable crossover during homologous recombination. (For interpretation of the references to color in this figure legend, the reader is referred to the web version of this article.)

through homologous recombination in host cells.

3.2. The maintenance of recombinant plasmids in D. radiodurans

The recombinant plasmids viz. pNOKOUT, pNOCOUT, pNOSOUT and pNOGOUT were transformed into *E. coli* and *D. radiodurans* R1 as described in the method. The survival of recombinant cells was monitored in presence of respective antibiotics as described in methods. As expected, the *E. coli* cells harboring different plasmids were able to grow similar to *E. coli* harboring pBSK(+) in the presence of ampicillin (data not shown). Subsequently, we constructed knockout plasmids by cloning homologous sequences from the upstream and downstream of target genes into these plasmids as detailed in materials and methods. For example, *parA* and *parB* of chromosome II (*parA2* and *parB2*, respectively), *parA and parB* of megaplasmid (*parA3* and *parB3*, respectively) were selected as target genes and required sequences were cloned in plasmids pNOKOUT, pNOCOUT, pNOSOUT and pNOGOUT, respectively. All four vectors bearing homologous sequences of respective target genes of *D. radiodurans* flanking to the selection markers were named as pNOKA2UD, pNOCB2UD, pNOSA3UD and pNOGB3UD plasmids, respectively (Fig. 2). These constructs were subsequently used for generating single, double and triple deletion mutation in *D. radiodurans* in the same background. These cells were grown till 30–35 passages under required selection pressure of antibiotics and the replacement of target genes with corresponding antibiotic cassettes was monitored by diagnostic PCR amplification using internal primers for selection marker and flanking primers for specific gene knockouts. It was observed that all four plasmids (pNOKOUT, pNOCOUT, pNOSOUT and pNOGOUT) did not survive independently or in different combinations in *D. radiodurans* (Fig. 3). However, the recombinant plasmids (pNOKA2UD, pNOCB2UD, pNOSA3UD and pNOGB3UD) bearing homologous sequences from respective targets genes flanking the antibiotic cassette could support the growth of *D. radiodurans* under selection pressures (Fig. 3). This suggests the possible replacement of target genes with respective antibiotic cassettes through classical homologous recombination. This confirmed that these plasmids are not maintaining in *D. radiodurans* and are suitable for making gene knockouts in this bacterium. In addition to these scorable markers, the tetracycline and hygromycin resistance genes have also been shown useful for gene disruption in *D. radiodurans* (Pasternak et al., 2010; Dulermo et al., 2015) and these can be used in combination with our plasmids for widening the genetic resources for creating multiple mutations in different combinations.

3.3. Generation of single and multiple deletion mutations under same genetic background in D. radiodurans

Since all 4 plasmids express different antibiotic resistance these

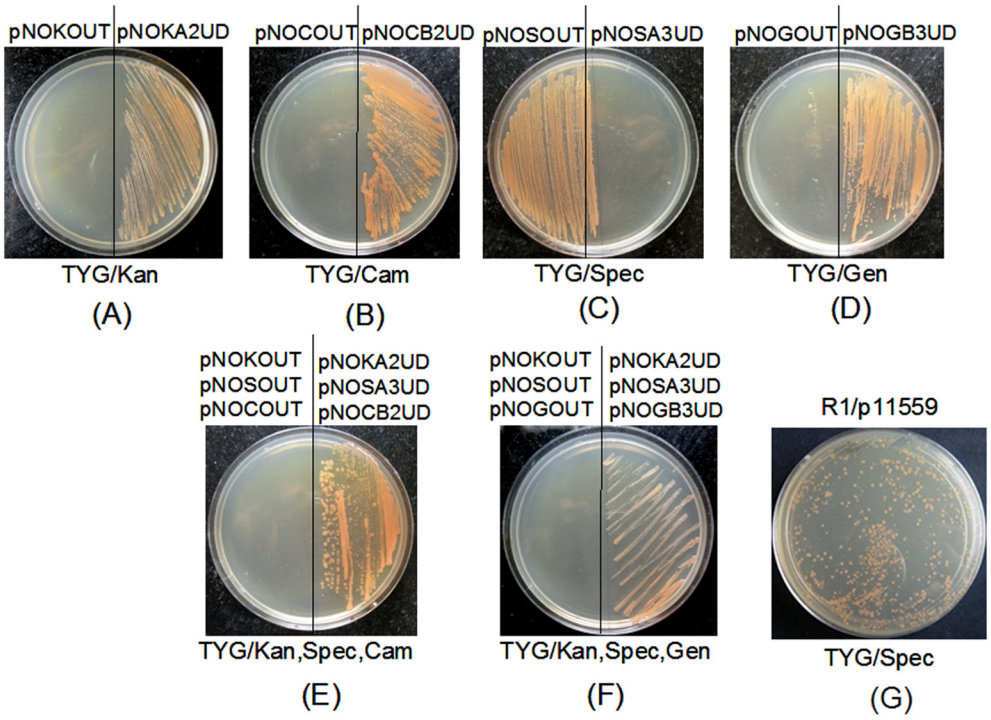

Fig. 3. Survival of *D. radiodurans* transformed with different plasmids. The *D. radiodurans* cells were transformed with linearized vectors (pNOKOUT (A), pNOCOUT (B), pNOSOUT (C) and pNOGOUT (D)) and their derivatives carrying upstream and downstream fragment of different target genes (pNOKA2UD (**A**), pNOCB2UD (**B**), pNOSA3UD (**C**) and pNOGB3UD (**D**)) in different combinations in *D. radiodurans*. Similarly, the triple mutants of *parA2*, *parA3* and *parB2* (**E**) and *parA2*, *parA3* and *parB3* (**F**) were also monitored for their survival in the presence of all three antibiotics. Transformants were streaked on TGY agar plates supplemented with applicable antibiotics and survival was monitored after 48 h. The *D. radiodurans* cells transformed with shuttle plasmid p11559 was used as transformation control (**G**).

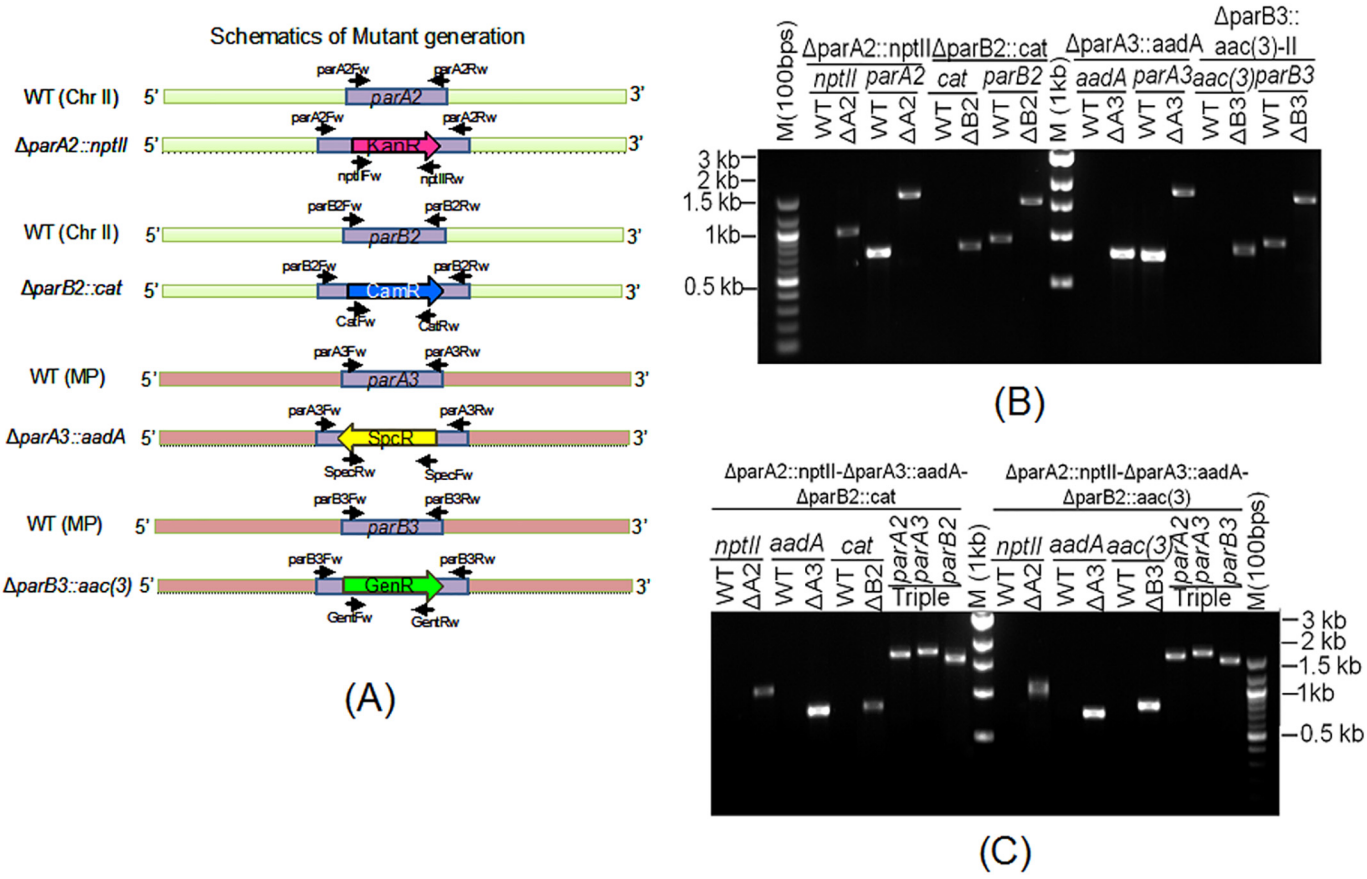

Fig. 4. Confirmation of gene disruption in the genome of *D. radiodurans* using flanking primers. Schematic representation and position of the primers used for PCR amplification are shown (**A**). The genomic DNA of single mutants (*ΔparA2, ΔparB2, ΔparA3* and *ΔparB3*) (**B**) and triple mutants (*ΔparA2-ΔparA3-ΔparB2* and *ΔparA2-ΔparA3-ΔparB3*) (**C**) were prepared and PCR amplified using gene-specific flanking primers (Table S1) of the target genes like *ΔparA2, ΔparB2, ΔparA3* and *ΔparB3* as well as antibiotics markers gene (*nptII, cat, aadA, aac(3)*) as depicted in scheme (**A**). The sizes of the PCR products were estimated using known size DNA markers (M).

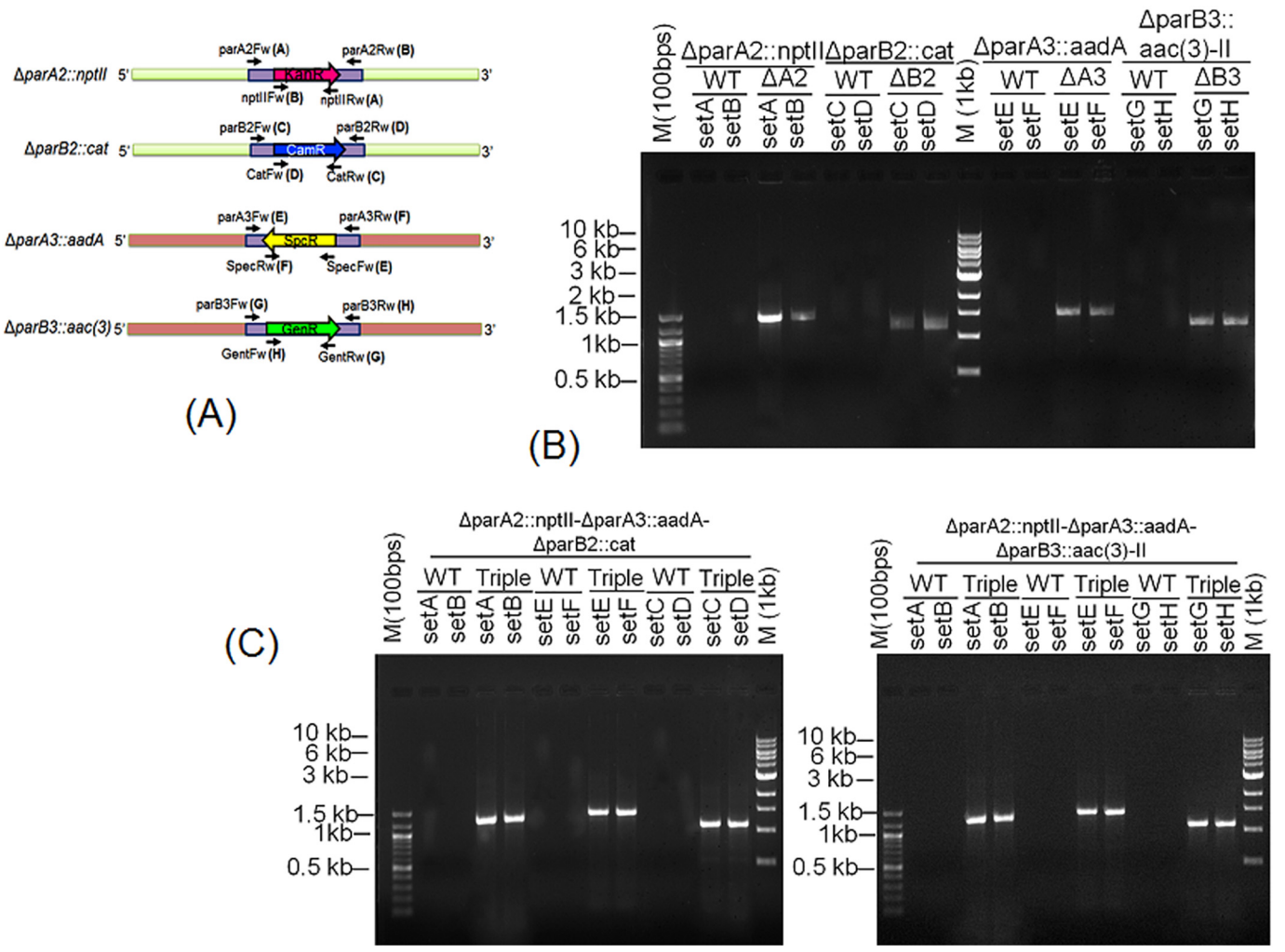

Fig. 5. Confirmation of single and triple genes disruption in *D. radiodurans* by diagnostic PCR. In brief, single mutants (*ΔparA2, ΔparB2, ΔparA3* and *ΔparB3*) and triple mutants (*ΔparA2-ΔparA3-ΔparB2* and *ΔparA2-ΔparA3-ΔparB3*) were subjected to diagnostic PCR using different primer sets (set A-H) as given in Table S1, which include one primer from the target gene and other from the antibiotic marker (**A**) in different combinations. The PCR products were electrophoresed in 1% agarose gel with 1 kb (N3232 L) and 100 bps (N3231S) DNA markers (**B** & **C**). Here, M denotes DNA size markers.

could be used for creating deletions of multiple genes in the same genetic background. For that *D. radiodurans* was transformed with all four plasmids separately and in combinations and the transformants were purified by repeated sub-culturing till 35 passages as described in methods. Results showed that cells transformed with different plasmids that were aimed to create single mutant of *parA2* (*ΔparA2::nptII*), *parB2* (*ΔparB2::cat*), *parA3* (*ΔparA3::aadA*) and *parB3* (*ΔparB3::aac*(3)) and triple mutants like *ΔparA2::nptIIΔparA3::aadAΔparB2::cat* and *ΔparA2::nptIIΔparA3::aadAΔparB3::aac(3)*) survived under selection pressure of required antibiotics. Further, it showed that plasmids without target sequences failed to support the growth of *D. radiodurans* in the presence of antibiotics. These transformants were maintained under selection pressure for several rounds of sub-culture and subjected to diagnostic PCR assay using gene-specific as well as antibiotic marker-specific primers in different combinations (Figs. 4A and 5A). The result showed the amplification of ~1.1 kb amplicon in *ΔparA2::nptII* using nptIIFw and nptIIRw primers, 0.816 kb amplicon in *ΔparB2::cat* using catFw and catRw primers, 0.792 kb amplicon in *ΔparA3::aadA* using aadAFw and aadARw primers and 0.804 kb amplicon in *ΔparB3::aac(3)* using GentFw and GentRw primers only in respective transformants (Fig. 4B). The wild type *D. radiodurans* cells did not amplify any product using antibiotic cassettes specific primers. This suggested that different antibiotic cassettes seem to have integrated at the target gene site in the genome by homologous recombination. The integration of antibiotic cassettes into target genes was diagnosed using different sets of primers; (i) flanking primers of the target genes and (ii) one primer of the flanking region in the genome and other specific to antibiotic resistance gene. Using flanking primers, the size of PCR products was total of the size of antibiotic gene plus target gene regions flanking to antibiotic cassette. For example, the PCR products of 0.783 kb amplicon with parA2Fw and parA2Rw primers, 0.882 kb amplicon with parB2Fw and parB2Rw primers, 0.777 kb amplicon with parA3Fw and *par*A3Rw primers and 0.876 kbp amplicon with parB3Fw and parB3Rw primers were obtained from the genomic DNA of wild type genome. On the other hand, the respective target gene-specific primers could amplify larger size fragment presumably containing antibiotic cassettes along with the flanking regions in the genome. We observed the amplification of 1.65 kbp amplicon with parA2Fw and parA2Rw primers in *ΔparA2::nptII* cells, 1.58 kbp amplicon with parB2Fw and parB2Rw primers in *ΔparB2::cat* cells, 1.75 kbp amplicon with parA3Fw and parA3Rw primers in *ΔparA3::aadA* cells and 1.55 kbp amplicon with parB3Fw and parB3Rw primers in *ΔparB3::aac(3)* cells (Fig. 4B). Similar patterns of PCR amplicon as stated above were found in triple mutants also (Fig. 4C). Using a combination of flanking region primer and antibiotic gene-specific primer, we observed that these primers did not amplify any amplicon in wild type (Fig. 5B, C). However, they amplified the expected size fragments from the mutants. For instance, parA2Fw & nptIIRw (setA) and nptIIFw & parA2Rw (setB) amplified

~1.4 kb in Δ*parA2::nptII*, parB2Fw & catRw (setC) and catFw & parB2Rw (setD) amplified an amplicon of ~1.2 kb in Δ*parB2::cat,* parA3Fw & aadARw (setE) and aadAFw & parA3Rw (setF) amplified PCR product of ~1.5 kb in Δ*parA3::aadA* and parB3Fw & GentRw (setG) and GentFw & parB3Rw (setH) amplified ~1.2 kb product in Δ*parB3::aac(3)* mutants (Fig. 5B). Similar patterns of PCR amplification were found in triple mutants (Fig. 5C). Earlier, the disruption of up to three genes has been shown in *D. radiodurans albeit* using constructs made using PCR based methods (Hua et al., 2012). These results together suggested that knockout of multiple genes can be generated in the same background using the plasmids constructs as used in this study at least in *D. radiodurans*. These plasmids could be useful for genetic manipulation in other microorganism that expresses antibiotic cassettes and do not support independent maintenance of *colE1* plasmids.

3.4. Phenotype of single, double and triple mutants of par genes in D. radiodurans

The mutation in genome partitioning components may lead to defect in segregation process which theoretically will reflect in form of a reduction in colony forming units (CFU) under selection pressure for which the expressing cassettes of the antibiotic gene is integrated into respective target gene. Interestingly, we observed that single mutants of *parA2, parA3, parB2* and *parB3* have no significant reduction in CFU in the presence of corresponding antibiotics. On the other hand, the number of antibiotic-resistant colonies of double and triple mutants had reduced to approximately 50–60% as compared to the colonies appeared without antibiotics. This indicated that double or triple mutants have less number of cells bearing secondary genome elements (chromosome II and megaplasmid) as represented by the loss of antibiotic resistance conferring on them, as compared to single mutants, and thus suggesting the segregation defect in multiple mutants as compared to single disruption (Fig. 6A). These results suggest a possibility of functional redundancy amongst the "Par" proteins encoded on secondary genome elements. Further, we have compared the growth kinetics of all the mutants with wild type under required selection pressure in absence and presence of nalidixic acid (an inhibitor of topoisomerase II). We found that the growth of double and triple mutants is very slow in comparison to wild type and single mutants under the required selection pressure of antibiotics (Fig. 6 B, C). This result is in correlation with data of CFU counts as mentioned above (Fig. 6A–C). In addition, double and triple mutants have shown very high sensitivity toward nalidixic acid in comparison to wild type and single mutants of *par* genes. The sensitivity for nalidixic acid indicated the defects in segregation of duplicated genome elements. These results suggested that double and triple mutants of secondary genome *par* genes show defective segregation, which seems to be similar to that observed with topoisomerase II inhibitors. Further, the mechanisms underlying the defective segregation or multiplication or both in multipartite genome system in *D. radiodurans* are yet to be ascertained and would be addressed independently.

In conclusion, we report the construction of different non-replicative plasmids in *D. radiodurans*, for simultaneous deletion of multiple genes in the same background in this bacterium. We demonstrated that all 4 plasmids like pNOKOUT, pNOCOUT, pNOSOUT and pNOGOUT expressing separate antibiotic resistance marker could be used for creating deletion mutation of 4 genes separately and 3 of them together in *D. radiodurans*. *E. coli* harboring these constructs did not show any adverse effects on growth. *D. radiodurans* harboring these plasmids could express antibiotic resistance only when target gene sequences were cloned flanking antibiotic-resistant cassette. These cells were found to have antibiotic cassette integrated in the target genes like *parA2, parB2, parA3* and *parB3*, respectively. This indicated that the plasmids bearing homologous region of the target genes located in the genome could undergo double crossover events leading to integration into target genes with a marker. Phenotypically, we found that double and triple mutants of *parAs* and *parBs* show a significant decrease in survival as compared to wild type and single mutants. Since, antibiotic resistance is conferred on respective genome elements, the decrease in the number of colony forming units per ml in the presence of antibiotic (s) would be an indicative to the loss of corresponding element(s) in certain proportion of daughter cells. Further, this indicates a possible defect in segregation of respective genome elements. Higher number of CFU in the absence of antibiotics in all *par* mutants of secondary genome elements argues in favour of faithful segregation of primary chromosome supporting ~100% cell survival, while an arrest in

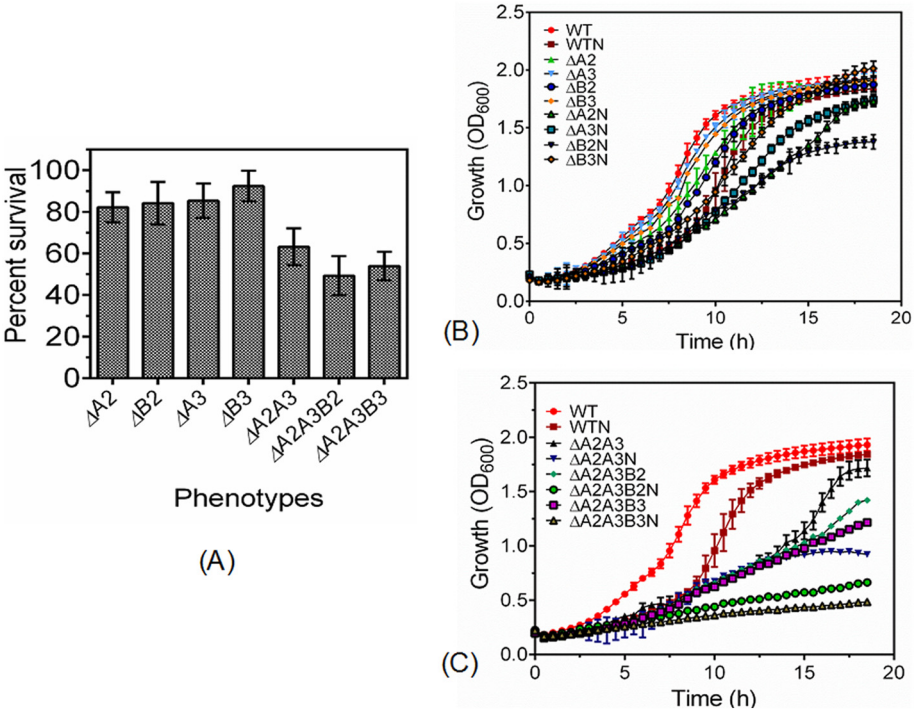

Fig. 6. Cell survival of different *par* mutants of *D. radiodurans*. The survival of Δ*parA2* (ΔA2), Δ*parB2* (ΔB2), Δ*parA3* (ΔA3) *and* Δ*parB3* (ΔB3) single mutants, Δ*parA2*-Δ*parA3* (ΔA2A3) double mutant, Δ*parA2*-Δ*parA3*-Δ*parB2* (ΔA2A3B2) and Δ*parA2*-Δ*parA3*-Δ*parB3* (ΔA2A3B3) triple mutants was monitored as CFU per ml in the presence and absence of antibiotics (8 μg/ml of kanamycin for ΔA2; 5 μg/ml of chloramphenicol for ΔB2; 70 μg/ml of spectinomycin for ΔA3; 10 μg/ml of gentamycin for ΔB3; and their respective combinations for double and triple mutants) (**A**). Percent survival in the presence of antibiotics was calculated with respect to the number of CFU per ml in the absence of antibiotics. The 100% survival was equivalent to the CFU / ml 5.26×10^7, 5.32×10^7, 5.52×10^7, 5.19×10^7, 4.85×10^7, 4.72×10^7 and 4.5×10^7 for ΔA2, ΔB2, ΔA3, ΔB3, ΔA2A3, ΔA2A3B2 and ΔA2A3B3 mutants, respectively in the absence of antibiotic(s). The data given here is Mean ± SD ($n = 9$). The growth kinetics of single, double and triple mutants of secondary genome *par* genes with wild type cells under required antibiotics selection in absence and presence of nalidixic acid (30 μg/ml) was monitored in microplate reader at wavelength of 600 nm (**B** and **C**). The data given here is Mean ± SD ($n = 6$). Here suffix N in name of mutant reflects presence of nalidixic acid.

segregation of secondary genome elements. Further, double and triple mutants of *par* genes were found highly sensitive to nalidixic acid in comparison to wild type and single mutants. Thus, these plasmids would give a reliable tool for genome-editing in *Deinococcus*. This technology will allow us to (i) disrupt several genes by replacing the expressing cassette of different antibiotics in the same genetic background, (ii) subcellular co-localization studies of proteins fused with different fluorescent proteins through double crossover recombination and (iii) stable integration and expression of homologous or heterologous genes with their promoters from chromosomal copies of the genome. Although, this study has confirmed the use of these plasmids in creating multiple gene disruptions in *D. radiodurans*, the possibility of these plasmids usefulness in any bacteria not maintaining *E. coli* plasmid cannot be ruled out.

Acknowledgments

GKM is grateful to Department of Atomic Energy, Government of India for providing research fellowship.

Appendix A. Supplementary data

Supplementary data to this article can be found online at https://doi.org/10.1016/j.plasmid.2018.09.003.

References

Battista, J.R., Park, M.J., McLemore, A.E., 2001. Inactivation of two homologues of proteins presumed to be involved in the desiccation tolerance of plants sensitizes Deinococcus radiodurans R1 to desiccation. Cryobiology 43 (2), 133–139.

Charaka, V.K., Misra, H.S., 2012. Functional characterization of the role of the chromosome I partitioning system in genome segregation in *Deinococcus radiodurans*. J. Bacteriol. 194, 5739–5748.

Daly, M.J., 2009. A new perspective on radiation resistance based on *Deinococcus radiodurans*. Nat. Rev. Microbiol. 7, 237–245.

Dulermo, R., Onodera, T., Coste, G., Passot, F., Dutertre, M., Porteron, M., Confalonieri, F., Sommer, S., Pasternak, C., 2015. Identification of new genes contributing to the extreme radioresistance of *Deinococcus radiodurans* using a Tn5-based transposon mutant library. PLoS One 10 (4), e0124358.

Gutman, P.D., Carroll, J.D., Lan Masters, C., Minton, K.W., 1994. Sequencing, targeted mutagenesis and expression of a recA gene required for the extreme radioresistance of *Deinococcus radiodurans*. Gene 141 (1), 31–37.

Harsojo Kitayama, S., Matsuyama, A., 1981. Genome multiplicity and radiation resistance in *Micrococcus radiodurans*. J. Biochem. 90 (3), 877–880.

Hua, X., Xu, X., Li, M., Wang, C., Tian, B., Hua, Y., 2012. Three nth homologs are all required for efficient repair of spontaneous DNA damage in *Deinococcus radiodurans*. Extremophiles 16 (3), 477–484.

Khairnar, N.P., Kamble, V.A., Misra, H.S., 2008. RecBC enzyme overproduction affects UV and gamma radiation survival of *Deinococcus radiodurans*. DNA Repair 7, 40–47.

Kota, S., Charaka, V.K., Ringgaard, S., Waldor, M.K., Misra, H.S., 2014. PprA contributes to *Deinococcus radiodurans* resistance to nalidixic acid, genome maintenance after DNA damage and interacts with deinococcal topoisomerases. PLoS One 9 (1), e85288.

Lau, I.F., Filipe, S.R., Søballe, B., Økstad, O.A., Barre, F.X., Sherratt, D.J., 2003. Spatial and temporal organization of replicating *Escherichia coli* chromosomes. Mol. Microbiol. 49 (3), 731–743.

Makarova, K.S., Aravind, L., Wolf, Y.I., Tatusov, R.L., Minton, K.W., Koonin, E.V., Daly, M.J., 2001. Genome of extremely radiation-resistant bacterium *Deinococcus radiodurans* viewed from the perspectives of comparative genomic. Microbiol. Mol. Biol. Rev. 65 (2001), 44–79.

Markillie, L.M., Varnum, S.M., Hradecky, P., Wong, K.K., 1999. Targeted mutagenesis by duplication insertion in the radioresistant bacterium *Deinococcus radiodurans*: radiation sensitivities of catalase (katA) and superoxide dismutase (sodA) mutants. J. Bacteriol. 181 (2), 666–669.

Meima, R., Lidstrom, M.E., 2000. Characterization of the minimal replicon of a cryptic *Deinococcus radiodurans* SARK plasmid and development of versatile *Escherichia coli-D. radiodurans* shuttle vectors. Appl. Environ. Microbiol. 66 (2000), 3856–3867.

Mennecier, S., Coste, G., Servant, P., Bailone, A., Sommer, S., 2004. Mismatch repair ensures fidelity of replication and recombination in the radioresistant organism *Deinococcus radiodurans*. Mol. Gen. Genomics. 272, 460–469.

Misra, H., Rajpurohit, Y.S., Kota, S., 2013. Physiological and molecular basis of extreme radioresistance in *Deinococcus radiodurans*. Curr. Sci. 104, 194–206.

Narumi, I., Satoh, K., Cui, S., Funayama, T., Kitayama, S., Watanabe, H., 2004. PprA: a novel protein from *Deinococcus radiodurans* that stimulates DNA ligation. Mol. Microbiol. 54, 278–285.

Pasternak, C., Ton-Hoang, B., Coste, G., Bailone, A., Chandler, M., Sommer, S., 2010. Irradiation-induced *Deinococcus radiodurans* genome fragmentation triggers transposition of a single resident insertion sequence. PLoS Genet. 6 (1), e1000799.

Rajpurohit, Y.S., Misra, H.S., 2010. Characterization of a DNA damage-inducible membrane protein kinase from *Deinococcus radiodurans* and its role in bacterial radioresistance and DNA strand break repair. Mol. Microbiol. 77, 1470–1482.

Sambrook, J., Russell, D.W., 2001. Molecular Cloning: A Laboratory Manual. Cold Spring Harbor Laboratory Press, N.Y.

Schaefer, M.C., Schmitz, R., Facius, G., Horneck, B., Milow, K.H., Ortner, J., 2000. Systematic study of parameters influencing the action of Rose Bengal with visible light on bacterial cells: comparison between biological effect and singlet-oxygen production. Photochem. Photobiol. 71, 514–523.

Slade, D., Radman, M., 2011. Oxidative stress resistance in *Deinococcus radiodurans*. Microbiol. Mol. Biol. Rev. 75, 133–191.

Slade, D., Lindner, A.B., Paul, G., Radman, M., 2009. Recombination and replication in DNA repair of heavily irradiated *Deinococcus radiodurans*. Cell 136 (6), 1044–1055.

Udupa, K.S., O'Cain, P.A., Mattimore, V., Battista, J.R., 1994. Novel ionizing radiation-sensitive mutants of *Deinococcus radiodurans*. J. Bacteriol. 176 (24), 7439–7446.

White, O., Eisen, J.A., Heidelberg, J.F., Hickey, E.K., Peterson, J.D., Dodson, R.J., et al., 1999. Genome sequence of the radioresistant bacterium *Deinococcus radiodurans* R1. Science 286, 1571–1577.

Microbiology (2016), **162**, 1321–1334 DOI 10.1099/mic.0.000330

Divisome and segrosome components of *Deinococcus radiodurans* interact through cell division regulatory proteins

Ganesh K. Maurya,[1,2] Kruti Modi[1] and Hari S. Misra [1,2]

Correspondence
Hari S. Misra
hsmisra@barc.gov.in

[1]Molecular Biology Division, Bhabha Atomic Research Centre, Mumbai, India
[2]Life Sciences, Homi Bhabha National Institute (DAE-Deemed University), Mumbai- 400094, India

The *Deinococcus radiodurans* genome encodes many of the known components of divisome as well as four sets of genome partitioning proteins, ParA and ParB on its multipartite genome. Interdependent regulation of cell division and genome segregation is not understood. *In vivo* interactions of *D. radiodurans'* sdivisome, segrosome and other cell division regulatory proteins expressed on multicopy plasmids were studied in *Escherichia coli* using a bacterial two-hybrid system and confirmed by co-immunoprecipitation with the proteins made in *E. coli*. Many of these showed interactions both with the self and with other proteins. For example, DrFtsA, DrFtsZ, DrMinD, DrMinC, DrDivIVA and all four ParB proteins individually formed at least homodimers, while DrFtsA interacted with DrFtsZ, DrFtsW, DrFtsE, DrFtsK and DrMinD. DrMinD also showed interaction with DrFtsW, DrFtsE and DrMinC. Interestingly, septum site determining protein, DrDivIVA showed interactions with secondary genome ParAs as well as ParB1, ParB3 and ParB4 while DrMinC interacted with ParB1 and ParB3. PprA, a pleiotropic protein recently implicated in cell division regulation, neither interacted with divisome proteins nor ParBs but interacted at different levels with all four ParAs. These results suggest the formation of independent multiprotein complexes of 'DrFts' proteins, segrosome proteins and cell division regulatory proteins, and these complexes could interact with each other through DrMinC and DrDivIVA, and PprA in *D. radiodurans*.

Received 6 February 2016
Accepted 29 June 2016

INTRODUCTION

Cellular processes including chromosome duplication, segregation and cell division occur through the coordinated actions of various proteins that form macromolecular complexes. These processes are tightly regulated both temporally and spatially. In prokaryotes, chromosome duplication followed by segregation is a pre-requisite for cell division. In a few rod-shaped bacteria like *Escherichia coli* and *Bacillus subtilis*, the functional interactions of these processes have been shown and the involvement of some common proteins in both these processes has been demonstrated (Thanbichler, 2010). Cell division in these bacteria occurs through interactions among a dozen proteins forming a higher order structure called the divisome (Vicente & Rico, 2006). FtsZ is the main component of divisome and various proteins regulate its activity both temporally and spatially. Using classical genetics, a bacterial two-hybrid system, fluorescence microscopy, etc., it has been shown that FtsZ localization at the mid cell position is spatially regulated by the 'Min' system comprising MinC, MinD and MinE mostly in Gram-negative bacteria and DivIVA instead of MinE in Gram-positive bacteria (Lutkenhaus, 2007; Conti *et al.*, 2015). Subsequently, FtsA tethers FtsZ to the membrane followed by assembly of other divisome components in a sequential manner as shown in *E. coli* (Di Lallo *et al.*, 2003; Vicente & Rico, 2006). This helps in the progression of FtsZ polymerization into the Z-ring and its subsequent contraction. This process is stalled if any anomalies caused by unresolved duplicated DNA are encountered and does not progress further till duplicated DNA is resolved. A number of regulatory proteins are known to regulate the resolution of duplicated intertwined circular DNA and consequently FtsZ ring dynamics (Goehring *et al.*, 2006; Cho *et al.*, 2011; Tonthat *et al.*, 2011; Bailey *et al.*, 2014). These include DNA topoisomerases, nucleoid occlusion (NOC) proteins and the FtsK-XerCD system. FtsK is a multifunctional DNA translocase and divisome component. It is recruited by FtsA and plays a role in coordination of chromosome segregation (Ip *et al.*, 2003; Massey *et al.*, 2006; Bigot *et al.*, 2007).

Ten supplementary tables are available with the online Supplementary Material.

Bacterial genome segregation involves mostly a tripartite partitioning system (segrosome) consisting of (i) a centromere-like sequence or *cis*-element, (ii) a centromere-binding protein (Schumacher *et al.*, 2010; Vecchiarelli *et al.*, 2010) called ParB or its homologues and (iii) an NTPase called ParA or ParA-like proteins. The dynamics created during polymerization/depolymerization of ParA provide the force for the separation of duplicated plasmids or chromosomes in opposite directions (Ebersbach & Gerdes, 2001; Fogel & Waldor, 2006; Salje *et al.*, 2010; Shebelut *et al.*, 2010; Gerdes *et al.*, 2010). Recently, it has been shown that an appropriate ratio of ParA to ParB within the cell is required for Z-ring formation and cell division in *Caulobacter crescentus*. Depletion of ParB and/or increase in ParA could inhibit Z-ring formation and cell division in *C. crescentus* (Mohl *et al.*, 2001) and *Mycobacterium smegmatis* (Ginda *et al.*, 2013). Similar observation has also been reported in *D. radiodurans* where the role of ParA of chromosome II (ParA2) in the regulation of cell division, in the context of its stoichiometric balance with ParB2, was observed (Charaka & Misra, 2012). DivIVA a tropomyocin-like coiled-coil protein appears as a bifunctional protein with distinct roles in division-site selection as well as during chromosome segregation at least in *B. subtilis* (Thomaides *et al.*, 2001). *In vivo* interaction of cell division proteins (Di Lallo *et al.*, 2003; Ginda *et al.*, 2013) and proteins involved in genome maintenance (Donovan *et al.*, 2012; Ringgaard *et al.*, 2011) has been demonstrated in other bacteria using a bacterial two-hybrid system.

D. radiodurans R1, a Gram-positive bacterium, shows extraordinary tolerance to DNA-damaging agents including radiation and desiccation (Minton, 1994; Slade & Radman, 2011; Misra *et al.*, 2013). Apart from these features, it shows ploidy of its four genomic elements, chromosome I (2.65 Mb), chromosome II (412 kb), a megaplasmid (177 kb) and a small plasmid (46 kb) (White *et al.*, 1999). Its genome encodes nearly all the 'Fts' proteins annotated in *E. coli*, the 'Min' system that includes MinC, MinD and DivIVA. It also possesses the 'Par' system comprising one set of ParAB each on chromosome I (ParA1/ParB1) and chromosome II (ParA2/ParB2) and two sets on its megaplasmid (ParA3/ParB3 and ParA4/ParB4). The mechanisms underlying maintenance and faithful inheritance of its multipartite genome and the regulation of cell division are not known in this bacterium and would be worth investigating. Characterization of chromosome I partitioning proteins and their functional interaction with newly identified centromeric sequences in chromosome I of *D. radiodurans* have been reported recently (Charaka & Misra, 2012). Further, deinococcal FtsZ (DrFtsZ) and FtsA (DrFtsA) have been characterized both *in vitro* and *in vivo* (Modi & Misra, 2014; Modi *et al.*, 2014). PprA was characterized as a pleiotropic protein involved in radiation resistance (Narumi *et al.*, 2004). Recently, the role of PprA in genome maintenance and cell division has been reported (Devigne *et al.*, 2013; Kota *et al.*, 2014a). It has also been demonstrated that PprA interacts with deinococcal DNA topoisomerase *in vivo* and modulates its functions *in vitro* (Kota *et al.*, 2014b, 2016; Devigne *et al.*, 2016).

Here we have used BACTH (Bacterial Adenylate Cyclase-based Two Hybrid) system (Karimova *et al.*, 1998) and monitored protein–protein interactions *in vivo*. We produced fusions of all annotated divisome and segrosome proteins in BACTH vectors, confirmed expression of tagged fusion proteins by immunoblotting using antibodies to the respective tags' antibodies and subsequently demonstrated their *in vivo* interactions that were demonstrated in the *cyaA*$^-$ deficient *E. coli* strain BTH101. Some of these interactions were confirmed by co-immunoprecipitation (co-IP) using representative examples of qualitatively defined strong interactions, weak interactions and no interactions. We observed *in vivo* interaction among 'Fts' proteins and segrosome proteins (hereafter referred to as 'Par'). Cell division spatial regulatory proteins like DrMinC, DrMinD and DrDivIVA also interacted selectively with certain components of both these macromolecular complexes, thus suggesting their possible involvement in the recruitment and regulation of these two important functions in *D. radiodurans*.

METHODS

Bacterial strains, plasmids and materials. *D. radiodurans* R1 (ATCC13939), a kind gift from Professor J. Ortner, Germany (Schäefer *et al.*, 2000) was grown in TGY [Bacto tryptone (1 %), glucose (0.1 %) and yeast extract (0.5 %)] medium with shaking at 180 rpm at 32° °C. *E. coli* strains DH5α and NovaBlue were grown at 37 °C, while *E. coli* BTH101 (*cyaA*$^-$) was grown at 30 °C with shaking at 180 rpm in Luria-Bertani (LB) broth. *E. coli* strain DH5α and NOVABLUE were used for cloning and maintenance of all the plasmids. BACTH vectors like pUT18 and pUT18C expressing 'T18' domain and pKT25 and pKNT25 expressing 'T25' domain of adenylate cyclase will be referred to as T18 and T25, respectively, throughout the paper. *E. coli* strain BTH101 (hereafter referred as BTH101) was used for co-expression of these proteins on BACTH plasmids for *in vivo* protein–protein interactions. Recombinant *E. coli* harbouring different BACTH plasmid derivatives were grown in the presence of both ampicillin (100 μg ml^{-1}) and kanamycin (50 μg ml^{-1}) as required. Standard protocols for all recombinant DNA techniques were used as described in Green & Sambrook (2012). Antibodies against T18 (SC-33620) and T25 (SC-13582) domains of CyaA of *Bordetella pertussis*, respectively, were procured commercially (Santacruz Biotechnology, Inc). Molecular biology grade chemicals and enzymes were procured from Sigma Chemicals Company, USA, Roche Biochemicals, Mannheim, Germany, New England Biolabs, USA and Merck India, Mumbai.

Construction of recombinant plasmids. The genomic DNA of *E. coli* MG1655 and *D. radiodurans* R1 were isolated as described in Battista *et al.*(2001). Details of the primers used for the cloning of various components of divisome and segrosome are given in Table S1 (available in the online Supplementary Material). BACTH vectors were used for making fusions with target proteins as described earlier (Karimova *et al.*, 1998). In brief the coding sequences of divisome proteins (FtsA, FtsE, FtsK, FtsW, FtsQ, FtsZ, MinC, MinD and DivIVA) and genome partitioning proteins ParA1 (DR_0013), ParA2 (DR_A0001), ParA3 (DR_B0001) and ParA4 (DR_B0031) as well as ParB1 (DR_0012), ParB2 (DR_A0002), ParB3 (DR_B0002) and ParB4 (DR_B0030) of *D. radiodurans* were PCR amplified from genomic DNA using appropriate primers. The required restriction enzymes sites were incorporated at the 5′ end of these primers. PCR products were digested with appropriate restriction enzymes and ligated at compatible ends in BACTH plasmids as detailed in Table S2. For the reader's convenience, all the proteins of *D. radiodurans* have been named with a prefix '*Dr*' before their standard

names (e.g. DrFtsZ) and will be referred to accordingly throughout the manuscript. Likewise, proteins expressed on constructs made using pUT18 and pKNT25, which would have T18/T25 at the C-terminus of the target proteins are denoted by the suffix C18/C25, respectively (e.g. DrFtsZ-C18/DrFtsZ-C25), and those made using pUT18C and pKT25 plasmids, which would have had T18 and T25 at the N-terminus of the protein are denoted by a prefix of N18/N25, respectively (e.g. N18-DrFtsZ/N25-DrFtsZ). Similarly, the coding sequences of FtsA and FtsZ of *E. coli* were also PCR amplified and cloned for use as positive control and will be referred as EcFtsA and EcFtsZ, respectively.

Immunoblotting of target proteins fused with T18/T25 domains. Different derivatives of BACTH plasmids harbouring coding sequences of divisome and segrosome proteins of *D. radiodurans* (Table S2) were transformed into BTH101. The production and stability of fusion proteins were monitored by immunoblotting with antibodies against T18 and T25 domains of adenylate cyclase using a protocol as described earlier (Rajpurohit & Misra, 2010). In brief, the total proteins of *E. coli* BTH101 expressing recombinant proteins, which were tagged with either T18 or T25 domains of CyaA, were separated on 12 % SDS-PAGE. The proteins were transferred on PVDF (Millipore) membrane and hybridized with primary antibodies against T18 or T25, respectively.

For co-IP, the representative sets of recombinant cells co-expressing these constructs in different combinations were selected for validating BACTH data. The cell-free extracts of these cells were made using RIPA buffer (50 mM Tris-base, 150 mM NaCl, 5 mM EDTA, containing 0.5 % Triton-X 100, 1 mM PMSF, 1 mM DTT, 0.5 mg ml^{-1} lysozyme and 50 µg protease inhibitor cocktail tablet (Cat No S8830, Sigma-Aldrich, Inc.)) followed by sonication. Total proteins incubated with polyclonal antibodies against T25 and T25 tagged proteins were co-immunoprecipitated using standard protocol as described in the Protein G immunoprecipitation kit (Cat. No. IP50, Sigma-Aldrich. Inc.). Immunoprecipitate was separated on SDS-PAGE, blotted on PVDF membrane, and hybridized with monoclonal antibodies against T18. Hybridization signals were detected using anti-mouse and anti-rabbit secondary antibodies conjugated with alkaline phosphatase as required, using BCIP/NBT substrates (Roche Biochemical, Mannheim).

BACTH complementation assays. For BACTH complementation assays, the recombinant BACTH plasmids (Table S2) expressing divisome and genome partitioning genes were transformed into BTH101 in different combinations. Recombinant cells were scored on LB agar plates supplemented with ampicillin 100 µg ml^{-1} and kanamycin 50 µg ml^{-1}. Recombinant clones were inoculated into 96-well titre plates containing 100 µl LB with appropriate antibiotics in triplicate and allowed to grow overnight. For plate assay, 5 µl of overnight grown culture was spotted on an LB agar plate supplemented with 5-bromo-4-chloro-3-indolyl-β-D-galactopyranoside (X-Gal) (40 µg ml^{-1}) and isopropyl-β-D-thiogalactopyranoside (IPTG) (0.5 mM) with required antibiotics. Plates were incubated at 30 °C overnight and appearance of white-blue colonies was recorded. In parallel, 5 µl of overnight grown cultures was used to inoculate 150 µl LB broth supplemented with 0.5 mM IPTG and appropriate antibiotics, and grown overnight at 30 °C. β-Galactosidase activity was measured from liquid cultures as described earlier (Battesti & Bouveret, 2012; Kota *et al.*, 2014b). In brief, the cultures were diluted 1 : 4 into LB medium and the optical density at 600 nm (OD_{600}) was normalized; 100 µl of each culture was suspended in 400 µl Z- buffer (60 mM Na_2HPO_4, 40 mM NaH_2PO_4, 10 mM KCl, 10 mM Mg SO_4, 50 mM β-mercaptoethanol, pH 7.0). To this 0.01 % SDS and 20 µl chloroform was added to permeabilize cells and cell debris were removed. Enzyme activity was assayed in triplicate with 50 µl of supernatant using 0.4 % O-nitrophenyl-β-D-galactoside (ONPG) as a substrate. Optical density at 420 nm was measured at 2 min intervals. β-Galactosidase activity was calculated in Miller units (MUs) as described in Kota *et al.* (2014). The formula used for calculating MUs was as follows: (500 ($OD_{420\,nm}$ at time t2- $OD_{420\,nm}$ at time t1)/t2-t1 (min))/$OD_{600\,nm}$, where the optical density 1.0 at 600 nm for 1 ml culture was considered as 300 µg of total protein equivalent dry weights as estimated earlier (Karimova *et al.*, 2005; Robichon *et al.*, 2011). A significant increase in β-galactosidase activity by twofold or more as compared to controls is considered a positive interaction in a majority of the cases. However, there are cases where fold increases were less than two-fold but these were reproducible in both spot assay and liquid cultures assay and therefore have been considered as positive interactions.

RESULTS

Translational fusions of divisome and segrosome proteins with BACTH partners

The coding sequences of cell division proteins like DrFtsZ, DrFtsA, DrFtsK, DrFtsE, DrFtsW, DrFtsQ, DrMinC, DrMinD and DrDivIVA and genome partitioning proteins like ParA1, ParB1, ParA2, ParB2, ParA3, ParB3, ParA4 and ParB4 were cloned in BACTH plasmids. The recombinant plasmids generated in this study and the expected size of the corresponding target proteins fused with either T18 or T25 of BACTH system are given in Table S2. The plasmids were transformed into BTH101 and expression of fusion proteins was confirmed by immunoblotting using antibodies against T18 and T25. Immunodetection using these antibodies showed expression of fusion proteins of the expected sizes in all the recombinant strains. These antibodies cross-reacted with a protein from the cells expressing anticipated protein, and immunosignals of the expected size of fusion proteins were detected (Fig. 1). The majority of the constructs tested for expression contained C-terminal tags and some were N-terminal fusions with T25. We observed that all these proteins express as fusion with T25 on respective BACTH plasmids. Interestingly, we noticed that the signal intensities of N25-DrFtsE (Fig. 1g) and DrDivIVA-C18 (Fig. 1b) were consistently lower than DrFtsE-C25 and DrDivIVA-C25, respectively. This confirmed the expression of divisome and genome partitioning proteins of *D. radiodurans* as translational fusion with T18/T25, on BACTH plasmids in BTH101. Since, T25 antibodies were polyclonal and were suspected for cross-reactivity with T18, hybridization conditions were standardized so that only specific hybridization of T18 (Fig. 1c) and T25 (Fig. 1d) antibodies was detected. These results ascertained the expression of target proteins with respective tags on recombinant BACTH plasmids in BTH101.

Cell division proteins (Fts) interact *in vivo*

It was shown earlier that when the T18 and T25 domains of CyaA are fused separately with two interacting proteins, the activity of CyaA is restored when the domains come together leading to the dimerization of T18 and T25 domains. Reconstitution of activity of CyaA is monitored as the expression of β-galactosidase in BTH101 (*cyaA*$^-$) cells. Therefore, BTH101 was co-transformed with constructs expressing 'Fts' proteins fused with either T18 or T25 in different combinations, and the expression of β-galactosidase was monitored as an indication of the intraction of two proteins *in vivo*. We observed that only certain combinations showed the expression of β-galactosidase in the spot assay

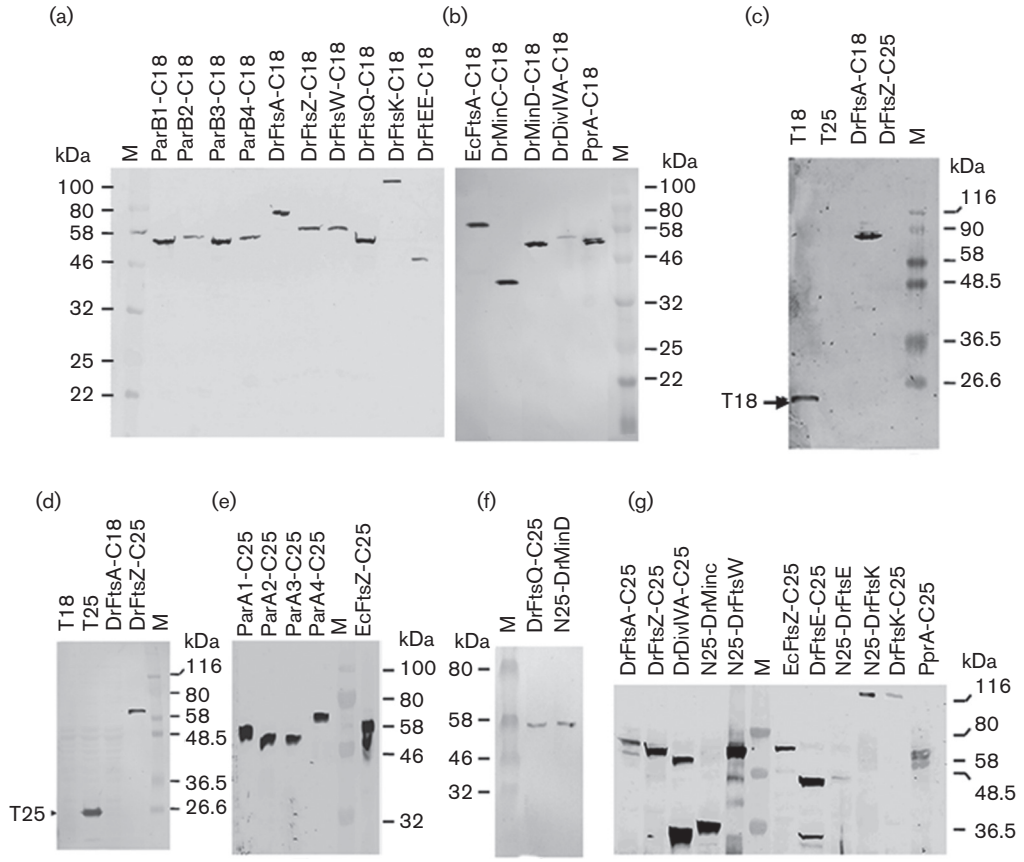

Fig. 1. Confirmation of expression of target proteinsn as T18/T25 fusions in *E. coli*. *E. coli* BTH101 cells were transformed with recombinant plasmids constructed for expressing different target proteins in fusion with T18 or T25 domains of CyaA enzyme and grown appropriately. Expression of proteins tagged with T18 at the C-terminus was probed using antibodies against T18 (a–c). Cells expressing T18 were used as positive control, while T25 alone and T25 with DrFtsZ (DrFtsZ-C25) were used as negative controls (c). Similarly, cells expressing T25 at C-termini were probed for expression of fusion proteins using T25 antibodies (d–g). Cells expressing T25 were used as positive control, while those expressing T18 or DrFtsA-C18 were used as negative controls (d). The size of fused proteins was compared with different molecular weight markers (M). Data shown are representative of a reproducible experiment repeated two times independently.

as detected by blue colour colonies as well as β-galactosidase activity in solution (Fig. 2). For example, DrFtsA-C25 co-expression with —DrFtsA-C18 and N25-DrFtsZ co-expression with DrFtsZ-C18 produced blue colour colonies and high levels of β-galactosidase (Fig. 2). Similarly, the cells co-expressing DrFtsZ-C25 with DrFtsA-C18 (Fig. 2)/ N18-DrFtsA (Table S3) showed β-galactosidase expression. However, in a majority of the cases, co-expression of target proteins including DrFtsZ with DrFtsQ, when fused with either tags did not induce reporter gene expression significantly (Table S3). These results indicated that DrFtsZ and DrFtsA proteins form at least homodimers as well as interacting with each other. Since, the position of T18/T25 tags at N- or C-termini in the proteins is known to affect their possible interactions, the possibility of the tag position affecting target proteins' interaction and, therefore, resulting in no induction of β-galactosidase expression in some combinations would be worth investigating. To address this, both T18 and T25 tags were fused at the N- as well as the C-terminus in the majority of the 'DrFts' proteins. These were co-expressed in different combinations and development of blue colour colonies and the inducible expression of β-galactosidase were monitored.

DrFtsA-C18 interacted with DrFtsE-C25, N25-DrFtsK and DrFtsW-C25 (Fig. 3) as well as with N25-DrFtsW (Table S3). However, when T25 was placed at the N-terminus of DrFtsE (N25-DrFtsE) and C-terminus of DrFtsK (DrFtsK-C25), the co-expression of proteins with DrFtsA-C18 did not induce β-galactosidase expression in BTH101 (Fig. 3). Similarly, DrFtsE-C18 showed interaction with N25-DrFtsW (Fig. 3), while DrFtsE-C18 was not observed to interact with DrFtsW-C25. N18-DrFtsE interacted poorly with DrFtsW having T25 at either end (Table S3). But the co-expression of N25-DrFtsZ with DrFtsW-C18 did not induce β-galactosidase expression at least in BTH101 background (Table S3). Interaction of DrFtsQ with DrFtsA was

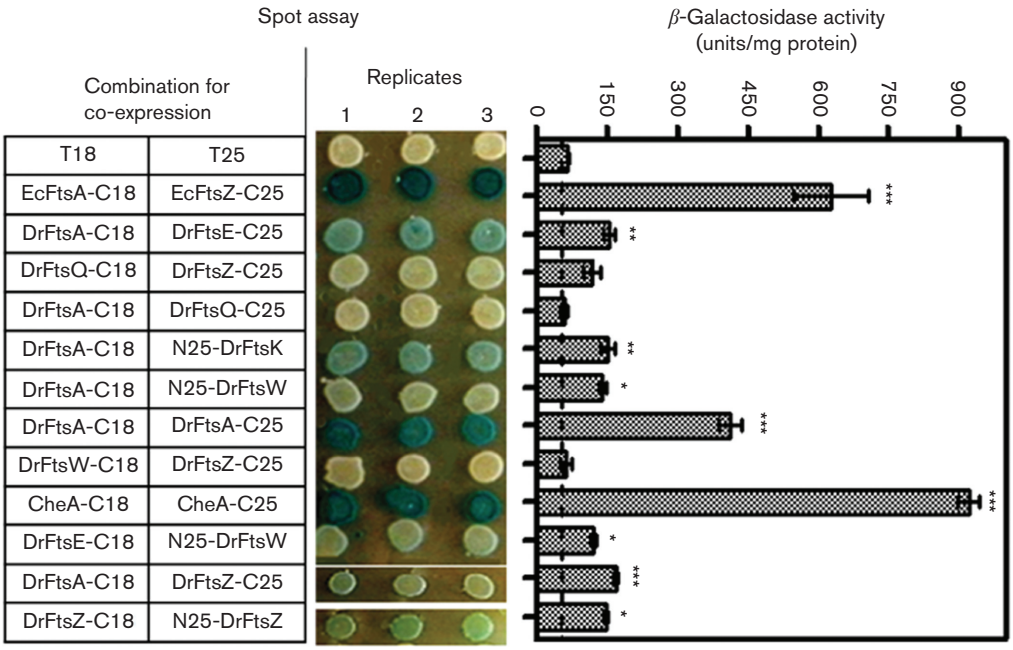

T18	T25
EcFtsA-C18	EcFtsZ-C25
DrFtsA-C18	DrFtsE-C25
DrFtsQ-C18	DrFtsZ-C25
DrFtsA-C18	DrFtsQ-C25
DrFtsA-C18	N25-DrFtsK
DrFtsA-C18	N25-DrFtsW
DrFtsA-C18	DrFtsA-C25
DrFtsW-C18	DrFtsZ-C25
CheA-C18	CheA-C25
DrFtsE-C18	N25-DrFtsW
DrFtsA-C18	DrFtsZ-C25
DrFtsZ-C18	N25-DrFtsZ

Fig. 2. *In vivo* interaction of divisome components of *D. radiodurans*. *E. coli* BTH101 cells co-expressing 'Fts' proteins tagged with T18/T25 at either terminals as required, in different combinations were checked for the expression of β-galactosidase activity both by spot assay and in liquid culture. Cells co-expressing T18 or T25 tag on vectors were used as negative control while *E. coli* FtsA (EcFtsA-C18) with *E. coli* FtsZ (EcFtsZ-C25) as well as chemotaxis protein (CheA-C18 with CheA-C25) were used as positive control. β-Galactosidase activity (units/mg protein) is shown here as mean±SD (n=9) and the significance of the possible difference was analysed using Student's t-test, and P values, obtained at 95 % confidence intervals, are shown as (*) for <0.05, (**) for <0.01 and (***) for <0.001. Total results obtained in several other combinations are provided in supplementary materials (Table S3).

also checked by co-expressing these two proteins in all possible combinations. DrFtsQ having T25/T18 at the C-terminus when co-expressed with DrFtsA-C18 did not induce expression of β-galactosidase (Table S3). These results suggested that many of the cell division proteins of *D. radiodurans* interact with each other as assayed in *E. coli*. However, some expected interactions were not observed in BACTH analysis. Since, BTH is known to give false positive and false negative results it could explain the lack of some of the expected interactions.

Cell division spatial regulatory proteins (Min) interact selectively

Likewise, interaction of DrMinC, DrMinD and DrDivIVA among each other was also monitored using the BACTH system. Results showed self-interaction of DrMinC, DrMinD and DrDivIVA fused with T18 and T25 tags, respectively, as well as DrMinC-C18 interaction with DrMinD-C25 (Fig. 4). However, the levels of interactions vary depending upon the tag's position in these proteins (Fig. 3). Interestingly, DrMinC-C18 co-expression with DrDivIVA in all four combinations could induce β-galactosidase expression, which was not observed when DrMinD was co-expressed with DrDivIVA (Table S4). This suggested that DrMinC, DrMinD and DrDivIVA at least form homodimers in addition to DrMinC forming heterodimers with DrMinD. Interaction of DrMinC with other two 'Min' regulatory proteins (DrMinD and DrDivIVA) may be required to bring these proteins together for their possible coordinated functions. Subsequently, these constructs of DrMinC, DrMinD and DrDivIVA were used for monitoring the interaction of these proteins with other divisome and segrosome proteins in different combinations. DrMinD tagged at different termini showed interaction with DrFtsE-C18, DrFtsA-C25 and N25-DrFtsW (Fig. 4). However, BTH101 co-expressing DrMinD-C25 with N18-DrFtsE or DrFtsE-C18, N25-DrMinD with DrFtsW tagged with T18 at either terminus as well as DrMinD-C18 with DrFtsW-C25 did not induce β-galactosidase expression (Table S5). In addition, many of these proteins co-expressed with other proteins in different combinations did not show β-galactosidase expression (Tables S4 and S5). This suggested that interactions of DrMinD with DrFtsE and DrFtsA and DrFtsW interaction with DrMinD were affected by the position of the tag in these proteins. Strikingly, DrMinC having T18 or T25 at its C-terminus interacted with some proteins but did not induce β-galactosidase expression with the majority of

divisome components tagged with either T18/T25 (Table S5). This indicated that DrMinC does not interact directly with 'DrFts' proteins, at least those monitored here, while DrMinD interacts with DrFtsE, DrFtsA and DrFtsW. Absence of interaction between DrMinC and DrFtsZ monitored as the expression of β-galactosidase is again a surprising result because MinC interaction with both FtsZ and MinD has been unambiguously reported in other microbes, albeit mostly rod-shaped bacteria (Shen & Lutkenhaus, 2011; Ghosal *et al.*, 2014). Since DrFtsZ does not interact with either DrMinD or DrMinC but shows interaction with other 'DrFts' proteins, the possibility of DrFtsZ interacting with the DrMinCD copolymer through other DrFts proteins cannot be ruled out.

Interactions of DivIVA with 'Fts' proteins have not been studied in much detail, perhaps because DivIVA is not found universally in all bacteria. Here, we monitored DrDivIVA interaction with all the 'Fts' proteins in different possible combinations. Though all the fusions of DrDivIVA interacted with at least one other protein of *D. radiodurans*, DrDivIVA co-expression with any of the 'DrFts' proteins did not induce β-galactosidase expression (Table S5). This might suggest that DrDivIVA does not interact directly with 'Fts' proteins of *D. radiodurans*. However, *D. radiodurans* also contains MinE, which appears to be truncated as compared to Min E of other bacteria (White *et al.*, 1999) but the possibility of involvement of this protein in *in vivo* interaction of the 'Min' system cannot be ruled out. Molecular mechanism(s) pertaining to roles of MinC, MinD and DivIVA roles in FtsZ localization and divisome assembly have largely been studied in rod-shaped bacteria. Further, the role of DivIVA in bacterial shape determination and genome segregation has also been shown recently (Thomaides *et al.*, 2001; Vicente & Garcia-Ovalle, 2007; Lenarcic *et al.*, 2009). Therefore, the possibility of DrDivIVA regulating cell division through the interaction of genome maintenance proteins would be worth speculating on.

Genome partitioning proteins interact *in vivo*

The *D. radiodurans* genome encodes four ParAs and 4 ParBs on different genome elements (White *et al.*, 1999). The C-terminal fusion of ParA proteins of *D. radiodurans* with T25 was made and expressed (Fig. 1). Similarly, all four ParB proteins were tagged at the C-terminus with T18 (-C18), and at the N-terminus with either T18 (N18-) and T25 (N25-) tags (Table S2). These were transformed into

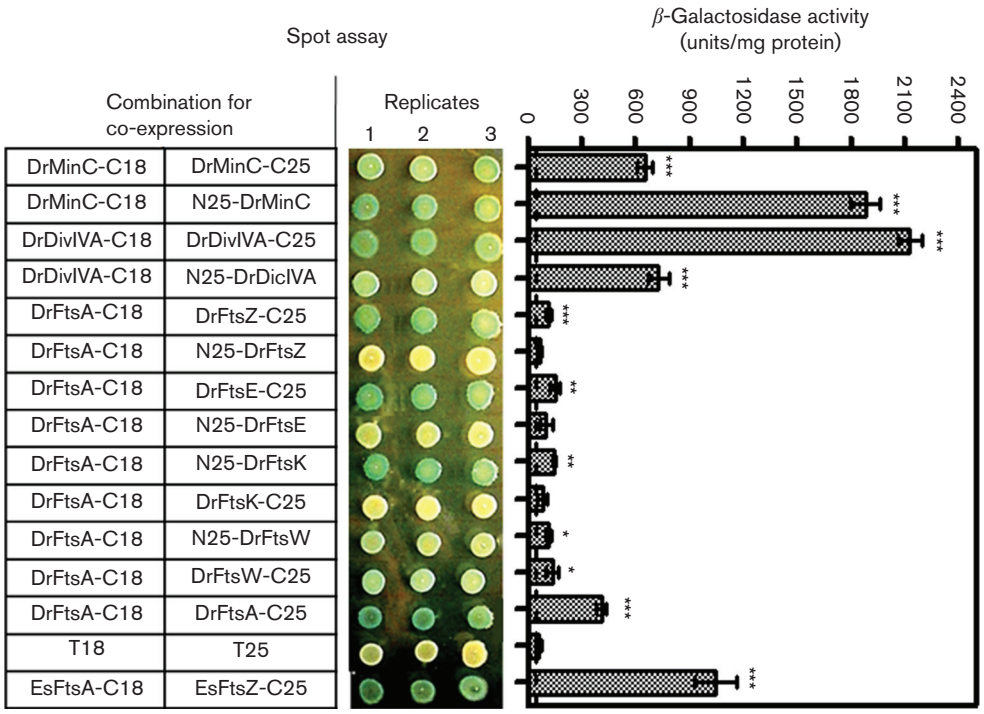

Fig. 3. Effect of BACTH tag position on protein–protein interaction. *E. coli* BTH101 cells co-expressing all the proteins tagged with T18/T25 at either terminus in different combinations were checked for the expression of β-galactosidase activity both by spot assay (a) and in liquid culture (b). Cells co-expressing T18 or T25 tag on vectors were used as negative control and *E. coli* FtsA (EcFtsA-C18) with *E. coli* FtsZ (EcFtsZ-C25) was used as positive control. β-Galactosidase activity (units/mg protein) is shown here as mean±SD (n=9) and the significance of the possible difference was analysed using Student's t-test and P values obtained at 95 % confidence intervals are shown as (*) for <0.05, (**) for <0.01 and (***) for <0.001. Total results obtained in several other combinations are provided in supplementary materials (Table S4).

BTH101 in different combinations for their co-expression and their interaction, if any, was monitored as the expression of β-galactosidase. Results showed that all four deinococcal ParBs dimerize and interestingly, ParB3 also dimerizes with other ParBs except ParB2 at least in *E. coli* (Fig. 5). Interactions of ParAs with ParBs were checked using C-terminal fusion of T25 tag with all four ParAs. ParA1-C25 showed interaction with N18-ParB1 and ParB4-C18 (additional ParB on megaplasmid). Similarly, ParA2-C25 and ParA4-C25 interacted with both the ParBs (ParB3 and ParB4) of megaplasmid, *albeit* having tags at different termini (Fig. 6). None of the other combinations of ParAs and ParBs could induce β-galactosidase expression in BTH101 (Table S6). Interactions of the megaplasmid-encoded ParB4 with both ParA1 and ParA2 chromosomal ParAs are notable. Earlier, it was shown that interaction of deinococcal ParA1 and ParB1 is required for stable maintenance of unstable *mini-F* plasmid carrying *cis* elements of *D. radiodurans* in *E. coli* (Charaka & Misra, 2012). These results suggest that all four ParBs undergo dimerization *in vivo* and ParB4 could interact with ParA1, ParA2 and ParA4 while ParB3 interacted with ParA4 alone.

Min proteins talk with Par proteins

The genome duplication followed by segregation is a prerequisite for productive cytokinesis (except in mini cell formation) and both occur in tandem. Therefore, the interdependent regulation of these processes can be partly understood if we understand the interaction of divisome proteins with genome partitioning proteins. The fusions of DrFts and DrMin proteins with T18 or T25, which had previously shown interaction with other proteins, were co-expressed with 'Par' proteins tagged with T18/T25 at their C-terminus, respectively. BTH101 cells co-expressing deinococcal ParAs and ParBs with different 'DrFts' proteins on BTH plasmids did not induce β-galactosidase expression (data not shown). However, *in vivo* interactions of certain 'Min' proteins with a few 'Par' proteins were observed (Fig. 7). For example, N25-DrMinC showed interaction with ParB1 and ParB3. Similarly, DrDivIVA having T18 or T25 tags on different termini interacted with ParA2, ParA3 and ParA4 as well as with ParB1, ParB3 and ParB4 (Fig. 6). However, the co-expression of DrMinC with ParB2, ParB4 and all four ParAs, DrDivIVA with ParA1 and ParB3 and of DrMinD with all the segrosome proteins in different combinations did not induce β-galactosidase expression (Table S7). This indicated that DrMinC and DrDivIVA talk to some of the 'Par' proteins of this bacterium while DrMinD does not do so with any of them. Further, DrMinD interaction with some of the 'DrFts' proteins as well as DrMinC and DrDivIVA interaction with 'Par' proteins together indicated the possible crosstalk between divisome and genome segregation complexes in the regulation of cell division in *D. radiodurans*.

PprA interacts with ParA but not cell division proteins

PprA, a pleiotropic protein associated with radiation resistance in *D. radiodurans* is found to be unique to the members of the *Deinococcaceae* family. The role of PprA in cell division and genome segregation has been reported in *D. radiodurans* (Devigne *et al.*, 2013; Kota *et al.*, 2014a). In

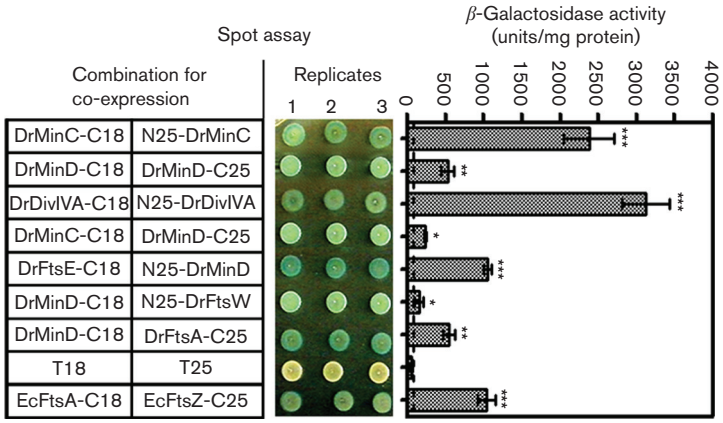

Fig. 4. Interaction of DrMin proteins with cell division proteins of *D. radiodurans*. The T18 or T25 tags fused to DrMinC (DrMin-C18/DrMin-C25), DrMinD (DrMinD-C18/DrMinD-C25/N25-DrMinD) and DrDivIVA (DrDivIVA-C18/N25-DrDivIVA) regulatory proteins and cell division proteins DrFtsA (DrFtsA-C25), DrFtsE (DrFtsE-C18) and DrFtsW (N25-DrFtsW) were co-expressed in *E. coli* BTH101 in different combinations. Expression of β-galactosidase activity was monitored both by spot assay (a) and in liquid culture (b). Cells co-expressing T18 or T25 tag on vectors were used as negative control, while *E. coli* FtsA (EcFtsA-C18) with *E. coli* FtsZ (EcFtsZ-C25) were used as positive control. β-Galactosidase activity (units/mg protein) is shown here as mean±SD (n=9) and the significance of the possible difference was analysed using Student's t-test, and P values obtained at 95 % confidence intervals are shown as (*) for <0.05, (**) for <0.01 and (***) for <0.001. Total results obtained in several other combinations are provided in supplementary materials (Table S5).

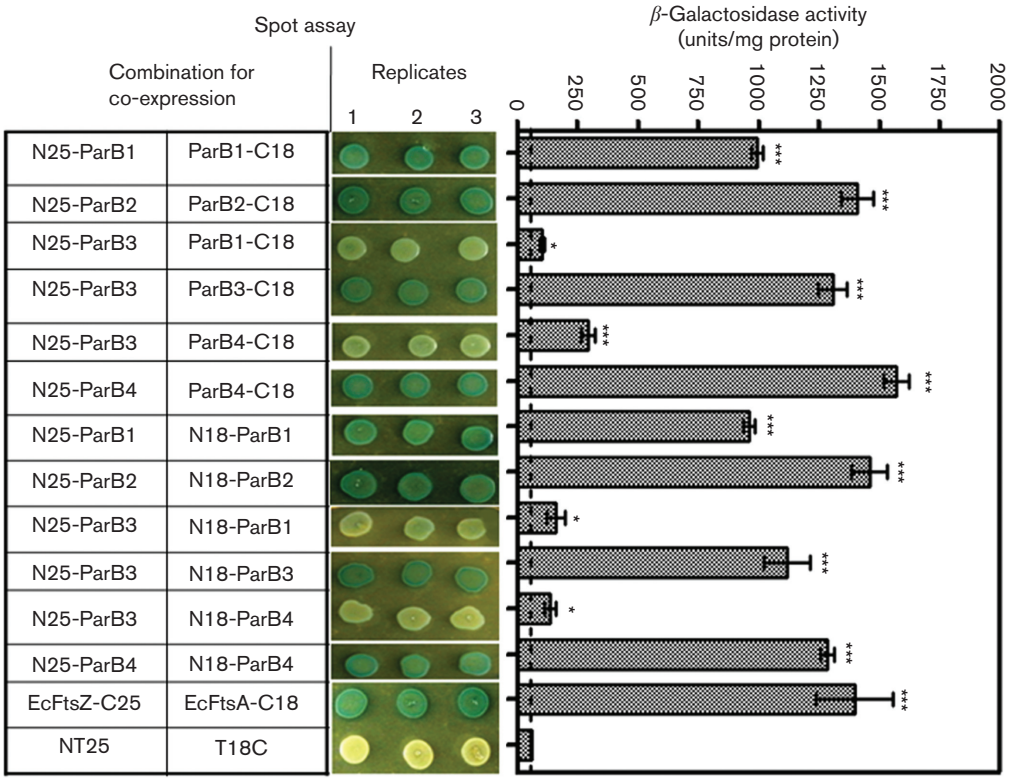

Fig. 5. *In vivo* interaction of genome partitioning proteins ParBs of *D. radiodurans*. *E. coli* BTH101 cells co-expressing T18 or T25 fusions of ParB1, ParB2, ParB3 and ParB4 in different combinations were checked for the expression of β-galactosidase both by spot assay (a) and in liquid culture (b). Vector expressing either T18 or T25 tag was used as negative control while *E. coli* FtsA (EcFtsA-C18) with *E. coli* FtsZ (EcFtsZ-C25) was used as positive control. β-Galactosidase activity (units/mg protein) is shown here as mean±SD (n=9) and the significance of the possible difference was analysed using Student's t-test, and P values obtained at 95 % confidence intervals are shown as (*) for <0.05 and (***) for <0.001. Data obtained from other combinations of different ParB proteins are shown in supplementary materials (Table S6).

order to get mechanistic insights on PprA function(s) in cell division and genome segregation. Interactions of PprA with all the cell division proteins including DrFtsZ and DrFtsA and 'Par' proteins were monitored using the BACTH system. Cells co-expressing PprA-C18 with either ParA1-C25 or ParA4-C25 expressed significantly high levels of β-galactosidase activity (Fig. 8). The levels of β-galactosidase activity in cells co-expressing PprA-C18 with ParA2-C25 or ParA3-C25 were low as compared to ParA1-C25 with ParA4-C25 but significantly more than vector control (Fig. 8). Notably, PprA-C18 did not show interaction with some of the 'Fts' and 'Min' proteins tested in different combinations (Table S9). However, the expression of β-galactosidase was not observed in cases where PprA-C25/PprA-C18 were co-expressed with any one of the four ParBs (Table S8) as well as in cases where ParBs were co-expressed with Min system proteins or Fts proteins (Table S10). These results suggested that PprA plays a role in genome partitioning and cell division perhaps by directly interacting with ParAs and indirectly with DrDivIVA, through ParA.

Co-immunoprecipitation confirmed *in vivo* interaction of deinococcal proteins

The results obtained from BACTH analyses indicated possible *in vivo* interaction of different cell division and genome segregation proteins of *D. radiodurans*. Some of these results were further confirmed by co-IP using antibodies against T25 (fused with one partner) followed by detection of the interacting partner using antibodies against T18 (fused with other partners) as described in Methods. This study reports a huge number of interactions between 'Fts', 'Min', 'Par' and PprA proteins. Although, it is possible to conduct co-IPs for all the tested interactions, we understandably decided to select a few representative samples expressing different levels of β-galactosidase activity. All the samples were qualitatively divided into three categories, i.e. strong, weak and no interactions. A few representatives from each category that were also to be further studied independently were selected. For instance, DrFtsZ-C25 with DrFtsA-C18, ParA2/ParA3/ParB1 with DrDivIVA, PprA with ParA4 represented strong interaction; DrFtsW with

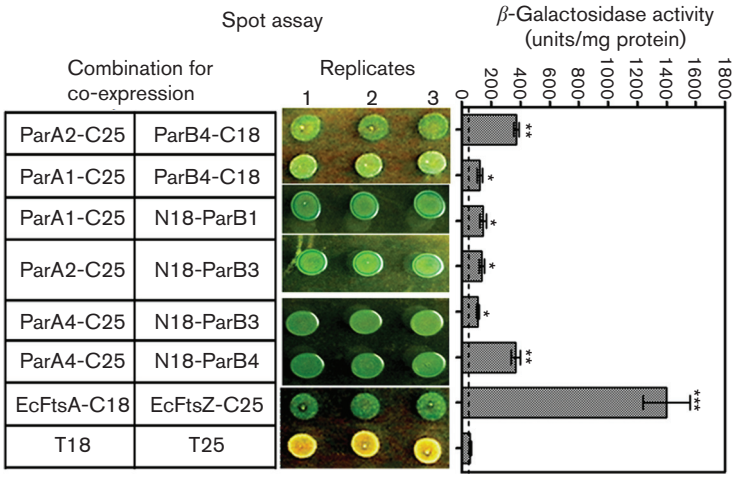

Fig. 6. *In vivo* interaction of different genome partitioning proteins ParAs and ParBs of *D. radiodurans*. *E. coli* BTH101 cells co-expressing T18 or T25 fusion of ParA1 (ParA1-C25), ParA2 (ParA2-C25), ParA3 (ParA3-C25), ParA4 (ParA4-C25), and ParB1, ParB2, ParB3 and ParB4 tagged with T18 and T25 at either terminus in different combinations was checked for the expression of β-galactosidase both by spot assay (a) and in liquid culture (b). Vector expressing either T18 or T25 tag was used as negative control while *E. coli* FtsA (EcFtsA-C18) with *E. coli* FtsZ (EcFtsZ-C25) was used as positive control. β-Galactosidase activity (units/mg protein) is shown here as mean±SD (n=9) and the significance of the possible difference was analysed using Student's t-test, and P values obtained at 95 % confidence intervals are shown as (*) for <0.05, (**) for <0.01 and (***) for <0.001. Data obtained from other combinations of ParA and ParB proteins are shown in supplementary materials (Table S6).

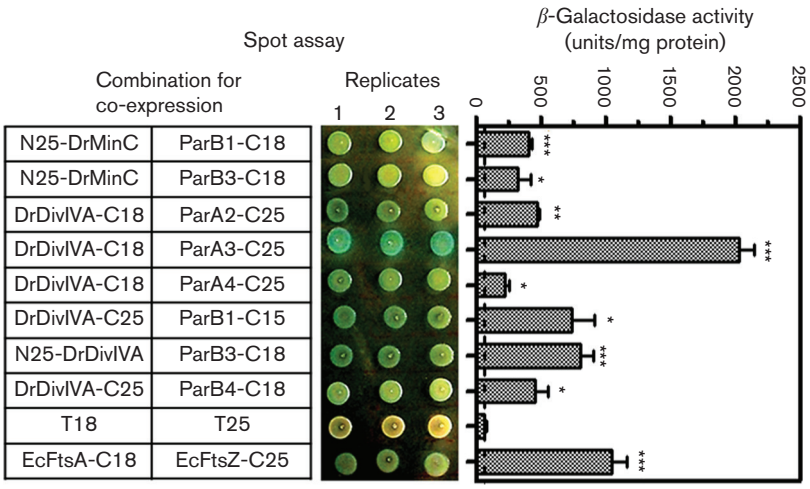

Fig. 7. *In vivo* interaction of cell division regulatory proteins with genome partitioning proteins of *D. radiodurans*. The genome partitioning proteins ParB1 (ParB1-C18), ParB3 (ParB3-C18), ParB4 (ParB4-C18), ParA2 (ParA2-C25), ParA3 (ParA3-C25) and ParA4 (ParA4-C25) were co-expressed with DrMinC (DrMinC-C25) and DrDivIVA (DrDivIVA-C18/DrDivIVA-C25/N25-DrDivIVA) in different combinations. Expression of β-galactosidase was monitored both by spot assay (a) and in liquid culture (b). Vector expressing either T18 or T25 tag was used as negative control while *E. coli* FtsA (EcFtsA-C18) with *E. coli* FtsZ (EcFtsZ-C25) was used as positive control. β-Galactosidase activity (units/mg protein) is shown here as mean±SD (n=9) and the significance of the possible difference was analysed using Student's t-test, and P values obtained at 95 % confidence intervals are shown as (*) for <0.05, (**) for <0.01 and (***) for <0.001. Data obtained from other possible combinations of Par proteins and Min proteins are provided as supplementary materials (Table S7).

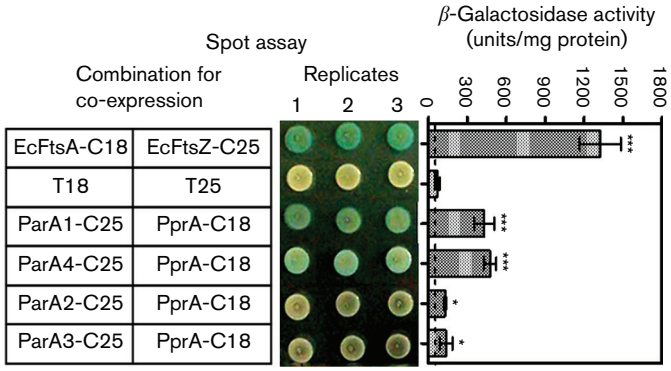

Fig. 8. *In vivo* interaction of genome partitioning proteins with PprA of *D. radiodurans*. *E. coli* BTH101 cells co-expressing ParA1 (ParA1-C25), ParA2 (ParA2-C25), ParA3 (ParA3-C25) or ParA4 (ParA4-C25) with PprA (PprA-C18) were checked for expression of β-galactosidase both by spot assay (a) and in liquid culture (b). Vector expressing either T18 or T25 tag was used as negative control while *E. coli* FtsA (EcFtsA-C18) with *E. coli* FtsZ (EcFtsZ-C25) was used as positive control. β-Galactosidase activity (units/mg protein) is shown here as mean±SD (n=9) and the significance of the possible difference was analysed using Student's t-test, and P values obtained at 95 % confidence intervals are shown as (*) for <0.05 and (***) for <0.001. Data obtained from various other possible combinations are shown in supplementary materials (Tables S8, S9 and S10).

DrFtsE, ParA2 with ParB4, DrMinD with DrFtsE represented weak interactions; and DrFtsA with ParB1, PprA with ParB1 and T18 with T25 represented no interaction categories. Cell-free extracts of such cells were incubated with polyclonal antibodies against T25 and immunoblotted using monoclonal antibodies against T18. The polyclonal antibodies against T25, which also showed specific hybridization in Western blotting (Fig. 1), did not immunoprecipitate T18 fused target proteins in the absence of T25 tagged partner or in the absence of interaction. On the other hand, T25 antibodies could immunoprecipitate T18 tagged proteins and the expected size fusion protein bands were detected in samples expressing β-galactosidase (Fig. 9). The signal intensities were also found to be nearly proportional to the levels of β-galactosidase expression. The combinations not supporting reporter gene (*lacZ*) expression also did not show any hybridization signal with anti-T18 monoclonal antibodies (Fig. 9). Absence of signals on using T18 antibodies in controls expressing only T18 fused proteins and its presence in samples expressing both T25 and T18 fused proteins, which also expressed β-galactosidase activity, further suggested a strong correlation between partners' interaction and β-galactosidase activity levels. These results indicated, though indirectly, that various proteins that showed *in vivo* interaction of divisome and segrosome proteins of *D. radiodurans* as demonstrated using BACTH system in BTH101 are true interacting partners, at least in the synthetic *E. coli* system.

DISCUSSION

D. radiodurans is a Gram-positive round-shaped radioresistant bacterium, which divides in alternate planes with a doubling time of ~90 min under normal growth conditions in a rich medium (Harris *et al.*, 2004). Earlier, bacterial cell division was studied mostly in rod-shaped/filamentous bacteria, which apparently have well-defined poles. In such cases, the regulation of FtsZ localization in mid cell position and the polarity for genome segregation could be better modelled and explained. In cocci, however, these aspects are not clearly understood, except that the second division is perpendicular to first plane of cell division in *Staphylococcus*-like bacteria. Here, we made translational fusions of almost all annotated cell division proteins ('Fts' and 'Min'), 'Par' proteins and PprA of *D. radiodurans*, with T25 and T18 in different combinations. Although this study has ascertained all the possible interactions of cell division proteins by taking into consideration a majority of the combinations of cell division proteins, the possibility of some of these interactions being affected by the position and size of the tags as well as the differences in the microenvironment of *D. radiodurans* and *E. coli* cannot be ruled out. The poor interaction of DrFtsA with DrFtsZ in *E. coli* background as reported earlier has been attributed to the differences in the microenvironment between *E. coli* and *D. radiodurans* (Modi & Misra 2014). Absence of interactions of some of the *D. radiodurans* proteins came as a surprise because such interactions are conserved in other bacteria. For example, interaction of FtsA with FtsQ has been found functionally critical in the assembly of FtsK, FtsL and FtsB components in the divisome of other bacteria (Buddelmeijer & Beckwith, 2002; Gonzalez & Beckwith, 2009). The results presented here clearly indicated that DrFtsA, DrFtsZ, DrFtsE, DrFtsK and DrFtsW proteins interact with their respective partners at least in *E. coli*. Several of these interactions amongst the divisome, segrosome and 'Min' system

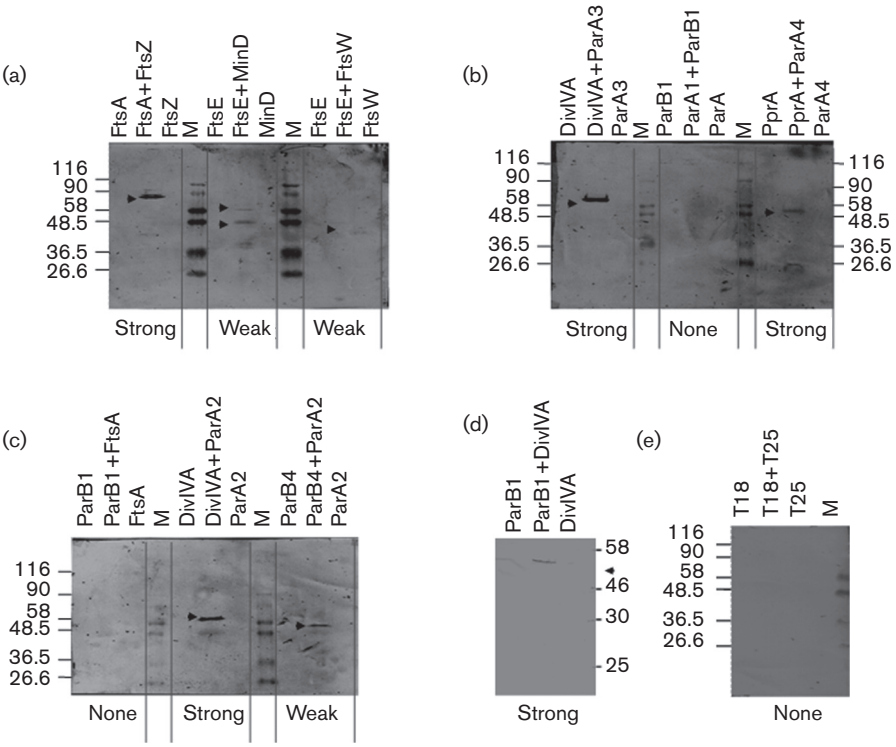

Fig. 9. Co-immunoprecipitation of proteins of the cells expressing target proteins using T25 antibodies. Total interactions were qualitatively divided into three categories like relatively strong interaction (Strong), weak interaction (Weak) and no interaction (None). DrFtsZ-C25 with DrFtsA-C18, ParA2-C18/ParA3-C18/ParB1-C18 with DrDivIVA-C25 and PprA-C18 with ParA4-C25 represented stronger interactions. DrFtsE-C18 interaction with DrFtsW-C25 and DrMinD-C25 and ParA2-C18 with ParB4-C25 represented a relatively weaker interaction while DrFtsA-C18 with ParB1-C25, PprA-C18 with ParB1-C25 and T18 tag and T25 tag co-expression represented non-interacting partners. Total proteins of the cells expressing either one of these partners or both the partners were immunoprecipitated using polyclonal antibodies against T25, and the interacting partner was immunodetected using monoclonal antibodies against T18. The sizes of the signals represent the size of target proteins fused with T18. Data shown here are the representatives of the reproducible experiments repeated two times.

components of *D. radiodurans* have been depicted diagrammatically (Fig. 10).

Here, we observed that several cell division, genome segregation and regulatory proteins of *D. radiodurans* interact in synthetic *E. coli* expressing recombinant proteins on multicopy plasmids. For example, the absence of interaction among the following proteins: (1) DrDivIVA with DrMinD, (2) DrMinD with 'Par' proteins and (3) none of the 'DrMin' proteins with DrFtsZ, is intriguing. On the other hand, interaction of DrMinC and DrDivIVA with a few 'Par' proteins (Fig. 10d) and interaction of DrMinD directly with DrFtsA, DrFtsW and DrFtsE (Fig. 10e) also suggest the possibility of different mechanism(s) of 'Min' proteins regulation in septum site selection in *D. radiodurans*. Earlier, interaction of MinC with both MinD and DrFtsZ in *E. coli* (Shen & Lutkenhaus, 2011; Ghosal *et al.*, 2014), interaction of DivIVA with ParB in *Corynebacterium glutamicum*, Wag31 (DivIVA homologue) of *Mycobacterium tuberculosis* and DivIVA of *Streptomyces coelicolor* with its ParB in synthetic *E. coli* (Donovan *et al.*, 2012) have already been demonstrated. Similarly, in *M. smegmatis*, Wag31 and ParA co-localization at poles (Ginda *et al.*, 2013) and effect of *minD* mutation on Soj protein (ParA homologue) and localization at poles in *B. subtilis* (Autret & Errington, 2003; Marston *et al.*, 1998) are other examples that suggest interaction of the Min system with the genome partitioning system in bacteria. Therefore, interactions of DrMinC and DrDivIVA with 'Par' proteins as demonstrated here indicate the importance of these interactions in the regulation of cell division and genome segregation in this bacterium. The functional significance of the interaction of 'Min' proteins with 'Par' proteins is not clear yet. However, it has been shown that MinC-MinD dimers localize at the septum site towards the late stage of cell division, and thus, predetermine the poles for the next cycle of cell division in some bacteria (Treuner-Lange & Søgaard-Andersen, 2014). DivIVAs from several bacteria have been shown to interact with their cognate ParB and RodA and co-localize at the poles in respective hosts (Laloux & Jacobs-Wagner, 2014; Sieger & Bramkamp, 2015). Our results provided evidence of such

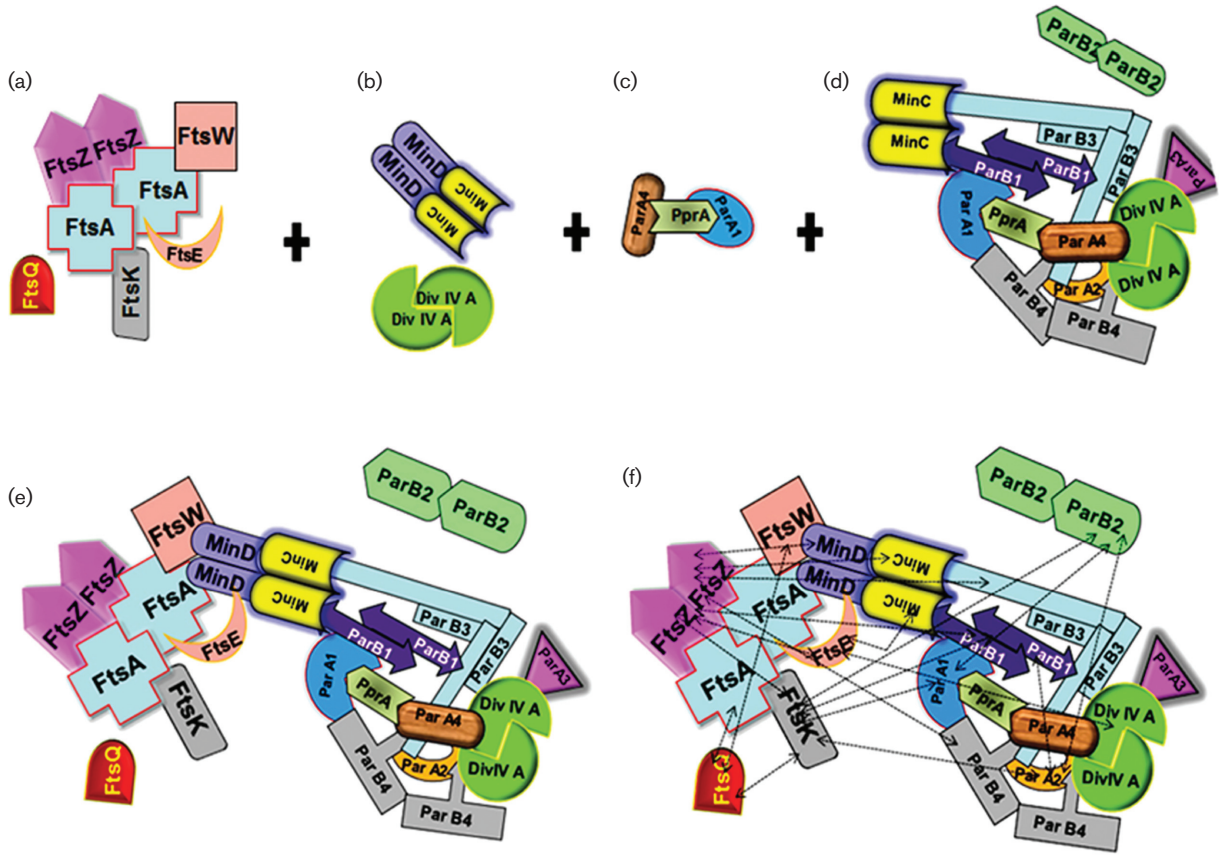

Fig. 10. Diagrammatic representation of cell division and genome segregation multiprotein complexes of *D. radiodurans*. The core components of cell division (a), Min system proteins (b), Par proteins with PprA (c) and Par proteins with PprA and Min system proteins (d) of *D. radiodurans* in *in vivo* interaction with their partners are shown. Integrating all four independent proteins complexes through some common partners yielded a higher order multiprotein complex of divisome and segrosome (e). Some of the components studied here, which have not shown *in vivo* interaction directly, are actually the STRING partners reported in other bacteria and therefore shown through dotted lines (f).

interactions in *D. radiodurans* also. Since the poles in cocci including *D. radiodurans* are not predefined, the possibility that interactions of DrDivIVA and DrMinC with Par proteins may somehow help this bacterium in determining the next plane of cell division would be worth speculating on.

Since PprA is found to be involved in cell division and genome maintenance in *D. radiodurans*, its interaction with cell division and genome partitioning proteins was investigated. Interactions of PprA with 'Fts' proteins were not observed using the BACTH system (Table S9). However, PprA did show interaction with ParA homologues of *D. radiodurans* (Fig. 10c). ParAs also showed interaction with 'DrMin' proteins (Fig. 10d). Earlier, BACTH analyses have been used for determining cell division and interaction of genome maintenance proteins and the results have been validated by other approaches (Karimova *et al.*, 2005).

Furthermore, we demonstrated by BACTH analyses and co-IP that a large number of *D. radiodurans* proteins whose homologues have roles in cell division and genome maintenance in other bacteria do not interact in *E. coli* as host (Tables S3–S9). The reason for this is not clear yet. However, it is important to know that BACTH analysis can give false positive and false negative results, which may have influenced some interactions. Additionally, there are other factors that can also influence interaction of deinococcal proteins in *E. coli*. These could be (i) the competition by *E. coli* homologues of many of these proteins, (ii) the effect of phosphorylation by serine/threonine protein kinases (S/TPKs) on the interaction of deinococcal proteins and (iii) the absence of some other deinococcal proteins that are required for interaction of these proteins in *E. coli*. The *D. radiodurans* genome encodes a large number of S/TPKs (White *et al.*, 1999). One such S/TPK (RqkA) has been characterized and its role in radioresistance and DSB repair has been demonstrated in *D. radiodurans* (Rajpurohit & Misra, 2010). Recently, it has been shown that RqkA plays a role in radiation resistance through phosphorylation-mediated

activity modulation of DNA repair proteins (Rajpurohit & Misra, 2013). We have also shown earlier, that DrFtsZ interaction with DrFtsA is less efficient compared to DrFtsZ interaction with EcFtsA in *E. coli* as host (Modi & Misra, 2014). The effect of phosphorylation of genome partitioning proteins by S/T protein kinase on functions of these proteins has also been demonstrated in *M. tuberculosis* (Baronian *et al.*, 2015). Since we know that RqkA could phosphorylate a few other *D. radiodurans* cell division and genome segregation proteins *in vitro* (H. S. Misra and colleagues, unpublished data), determining whether any of these factors affect the interaction of *D. radiodurans* proteins in *E. coli* would be worth speculating on and investigating independently.

In summary, using the bacterial two-hybrid system and co-IP, we showed that divisome, segrosome and cell division regulatory proteins of *D. radiodurans* when overexpressed from the plasmids interact with each other, which possibly suggests the formation of multiprotein complexes of such deinococcal proteins, at least in *E. coli*. Such macromolecular complexes appear to interact with each other through cell division regulatory proteins like PprA and 'Min' proteins of *D. radiodurans* and may play important roles in interdependent regulation of cell division and genome segregation in this bacterium.

ACKNOWLEDGEMENTS

The authors are grateful to Professor S. Chattopadhyay for his constant support and encouragement. We thank Dr Chitra Seetharam Misra and Dr Swathi Kota for technical comments in the manuscript. G. K. M. and K. M. are grateful to the Department of Atomic Energy, Government of India for research fellowships.

REFERENCES

Autret, S. & Errington, J. (2003). A role for division-site-selection protein MinD in regulation of internucleoid jumping of Soj (ParA) protein in *Bacillus subtilis*. *Mol Microbiol* **47**, 159–169.

Bailey, M. W., Bisicchia, P., Warren, B. T., Sherratt, D. J. & Männik, J. (2014). Evidence for divisome localization mechanisms independent of the Min system and SlmA in *Escherichia coli*. *PLoS Genet* **10**, e1004504.

Baronian, G., Ginda, K., Berry, L., Cohen-Gonsaud, M., Zakrzewska-Czerwińska, J., Jakimowicz, D. & Molle, V. (2015). Phosphorylation of *Mycobacterium tuberculosis* ParB participates in regulating the ParABS chromosome segregation system. *PLoS One* **10**, e0119907.

Battesti, A. & Bouveret, E. (2012). The bacterial two-hybrid system based on adenylate cyclase reconstitution in *Escherichia coli*. *Methods* **58**, 325–334.

Battista, J. R., Park, M. J. & McLemore, A. E. (2001). Inactivation of two homologues of proteins presumed to be involved in the desiccation tolerance of plants sensitizes *Deinococcus radiodurans* R1 to desiccation. *Cryobiology* **43**, 133–139.

Bigot, S., Sivanathan, V., Possoz, C., Barre, F. X. & Cornet, F. (2007). FtsK, a literate chromosome segregation machine. *Mol Microbiol* **64**, 1434–1441.

Buddelmeijer, N. & Beckwith, J. (2002). Assembly of cell division proteins at the *E. coli* cell center. *Curr Opin Microbiol* **5**, 553–557.

Charaka, V. K. & Misra, H. S. (2012). Functional characterization of the role of the chromosome I partitioning system in genome segregation in *Deinococcus radiodurans*. *J Bacteriol* **194**, 5739–5748.

Cho, H., McManus, H. R., Dove, S. L. & Bernhardt, T. G. (2011). Nucleoid occlusion factor SlmA is a DNA-activated FtsZ polymerization antagonist. *Proc Natl Acad Sci U S A* **108**, 3773–3778.

Conti, J., Viola, M. G. & Camberg, J. L. (2015). The bacterial cell division regulators MinD and MinC form polymers in the presence of nucleotide. *FEBS Lett* **589**, 201–206.

Devigne, A., Mersaoui, S., Bouthier-de-la-Tour, C., Sommer, S. & Servant, P. (2013). The PprA protein is required for accurate cell division of γ-irradiated *Deinococcus radiodurans* bacteria. *DNA Repair* **12**, 265–272.

Devigne, A., Guerin, P., Lisboa, J., Quevillon-Cheruel, S., Armengaud, J., Sommer, S., Bouthier de la Tour, C. & Servanta, P. (2016). PprA protein is involved in chromosome segregation via its physical and functional interaction with DNA gyrase in irradiated *Deinococcus radiodurans* bacteria. *Mol Biol Physiol* **1**, e00036–15.

Di Lallo, G., Fagioli, M., Barionovi, D., Ghelardini, P. & Paolozzi, L. (2003). Use of a two-hybrid assay to study the assembly of a complex multicomponent protein machinery: bacterial septosome differentiation. *Microbiology* **149**, 3353–3359.

Donovan, C., Sieger, B., Krämer, R. & Bramkamp, M. (2012). A synthetic *Escherichia coli* system identifies a conserved origin tethering factor in Actinobacteria. *Mol Microbiol* **84**, 105–116.

Ebersbach, G. & Gerdes, K. (2001). The double par locus of virulence factor pB171: DNA segregation is correlated with oscillation of ParA. *Proc Natl Acad Sci U S A* **98**, 15078–15083.

Fogel, M. A. & Waldor, M. K. (2006). A dynamic, mitotic-like mechanism for bacterial chromosome segregation. *Genes Dev* **20**, 3269–3282.

Gerdes, K., Howard, M. & Szardenings, F. (2010). Pushing and pulling in prokaryotic DNA segregation. *Cell* **141**, 927–942.

Ghosal, D., Trambaiolo, D., Amos, L. A. & Löwe, J. (2014). MinCD cell division proteins form alternating copolymeric cytomotive filaments. *Nat Commun* **5**, 5341.

Ginda, K., Bezulska, M., Ziółkiewicz, M., Dziadek, J., Zakrzewska-Czerwińska, J. & Jakimowicz, D. (2013). ParA of *Mycobacterium smegmatis* co-ordinates chromosome segregation with the cell cycle and interacts with the polar growth determinant DivIVA. *Mol Microbiol* **87**, 998–1012.

Goehring, N. W., Gonzalez, M. D. & Beckwith, J. (2006). Premature targeting of cell division proteins to midcell reveals hierarchies of protein interactions involved in divisome assembly. *Mol Microbiol* **61**, 33–45.

Gonzalez, M. D. & Beckwith, J. (2009). Divisome under construction: distinct domains of the small membrane protein FtsB are necessary for interaction with multiple cell division proteins. *J Bacteriol* **191**, 2815–2825.

Green, M. R. & Sambrook, J. (2012). *Molecular Cloning: A Laboratory Manual*. Cold Spring Harbor, NY: Cold Spring Harbor Laboratory Press.

Harris, D. R., Tanaka, M., Saveliev, S. V., Jolivet, E., Earl, A. M., Cox, M. & Battista, J. R. (2004). Correction: preserving genome integrity: the DdrA protein of *Deinococcus radiodurans* R1. *PLoS Biol* **4**, e385.

Ip, S. C., Bregu, M., Barre, F. X. & Sherratt, D. J. (2003). Decatenation of DNA circles by FtsK-dependent Xer site-specific recombination. *EMBO J* **22**, 6399–6407.

Karimova, G., Pidoux, J., Ullmann, A. & Ladant, D. (1998). A bacterial two-hybrid system based on a reconstituted signal transduction pathway. *Proc Natl Acad Sci U S A* **95**, 5752–5756.

Karimova, G., Ullmann, A. & Ladant, D. (2001). Protein-protein interaction between *Bacillus stearothermophilus* tyrosyl-tRNA synthetase subdomains revealed by a bacterial two-hybrid system. *J Mol Microbiol Biotechnol* **3**, 73–82.

Karimova, G., Dautin, N. & Ladant, D. (2005). Interaction network among *Escherichia coli* membrane proteins involved in cell division as revealed by bacterial two-hybrid analysis. *J Bacteriol* **187**, 2233–2243.

Kota, S., Charaka, V. K. & Misra, H. S. (2014a). PprA, a pleiotropic protein for radioresistance, works through DNA gyrase and shows cellular dynamics during postirradiation recovery in *Deinococcus radiodurans*. *J Genet* **93**, 349–354.

Kota, S., Charaka, V. K., Ringgaard, S., Waldor, M. K. & Misra, H. S. (2014b). PprA contributes to *Deinococcus radiodurans* resistance to nalidixic acid, genome maintenance after DNA damage and interacts with deinococcal topoisomerases. *PLoS One* **9**, e85288.

Kota, S., Rajpurohit, Y. S., Charaka, V. K., Satoh, K., Narumi, I. & Misra, H. S. (2016). DNA gyrase of *Deinococcus radiodurans* is characterized as Type II bacterial topoisomerase and its activity is differentially regulated by PprA in vitro. *Extremophiles* **20**, 195–205.

Laloux, G. & Jacobs-Wagner, C. (2014). How do bacteria localize proteins to the cell pole? *J Cell Sci* **127**, 11–19.

Lenarcic, R., Halbedel, S., Visser, L., Shaw, M., Wu, L. J., Errington, J., Marenduzzo, D. & Hamoen, L. W. (2009). Localisation of DivIVA by targeting to negatively curved membranes. *EMBO J* **28**, 2272–2282.

Lutkenhaus, J. (2007). Assembly dynamics of the bacterial MinCDE system and spatial regulation of the Z ring. *Annu Rev Biochem* **76**, 539–562.

Marston, A. L., Thomaides, H. B., Edwards, D. H., Sharpe, M. E. & Errington, J. (1998). Polar localization of the MinD protein of *Bacillus subtilis* and its role in selection of the mid-cell division site. *Genes Dev* **12**, 3419–3430.

Massey, T. H., Aussel, L., Barre, F. X. & Sherratt, D. J. (2004). Asymmetric activation of Xer site-specific recombination by FtsK. *EMBO Rep* **5**, 399–404.

Massey, T. H., Mercogliano, C. P., Yates, J., Sherratt, D. J. & Löwe, J. (2006). Double-stranded DNA translocation: structure and mechanism of hexameric FtsK. *Mol Cell* **23**, 457–469.

Minton, K. W. (1994). DNA repair in the extremely radioresistant bacterium *Deinococcus radiodurans*. *Mol Microbiol* **13**, 9–15.

Misra, H., Rajpurohit, Y. S. & Kota, S. (2013). Physiological and molecular basis of extreme radioresistance in *Deinococcus radiodurans*. *Curr Sci* **104**, 194–206.

Modi, K. & Misra, H. S. (2014). Dr-FtsA, an actin homologue in *Deinococcus radiodurans* differentially affects Dr-FtsZ and Ec-FtsZ functions in vitro. *PLoS One* **9**, e115918.

Modi, K. M., Tewari, R. & Misra, H. S. (2014). FtsZDr, a tubulin homologue in radioresistant bacterium *Deinococcus radiodurans* is characterized as a GTPase exhibiting polymerization/depolymerization dynamics *in vitro* and FtsZ ring formation *in vivo*. *Int J Biochem Cell Biol* **50**, 38–46.

Mohl, D. A., Easter, J. & Gober, J. W. (2001). The chromosome partitioning protein, ParB, is required for cytokinesis in *Caulobacter crescentus*. *Mol Microbiol* **42**, 741–755.

Narumi, I., Satoh, K., Cui, S., Funayama, T., Kitayama, S. & Watanabe, H. (2004). PprA: a novel protein from *Deinococcus radiodurans* that stimulates DNA ligation. *Mol Microbiol* **54**, 278–285.

Rajpurohit, Y. S. & Misra, H. S. (2010). Characterization of a DNA damage-inducible membrane protein kinase from *Deinococcus radiodurans* and its role in bacterial radioresistance and DNA strand break repair. *Mol Microbiol* **77**, 1470–1482.

Rajpurohit, Y. S. & Misra, H. S. (2013). Structure-function study of deinococcal serine/threonine protein kinase implicates its kinase activity and DNA repair protein phosphorylation roles in radioresistance of *Deinococcus radiodurans*. *Int J Biochem Cell Biol* **45**, 2541–2552.

Ringgaard, S., Schirner, K., Davis, B. M. & Waldor, M. K. (2011). A family of ParA-like ATPases promotes cell pole maturation by facilitating polar localization of chemotaxis proteins. *Genes Dev* **25**, 1544–1555.

Robichon, C., Karimova, G., Beckwith, J. & Ladant, D. (2011). Role of leucine zipper motifs in association of the *Escherichia coli* cell division proteins FtsL and FtsB. *J Bacteriol* **193**, 4988–4992.

Salje, J., Gayathri, P. & Löwe, J. (2010). The ParMRC system: molecular mechanisms of plasmid segregation by actin-like filaments. *Nat Rev Microbiol* **8**, 683–692.

Schäfer, M., Schmitz, C., Facius, R., Horneck, G., Milow, B., Funken, K. H. & Ortner, J. (2000). Systematic study of parameters influencing the action of Rose Bengal with visible light on bacterial cells: comparison between the biological effect and singlet-oxygen production. *Photochem Photobiol* **71**, 514–523.

Schumacher, M. A., Piro, K. M. & Xu, W. (2010). Insight into F plasmid DNA segregation revealed by structures of SopB and SopB-DNA complexes. *Nucleic Acids Res* **38**, 4514–4526.

Shebelut, C. W., Guberman, J. M., van Teeffelen, S., Yakhnina, A. A. & Gitai, Z. (2010). *Caulobacter* chromosome segregation is an ordered multistep process. *Proc Natl Acad Sci U S A* **107**, 14194–14198.

Shen, B. & Lutkenhaus, J. (2011). Differences in MinC/MinD sensitivity between polar and internal Z rings in *Escherichia coli*. *J Bacteriol* **193**, 367–376.

Sieger, B. & Bramkamp, M. (2015). Interaction sites of DivIVA and RodA from *Corynebacterium glutamicum*. *Front Microbiol* **5**, 738.

Slade, D. & Radman, M. (2011). Oxidative stress resistance in *Deinococcus radiodurans*. *Microbiol Mol Biol Rev* **75**, 133–191.

Thanbichler, M. (2010). Synchronization of chromosome dynamics and cell division in bacteria. *Cold Spring Harb Perspect Biol* **2**, a000331.

Thomaides, H. B., Freeman, M., El Karoui, M. & Errington, J. (2001). Division site selection protein DivIVA of *Bacillus subtilis* has a second distinct function in chromosome segregation during sporulation. *Genes Dev* **15**, 1662–1673.

Tonthat, N. K., Arold, S. T., Pickering, B. F., Van Dyke, M. W., Liang, S., Lu, Y., Beuria, T. K., Margolin, W. & Schumacher, M. A. (2011). Molecular mechanism by which the nucleoid occlusion factor, SlmA, keeps cytokinesis in check. *EMBO J* **30**, 154–164.

Treuner-Lange, A. & Søgaard-Andersen, L. (2014). Regulation of cell polarity in bacteria. *J Cell Biol* **206**, 7–17.

Vecchiarelli, A. G., Han, Y. W., Tan, X., Mizuuchi, M., Ghirlando, R., Biertümpfel, C., Funnell, B. E. & Mizuuchi, K. (2010). ATP control of dynamic P1 ParA-DNA interactions: a key role for the nucleoid in plasmid partition. *Mol Microbiol* **78**, 78–91.

Vicente, M. & Rico, A. I. (2006). The order of the ring: assembly of *Escherichia coli* cell division components. *Mol Microbiol* **61**, 5–8.

Vicente, M. & García-Ovalle, M. (2007). Making a point: the role of DivIVA in streptococcal polar anatomy. *J Bacteriol* **189**, 1185–1188.

White, O., Eisen, J. A., Heidelberg, J. F., Hickey, E. K., Peterson, J. D., Dodson, R. J., Haft, D. H., Gwinn, M. L., Nelson, W. C. & other authors (1999). Genome sequence of the radioresistant bacterium *Deinococcus radiodurans* R1. *Science* **286**, 1571–1577.

Edited by: F. Sargent

Journal of Genetics, Vol. 97, No. 4, September 2018, pp. 1013–1038
https://doi.org/10.1007/s12041-018-0969-x

REVIEW ARTICLE

Maintenance of multipartite genome system and its functional significance in bacteria

HARI SHARAN MISRA[1,2]*, GANESH KUMAR MAURYA[1,2], SWATHI KOTA[1,2] and VIJAYA KUMAR CHARAKA[2]

[1] *Molecular Biology Division, Bhabha Atomic Research Centre, Mumbai 400 085, India*
[2] *Homi Bhabha National Institute, Mumbai 400 094, India*
*For correspondence. E-mail: hsmisra@barc.gov.in.

Received 30 June 2017; revised 17 November 2017; accepted 29 November 2017; published online 11 August 2018

Abstract. Bacteria are unicellular organisms that do not show compartmentalization of the genetic material and other cellular organelles as seen in higher organisms. Earlier, bacterial genomes were defined as single circular chromosome and extrachromosomal plasmids. Recently, many bacteria were found harbouring multipartite genome system and the numbers of copies of genome elements including chromosomes vary from one to several per cell. Interestingly, it is noticed that majority of multipartite genome-harbouring bacteria are either stress tolerant or pathogens. Further, it is observed that the secondary genomes in these bacteria encode proteins that are involved in bacterial genome maintenance and also contribute to higher stress tolerance, and pathogenicity in pathogenic bacteria. Surprisingly, in some bacteria the genes encoding the proteins of classical homologous recombination pathways are present only on the secondary chromosomes, and some do not have either of the classical homologous recombination pathways. This review highlights the presence of ploidy and multipartite genomes in bacterial system, the underlying mechanisms of genome maintenance and the possibilities of these features contributing to higher abiotic and biotic stress tolerance in these bacteria.

Keywords. bacterial pathogenesis; genome segregation; multipartite genome maintenance; radioresistance; recombination pathways; serine/threonine protein kinases; stress tolerance.

Brief account on bacterial genome systems

Mostly bacteria harbour single circular chromosome as primary genetic material and plasmids as extrachromosomal genome elements. Chromosomes encode proteins required for essential functions like cell division, DNA replication, translation etc., and therefore are indispensable. Physical organization of these elements is found to be different in different bacteria studied. In majority of the cases, circular chromosome and plasmids are located separately in the cell, but in some bacteria including *Deinococcus radiodurans* the genome is packaged together in the form of a highly compact nucleoid structures (Minsky *et al.* 2006). Although not fully understood, the negative supercoiling by topoisomerases and DNA condensation by structural proteins like H-NS, IHF, Hu etc. contribute to genome compactness in bacteria. Negative supercoiling also favours DNA unwinding and thus regulates many cellular processes, including DNA–protein interaction *in vivo*. The structural repertoire of DNA-binding proteins varies with growth rate and is associated with the topological remodelling of the nucleoid, which could further contribute to the survival of these organisms under adverse conditions.

Genome duplication and segregation are vital processes that ensure the stable transmission of genetic materials to daughter cells. The basic mechanism of genome segregation is relatively better understood in eukaryotes where the chromosome duplication, segregation and cell division are temporally separated (Yanagida 2005). Chromosomes are duplicated in S phase and remain together till G2 phase and partitioning occurs in M phase. This ensures that every cell has acquired at least one set of chromosomes. A large number of proteins involved in replication and segregation were characterized and their roles in eukaryotic genome segregation are better described. Centromere is a region where two identical sister chromatids come close in contact and microtubule filaments interact with the centromere

sequence binding proteins and separates sister chromatids to opposite poles by a series of events and finally cells divide. However in bacteria the genome partitioning mechanisms are not fully known. The interdependent regulation of DNA duplication, segregation and cytokinesis has been fairly worked out in some rod-shaped bacteria harbouring single circular chromosome and low-copy plasmids. Recent advances in genome sequencing technology helped in discovering bacterial genomes beyond a set paradigm. Further this knowledge may help in understanding the mechanisms underlying both abiotic stress tolerance and biotic stress tolerance particularly in pathogenic bacteria. In this review, we have made a good attempt and brought forth some useful information from the literature, particularly for the readers who may like to revisit the understanding of bacterial genome biology for both basic and applied research.

Bacteria harbouring multipartite genome and their occurrence

Since the discovery of DNA structure between 1950 and 1980, it was largely believed that bacteria have single circular chromosome (Jacob *et al.* 1963). In the late 1980s, it was reported that in certain bacteria, the DNA content per cell is more than one chromosome. Now it is known that many bacterial genomes consist of more than one chromosome and megaplasmid. In general, the primary chromosome is larger and tends to have significantly more conserved housekeeping genes encoding core cellular functions and a greater conservation of the contents. On the other hand, the secondary genome elements show a greater variability and encode accessory functions associated with adaptation and survival in different niches and largely contribute to stress tolerance (Holden *et al.* 2004; Cooper *et al.* 2010; Lykidis *et al.* 2010). The secondary chromosomes are normally smaller than primary chromosomes (Prozorov 2008). These can also encode some essential elements required for survival under both normal as well as stressed conditions, and in many cases these have been found indispensable like primary chromosomes. Theoretically, the additional chromosomes can originate by mechanisms like split of a single chromosome, chromosome duplication or acquisition of a large plasmid with essential genes. The similarity in the origin of replication between some secondary chromosomes and plasmids supports the greater possibility of secondary chromosomes evolution through plasmids acquiring some essential genes for its prolonged maintenance (Egan *et al.* 2005).

The first report of MGH system came in 1989 when pulsed-field gel electrophoresis studies showed that the genome of *Rhodobacter sphaeroides*, a phototrophic alphaproteobacterium, contains two circular chromosomes and five large plasmids (Suwanto and Kaplan 1989). The genome sequencing has revealed that many bacteria have multipartite genome systems with more than one chromosome and large plasmids. It is also noticed that almost all multipartite genome-harbouring (MGH) bacteria are either pathogenic to animals, human and plants or confer higher tolerance to abiotic stresses (table 1). At the same time there are many pathogenic and symbiotic bacteria that have single circular chromosomes as their genetic material. Currently, the cytogenetic features and cellular organization of multipartite genome elements are better known in only a few MGH bacteria such as *Vibrio cholerae*, *Burkholderia cenocepacia* and *D. radiodurans*. The alphaproteobacteria like brucellas; *Brucella melitensis*, *B. abortus*, *B. suis* and *B. ovis*, *Ochrobacterium anthropi* (Jumas-Bilak *et al.* 1998) and plant pathogen; *Agrobacterium tumefaciens*, *A. rubi* (Allardet-Servent *et al.* 1993) have MGH system (table 1). Among betaproteobacteria, *Burkholderia* (earlier known as *Pseudomonas*) was reported for the presence of additional chromosomes as part of their genome (Cheng and Lessie 1994). Three circular chromosomes have been reported in the species of the *B. cepacia* complex (Bcc). The members of Bcc include both plant pathogens and opportunistic human pathogens of patients with cystic fibrosis (Komatsu *et al.* 2003; Holden *et al.* 2004; Nierman *et al.* 2004) and maintain all the three chromosomes independently (Komatsu *et al.* 2003; Holden *et al.* 2009; Agnili *et al.* 2012). Among gammaproteobacteria, the first report on the genomic composition of vibrios came in 1998 and 1999 from *V. cholerae*, which showed the presence of two circular chromosomes (Trucksis *et al.* 1998; Yamaichi *et al.* 1999; Okada *et al.* 2005). Later on, many vibrios and related bacteria belonging to gammaproteobacteria were found to contain additional chromosomes in their genomic composition (Okada *et al.* 2005 and table 1 therein). In *V. cholerae*, both chromosomes carry their nearly nonredundant and independent machinery for genome duplication and segregation (Fogel and Waldor 2005, 2006). *D. radiodurans* has multipartite genome system with ploidy and all molecules seem to be packaged in the form of a highly compact single doughnut-shaped toroidal nucleoid (Minsky *et al.* 2006). The nucleoid of *Thermus aquaticus* is uncondensed and distributed throughout the cytosol, nearly similar to that of *Escherichia coli* (Zimmerman and Battista 2005). Nucleoid of *Rubrobacter radiotolerans* appears to be highly compact but does not have any fixed shape and most of these cells contain more than two different nucleoid structures.

Mechanism of bacterial genome segregation

Mechanisms of bacterial genome segregation have been modelled mostly based on the findings from bacteria that harbour single circular chromosome and low-copy plasmid(s). Initially it was believed that the segregation of

Table 1. List of known MGH bacteria, their genome composition and inhabitants.

Bacteria	Replicons	Size (Mbp)	Specific features	Sources
A. radiobacter K84	Chr I	4	Biological control agent againt some pathogenic bacteria.	Slater *et al.* (2009)
	Megareplicon	2.65		
	pAgK84B	0.184		
A. tumefaciens C58	Chr I	2.84	Plant pathogen	Goodner *et al.* (2001)
	Chr II	2.08		
	pAtC58	0.54		
A. vitis S4	Chr I	3.72	Grapevine plant pathogen	Slater *et al.* (2009)
	Chr II	1.28		
	pAtS4e	0.631		
	pTiS4	0.258		
	pAtS4c	0.211		
	pAtS4b	0.13		
	pAtS4a	0.078		
Anabaena sp. 90	Chr I	4.32	Stress-tolerant cyanobacteria	Wang *et al.* (2012)
	Chr II	0.81		
	Plasmid A	0.080		
	Plasmid B	0.056		
B. abortus A13334	Chr I	2.12	Cattle pathogen	Kim *et al.* (2012)
	Chr II	1.16		
B. canis	Chr I	2.01	Canine pathogen	Kim *et al.* (2012)
	Chr II	1.17		
B. ceti TE10759-12	Chr I	2.11	Dolphins pathogen	Ancora *et al.* (2014)
	Chr II	1.16		
B. melitensis NI	Chr I	2.11	Causes zoonotic brucellosis	Michaux *et al.* (1993); Jumas-Bilak *et al.* (1998)
	Chr II	1.17		
B. ovis ATCC 25840	Chr I	2.11	Veterinary sheep pathogen	Paulsen *et al.* (2002); Tsolis *et al.* (2009)
	Chr II	1.16		
B. pinnipedialis B2	Chr I	2.13	Pinnipeds (Seal) pathogen	Audic *et al.* (2009)
	Chr II	1.26		
B. suis VBI22	Chr I	2.1	Causes brucellosis in animals	Tae *et al.* (2011)
	Chr II	1.2		
Burkholderia ambifaria	Chr I	3.44	Causes cystic fibrosis in human	CP001025.1
	Chr II	2.77		CP001026.1
	Chr III	1.13		CP001027.1
	Plasmid	0.3		CP001028.1
Burkholderia cenocepacia J2315	Chr I	3.87	Causes cystic fibrosis in human	Holden *et al.* (2009)
	Chr II	3.21		
	Chr III	0.87		
	Plasmid	0.092		
Burkholderia dolosa	Chr I	3.31	Opportunistic pathogen in human	Workentine *et al.* (2014)
	Chr II	2.16		
	Chr III	0.82		
Burkholderia gladioli	Chr I	4.41	Plant pathogen and opportunistic pathogen in human	Seo *et al.* (2011)
	Chr II	3.7		
	bgla_1p	0.28		
	bgla_2p	0.13		
	bgla_3p	0.13		
	bgla_4p	0.4		
Burkholderia mallei	Chr I	3.51	Aetiological agent of glanders	Nierman *et al.* (2004)
	Chr II	2.33		
Burkholderia multivorans ATCC 17616	Chr I	3.45	Infectious in cystic fibrosis patients	Komatsu *et al.* (2003)
	Chr II	2.47		
	Chr III	0.92		
	Plasmid	0.17		
Burkholderia phenoliruptrix BR3459a	Chr I	4.15	Stress-tolerant symbiont of *Mimosa flocculosa*	Zuleta *et al.* (2014)
	Chr II	2.71		
	Plasmid	0.78		
Burkholderia pseudomallei	Chr I	4.07	Causative agent of melioidosis	Holden *et al.* (2004)
	Chr II	3.17		

Table 1 (*contd*)

Bacteria	Replicons	Size (Mbp)	Specific features	Sources
Burkholderia thailandensis MSMB121	Chr I	3.67	Nonpathogenic but opportunistic	Tuanyok *et al.* (2017)
	Chr II	2.76		
Burkholderia vietnamiensis G4	Chr I	3.65	TCE degrador and cystic fibrosis pathogen	CP000614.1
	Chr II	2.41		CP000615.1
	Chr III	1.24		CP000616.1
	pBVIE01	0.4		CP000617.1
	pBVIE02	0.27		CP000618.1
	pBVIE03	0.23		CP000619.1
	pBVIE04	0.11		CP000620.1
	pBVIE05	0.09		CP000621.1
Burkholderia xenovorans	Chr I	4.89	A polychlorinated biphenyl (PCB) degrader	Chain *et al.* (2006)
	Chr II	3.36		
	MP	1.47		
Butyrivibrio proteoclasticus	Chr I	3.55	Rumen bacterium help in plant polysaccharide degradation	Kelly *et al.* (2010)
	Chr II	0.3		
	pCY360	0.36		
	pCY186	0.19		
Candidatus Chloracidobacterium thermophilum	Chr I	2.68	Biocidal to microbial mat of alkaline siliceous hot springs	Garcia Costas *et al.* (2012)
	Chr II	1.01		
C. taiwanensis LMG 19424	Chr I	3.41	Nitrogen fixing symbiont	Amadou *et al.* (2008)
	Chr II	2.5		
	pRalta	0.55		
Cyanothece 51142	Chr I Cir.	4.93	Diazotrophic cyanobacterium	Welsh *et al.* (2008)
	Chr II Lin.	0.42		
Deinococcus radiodurans R1	Chr I	2.64	Extraordinary radioresistance	White *et al.* (1999)
	Chr II	0.41		
	MP	0.17		
Leptospira interrogans	Chr I	4.33	Leptospirosis in human	Ren *et al.* (2003)
	Chr II	0.36		
Ochrobactrum anthropi	Chr I	2.89	An opportunistic human pathogen	Jumas-Bilak *et al.* (1998); Chain *et al.* (2011)
	Chr II	1.9		
	pOANT01	0.17		
	pOANT02	0.1		
	pOANT03	0.09		
	pOANT04	0.06		
O. intermedium	Chr I	2.6	Opportunistic gut pathogen in human	Kulkarni *et al.* (2013)
	Chr II	1.91		
	Plasmid	0.06		
Photobacterium angustum	Chr I	3.2	Bioluminescent and a symbiont marine fish	Bjornsdottir-Butler *et al.* (2015)
	Chr II	1.8		
Photobacterium damselae	Chr I	3.2	Pathogenic to marine fishes	NZ_ADBS00000000.1
	Chr II	1.4		
Photobacterium leiognathi	Chr I	3.3	Bioluminescent and a symbiont of ponyfish	NZ_JZSK00000000.1
	Chr II	1.6		
P. profundum SS9	Chr I	4.09	A barophilic marine bacterium	Vezzi *et al.* (2005)
	Chr II	2.24		
	pPBPR1	0.08		
Prevotella dentalis DSM	Chr I	1.89	Dental root canal infections	NC_019960.1
	Chr II	1.45		NC_019961.1
Prevotella intermedia	Chr I	0.58	Causes peridontal disease and gingivitis	Nambu *et al.* (2015)
	Chr II	2.12		
Prevotella melaninogenica ATCC 25845	Chr I	1.8	Lives in oral cavity and infects teeth	NC_014370.1
	Chr II	1.37		NC_014371.1
Pseudoalteromonas haloplanktis TAC125	Chr I	3.21	A psychrophilic bacterium	Medigue *et al.* (2005)
	Chr II	0.635		

Table 1 (*contd*)

Bacteria	Replicons	Size (Mbp)	Specific features	Sources
Pseudoalteromonas sp. *SM 9913*	Chr I	3.33	Adapted to deep-sea sedimentary life	Qin *et al.* (2011)
	Chr II	0.7		
Ralstonia eutropha JMP134 (pJP4)	Chr I	3.81	Chloroaromatic pollutants degrader	NC_007347.1
	Chr II	2.73		NC_007348.1
	MP	0.63		NC_007336.1
	Plasmid1	0.087		NC_007337.1
Ralstonia pickettii DTP0602	Chr I	4.49	Degrades 2,4,6-trichlorophenol	Ohtsubo *et al.* (2013)
	Chr II	2.88		
	Chr III	0.73		
Rhizobium sp. *IRBG74*	Chr I	2.84	Legume symbiont diazotroph	Crook *et al.* (2013)
	Chr II (linear)	2.03		
	pIRBG74a	0.58		
Rhodobacter sphaeroides KD131	Chr I	3.05	Purple nonsulfur photosynthetic bacterium	Suwanto and Kaplan (1989); Lim *et al.* (2009)
	Chr II	0.91		
Salinivibrio costicola	Chr I	3.2	Halotolerant facultative anaerobe	AQOF00000000.1
	Chr II	1.3		
S. meliloti	Chr I	3.65	Legumes symbiotic bacterium	Sobral *et al.* (1991); Galardini *et al.* (2013)
	pSymA	1.35		
	pSymB	1.68		
S. japonicum UT26S	Chr I	3.51	Hexachlorocyclohexan degrador	Nagata *et al.* (2010)
	Chr II	0.68		
	pCHQ1	0.19		
V. paradoxus S110	Chr I	5.8	Biogenic and anthropogenic contaminants degrader	NC_012791.1
	Chr II	1.35		NC_012792.1
V. alginolyticus	Chr I	3.33	Humans and marine animals pathogen	Liu *et al.* (2015)
	Chr II	1.81		
V. campbellii ATCC BAA-1116	Chr I	3.77	A bioluminescent marine bacterium	Lin and Grossman (1998); Wang *et al.* (2013)
	Chr II	2.2		
	Plasmid	0.09		
V. cholerae O1 biovar eltor str. N16961	Chr I	2.96	An aetiological agent of cholera	Heidelberg *et al.* (2000)
	Chr II	1.07		
V. fischeri ES114	Chr I	2.9	Infectious agent of certain fishes and squids	Ruby *et al.* (2005)
	Chr II	1.3		
V. furnissii	Chr I	3.29	Acute gastroenteritis infections	Lux *et al.* (2011)
	Chr II	1.62		
V. parahaemolyticus RIMD 2210633	Chr I	3.28	Gastroenteritis infections	Makino *et al.* (2003)
	Chr II	1.87		
V. splendidus LGP 32	Chr I	3.3	Oyster pathogen	Le Roux *et al.* (2009)
	Chr II	1.68		
V. vulnificus	Chr I	3.35	Causes seafood-borne infections in human	Chen *et al.* (2003)
	Chr II	1.85		
V. nigripulchritudo	Chr I	4.11	Causes Summer syndrome in shrimps	Goudenege *et al.* (2013)
	Chr II	2.41		
V. mediterranei	Chr I	3.6	Nonpathogenic, gut colonizer of turbot larvae	NZ_BCUE00000000.1
	Chr II	2.3		
Alivibrio salmonicida	Chr I	3.3	Causes Hitra disease in Atlantic salmon and rainbow trout	Hjerde *et al.* (2008)
	Chr II	1.21		
	pVSAL84	0.08		
V. tubiashii	Chr I	3.3	Pathogenic for oyster and clam larvae	Temperton *et al.* (2011)
	Chr II	1.77		
	P251	0.25		
	P123	0.122		
	P57	0.057		
V. natriegens	Chr I	3.3	Nonpathogenic, halophile	Wang *et al.* (2013)
	Chr II	1.9		
V. nereis	Chr I	3.3	Nonpathogenic, halophile	NZ_BCUD00000000.1
	Chr II	1.9		

Table 1 (*contd*)

Bacteria	Replicons	Size (Mbp)	Specific features	Sources
V. fluvialis	Chr I	3.3	Causes gastroenteritis in humans	de Oliveira Veras *et al.* (2015)
	Chr II	1.9		
V. orientalis	Chr I	3.3	Associated with aquaculture farm	NZ_ACZV00000000.1
	Chr II	1.7		
V. aestuarianus	Chr I	3.2	Pathogenic to oyster	Okada *et al.* (2005)
	Chr II	1.8		
V. pelagius	Chr I	3.2	Nonpathogenic	Okada *et al.* (2005)
	Chr II	1.7		
V. wodanis	Chr I	3.3	Fish pathogen	NZ_LN554846.1
	Chr II	1.52		NZ_LN554847.1
	pAWOD9	0.091		NZ_LN554848.1
V. proteolyticus	Chr I	3.2	Marine pathogen in corals	NZ_BATJ00000000.1
	Chr II	1.7		
V. ichthyoenteri	Chr I	3.2	Pathogens of Japanese flounder larvae	Hoffmann *et al.* (2012)
	Chr II	1.4		
V. pectenicida	Chr I	3.2	A pathogen of scallop larvae	Okada *et al.* (2005)
	Chr II	1.4		
V. logei	Chr I	3	Bioluminscent organism	AJYJ00000000.2
	Chr II	1.5		
V. mimicus	Chr I	2.97	Human pathogen	Hasan *et al.* (2010)
	Chr II	1.3		
V. mytili	Chr I	3	Hosted in Mussels	NZ_JXOK00000000.1
	Chr II	1.5		
V. rumoiensis	Chr I	3	Facultatively Psychrophilic Bacterium	NZ_AJYK00000000.2
	Chr II	1.3		
V. anguillarum	Chr I	3.06	Pathogenic to marine fishes	Naka *et al.* (2011)
	Chr II	0.98		
	pJM1	0.065		
V. gazogenes	Chr I	3	Nonpathogenic to human, marine bacteria	FQUH00000000.1
	Chr II	1.2		
V. halioticoli	Chr I	3	Alginolytic marine bacterium isolated from the gut	NZ_BAUJ00000000.1
	Chr II	1.1		
V. hollisae	Chr I	3.22	Occasional human pathogen	NZ_CP014055.1
	Chr II	0.78		NZ_CP014056.1
V. ordalii	Chr I	3	Pathogenic to marine fishes	Naka *et al.* (2011)
	Chr II	0.9		
V. metschnikovii	Chr I	3	Occasional human pathogen	NZ_ACZO00000000.1
	Chr II	0.9		

Details of the chromosomes (Chr) and more than 50-kb plasmids are given.

duplicated chromosome is a passive process, which later was found to be a highly dynamic and regulated process (Jensen and Shapiro 1999). However, the driving force or tension required for bringing bacterial chromosomes steadily apart was intriguing. Later, the characterization of conditional mutants led to the identification of many factors or proteins that are involved in active genome partitioning in bacteria (Jensen and Shapiro 1999). Several mechanisms that could explain bacterial genome segregation have been reviewed in detail (Egan *et al.* 2005; Errington *et al.* 2005; Leonard *et al.* 2005; Ringgaard *et al.* 2009; Gerdes *et al.* 2010; Hatano and Niki 2010) and are out of the scope of this review. For the benefit of the readers to understand the subject covered in this review we have briefly summarized the various aspects of tripartite genome segregation (TGS) system. The TGS was initially identified in plasmids and later in chromosomes of *Bacillus subtilis* and *Caulobater crescentus*. TGS comprises of two *trans*-acting factors like ParA (or ParA-like) and ParB (or ParB-like) proteins and one *cis* element called centromeric sequences. ParAs or its homologues are NTPase, while ParBs or its homologues are centromere-binding proteins in bacteria. ParA homologues are both structurally and functionally diverse in bacteria. Genetic organization of TGS components differ from genome to genome and that tentatively defines three types of bacterial genome partitioning systems, such as type I, type II and type III (figure 1). Functional homologues of these elements are present on both plasmids and chromosomes in different bacteria. Some of these have been functionally

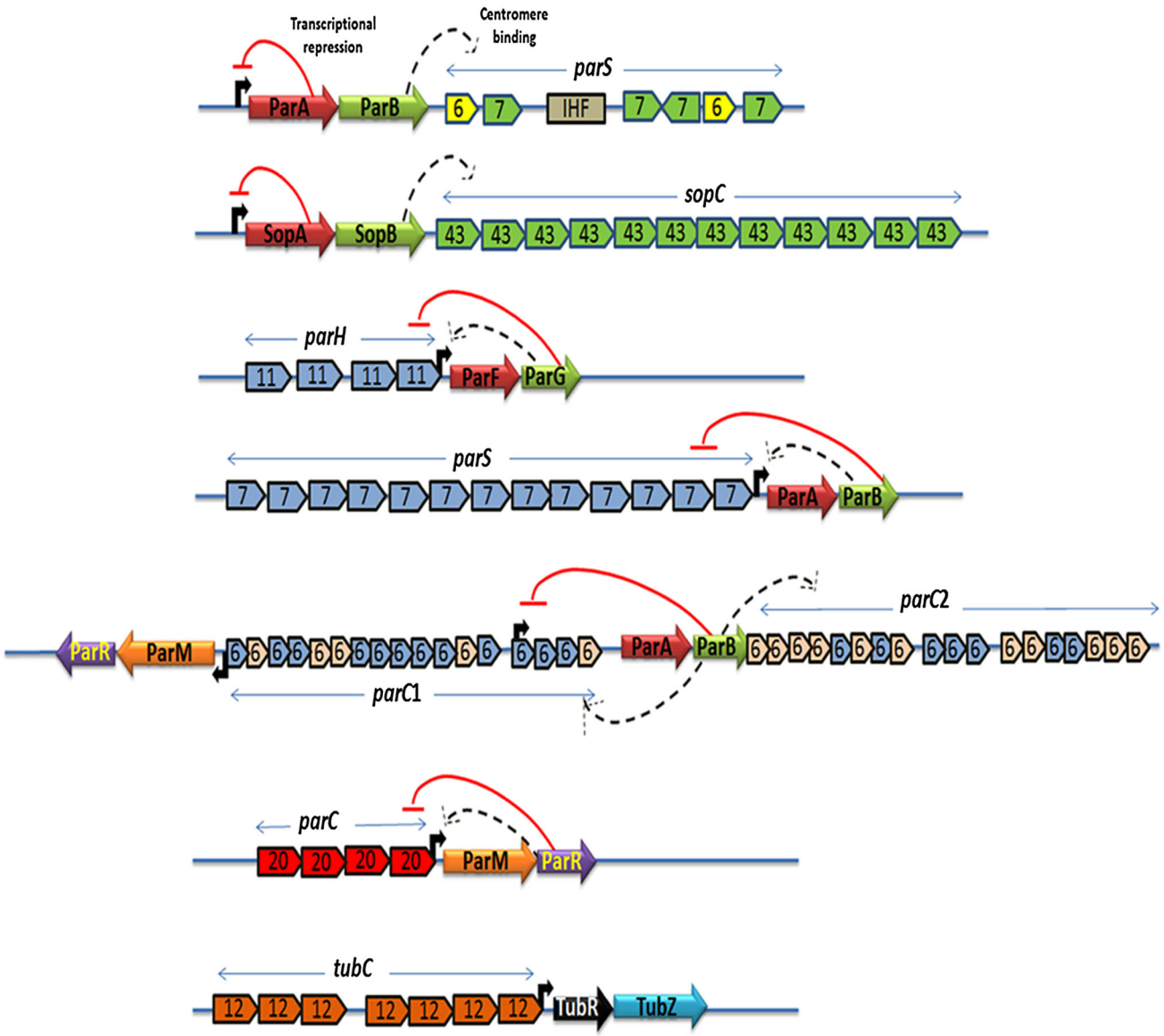

Figure 1. Genetic organization of *par* loci in different genome partitioning systems as observed in low-copy plasmid and chromosome. Type Ia *par* loci characterized from plasmids P1, F and RK2 encodes large ParAs with N-terminal DNA-binding domains and large ParBs while type Ib *par* loci are small ParAs and ParBs characterized from plasmidsTP228 and pTAR encoding single set of 'Par' proteins while plasmid pB171 contains double *par* loci as *par*1 and *par*2. (a) Type II *par* loci encoding actin homologues and found in plasmids R1, pSK41 and pBET131. (b) Type III *par* loci encoding tubulin homologues as reported from plasmids pBtoxis and pXO1. (c) Solid arcs indicate regulation of promoter activity and dashed arcs show centromere binding. The boxes represent repeat elements within each centromere and are schematic. The number of nucleotides in each repeat is indicated in numeric in each box.

characterized and are listed in table 2. The centromeric sequences are different in different plasmids and chromosomes. General mechanism of segregation involves the sequence-specific interaction of ParB proteins with centromeric sequences to form the nucleoprotein complexes. ParA proteins interact with respective ParB-centromere nucleoprotein complex. The polymerization and depolymerization dynamics of different ParAs (NTPase protein) are differentially regulated upon their interaction with respective centromere-ParB nucleoprotein complex and ATP. Based on the mode of actions of ParA proteins, three types of mechanisms have been characterized for bacterial genome segregations. The pulling mechanism, a predominant mechanism of bacterial genome segregation (figure 2) involves P-loop ATPase having Walker type or its deviant motif. These ATPases have been reported in plasmids like P1, F, pB171, pTAR and pTP228 and in the chromosomes of many bacteria. These ATPases differ in their sizes and that would account for their different mechanisms of action as elaborated in Gerdes *et al.* (2010). Some bacteria where mechanisms of action of TGS components are different from that of those involved in pulling

Table 2. Summary of characterized elements of TGS systems.

Name of bacteria	Genome elements	Partitioning elements			References
		NTPase	Adaptor	Centromere	
E. coli	P1 plasmid	ParA	ParB	P1*parS*	Ebersbach and Gerdes (2005); Leonard *et al.* (2005); Ghosh *et al.* (2006); Gitai (2006)
E. coli	F plasmid	SopA	SopB	*sopC*	Ebersbach and Gerdes (2005); Leonard *et al.* (2005); Ghosh *et al.* (2006); Gitai (2006)
B. subtilis	Chromosome	Soj	Spo0J	*parS*	Draper and Gober (2002); Lee *et al.* (2003)
C. crescents	Chromosome	ParA	ParB	*parS*	Mohl and Gober (1997); Mohl *et al.* (2001)
D. radiodurans	Chromosome	ParA1	ParB1	*segS* (1–3)	Charaka and Misra (2012)
S. enterica	pTP228	ParF	ParG	*parH*	Dobruk-Serkowska *et al.* (2012)
	pB171	ParA	ParB	*parC*	Ebersbach and Gerdes (2005)
	pSM19035	δ/ω			Volante *et al.* (2015)
S. aureus	PSK41	ParM	ParR	*parC*	Gerdes *et al.* (2010)

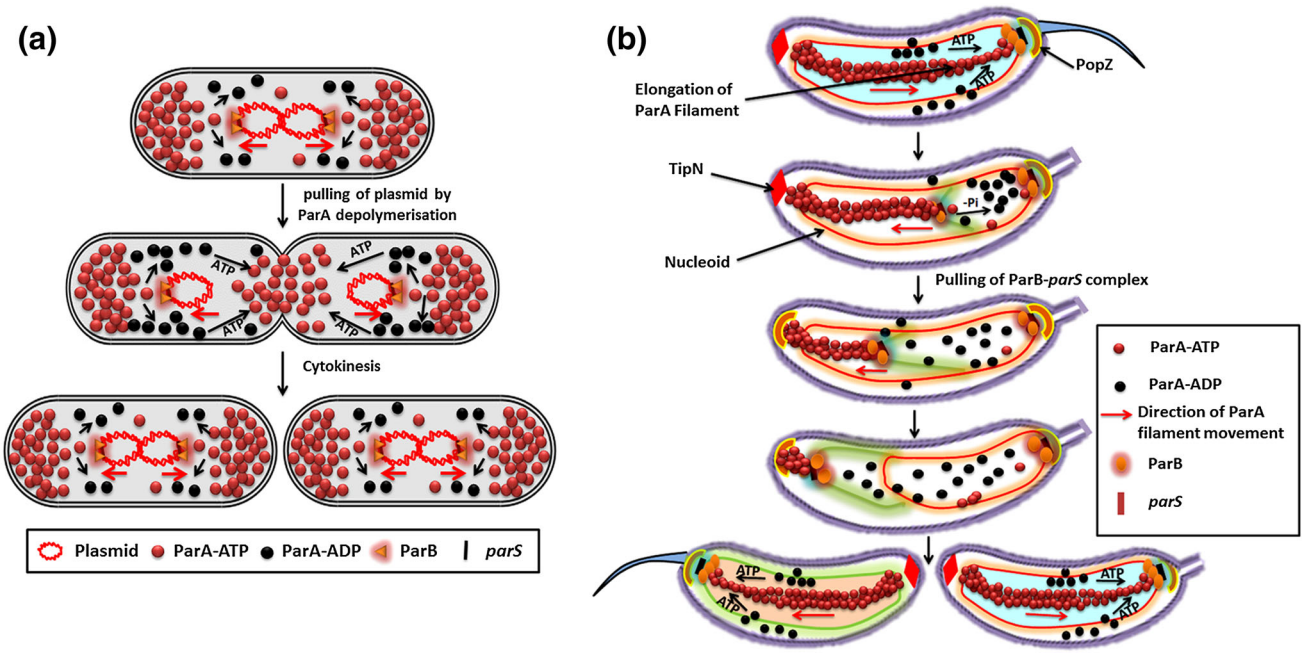

Figure 2. Type I partitioning system depicted the pulling mechanism of genome segregation. (a) Low-copy plasmids like F and P1 duplicated at mid-cell position of *E. coli*. ParA-ATP polymerizes from poles and its depolymerization starts from proximal to ParB bound to centromeres generating Par-ADP and DNA is pulled toward poles. ParA-ADP gets recycled to ParA-ATP, which takes part in next round to segregation. (b) Chromosomal DNA segregation is shown in *C. crescentus*. Chromosomal DNA duplication initiates at one pole in Swarmer cells and ParA-ATP polymerization starts from its opposite pole. After ParA polymers interact with ParB bound to centromere, depolymerization of ParA begins from the ends interacting with ParB-centromere and one of the duplicated DNA molecule gets pulled to the other end by the force generated through progressive depolymerization of ParA polymer.

mechanism, they apparently follow other mechanisms like pushing mechanisms (figure 3) and Tram model (figure 4) (Ebersbach and Gerdes 2005; Larsen *et al.* 2007; Schumacher 2007; Ni *et al.* 2010). There are bacteria whose genomes do not encode the typical TGS and in such cases the molecular basis of genome partitioning would be different. For instance, *E. coli* chromosome does not encode typical TGS and various mechanisms have been proposed. Recently, MatP and *matS* system has been discovered and shown to be involved in partitioning of duplicated circular chromosome. It was observed that 800-kb region in *ter* macrodomain of *E. coli* chromosome contains 23 direct repeats of a 13-bp long sequence called *matS* (Mercier *et al.* 2008). MatP protein binds to *matS* and helps in segregation. MatP also interacts with FtsZ through cell division regulatory protein ZapB (Espeli *et al.* 2012) and suggests

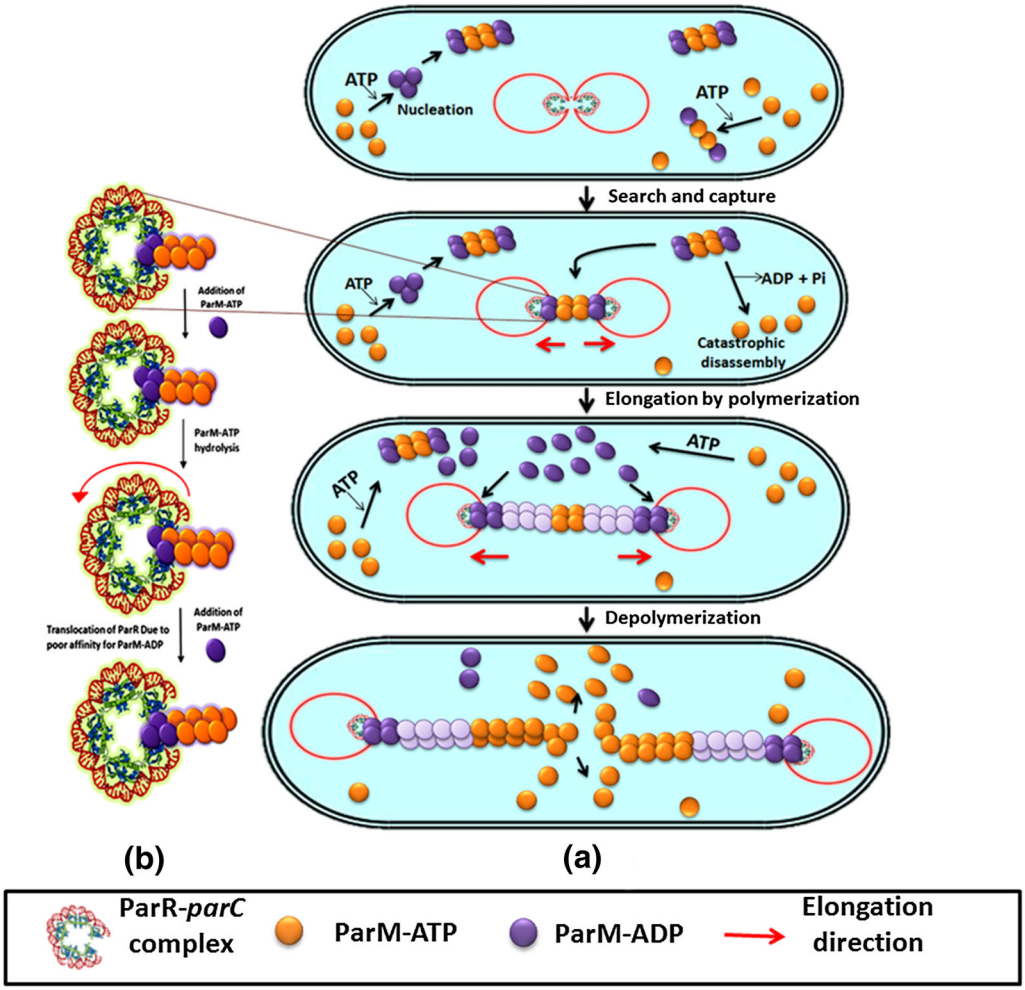

Figure 3. Type II partitioning system depicting pushing mechanism of genome segregation in plasmid pSK41. (a) Schematic representation of ParR interaction with *parC* followed by nucleation and polymerization of ParM, which pushes duplicated plasmid molecules in the opposite direction. (b) Molecular assembly of ParR–*parC* complex (PDB ID: 1Q2 K) depicting the processive ParM polymerization mechanism. At a time only one subunit of ParM-ATP is added to ParR–*parC* complex and undergoes ATPase activation leading to ATP hydrolysis and addition of ParM monomer on growing chain of ParM protofilament. This results in the growth of ParM filaments and pushing of daughter DNA molecules in the opposite direction.

being a protein that regulates the interdependence of cell division and genome segregation in *E. coli*.

Genome partitioning system in MGH bacteria

Molecular mechanisms underlying evolution, maintenance of multipartite genome system, its inheritance into daughter cells, maintenance of ploidy and the functional significance of multipartite genomes are some exciting areas in prokaryotic genome biology and would be worth studying. A large number of genes repeated on different genome elements can cause genetic redundancy and would have equipped these bacteria for better resistance to DNA assaults. The understanding of genome maintenance in these bacteria would help in unearthing the molecular basis of stress tolerance and possibly bacterial pathogenesis. The primary chromosome in almost all MGH bacteria contains *parAB* operon-type genetic organization of Par proteins. In addition, these bacteria also encode orphan ParAs and ParBs proteins in their primary chromosome (table 1 in electronic supplementary material at http://www.ias.ac.in/jgenet/). Very interestingly, the secondary genome elements in many MGH bacteria do not contain ParA and ParB homologues (table 3). Some bacteria like *A. vitis* S4, *Brucella canis*, *B. ovis* ATCC 25840, *B. pinnipedialis* B2/94, *Burkholderia pseudomallei* strain MSHR30,*B. thailandensis* MSMB121, *Cyanothece*, *Ochrobactrum intermedium*, all the species of *Prevotella*, *Sphingobium japonicum* UT26S and *Variovorax paradoxus* S110 do not have ParA and ParB proteins on any of the secondary genome elements. The presence of TGS on secondary genome elements and its absence on primary chromosome are intriguing and suspects some possible cross-talks of secondary genome segregation

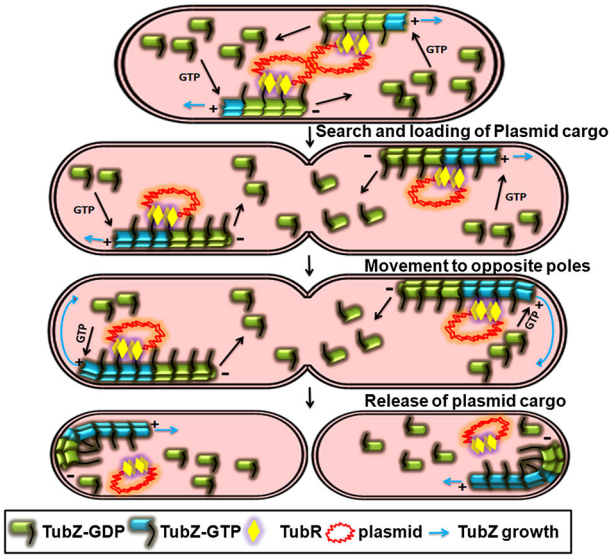

Figure 4. Type III partitioning model of genome segregation. Certain plasmids including pBtoxis do not encode ATPase–type tripartite genome partitioning system but GTPase-type system. TubZRC tripartite system contains TubZ a GTPase, TubR adaptor and *tubC* centromere. TubR binds to *tubC* and then TubZ-GTP binds to this complex. TubZ-GTP polymerizes at growing ends of the polymer and then gets converted at TubZ-GDP, which leaves polymer and apparently does not have affinity to TubR–*tubC* complex. As a result, DNA molecules move along with the growth of the TubZ polymer like a Tram. Hence, named as 'Tram' model of genome segregation.

elements with primary chromosome segregation and would be worth understanding. Direct repeats located near the putative *ori* regions and upstream to *parAB* operon may work as potential centromers for genome partitioning. Among different MGH bacteria, the limited studies on genome partitioning have been carried out in *V. cholerae*, *D. radiodurans*, *Thermus thermophilus* and *B. cenocepacia*. *V. cholerae* harbours two chromosomes, chromosome I (2,961,149 bp) and chromosome II (1,072,315 bp), and each encodes independent partition system (Egan *et al.* 2005). Genetic and microscopic studies show that chromosome I is localized at 3/4th position from the cell pole and chromosome II in the mid-cell position. They follow bidirectional yet asymmetric chromosome segregation. Interestingly, the partitioning systems in both chromosomes are nonredundant and segregate independently (Fogel and Waldor 2005). *In vivo* interaction of ParA protein of chromosome I with its cognate ParB–*parS* complex and regulation of its activity suggests a pulling type mechanism for chromosome I segregation (Fogel and Waldor 2006). Unlike chromosome I which has one *parS* site, chromosome II has nine repeats in *parS* (*parS2*) (Yamaichi *et al.* 2007). Functional interaction of ParA of chromosome II (ParA2) with DNA is different from ParA of chromosome I (ParA1), and ParA2 does not complement ParA1 loss in *V. cholerae*. The cystic fibrosis pathogen *B. cenocepacia* genome comprises three chromosomes and one low-copy plasmid. A single *parABS* system is present near the origin of each replicon. ParA and ParB of the largest chromosome are phylogenetically similar to primary chromosome in other bacteria but are distinct from ParAs encoded on secondary genome elements. Plasmid stabilization test in *E. coli* showed that each *parAB* exhibits partitioning activity only with its cognate *parS* (Dubarry *et al.* 2006). This study concluded that the functions of *parABS* system are independently regulated on individual genome elements and the expression of *parAB* operons of smaller chromosome and plasmid are autoregulated in this bacterium (Dubarry *et al.* 2006). Notably, ParB of chromosome III binds specifically to the centromeres of all the genome elements in spite of great sequence diversity. Based on these results and other evidences, investigators suggested that the ancestral features in genome partitioning are preserved during evolution at least in *B. cenocepacia* (Passot *et al.* 2012). The *T. thermophilus* genome consists of a chromosome (1.85 Mb), a megaplasmid pTT27 (0.26 Mb), a plasmid pTT8 (9.3 kb) and each of them is present in multiple copies (Ohtani *et al.* 2010). Each genome element encodes ParAB homologues. Using molecular genetics and imaging approaches, it has been shown that *par* locus of chromosome is neither required for chromosomal nor megaplasmid bulk DNA replication and segregation. However, megaplasmid 'Par' system is needed for the proper replication and segregation of megaplasmid (Ohtani *et al.* 2015). This might suggest that chromosome segregation in *T. thermophilus* follows some other mechanism. *D. radiodurans* is an extremotolerant bacterium and its multipartite genome consists of chromosome I (2,648,638 bp), chromosome II (412,348 bp), a megaplasmid (177,466 bp) and a small plasmid (45,704 bp) (White *et al.* 1999; Slade and Radman 2011; Misra *et al.* 2013). This bacterium also confers ploidy with 4–8 copies of its genome per cell, which vary in different growth phases. Recently, chromosome I partitioning system was characterized and centromeric sequences (*segS*) have been identified in chromosome I in *D. radiodurans* (Charaka and Misra 2012). ParA and ParB proteins of chromosome I (termed ParA1 and ParB1) are functionally characterized as nonspecific DNA-binding ATPase and centromere-binding protein, respectively. ParA1-GFP expressing in synthetic *E. coli* showed pole-to-pole oscillation only when its cognate ParB1 and centromeric sequences are present. Further, the ATPase activity of ParA1 was stimulated in the presence of ParB–segS complex. These results together suggest that chromosome I segregation in this bacterium is likely following pulling mechanism of genome segregation (Charaka and Misra 2012). ParA-GFP localization in *D. radiodurans* was observed irrespective of the presence of ParB but genome segregation was significantly affected in *parB* mutant. Although centromere sequences for secondary genome elements are not known, overexpression of ParA of chromosome II inhibited cell division in the

absence of its cognate member ParB in *D. radiodurans* as well as in synthetic *E. coli* expressing ParA2 (Charaka *et al.* 2013). While roles of Par system in segregation of secondary genome elements of *D. radiodurans* are not completely understood, PprA a pleiotropic protein of chromosome II having a role in radioresistance in *D. radiodurans* has also been implicated in cell division and genome segregation (Devigne *et al.* 2013; Kota *et al.* 2014a). The *D. radiodurans* genome encodes topoisomerase IB (DrTopoIB) and both the subunits of DNA gyrase (DrGyr). Both physical and functional interactions of PprA with DrGyr and DrTopoIB have been shown (Kota *et al.* 2014a, b), which indicated the roles of PprA in cell division and genome maintenance perhaps through modulating the functions of DNA topoisomerases (Devigne *et al.* 2016; Kota *et al.* 2016).

Stress tolerance determinants on secondary genome elements in MGH bacteria

Stress kinases

The presence of stress sensor kinases in bacteria is attributed to their better stress tolerance. The presence of protein kinases in the genomes of MGH bacteria was checked. Interestingly, a large number of protein kinases are also found on secondary genome elements in these bacteria (table 2 in electronic supplementary material). The histidine kinases and their cognate response regulators constituting the typical two-component system (TCS) are highest (figure 5) followed by others including serine/threonine protein kinases. In majority of the cases, abundance of these kinases was higher on the primary chromosome as compared to secondary genome elements. However, in some MGH bacteria, the numbers of open reading frames (ORFs) encoding these protein kinases are relatively more on secondary chromosomes and on plasmids. For instance, bacteria belonging to genus *Burkholderia*, *Vibrio*, *Agrobacterium* and *Rastolnia* were found to have more number of protein kinases on their secondary genome elements. The other members like *Cupriavidus taiwanensis* LMG 19424, *Sinorhizobium meliloti*, *Rhizobium* sp. IRBG74, *Photobacterium profundum* SS9, *Candidatus Chloracidobacterium thermophilum*, *Anabaena*, *D. radiodurans* also showed high number of protein kinases on their secondary genome elements. Notably, burkholderias and vibrios are mostly pathogens to mammals while *Agrobacterium* and *Rastolnia* are highly infectious to plants.

Since the role of TCS as stress response regulator is well characterized, the presence of TCS components on secondary genome elements should be an added advantage to the stress tolerance in MGH bacteria (figure 5). Peculiarly, Ser/Thr protein kinases (STPKs), aspartate and tyrosine protein kinases are found to be distributed on both primary and secondary genome elements in several MGH bacteria (figure 6). However, number of the STPKs and tyrosine kinases are lesser than histidine kinases. The correlation between higher number of signalling kinases especially on secondary genomes with pathogenesis and abiotic stress tolerance would be worth investigating.

Oxidative stress response genes

Bacteria exhibiting resistance to different stresses are known to have higher tolerance to oxidative stress. Since, majority of the MGH bacteria are infectious, the possibility of these having higher tolerance to oxidative stress would be anticipated. The distributions of known and ubiquitous stress response proteins like OxyR, SoxRS, RpoS, catalases and superoxide dismutases (SODs) on different genome elements have been reviewed in this article. Although the distribution of OxyR, SoxRS, RpoS, catalases and SODs on primary or secondary genome elements does not follow a pattern, a large number of ubiquitous antioxidant enzymes like catalases and SODs are found on secondary genome elements (table 4). For example, catalases like Mn-catalase, KatA, KatE, KatG, KatN and superoxide dismutases like Mn–SODs, Cu–FeSOD and Mn–Fe SODs are mostly found on secondary genome elements. Although OxyR or its homologues are mostly found on primary chromosome, some of the MGH bacteria also have the additional copies of OxyR/SoxR on secondary genomes (table 4). Similarly, DsqI and DqsR proteins are found in secondary genome elements. Some of them have both OxyR and SoxR regulators on their secondary genome elements. Secondary genome also has RpoS, a stationary phase sigma factor in many MGH bacteria. Although the oxidative stress management system in these bacteria spread over all the genome, a large number of catalases and superoxide dismutases are also present on their secondary genome elements. Earlier, it has been shown that catalases are required to fight against the oxidative bursts of phagocytes in pathogenic bacteria (Ng *et al.* 2004; Cosgrove *et al.* 2007; Italiani *et al.* 2011). Although not studied in greater detail, plants also exert hypersensitive response mainly through oxidative stress. The catalases in plant pathogenic bacteria might play the same role in plant cell infection as articulated during the infection of pathogenic bacteria to mammalian cells. These observations might together support the hypothesis that secondary genome elements provide an additional dose of oxidative stress management enzymes to fight against oxidative stress posed by the host system upon infection by these bacteria.

DNA repair pathways

Bacterial cells exposed to stress conditions damage DNA. Since the majority of MGH bacteria are stress

Table 3. Occurrence of ParA and ParB homologs in secondary genome elements.

Name of bacteria	Secondary chromosome		Plasmid	
	ParA	ParB	ParA	ParB
A. radiobacter K84	Arad_7000	Arad_7001	Arad_15017	–
Anabaena	–	–	ANA_P10019	ANA_P10018
B. abortus A13334	BAA13334_II00213	BAA13334_II00214	–	–
B. ceti TE10759-12	V910_200092	V910_200091	–	–
B. melitensis NI	BMNI_II1147	BMNI_II1148	–	–
B. suisVBI22	BSVBI22_B1192	BSVBI22_B1193	–	–
Burkholderia ambifaria	BamMC406_5102 BamMC406_6362	BamMC406_3107 BamMC406_5757	–	–
B. cenocepacia J2315	BCAM0003 BCAS0003	BCAM0004 BCAS0002	pBCA001	pBCA002
Burkholderia dolosa	BDSB_24405	BDSB_24410 BDSB_26075	–	–
Burkholderia gladioli	bgla_2g00010	bgla_2g00020	bgla_1p0010 +4 ParA like	bgla_1p0020 +3 ParB like
Burkholderia mallei	BMAA2114	BMAA2115	–	–
Burkholderia multivorans ATCC 17616	BMULJ_05360 BMULJ_05370	BMULJ_05361 BMULJ_05369	BMULJ_06310	BMULJ_06311
Burkholderia phenoliruptrix BR3459a	BUPH_01337	–	–	BUPH_08203
Burkholderia vietnamiensis G4	Bcep1808_3795 Bcep1808_5481	Bcep1808_3794 Bcep1808_5482	Bcep1808_6797 +2 Par A Like	Bcep1808_6798 +2 ParB like
Burkholderia xenovorans	Bxe_B3028 Bxe_C1369	Bxe_B3027	–	–
Butyrivibrio proteoclasticus	bpr_III214	–	bpr_IV197 bpr_II428	bpr_IV199
C. taiwanensis LMG 19424	RALTA_B0004	RALTA_B0003	pRALTA_0307	pRALTA_0306
D. radiodurans	DR_A0001	DR_A0002	DR_B0001 DR_B0031	DR_B0002 DR_B0030
Leptospira interrogens serovar Lai str. 56601	LB_026 LB_365	LB_027 LB_366	–	–
P. profundum SS9	PBPRB2025	PBPRB2024	PBPRC0026	PBPRC0027
Pseudoalteromonas haloplanktis TAC125	PSHAb0001	PSHAb0002	–	–
Pseudoalteromonas sp. *SM9913*	PSM_B0001	PSM_B0002	–	–
Ralstonia eutropha JMP (pJP4)	Reut_B5343	Reut_B5344	–	Reut_C6163
Ralstonia pickettii DTP0602	– N234_34400	N234_20970 N234_34405	–	–
Rhizobium sp. *IRBG74*	BN877_II0976	BN877_II0977	BN877_p0001	BN877_p0002
R. sphaeroides KD131	–	RSKD131_3309 RSKD131_3783 RSKD131_3815 RSKD131_3816	RSKD131_4385 RSKD131_45 46	RSKD131_4386 RSKD131_4545
S. meliloti	Sinme_4124 Sinme_4233 Sinme_5507	Sinme_4125 Sinme_4234 Sinme_5508	Sinme_6884	Sinme_6883
V. alginolyticus NBRC 15630 = ATCC 17749	N646_3464	N646_3463	–	–
V. campbellii ATCC BAA-1116	M892_27710	M892_27705	M892_28710	M892_28705
V. cholerae O1 biovar eltor str. N16961	VC_A1115	VC_A1114	–	–

Table 3 (*contd*)

Name of bacteria	Secondary chromosome		Plasmid	
	ParA	ParB	ParA	ParB
V. fischeri ES114	VF_A1172	VF_A1171	–	–
V. furnissii	vfu_B00989	vfu_B00988	–	–
V. parahaemolyticus BB22OP	VPBB_A1600+2 ParA like	VPBB_A1599+2 ParA like	SJA_P1-00020+3 ParA like	SJA_P1-00030+3 ParB like
V. splendidus LGP 32	VS_II0001	VS_II0002	–	–
V. vulnificus	VVA1697	–	VVP64	–
Alivibrio salmonicida	VSAL_RS21715	VSAL_RS21710	–	–
V. anguillarum	VAA_RS16255, VAA_RS16385	VAA_RS16380	–	–
V. fluvialis	AL536_RS20315	AL536_RS20320	–	–
V. hollisae	AL542_RS00130	AL542_RS00135	–	–
V. mimicus	AL543_RS01115, AL543_RS01310, AL543_RS02545	AL543_RS01305	–	–
V. natriegens	PN96_RS16485	PN96_RS1648	–	–
V. nigripulchritudo	VIBNI_RS18690, VIBNI_RS18850	VIBNI_RS18695	–	–
V. tubiashii	IX91_RS15165	IX91_RS15170	–	–
V. wodanis	AWOD_RS18155, AWOD_RS19730, AWOD_RS20355	AWOD_RS20350	–	–

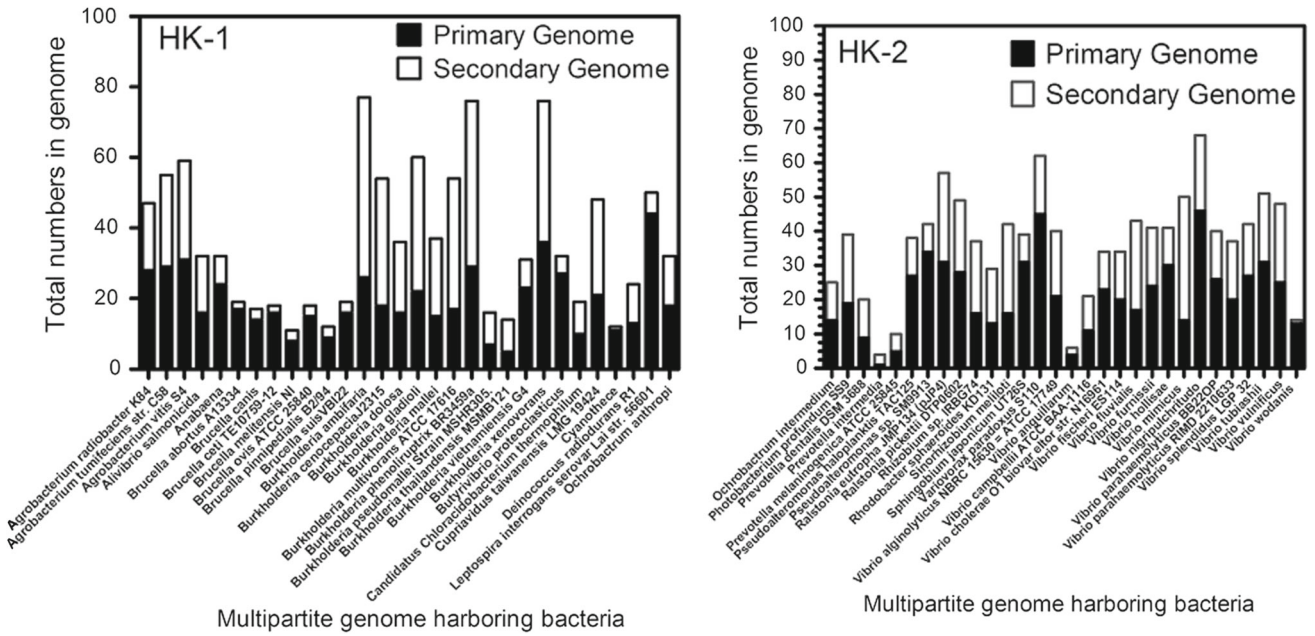

Figure 5. Distribution and density of histidine kinases in the primary and secondary genome elements of different MGH bacteria. For presentation purpose, the total MGH bacteria containing histidine kinase have been divided into two graphs (HK1 and HK2).

tolerant, the possibility of these having efficient DNA repair mechanisms encoded on secondary genome elements could be speculated. When the presence of DNA repair and recombination proteins on secondary genome elements are searched, the distribution observed was sporadic (table 5). The genomes of majority of the MGH bacteria considered under this study, encode for the components of RecF and RecBC types (*Rec*BCD enzymes or *Add*AB enzymes) homologous recombination pathways. Notably, however, the genomes of some MGH bacteria such as *Anabaena* sp. PCC 7120, *C. chloracidobacterium thermophilum*, *C. taiwanensis* LMG, *Cyanothece*, *D. radiodurans* R1, *P. dentalis* DSM, *P. intermedia*, *Pseudoalteromonas* sp. SM9913, *V. paradoxus* S110, *A. salmonicida*, *V. hollisae* do not encode *Rec*BC or *Add*AB enzymes (table 6). On the other hand, there are MGH bacteria that

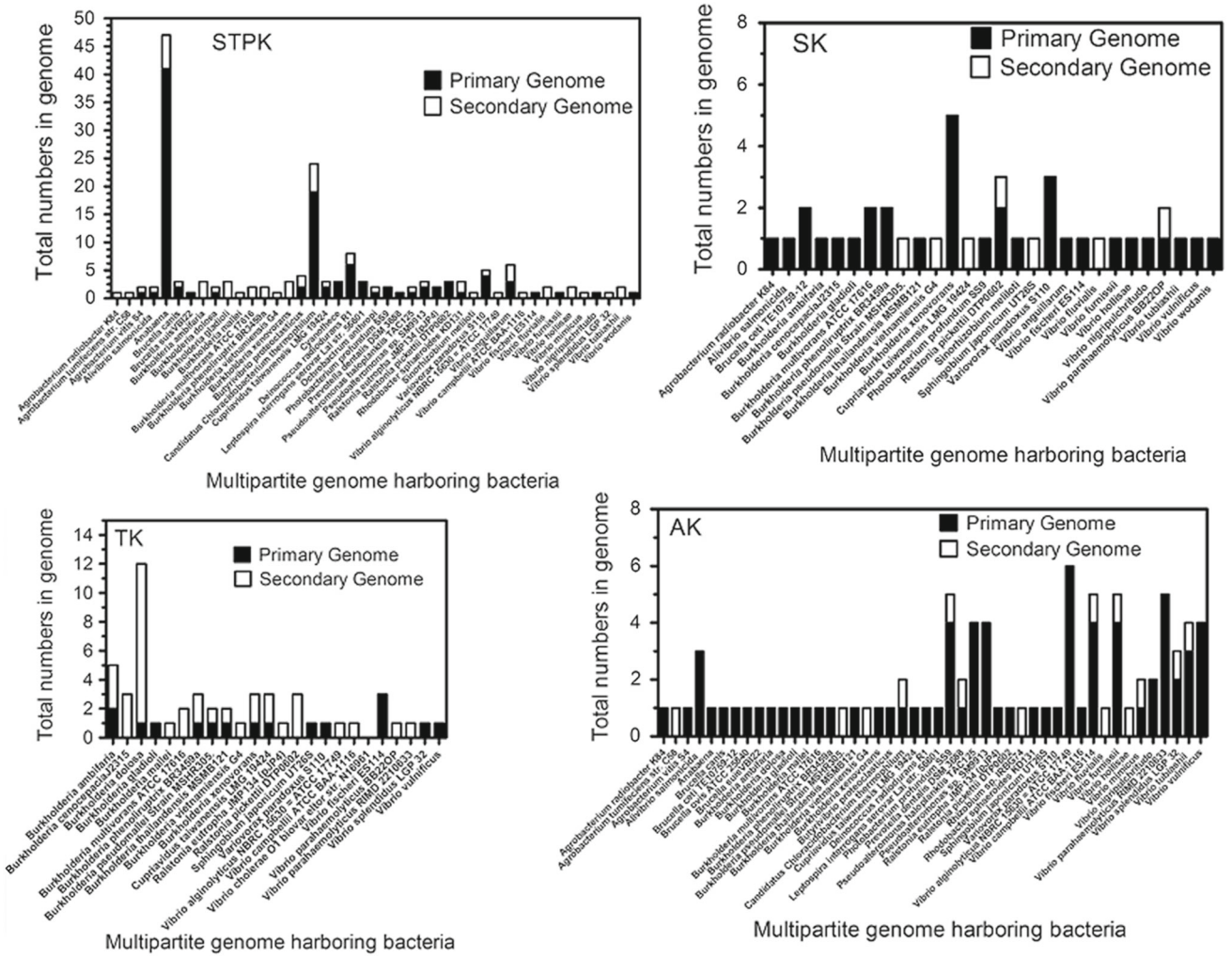

Figure 6. Distribution and density of other kinases besides histidine kinases in the primary and secondary genome elements of different MGH bacteria. Number of ORFs encoding serine/threonine (STPK), serine (SK), tyrosine (TK) and aspartate (AK) kinases on the genome of MGH bacteria are depicted.

harbour either RecBC or RecF recombination pathway components (table 3 in electronic supplementary material). For instance, the genome of all species of *Burkholderia* except *B. pseudomallei* strain MSHR305 encodes *E. coli* type *Rec*B, *Rec*C and *Rec*D enzymes but not RecF protein. Surprisingly, there are bacteria such as *C. taiwanensis* LMG 19424, *R. eutropha* JMP134 (pJP4) and *R. pickettii* DTP0602 that have neither classical RecBC complex nor RecF pathway enzymes of homologous recombination. The most puzzling information derived from the analysis of annotated protein database of MGH bacteria is that the RecF pathway proteins are found on secondary chromosome rather than primary chromosome in *Prevotella* sps like *P. dentalis* DSM 3688, *P. melaninogenica* ATCC 25845 and *P. intermedia* and these bacteria do not have LexA homologues on either of the chromosomes. On the other hand genomes of all the *Vibrio* species have both RecBC and RecF pathway components, RecA and RadA as well as LexA. The MGH bacteria also have a large number of proteins involved in excision and mismatch repair on their secondary genomes. Some bacteria have only one or two DNA repair proteins on secondary genomes but these are regulatory in nature. For instance, the photolyase (Phr) enzyme is found on secondary genome elements in *B. xenovorans*, *Pseudoalteromonas haloplanktis* TAC125, *V. fischeri* ES114, *O. intermedium*, *Anabaena*, *B. multivorans* ATCC 17616, *B. abortus* A13334, *B. pseudomallei strain* MSHR305 and in some vibrio species. This might suggest that the photoreactivation repair of UV-damaged lesions is supported by secondary genome elements in these bacteria. Similarly, Ku80 homologues are present in *C. taiwanensis* LMG 19424, *R. pickettii* DTP0602, *B. dolosa* and *R. eutropha* JMP134 (pJP4). Thus, the possibility of cross talk between different homologous recombination pathways in the regulation of multipartite genome maintenance cannot be ruled out in these bacteria. Earlier, the role of RecBCD in plasmidic recombination leading to formation of plasmid

Table 4. Distribution of some selected oxidative stress tolerance markers on secondary genome elements in MGH bacteria.

Names of the bacteria	Oxidative stress response managers		
	Response regulator	Catalases	Superoxide dismutases
A. radiobacter K84	Arad7240 (OxyR) Arad8448 (OxyR) Arad9369 (OxyR)	Arad7339 (KatE) Arad9370 (KatG)	–
A. tumefaciens C58	Atu4641 (OxyR) Atu3915 (SoxR)	Atu4642 (KatA) Atu5491 (KatE)	Atu4583 (Fe-SOD) Atu4726 (Fe-SOD) Atu0876 (Fe-SOD)
A. vitis S4	Avi_5771 (OxyR)	Avi_5326 (KatE) Avi_5190 (KatA)	
B. abortus A13334	BAA13334_II01548 (OxyR)	BAA13334_II01546 (KatE)	BAA13334_II01076 (Cu–Zn SOD)
B. canis	BCA52141_II0695 (OxyR)	BCA52141_II0693 (KatE)	BCA52141_II0228 (Cu–Zn SOD)
B. ceti TE10759-12	BCA52141_II0695 (OxyR)	V910_RS14490 (KatE)	V910_RS12985 (Cu–Zn SOD)
B. melitensis NI	–	BMNI_II0336 (KatE)	BMNI_II0654 (Cu–Zn SOD)
B. ovis ATCC 25840	BOV_A0321 (OxyR) BOV_A0665 (OxyR)	BOV_A0322 (KatA)	BOV_A0659 (Cu–Zn SOD)
B. pinnipedialis B2/94	BPI_II352 (OxyR)	BPI_II353 (KatA)	BPI_II757 (Cu–Zn SOD)
B. suisVBI22	BSVBI22B0350 (OxyR)	BSVBI22_B0351 (KatA)	BSVBI22_B0695 (Cu–Zn SOD)
Burkholderia ambifaria	–	BamMC406_6342 (KatE) BamMC406_5625 (KatG)	BamMC406_4594 (Fe-SOD)
B. cenocepacia J2315	–	BCAS0635 (Mn-catalase) BCAM2107 (KatA)	–
Burkholderia dolosa	AK34_3727 (SoxR)	BDSB_28020 (Mn-catalase)	–
Burkholderia gladioli	–	bgla_2g20310 (Mn-catalase) bgla_2g27370 (KatE) bgla_2g27730 (KatE) bgla_2g28310 (KatG)	bgla_2g28560 (Fe-SOD)
Burkholderia vietnamiensis G4	Bcep1808_4695 (RpoS)	Bcep1808_5181 (Mn-catalase) Bcep1808_5870 (Mn-catalase) Bcep1808_5733 (KatE) Bcep1808_5214 (KatG)	Bcep1808_6106 (Mn–Fe SOD) Bcep1808_7479 (Mn–Fe SOD)
Burkholderia xenovorans	–	Bxe_B0318 (KatN) Bxe_B1215 (KatE) Bxe_B1668 (KatE)	Bxe_C1205 (Mn–Fe SOD)

Table 4 (*contd*)

Names of the bacteria	Oxidative stress response managers		
	Response regulator	Catalases	Superoxide dismutases
C. taiwanensis LMG 19424	RALTA_B2083 (SoxR)	RALTA_B1505 (KatN) RALTA_B0345 (KatE)	RALTA_B0932 (Cu–Zn SOD)
D. radiodurans R1	DR_A0336 (OxyR)	DR_A0259 (KatA) DR_A0146 (KatA)	DR_A0202 (Cu–Zn SOD)
Ochrobactrum anthropi	OANT_RS15285 (SoxR)	OANT_RS15805 (KatE)	OANT_RS19760 (Cu–Zn SOD)
O. intermedium	OINT_2000242 (SoxR)	OINT_2000336 (KatE) OINT_2001566 (KatE) OINT_2001849 (KatE)	OINT_2000919 (Cu–Zn SOD)
P. profundum SS9	PBPRB1505 (SoxR)	PBPRB0286 (KatE)	–
Ralstonia eutropha H16	h16_B2319 (SoxR)	H16_A3109 (KatE) H16_A2777 (KatG) H16_B1428 (KatE)	H16_A0610 (Mn–Fe SOD) h16_B1110 (Cu–Zn SOD)
Ralstonia eutropha JMP134 (pJP4)	–	Reut_B4409 (Mn-catalase)	Reut_B4338 (Cu–Zn SOD)
Ralstonia pickettii DTP0602	N234_33075 (SoxR)	N234_24060 (KatE)	N23426615 (Cu–Zn SOD) N23435130 (Mn–Fe SOD)
Rhizobium sp. *IRBG74*	BN877_II1722 (OxyR) BN877_II0984 (SoxR)	BN877_II1832 (KatE) BN877_II1723 (KatG)	BN877_II1666 (Mn–Fe SOD) BN877_II1885 (Mn–Fe SOD)
V. alginolyticus NBRC 15630 = ATCC 17749	N646_3759 (Sox R)	N646_3134 (KatE) N646_4164 (KatG)	N646_3233 (Cu–Zn SOD)
V. campbellii ATCC BAA-1116	–	M892_19460 (KatE) M892_25335 (KatE)	M892_19470 (Cu–Zn SOD)
V. parahaemolyticus BB22OP	VPBB_A0311 (SoxR)	VPBB_A12 91 (KatE) VPBB_A02 85 (KatE) VPBB_A0408 (KatG) VPBB_A0708 (KatG)	–
V. parahaemolyticus RIMD 2210633	VPA0335 (SoxR)	VPA0305 (KatE) VPA1418 (KatE) VPA0453 (KatG) VPA0768 (KatG)	VPA1514 (Cu–Zn SOD)
V. splendidus LGP 32	VS_II0853(RpoS)	VS_II0148 (KatE)	–
V. vulnificus	–	VVA0294 (KatE)	VVA0291 (Cu–Zn SOD)
Alivibrio salmonicida	VSAL_RS17285 (SoxR)	VSAL_RS17235 (KatE)	VSAL_RS18750 (Cu–Zn SOD)

Table 4 (*contd*)

Names of the bacteria	Oxidative stress response managers		
	Response regulator	Catalases	Superoxide dismutases
V. fluvialis	AL536_RS21800 (OxyR) AL536_RS14685 (SoxR)	–	AL536_RS21525 (SodA) AL536_RS10230 (SodB)
V. natriegens	PN96_RS17565 (SoxR)	–	PN96_RS15615 (Cu–Zn SOD)
V. nigripulchritudo	VIBNI_RS18965 (SoxR)	VIBNI_RS21325, (KatE) VIBNI_RS19155 (KatE)	–
V. tubiashii	IX91_RS17995 (SoxR)	IX91_RS24110 (KatE)	–
V. wodanis	AWOD_RS13900 (SoxR)	AWOD_RS13805 (KatE)	–

multimers has been shown (Mythili and Muniyappa 1993). *D. radiodurans*, an MGH bacterium does not seem to have RecBC recombination pathway and in *trans* expression of *E. coli* RecB and RecC homologues made these cells sensitive to γ radiation (Khairnar *et al.* 2008).

Pathogenic determinants on secondary genome elements

Molecular mechanisms underlying bacterial pathogenesis are not fully understood. However, we searched some known virulence factors associated with the bacterial pathogenicity in the genome of MGH bacteria. These include capsular polysaccharide (CPS) that confers resistance to phagocytosis and serum killing, secretory systems, iron acquisition and extracellular enzymes and toxins, proteins that control cell motility, type IV pilus formation and RTX toxin. The presence of these pathogenicity markers, if any, on secondary genome elements, was therefore reviewed in some notable pathogenic MGH bacteria.

The vibrios are well-known human pathogens having multipartite genome systems. The pathogenic factors in *V. cholerae* are mainly distributed on its primary chromosome. However, chromosome II of this bacterium also encodes virulence factors like VCA0865 encoding for *hap*, a secretory haemaglutinin metalloprotease; VCA0219 for *hlyA* a secretory haemolysin with enterotoxic activity; VCA0594 for haemolysin (*hlx*) and VCA0218 and VCA1111 for thermolabile and thermostable haemolysin (*tdh*), respectively. In addition, chromosome II in *V. cholerae* encodes haemagglutinin (VCA0446) and its associated protein (VCA0447), as well as other hypothetical haemolysin and haemagglutinin-type proteins etc. (Heidelberg *et al.* 2000). Likewise, *V. vulnificus* YJ016, a highly invasive agent causing fulminant septicaemia in humans has multiple virulence factors like the CPS, five groups of genes (type IV pilus, iron acquisition, extracellular enzyme and toxin, and RTX toxin) on its secondary chromosome (Chen *et al.* 2003). In addition to a cytolysin gene *vvhA* (VVA0965) uniquely present only on small chromosome, it also encodes a metalloprotease (VVA1465), a phospholipase (VVA0303), the clusters of RTX A–D homologues (VVA1030, VVA1032, VVA1034, VVA1035 and VVA1036) (Chen *et al.* 2003). *V. fischeri* is a symbiont in a few squids and fishes, and is nonpathogenic. It carries many homologues of toxin-encoding genes from vibrios and the virulence factors are encoded on chromosome I (Ruby *et al.* 2005). Chromosome II encodes Flp1 pilus and PilA2 pilus for efficient colonization by bacteria in light organ of the host. In addition, the cholera toxin (CTX) phage-like mobile elements composed of eight ORFs, including four homologues of CTX-phage genes: *cep*, *orfU*, *ace* and *zot*, and the majority of toxin coregulated pilus (TCP) proteins are encoded on chromosome II. The *V. fischeri* genome contains 10 separate

Table 5. DNA recombination and repair proteins in secondary genome elements.

Bacteria	Names of the ORFs and proteins in parentheses	
	Recombination	Repair
Anabaena	ANA_C20356 (RecQ) ANA_C20436 (RecJ) ANA_C20139 (RecF) ANA_C20032 (RecG)	ANA_C20446 (MutS) ANA_C20598 (PhrB)
B. abortus A13334	–	BAA13334_II0133 (AlkB) BAA13334_II00265 (Phr) BAA13334_II00555 (MutL)
B. canis	BCA52141_II0352 (RecG)	BCA52141_II0896 (MutL) BCA52141_II0896 (AlkB)
B. ceti TE10759-12	V910_200672 (RecG)	V910_200990 (MutL) V910_200719 (AlkB)
B. ovis ATCC 25840	BOV_A0546 (RecG)	BOV_A0198 (MutL) BOV_A0463 (AlkB)
B. pinnipedialis B2/94	BPI_II633 (RecG)	BPI_II216 (MutL) BPI_II516 (AlkB)
Burkholderia dolosa	BDSB_17505 (RecQ)	BDSB_29025 (Ku80)
Burkholderia gladioli		bgla_2g27310 (AlkB)
Burkholderia multivorans 17616	BMULJ_03921(RecQ)	BMULJ_03823(Phr) BMULJ_04524(AlkB)
Burkholderia pseudomallei strain MSHR305	BDL_2177 (RecQ) BDL_1251 (RecQ) BDL_738 (RecD) BDL_739 (RecB) BDL_740 (RecC) BDL_3210 (RecJ) BDL_3521 (RecF) BDL_3014 (RecO) BDL_47 (RecR) BDL_2611 (RecN) BDL_2576 (RecG) BDL_1250 (RecX) BDL_3370 (RecA) BDL_1106 (RadA) BDL_1856 (RadC)	BDL_2630 (LexA) BDL_3237 (MutL) BDL_3140 (MutS) BDL_1988 (Phr) BDL_1847 (Ada)
Butyrivibrio proteoclasticus	bpr_IV188 (RecD)	bpr_IV158 (UmuC)
Cupriavidus taiwanensis LMG 19424	–	RALTA_B0289 (Ku80) RALTA_B2123 (Ku80) RALTA_B1379 (UvrA)
Cyanothece	cce_5212 (RuvC)	cce_5074 (LexA) cce_5035 (XseA) cce_5034 (XseB)
Ochrobactrum anthropi	OANT_RS18815 (RecG)	OANT_RS16275 (SbcC) OANT_RS15780 (MutL) OANT_RS18980 (MutT)
Ochrobactrum intermedium	OINT_2000735 (RecG)	OINT_2000330 (MutL) OINT_2000372 (Methyl transferase) OINT_2001883 (Phr) OINT_2001414 (Ung)
Photobacterium profundum SS9	PBPRB0507 (RecQ)	PBPRB0972 (UmuC) PBPRB0973 (UmuD)
Prevotella intermedia	PIN17_A0096 (RecB) PIN17_A1674 (RecJ) PIN17_A1308 (RecF) PIN17_A0335 (RecO) PIN17_A1532 (RecR) PIN17_A0189 (RecG) PIN17_A0655 (RecX) PIN17_A1062 (RecA) PIN17_A0441 (RadC)	PIN17_A0707 (Vsr) PIN17_A0090 (MutL) PIN17_A0541 (MutS) PIN17_A0405 (MutT) PIN17_A1375 (MutT) PIN17_A1998 (MutY) PIN17_A1641 (UvrD) PIN17_A1644 (UvrD) PIN17_A0525 (UvrC)

Table 5 (*contd*)

Bacteria	Names of the ORFs and proteins in parentheses	
	Recombination	Repair
	PIN17_A0453 (RuvB) PIN17_A1083 (RuvA)	PIN17_A1504 (UvrB) PIN17_A1486 (UvrA1) PIN17_A1743 (UvrA2) PIN17_A1338 (XseB) PIN17_A1904 (XthA) PIN17_A1373 (LigA) PIN17_A0341 (Ung) PIN17_A0342 (Ung) PIN17_A0934 (PriA) PIN17_A1704 (AlkD)
Prevotella melaninogenica ATCC 25845	HMPREF0659_A6930 (RecF) HMPREF0659_A7398 (RecR) HMPREF0659_A6927 (RadA) HMPREF0659_A7215 (RadC) HMPREF0659_A6842 (RuvC)	HMPREF0659_A6530 (UvrD) HMPREF0659_A6762 (UvrD) HMPREF0659_A6764 (UvrD) HMPREF0659_A7124 (UvrB) HMPREF0659_A6927 (LexA)
Pseudoalteromonas haloplanktis TAC125	–	PSHAb0293 (OgtA) PSHAb0453 (Phr)
Ralstonia eutropha JMP134	Reut_B4547 (RecQ)	Reut_B4423 (Ku80)
Ralstonia pickettii DTP0602	–	RALTA_B1379 (UvrA) RALTA_B0289 (Ku80) RALTA_B2123 (Ku80)
Rhizobium sp. IRBG74	BN877_II1155 (RecX) BN877_II0672 (RuvA) BN877_II0671 (RuvB) BN877_II0673 (RuvC)	–
V. fischeri ES114	VF_A1156 (RecQ) VF_A0522 (RadC) VF_B0007 (RadC)	VF_A0753 (Phr)
V. furnissii	–	vfu_B01401 (MutT) vfu_B00078 (MutT) vfu_B00126 (MutT) vfu_B00768 (AlkB)
V. vulnificus	–	VVA0562 (MutT) VVA0615 (MutT) VVA0357 (Phr) VVA0455 (AlkA)
Alivibrio salmonicida	VSAL_RS16195 (RecQ)	VSAL_RS18510 (MutT) VSAL_RS18710 (methyl transferase) VSAL_RS17155 (Mmethyl transferase) VSAL_RS16915 (AlkB)
V. fluvialis	–	AL536_RS07165 (photolyase AL536_RS03210, (MutT) AL536_RS04435, (MutT) AL536_RS05340 (MutT) AL536_RS00850 (AlkB)
V. hollisae	–	AL542_RS01910 (photolyase)
V. mimicus	–	AL543_RS01565 (photolyase) AL543_RS03960, (MutT) AL543_RS04165, (MutT) AL543_RS00715 (AlkB)
V. natriegens	–	PN96_RS15445 (photolyase) PN96_RS17385, (MutT) PN96_RS20200 (MutT) PN96_RS17160 (AlkA)

Table 5 (*contd*)

Bacteria	Names of the ORFs and proteins in parentheses	
	Recombination	Repair
V. nigripulchritudo	–	VIBNI_B1750 (photolyase) VIBNI_B1039 (MutT) VIBNI_RS27630 (UvrD VIBNI_RS23040, (Methyl transferase) VIBNI_RS23045, (methyl transferase) VIBNI_RS23580 (methyl transferase)
V. tubiashii	–	IX91_RS21430 (photolyase) IX91_RS23940 (RadC) IX91_RS17725, (MutT) IX91_RS18650, (MutT) IX91_RS19680 (MutT)
V. wodanis	AWOD_RS20280 (RecQ) AWOD_RS18700 (RecX)	AWOD_RS17980 (photolyase) AWOD_RS15880, (MutT) AWOD_RS15880 (MutT)

pilus gene clusters including eight type-IV pilus loci (five on chromosome I and three on chromosome II) and these are required for colonization and pathogenesis by this bacterium.

These features were also found in the members of genus *Burkholderia* another potent human pathogen that contains multipartite genome system. The distribution of pathogenic determinants in most of the *Burkholderia* strains was found to be on secondary chromosomes. For instance in *B. Mallei*, 21 of 33 genes for nonribosomal peptide synthases and polyketide synthases that are associated with virulence in this bacterium are located primarily in clusters on the smaller chromosome (Nierman *et al.* 2004). The chromosome II of this bacterium encodes the enzymes that are involved in toxins and extracellular capsule production, and also encodes a *S. typhimurium*-like type III secretion system. When the genomes of 10 *B. mallei* strains (seven virulent and three avirulent tested in Syrian golden hamsters) were hybridized and compared, there were 162 genes which were either diverged or absent in the avirulent isolates but present on both the chromosomes of virulent strains. In *B. pseudomallei* K96243, the virulence functions are encoded on the secondary genome. These include three sets of type III secretion systems (TTS1, BPSS1390–BPSS1408; TTS2, BPSS1613–BPSS1629; TTS3, BPSS1543–BPSS1552), two potential surface polysaccharide clusters (BPSS1825–BPSS1834 and BPSS0417–BPSS0429), one of three phospholipases C (BPSS0067), metalloprotease A (BPSS1993) and a putative collagenase (BPSS0666), few Hep-Hag repeat family proteins (BPSS0796, BPSS0908, BPSS1434 and BPSS 1439) that potentially modulate host–cell interactions (Holden *et al.* 2004; Chain *et al.* 2006). Presence of both survival and virulence functions in the secondary genome of this organism reflects the importance of secondary replicon in the survival and success of such bacteria in different environments. The *B. cenocepacia* strain J2315 which is more fatal, encodes the core functions (cell division, central metabolism and other 'house-keeping' functions) on chromosome I. However, chromosome II also encodes many potential virulence factors like LPS and other surface polysaccharides biosynthesis (BCAL2402–BCAL2408; BCAL3110–BCAL3125; BCAL1929–BCAL1935), phospholipase C (BCAL0443; BCAL1046; BCAM0408; BCAM1969; BCAM2429; BCAM2720), all types of secretion system (type I–type VI) and quorum sensing genes like *N*-acylhomoserine lactone regulons. Several proteins responsible for pilli formation, motility and adhesiveness of this bacterium are also present on secondary genome elements (Holden *et al.* 2009).

Leptospira interrogans, an obligately aerobic and tightly coiled spirochaete produces a fatal medical pathology in human, leptospirosis. Leptospiras exhibit structural differences in the carbohydrate moiety of LPS that determines antigenic diversity (Evangelista and Cobum 2010). It contains multipartite genome system comprised of two chromosomes. Although most of the genes required for growth and viability are located on chromosome I, some pathogenic genes also lie on chromosome II (Ren *et al.* 2003). These include LPS, haemolysins, outer membrane proteins (OMPs), chemotaxis system, sphingomyelinase like haemolysins (*sph* 1 and *sphH*) and four genes for nonsphingomyelinase-like haemolysins (*tlyA*, *hlyX*, *hlpA* and *hlyC*) and host extracellular matrix (ECM) interacting system, which makes this bacterium the most effective pathogen.

Since MGH group also includes plant pathogenic bacteria, the distribution of virulence factors on secondary genome elements of these bacteria was analysed. It was

Table 6. Absence/incomplete RecBC/RecF types homologous recombination pathway genes in the genome of some MGH bacteria.

Bacteria	RecB	RecC	RecD	AddAB	RecF	RecA	LexA	RadA
Anabaena	–	–	–		ANA_C12201	ANA_C12885	ANA_C12996	ANA_C11844
Candidatus Chloracidobacterium thermophilum	Cabther_A1450	–	Cabther_A2066	–	Cabther_A0743	Cabther_A0040	–	Cabther_A1430
Cupriavidus taiwanensis LMG	–	–	–	–	–	RALTA_A0499	RALTA_A1825	RALTA_A1733
Cyanothece	–	–	–	–	cce_2613	cce_4639	cce_1899 cce_5074	cce_4001
Deinococcus radiodurans R1	–	–	DR_1902	–	DR_1089	DR_2340	–	DR_1105
Prevotella dentalis DSM	–	–	–	–	–	Prede_0960	–	Prede_0402
Prevotella intermedia	–	–	–	–	–	PIN17_A1062	–	PIN17_0360
Pseudoalteromonas sp. *SM9913*	–	–	–	–	PSM_A0003	–	PSM_A2971	PSM_A2399
Ralstonia eutropha	Reut_A2115	–	Reut_A2114	–	–	Reut_A0527	Reut_A2008	Reut_A1933
Ralstonia pickettii	N234_13810	–	–	–	–	N234_02680	N234_13250	N234_11755
Rhodobacter sphaeroides	RSKD131_2919		RSKD131_2744	–	RSKD131_1784	RSKD131_0299	RSKD131_0770	RSKD131_2919
Variovorax paradoxus S110	–	–	–	–	VAPA_1c12300	VAPA_1c54021	VAPA_1c29160	VAPA_1c03050
Alivibrio salmonicida	–	–	–	–	VSAL_RS00155	VSAL_RS03540	VSAL_RS15215	VSAL_RS03500

observed that the secondary genome elements like pSymA and pSymB in *S. meliloti*, a symbiont of the legume alfalfa encode the majority of the proteins required for the symbiotic association with plants (Galibert *et al.* 2001). These include ABC transporters (~12% of whole genome) and regulatory functions like LysR family, GntR regulators, histidine kinases, response regulators and nucleotide cyclases that occupied ~8.7% in the whole genome. In addition, genes for exopolysaccharide synthesis, multidrug efflux permeases (SMb20345, SMb20346 and SMb20698), putative acriflavine resistance proteins (*acre*; SMb21497 and *acrF*; SMb21498), C4-dicarboxylate (*dctA*) and phosphate transport (*phoCDET*) as well as the complete nitrogen fixation machinery including those required for N_2-fixing root nodule formation (*bacA*) are reported on pSymB (Finan *et al.* 2001). Similarly, *A. tumefaciens*, a well-known plant pathogen consists of a circular chromosome, a linear chromosome and two plasmids (pAtC58 and pTiC58) (Wood *et al.* 2001). All four replicons of *A. tumefaciens* contains orthologues of those present in *S. meliloti* pSymA and pSymB plasmids except nitrogen fixation operon *fixNOQP* of pSymA, on the circular chromosome in *A. tumefaciens*. The presence of *chvAB* genes involved in the synthesis of the extracellular β-1, 2-glucan for adhesion to plant cells on its primary chromosome, the *chvGI*, *chvE* and *ros* genes involved in regulation of *vir* genes on Ti plasmid; the *chvD*, *chvH* and *acvB* genes on linear chromosomes (Goodner *et al.* 2001) have been found. Ti plasmid encodes for proteins involved in virulence functions as well as control opines metabolism during and after infection to plants. Interestingly, the linear chromosome of *A. tumefaciens* encodes a highly potent virulence factor pectinase (*kdgF*). The presence of other important factors like ligninase (*ligE*) on Ti plasmid, and xylanase as well as regulators of pectinase and cellulase production (*pecS*/*pecM*) on circular chromosome has been observed. These information suggest that secondary genome elements with their higher copies in some cases might provide the strong support to pathogenic bacteria to invade the host defense system and causes pathogenicity.

Correlation between multipartite genome system and stress tolerance

Since the discovery of multipartite genome system and its biology in bacteria is relatively new, the role of multipartite genome system and ploidy in bacterial response to various stresses is less characterized. Conceptually, the genetic redundancy because of the ploidy and/or multiple copies of a gene could provide substrates during the recombination repair of damaged DNA, and that helps the organisms for maintaining genome integrity. Therefore, the possibility of higher DNA damage tolerance in these bacteria if due to its multipartite genome and ploidy nature cannot be

ruled out. Microscopic examination of different members of Deinococacceae family showing almost similar levels of radioresistance and the *D. radiodurans* mutants that have compromised radioresistance did not support this hypothesis. For instance, *rec30* strain of *D. radiodurans* is highly sensitive to γ radiation but its ploidy and nucleoid structure did not change. Further, *D. geothermalis* and *D. radiopugnans* are as resistant to γ radiation as *D. radiodurans* but their nucleoid compactness differed widely (Ferreira *et al.* 1997). On the other hand, *D. geothermalis* and *D. pugnans* as well as *T. aquaticus* and *E. coli*'s nucleoid are less compact and have more fluid genome structure than *D. radiodurans*, also show different levels of radioresistance.

Deletion of *parABS* system from the genome of bacteria harbouring single circular chromosome had affected survival and growth characteristics of wild-type cells (Lasocki *et al.* 2007; Donovan *et al.* 2010; Donczew *et al.* 2016). Genome partitioning mechanisms in four MGH bacteria have been studied as described above. ParB1 and ParB2 have been deleted from chromosomes I and II in *V. cholerae* and the roles of these proteins in polarization of respective chromosomal *ori* regions have been shown (Fiebig *et al.* 2006; Yamaichi *et al.* 2007; Kadoya *et al.* 2011). When pathogenesis of these mutants was checked, interestingly it was observed that both ParBs in *V. cholerae* controls respective chromosome segregation. These cells lose many characteristics linked to the pathology of *V. cholerae* like arrest of growth after one cycle of division, cell enlargement, nucleoid condensation, degradation and loss of membrane integrity (Yamaichi *et al.* 2007). However, the absence of ParA1 did not affect segregation of chromosome I. Transcriptome analysis and the screening of genes responsible for pathogenesis in *V. cholerae* showed that quite a large number of proteins that are involved in bacterial pathogenesis are encoded on chromosome II (Kamp *et al.* 2013). *D. radiodurans* harbours two chromosomes and two plasmids. ParBs of chromosome II and megaplasmid were deleted and deletion mutants show loss of respective genome elements. These cells also significantly compromised radioresistance and oxidative stress tolerance as compared to wild-type *D. radiodurans* (Misra *et al*., *unpublished data*). The *parB1* mutant of *D. radiodurans* showed growth defect and prolonged cell division (Charaka *et al.* 2014). In case of *B. cepacia*, the chromosome 3 (C3) deletion mutant was isolated through transposon mutagenesis and this mutant becomes non-infectious to *Caenorhabditis elegans* (Agnili *et al.* 2012). When C3-based mini-chromosome was constructed and used for curing chromosome 3 in several strains of *B. cepacia* complex species, all C3-null mutants lost virulence in multiple infection hosts. From these available evidences it appears that secondary genome elements that could be either extra chromosomes or plasmids do not seem to be required for normal growth of MGH bacteria but might contribute in stress tolerance and pathogenesis.

Concluding remarks and future perspectives

Similar to bacteria harbouring single circular chromosome, MGH bacteria also encode 'Par' protein homologues of tripartite partitioning systems. The centromeric sequences have not been identified in most of MGH bacteria except in case of *V. cholerae*, *D. radiodurans* and *B. cenocepacia* where genome segregation mechanisms have been partly studied. Primary chromosome in these three MGH bacteria appears to segregate through pulling mechanism. Not much has been studied about the segregation mechanism of secondary chromosomes and plasmids. Primary chromosome in MGH bacteria is nearly similar to the chromosome of the single chromosome harbouring bacteria, particularly for the genes encoded on these elements. Genomewide scanning showed that a large number of stress response kinases and cognate regulators, DNA damage repair proteins and the machinery for their maintenance in these bacteria are encoded on secondary genome elements. Information on the presence and distribution of RecBC and RecF recombination pathways on both primary chromosome and secondary genome elements might open up further debate on the essentiality of *E. coli*-type homologous recombination pathways for maintaining genomic integrity in MGH bacteria. This is also because there are some MGH bacteria, where neither of these homologous recombination pathways exists while in some cases only one is found. Understanding the underlying mechanisms of multipartite genome maintenance and its ploidy, and its relation with microbial infections could be one of the most exciting and demanding directed basic research areas in bacterial genome biology and pathogenesis.

Although not much work has been reported on the curing of secondary genome elements and its effect on phenotypes, the available information clearly supports that secondary genome elements have roles in abiotic and biotic stress tolerance in MGH bacteria. Curing of secondary genome in *B. cenocepacia* has resulted in the loss of infectivity and therefore, the use of this approach in the management of bacterial infections would be a hypothesis worth testing. Further studies on understanding the underlying mechanisms of secondary genome maintenance in these bacteria and the anucleation strategy if it leads to the altered phenotypes might help in designing the effective and sustainable technologies in the development of live vaccines for the management of microbial pathogenesis.

Acknowledgements

The authors are grateful to Dr Subrata Chattopadhyay and Dr Chitra Seetharam Misra for critical reading of the manuscript and their comments.

References

Agnili K., Schwager S., Uehlinger S., Vergunst A., Viteri D. F., Nguyen D. T. *et al.* 2012 Exposing the third chromosome of *Burkholderia cepacia* complex strains as a virulence plasmid. *Mol. Microbiol.* **83**, 362–378.

Allardet-Servent A., Michaux-Charachon S., Jumas-Bilak E., Karayan L. and Ramuz M. 1993 Presence of one linear and one circular chromosome in the *Agrobacterium tumefacience* C58 genome. *J. Bacteriol.* **175**, 7869–7874.

Amadou C., Pascal G., Mangenot S., Glew M., Bontemps C., Capela D. *et al.* 2008 Genome sequence of the β-rhizobium *Cupriavidus taiwanensis* and comparative genomics of rhizobia. *Genome Res.* **18**, 1472–1483.

Ancora M., Marcacci M., Orsini M., Zilli K., Di Giannatale E., Garofolo G. *et al.* 2014 Complete genome sequence of a *Brucella ceti* ST26 strain isolated from a striped dolphin (*Stenella coeruleoalba*) on the Coast of Italy. *Genome Announc.* **6**, 2.

Audic S., Lescot M., Claverie J. M., Cloeckaert A. and Zygmunt M. S. 2009 The genome sequence of *Brucella pinnipedialis* B2/94 sheds light on the evolutionary history of the genus *Brucella*. *BMC Evol. Biol.* **11**, 200.

Bjornsdottir-Butler K., McCarthy S. A., Dunlap P. V., Timme R. E. and Benner R. A. Jr. 2015 Draft genome sequences of histamine-producing *Photobacterium kishitanii* and *Photobacterium angustum*, isolated from albacore (*Thunnus alalunga*) and yellowfin (*Thunnus albacares*) tuna. *Genome Announc.* **3**, e00400–e00415.

Chain P. S., Denef V. J., Konstantinidis K. T., Vergez L. M., Agullo L., Reyes V. L. *et al.* 2006 *Burkholderia xenovorans* LB400 harbors a multi-replicon, 9.73-Mbp genome shaped for versatility. *Proc. Natl. Acad. Sci. USA* **103**, 15280–15287.

Chain P. S., Lang D. M., Comerci D. J., Malfatti S. A., Vergez L. M., Shin M. *et al.* 2011 Genome of *Ochrobactrum anthropi* ATCC 49188 T, a versatile opportunistic pathogen and symbiont of several eukaryotic hosts. *J. Bacteriol.* **193**, 4274–4275.

Charaka V. K. and Misra H. S. 2012 Functional characterization of the role of the chromosome I partitioning system in genome segregation in *Deinococcus radiodurans*. *J. Bacteriol*. **194**, 5739–5748.

Charaka V. K., Mehta K. P. and Misra H. S. 2013 ParA encoded on chromosome II of *Deinococcus radiodurans* binds to nucleoid and inhibits cell division in *Escherichia coli*. *J. Biosci*. **38**, 487–497.

Charaka V. K., Kota S. and Misra H. S. 2014 ParA encoded on chromosome I of *Deinococcus radiodurans* requires its cognate ParB and centromere for its dynamics. *Proc. Ind. Natl. Sci. Acad.* **80**, 663–674.

Chen C. Y., Wu K. M., Chang Y. C., Chang C. H., Tsai H. C., Liao T. L. *et al.* 2003 Comparative genome analysis of *Vibrio vulnificus*, a marine pathogen. *Genome Res.* **13**, 2577–2587.

Cheng H. P. and Lessie T. G. 1994 Multiple replicons constituting the genome of *Pseudomonas cepacia* 17616. *J. Bacteriol.* **176**, 4034–4042.

Cooper V. S., Vohr S. H., Wrocklage S. C. and Hatcher P. J. 2010 Why genes evolve faster on secondary chromosomes in bacteria. *PLoS Comput. Biol.* **6**, e1000732.

Cosgrove K., Coutts G., Jonsson I.-M., Tarkowski A., Kokai-Kun J.-F., Mond J. J. *et al.* 2007 Catalase (KatA) and alkyl hydroperoxide reductase (AhpC) have compensatory roles in peroxide stress resistance and are required for survival, persistence, and nasal colonization in *Staphylococcus aureus*. *J. Bacteriol*. **189**, 1025–1035.

Crook M. B., Mitra S., Ane J. M., Sadowsky M. J. and Gyaneshwar P. 2013 Complete genome sequence of the Sesbania symbiont and rice growth-promoting endophyte *Rhizobium* sp. strain IRBG74. *Genome Announc*. **1**, e00934–e00913.

De Oliveira Veras A. A., da Silva M. L., Gomes J. C., Dias L. M., de Sá P. C., Alves J. T. *et al*. 2015 Draft genome sequences of *Vibrio fluvialis* strains 560 and 539, isolated from environmental samples. *Genome Announc*. **3**, e01344-14.

Devigne A., Mersaoui S., Bouthier-de-la-Tour C., Sommer S. and Servant P. 2013 The PprA protein is required for accurate cell division of γ-irradiated *Deinococcus radiodurans* bacterium. *DNA Repair* **12**, 265–272.

Devigne A., Guerin P., Lisboa J., Quevillon-Cheruel S., Armengaud J., Sommer S. *et al.* 2016 PprA protein is involved in chromosome segregation via its physical and functional interaction with DNA gyrase in irradiated *Deinococcus radiodurans* bacterium. *Mol. Biol. Physiol*. **1**, e00036–e000315.

Dobruk-Serkowska A., Caccamo M., Rodriguez-Castaneda F., Wu M., Bryce K., Ng I. *et al.* 2012 Uncoupling of nucleotide hydrolysis and polymerization in the ParA protein superfamily disrupts DNA segregation dynamics. *J. Biol. Chem*. **287**, 42545–42553.

Donczew M., Mackiewicz P., Wróbel A., Flärdh K., Zakrzewska-Czerwińska J. and Jakimowicz D. 2016 ParA and ParB coordinate chromosome segregation with cell elongation and division during *Streptomyces* sporulation. *Open Biol*. **6**, 150263.

Donovan C., Schwaiger A., Krämer R. and Bramkamp M. 2010 Subcellular localization and characterization of the ParAB system from *Corynebacterium glutamicum*. *J. Bacteriol.* **192**, 3441–3451.

Draper G. C. and Gober J. W. 2002 Bacterial chromosome segregation. *Annu. Rev. Microbiol.* **56**, 567–597.

Dubarry N., Pasta F. and Lane D. 2006 ParABS systems of the four replicons of *Burkholderia cenocepacia*: new chromosome centromeres confer partition specificity. *J. Bacteriol.* **188**, 1489–1496.

Ebersbach G. and Gerdes K. 2005 Plasmid segregation mechanisms. *Annu. Rev. Genet*. **39**, 453–479.

Egan E. S., Fogel M. A. and Waldor M. K. 2005 Divided genomes: negotiating the cell cycle in prokaryotes with multiple chromosomes. *Mol. Microbiol.* **56**, 1129–1138.

Errington J., Murray H. and Wu L. J. 2005 Diversity and redundancy in bacterial chromosome segregation mechanisms. *Philos. Trans. R. Soc. London, B* **360**, 497–505.

Espeli O., Borne R., Dupaigne P., Thiel A., Gigant E., Mercier R. *et al.* 2012 MatP–divisome interaction coordinates chromosome segregation with cell division in *E. coli*. *EMBO J.* **31**, 3198–3211.

Evangelista K. V. and Cobum J. 2010 Leptospiraas an emerging pathogen: a review of its biology, pathogenesis and host immune responses. *Future Microbiol.* **5**, 1413–1425.

Ferreira A. C., Nobre M. F., Rainey F. A., Silva M. T., Wait R. and Burghardt J. 1997 *Deinococcus geothermalis* sp. Nov., and *Deinococcus murrayi* sp. nov., two extremely radiation-resistant and slightly thermophilic species from hot springs. *Int. J. Syst. Bacteriol.* **47**, 939–947.

Fiebig A., Keren K. and Theriot J. A. 2006 Fine-scale time-lapse analysis of the biphasic, dynamic behaviour of the two *Vibrio cholerae* chromosomes. *Mol. Microbiol.* **60**, 1164–1178.

Finan T. M., Weidner S., Wong K., Buhrmester J., Chain P., Vorholter F. J. *et al.* 2001 The complete sequence of the 1,683-kb pSymB megaplasmid from the N2-fixing endosymbiont *Sinorhizobium meliloti*. *Proc. Natl. Acad. Sci. USA* **98**, 9889–9894.

Fogel M. A. and Waldor M. K. 2005 Distinct segregation dynamics of the two *Vibrio cholerae* chromosomes. *Mol. Microbiol.* **55**, 125–136.

Fogel M. A. and Waldor M. K. 2006 A dynamic, mitotic-like mechanism for bacterial chromosome segregation. *Genes Dev.* **20**, 3269–3282.

Galardini M., Pini F., Bazzicalupo M., Biondi E. G. and Mengoni A. 2013 Replicon-dependent bacterial genome evolution: the case of *Sinorhizobium meliloti*. *Genome Biol. Evol*. **5**, 542–558.

Galibert F., Finan T. M., Long S. R., Puhler A., Abola P., Ampe F. *et al.* 2001 The composite genome of the legume symbiont *Sinorhizobium meliloti*. *Science* **293**, 668–672.

Garcia Costas A. M., Tsukatani Y., Rijpstra W. I., Schouten S., Welander P. V., Summons R. E. *et al.* 2012 Identification of the bacteriochlorophylls, carotenoids, quinones, lipids, and hapanoids of *Cadidatus Chloracidobacterium thermophilum*. *J. Bacteriol.* **194**, 1158–1168.

Gerdes K., Howard M. and Szardenings F. 2010 Pushing and pulling in prokaryotic DNA segregation. *Cell* **121**, 927–942.

Ghosh S. K., Hajra S., Paek A. and Jayaram M. 2006 Mechanisms for chromosome and plasmid segregation. *Annu. Rev. Biochem.* **75**, 211–241.

Gitai Z. 2006 Plasmid segregation: a new class of cytoskeletal proteins emerges. *Curr. Biol*. **16**, R133–R136.

Goodner B., Hinkle G., Gattung S., Miller N., Blanchard M., Qurollo B. *et al.* 2001 Genome sequence of the plant pathogen and biotechnology agent *Agrobacterium tumefaciens* C58. *Science* **294**, 2323–2328.

Goudenege D., Labreuche Y., Krin E., Ansquer D., Mangenot S. and Calteau A. 2013 Comparative genomics of pathogenic lineages of *Vibrio nigripulchritudo* identifies virulence-associated traits. *ISME J.* **7**, 1985–1996.

Hasan N. A., Grim C. J., Haley B. J., Chun J., Alam M., Taviani E. *et al.* 2010 Comparative genomics of clinical and environmental *Vibrio mimicus*. *Proc. Natl. Acad. Sci. USA* **107**, 21134–21139.

Hatano T. and Niki H. 2010 Partitioning of P1 plasmids by gradual distribution of the ATPase ParA. *Mol. Microbiol.* **78**, 1182–1198.

Heidelberg J. F., Eisen J. A., William C. N., Rebecca A. C., Michelle L. G., Robert J. D. *et al.* 2000 DNA sequence of both chromosomes of the cholera pathogen *Vibrio cholerae*. *Nature* **406**, 477–483.

Hjerde E., Lorentzen M. S., Holden M. T., Seeger K., Paulsen S., Bason N. *et al.* 2008 The genome sequence of the fish pathogen *Alivibrio salmonicida* strain LFI1238 shows extensive evidence of gene decay. *BMC Genomics* **9**, 616.

Hoffmann M., Monday S. R., Allard M. W., Strain E. A., Whittaker P., Naum M. *et al.* 2012 *Vibrio caribbeanicus* sp. nov., isolated from the marine sponge *Scleritoderma cyanea*. *Int. J. Syst. Evol. Microbiol.* **62**, 1736–1743.

Holden M. T., Seth-Smith H. M., Crossman L. C., Sebaihia M., Bentley S. D., Cerdeno-Tarraga A. M. *et al.* 2009 The genome of *Burkholderia cenocepacia* J2315, an epidemic pathogen of cystic fibrosis patients. *J. Bacteriol.* **191**, 261–277.

Holden M. T., Titball R. W., Peacock S. J., Cerdeno-Tarraga A. M., Atkins T., Crossman L. C. *et al.* 2004 Genomic plasticity of the causative agent of melioidosis, *Burkholderia pseudomallei*. *Proc. Natl. Acad. Sci. USA* **101**, 14240–14245.

Italiani V. C., da Silva Neto J. F., Braz V. S. and Marques M. V. 2011 Regulation of catalase-peroxidase KatG is OxyR dependent and Fur independent in *Caulobacter crescentus*. *J. Bacteriol.* **193**, 1734–1744.

Jacob F., Brenner S. and Cuzin F. 1963 On the regulation of DNA replication in bacteria. *Cold Spring Harbor Symp. Quant. Biol.* **23**, 329–348.

Jensen R. B. and Shapiro L. 1999 The *Caulobacter crescentus* smc gene is required for cell cycle progression and chromosome segregation. *Proc. Natl. Acad. Sci. USA* **96**, 10661–10666.

Jumas-Bilak E., Michaux-Charachon S., Bourg G., Ramuz M. and Allardet-Servent A. 1998 Unconventional genomic organization in the alpha subgroup of the proteobacteria. *J. Bacteriol.* **180**, 2749–2755.

Kadoya R., Baek J.-H., Sarker A. and Chattoraj D. K. 2011 Participation of chromosome segregation protein ParAI of *Vibrio cholerae* in chromosome replication. *J. Bacteriol.* **193**, 1504–1514.

Kamp H. D., Patimalla-Dipali B., Lazinski D. W., Wallace-Gadsden F. and Camilli A. 2013 Gene fitness landscapes of *Vibrio cholerae* at important stages of its life cycle. *PLoS Pathog.* **9**, e1003800.

Kelly W. J., Leahy S. C., Altermann E., Yeoman C. J., Dunne J. C., Kong Z. *et al.* 2010 The glycobiome of the rumen bacterium *Butyrivibrio proteoclasticus* B316 (T) highlights adaptation to a polysaccharide-rich environment. *PLoS One* **5**, e11942.

Khairnar N. P., Kamble V. A. and Misra H. S. 2008 RecBC enzyme overproduction affects UV and gamma radiation survival of *Deinococcus radiodurans*. *DNA Repair* **7**, 40–47.

Kim H., Jeong W., Jeoung H. Y., Song J. Y., Kim J. S., Beak J. H. *et al.* 2012 Complete genome sequence of *Brucella abortus* A13334, a new strain isolated from the fetal gastric fluid of dairy cattle. *J. Bacteriol.* **194**, 5444.

Komatsu H., Imura Y., Ohori A., Nagata Y. and Tsuda M. 2003 Distribution and organization of auxotrophic genes on the multichromosomal genome of *Burkholderia multivorans* ATCC 17616. *J. Bacteriol.* **185**, 3333–3343.

Kota S., Charaka V. K., Ringgaard S., Waldor M. K. and Misra H. S. 2014a PprA contributes to *Deinococcus radiodurans* resistance to nalidixic acid, genome maintenance after DNA damage and interacts with deinococcal topoisomerases. *PLoS One* **9**, e85288.

Kota S., Charaka V. and Misra H. S. 2014b PprA, a pleiotropic protein for radioresistance, works through DNA gyrase and shows cellular dynamics during postirradiation recovery in *Deinococcus radiodurans*. *J. Genet.* **93**, 349–354.

Kota S., Rajpurohit Y. S., Satoh K., Narumi I. and Misra H. S. 2016 DNA gyrase of *Deinococcus radiodurans* is characterized as type II bacterial topoisomerase and its activity is differentially regulated by PprA *in vitro*. *Extremophiles* **20**, 195–205.

Kulkarni G., Dhotre D., Dharne M., Shetty S., Chowdhury S., Misra V. *et al.* 2013 Draft genome of *Ochrobactrum intermedium* strain M86 isolated from non-ulcer dyspeptic individual from India. *Gut. Pathog.* **5**, 7.

Larsen R. A., Cusumano C., Fujioka A., Lim-Fong G., Patterson P. and Pogliano J. 2007 Treadmilling of a prokaryotic tubulin-like protein, TubZ, required for plasmid stability in *Bacillus thuringiensis*. *Genes Dev.* **21**, 1340–1352.

Lasocki K., Bartosik A. A., Mierzejewska J., Thomas C. M. and Jagura-Burdzy G. 2007 Deletion of the parA (soj) homologue in *Pseudomonas aeruginosa* causes ParB instability and affects growth rate, chromosome segregation, and motility. *J. Bacteriol.* **189**, 5762–5772.

Lee P. S., Lin D. C., Moriya S. and Grossman A. D. 2003 Effects of the chromosome partitioning protein Spo0J (ParB) on oriC positioning and replication initiation in *Bacillus subtilis*. *J. Bacteriol.* **185**, 1326–1337.

Leonard T. A., Møller-Jensen J. and Löwe J. 2005 Towards understanding the molecular basis of bacterial DNA segregation. *Philos. Trans. R. Soc. Lond. B Biol. Sci.* **360**, 523–535.

Le Roux F., Zouine M., Chakroun N., Binesse J., Saulnier D., Bouchier C. *et al.* 2009 Genome sequence of *Vibrio splendidus*: an abundant planctonic marine species with a large genotype diversity. *Environ Microbiol.* **11**, 1959–1970.

Lim S. K., Kim S. J., Cha S. H., Oh Y. K., Rhee H. J., Kim M. S. *et al.* 2009 Complete genome sequence of *Rhodobacter sphaeroides* KD131. *J. Bacteriol.* **191**, 1118–1129.

Lin D. C. and Grossman A. D. 1998 Identification and characterization of a bacterial chromosome-partitioning site. *Cell* **92**, 675–685.

Liu X. F., Cao Y., Zhang H. L., Chen Y. J. and Hu C. J. 2015 Complete genome sequence of *Vibrio alginolyticus* ATCC 17749T. *Genome Announc.* **3**, e01500–e01514.

Lux T. M., Lee R. and Love J. 2011 Complete genome sequence of a free-living *Vibrio furnissii* sp. nov.strain (NCTC 11218). *J. Bacteriol.* **193**, 1487–1498.

Lykidis A., Pérez-Pantoja D., Ledger T., Mavromatis K., Anderson I. J., Ivanova N. N. *et al*. 2010 The complete multipartite genome sequence of *Cupriavidus necator* JMP134, a versatile pollutant degrader. *PLoS One* **5**, e9729.

Makino K., Oshima K., Kurokawa K., Yokoyama K., Uda T., Tagomori K. *et al.* 2003 Genome sequence of *Vibrio parahaemolyticus*: a pathogenic mechanism distinct from that of *V. cholerae*. *Lancet* **361**, 743–749.

Medigue C., Krin E., Pascal G., Barbe V., Bernsel A., Bertin P. N. *et al.* 2005 Coping with cold: the genome of the versatile marine antarctica bacterium *Pseudoalteromonas haloplanktis* TAC125. *Genome Res.* **15**, 1325–1335.

Mercier R., Petit M. A., Schbath S., Robin S. E., Karoui M., Boccard F. *et al.* 2008 The MatP/matS site-specific system organizes the terminus region of the *E. coli* chromosome into a macrodomain. *Cell* **135**, 475–485.

Michaux S., Paillisson J., Carles-Nurit M. J., Bourg G., Allardet-Servent A. and Ramuz M. 1993 Presence of two independent chromosomes in the *Brucella melitensis* 16 M genome. *J. Bacteriol.* **175**, 701–705.

Minsky A., Shimoni E. and Englander J. 2006 Ring-like nucleoids and DNA repair through error-free non-homologous end joining in *Deinococcus radiodurans*. *J. Bacteriol.* **188**, 6047–6051.

Misra H., Rajpurohit Y. S. and Kota S. 2013 Physiological and molecular basis of extreme radioresistance in *Deinococcus radiodurans*. *Curr. Sci.* **104**, 194–206.

Mohl D. A. and Gober J. W. 1997 Cell cycle-dependent polar localization of chromosome partitioning proteins in *Caulobacter crescentus*. *Cell* **88**, 675–684.

Mohl D. A., Easter J. Jr and Gober J. W. 2001 The chromosome partitioning protein, ParB, is required for cytokinesis in *Caulobacter crescentus*. *Mol. Microbiol.* **42**, 741–755.

Mythili E. and Muniyappa K. 1993 Formation of linear plasmid multimers promoted by the phage lambda red-system in lon mutants of *Escherichia coli*. *J. Gen. Microbiol.* **139**, 2387–2397.

Nagata Y., Ohtsubo Y., Endo R., Ichikawa N., Ankai A., Fukui S. *et al.* 2010 Complete genome sequence of the representative γ-hexachlorocyclohexane-degrading bacterium *Sphingobium japonicum* UT26. *J. Bacteriol.* **192**, 5852–5853.

Naka H., Dias G. M., Thompson C. C., Dubay C., Thompson F. L. and Crosa J. H. 2011 Complete genome sequence of the marine fish pathogen *Vibrio anguillarum* harboring the pJM1 virulence plasmid and genomic comparison with other virulent strains of *V. anguillarum* and *V. ordali*. *Infect Immun*. **79**, 2889–2900.

Nambu T., Yamane K., Maruyama H., Mashimo C. and Yamanaka T. 2015 Complete genome sequence of *Prevotella intermedia* strain 17-2. *Genome Announc.* **3**, e00951–e00915.

Ng V. H., Cox J. S., Sousa A. O., MacMicking J. D. and McKinney J. D. 2004 Role of KatG catalase-peroxidase in mycobacterial pathogenesis: countering the phagocyte oxidative burst. *Mol. Microbiol.* **52**, 1291–1302.

Ni T., Corcoran D. L., Rach E. A., Song S., Spana E. P., Gao Y. *et al.* 2010 A paired-end sequencing strategy to map the complex landscape of transcription initiation. *Nat. Methods* **7**, 521–527.

Nierman W. C., DeShazer D., Kim H. S., Tettelin H., Nelson K. E., Feldblyum T. *et al.* 2004 Structural flexibility in the *Burkholderia mallei* genome. *Proc. Natl. Acad Sci. USA* **101**, 14246–14255.

Ohtani N., Tomita M. and Itaya M. 2010 An extreme thermophile, *Thermus thermophilus*, is a polyploid bacterium. *J. Bacteriol.* **192**, 5499–5505.

Ohtani N., Tomita M. and Itaya M. 2015 Curing the megaplasmid pTT27 from *Thermus thermophilus* HB27 and maintaining exogenous plasmids in the plasmid-free strain. *Appl. Environ. Microbiol.* **82**, 1437–1448.

Ohtsubo Y., Fujita N., Nagata Y., Tsuda M., Iwasaki T. and Hatta T. 2013 Complete genome sequence of *Ralstonia pickettii* DTP0602, a 2,4,6-trichlorophenol degrader. *Genome Announc.* **1**, e00903–e00913.

Okada K., Iida T., Tsukamoto K. K. and Honda T. 2005 Vibrios commonly possess two chromosomes. *J. Bacteriol.* **187**, 752–757.

Passot F. M., Calderon V., Fichant G., Lane D. and Pasta F. 2012 Centromere binding and evolution of chromosomal partition systems in the burkholderiales. *J. Bacteriol.* **194**, 3426–3436.

Paulsen I. T., Seshadri R., Nelson K. E., Eisen J. A., Heidelberg J. F., Read T. D. *et al.* 2002 The *Brucella suis* genome reveals fundamental similarities between animal and plant pathogens and symbionts. *Proc. Natl. Acad. Sci. USA* **99**, 13148–13153.

Prozorov A. A. 2008 Additional chromosomes in bacteria: properties and origin. *Microbiology* **77**, 385–394.

Qin Q. L., Li Y., Zhang Y. J., Zhou Z. M., Zhang W. X., Chen X. L. *et al.* 2011 Comparative genomics reveals a deep-sea sediment-adapted life style of *Pseudoalteromonas* sp. SM9913. *ISME J.* **5**, 274–284.

Ren S. X., Fu G., Jiang X. G., Zeng R., Miao Y. G., Xu H. *et al.* 2003 Unique physiological and pathogenic features of *Leptospira interrogans* revealed by whole-genome sequencing. *Nature* **422**, 888–892.

Ringgaard S., van Zon J., Howard M. and Gerdes K. 2009 Movement and equipositioning of plasmids by ParA filament disassembly. *Proc. Natl. Acad. Sci. USA* **106**, 19369–19374.

Ruby E. G., Urbanowski M., Campbell J., Dunn A., Faini M., Gunsalus R. *et al.* 2005 Complete genome sequence of *Vibrio fischeri*: A symbiotic bacterium with pathogenic congeners. *Proc. Natl. Acad Sci. USA* **102**, 3004–3009.

Schumacher M. A. 2007 Structural biology of plasmid segregation proteins. *Curr. Opin. Struct. Biol.* **17**, 103–109.

Seo Y. S., Lim J., Choi B. S., Kim H., Goo E., Lee B. *et al.* 2011 Complete genome sequence of *Burkholderia gladioli* BSR3. *J. Bacterial.* **193**, 3149.

Slade D. and Radman M. 2011 Oxidative stress resistance in *Deinococcus radiodurans*. *Microbiol. Mol. Biol. Rev.* **75**, 133–191.

Slater S. C., Goldman B. S., Goodner B., Setubal J. C., Farrand S. K., Nester E. W. *et al.* 2009 Genome sequences of three *Agrobacterium biovars* help elucidate the evolution of multichromosome genomes in bacteria. *J. Bacteriol.* **191**, 2501–2511.

Sobral B. W., Honeycutt R. J., Atherly A. G. and McClelland M. 1991 Electrophoretic separation of the three *Rhizobium meliloti* replicons. *J. Bacteriol.* **173**, 5173–5180.

Suwanto A. and Kaplan S. 1989 Physical and genetic mapping of the *Rhodobacter spahaeroides* 2.4.1 genome: presence of two unique circular chromosomes. *J. Bacteriol.* **171**, 5850–5859.

Tae H., Shallom S., Settlage R., Preston D., Adams L. G. and Garner H. R. 2011 Revised genome sequence of *Brucella suis* 1330. *J. Bacteriol.* **193**, 6410.

Temperton B., Thomas S., Tait K., Parry H., Emery M., Allen M. *et al.* 2011 Permanent draft genome sequence of *Vibrio tubiashii* strain NCIMB 1337 (ATCC19106). *Stand Genomic Sci.* **4**, 183–190.

Trucksis M., Michalski J., Deng Y. K. and Kaper J. B. 1998 The *Vibrio cholerae* genome contains two unique circular chromosomes. *Proc. Natl. Acad. Sci. USA* **95**, 14464–14469.

Tsolis R. M., Seshadri R., Santos R. L., Sangari F. J., Lobo J. M., de Jong M. F. *et al.* 2009 Genome degradation in *Brucella ovis* corresponds with narrowing of its host range and tissue tropism. *PLoS One* **4**, e5519.

Tuanyok A., Mayo M., Scholz H., Hall C. M., Allender C. J., Kaestli M. *et al.* 2017 *Burkholderia humptydooensis* sp. Nov., a new species related to *Burkholderia thailandensis* and the fifth member of the *Burkholderia pseudomallei* complex. *App. Environ. Microbiol.* **83**, e02802.

Vezzi A., Campanaro S., D'Angelo M., Simonato F., Vitulo N., Lauro F. M. *et al.* 2005 Life at depth: *Photobacterium profundum* genome sequence and expression analysis. *Science* **307**, 1459–1461.

Volante A., Carrasco B., Tabone M. and Alonso J. C. 2015 The interaction of ω2 with the RNA polymerase β' subunit functions as an activation to repression switch. *Nucleic Acids Res.* **43**, 9249–9261.

Wang H., Sivonen K., Rouhiainen L., Fewer D. P., Lyra C., Rantala-Ylinen A. *et al.* 2012 Genome-derived insights into the biology of the hepatotoxic bloom-forming cyanobacterium *Anabaena* sp. strain 90. *BMC Genomics* **13**, 613.

Wang Z., Lin B., Hervey W. J. and Vora G. J. 2013 Draft genome sequence of the fast-growing marine bacterium *Vibrio natriegens* strain ATCC 14048. *Genome Announc.* **1**, e00589-13.

Welsh E. A., Liberton M., Stockel J., Loh T., Elvitigala T., Wang C. *et al.* 2008 The genome of*Cyanothece* 51142, a unicellular diazotrophic cyanobacterium important in the marine nitrogen cycle. *Proc. Natl. Acad. Sci. USA* **105**, 15094–15099.

White O., Eisen J. A., Heidelberg J. F., Hickey E. K., Peterson J. D., Dodson R. J. *et al.* 1999 Genome sequence of the radioresistant bacterium *Deinococcus radiodurans* R1. *Science* **286**, 1571–1577.

Wood D. W., Setubal J. C., Kaul R., Monks D. E., Kitajima J. P., Okura V. K. *et al.* 2001 The genome of the natural genetic engineer *Agrobacterium tumefaciens* C58. *Science* **294**, 2317–2323.

Workentine M. L., Surette M. G. and Bernier S. P. 2014 Draft genome sequence of *Burkholderia dolosa* PC543 isolated from cystic fibrosis airways. *Genome Announc.* **13**, 2.

Yamaichi Y., Iida T., Park K. S., Yamamoto K. and Honda T. 1999 Physical and genetic map of the genome of *Vibrio parahaemolyticus*: presence of two chromosomes in *Vibrio* species. *Mol. Microbiol*. **31**, 1513–1521.

Yamaichi Y., Fogel M. A. and Waldor M. K. 2007 par genes and the pathology of chromosome loss in *Vibrio cholerae*. *Proc. Natl. Acad. Sci. USA* **104**, 630–635.

Yanagida M. 2005 Basic mechanism of eukaryotic chromosome segregation. *Philos. Trans. R. Soc. London, B* **360**, 609–621.

Zimmerman J. M. and Battista J. R. 2005 A ring-like nucleoid is not necessary for radioresistance in the *Deinococcaceae*. *BMC Microbiol.* **5**, 17.

Zuleta L. F. G., Cunha C. de O., de Carvalho F. M. *et al.* 2014 The complete genome of *Burkholderia phenoliruptrix* strain BR3459a, a symbiont of *Mimosa flocculosa*: highlighting the coexistence of symbiotic and pathogenic genes. *BMC Genomics.* **15**, 535.

Corresponding editor: Umesh Varshney

Microbiological Research 208 (2018) 12–24

Contents lists available at ScienceDirect

Microbiological Research

journal homepage: www.elsevier.com/locate/micres

Interdependence of bacterial cell division and genome segregation and its potential in drug development

Hari S. Misra*, Ganesh K. Maurya, Reema Chaudhary, Chitra S. Misra

Molecular Biology Division, Bhabha Atomic Research Centre, Mumbai, 400085, India

ARTICLE INFO

Keywords:
Antibacterial drug development
Cell cycle regulation
Cell division and genome segregation
DivIVA
FtsK
Multifunctional protein regulators
'Par' proteins
Ser/Thr protein kinase
Ser/Thr protein phopshorylation

ABSTRACT

Cell division and genome segregation are mutually interdependent processes, which are tightly linked with bacterial multiplication. Mechanisms underlying cell division and the cellular machinery involved are largely conserved across bacteria. Segregation of genome elements on the other hand, follows different pathways depending upon its type and the functional components encoded on these elements. Small molecules, that are known to inhibit cell division and/or resolution of intertwined circular chromosome and maintenace of DNA topology have earlier been tested as antibacterial agents. The utility of such drugs in controlling bacterial infections has witnessed only partial success, possibly due to functional redundancy associated with targeted components. However, in due course, literature has grown with newer information. This review has brought forth some recent findings on bacterial cell division with special emphasis on crosstalk between cell division and genome segregation that could be explored as novel targets in drug development.

1. Introduction

Bacterial cell division involves the interaction of a large number of proteins forming a macromolecular complex called divisome. There are more than a dozen divisome components have been identified in bacteria including *Escherichia coli*, *Bacillus subtilis* and *Caulobacter crescentus*. A productive cell division requires the coordinated action of all the divisome components. The process of dividing a bacterial cell into two daughter cells sequentially involves invagination of inner membrane, remodeling of the peptidoglycan cell wall and the constriction of the outer membrane at least in case of Gram-negative bacteria (Nanninga, 1991). Majority of the divisome components are conserved across bacteria and are represented in all sequenced bacterial genome while a few of them are organism specific. The regulation of the molecular processes involved in cell division is found to be largely different in different bacteria studied so far. Cell division has been studied in many bacteria including *E. coli*, *B. Subtilis*, *C. crescentus*, *Mycobacterium tuberculosis* (Mtb) and *Deinococcus radiodurans* (Haeusser and Margolin, 2016; Modi et al., 2014; Modi and Misra, 2014). Most of the concepts, models and understanding of cell division regulation in bacteria are centred arround *E. coli* as a model organism. The proteins associated with cell division are denoted as "Fts" (filamentation temperature sensitive) based on the conditional filamentation phenotype of mutants lacking them. Assembly of cell division proteins in divisome is a highly ordered, well-orchestrated process. FtsZ, a tubulin homologue in bacteria is the central player, which is found to be largely conserved across bacteria.

Cell division is well co-ordinated with genome duplication and segregation to ensure that each daughter cell receives one copy of duplicated chromosome (Thanbichler, 2010). The process is complex since, it is now known that except under the slowest growing conditions, in *E. coli*, chromosomes replicate continuously and cell cycles overlap. Further it is argued that the positions of origins, replication forks, and segregation zones in *E. coli* are dynamically favoured so that the developing nucleoid can move apart without requirement of any specialized segregation function with the exception of the terminus translocation mechanism (Youngren et al., 2014). Regarding the terminus translocation, several mechanisms starting from the decatenation of duplicated intertwined circular chromosome by DNA topoisomerases and FtsK/XerCD tyrosine recombinases, separation of the newly synthesised copy of chromosome by macromolecular DNA replication complex and eventually employment of a tripartite genome partitioning system have been suggested (Zaritsky and Woldringh, 2015). Majority of the bacterial genomes, except interestingly *E. coli,* encode proteins of the typical triparite genome partitioning system, which comprises of two *trans* acting factors (ParA and ParB) and one *cis* element (centromere like sequence) (Gerdes et al., 2010). The genome segregation mechanisms are largely studied in plasmids and only in some bacterial chromosomes (Table 1). General mechanism of segregation involves the sequence specific interaction of adapter protein with centromere like

* Corresponding author at: Molecular Biology Division, Bhabha Atomic Research Centre, Mumbai, 400085, India.
E-mail address: hsmisra@barc.gov.in (H.S. Misra).

https://doi.org/10.1016/j.micres.2017.12.013
Received 3 September 2017; Received in revised form 5 December 2017; Accepted 31 December 2017
Available online 05 January 2018
0944-5013/

Table 1
Summary of genome partitioning system characterized in selected plasmids and chromosome of some bacteria.

Name of Bacteria	Genome elements	Tripartite partitioning elements			Mechanism of genome partitioning	References
		NTPase	Adaptor	Centromeric sequences		
E. coli	P1 plasmid	ParA	ParB	parS	Pushing	Schumacher and Funnell (2005)
	F plasmid	SopA	SopB	sopC	Pushing	Ravin et al. (2003); Vecchiarelli et al. (2010)
	R plasmid	ParM	ParR	parC	Pushing	Ebersbach and Gerdes (2001)
	pSK1	Classical TGS is replaced by different mechanism			Pilot-fish like mechanism	Guynet and de la Cruz (2011)
	R338					
Bacillus subtilis	pX101	TubZ*	TubR	tubC	Tram model	Larsen et al. (2007); Ni et al. (2010)
	Chromosome	Soj	Spo0J	parS	Pulling	Lin and Grossman (1998); Draper and Gober (2002)
Bacillus anthracis	pBToxis	TubZ*	TubR	tubC	Tram model	Larsen et al. (2007); Ni et al. (2010)
Bacillus thuringiensis	pBToxis	TubZ*	TubR	tubC	Tram model	Larsen et al. (2007); Ni et al. (2010)
S. enterica	pTP228	ParF	ParG	parH	Pulling	Ringgaard et al. (2009)
	pB171	Par A	ParB	parC	Pulling	
	pSM19035	δ protein	ω protein	Not known	Pulling	
S. aureus	pSK41	ParM	ParR	ParC	Pushing	Gerdes et al. (2010)
Caulobacter crescents	Chromosome	ParA	ParB	parS	Pulling	Mohl et al. (2001); Mohl and Gober (1997)
Deinococcus radiodurans	Chromosome I	ParA1	ParB1	SegS (1–3)	Pulling	Charaka and Misra (2012)

Note: *GTPase and all other NTPases are ATPases

sequences to form the nucleoprotein complexes. A great diversity in both structure and functions of NTPase proteins has been observed across bacteria and their mode of action determines the mechanism of genome segregation. It has been observed that the directionality of DNA movement depends upon the concentration gradient of nucleoid bound NTPase protein in the cell. In majority of the plasmid segregation, the NTPase protein polymerization nucleates at the ParB-centromere complex, and as the length of the polymer increases the daughter molecules are pushed into opposite directions (Gerdes et al., 2010). In certain cases, when ParA polymers encounter to ParB bound to centromere, it stimulates ATP hydrolysis at the junction of ParB-*parC* causing depolymerization of ParA filament. This leads to the retraction of ParA from one end while holding ParB nucleoprotein from other end and eventually the pulling of plasmid DNA towards higher ParA-ATP concentration (Gordon and Wright, 2000; Ebersbach and Gerdes, 2005; Leonard et al., 2005; Gitai, 2006). Both pulling and pushing models of genome segregation suggest that ParAs form a continuous helical filament type structure through polymerization on DNA. There are plasmids such as pX101 of *Bacillus subtilis* and pBToxis in *Bacillus anthracis* and *Bacillus thuringiensis* where motor protein is GTPase (TubZ) and not ATPase while adaptor protein is TubR and centromere sequence is *tubC*. In such cases, two sets of TubZ-GDP polymers bind to duplicated DNA through TubR and both these polymers pulls the nucleoprotein cargo bound to DNA species in opposite directions mimicking like Tram movement, hence named as Tram Model (Larsen et al., 2007; Ni et al., 2010). In some plasmids like pSK1 and plasmid R388 of *E. coli*, the classical tripartite system is functionally replaced by a different mechanism where chromosome segregation drives plasmid movement through a “pilot-fish”-like mechanism (Guynet and de la Cruz, 2011). This involves a single plasmid encoded DNA binding protein and a conjugation machinery. Microscopic imaging using immunofluorescence, fluorescence *in situ* hybridization (FISH) and fluorescence repressor operator system (FROS) approaches have provided evidence that P1 and F plasmid segregation is asymmetric *i.e.* one copy of the plasmid remains either in mid cell or 1/4th position while other copy moves to new 1/4th position in a time dependent manner (Erdmann et al., 1999; Onogi et al., 2002; Mascarenhas et al., 2005; Ringgaard et al., 2009). Visualization of ParA by immunofluorescence or through GFP fusion shows its association with the nucleoid (Erdmann et al., 1999; Gordon et al., 2004; Hatano and Niki, 2010; Li and Austin, 2002; Sengupta et al., 2010; Charaka et al., 2013). Genetic organization of tripartite components as well as regulation of Par proteins expression shows great diversity amongst different genome elements following different mechanisms. Detailed discussion on various aspects of genome partitioning is outside the scope of this review and therefore, readers are referred to other reviews published in recent past for this information (Gerdes et al., 2010). However, a brief discription on genome partitioning processes has been brought here to emphasize that any defect in genome segregation may lead to the inhibition of cell division. DNA metabolism plays a great role in regulation of cell cycle in bacteria. It is also known that DNA damage in bacteria leads to cell cycle arrest. Proteins involved in the classical SOS response, a typical DNA damage response in bacteria, play significant roles in regulation of cell division. The interface between genome segregation and cell division, though extensively studied still has a few grey areas, which are only just being revealed.

Antibacterial drugs have been developed for targeting both cell division and genome maintenance machineries in bacteria. Inhibition of cell division has centred on FtsZ activity and dynamics while DNA topoisomerases have been targeted for disrupting the topological integrity of bacterial genome. Both these approaches have been used separately, and have witnessed partial success. One of the reasons attributed to the inefficacy of such drugs developed based on FtsZ and topoisomerases is the occurence of functional redundancy for both these targets. Further, certain bacteria do not need FtsZ or its homologues for cell division, which may indicate that cell division, can occur without FtsZ activity. Similarly, DNA topology could be maintained by the contribution of functionally redundant topoisomerases. In fact, it has been observed that topoisomerase inhibitors function not only by tempering DNA topology but also by generating a high density of DNA strand breaks, which if not repaired, kill cells. Quite obviously, a bacterium, which has an efficient DNA strand break repair system, would survive such drugs. Hence, efforts for developing antibacterial drug based on combinatorial approaches would be worth aiming. Over time, the basic understanding on the interdependence of cell division and genome segregation at molecular levels has grown and a large amount of information has accumulated in literature. This review presents the most recent research published at the interface of cell division and genome segregation under both normal and stressed growth conditions. The review starts out highlighting the interdependence of these two important processes leading up to the identification of targets for the development of antibacterial drugs. For easy understanding of the subject, we have provided a brief introduction to cell division and its regulation. In addition, the regulatory components that facilitate interaction between cell division and genome segregation, and divisome assembly regulation by post translation modification of FtsZ in some bacteria are also reviewed.

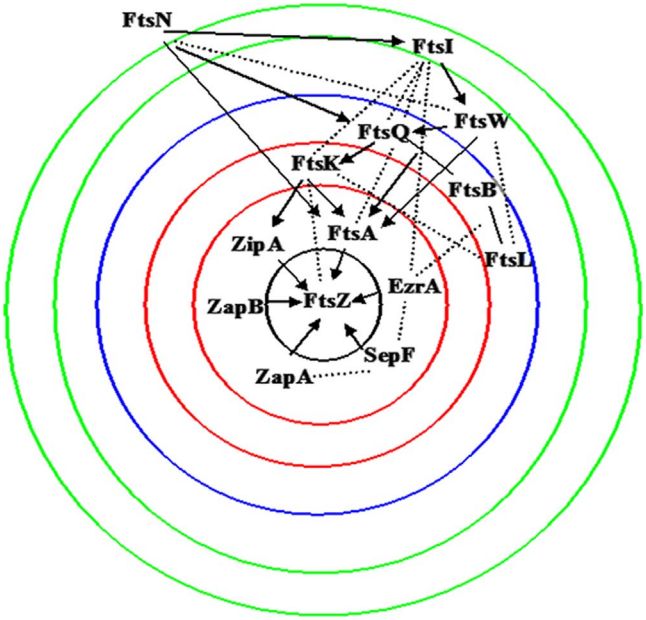

Fig. 1. Schematic representation of cell division proteins' assembly in divisome. Assembling order of conserved divisome components are shown.

The latter portion of the review highlights the importance of understanding these processes for developing an effective strategy to combat bacterial infections. However, we still do not claim to have covered all aspect of this biology and therefore, refer readers to other recent reviews published on related aspects for more information (Kleckner et al., 2014; Hajduk et al., 2016; Rowlett and Margolin, 2015; Zaritsky and Woldringh, 2015; den Blaauwen et al., 2017).

2. Divisome assembly and FtsZ dynamics in bacteria

Divisome is a higher ordered structure made of a large number of proteins associated with FtsZ in the Z-ring that forms at the longitudinal midpoint or septum of the cell during cell division. The divisome assembly has been studied in *E. coli*, *B. subtilis* and *C. crescentus* and some common components and the order in which they assemble in all the three bacteria are depicted schematically (Fig. 1). In these bacteria, it follows either a linear hierarchy of proteins or its components are assembled temporally? Since the mechanisms of divisome assembly are outside the scope of this review, here we have only summarised the divisome components and the functions of only some of the crucial proteins in these three bacteria. In *E. coli*, the divisome is comprised of FtsZ bound with FtsA, ZipA, ZapA, FtsK, FtsQ-FtsL-FtsB, FtsW, FtsI and FtsN (Aarsman et al., 2005; Goehring and Beckwith, 2005; Vincente and Rico, 2006; Liu et al., 1999; Pazos et al., 2012). FtsA and ZipA help in membrane anchoring of FtsZ while ZipA and ZapA stabilize the FtsZ-ring. FtsA or FtsQ (in the absence of FtsA) recruits FtsK, which coordinates chromosome segregation with cell division. Bacteria contain a battery of hydrolytic enzymes that regulate peptidoglycans modelling and some of these are required for splitting of septum during final stage of cell division (Vollmer et al., 2008). Among these, AmiC and the LytM-domain containing proteins like EnvC and NlpD that accumulate at the septum during constriction, the AmiC recruitment to midcell was shown to be dependent on the cell division protein FtsN (Bernhardt and de Boer, 2005). The recruitment of various proteins implicated or involved in constriction of the peptidoglycan layer, such as PBP3 (also called FtsI), the putative membrane transporter FtsW, and the murein-binding protein FtsN occurs at the septum site (Egan et al., 2016). FtsQLB complex a relatively less characterized complex, acts as a connector between the cytoplasmic early divisome components and the peptidoglycan modelling components, FtsW and FtsI (Alvarez et al., 2014). Although, FtsA and ZipA function alike in terms of their support to FtsZ, ZipA carry out other functions, which FtsA does not do. For example, unlike FtsA, ZipA induces bundling of FtsZ protofilament *in vitro* (Hale et al., 2000), is involved in pre-septal peptidoglycan synthesis (Potluri et al., 2012) and in cell membrane invagination (Cabre et al., 2013). ZapA is dispensable for normal growth but becomes essential under stress conditions (Gueiros-Filho and Losick, 2002). Recent studies demonstrate that ZapA exists in a dimer to tetramer equilibrium *in solution* and its tetramerization is essential for bundling of FtsZ (Pacheco-Gomez et al., 2013). In *B. subtilis*, the divisome is a multiprotein complex constituting FtsZ, FtsA, ZapA, EzrA and SepF, GpsB, FtsL, DivIB, FtsW, Pbp2B (FtsI), and DivIVA. But unlike in *E. coli*, the recruitments of proteins like FtsL, DivIB (FtsQ), DivIC (FtsB), and Pbp2B to divisome are found to be interdependent, and also depend on the stability of FtsQLB complex in *B. subtilis* (Gamba et al., 2009). In *C. crescentus* the components of divisome are MipZ, FtsZ, ZapA, FzlC, FtsE, FzlA, MurG, DipN, MreB, FtsA, TolQ, FtsN, FtsQ, FtsI, FtsK, FtsL, FtsW, FtsB, KidO and TipN. Out of these MurG, DipN and MreB are characterized for their roles in peptidoglycan modelling in *C. crescentus*. The divisome assembly processes in *C. crescentus* is similar to *E. coli* except that in *C. crescentus* FtsA is recruited at a much later stage and not immediately after FtsZ and that FtsW is not required for the recruitement of FtsI (Goley et al., 2011).

3. FtsZ, a tubulin homologue in bacteria is largely conserved

FtsZ is the primary cytoskeletal protein of bacterial cell division that forms the Z-ring at the site of cell division. It polymerizes in a head to tail fashion, very much like tubulin (Adams and Erington, 2009). This pattern of polymerization places the GTP hydrolysis loop (NxDxxK) of one subunit in close contact with the GTP binding site of the incoming adjacent subunit (Fig. 2). This mechanism of GTP hydrolysis by FtsZ makes it a tubulin-like protein, a self-activating GTPase. The extreme C-terminus of FtsZ is highly disordered and a stretch of conserved 12 amino acids of this region are essential for it's interaction with other divisome components (Ma and Margolin, 1999; Durand-Heredia et al., 2012). FtsZ polymerizes to form protofilaments, which are highly dynamic (Adams and Erington, 2009; Oliva et al., 2004). Under conditions that support maximum GTPase activity, these filaments are about 30 subunits long as seen in *E. coli* (Chen and Erickson, 2005). The polymerization and depolymerization dynamics of FtsZ associated with FtsZ ring (Z-ring) generate the constriction force that leads to septum invagination (Fig. 3). GTP hydrolysis and FtsZ subunit turnover are very important processes associated with septum invagination. Using liposomal membrane model, GTP hydrolysis mediated conformational change in membrane curvature and the generation of bending force have been demonstrated (Osawa et al., 2009). However, the completion of invagination requires coordination with peptidoglycan synthetic machinery as the inhibition of septal peptidolycan synthesis could inhibit invagination of inner membrane (Joseleau-Petit et al., 2007). Though FtsZ is an absolutely essential cell division protein in most of the bacteria, several archeal and bacterial phyla including the entire phylum of *Crenarcheota*, *Chlamydiaceae*, and *Planctomycetes* as well as thermophilic archeon like *Aeropyrum pernix*, intracellular symbionts like *Calyptogena okutanii* and *Carsonella ruddi* and mycoplasma species like *Ureaplasma urealyticum* and *Mycoplasma mobile* do not contain FtsZ (Erickson and Osawa, 2010) and yet divide. Several of these bacteria use a completely different cytoskeletal system related to eukaryotic Endosomal Sorting Complexes Required for Transport (ESCRT) system (Lindas et al., 2008; Samson et al., 2008; Wollert et al., 2009).

4. FtsA homologues are structurally diverse and functionally redundant

The second most important, yet diverse protein in bacterial cell division is FtsA. FtsA, an approximately 43 kDa cytoplasmic protein has

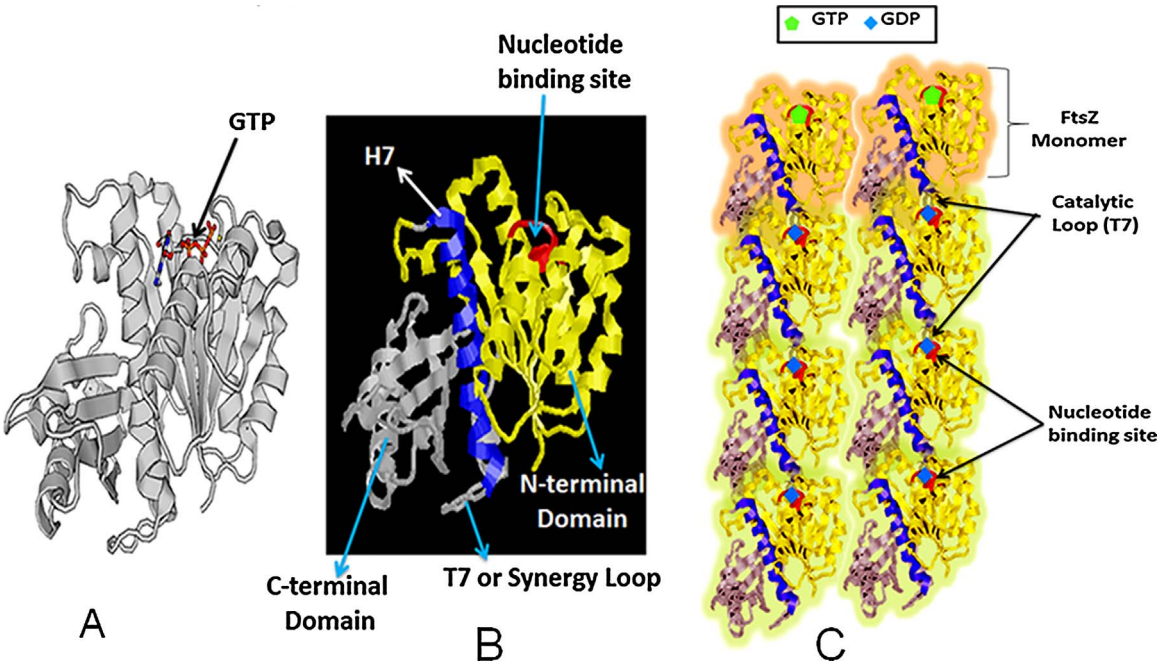

Fig. 2. FtsZ structure and its polymerization mechanism. Structure of *Bacillus subtilis* FtsZ showing GTP interaction (PDB No. 2RHO) (A) was used for information. Different functional domains like N-terminal domain (Yellow), GTP binding site (Red), C-terminal domain (Gray) along with GTP hydrolysis loop (T7 Loop) (PDB No. 2RHO) are shown (B). Schematic representation of head to tail mode of FtsZ polymerization was made based on information obtained from FtsZ structure (A and B) is shown (C). (For interpretation of the references to colour in this figure legend, the reader is referred to the web version of this article).

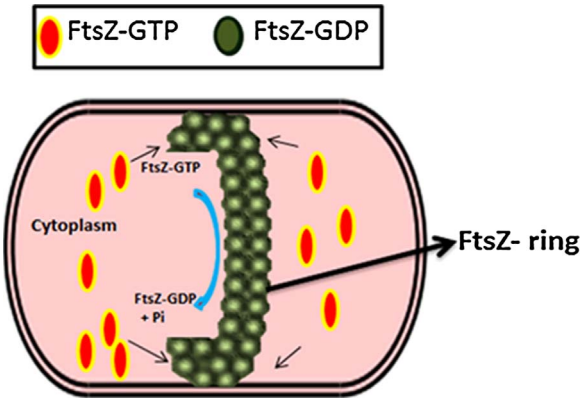

Fig. 3. Schematic representation of FtsZ-GTP subunit turnover during its polymerization and FtsZ ring formation *in vivo*.

been found to be functionally dispensable as it is made redundant by other proteins. FtsA from *B. subtilis* (Feucht et al., 2001), *E. coli* (Yim et al., 2000), *S. pneumoniae* (Lara et al., 2005), *Staphylococcus aureus* (Fujita et al., 2014) have been shown to bind ATP. However, significant ATPase activity has been reported only for FtsA from *B. subtilis* and *Pseudomonas aeruginosa* (Paradis-Bleau et al., 2005). FtsA homologues are found to be structurally diverse with different levels of amino acid similarities but these differences neither influence its interaction with FtsZ nor its nucleotide binding ability, hydrolysis or polymerization functions (Pichoff and Lutkenhaus, 2007). *In vivo* stoichiometric ratio of FtsZ: FtsA is 5:1 in *E.coli* and *B. subtilis* (Feucht et al., 2001) while it is 1.5:1 in *S. pneumoniae* (Lara et al., 2005). In *D. radiodurans*, the sedimentation analysis of Dr-FtsZ in presence of different molar ratios of Dr-FtsA showed a significantly increased amount of Dr-FtsZ in the supernatant when Dr-FtsA and Dr-FtsZ were present in a 1:1 molar ratio (Modi and Misra, 2014). Effect of FtsA on GTPase activity of FtsZ varies in different bacteria. For instance, *E. coli* FtsA neither affects GTPase activity nor polymerization of FtsZ (Beuria et al., 2009). On the other hand, FtsA from *S. aureus* and *D. radiodurans* stimulates the GTPase activity of respective FtsZ homologues (Fujita et al., 2014; Modi and Misra, 2014). Realtime imaging studies showed that FtsA has dual function in FtsZ dynamics. Initially it recruits the highly dynamic FtsZ polymers to the membrane and supports polymerization and at a later stage it causes destabilization of FtsZ polymer. This dual effect of FtsA on FtsZ's GTPase activity and bundling of FtsZ filaments gives rise to rotating rings (Loose and Mitchison, 2013) and provides the most plausible explanation to FtsA's regulatory role in FtsZ dynamics. The highly conserved C-terminus of FtsZ is involved in interaction with FtsA in *E.coli* (Pichoff and Lutkenhaus, 2007). Crystal structure of *Thermotoga maritima* FtsA (van den Ent and Lowe, 2000) reveals the presence of two domains, which are further subdivided into two subdomains each – 1A, 1C, 2A and 2B. The, subdomain 2B establishes contact with C-terminus of FtsZ (Szwedziak et al., 2012). Data from mutational studies of *E. coli* FtsA concurred with the information obtained on interaction of FtsA with FtsZ in *T. maritima*. FtsA from *B. subtilis* (Feucht et al., 2001) and *S. aureus* (Fujita et al., 2014) exist as dimers while that from *T. maritima* (van den Ent and Lowe, 2000) and *E. coli* (Martos et al., 2012) exist as monomers. Although, crystal structures of FtsA homologues are not available for comparision, the available evidence suggests that FtsA or its functional homologues are very diverse among different bacteria indicating the possibility of variations in the interaction between FtsA and FtsZ. In addition to FtsZ and FtsA, there are many other proteins that take part in regulation of divisome formation and cytokinesis but discussion on those have been kept outside the scope of this review.

4.1. Regulation of cell division under normal growth of bacteria

The bacterial cell division is regulated by FtsZ localization in the membrane, FtsZ ring formation and dynamics. FtsZ is both functionally and structurally conserved across all bacteria and cytokinesis depends upon the regulation of FtsZ activity and polymer dynamics in respective bacteria. In rod shaped bacteria, these processes are spatially regulated by 'Min' system (Lutkenhaus, 2007), and nucleoid occlusion (NOC) system (Wu and Errington, 2004; Bernhardt and de Boer, 2005; Charaka and Misra, 2012) (Fig. 4). Temporal regulation is normally observed

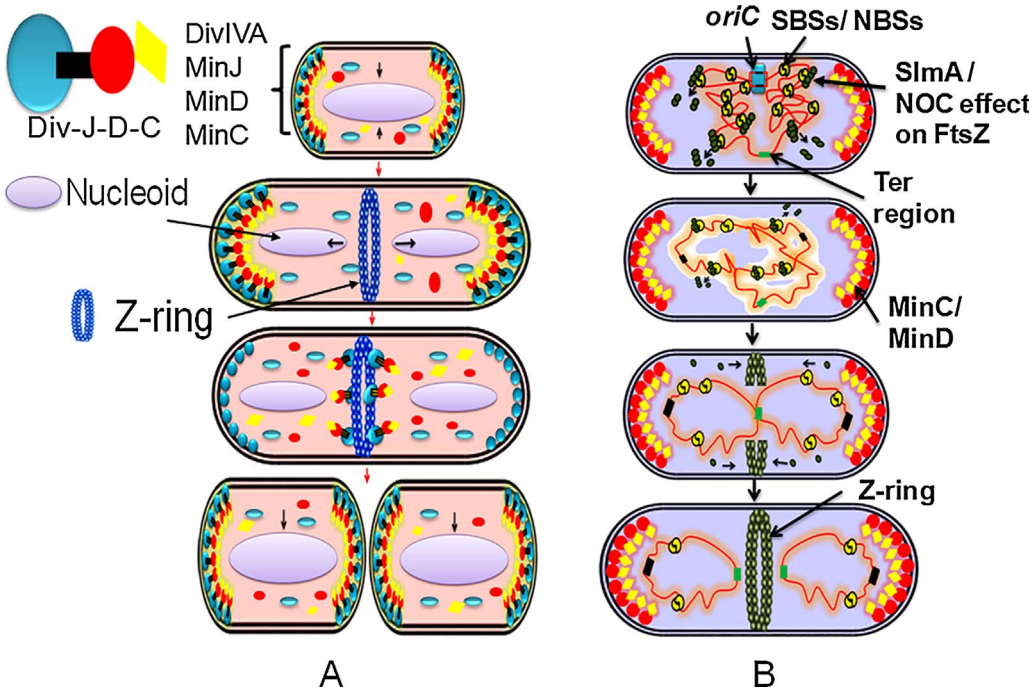

Fig. 4. Spatial regulation of FtsZ localization in mid cell position and polymerization in rod shaped bacteria. Schematic representation of 'Min' system (A) and 'NOC' system (B) regulating FtsZ localization and polymerization for productive cell division is shown.

under stress conditions when cell division is arrested till genome is repaired and duplication and segregation is completed.

Spatial regulation of cell division in rod shaped bacteria involves the correct placement of the Z-ring at the mid cell position, away from the poles. The Min system that regulates FtsZ localization in mid cell position consists of primarily MinC, MinD and MinE in *E. coli* while DivIVA replaces MinE in some Gram-positive bacteria including *B. subtilis*. In *D. radiodurans,* the Min system consists of MinC, MinD and both DivIVA as well as a truncated form of Min E (White et al., 1999). Functions of these proteins are believed to be conserved across bacteria and together decide the localization of FtsZ at mid cell position and prevent septum formation at cell poles (Lutkenhaus, 2007). For instance, Min D forms a dimer with Min C (de Boer et al., 1991) that gets restricted to the poles through Min E in rod shaped bacteria (Fig. 4A). Since Min C prevents formation of the Z ring, its localization in the membrane at the poles restricts septum formation only to the mid cell position (Johnson et al., 2004; Ghosal et al., 2014; Conti et al., 2015). DivIVA in *B. subtilis* as well as in many other Gram-positive bacteria including cocci behaves like Min E (Marston et al., 1998; Lutkenhaus, 2007). The exact mechanism of DivIVA action is not known yet but it localizes at the extreme end of the poles and remains there (Gamba et al., 2009). This allows for speculation on the role of DivIV in determining the plane of second division at least in *cocci* that is perpendicular to first division plane. In other words, DivIVA determines the polarity in *cocci* (Bramkamp et al., 2008) and restricts FtsZ localization from the pole that already had MinCD-DivIVA localized in the membrane.

The other mechanism that determines the spatial regulation of cell divison is the negative control of Z-ring formation by the nucleoid, referred to as nucleoid occlusion mechanism (Fig. 4B). Totally unrelated proteins, 'Noc' in *B. subtilis* (Wu and Errington, 2004) and SlmA in *E. coli* (Bernhardt and de Boer, 2005) are keys to the nucleoid occlusion mechanism in these bacteria. Both Noc and SlmA bind to specific DNA sequences which are distributed in proximal 2/3 part of the origin of replication present on the chromosome and are mostly absent in the terminus region (Wu et al., 2009; Tonthat et al., 2011). Mechanism that explains this control is that NOC proteins binding to the sequences proximal to *ori* region keeps them in mid cell position, until its gets cleared when genome is duplicated and segregated. During cell division, when FtsZ ring starts to progress, it encounters the proteins present on the nucleoid, which presumably arrests FtsZ polymerization. SlmA is shown to function as an antagonist of FtsZ polymerization. This activity of SlmA is stimulated by its binding to specific DNA sequences (Cho et al., 2011). SlmA forms higher order structures on DNA and that inhibits Z-ring formation over the nucleoid (Tonthat et al., 2013; Du and Lutkenhaus, 2014) (Fig. 4B). In NOC mechanism of cell division regulation, the regulation of DNA duplication cum segregation in coordination with FtsZ ring progression is more important than the type of proteins involved in this regulation. There is a possibility that other factors that regulate genome duplication and sergegation are also involved in spatial regulation. Furthermore, factors that govern decision on FtsZ localization and the plane of second cell division in oval shaped bacteria are not clear yet and would be worth unearthing.

MinCDE and NOC system in rod shaped bacteria primarily regulate spatial regulation of FtsZ ring formation under normal growth conditions. However, in the absence of MinCDE systems, the placement of FtsZ in mid position is achieved with the help of other protein. For example, EzrA, a protein reported from *B. subtilis* acts as a spatial regulator of FtsZ ring placement in the absence of 'Min' system (Haeusser et al., 2004; Steele et al., 2011). EzrA localizes to membrane through its N-terminus and inhibits FtsZ function through its C-terminal cytoplasmic domain (Land et al., 2014). In *B. subtilis* using Bacterial Two Hybrid (BACTH) system based on adenylate cyclase reconstitution, the interaction of EzrA with FtsA, Pbp1, SepF, and GpsB has been established. In *S. aureus*, BACTH analysis suggested that EzrA interacts directly not only with FtsZ, GpsB, PBP1, and SepF, but also with Pbp3, Pbp2, DivIB, DivIC, FtsL, and RodA (Ishikawa et al., 2006; Claessen et al., 2008; Tavares et al., 2008).

More recently, the 'Ter' macrodomain in conjunction with MatP, ZapB and ZapA proteins have been demonstrated to ensure midcell positioning of Z-ring in *min* and *slm* mutants of *E. coli* by positive regulation (Bailey et al., 2014). In *C. crescentus* that lacks 'Min' system, MipZ has been identified as the spatial regulator of FtsZ ring placement. MipZ regulates cell division through chromosome partitioning system. Mechanistically, it localizes as a gradient with highest concentration at the stalked pole and interacts with ParB bound to *par S*. Subsequently, the entire MipZ-ParB complex along with replicated chromosome moves to opposite pole and dislodges FtsZ from the opposite pole. This

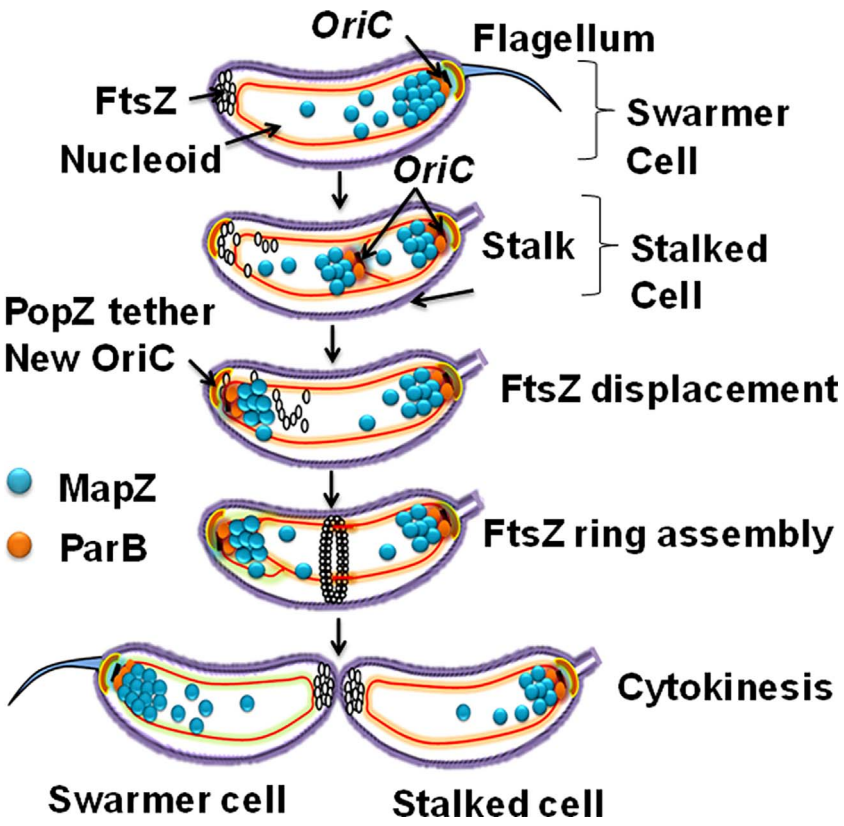

Fig. 5. Regulation of FtsZ localization and its polymerization dynamics in *Caulobacter crescentus*. Schematic model showing conversion of Swammer cells to Stalk cells in *C. crescentus* leading to the displacement of FtsZ and its localization in mid cell position is fascilitated by MapZ and ParB interaction.

makes FtsZ move to the midcell position and form a ring where MipZ concentration is now low. *In vitro,* MipZ stimulates GTPase activity of FtsZ and inhibits its polymerization (Thanbichler and Shapiro, 2006) (Fig. 5). In *S. pneumonia*, a cell wall structure called equatorial ring, marks the site of septation and a novel protein MapZ was identified as septum site determinant. MapZ *via* its extracellular domain binds to the equatorial ring and recruits FtsZ by interacting through the cytoplasmic C-terminal domain of FtsZ (Bramkamp, 2015). Another ParA like protein PomZ has been identified in *Myxococcus xanthus* which localizes to division site before FtsZ and then recruits it at the midcell following chromosome segregation (Treuner-Lange et al., 2013). In *Streptomyces coelicolor*, SsgB recruits FtsZ at the division site during sporulation (Willemse et al., 2012).

5. Regulation of cell division under stressed conditions

Majority of bacteria do not have protein kinases similar to cell cycle checkpoint kinases found in eukaryotes. However, they do regulate cell cycle. Temporal regulation ensures the correct, time dependent entry of the cell into division phase with respect to nutrient availability, integrity of genome, integrity of cytoplasm and effect of external environment.

Bacteria exposed to DNA damaging agents including UV, ionizing radiations or DNA cross-linking agents like mitomycin C arrest their cell division till damaged DNA is repaired. The best-characterized response to DNA damage induced cell division inhibition is SOS response (Fig. 6). Certain bacteria employ classical SOS response as the mechanism for restricting cell division by controlling FtsZ levels and activity while concurrently promoting DNA repair. SulA, a SOS response protein is found to be a cell division inhibitor in *E. coli* (Huisman et al., 1984). It directly affects FtsZ activity and FtsZ ring dynamics (Bi and Lutkenhaus, 1993; Dajkovic et al., 2008) thus causing cell cycle arrest. YneA of *B. subtilis*, DivS of *Corynebacterium glutamicum,* Rv2719c in *M. tuberculosis* and SidA in *C. crescentus* also inhibit cell division in response to DNA damage by different mechanisms. While YneA acts at later stages of cell division (Kawai et al., 2003), DivS works possibly by interfering with Z-ring assembly and septum wall synthesis (Ogino et al., 2008) and Rv2719c acts as a cell wall hydrolase in the peptidoglycan synthesis zone affecting FtsZ localization (Chauhan et al., 2006). SidA down-regulates CtrA, a key regulator of cell division and DNA replication (Laub et al., 2002) and affects constriction of septum by directly interacting with late cell division proteins FtsN and FtsW (Modell et al., 2011). Interestingly, these are not functional homologoues of SulA.

In response to nutritional stress like amino acid and carbon starvation, the production of (p)ppGpp (guanosine pentaphosphate or tetraphosphate) causes inhibition of replication initiation and thus arrest of cell division in *E. coli* and *C. crescentus* (Boutte et al., 2012). In *E. coli*, (p)ppGpp inhibits the transcription of DnaA, a replication initiator protein (Chiaramello and Zyskind, 1990) while in *C. crescentus* it affects the stability of replication factors and their abundance (Boutte et al., 2012). In *B. subtilis*, (p)ppGpp causes replication fork arrest by directly interacting with primase and thus interfering with replication elongation (Wang et al., 2007). Replication fork arrest helps cells in maintaining genome integrity during transient phases of nutrient deprivation (Denapoli et al., 2013). Prolonged starvation leads to sporulation in *B. subtilis*, where two proteins SirA and MciZ are induced. These proteins inhibit DNA replication and cell division by directly interacting with DnaA and FtsZ respectively (Handler et al., 2008; Wagner et al., 2009). FtsZ activity and Z ring dynamics are also regulated during carbohydrate starvation. For instance, UgtP, a terminal sugar transferase that uses UDP-glucose in synthesis of lipotechoic acid causes FtsZ assembly inhibition in *B. subtilis* (Weart et al., 2007). OpgH, a glucosyltransferase enzyme in *E. coli* (Hill et al., 2013) and KidO, a NADH oxidoreductase homolog in *C. crescentus* (Radhakrishnan et al., 2010), also regulate cell division in these bacteria.

6. DNA metabolism during cell division

Genome duplication followed by segregation is a prerequisite for productive cell division (Männik and Bailey, 2015). As bacterial

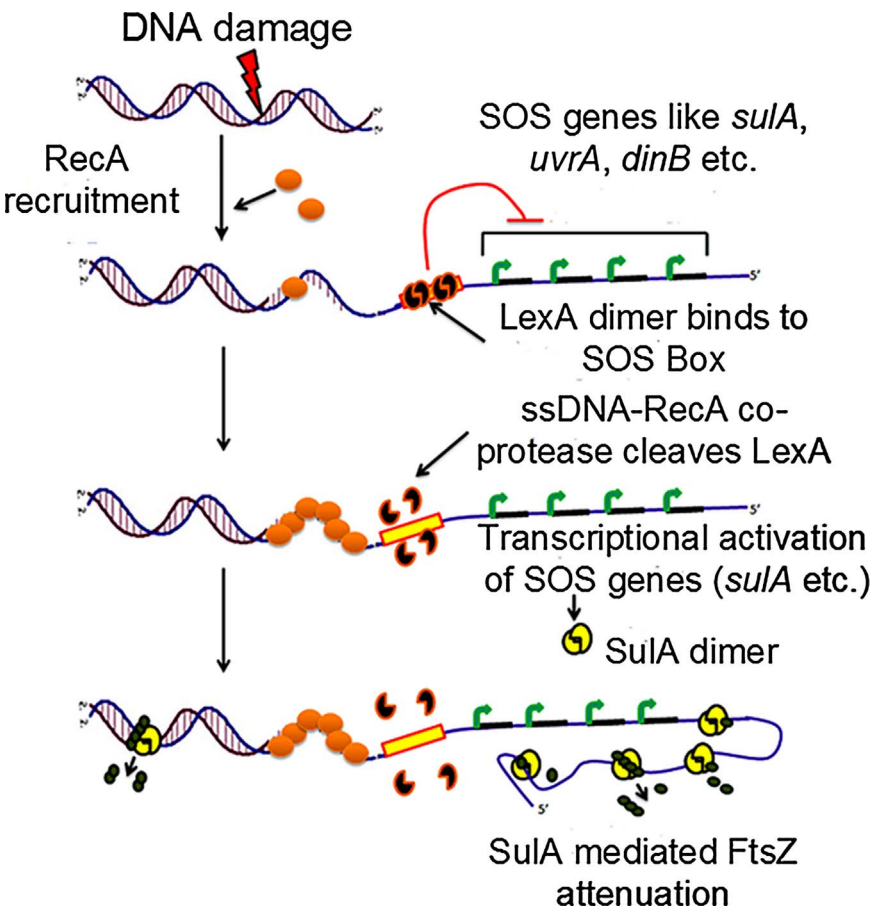

Fig. 6. Cell cycle regulation in response to DNA damage. DNA damage mediated SOS response triggering activation of DNA repair mechanism on one hand and the attenuation of cell division machinery on the other hand as was observed in *E. coli* is depeicted.

chromosomes are mostly circular and their replication is bidirectional, the fully duplicated chromosome forms intertwined circular DNA structures (Sogo et al., 1999). The resolution of such structures is the first step in daughter chromosomes segregation. This step is largely accomplished by DNA topoisomerase IV at least in *E. coli* (Peng and Marians, 1993; Zechiedrich et al., 1997; Espeli et al., 2003). When replication has reached termination sites and some of these structures have escaped topoisomerase attention, such structures are likely to get resolved by the combined action of FtsK/XerCD recombinases (Aussel et al., 2002; Sherratt, 2003). In bacteria, several hypotheses or models have been proposed for explaining genome segregation processes. Initially, it was believed that duplicated chromosome segregation is a passive process, but it was later found to involve several accessory factors and shown to be a highly energy- intensive, regulated process (Jensen and Shapiro, 1999; Lemon and Grossman, 2000; Sawitzke and Austin, 2000). Several mechanisms that could explain bacterial genome segregation have been reviewed in detail but have deliberately been kept outside the scope of this review. They can be found in specialized reviews published in recent past (Errington et al., 2005; Leonard et al., 2005).

The tripartite genome segregation (TGS) mechanism is found to be almost ubiquitous in bacteria but is conspicuously absent in *E. coli*. TGS system comprises of two *trans* acting factors (ParA and ParB) and one *cis* element (centromere like sequence). TGS based partitioning of duplicated genome elements has been shown in both plasmid, as well as chromosomal DNA segregation in *B. subtilis* and *C. crescentus* (Reyes-Lamothe et al., 2012; Lindas and Bernander, 2013). Functional homologues of these elements are also present on both, plasmids and chromosome in different bacteria. Some of these have been functionally characterized. It has been observed that the polymerization and depolymerization dynamics of NTPase protein is differentially regulated upon its interaction with centromere-ParB nucleoprotein complex, which results in different mechanisms of genome segregation. A great diversity in both structure and functions of NTPase proteins has been observed across bacteria. Both pulling and pushing models of genome segregation suggest that ParAs form a continuous helical filament type structure through polymerization on DNA. However, there are proteins including MreB that do not form continuous helical filament *in vivo* yet have roles in genome segregation and cell division. Recently, it has been observed that ParAs of certain plasmids pattern *via* interactions with the bacterial nucleoid, and the movement of cargoes is not always filamentous rather can follow the “diffusion-ratchet” mechanism driven by concentration gradient of ParAs on DNA carpet (Vecchiarelli et al., 2012, 2013). For further details on “diffusion-ratchet” mechanism, readers may refer recently published article (Vecchiarelli et al., 2014). Thus, it is clear that ParA ATPases interact with ParB bound to DNA and form the macromolecular complexes termed segrosome, which plays the crucial role in segregation of duplicated genome in bacteria by various mechanisms. However, the recent studies on protein–protein interactions showed that ParA and ParB proteins can also interact with other proteins including orphan ATPases and cell division regulatory proteins (Maurya et al., 2016 and reference *there in*). This might suggest that the composition and size of segrosome complex contributing in genome partitioning in bacteria could be beyond ParA and ParB complexes and would be worth investigating.

The *E. coli* chromosome is highly condensed and organized. A number of SMC proteins including MukBEF family of condensins play important roles in maintenance of the *E. coli* genome integrity. The mutational studies have shown the roles of these proteins in chromosome organization, condensation and precise cell division. Similar defects in condensin deficient strains of *B. subtilis* and *C. crescentus* have also been reported (Rybenkov, 2015). On the otherhand, the *E. coli* chromosome does not encode a typical TGS system. But the Ter macrodomain region in the *E. coli* chromosome was found to contain 23

repeats of 13 bp long elements named as *mat S* (Mercier et al., 2008). MatP, a protein that is crucial for organization and proper segregation of the Ter macrodomain in *E. coli* was found to bind the *matS* motifs. MatP, in turn establishes contact with FtsZ through a cell division regulatory protein ZapB (Espeli et al., 2012). Thus, MatP-ZapB-FtsZ interaction seems to be a novel mechanism that regulates the cell division and genome segregation, at least in *E. coli*.

7. Proteins at the interface of cell division and genome sergegation

7.1. FtsK – a multifunctional DNA resolvase

FtsK is widely distributed across bacterial species and belongs to FtsK/SpoIIIE/Tra family of DNA translocases. It is a multidomain, multifunctional; membrane bound translocase (Bigot et al., 2007) and an early component of divisome (Wang and Lutkenhaus, 1998). FtsK can be divided primarily into three domains – the N-terminal domain, the linker region and the C-terminal domain. It primarily stabilizes the divisome (Draper et al., 1998) and is involved in interaction with FtsZ and other divisome components (Buddelmeijer and Beckwith, 2002). FtsK helps in tethering FtsZ to the membrane at the division site and is indispensable for cellular viability (Draper et al., 1998). The linker region located between the N and C-terminal domains is poorly conserved and varies in length among bacterial species (Bigot et al., 2007). In spite of its poorly conserved nature, this region is involved in interaction with FtsI and to a lesser extent with FtsQ and possibly, also in their recruitment to the septum (Grenga et al., 2008; Grainge, 2010). The C-terminus is the signature domain of FtsK which is a highly conserved region involved in chromosome resolution. The C-terminal domain is further subdivided into three subdomains – α, β and γ (Yates et al., 2003). The α and β subdomains form a DNA pump (Massey et al., 2006) while the γ subdomain regulates this activity (Yates et al., 2006). The C-terminus is involved in activation of chromosome dimer resolution through a dedicated XerCD/*dif* resolvase system. XerC and XerD are two tyrosine recombinases, which act at *dif* sites (the site of chromosome dimer resolution) located near the terminus region of the chromosome. Unlike XerC, XerD is functional only when activated by the C-terminal region of FtsK (Ip et al., 2003; Massey et al., 2004). The *E. coli* chromosome contains the over-represented FtsK orienting polar sequence (KOPS) motifs (GGGNAGGG), which are directed towards the *dif* region (Levy et al., 2005). The γ subdomain recognizes this KOPS sequences (Ptacin et al., 2006) and orients FtsK towards the *dif* region (Sivanathan et al., 2006) with the α and β subdomains providing the pumping force for DNA translocation using energy from ATP hydrolysis. At the *dif* site, FtsK γ domain brings together the XerCD/*dif* complex along with TopoIV in a productive conformation activating the synaptic junction. It then activates XerD catalytic activity bringing about chromosome decantenation (Ip et al., 2003; Massey et al., 2004). The crystal structures of α and β subdomains reveal the hexameric ring structure, which can accommodate dsDNA (Massey et al., 2006). At a translocation speed of 7 kb per second, FtsK is the fastest moving translocase on dsDNA (Pease et al., 2005). Although the linker region fused to a membrane binding divisome component is completely able to restore resolution of chromosome dimers even when FtsK does not have its transmembrane domain in *E. coli* (Dubarry and Barre, 2010; Dubbary et al., 2010), the C-terminal region also plays a role in cell division perhaps through resolution of intertwined circular duplicated chromosome (Bigot et al., 2004). Involvement of FtsK in the dual role of genome segregation as well as septum formation could also implicate it in a mechanism that would delay membrane fusion in the presence of unsegregated DNA at the septum (Dubarry and Barre, 2010), thus making FtsK a very crucial protein at the interface of bacterial cell division and genome maintenance that could be a potential target of drug development. Additionally, this protein has no human homologue and the structural data is also available (Lock and Harry, 2008). There are however, reservations about this protein to be investigated as an antibacterial drug target because of it's large size making it difficult to study its structure/function relationship and functional redundancy in interaction of the N terminal and C terminal domains with divisome and segrosome complexes.

7.2. DivIVA, a species specifc multifunctional protein

DivIVA is a coiled-coil tropomyosin-like protein in Gram-positive bacteria that has a role in sequestering MinCD to the cell poles, thereby aiding in directing cell division to the correct midcell site. It has been shown that DivIVA has a second function, which is quite different in sporulating cells of *B. subtilis*. In such cells, it interacts with the chromosome segregation machinery and helps in positioning *oriC* of the chromosome at the cell pole. A *divIVA* mutant that distinguishes this protein's role in genome segregation during sporulation from its vegetative function in cell division suggested that DivIVA is a bifunctional protein with distinct roles in division-site selection and chromosome segregation (Thomaides et al., 2001). DivIVA has been studied in many Gram-positive bacteria like *S. pneumoniae* (Fadda et al., 2007), *E. faecalis* (Ramirez-Arcos et al., 2005), *S. aureus* (Pinho and Errington, 2004), *S. coelicolor* (Flardh, 2003), *M. tuberculosis* (Wag31;antigen 84) (Kang et al., 2008) and *Bacillus lactofermentum* (Ramos et al., 2003). *E. faecalis* DivIVA has been established to be an essential gene having roles in cell division and chromosome segregation (Ramirez-Arcos et al., 2005). When this gene was disrupted by insertional inactivation creating *E. faecalis* JHSR1, the cell division led to abnormal cell clustering and improper nucleoid segregation. DivIVA is perceived as a species-specific multifunctional protein implicated in cell division and chromosome segregation. DiviVA's role in genome segregation and in defining the first plane of cell division in *cocci*, where poles are not structurally defined, would be an exciting area of research worth undertaking. Since, this protein acts as a regulatory link between cell division and genome segregation in bacteria it could be an ideal target for developing an effective antibacterial drug. Fortunately, human homologue(s) of DivIVA have not been identified yet and an assay system has been developed for studying *in vivo* interaction of DivIVA with other genome segregation and divisome components. Min D is another FtsZ mid-cell localizaing protein that has been shown to interact with genome partitioning system in both pathogenic and non-pathogenic strains (Ramirez-Arcos et al., 2005; Bramkamp, 2015). Although, further studies would require understanding the differential roles of DivIVA and MinD in these two major processes during bacterial growth, an inhibitior that could inhibit functions of both these proteins would be an ideal antibacterial drug.

7.3. Genome partitioning proteins (Par)

Tripartite genome partitioning in bacteria requires ParA and ParB proteins and a ParB binding *cis* regulatory element. Deletion of *parAB* genes induces a plethora of phenotypes including altered growth rates and cell lengths, anucleate cells and, perturbed chromosome organization in many bacteria. For instance, the absence of ParA and ParB proteins leads to disorganised chromosomes, which additionally impacts division site selection and growth in *C. glutamicum* (Donovan et al., 2013). In *C. crescentus*, ParA and ParB are found to be essential for growth and cells lacking ParB showed altered FtsZ ring formation at mid cell position. Inhibitors that targeted the ParA protein in *M. tuberculosis* resulted in a bacteriostatic effect (Nisa et al., 2010). Depletion of ParB and/or increase in ParA could inhibit Z-ring formation and cell division in *C. crescentus* (Figge et al., 2003) and *Mycobacterium smegmatis* (Ginda et al., 2013). This phenotypic effect of ParB deletion has been attributed to the change in the ratio of ParA to ParB in *parB* mutant of *C. crescentus*. Similar observation is also reported from *D. radiodurans* where role of ParA of chromosome II (ParA2) in the regulation of cell division in the context of its stoichiometric balance with

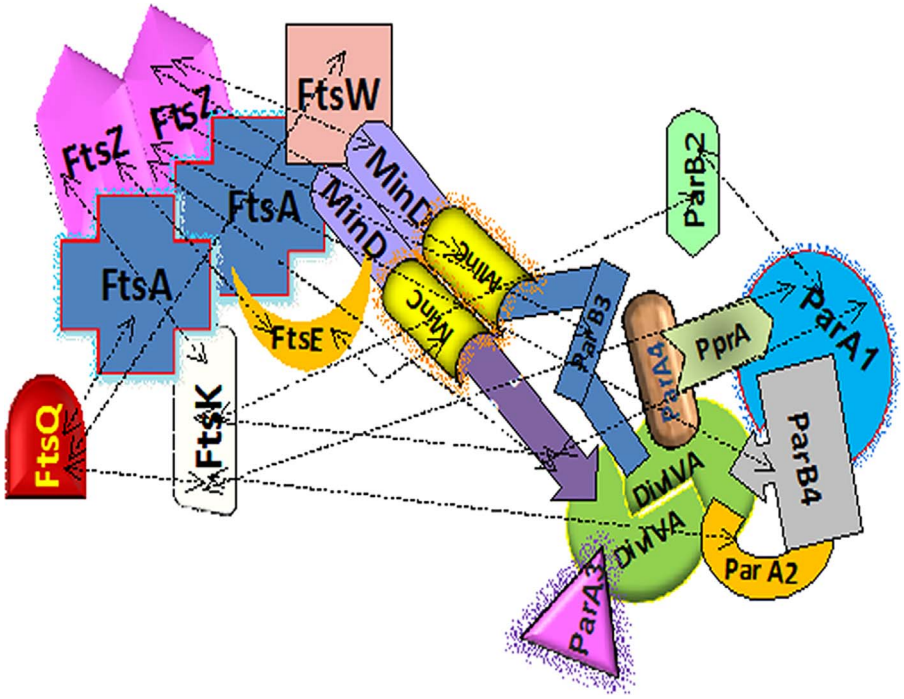

Fig. 7. *In vivo* interaction of cell division and genome segregation proteins of *D. radiodurans*. *In vivo* interaction of various divisome and segrosome proteins were determined using bacterial 2-hybrid system and shown. There are other probable interactions, which could not be observed using bacterial two-hybrid system were also deduced using STRING software and shown as dotted line.

ParB2 has been articulated (Charaka et al., 2013). The Par proteins therefore form another link between genome segregation machinery and cell division making it a target with high potential for antibacterial activity.

Further, recruitment of components involved in Structural Maintenance of Chromosome (MukBEF) by ParABS has been demonstrated and a weak interaction between ParC and Muk has also been discovered. Mutations that disrupt Muk-ParC interface adversely affect *E. coli* viability. *In vivo* interactions of chromosome segregation and cell division proteins have been demonstrated using bacterial two-hybrid system in other bacteria (Donovan et al., 2012; Ginda et al., 2013; Ringgaard et al., 2014) as well as in *D. radiodurans* (Fig. 7), which could be explored further.

8. Protein phosphorylation in cell cycle regulation

The phosphorylation-mediated regulation of protein functions and macromolecular interactions is not a new area of research. We know that protein kinases play a very important regulatory role in cell cycle regulation in eukaryotes. In bacteria too, the evidence for involvement of protein phosphorylation in cell division exists (Manuse et al., 2015). Recently, several studies have shown the involvement of eukaryotic-type Serine-threonine protein kinases (eSTPK) in genome segregation and cell division as well as in the crosstalk with other phosphorylation systems in intermediary metabolism (Jers et al., 2011; Shi et al., 2014; Libby et al., 2015). Involvement of tyrosine kinase (Wu et al., 1999) and serine threonine protein kinase (STPK) (Av-Gay and Everett, 2000; Bakal and Davies, 2000; Cozzone, 2005; Pereira et al., 2011) in bacterial cell division has been demonstrated. For instance, the roles of Ser/Thr phosphorylation in FtsZ activity regulation have been shown in many bacteria (Thakur and Chakraborti, 2006; Sureka et al., 2010; Manuse et al., 2015). Recently, a number of bacteria that harbour a multipartite genome system have been identified. The density of STPKs and tyrosine kinases on the genome of such bacteria are found to be relatively higher than the bacteria harbouring single circular chromosome (Misra et al., 2018). A DNA damage responsive STPK characterized for its role in radiation resistance in a multipartite genome harbouring radioresistant bacterium *D. radiodurans* is found to phosphorylate cell division proteins and is speculated to have roles in cell cycle regulation (Rajpurohit and Misra, 2010, 2013). The study on the effect of FtsZ phosphorylation has been mostly restricted to change in FtsZ activities *in vitro*. In *Streptococcus pneumoniae*, the MapZ an important protein contributing in FtsZ function is phosphorylated *in vivo* by STPK on two threonine residues (threonines 67 and 78) (Beilharza et al., 2012; Fleurie et al., 2014; Holeckova et al., 2015). On the other hand, the phoshorylation of ParB affecting the recruitment of ParB-centromere complex during genome partitioning has been shown in *Mycobacterium* (Baronian et al., 2015). DivIVA and FtsK, the proteins that work at the crossroad of cell division and genome partitioning are phosphorylated in some pathogenic bacteria. Since there are a number of other divisome components that are phosphphorylated by STPKs (Dasgupta et al., 2006), the possibility that these modifications change their *in vivo* interaction as well as function differently than *in vitro* need to be addressed? This could provide a new dimension to antibacterial drug development that would be worth undertaking.

9. Putative targets for antibacterial drug development

Bacterial multiplication and its regulation under biotic stress is linked to bacterial pathogenesis and therefore, growth inhibitors are normally used to cure bacterial infections. As said earlier, FtsZ is at the core of the divisome assembly and if the activity of FtsZ is inhibited it should control bacterial infection. A large number of both natural and chemically synthesised compounds mostly affecting functions of FtsZ have been identified as antibacterial drugs (Kumar et al., 2011; Awasthi et al., 2013). Many of these drugs for some reasons, have failed to control bacterial infection. One of the reasons could be that FtsZ function has become reductant to bacterial cell division in the presence of such drugs. Alternatively, the accessory proteins that aid FtsZ in its dynamics could protect its activity from such drugs. The other prominent candidates of bacterial cell division that have been targeted for developing antibacterial drugs include FtsA, FtsE, FtsI, ZapA, ZipA and SepF (Lock and Harry, 2008 and *therein* Table 1). There are proteins that regulate FtsZ functions and also interact with many other cell division and genome segregation proteins. While further work on killing pathogenic bacteria by blocking these proteins functions would continue, the possibility of disrupting bacterial growth by inhibiting cell division along with genome segregation would be worth exploring. The

earlier paradigm that genome maintenance proteins can inhibit cell division only through inhibiting the separation of duplicated genomes from the site of cell division is changing very fast. The evidences of genome partitioning system directly interacting with divisome and cell division regulatory proteins have grown significantly. In addition to FtsK, DivIVA and Par proteins, MatP-ZapB-FtsZ interaction has been charatcerized for their regulation of both cell division and genome segregation. If such proteins are present in pathogenic bacteria and exhibit functional analogy, these could be studied in detail for developing targets for antibacterial drugs. Structural dissimilarities in homologues in a few cases may even help in developing selective inhibitors for pathogenic bacteria. There are many proteins that provide a bridge between genome segregation and cell division. If they were present in pathogenic bacteria, would be the ideal candidates for targeting both the processes simultaneously.

10. Conclusion and future perspectives

Genome duplication, followed by segregation and cytokiensis are mutually interdependent processes that determine the growth of an organism. These two macromolecular events have been studied in isolation mostly in rod shaped bacteria. Information on the molecular mechanisms interlinking cytokinesis and genome partitioning have started growing in the very recent past and certain components that regulate both these processes have been discovered. This has offered a great oppurtunity to understand the interdependent regulation of cell division and genome maintenance and design approaches for developing antibacterial drugs. Antibacterial drugs have been developed primarily by targeting cell division and maintenance of DNA topology. However, a large number of such drugs have not seen expected success. Although, several reviews have been published on cell division and genome segregation separately, reviews interlinking these two events in bacterial physiology have been very few in numbers. This review is written for researcher to enable them to find literature that comments on the interdependence of cell division and genome segregation in bacteria. It has also brought forth some discussion on this and suggested possible alternatives for better sustainability in antibacterial drug development. Targeting common regulators that coordinate molecular events occuring during genome segregation and cell division may strengthen antibacterial drug research. One of the major bottlenecks in this approach in the authors' opinion could be lack of availability of structures of these proteins, which would necessitate screening of a large number of molecules that would effectively attenuate their functions thus proving bactericidal. Among spatial regulators of cell division, it was found that none of the known molecular systems are strictly essential in *E. coli*. This indicates that the organism may have as yet unrevealed molecular mechanisms, which could hold potential for drug targeting (Männik and Bailey, 2015). The involvement of different kinases in the coordination between cell division and genome maintenance with other cellular processes would be another strong area that demands continuous update. The mechanism by which kinases regulate cell division and growth of bacteria is however not yet clear. Further research to understand how protein phosphorylation can regulate bacterial cell cycle would be an excellent question worth looking at in addition to identifying putative targets in the development of antibacterial drugs.

References

Aarsman, M.E., Piette, A., Fraipont, C., Vinkenvleugel, T.M., Nguyen-Distèche, M., den Blaauwen, T., 2005. Maturation of the *Escherichia coli* divisome occurs in two steps. Mol. Microbiol. 55, 1631–1645.

Adams, D.W., Erington, J., 2009. Bacterial cell division: assembly, maintenance and disassembly of the Z ring. Nat. Rev. Microbiol. 7, 642–653.

Alvarez, L., Espaillat, A., Hermoso, J.A., de Pedro, M.A., Cava, F., 2014. Peptidoglycan remodeling by the coordinated action of multispecific enzymes. Microb. Drug Resist. 20, 190–198.

Aussel, L., Barre, F.X., Aroyo, M., Stasiak, A., Stasiak, A.Z., Sherratt, D., 2002. FtsK is a DNA motor protein that activates chromosome dimer resolution by switching the catalytic state of the XerC and XerD recombinases. Cell 108, 195–205.

Av-Gay, Y., Everett, M., 2000. The eukaryotic-like Ser/Thr protein kinases of *Mycobacterium tuberculosis*. Trends Microbiol. 8, 238–244.

Awasthi, D., Kumar, K., Knudson, S.E., Slaydon, R.A., Ojima, I.J., 2013. SAR studies on trisubstituted benzimidazoles as inhibitors of Mtb FtsZ for the development of novel antitubercular agents. J. Med .Chem. 56, 9756–9770.

Bailey, M.W., Bisicchia, P., Warren, B.T., Sherratt, D.J., Mannik, J., 2014. Evidence for divisome localization mechanisms independent of the Min system and SlmA in *Escherichia coli*. PLoS Genet. 10, e1004504.

Bakal, C.J., Davies, J.E., 2000. No longer an exclusive club: eukaryotic signalling domains in bacteria. Trends Cell. Biol. 10, 32–38.

Baronian, G., Ginda, K., Berry, L., Cohen-Gonsaud, M., Zakrzewska-Czerwinska, J., Jakimowicz, D., Molle, V., 2015. Phosphorylation of *Mycobacterium tuberculosis* ParB participates in regulating the ParABS chromosome segregation system. PLoS One 10, e0119907.

Beilharza, K., Novakovab, L., Fadda, D., Branny, P., Massidda, O., Veening, J.W., 2012. Control of cell division in *Streptococcus pneumoniae* by the conserved Ser/Thr protein kinase StkP. Proc. Natl. Acad. Sci. U. S. A. 109, E905–E913.

Bernhardt, T.G., de Boer, P.A., 2005. SlmA a nucleoid-associated, FtsZ binding protein required for blocking septal ring assembly over chromosomes in *E. coli*. Mol. Cell 18, 555–564.

Beuria, T.K., Mullapudi, S., Mileykovskaya, E., Sadasivam, M., Dowhan, M., Margolin, W., 2009. Adenine nucleotide-dependent regulation of assembly of bacterial tubulin-like FtsZ by a hypermorph of bacterial actin-like FtsA. J. Biol. Chem. 284, 14079–14086.

Bi, E., Lutkenhaus, J., 1993. Cell division inhibitors SulA and MinCD prevent formation of the FtsZ ring. J. Bacteriol. 175, 1118–1125.

Bigot, S., Corre, J., Louarn, J.M., Cornet, F., Barre, F.X., 2004. FtsK activities in Xer recombination, DNA mobilization and cell division involve overlapping and separate domains of the protein. Mol. Microbiol. 54, 876–886.

Bigot, S., Sivanathan, V., Possoz, C., Barre, F.X., Cornet, F., 2007. FtsK, a literate chromosome segregation machine. Mol. Microbiol. 64, 1434–1441.

Boutte, C.C., Henry, J.T., Crosson, S., 2012. ppGpp and polyphosphate modulate cell cycle progression in *Caulobacter crescentus*. J. Bacteriol. 194, 28–35.

Bramkamp, M., Emmins, R., Weston, L., Donovan, C., Daniel, R.A., Errington, J., 2008. A novel component of the division-site selection system of *Bacillus subtilis* and a new mode of action for the division inhibitor MinCD. Mol. Microbiol. 70, 1556–1569.

Bramkamp, M., 2015. Following the equator: division site selection in *Streptococcus pneumoniae*. Trends Microbiol. 23, 121–122.

Buddelmeijer, N., Beckwith, J., 2002. Assembly of cell division proteins at *the E. coli* cell center. Curr. Opin. Microbiol. 5, 553–557.

Cabre, E.J., Gorostiaga, A., Carrara, P., Ropero, N., Casanova, M., Palacios, P., Stano, P., Jimenez, M., Rivas, G., Vicente, M., 2013. Bacterial division proteins FtsZ and ZipA induce vesicle shrinkage and cell membrane invagination. J. Biol. Chem. 288, 26625–26634.

Charaka, V.K., Misra, H.S., 2012. Functional characterization of the role of the chromosome I partitioning system in genome segregation in *Deinococcus radiodurans*. J. Bacteriol. 194, 5739–5748.

Charaka, V.K., Mehta, K.P., Misra, H.S., 2013. ParA encoded on chromosome II of *Deinococcus radiodurans* binds to nucleoid and inhibits cell division in *Escherichia coli*. J. Biosci. 38, 487–497.

Chauhan, A., Lofton, H., Maloney, E., Moore, J., Fol, M., Madiraju, M.V., Rajgopalan, M., 2006. Interference of *Mycobacterium tuberculosis* cell division by Rv2719c, a cell wall hydrolase. Mol. Microbiol. 62, 132–147.

Chen, Y., Erickson, H.P., 2005. Rapid *in vitro* assembly dynamics and subunit turnover of FtsZ demonstrated by fluorescence resonance energy transfer. J. Biol. Chem. 280, 22549–22554.

Chiaramello, A.E., Zyskind, J.W., 1990. Coupling of DNA replication to growth rate in *Escherichia coli*: a possible role for guanosine tetraphosphate. J. Bacteriol. 172, 2013–2019.

Cho, H., McManus, H.R., Dove, S.L., Bernhardt, T.G., 2011. Nucleoid occlusion factor SlmA is a DNA-activated FtsZ polymerization antagonist. Proc. Natl. Acad. Sci. U. S. A. 108, 3773–3778.

Claessen, D., Emmins, R., Hamoen, L.W., Daniel, R.A., Errington, J., Edwards, D.H., 2008. Control of the cell elongation-division cycle by shuttling of PBP1 protein in *Bacillus subtilis*. Mol. Microbiol. 68, 1029–1046.

Conti, J., Viola, M.G., Camberg, J.L., 2015. The bacterial cell division regulators MinD and MinC form polymers in the presence of nucleotide. FEBS Lett. 589, 201–206.

Cozzone, A.J., 2005. Role of protein phosphorylation on serine/threonine and tyrosine in the virulence of bacterial pathogens. J. Mol. Microbiol. Biotechnol. 9, 198–213.

de Boer, P.A.J., Crossley, R.E., Hand, A.R., Rothfield, L.I., 1991. The MinD protein is a membrane ATPase required for the correct placement of the *Escherichia coli* division site. EMBO J. 10, 4371–4380.

den Blaauwen, T., Hamoen, L.W., Levin, P.A., 2017. The divisome at 25: the road ahead. Curr. Opin. Microbiol. 36, 85–94.

Dajkovic, A., Mukherjee, A., Lutkenhaus, J., 2008. Investigation of regulation of FtsZ assembly by SulA and development of a model for FtsZ polymerization. J. Bacteriol. 190, 2513–2526.

Dasgupta, A., Datta, P., Kundu, M., Basu, J., 2006. The serine/threonine kinase PknB of *Mycobacterium tuberculosis* phosphorylates PBPA, a penicillin-binding protein required for cell division. Microbiology 152, 493–504.

Denapoli, J., Tehranchi, A.K., Wang, J.D., 2013. Dose-dependent reduction of replication elongation rate by (p)ppGpp in *Escherichia coli* and *Bacillus subtilis*. Mol. Microbiol. 88, 93–104.

Donovan, C., Sieger, B., Kramer, R., Bramkamp, M., 2012. A synthetic Escherichia coli

system identifies a conserved origin-tethering factor in Actinobacteria. Mol. Microbiol. 84, 105–116.
Donovan, C., Schauss, A., Krämer, R., Bramkamp, M., 2013. Chromosome segregation impacts on cell growth and division site selection in *Corynebacterium glutamicum*. PLoS One 8, e55078.
Draper, D.C., McLennan, N., Begg, K., Masters, M., Donachie, W.D., 1998. Only the N-terminal domain of FtsK functions in cell division. J. Bacteriol. 180, 4621–4627.
Du, S., Lutkenhaus, J., 2014. SlmA antagonism of FtsZ assembly employs a two-pronged mechanism like MinCD. PLoS Genet. 10, e1004460.
Dubarry, N., Barre, F.X., 2010. Fully efficient chromosome dimer resolution in *Escherichia coli* cells lacking the integral membrane domain of FtsK. EMBO J. 29, 597–605.
Durand-Heredia, J., Rivkin, E., Fan, G., Morales, J., Janakiraman, A., 2012. Identification of ZapD as a cell division factor that promotes the assembly of FtsZ in *Escherichia coli*. J. Bacteriol. 194, 3189–3198.
Ebersbach, G., Gerdes, K., 2005. Plasmid segregation mechanisms. Ann. Rev. Genet. 39, 453–479.
Egan, A.J., Cleverley, R.M., Peters, K., Lewis, R.J., Vollmer, W., 2016. Regulation of bacterial cell wall growth. FEBS J. 284, 851–867.
Erdmann, N., Petroff, T., Funnell, B., 1999. Intracellular localization of P1 ParB protein depends on ParA and parS. Proc. Natl. Acad. Sci. U. S. A. 96 14905-14901.
Erickson, H.P., Osawa, M., 2010. Cell division without FtsZ–a variety of redundant mechanisms. Mol. Microbiol. 78, 267–270.
Errington, J., Murray, H., Wu, L.J., 2005. Diversity and redundancy in bacterial chromosome segregation mechanisms. Philos. Trans. R. Soc. Lond. B Biol. Sci. 360, 497–505.
Espeli, O., Levine, C., Hassing, H., Marians, K.J., 2003. Temporal regulation of topoisomerase IV activity in *E. coli*. Mol. Cell 11, 189–201.
Espeli, O., Borne, R., Dupaigne, P., Thiel, A., Gigant, E., Mercier, R., Boccard, F., 2012. MatP–divisome interaction coordinates chromosome segregation with cell division in *E. coli*. EMBO J. 31, 3198–3211.
Fadda, D., Santona, A., D'Ulisse, V., Ghelardini, P., Ennas, M.G., Whalen, M.B., Massidda, O., 2007. *Streptococcus pneumoniae* DivIVA: localization and interactions in a MinCD-free context. J. Bacteriol. 189, 1288–1298.
Feucht, A., Lucet, I., Yudkin, M.D., Errington, J., 2001. Cytological and biochemical characterization of the FtsA cell division protein of *Bacillus subtilis*. Mol. Microbiol. 40, 115–125.
Figge, R.M., Easter, J., Gober, J.W., 2003. Productive interaction between the chromosome partitioning proteins, ParA and ParB: is required for the progression of the cell cycle in *Caulobacter crescentus*. Mol. Microbiol. 47, 1225–1237.
Flardh, K., 2003. Essential role of DivIVA in polar growth and morphogenesis in *Streptomyces coelicolor* A3(2). Mol. Microbiol. 49, 1523–1536.
Fleurie, A., Lesterlin, C., Manuse, S., Zhao, C., Cluzel, C., Lavergne, J.P., Franz-Wachtel, M., Macek, B., Combet, C., Kuru, E., et al., 2014. MapZ marks the division sites and positions FtsZ rings in *Streptococcus pneumoniae*. Nature 516, 259–262.
Fujita, J., Maeda, Y., Nagao, C., Tshuchiya, Y., Miyazaki, Y., Hirose, M., Mizohata, E., Matsumoto, Y., Inoue, T., Mizuguchi, K., Matsumura, H., 2014. Crystal structure of FtsA from *Staphylococcus aureus*. FEBS Lett. 588, 1879–1885.
Gamba, P., Veening, J.W., Saunders, N.J., Hamoen, L.W., Daniel, R.A., 2009. Two-step assembly dynamics of the *Bacillus subtilis* divisome. J. Bacteriol. 191, 4186–4194.
Gerdes, K., Howard, M., Szardenings, F., 2010. Pushing and pulling in prokaryotic DNA segregation. Cell 121, 927–942.
Ghosal, D., Trambaiolo, D., Amos, L.A., Lowe, J., 2014. MinCD cell division proteins form alternating copolymeric cytomotive filaments. Nat. Commun. 5, 5341.
Ginda, K., Bezulska, M., Ziołkiewicz, M., Dziadek, J., Zakrzewska-Czerwinska, J., Jakimowicz, D., 2013. ParA of *Mycobacterium smegmatis* co-ordinates chromosome segregation with the cell cycle and interacts with the polar growth determinant DivIVA. Mol. Microbiol. 87, 998–1012.
Gitai, Z., 2006. Plasmid segregation: a new class of cytoskeletal proteins emerges. Curr. Biol. 16, R133–R136.
Goehring, N.W., Beckwith, J., 2005. Diverse paths to midcell: assembly of the bacterial cell division machinery. Curr. Biol. 15, R514–R526.
Goley, E.D., Yeh, Y.C., Hong, S.H., Fero, M.J., Abeliuk, E., McAdams, H.H., Shapiro, L., 2011. Assembly of the *Caulobacter* cell division machine. Mol. Microbiol. 80, 1680–1698.
Gordon, G.S., Wright, A., 2000. DNA segregation in bacteria. Annu. Rev. Microbiol. 54, 681–708.
Gordon, G.S., Sitnikov, D., Webb, C.D., Teleman, A., Straight, A., Losick, R., Murray, A.W., Wright, A., 2004. Chromosome and low copy plasmid segregation in E. coli: visual evidence for distinct mechanisms. Cell 90, 1113–1121.
Grainge, I., 2010. FtsK–a bacterial cell division checkpoint? Mol. Microbiol. 78, 1055–1057.
Grenga, L., Luzi, G., Paolozzi, L., Gheraldini, P., 2008. The *Escherichia coli* FtsK functional domains involved in its interaction with its divisome protein partners. FEMS Microbiol. Lett. 287, 163–167.
Gueiros-Filho, F.J., Losick, R., 2002. A widely conserved bacterial cell division protein that promotes assembly of the tubulin-like protein FtsZ. Genes Dev. 16, 2544–2556.
Guynet, C., de la Cruz, F., 2011. Plasmid segregation without partition. Mob. Genet. Elem. 1, 236–241.
Haeusser, D.P., Margolin, W., 2016. Splitsville: structural and functional insights into the dynamic bacterial Z ring. Nat. Rev. Microbiol. 14, 305–319.
Haeusser, D.P., Schwartz, R.L., Smith, A.M., Oates, M.E., Levin, P.A., 2004. EzrA prevents aberrant cell division by modulating assembly of the cytoskeletal protein FtsZ. Mol. Microbiol. 52, 801–814.
Hajduk, I.V., Rodrigues, C.D., Harry, E.J., 2016. Connecting the dots of the bacterial cell cycle: coordinating chromosome replication and segregation with cell division. Semin Cell Dev. Biol. 53, 2–9.
Hale, C.A., Rhee, A.C., de Boer, P.A., 2000. ZipA-induced bundling of FtsZ polymers mediated by an interaction between C-terminal domains. J. Bacteriol. 182, 5153–5166.
Handler, A.A., Lim, J.E., Losick, R., 2008. Peptide inhibitor of cytokinesis during sporulation in *Bacillus subtilis*. Mol. Microbiol. 68, 588–599.
Hatano, T., Niki, H., 2010. Partitioning of P1 plasmids by gradual distribution of the ATPase ParA. Mol. Microbiol. 78, 1182–1198.
Hill, N.S., Buske, P.J., Shi, Y., Levin, P.A., 2013. A moonlighting enzyme links *Escherichia coli* cell size with central metabolism. PLoS Genet. 9, e1003663.
Holeckova, N., Doubravova, L., Massidda, O., Molle, V., Buriánková, K., Benada, O., Kofroňová, O., Ulrych, A., Branny, P., 2015. LocZ is a new cell division protein involved in proper septum placement in *Streptococcus pneumoniae*. mBio 6, e01700–14.
Huisman, O., D'Ari, R., Gottesman, S., 1984. Cell-division control in *Escherichia coli*: specific induction of the SOS function SfiA protein is sufficient to block septation. Proc. Natl. Acad. Sci. U. S. A. 81, 4490–4494.
Ip, S.C., Bregu, M., Barre, F.X., Sherratt, D.J., 2003. Decatenation of DNA circles by FtsK-dependent Xer site-specific recombination. EMBO J. 22, 6399–6407.
Ishikawa, S., Kawai, Y., Hiramatsu, K., Kuwano, M., Ogasawara, N., 2006. A new FtsZ-interacting protein, YlmF, complements the activity of FtsA during progression of cell division in *Bacillus subtilis*. Mol. Microbiol. 60, 1364–1380.
Jensen, R.B., Shapiro, L., 1999. The *Caulobacter crescentus smc* gene is required for cell cycle progression and chromosome segregation. Proc. Natl. Acad. Sci. U. S. A. 96, 10661–10666.
Jers, C., Kobir, A., Sondergaard, E.O., Jensen, P.R., Mijakovic, I., 2011. Bacillus subtilis two-component system sensory kinase DegS is regulated by serine phosphorylation in its input domain. PLoS One 6, e14653.
Johnson, J.E., Lackner, L.L., Hale, C.A., de Boer, P.A., 2004. ZipA is required for targeting of DMinC/DicB, but not DMinC/MinD, complexes to septal ring assemblies in Escherichia coli. J. Bacteriol. 186, 2418–2429.
Joseleau-Petit, D., Liebart, J.C., Ayala, J.A., D'Ari, R., 2007. Unstable *Escherichia coli* L forms revisited: growth requires peptidoglycan synthesis. J. Bacteriol. 189, 6512–6520.
Kang, C.M., Nyayapathy, S., Lee, J.Y., Suh, J.W., Husson, R.N., 2008. Wag31, a homologue of the cell division protein DivIVA, regulates growth, morphology and polar cell wall synthesis in mycobacteria. Microbiology 154, 725–735.
Kawai, Y., Moriya, S., Ogasawara, N., 2003. Identification of a protein, YneA, responsible for cell division suppression during the SOS response in *Bacillus subtilis*. Mol. Microbiol. 47, 1113–1122.
Kleckner, N., Fisher, J.K., Stouf, M., White, M.A., Bates, D., Witz, G., 2014. The bacterial nucleoid: nature, dynamics and sister segregation. Curr. Opin. Microbiol. 22, 127–137.
Kumar, K., Awasthi, D., Lee, S., Zanardi, I., Ruzsicska, B., Knudson, S., Tonge, P.J., Slaydon, R.A., Ojima, I.J., 2011. Novel trisubstituted benzimidazoles, targeting Mtb FtsZ, as a new class of antitubercular agents. J. Med. Chem. 54, 374–381.
Land, A.D., Luo, Q., Levin, P.A., 2014. Functional domain analysis of the cell division inhibitor EzrA. PLoS One 9, e102616.
Lara, B., Rico, A.I., Petruzzelli, S., Santona, A., Dumas, J., Biton, J., Vicente, M., Mingorance, J., Massidda, O., 2005. Cell division in cocci: localization and properties of the *Streptococcus pneumoniae* FtsA protein. Mol. Microbiol. 55, 699–711.
Larsen, R.A., Cusumano, C., Fujioka, A., Lim-Fong, G., Patterson, P., Pogliano, J., 2007. Treadmilling of a prokaryotic tubulin-like protein, TubZ, required for plasmid stability in *Bacillus thuringiensis*. Genes Dev. 21, 1340–1352.
Laub, M.T., Chen, S.L., Shapiro, L., McAdams, H.H., 2002. Genes directly controlled by CtrA, a master regulator of the *Caulobacter* cell cycle. Proc. Natl. Acad. Sci. U. S. A. 99, 4632–4637.
Lemon, K.P., Grossman, A.D., 2000. Movement of replicating DNA through a stationary replisome. Mol. Cell 6, 1321–1330.
Leonard, T.A., Møller-Jensen, J., Löwe, J., 2005. Towards understanding the molecular basis of bacterial DNA segregation. Philos. Trans. R. Soc. Lond. B Biol. Sci. 360, 523–535.
Levy, O., Ptacin, J.L., Pease, P.J., Gore, J., Eisen, M.B., Bustamante, C., Cozzarelli, N.R., 2005. Identification of oligonucleotide sequences that direct the movement of the *Escherichia coli* FtsK translocase. Proc. Natl. Acad. Sci. U. S. A. 102, 17618–17623.
Li, Y., Austin, S., 2002. The P1 plasmid in action: time-lapse photomicroscopy reveals some unexpected aspects of plasmid partition. Plasmid 48, 174–178.
Libby, E.A., Goss, L.A., Dworkin, J., 2015. The Eukaryotic-like Ser/Thr kinase PrkC regulates the essential WalRK two-component system in *Bacillus subtilis*. PLoS Genet. 11, e1005275.
Lindas, A.-C., Bernander, R., 2013. The cell cycle of archaea. Nat. Rev. Microbiol. 11, 627–638.
Lindas, A.C., Karlsson, E.A., Lindgren, M.T., Ettema, T.J., Bernander, R., 2008. A unique cell division machinery in the *Archaea*. Proc. Natl. Acad. Sci. U. S. A. 105, 18942–18946.
Liu, Z., Mukherjee, A., Lutkenhaus, J., 1999. Recruitment of ZipA to the division site by interaction with FtsZ. Mol. Microbiol. 31, 1853–1861.
Lock, R.L., Harry, E.J., 2008. Cell-division inhibitors: new insights for future antibiotics. Nat. Rev. Drug Discov. 7, 324–338.
Loose, M., Mitchison, T.J., 2013. The bacterial cell division proteins FtsA and FtsZ self-organize into dynamic cytoskeletal patterns. Nat. Cell. Biol. 16, 38–46.
Lutkenhaus, J., 2007. Assembly dynamics of the bacterial MinCDE system and spatial regulation of the Z ring. Annu. Rev. Biochem. 76, 539–562.
Männik, J., Bailey, M.W., 2015. Spatial coordination between chromosomes and cell division proteins in *Escherichia coli*. Front. Microbiol. 6, 306.
Ma, X., Margolin, W., 1999. Genetic and functional analyses of the conserved C-terminal core domain of *Escherichia coli* FtsZ. J. Bacteriol. 181, 7531–7544.
Manuse, S., Fleurie, A., Zucchini, L., Lesterlin, C., Grangeasse, C., 2015. Role of

eukaryotic-like serine/threonine kinases in bacterial cell division and morphogenesis. FEMS Microbiol. Rev. 40 (1), 41–56.
Marston, A.L., Thomaides, H.B., Edwards, D.H., Sharpe, M.E., Errington, J., 1998. Polar localization of the MinD protein of *Bacillus subtilis* and its role in selection of the mid-cell division site. Genes Dev. 12, 3419–3430.
Martos, A., Monterroso, B., Zorrilla, S., Reija, B., Alfonso, C., Mingorance, J., Rivas, G., Jimenez, M., 2012. Isolation, characterization and lipid-binding properties of the recalcitrant FtsA division protein from *Escherichia coli*. PLoS One 7, e39829.
Mascarenhas, J., Volkov, A.V., Rinn, C., Schiener, J., Guckenberger, R., Graumann, P.L., 2005. Dynamic assembly, localization and proteolysis of the *Bacillus subtilis* SMC complex. BMC Cell Biol. 6, 28.
Massey, T.H., Aussel, L., Barre, F.X., Sherratt, D.J., 2004. Asymmetric activation of Xer site-specific recombination by FtsK. EMBO Rep. 5, 399–404.
Massey, T.H., Mercogliano, C.P., Yates, J., Sherratt, D.J., Lowe, J., 2006. Double-stranded DNA translocation: structure and mechanism of hexameric FtsK. Mol. Cell 23, 457–469.
Maurya, G.K., Modi, K., Misra, H.S., 2016. Divisome and segrosome components of *Deinococcus radiodurans* interact through cell division regulatory proteins. Microbiology 162, 1321–1334.
Mercier, R., Petit, M.A., Schbath, S., Robin, S.E., Karoui, M., Boccard, F., Espeli, O., 2008. The MatP/matS site-specific system organizes the terminus region of the *E. coli* chromosome into a macrodomain. Cell 135, 475–485.
Misra, H.S., Maurya, G.K., Kota, S., Charaka, V.K., 2018. Maintenance of multipartite genome system and its functional significance in bacteria. J. Genet In Press.
Modell, J.W., Hopkins, A.C., Laub, M.T., 2011. A DNA damage checkpoint in *Caulobacter crescentus* inhibits cell division through a direct interaction with FtsW. Genes Dev. 25, 1328–1343.
Modi, K.M., Misra, H.S., 2014. Dr-FtsA, an actin homologue in *Deinococcus radiodurans* differentially affects Dr-FtsZ and Ec-FtsZ functions in vitro. PLoS One 9, e115918.
Modi, K.M., Tewari, R., Misra, H.S., 2014. FtsZDr, a tubulin homologue in radioresistant bacterium *Deinococcus radiodurans* is characterized as a GTPase exhibiting polymerization/depolymerization dynamics in vitro and FtsZ ring formation *in vivo*. Int. J. Biochem. Cell Biol. 50, 38–46.
Mohl, D.A., Gober, J.W., 1997. Cell cycle–dependent polar localization of chromosome partitioning proteins in Caulobacter crescentus. Cell 88 (5), 675–684.
Nanninga, N., 1991. Cell division and peptidoglycan assembly in *Escherichia coli*. Mol. Microbiol. 5, 791–795.
Ni, T., Corcoran, D.L., Rach, E.A., Song, S., Spana, E.P., Gao, Y., Ohler, U., Zhu, J., 2010. A paired-end sequencing strategy to map the complex landscape of transcription initiation. Nat. Methods 7, 521–527.
Nisa, S., Blokpoel, M.C., Robertson, B.D., Tyndall, J.D., Lun, S., Bishai, W.R., O'toole, R., 2010. Targeting the chromosome partitioning protein ParA in tuberculosis drug discovery. J. Antimicrob. Chemother. 65 (11), 2347–2358.
Ogino, H., Teramoto, H., Inui, M., Yukawa, H., 2008. DivS, a novel SOS-inducible cell-division suppressor in Corynebacterium glutamicum. Mol. Microbiol. 67 (3), 597–608.
Oliva, M.A., Cordell, S.C., Lowe, J., 2004. Structural insights into FtsZ protofilament formation. Nat. Struct. Mol. Biol. 11, 1243–1250.
Onogi, T., Ohsumi, K., Katayama, T., Hiraga, S., 2002. Replication-dependent recruitment of the beta-subunit of DNA polymerase III from cytosolic spaces to replication forks in *Escherichia coli*. J. Bacteriol. 184, 867–870.
Osawa, M., Anderson, D.E., Erickson, H.P., 2009. Curved FtsZ protofilaments generate bending forces on liposome membranes. EMBO J. 28, 3476–3484.
Pacheco-Gomez, R., Cheng, X., Hicks, M.R., Smith, C.J.I., Roper, D.I., Addinall, S., Rodger, A., Dafforn, T.R., 2013. Tetramerization of ZapA is required for FtsZ bundling. Biochem. J. 449, 795–802.
Paradis-Bleau, C., Sanschagrin, F., Levesque, R.C., 2005. Peptide inhibitors of the essential cell division protein FtsA. Protein Eng. Des. Sel. 18, 85–91.
Pazos, M., Natale, P., Vicente, M., 2012. A specific role for the ZipA protein in cell division: stabilization of the FtsZ protein. J. Biol. Chem. 288, 3219–3226.
Pease, P.J., Levy, O., Cost, G.J., Gore, J., Ptacin, J.L., Sherratt, D., Bustamante, C., Cozzarelli, N.R., 2005. Sequence-directed DNA translocation by purified FtsK. Science 307, 586–590.
Peng, H., Marians, K., 1993. Decatenation activity of topoisomerase IV during *oriC* and pBR322 DNA replication *in vitro*. Proc. Natl. Acad. Sci. U. S. A. 90, 8571–8575.
Pereira, S.F., Goss, L., Dworkin, J., 2011. Eukaryote-like serine/threonine kinases and phosphatases in bacteria. Microbiol. Mol. Biol. Rev. 75, 192–212.
Pichoff, S., Lutkenhaus, J., 2007. Identification of a region of FtsA required for interaction with FtsZ. Mol. Microbiol. 64, 1129–1138.
Pinho, M.G., Errington, J., 2004. A *divIVA* null mutant of *Staphylococcus aureus* undergoes normal cell division. FEMS Microbiol. Lett. 240, 145–149.
Potluri, L.P., Kannan, S., Young, K.D., 2012. ZipA is required for FtsZ-dependent preseptal peptidoglycan synthesis prior to invagination during cell division. J. Bacteriol. 194, 5334–5342.
Ptacin, J.L., Nollmann, M., Bustamante, C., Cozzarelli, N.R., 2006. Identification of the FtsK sequence-recognition domain. Nat. Struct. Mol. Biol. 13, 1023–1025.
Radhakrishnan, S.K., Pritchard, S., Viollier, P.H., 2010. Coupling prokaryotic cell fate and division control with a bifunctional and oscillating oxidoreductase homolog. Dev. Cell 18, 90–101.
Rajpurohit, Y.S., Misra, H.S., 2010. Characterization of a DNA damage-inducible membrane protein kinase from *Deinococcus radiodurans* and its role in bacterial radioresistance and DNA strand break repair. Mol. Microbiol. 77, 1470–1482.
Rajpurohit, Y.S., Misra, H.S., 2013. Structure-function study of deinococcal serine/threonine protein kinase implicates its kinase activity and DNA repair protein phosphorylation roles in radioresistance of *Deinococcus radiodurans*. Int. J. Biochem. Cell Biol. 45, 2541–2552.
Ramirez-Arcos, S., Liao, M., Marthaler, S., Rigden, M., Dillon, J.-A.R., 2005. *Enterococcus faecalis divIVA*: an essential gene involved in cell division, cell growth and chromosome segregation. Microbiology 151, 1381–1393.
Ramos, A., Honrubia, M.P., Valbuena, N., Vaquera, J., Mateos, L.M., Gil, J.A., 2003. Involvement of DivIVA in the morphology of the rod-shaped actinomycete *Brevibacterium lactofermentum*. Microbiology 149, 3531–3542.
Ravin, N.V., Rech, J., Lane, D., 2003. Mapping of functional domains in F plasmid partition proteins reveals a bipartite SopB-recognition domain in SopA. J. Mol. Biol. 329, 875–889.
Reyes-Lamothe, R., Nicolas, E., Sherratt, D.J., 2012. Chromosome replication and segregation in bacteria. Annu. Rev. Genet. 46, 121–143.
Ringgaard, S., van Zon, J., Howard, M., Gerdes, K., 2009. Movement and equipositioning of plasmids by ParA filament disassembly. Proc. Natl. Acad. Sci. U. S. A. 106 (46), 19369–19374.
Ringgaard, S., Zepeda-Rivera, M., Wu, X., Schirner, K., Davis, B.M., Waldor, M.K., 2014. ParP prevents dissociation of CheA from chemotactic signaling arrays and tethers them to a polar anchor. Proc. Natl. Acad. Sci. U. S. A. 111, E255–E264.
Rowlett, V.W., Margolin, W., 2015. The bacterial divisome: ready for its close-up. Philos. Trans. R. Soc. Lond. B Biol. Sci. 370, 1679.
Samson, R.Y., Obita, T., Freund, S.M., Williams, R.L., Bell, S.D., 2008. A role for the ESCRT system in cell division in archaea. Science 322, 1710–1713.
Sawitzke, J.A., Austin, S., 2000. Suppression of chromosome segregation defects of *Escherichia coli* muk mutants by mutations in topoisomerase I. Proc. Natl. Acad. Sci. U. S. A. 97, 1671–1676.
Sengupta, M., Nielsen, H.J., Youngren, B., Austin, S., 2010. P1 plasmid segregation: accurate redistribution by dynamic plasmid pairing and separation. J. Bacteriol. 192, 1175–1183.
Sherratt, D.J., 2003. Bacterial chromosome dynamics. Science 301, 780–785.
Shi, L., Pigeonneau, N., Ravikumar, V., Dobrinic, P., Macek, B., Franjevic, D., Noirot-Gros, M.F., Mijakovic, I., 2014. Cross-phosphorylation of bacterial serine/threonine and tyrosine protein kinases on key regulatory residues. Front. Microbiol. 5, 495.
Sivanathan, V., Allen, M.D., de Bekker, C., Baker, R., Arciszewska, L.K., Freund, S.M., Bycroft, M., Löwe, J., Sherratt, D.J., 2006. The FtsK gamma domain directs oriented DNA translocation by interacting with KOPS. Nat. Struct. Mol. Biol. 13, 965–972.
Sogo, J.M., Stasiak, A., Martinez-Robles, M.L., Krimer, D.B., Hernandez, P., Schvartzman, J.B., 1999. Formation of knots in partially replicated DNA molecules. J. Mol. Biol. 286, 637–643.
Steele, V.R., Bottomley, A.L., Garcia-Lara, J., Kasturiarachchi, J., Foster, S.J., 2011. Multiple essential roles for EzrA in cell division of *Staphylococcus aureus*. Mol. Microbiol. 80, 542–555.
Sureka, K., Hossain, T., Mukherjee, P., Chatterjee, P., Datta, P., Kundu, M., Basu, J., 2010. Novel role of phosphorylation-dependent interaction between FtsZ and FipA in mycobacterial cell division. PLoS One 5, e8590.
Szwedziak, P., Wang, Q., Freund, S.M., Lowe, J., 2012. FtsA forms actin-like protofilaments. EMBO J. 31, 2249–2260.
Tavares, J.R., de Souza, R.F., Meira, G.L., Gueiros-Filho, F.J., 2008. Cytological characterization of YpsB, a novel component of the *Bacillus subtilis* divisome. J. Bacteriol. 190, 7096–7107.
Thakur, M., Chakraborti, P.K., 2006. GTPase activity of mycobacterial FtsZ is impaired due to its transphosphorylation by the eukaryotic-type Ser/Thr kinase, PknA. J. Biol. Chem. 281, 40107–40113.
Thanbichler, M., Shapiro, L., 2006. MipZ, a spatial regulator coordinating chromosome segregation with cell division in *Caulobacter*. Cell 126, 147–162.
Thanbichler, M., 2010. Synchronization of chromosome dynamics and cell division in bacteria. Cold Spring Harbor Perspect. Biol. 2, a000331.
Thomaides, H.B., Freeman, M., Karoui, M.E., Errington, J., 2001. Division site selection protein DivIVA of *Bacillus subtilis* has a second distinct function in chromosome segregation during sporulation. Genes Dev. 15, 1662–1673.
Tonthat, N.K., Arold, S.T., Pickering, B.F., Van Dyke, M.W., Liang, S., Lu, Y., Beuria, T.K., Margolin, W., Schumacher, M.A., 2011. Molecular mechanism by which the nucleoid occlusion factor, SlmA, keeps cytokinesis in check. EMBO J. 30, 154–164.
Tonthat, N.K., Milam, S.L., Chinnam, N., Whitfill, T., Margolin, W., Schumacher, M.A., 2013. SlmA forms a higher-order structure on DNA that inhibits cytokinetic Z-ring formation over the nucleoid. Proc. Natl. Acad. Sci. U. S. A. 110, 10586–10591.
Treuner-Lange, L., Aguiluz, K., van der Does, C., Gomez-Sanot, N., Harms, A., Schumacher, D., Lenz, P., Hoppert, M., Kahnt, J., Muñoz-Dorado, J., Søgaard-Andersen, L., 2013. PomZ, a ParA-like protein, regulates Z-ring formation and cell division in *Myxococcus xanthus*. Mol. Microbiol. 87, 235–253.
van den Ent, F., Lowe, J., 2000. Crystal structure of the cell division protein FtsA from *Thermotoga maritime*. EMBO J. 19, 5300–5307.
Vecchiarelli, A.G., et al., 2010. ATP control of dynamic P1 ParA-DNA interactions: a key role for the nucleoid in plasmid partition. Mol. Microbiol. 78 (1), 78–91.
Vecchiarelli A.G. et al., ATP control of dynamic P1 ParA-DNA interactions: A key role for the nucleoid in plasmid partition, Mol Microbiol, 78(1), 2010, 78–91. Vecchiarelli, A.G., Mizuuchi, K., Funnell, B.E., 2012. Surfing biological surfaces: exploring the nucleoid for partition and transport in bacteria. Mol. Microbiol. 86, 513–523.
Vecchiarelli, A.G., Hwang, L.C., Mizuuchi, K., 2013. Cell-free study of F plasmid partition provides evidence for cargo transport by a diffusion-ratchet mechanism. Proc. Natl. Acad. Sci. U. S. A. 110, E1390–7.
Vecchiarelli, A.G., Neuman, K.C., Mizuuchi, K., 2014. A propagating ATPase gradient drive transport of surface-confined cellular cargo. Proc. Natl. Acad. Sci. U. S. A. 111, 4880.
Vincente, M., Rico, A., 2006. The order of the ring: assembly of *Escherichia coli* cell division components. Mol. Microbiol. 61, 5–8.
Vollmer, W., Joris, B., Charlier, P., Foster, S., 2008. Bacterial peptidoglycan (murein) hydrolases. FEMS Microbiol. Rev. 32, 259–286.

Wagner, J.K., Marquis, K.A., Rudner, D.Z., 2009. SirA enforces diploidy by inhibiting the replication initiator DnaA during spore formation in *Bacillus subtilis*. Mol. Microbiol. 73, 963–974.
Wang, L., Lutkenhaus, J., 1998. FtsK is an essential cell division protein that is localized to the septum and induced as part of the SOS response. Mol. Microbiol. 29, 731–740.
Wang, J.D., Sanders, G.M., Grossman, A.D., 2007. Nutritional control of elongation of DNA replication by (p)ppGpp. Cell 128, 865–875.
Weart, R.B., Lee, A.H., Chien, A.C., Haeusser, D.P., Hill, N.S., Levin, P.A., 2007. A metabolic sensor governing cell size in bacteria. Cell 130, 335–347.
White, O., Eisen, J.A., Heidelberg, J.F., Hickey, E.K., Peterson, J.D., Dodson, R.J., Haft, D.H., Gwinn, M.L., Nelson, W.C., Richardson, D.L., et al., 1999. Genome sequence of the radioresistant bacterium *Deinococcus radiodurans* R1. Science 286, 1571–1577.
Willemse, J., Mommaas, A.M., van Wezel, G.P., 2012. Constitutive expression of ftsZ overrides the whi developmental genes to initiate sporulation of *Streptomyces coelicolor*. Antonie Van Leeuwenhoek 101, 619–632.
Wollert, T., Yang, D., Ren, X., Lee, H.H., Im, Y.J., Hurley, J.H., 2009. The ESCRT machinery at a glance. J. Cell Sci. 122, 2163–2166.
Wu, L.J., Errington, J., 2004. Coordination of cell division and chromosome segregation by a nucleoid occlusion protein in *Bacillus subtilis*. Cell 117, 915–925.
Wu, J., Ohta, N., Zhao, J.L., Newton, A., 1999. A novel bacterial tyrosine kinase essential for cell division and differentiation. Proc. Natl. Acad. Sci. U. S. A. 96, 13068–13073.
Wu, L.J., Ishikawa, S., Kawai, Y., Oshima, T., Ogasawara, N., Errington, J., 2009. Noc protein binds to specific DNA sequences to coordinate cell division with chromosome segregation. EMBO J. 28, 1940–1952.
Yates, J., Aroyo, M., Sherratt, D.J., Barre, F.X., 2003. Species specificity in the activation of Xer recombination at dif by FtsK. Mol. Microbiol. 49, 241–249.
Yates, J., Zhekov, I., Baker, R., Eklund, B., Sherratt, D.J., Arciszewska, L.K., 2006. Dissection of a functional interaction between the DNA translocase, FtsK, and the XerD recombinase. Mol. Microbiol. 59, 1754–1766.
Yim, L., Vandenbussche, G., Mingorance, J., Rueda, S., Casanova, M., Ruysschaert, J.M., Vicente, M., 2000. Role of the carboxy terminus of *Escherichia coli* FtsA in self-interaction and cell division. J. Bacteriol. 182, 6366–6373.
Youngren, B., Nielsen, H.J., Jun, S., Austin, S., 2014. The multifork *Escherichia coli* chromosome is a self-duplicating and self-segregating thermodynamic ring polymer. Genes Dev. 28, 71–84.
Zaritsky, A., Woldringh, C.L., 2015. Chromosome replication, cell growth, division and shape: a personal perspective. Front. Microbiol. 6, 756.
Zechiedrich, E.L., Khodursky, A.B., Cozzarelli, N.R., 1997. Topoisomerase IV, not gyrase, decatenates products of site-specific recombination in *Escherichia coli*. Genes Dev. 11, 2580–2592.